THEORETICA CHIMICA ACTA

edenda curat

Hermann Hartmann

adiuvantibus

C. J. Ballhausen, København
R. D. Brown, Clayton
E. Heilbronner, Basel
J. A. A. Ketelaar, Amsterdam
M. Kotani, Tokyo
J. Koutecký, Praha
J. W. Linnett, Cambridge
E. E. Nikitin, Moskwa
R. G. Pearson, Evanston
B. Pullman, Paris
K. Ruedenberg, Ames
C. Sandorfy, Montreal
M. Simonetta, Milano
O. Sinanoğlu, New Haven

Vol. 24, 1972

Springer-Verlag · Berlin · Heidelberg · New York

The exclusive copyright for all languages and countries, including the right for photomechanical and any other reproductions, also in microform, is transferred to the publisher.

The use in this journal of registered or trade names, trademarks etc. without special acknowledgement does not imply that such names, as defined by the relevant protections laws, may be regarded as unprotected and thus free for general use.

Alle Rechte, einschließlich das der Übersetzung in fremde Sprachen und das der fotomechanischen Wiedergabe oder einer sonstigen Vervielfältigung, auch in Mikroform, vorbehalten. Jedoch wird gewerblichen Unternehmen für den innerbetrieblichen Gebrauch nach Maßgabe des zwischen dem Börsenverein des Deutschen Buchhandels e. V. und dem Bundesverband der Deutschen Industrie abgeschlossenen Rahmenabkommens die Anfertigung einer fotomechanischen Vervielfältigung gestattet. Wenn für diese Zeitschrift kein Pauschalabkommen mit dem Verlag vereinbart worden ist, ist eine Wertmarke im Betrage von DM 0,40 pro Seite zu verwenden. *Der Verlag läßt diese Beträge den Autorenverbänden zufließen.*

Die Wiedergabe von Gebrauchsnamen, Handelsnamen, Warenbezeichnungen usw. in dieser Zeitschrift berechtigt auch ohne besondere Kennzeichnung nicht zu der Annahme, daß solche Namen im Sinne der Warenzeichen- und Markenschutz-Gesetzgebung als frei betrachtet wären und daher von jedermann benutzt werden dürften.

Springer-Verlag Berlin Heidelberg New York
Printed in Germany by Brühlsche Universitätsdruckerei, Gießen
© by Springer-Verlag Berlin · Heidelberg 1972

Index

Commentationes et Relationes

Alagona, G., Tomasi, J.: Contracted and Uncontracted Oscillator Orbitals in CI Calculations on Two Electron Systems . . . 42
Allen, L. C.: The Shape of Molecules . . . 117
Armstrong, D. R., Clark, D. T.: The Electronic Structures and Energies of Borazine, Boronimide and Dimeric Boronimide . . . 307

Ballhausen, C. J.: The Crystal Field Splittings in the 5 f Complexes . . . 234
Berke, T. D., s. Dannenberg, J. J. . . . 99
Blinder, S. M.: Spectral Variational Principle for Green's Functions . . . 382
Bonaccorsi, R., Pullman, A., Scrocco, E., Tomasi, J.: The Molecular Electrostatic Potentials for the Nucleic Acid Bases: Adenine, Thymine, and Cytosine . . . 51
Brett, A. C., Dingle, T. W.: Excited State Wave Functions. I. Comparison of the Messmer and Rayleigh-Ritz Variational Methods in the Case of Hydrogen . . . 111
Buemi, G., s. Favini, G. . . . 61
Buenker, R. J., Peyerimhoff, S. D.: Extension of Walsh's Rules to More General Systems 132

Clark, D. T., s. Armstrong, D. R. . . . 307
Coubeils, J. L., Pullman, B.: Molecular Orbital Study of the Conformational Properties of Phenothiazines . . . 35

Dannenberg, J. J., Berke, T. D.: Hyperconjugation in the 2-Butyl Cation . . . 99
DeArmond, M. K., s. Hauser, P. J., et al. . . . 78
Dingle, T. W., s. Brett, A. C. . . . 111

Favini, G., Buemi, G.: Configuration Analysis and Electronic States Properties. I. Four- and Six-π-Electron Systems . . . 61
Fischer, J., Veillard, A., Weiss, R.: Nature de la liaison dans l'ion tétraperoxochromate CrO_8^{3-}: une étude des structures cristalline et électronique . . . 317
Fraga, S., s. Lo, B. W. N., et al. . . . 71
— s. Lo, B. W. N., et al. . . . 300

Goodisman, J.: Energy Levels in Modified Quantum Statistical Potentials . . . 1
Gouterman, M., s. McHugh, A. J., et al. . . . 346
Gunter, J. D., s. Hauser, P. J., et al. . . . 78

Halton, M. P.: SCC—EH—MO Calculations on the Bonding and Electric Field Gradient in Oxyhaemoglobin and Other Haem Derivatives . . . 89
Hansen †, K. H., Koglin, E.: Polarisierte Kristallspektren einiger Hexaharnstoffkomplexe bei tiefen Temperaturen. Teil II. Lumineszenz . . . 216
— Schenk, H. J.: Polarisierte Kristallspektren einiger Hexaharnstoffkomplexe bei tiefen Temperaturen. Teil I. Absorption . . . 207
Hartmann, H.: Die Bewegung eines Körpers in einem ringförmigen Potentialfeld . . . 201
Hauser, P. J., Schreiner, A. F., Gunter, J. D., Mitchell, W. J., DeArmond, M. K.: Electronic Structures and MCD Spectra of Trigonal CR(III)S_6 Systems . . . 78
Helfrich, K.: Constants of Motion for Separable One-Particle Problems with Cylinder Symmetry . . . 271
Hensel, V., s. Kohlmaier, G. H., et al. . . . 251

Johansen, H., s. Ranck, J. P. . . . 334
Jørgensen, C. K.: Chemical Effects of Inner Shells Studied by Photo-Electron Spectrometry . . . 241
Jug, K., Labhart, H.: Über den Kontinuumseinfluß auf die Polarisierbarkeit von Molekülzuständen . . . 283
— Parr, R. G.: On the Rules of Scheibe . . . 147
Jungen, M., s. Staemmler, V. . . . 152

Kikuchi, O., s. Morikawa, T., et al. . . . 393
Koglin, E., s. Hansen †, K. H. . . . 216
Kohlmaier, G. H., Siré, E. O., Hensel, V.: Eine exakte klassische Behandlung der Schwingungs-Translations-Energieübertragung bei symmetrischen Zentralstößen . . . 251

Labhart, H., s. Jug, K. 283
Lischka, H., s. Russegger, P., et al. 191
Lo, B. W. N., Saxena, K. M. S., Fraga, S.: Electron Spin-Spin Contact Interaction in Many-Electron Atoms 71
— — — Mass-Variation and Darwin Relativistic Corrections in Many-Electron Atoms 300
McAloon, B. J., Perkins, P. G.: An SCF Study of P_4O_6 and P_4O_{10} 102
McHugh, A. J., Gouterman, M., Weiss, C., Jr.: Porphyrins XXIV. Energy, Oscillator Strength, and Zeeman Splitting Calculations (SCMO-CI) for Phthalocyanine, Porphyrins, and Related Ring Systems 346
Mechtler, R., s. Neckel, A., et al. 170
Mitchell, W. J., s. Hauser, P. J., et al. 78
Morikawa, T., Kikuchi, O., Somono, K.: SCF MO INDO Calculation of Anisotropic Hyperfine Coupling Tensors for σ-Type Radicals 393
Neckel, A., Rastl, P., Weinberger, P., Mechtler, R.: Berechnung der Bandstruktur vom Vanadiumcarbid VC 170
Parr, R. G., s. Jug, K. 147
Peat, F. D.: Suggested Calculations Using Transition Density Matrices 11
Perkins, P. G., s. McAloon, B. J. 102
Peters, D.: The Use of Symmetry in the Self-Consistent Field Theory of the Localised Molecular Orbital 16
Peyerimhoff, S. D., s. Buenker, R. J. 132
Polák, R., Rosmus, P.: Freie Elektronenpaare in lokalisierten CNDO/2-Wellenfunktionen der Stickstoffverbindungen 107
Porter, G. B.: Reversible Energy Transfer 265
Pullman, A., s. Bonaccorsi, R., et al. 51
Pullman B., s. Coubeils, J. L. 35
Raeber, P.: Zur Quantenchemie zyklischer und linearer Kohlenwasserstoffe 371
Ranck, J. P., Johansen, H.: Polarization Functions and Geometry Optimization in *ab initio* Calculations of the Rotational Barrier in Hydrogen Peroxide 334
Rastl, P., s. Neckel, A., et al. 170
Reinsch, E.-A.: Das Kastenmodell als Grundlage für ein *ab initio* Verfahren. II. Berechnung der Integrale 290
Rosmus, P., s. Polák, R. 107
Russegger, P., Lischka, H., Schuster, P.: Modellrechnungen zur Solvation einatomiger Ionen (LCAO—MO-Untersuchungen von Molekülstrukturen VIII) 191
Saxena, K. M. S., s. Lo, B W. N., et al. 71
— s. Lo, B. W. N., et al. 300
Schenk, H. J., Schwarz, W. H. E.: Spin-Bahn-Wechselwirkung und Jahn-Teller-Effekt. Analyse der $^4A_2 \to {}^2E$-Schwingungsprogression bei Crha$_6$ J$_3$ 225
— s. Hansen †, K. H. 207
Schreiner, A. F., s. Hauser, P. J., et al. 78
Schuster, P., s. Russegger, P., et al. 191
Schwarz, W. H. E.: Gombás Pseudopotential SCF Calculations for Atoms 29
— s. Schenk, H. J. 225
Scrocco, E., s. Bonaccorsi, R., et al. 51
Shchembelov, G. A., Ustynyuk, Yu. A.: CNDO/2 Calculation of Prototropic Rearrangement in Cyclopentadiene 389
Siré, E. O., s. Kohlmaier, G. H., et al. 251
Someno, K., s. Morikawa, T., et al. 393
Staemmler, V., Jungen, M.: The Direct Determination of Brueckner Orbitals with Application to the H_2 Molecule 152
Tomasi, J., s. Alagona, G. 42
— s. Bonaccorsi, R., et al. 51
Ustynyuk, Yu. A., s. Shchembelov, G. A. 389
Veillard, A., s. Fischer, J., et al. 317
Weinberger, P., s. Neckel, A., et al. 170
Weiss, C., Jr., s. McHugh, A. J., et al. 346
Weiss, R., s. Fischer, J., et al. 317

Theoret. chim. Acta (Berl.) 24, 1—10 (1972)
© by Springer-Verlag 1972

Commentationes

Energy Levels in Modified Quantum Statistical Potentials*

JERRY GOODISMAN

Department of Chemistry, Syracuse University, Syracuse, N. Y. 13210, USA

Received July 6, 1971

We calculate one-electron energy levels in potentials derived from the solution of the atomic Thomas-Fermi-Dirac equation. A local exchange potential is used. Corrections are made to a previous heory, which joins a TFD density to a quantum mechanical electron density near the nucleus, where the Thomas-Fermi-Dirac density has an incorrect singularity. Use of a potential derived from this theory leads to improvement in inner-shell energies. Changes in the potential, suggested in the literature as being reasonable for valence electrons, do not always give the expected improvement. Nor does naively correcting for self-energy lead to improved one-electron energy levels in general.

Es werden Einelektronen-Energieniveaus bezüglich Potentialen, die sich aus der Thomas-Fermi-Dirac Gleichung ergeben, berechnet, wobei ein lokales Austauschpotential benutzt wird. Es ergeben sich Korrekturen gegenüber einem früheren Verfahren, bei dem einerseits mit einer TFD Dichte und andererseits der quantenmechanischen Dichte in der Umgebung des Kernes, wo das TFD-Modell ein falsches Verhalten liefert, operiert wird. Auf diesem modifizierten Wege erhält man ein Potential, das zu besseren Funktionen für die inneren Schalen führt. Dagegen ergeben üblicherweise benützte Potentialänderungen für die Valenzelektronen, ebenso wenig wie naheliegende Korrekturen für die Selbstwechselwirkung, nicht die erstrebten Verbesserungen.

1. Introduction

Recently, we have been interested in calculating one-electron energies and wavefunctions in potentials derived from the solution of the Thomas-Fermi-Dirac equations for molecules. Hopefully, this could give results comparable to those of Hartree-Fock calculations but without the necessity of evaluating two-electron integrals or iterating to self-consistency. The potential used was the electrostatic potential which is the solution to the TFD equation (see Eqs. (6) et seq. below) plus an exchange potential proportional to the 1/3 power of the TFD electron density. The potential was modified far from the nuclei to give the proper behavior for an electron moving in the field of the nuclei and all the electrons but one.

The results [1] were qualitatively correct, but definitely inferior in accuracy to the Hartree-Fock. In particular, inner shell orbital energies were too high (by 2 a.u. for the Ar 1s electrons, for instance). We thus want to investigate improvements in the potential, testing these on atoms for simplicity, but requiring that the improvements be applicable to the molecular problem without increasing the complexity of the calculation. (This rules out use of the Weizsacker correction [2], for instance.)

---

* Supported by National Science Foundation under grant GP-20718.

It is well known that the Thomas-Fermi (TF) and Thomas-Fermi-Dirac (TFD) theories [3], while giving a roughly correct idea of the electron density for atoms, suffer from several serious deficiencies. One of these is that, because of the breakdown of the assumptions of the theory near a Coulombic singularity, they lead to an electron density which goes infinite as $r^{-3/2}$ instead of approaching a constant value as does the correct quantum mechanical density. This suggested to Ashby and Holtzman [4] and to the present author [5] the idea of using a density with the proper behavior for small r, and joining it to a density obtained from solution of the TF or TFD equation for larger r. The modified electron density led ot improved values for several electronic properties in the atomic [5] and molecular [6] cases. It was thought that the modification mentioned could improve the potential as it did the electron density. Examination of the modified theory [5] from the point of view of the potential revealed an inconsistency. In the next section, we give a slightly changed theory which is free from this problem. In Section 3 we calculate eigenvalues in the resulting modified potential.

Recently, Schwarz [7, 8] has pointed out that the Coulomb and exchange energies of the TFD theory actually both include the electrostatic interaction of each electron with itself, and that this self-interaction is a large quantity for atoms (larger [8] than the true exchange energy) where the electrons are localized. While the self-energy terms cancel out in the expression for the total energy, a modification in the potential seen by a single electron, with which we are concerned, is clearly called for. We investigate some simple corrections of this kind in Section 4.

The orbital energies for the valence shell electrons tended to be too low in our preceding work. In this connection, one can argue [9] that the exchange potential employed should be reduced by a factor of 2/3 for these electrons. The exchange potential used by us, given in terms of the density ϱ as $V_a = (3/2)(3/\pi)^{1/3} e\varrho^{1/3}$, may be derived as the *mean* exchange potential for the free-electron gas. However, for electrons with the maximum momentum, *i.e.*, in the highest filled energy state, the same theory gives the exchange potential as $(3/\pi)^{1/3} e\varrho^{1/3}$. This potential has been used successfully [9] to describe atomic valence electrons, and for all the electrons [8] in Hartree-Fock-Slater calculations (where the exchange interaction is approximated by a local exchange potential). The effect of modifying V_a in this way is investigated in Sect. 5.

2. Modified Thomas-Fermi-Dirac Theory

For an atom, let the electron density $\varrho(r)$ be given from $r = 0$ to $r = r_c$, and let the electron density for $r > r_c$ be varied to minimize the energy. Since we will use quantum statistical theories for the energy expression, we may anticipate that the outer boundary of the atom may be at a finite distance. We denote it by r_0, and minimize the energy with respect to r_0 as well as the density for $r > r_c$. The value of r_c is also to be determined.

The following conditions are imposed: (1) Continuity of ϱ at $r = r_c$; (2) continuity of $d\varrho/dr$ at $r = r_c$; (3) normalization of the total electron density; (4) vanishing of the electrostatic potential at $r = r_0$; (5) vanishing of the electric field at $r = r_0$. According to the quantum statistical theories [3] the kinetic energy is given by $\int \varkappa_k \varrho^{5/3} d\tau$ and the exchange energy by $-\int \varkappa_a \varrho^{4/3} d\tau$. Then the part of the energy which depends on the electron density for $r > r_c$ is

$$\begin{aligned} E = -Ze^2 \int_{r_c}^{r_0} \varrho r^{-1} \mathrm{d}\tau + \mathcal{J} e^2 \int_{r_c}^{r_0} \varrho r^{-1} \mathrm{d}\tau - \varkappa_a \int_{r_c}^{r_0} \varrho^{4/3} \mathrm{d}\tau \\ + \varkappa_k \int_{r_c}^{r_0} \varrho^{5/3} \mathrm{d}\tau + 1/2 e^2 \int_{r_c}^{r_0} \varrho(r)\, \mathrm{d}\tau \int_{r_c}^{r_0} \varrho(r')\, \mathrm{d}\tau' \, |r - r'|^{-1} . \end{aligned} \tag{1}$$

Here, Z is the nuclear charge, $\mathcal{J}$ is the total electron density contained in the sphere $r < r_c$, and the values of the constants in (1) are

$$\varkappa_a = 3/4 (3/\pi)^{1/3}\, e^2 \tag{2}$$

and

$$\varkappa_k = 3/10 (3\pi^2)^{2/3}\, e^2 a_0 , \tag{3}$$

where a_0 is the Bohr radius. The normalization condition for the total electron density is

$$(Z - \mathcal{J})\, e = e \int_{r_c}^{r_0} \varrho\, \mathrm{d}\tau . \tag{4}$$

We minimize the energy of Eq. (1) keeping the quantity (4) constant by means of a Lagrange multiplier λ. The result is

$$-e^2(Z - \mathcal{J})\, r^{-1} - 4/3 \varkappa_a \varrho^{1/3} + 5/3 \varkappa_k \varrho^{2/3} + e^2 \int \mathrm{d}\tau' \varrho(r')\, |r - r'|^{-1} + \lambda e = 0 . \tag{5}$$

Since the electrostatic potential is

$$V = (Z - \mathcal{J})\, r^{-1} - e \int \mathrm{d}\tau' \varrho(r')\, |r - r'|^{-1} \tag{6}$$

we can rewrite the equation as

$$5/3 \varkappa_k \varrho^{2/3} - 4/3 \varkappa_a \varrho^{1/3} + \mathrm{e}(\lambda - V) = 0 .$$

Combining this with the Poisson equation gives a second order non-linear differential equation for V or ϱ. We go over to the usual dimensionless variables

$$x = r/\mu \tag{7}$$

and

$$\psi = \frac{r}{Ze} (V - \lambda + \tau_0^2) , \tag{8}$$

where

$$\mu = 1/4 (3\pi)^{2/3} (2Z)^{-1/3} a_0 \tag{9}$$

and

$$\tau_0^2 = 4 \varkappa_a^2 / 15 \varkappa_k e . \tag{10}$$

The differential equation for $r > r_c$ is the usual TFD equation

$$\psi'' = x[(\psi/x)^{1/2} + \beta_0]^3 , \tag{11}$$

where

$$\beta_0 = \tau_0 (\mu/Ze)^{1/2} \tag{12}$$

and the density is given by

$$\varrho = \frac{Z}{4\pi\mu^3} [(\psi/x)^{1/2} + \beta_0]^3 . \tag{13}$$

Here, primes mean differentiation with respect to x. The normalization condition is then

$$Z-\mathscr{I}=Z\int_{x_c}^{x_0}(\psi''/x)\,x^2\,\mathrm{d}x=Z(x_0\psi_0'-\psi_0-x_c\psi_c'+\psi_c)\,, \tag{14}$$

where subscripts 0 and c mean values at x_0 and x_c.

We now have to determine r_0 by minimizing the energy expression (1) with respect to this quantity. Because of the conditions (1) and (2) on the density, the differential equation determines ϱ for all $r>r_c$, independently of r_0. Then we need consider only the explicit occurrences of r_0 in Eq. (1). Thus

$$\mathrm{d}E/\mathrm{d}r_0=0=\frac{(-Z+\mathscr{I})\,e^2\varrho_0}{r_0}-\varkappa_a\varrho_0^{4/3}+\varkappa_k\varrho_0^{5/3}$$
$$+e^2\varrho_0\int_{r_c}^{r_0}\varrho(r')\,\mathrm{d}\tau'|\boldsymbol{r}_0-\boldsymbol{r}'|^{-1}\,.$$

Here ϱ_0 is the value of the density at $r=r_0$. The last integral is just $(Z-\mathscr{I})/r_0$, so

$$\varrho_0=(\varkappa_a/\varkappa_k)^3 \tag{15}$$

which is eight times the value for the unmodified TFD theory.

Now we impose the conditions that V and $\mathrm{d}V/\mathrm{d}r$ must vanish at the boundary of the atom, $r=r_0$. Integrating the Poisson equation inward to some $r>r_c$, we have

$$V=\frac{e}{r}\int_r^{r_0}4\pi r^2\varrho\,\mathrm{d}r-e\int_r^{r_0}4\pi r\varrho\,\mathrm{d}r=er^{-1}\int_x^{x_0}Zx\psi''\,\mathrm{d}x$$
$$-e\mu^{-1}\int_x^{x_0}Z\psi''\,\mathrm{d}x=(eZ/r)(x_0\psi_0'-\psi_0+\psi-x\psi_0')\,.$$

Now this must equal $Ze\psi/r+\lambda-\tau_0^2$ according to (8), so we have

$$\lambda-\tau_0^2=\frac{Ze}{r}\,[x_0\psi_0'-\psi_0-x\psi_0']\,.$$

Since λ, τ_0^2, x_0, ψ_0', and ψ_0 are constants, this can hold for all r between r_c and r_0 only if

$$x_0\psi_0'-\psi_0=0 \tag{16}$$

and

$$\lambda-\tau_0^2=-Ze\psi_0'/\mu\,. \tag{17}$$

The condition (16) is automatically satisfied for the unmodified TFD theory, as is seen by putting $x_c=0$, $\mathscr{I}=0$, and $\psi_c=1$ in (14). In the present case, ψ_c and ψ_c' will be chosen to assure continuity of ϱ and $\mathrm{d}\varrho/\mathrm{d}r$ at r_c, assuming a particular density ϱ for $r<r_c$. We must satisfy (14), (16), and (17). The available parameters are r_c and λ. Combining (14) and (16) allows one to calculate r_c, and the cut-off point is determined by normalization, so can no longer be chosen by the variational criterion. λ is fixed by (17).

In the original modified theory [5], the small-r density was assumed to be that of the inner shell electrons. Thus

$$\varrho(r<r_c)=\frac{2Z^3}{\pi}\,e^{-2Zr} \tag{18}$$

which corresponds to two 1*s* electrons moving in the field of the nucleus. Then

$$\mathcal{J}=2[1-e^{-2Zr_c}(1+2Zr_c+2Z^2r_c^2)]\,.$$

According to (14) and (16),

$$1-Z^{-1}\mathcal{J}=-x_c\psi_c'+\psi_c \qquad (19)$$

and from (13)

$$\psi_c=\left[\left(\frac{4\pi\mu^3\varrho_c}{Z}\right)^{1/3}-\beta_0\right]^2 x_c\,. \qquad (20)$$

Insertion of (18) into (20) and differentiation allows computation of the right side of (19) as a function of r_c. Then (19) may be solved numerically for r_c. When this procedure is performed for Ar, it is found that r_c must be 0.0422 a_0 and that $\psi_c=0.7904$ and $\psi_c'=-0.1573$. If this is integrated outward, the electron density remains large out to r_0 so that it has a large discontinuity at this point, which is physically unacceptable.

To get something more reasonable for this model and to satisfy the condition of Eq. (15) for ϱ_0, it is necessary to relax one of the conditions we have imposed. For the density of (18) we substitute αe^{-2Zr} with the coefficient α to be determined. Unlike Ashby and Holtzman [4], who used the density $\varrho=\alpha e^{-\beta r}$ for $r<r_c$ with both α and β variable, we maintain $\beta=2Z$ to give the known correct behavior of the density at the nucleus (cusp condition) [10].

Now our procedure is as follows: (i) For a given α we find x_c by demanding that (19) be fulfilled. This is done by computing ϱ and ϱ' for different values of x, and from them deriving $\mathcal{J}$, ψ_c, and ψ_c'. (ii) Now one has initial values for ψ and ψ' and can integrate (11) outward. The integration is stopped at x_0 such that (16) is obeyed. (iii) ψ_0 and ψ_0' are now known, and ϱ_0 may be computed from (13). If (15) is not obeyed, α is changed and the process is repeated until it is. (iv) From ψ_0', λ may be computed according to (17). Now one knows V between r_c and r_0 according to (8). (v) For $r<r_c$, V is obtained by integrating the Poisson equation inward, using $\varrho=\alpha e^{-2Zr}$. Explicitly, this gives

$$V=\frac{\pi\alpha}{Z^3 r}\,[-1+e^{-2Zr}(1+Zr)]+\frac{Z}{r}+\frac{\pi\alpha}{Z^2}\,e^{-2Zr_c}(1+2Zr_c)-\frac{Z}{\mu}(\psi_0'-\psi_c')\,. \qquad (21)$$

3. Orbital Energies in Modified Potential

Having determined the electrostatic potential V according to the above procedure, we add the exchange potential

$$V_a=3/2(3/\pi)^{1/3}\,e\varrho^{1/3} \qquad (22)$$

to form the potential to be used in the calculation of one-electron energies. The density ϱ is $\alpha\cdot e^{-2Zr}$ for $r<r_c$ and the TFD density (13) for $r>r_c$. As we have mentioned, Eq. (22) represents an average exchange potential for all the electrons. The total exchange energy density (Eqs. (1) and (2)) is $-1/2\,eV_a\varrho$, the factor of 1/2 correcting the fact that the interaction between each pair of electrons is otherwise counted twice. For a neutral system, the total potential seen by one electron must become Coulombic at large distances from the nuclei. This is assured for the present

Table 1. Orbital energies for F in a.u. (Per cent differences from experimental results in parentheses)

	Experimental (Ref. [11])	SCF[1]	Unmodified TFD (Ref. [1])	Modified TFD (Section 3)
1s	−25.6	−26.38 (3.0)	−25.38 (0.9)	−26.01 (1.6)
2s	−1.48	−1.57 (6.0)	−1.68 (13.5)	−1.63 (10.1)
2p	0.96	−0.73 (6.0)	−0.96 (39.0)	−0.93 (35.0)

Table 2. Orbital energies for Ar in a.u. (Per cent difference from experimental results in parentheses)

	Experimental (Ref. [11])	SCF (Ref. [12])	Unmodified TFD (Ref. [1])	Modified TFD (Section 3)
1s	−118.1	−118.6 (0.4)	−116.4 (1.4)	−117.9 (0.2)
2s	12.1	−12.32 (1.8)	−11.54 (4.6)	−11.66 (3.6)
2p	9.25	−9.58 (3.6)	−9.31 (0.6)	−9.41 (1.7)
3s	−1.08	−1.28 (18.5)	−1.08 (0.0)	−1.01 (6.5)
3p	−0.58	−0.59 (2.0)	−0.62 (.0)	−0.53 (10.0)

case by replacing $V + V_a$ by er^{-1} whenever it falls below er^{-1}. This was done by Latter[1] in his computations for a related problem.

In Table 1 we give orbital energies for F, as derived from the present theory, the unmodified TFD theory [1], SCF calculations [11] and experiment [12]. The values found for α and r_c were 356.845 and $0.1015763 a_0$. An improvement for the inner shell electrons due to the modification is evident and expected: the error goes from 3.8% to 1.4% relative to the SCF result. For the other electrons, the modification also gives improvement, but it is slight for the $2p$ electrons, where the error is most serious. We believe that the fact that the SCF is farther from experiment than either TFD result for $1s$ is a coincidence for this case. Table 2 gives similar results for Ar. Here, $\alpha = 3134.98$ and $r_c = 0.0476648 a_0$. The K-shell energy here is in error by 0.2% relative to SCF, compared to 1.4% for the unmodified TFD theory. Other energies are sometimes improved, sometimes not; those for the outer electrons (M-shell) are relatively little affected. It may be noted that, in general, while inner shell orbital energies are lowered by the modification, outer shell energies are raised. In addition, the SCF does not reproduce the experimental term values as well as either TFD theory. The average per cent errors for the five levels are 5.2 for SCF, 2.7 for TFD and 4.5 for the modified TFD.

For the orbitals themselves we give in Table 3 the values of r for which nodes and extrema occur in the case of Ar. These are compared with the results of a Hartree-Fock calculation. The functions involved are actually r times the true radial wavefunctions. Since our method of determining the energies [1] involves outward numerical integration of the one-electron Schrödinger equation, our wavefunctions are less precisely determined at larger r. In particular, their tails are inaccurately determined, making it difficult to compute expectation values for the orbitals. It is seen that they have roughly the correct shapes.

---

[1] Latter, R.: Physic. Rev. 99, 510 (1955). The potential used by Latter was an approximation to $V + V_a$; the difference between the approximation and the potential leads to important differences in the computed energy levels as shown in Ref. [1].

Table 3. Characteristics of orbitals for Ar, distances in a_0[a]

Orbital	Extremum	Node	Extremum	Node	Extremum
1s	0.057	—	—	—	—
	0.051				
2s	0.045	0.118	0.34		
	0.039	0.102	0.28		
2p	0.29				
	0.24				
3s	0.044	0.115	0.29	0.52	1.19
	0.039	0.101	0.25	0.44	1.0
3p	0.22	0.42	1.29		
	0.19	0.40	1.10		

[a] First line is SCF from Czyzak, S. J.: Astrophys. J. Supp. 65, 7, 53 (1962); second is our result.

Table 4. Orbital energies for Zn, a.u. (Per cent deviation from experiment in parentheses)

Orbital	Experiment (Ref. [11])	This calculation	Herman and Skillman, Ref. [13]
1s	−356.0	−352.5 (0.8)	−349.2 (1.9)
2s	− 44.4	− 44.2 (0.5)	− 42.56 (4.1)
2p	− 38.1	− 39.6 (3.9)	− 37.78 (0.8)
3s	− 5.2	− 6.22 (20.)	− 4.89 (6.)
3p	− 3.5	− 4.64 (33.)	− 3.33 (5.)
3d	− 0.64	− 1.82 (180.)	− 0.63 (1.6)
4s	− 0.34_5	− 0.51 (48.)	− 0.309 (10.)

It is of interest to compare our results with those of the Hartree-Fock-Slater calculations of Herman and Skillman [13], a self-consistent field procedure in which a local approximation to the exchange potential is used. Their orbital energies are slightly better than ours for the outer shells, but inferior for the rest. The results for the orbitals are similar. The positions of the first extremum for the five orbitals are 0.057, 0.044, 0.28, 0.044, 0.22. This agrees very well – better than our results – with the SCF. The positions of the second extremum for 2s, 3s, and 3p are also in good agreement with SCF.

Finally, we give results for the 30-electron atom: Zn. Table 4 gives our calculated orbital energies, experimental ionization potentials, and the orbital energies of Herman and Skillman. Again, we do well for the inner shells and poorly for the outer electrons. Indeed, the errors for these orbital energies are very large, all being much too low. The evidence is, however, that *the small-r modification is successful in correcting the incorrect behavior of the potential as it affects the inner shell electrons, and permits reliable values to be calculated for inner-shell ionization potentials.*

4. Self-Energy Corrections

In this section, we investigate the effect on the one-electron energy levels of nple modifications of the Coulomb and exchange potentials, designed to remove correctly included self-energy terms. These would cancel for a correct Hartree-

Table 5. Energy levels for Ar (atomic units) with V_a, $(1-2Z^{-1})^{1/3}V_a$ and $(1-2Z^{-1})V_a$[a] compared with SCF values[b]

Atomic orbital	With full V_c and V_a	With $V_c x$ $(1-Z^{-1})$ and $V_a(1-2Z^{-1})^{1/3}$	With $V_c x$ $(1-Z^{-1})$ and $V_a(1-2Z^{-1})$	SCF result
1s	-116.4	-118.1	-117.4	-118.60
2s	11.54	12.97	-12.70	-12.32
2p	9.31	-10.78	-10.52	-9.58
3s	1.08	-1.76	-1.64	-1.28
3p	0.62	-1.19	-1.13	-0.59

[a] *The Coulombic potential is multiplied by $1-Z^{-1}$ in the latter two cases.*

[b] Czyzak, S. J.: Astrophys. J. Supp. 65, 7, 53 (1962).

Fock potential. For the Coulombic potential V_c, a simple and reasonable approximation is to multiply the electronic contribution to the electrostatic potential by $(Z-1)/Z$, Z being the number of electrons [7].

The correction to be made on the exchange potential is perhaps more problematical. Schwarz [8], following a suggestion of Gombás [14], favors reducing ϱ by $(Z-2)/Z$, noting that only half the electrons have an exchange interaction with any given electron. This menas V_a is to be multiplied by $(1-2Z^{-1})^{1/3}$. We think it is equally reasonable to argue that the potential itself should be multiplied by $(1-2Z^{-1})$. We may also note that Schwarz's V_a is only 2/3 of ours. Whether the factor of 3/2 does or does not appear in V_a may depend [7] on at what stage in the derivation one introduces the free-electron-gas model (but see next section). Irrespective of the coefficient of $\varrho^{1/3}$ in the exchange potential, the factor of $(1-Z^{-1})$ multiplying V_c assures that the overall potential approaches r^{-1} for large r as it should, with no additional modification.

In Table 5 we give the energies of the occupied one-electron levels for Ar, calculated with the unmodified TFD, with SCF, and the energies calculated when the Coulombic potential is multiplied by $1-Z^{-1}$ with the exchange potential reduced either by $(1-2Z^{-1})$ or by $(1-2Z^{-1})^{1/3}$. All energies are in atomic units (one a.u. = 27.21 eV).

It may be seen that the energies with the full V_c and V_a (and V replaced by r^{-1} when it falls below r^{-1}) are in fair agreement with the SCF values (average error = 6%). Modification of V_c and V_a in either way lowers all the energy levels and makes the overall agreement worse, although improving the 1s and 2s energies. We feel that the problem here is that the unmodified TFD model puts too much electron density near the nucleus. (The modification of Sections 2 and 3 lowers this density markedly.) Then the effective nuclear charge is too low near the nucleus, so that orbital energies will be too high for orbitals whose density is large here. Reducing V_c raises the effective charge everywhere, improving inner shell orbitals but overcompensating errors in others.

The situation may be contrasted with calculations such as those of Schwarz [8] or Herman and Skillman [13], where the exchange potential or some modification of it is used in SCF calculations to avoid the complications of the non-local Hamiltonian. There, the Coulombic potential includes correct behavior of the electron density near the nucleus. No iteration to self-consistency is involved in our work. Still, it is interesting to note that the errors in the orbital energies, using the full V_c and V_a, are comparable to those made in the approximate calculations. Schwarz [8] has given an extensive summary of such results for Ar. Our per cent errors are 1.9, 6.3, 2.8, 15.6, and 5.1; only about half of the ten methods tried by Schwarz do as well overall.

A recent article by Slater and Wood [15] discusses SCF calculations using local exchange approximations. The reason that good atomic orbitals, but poor orbital energies, are obtained in some cases (see end of Section 3) is explained. The orbital energy in Hartree-Fock calculations represents the change in energy on removal of one electron (Koopmans' Theorem), whereas in the calculations using local exchange potentials the orbital energy is the derivative of total energy with respect to the number of electrons. The difference may be written as a power series in which the derivative is the leading term, and higher terms may be used to give corrections. In the present case, where the potential is not constructed from the orbitals, the errors in orbital energies merely reflect the errors in the potential itself.

5. Modifications for the Valence Electrons

For some purposes, the valence electrons or electrons in the highest filled shell are of greatest interest. Thus we are interested in methods which may give reliable values for these. The errors in the present results are serious. We wish to explore methods for obtaining better values for the valence electrons, keeping in mind that our object is to apply such methods, eventually, to molecules with many electrons.

Errors in our potential for large r are of importance here. In particular, the effect of simply putting on a Coulombic tail must be examined. Yonei [16] remarked that the resulting discontinuity in $\mathrm{d}V/\mathrm{d}r$ may be of importance. Since we are interested in an electron moving in the field of the nucleus plus the other electrons, we could calculate their distribution and potential, and use this potential to treat the electron of interest. This automatically gives the correct large-r behavior with no discontinuity in $\mathrm{d}V/\mathrm{d}r$.

For the atom of atomic number Z, one should solve the TFD problem for the positive ion of nuclear charge Z and with $Z-1$ electrons. Then the electrostatic potential from this solution should be used, together with V_a derived from the electron density of the ion, to compute one-electron eigenvalues. Since the boundary conditions for the TFD equation change with degree of ionization [4] we have not done this. If one assumes the density for K^+ is well-approximated by that of Ar, one can use the Ar potential plus er^{-1} to obtain one-electron energies for K. The results were not good: orbital energies were always too low. This ignores the contraction of ϱ due to the additional nuclear charge, which increases the electrostatic shielding.

As we have mentioned, the exchange potential may be derived by averaging the exchange energy expression for an electron in a free-electron gas over all the electrons. One can also consider electrons with specific momenta individually, without averaging. For an electron with $p=0$, one obtains $2(3/\pi)^{1/3}e\varrho^{1/3}$ for the potential representing its exchange interaction with all the others. For an electron with p equal to the Fermi momentum, one gets half this. The last result is relevant for consideration of valence electrons, which are the highest filled orbitals. It may also be derived from the expression for the exchange energy density, $\varkappa_a \varrho^{4/3}$, by considering the effect of adding a small number of electrons, which must be at the Fermi momentum. The change in exchange energy density with change in ϱ is

$$d(-\varkappa_a e^2 \varrho^{4/3})/d(-e\varrho) = 4/3\,\varkappa_a e \varrho^{1/3}$$

so that $V_a = 4/3\,\varkappa_a e \varrho^{1/3}$ for these electrons.

Maintaining the small r modification of Sections 2 and 3, we change our exchange potential as above. For F, the $2p$ energy level goes from -0.93 a.u. to -0.52 a.u., which is equally far from the SCF value of -0.73 a.u. Now the $2p$ electrons represent 5/9 of the total number, so that the argument for using a potential appropriate to the top of the Fermi sea is not well-justified here. For Ar, the $3p$ electrons are 6/18 of the total, so the situation is somewhat better from the point of view of justification. Unfortunately, ε_{3p} is already too high and the modification must make things worse. In fact it goes to about -0.3 a.u.

However, for Zn, this modification leads to $\varepsilon = -0.32_2$ for the $4s$ orbital energy which is closer to the experimental orbital energy than the result of Herman and Skillman. The $3d$ energy increased to above -1. It is for this atom that one expects this idea to work best, since (a) the number of electrons is greatest and (b) the valence electrons are the smallest fraction (1/15) of the total number. The result is encouraging: in the future, we hope to extend these calculations to larger atoms and then to molecules, to see whether the results for Zn are typical.

References

1. Goodisman, J.: Theoret. chim. Acta (Berl.). Submitted for publication.
2. Yonei, K., Tomishima, Y.: J. Physic. Soc. Japan **20**, 1051 (1965).
3. Gombás, P.: Die statistische Theorie des Atoms und ihre Anwendungen, Vienna: Springer 1949.
4. Ashby, N., Holtzman, M. A.: Physic. Rev. A **1**, 764 (1970).
5. Goodisman, J.: Physic. Rev. A **2**, 1193 (1970).
6. Physic. Rev. A **3**, 1819 (1971).
7. Schwarz, W. H. E.: Z. Physik **214**, 149 (1968).
8. -- Z. Physik **239**, 162 (1970).
9. Gombás, P.: Pseudopotentiale, Wien-New York: Springer 1967.
10. Steiner, E.: J. chem. Physics **39**, 2365 (1963).
11. Clementi, E.: IBM J. Res. Devel. **9**, 2 (1965), supplement.
12. Slater, J. C.: Physic. Rev. **98**, 1039 (1955).
13. Herman, F., Skillman, S.: Atomic structure calculations, Englewood Cliffs, New Jersey: Prentice-Hall 1963.
14. Gombás, P.: Theoret. chim. Acta (Berl.) **5**, 112 (1966).
15. Slater, J. C., Wood, J. H: Int. J quant. Chemistry **4**, 3 (1971).
16. Yonei, K.: J. Physic. Soc. Japan **22**, 1127 (1967).

Prof. Dr. J. Goodisman
Department of Chemistry
Syracuse University
Syracuse, N.Y. 13210, USA

Theoret. chim. Acta (Berl.) 24, 11—15 (1972)
© by Springer-Verlag 1972

Suggested Calculations Using Transition Density Matrices

F. DAVID PEAT

Division of Chemistry, National Research Council of Canada, Ottawa, Canada

Received August 13, 1971

It is suggested that certain transition density matrices, N-representable in a limit, be used in a riational calculation. It is noted that such trial matrices should yield reasonable values for the ound state energies of small atoms or molecules provided a set of overlap integrals is maximised.

Es wird vorgeschlagen, bestimmte Übergangsdichtematrizen, die im Limit N-darstellbar sind, in einer Variationsrechnung zu benutzen. Es wird festgestellt, daß solche Näherungsmatrizen gute Werte für die Energie des Grundzustandes kleiner Atome oder Moleküle geben sollten, falls im Satz von Überlappungsintegralen maximiert wird.

On propose d'utiliser dans un calcul variationnel certaines matrices densité de transition, N représentables à la limite. Ces matrices d'essai devraient fournir des valeurs raissonnables pour l'énergie de l'état fondamental dans les petits atomes et les petites molécules à condition de maximiser un ensemble d'intégrales de recouvrement.

Introduction

Quantum chemistry has met with considerable success in calculating the ground state energies of atoms and atomic ions and more recently in computing molecular binding energies.

These calculations are normally performed on a computer by varying the different parameters which define a trial wave function, according to a minimisation procedure. Such minimisation procedures rely upon the Variation Theorem and hence upon totally antisymmetric trial functions.

Since full N-representability conditions have not been found for density matrices, any numerical work has been done in trivial cases or using density matrices formed by integration of an antisymmetric function. This compromise is motivated from fear of violating the Variation Principal during a minimisation procedure and may account for the lack of success of the density matrix in the field of quantum chemistry. For example although the density matrix was introduced seventeen years ago [1], no theory of valency has been advanced which has a basis in density matrix theory or uses the notation of geminals.

A resolution of the dilemma would be to adopt a perturbation approach to add corrections to the density matrix. The question of perturbation corrections and their relation to N-representability has never been properly discussed and there is no reason why a systematic approach along these lines should not be adopted.

It has also been suggested [2—4] that density matrices which are "approximately N-representable" may be used to obtain bounds upon the energy. It would not seem unreasonable therefore to relate such bounds to the particular order of the perturbation corrections. In this paper a scheme is outlined which uses transition density matrices which do not fulfill all the N-representability conditions.

The Transition Matrix

The discussion below is restricted to a system containing four electrons but may be extended to more general cases.

A totally antisymmetric wave function $\Psi(1234)$ may be expanded in terms of the eigenfunctions $\{\Phi_n(12)\}$ to the reduced two electron Hamiltonian $\boldsymbol{h}(12)$; that is

$$\Psi(1234) = \sum_n \Phi_n(12) f_n(34), \tag{1}$$

where

$$f_n(34) = \int_{34} \Phi_n^*(12)\,\Psi(1234). \tag{2}$$

The reduced Hamiltonian is related to the N-particle Hamiltonian $H(1234)$ by [5]

$$H(1234) = \frac{1}{2} NQ\boldsymbol{h}(12), \tag{3}$$

where Q is a projection operator formed from all even permutations $\boldsymbol{P}$ of the N-particles, that is

$$Q = \frac{2}{N!} \sum_{\text{even}} \boldsymbol{P}. \tag{4}$$

In the $\{\Phi_n\}$ representation the second order reduced density matrix is written

$$D^{(2)}(12:1'2') = \sum_{nm} B_{nm} \Phi_n(12)\,\Phi_m^*(1'2'), \tag{5}$$

where

$$B_{nm} = \int_{12} f_n(34) f_m^*(34). \tag{6}$$

The advantage of the density matrix formalism lies in the possibility of working with this function directly rather than with the wave function which becomes more difficult to define numerically with an increasing member of electrons. The drawback to this approach is that one does know how to choose the $\{f_n\}$ or $\{B_{nm}\}$ in order that the density matrix be N-representable [6]. (An N-representable density matrix is one derivable from an N-particle antisymmetric function or an ensemble of such functions.)

Grimley and Peat [5] suggested that as a first approximation to (5) the $\{f_n\}$ be projected from a zero order determinantal wave function $\Psi^0(1234)$ by zero order geminals $\{\Phi_n^{(0)}\}$ expanded in the same basis set. These zero order functions are Slater Determinants or linear combinations of such determinants with simple coefficients. That is

$$f_n^{(0)}(34) = \int_{34} \Phi_n^{*(0)}(12)\,\Psi^{(0)}(1234). \tag{7}$$

The approximate $\{B^{(0)}_{nm}\}$

$$B^{(0)}_{nm} = \int_{34} f^{(0)}_n(34)\, f^{(0)*}_m(34) \tag{8}$$

are inserted into (5), the correlated basis $\{\Phi_n\}$ being retained, and therefore define a trial density matrix $D^{(2)}_T(12:1'2')$,

$$D^{(2)}_T(12:1'2') = \sum_{nm} B^{(0)}_{nm}\Phi_n(12)\,\Phi^*_m(1'2')\,. \tag{9}$$

The energy computed using this trial density matrix generally falls below the true energy since the wave function

$$\Psi_T(1234) = \sum_n \Phi_n(12)\, f^{(0)}_n(34) \tag{10}$$

is not antisymmetric under the permutation (2, 3). (It can not, however, be proved hat the calculated energies form a lower bound.) Since the $\{\Phi_n\}$ are orthonormal he energy calculated using $D'^{(2)}_T(34:3'4')$, where

$$D'^{(2)}_T(34:3'4') = \int_{12} \Psi_T(1234)\,\Psi^*_T(123'4')\,, \tag{11}$$

ies above the true energy. If $\Psi^0_T(1234)$ is chosen to be the Hartree-Fock wave unction then the energy calculated using (11) is the Hartree-Fock energy.

The preceding discussion suggests that one may be able to improve upon the Grimley-Peat result employing the transition matrix defined by using the non antisymmetric wave functions;

$$\bar{D}^{(2)}_T(34:12) = \int_{1'2'} \Psi^*_T(1'2'34)\,\Psi_T(121'2') \tag{12}$$

$$= \Sigma\, \bar{B}_{nm} f^{*(0)}_n(34)\,\Phi_m(12)\,, \tag{13}$$

where

$$\bar{B}_{nm} = \int_{1'2'} \Phi^*_n(1'2')\, f^{(0)}_m(1'2')\,. \tag{14}$$

The energy calculated using this matrix is

$$\bar{E} = \frac{N}{2}\,\mathrm{Trace}\, h(1'2')\, D^{(2)}_T(12:1'2') + \mathrm{Trace}\,\bar{D}^{(2)}_T \tag{15}$$

$$= \frac{N}{2}\bar{B}^2_{nm}\varepsilon_m + \sum_n \bar{B}^2_{nm}\,, \tag{16}$$

where the ε_m are eigenvalues to $h(12)$ associated with the eigenfunctions Φ_n. The lower bound to $\bar{E}$ occurs if the overlaps $\{\bar{B}_{nm}\}$ are maximized with respect to the $\{f^{(0)}_m\}$, in such a limit $\bar{E}$ approaches the Grimley-Peat result. This limit is unobtainable of course since the zero order $\{f^{(0)}_m\}$ can never overlap completely with correlated $\{\Phi_n\}$. The expression (16) will therefore give an improvement over the Grimley-Peat result. Conversely the meaning of maximizing the $\{\bar{B}_{nm}\}$ with respect to the $\{\Phi_n\}$ may be investigated. Such a maximization could only be achieved if the $\{\Phi_n\}$ were limited to determinantal wave functions, with a corresponding increase in the energy; for example in the case of Hartree-Fock geminals, an upper bound $\bar{E}$ would be given by the Hartree-Fock energy. Therefore this transition matrix gives a calculated energy bracketed between the Grimley-Peat and Hartree-Fock results.

The example of anzats (12) suggests therefore that a more general transition matrix

$$D^{(2)}_{AB}(12:1'2') = \int_{34} \Psi^*_A(1234)\,\Psi_B(1'2'34) \tag{17}$$

could be used in calculations. Ψ_A is a Hartree-Fock or configurational interaction wave function while Ψ_B is a trial function built up from correlated geminals, possibly the eigenfunctions to $h(12)$, and may not be totally antisymmetric. Given the form $D^{(2)}_{AB}$ one would work directly with this density matrix rather than with the wave functions. An attempt would be made to maximize the overlap by varying Ψ_A and by selecting the geminals from the set $\{\Phi_n\}$ which are to be inserted in Ψ_B. For example in the case of the ground state to a four electron ion the dominant configuration in Ψ_A will be $(1S^2\,2S^2)$ indicating that the overlap may be maximised if the $\Phi(2S^2)$ geminal is included in Ψ_B. Since the energy corresponding to this geminal is quite large it would not have been included in Ψ_B on the grounds of energy minimisation alone.

No calculations have been performed using this program, however a simple argument gives an order of magnitude estimate of the success of the method. Consider Ψ_A to be the Hartree-Fock solution and Ψ_B to be composed of six eigenfunctions $\Phi(1s^2:{}^1S)$; $\Phi(1s\,2s:{}^1S)$; $\Phi(1s\,2s:{}^3S)$; $\Phi(2s^2;{}^1S)$ to $h(12)$. The energy calculated using $D^{(2)}_{AB}$ with these functions is

$$E_{AB} = \Sigma\, B^{(0)}_{nm}\Delta^2_{nm}\varepsilon_n \div \Sigma\, B^{(0)}_{nm}\Delta^2_{nm}\,, \tag{18}$$

where Δ_{nm} is the overlap between Φ_n and the relevant geminal projected out o Ψ_A, $B^{(0)}_{nm}$ is defined through (8) and the ε_n are the eigenvalues to $h(12)$. The overlap between the exact ground state of Beryllium and the Hartree-Fock result is 0.985 [7]. The significant deviations from an overlap of unity occur for the highly correlated $1S^2$ and $2S^2$ geminals [8] and it will be supposed that these overlaps occurring in equal proportion [8] give rise to the deficiency of 0.015 in the overlap of Ψ_A with the ground state.

Unfortunately the eigenvalues to $h(12)$ are not known in the case of Berryllium but they are known [5] for the ion C^{2+}. Since it is reasonable to suppose that the Δ_{nm} do not change rapidly with the nuclear charge in an isoelectronic series, the values for the Δ_{nm} obtained for Berryllium are inserted into (18). The ground state energy of C^{2+} is calculated to be 7981893 cm^{-1} and is 0.5% above the "experimental" non-relativistic energy of 8020746 cm^{-1} [9]. If a calculation were made using this technique it would be possible to improve upon this energy by maximizing the overlap integrals with respect to some configurational Ψ_A

The method suggested above is essentially that of taking the expectation value of the Hamiltonian over two different wave functions then passing to the reduced transition density matrix formation for convenience in performing the calculations. This approach is a special case of the problem of determining the eigenvalues to an operator H. In general the matrix elements

$$H_{nm} = \langle \Phi_n | H | X_m \rangle \tag{19}$$

over two basis sets $\{\Phi_n\}$ and $\{X_m\}$ are computed and the eigenvalue equation

$$\sum_n (H_{nm} - E\Delta_{nm})\, a_m = 0 \tag{20}$$

solved. The Δ_{nm} are overlap integrals between the two bases

$$\Delta_{nm} = \langle \Phi_n | X_m \rangle \tag{21}$$

and the a_m define an eigenfunction Ψ_E to H associated with the eigenvalue E, that is

$$a_m = \langle \Psi_E | X_m \rangle\,. \tag{22}$$

Use of different basis sets may give an advantage [10] over the calculation of matrix elements with a single basis. For example the $\{X_n\}$ may be expected to provide an excellent approximation to the eigenfunctions to H, however any integrals involved may be difficult to compute and the introduction of a set $\{\Phi_n\}$ which simplifies the integration without a significant reduction in accuracy would therefore be advisable. Recently use has been made of this convenience in making accurate calculations of the correlation energy of atoms [11].

Conclusion

If it is decided to work with wave functions which are not totally antisymmetric or density matrices which are not completely N-representable then it may be possible to develop successful computational procedures which would yield bounds upon the eigenvalues to the operators of interest. The particular anzats suggested in this paper enables one to work with a reduced density matrix directly rather than referring back to the wave function during any variation of the density matrix. Since the N-representability problem appears at present to be rather intractable investigations involving "almost N-representable" density matrices may prove to be profitable.

References

1. Löwdin, P. O.: Proc. Tenth Solvay Conference (1954).
   Physic. Rev. **97**, 1474 (1955).
2. Peat, F. D., Brown, R. J. C.: Int. J. quant. Chemistry **15**, 465 (1967).
3. — Physic. Rev. **173**, 69 (1968).
4. Simons, J., Harriman, J. E.: Physic. Rev. **2**, 1034 (1970).
5. Grimley, T. B., Peat, F. D.: Proc. physic. Soc. (London) **86**, 249 (1965).
6. Coleman, A. J.: Rev. mod. Physics **35**, 668 (1963).
7. Allen, T. L., Shull, H.: J. physic. Chem. **66**, 2281 (1962).
8. Tuan, D. F., Sinanoglu, O.: J. chem. Physics **41**, 2677 (1964).
9. Scheer, C. W., Silverman, J. N., Matsen, F. A.: Physic. Rev. **127**, 830 (1962).
10. Schwartz, C.: J. comput. Physics **2**, 90 (1967).
11. Boys, S. F., Hardy, N. C.: Proc. Roy. Soc. (London) A **310**, 43 (1969).

Dr. D. Peat
Department of Mathematics
Birkbeck College
Molet St.
London W.C.I., England

Theoret. chim. Acta (Berl.) 24, 16–28 (1972)
© by Springer-Verlag 1972

The Use of Symmetry in the Self-Consistent Field Theory of the Localised Molecular Orbital

DAVID PETERS

Royal Holloway College, University of London

Received March 22, 1971

It is shown how symmetry may be used in the context of the self-consistent field theory of the localised molecular orbital of the chemical bond. The results are (1) a reduction of the order of the secular determinant of the localised molecular orbital; (2) the classifying of the localised and canonical molecular orbitals under the various symmetry groups of the bonds and the molecule; (3) a clarification of the various types of symmetry group which are involved with the localised molecular orbitals.

Es wird gezeigt, wie Symmetrieeigenschaften im Zusammenhang mit der SCF-Theorie lokalisierter Molekülorbitale benutzt werden kann. Die Ergebnisse sind: 1. eine Reduktion der Ordnung der Säkulardeterminante des lokalisierten Molekülorbitals; 2. die Klassifizierung der lokalisierten und kanonischen Molekulorbitale nach den verschiedenen Symmetriegruppen der Bindungen und des Moleküls; 3. eine Klarung der verschiedenen Typen von Symmetriegruppen, die im Zusammenhang mit lokalisierten Molekülorbitalen stehen.

When we deal with the localised molecular orbitals (l.m.o.) which describe the chemical bond [1], it is not clear just what role symmetry plays in this type of theory. It is well known that the l.m.o.s transform as a reducible representation of the molecule's point group and it is less easy to deal with the reducible representations than with the irreducible ones. In addition, the nature of the relevant symmetry group is not obvious because l.m.o.s are confined in large measure to one part of a molecule and so it may seem that the symmetry group should be that of this part of the molecule. On the other hand, no l.m.o. is ever perfectly localised in one region of a molecule because it will generally have small but finite amplitude in all parts of the molecule.

In thinking about chemical bonds and l.m.o.s, we may either begin with an isolated bond and then expand our viewpoint to encompass the whole molecule or we may begin with the whole molecule and then narrow down our attention to the bond in question. The latter method is simpler and is generally used in this paper.

1. Introduction

The first step in applying symmetry to any molecule is to select the point group of the molecule in the usual way [2]. This group is now referred to as the "molecule group", G, and is of order g. If we are dealing with a closed shell ground state of a $2n$ electron molecule, then we have immediately

$$H\Psi = E\Psi \qquad R\Psi = +1\Psi \qquad = |\phi_1 \dots \phi_n \bar{\phi}_1 \dots \bar{\phi}_n| \tag{1}$$

where H is the hamiltonian of the molecule, Ψ is the many electron wavefunction of the Hartree-Fock approximation, R is any operation of the molecule group, the vertical bars denote a determinant and the ϕ are the familiar canonical m.o.s. In Eq. (1), we have labeled the m.o.s $1 \ldots n$. We may equally use three labels, one for the irreducible representation to which the m.o. belongs (i), one for the row of this representation (r) and a third label to distinguish m.o.s which are not distinguished by symmetry. This is a common notation and the standard sequence is a, i, r.

The equations which describe the symmetry of the canonical m.o.s are

$$R\phi_{air} = \sum_{s=1}^{d_i} D_i(R)_{sr}\phi_{ais} \tag{2}$$

together with the basic eigenvalue equation

$$F\phi_{air} = e_{ai}\phi_{air} \tag{3}$$

and the equations which result from the fact that R and F commute

$$\begin{aligned} R(F\phi_{air}) = F(R\phi_{air}) = F \sum_{s=1}^{d_i} D_i(R)_{rs}\phi_{ais} &= \sum_{s=1}^{d_i} D_i(R)_{rs} F\phi_{ais} \\ = e_{ai} \sum_{s=1}^{d_i} D_i(R)_{rs}\phi_{ais} \,. \end{aligned} \tag{4}$$

In these three equations, R is the operator of the molecule group G, and $D_i(R)_{rs}$ is the element of the r^{th} row and s^{th} column of the matrix D of the i^{th} irreducible representation.

The secular equation for the l.m.o.s is

$$\sum_{q=1}^{t-n+1} \left[c_{qi}(F_{pq} - e_{ii}S_{pq})\right] = 0 \qquad p = 1 - (t - n + 1) \tag{5}$$

where the c_{qi} are coefficients of the expansion of the l.m.o. over suitable basis functions earlier written [3] as $\chi_1 \ldots \chi_{(t-n+1)}$. In the earlier work [3] we chose these basis functions by guessing the final form of the eigenfunctions as well as possible and using these basis functions $u_1 \ldots u_{(t-n+1)}$ to form the secular determinant as in Fig. 1. Full details are given in the earlier work [3].

The two nuclei of the chosen bond establish a unique axis in the molecule. This is the "bond axis". We select from all the operations of the molecule group those operations which leave unchanged the two nuclei of the bond. Should we be dealing with a homopolar bond, A–A, we must extent this selection to include those operations which exchange the two nuclei.

Two possibilities arise now. If the bond in question is unique in the molecule, such as the C–Cl bond of methyl chloride, the selected operations will be the whole molecule group G. If there are other bonds in the molecule which are equivalent to the bond in question under the operations of the molecule group, such as the C–H bonds of methyl chloride, then the selected operations will be a subgroup, H, of the molecule group. The order of this subgroup is h. We refer to this group as the "bond-molecule" group (Table 1) to stress that this group is concerned with both the bond and the whole molecule. If we identify each bond in

$$\begin{array}{c|cc|ccc}
 & u_1 & u_1^* & u_2^* & u_3^* & u_4^* \ldots \\
\hline
u_1 & -0.5 & \delta & & \text{small} & \\
u_1^* & \delta & 0.5 & & & \\
\hline
u_2^* & & & 0.5 & & \\
u_3^* & \text{small} & & & 0.5 & \ldots \\
\vdots & & & & & \\
\end{array}$$

Fig. 1 The F matrix for the localised m.o.s before the use of symmetry. The quantity δ is a small quantity in general

Table 1 The bond-molecule groups

C_1	C_2	C_3	C_4	C_5	C_6	
	C_{2v}	C_{3v}	C_{4v}	C_{5v}	C_{6v}	
C_{1h}	C_{2h}	C_{3h}	C_{4h}	C_{5h}	C_{6h}	
	$S_2(C_i)$		S_4		S_6	
	D_2	D_3	D_4	D_5	D_6	
	D_{2d}	D_{3d}	D_{4d}	D_{5d}	D_{6d}	
	D_{2h}	D_{3h}	D_{4h}	D_{5h}	D_{6h}	
						$C_{\infty v}$
						$D_{\infty h}$

Taking the 37 groups in this table, removing the ten groups C_5, C_{5v}, C_{5h}, D_5, D_{5h}, D_{4d}, D_{5d}, D_{6d}, $C_{\infty v}$ and $D_{\infty h}$ and adding the groups T, T_d, O, O_h and T_h gives the familiar 32 point groups which occur in crystals. In a few molecules, other symmetries such as D_{7h} may occur.

the molecule with a label, α say, then we have H^α for a bond molecule group and S^α for its operations. The irreducible representations of H^α are either one dimensional or two dimensional.

Looking now at the forms of the m.o.s (not l.m.o.s) of the bond-molecule group, it is clear that we get the same m.o.s when we use the bond-molecule group as when we use the molecule group. This must be so if we use Eq. (3) to calculate the m.o.s since this equation uniquely determines the m.o.s regardless of any manipulation of symmetry groups. Some care is required with any degenerate levels but suitable choice of the functions spanning a degenerate level will make the above statement a valid one.

The formal equations for the use of symmetry with the bond-molecule group are straightforward. The equation which refer to the many electron wave function are essentially as before (Eq. (1)) while the equations which refer to the individual

Table 2. Examples of bond-molecule groups and bond groups

Molecule	Molecule group	Bond	Bond-molecule group	Bond group
H_2	$D_{\infty h}$	H–H	$D_{\infty h}$	$D_{\infty h}$
HF	$C_{\infty v}$	H–F	$C_{\infty v}$	$C_{\infty v}$
H_2O	C_{2v}	O–H	$C_{\infty v}$	$C_{\infty v}$
NH_3	C_{3v}	N–H	C_s	$C_{\infty v}$
CH_4	T_d	C–H	C_{3v}	$C_{\infty v}$
C_2H_4	D_{2h}	C–H	C_{1h}	$C_{\infty v}$
C_6H_6	D_{6h}	C–H	C_{2v}	$C_{\infty v}$
PCl_5	D_{3h}	P–Cl (axial)	C_{3v}	$C_{\infty v}$
PCl_5	D_{3h}	P–Cl (equatorial)	C_{2v}	$C_{\infty v}$
BF_3	D_{3h}	B–F	C_{2v}	$C_{\infty v}$
H_2O_2	C_2	O–H	C_1	$C_{\infty v}$
C_2H_6	D_{3h}	C–H	C_{1h}	$C_{\infty v}$
C_2H_6	D_{3h}	C–C	D_{3h}	$D_{\infty h}$

Table 3. Correlation tables for the bond groups $C_{\infty v}$ and $D_{\infty h}$

Heteronuclear case $C_{\infty v}$

$C_{\infty v}$	C_{6v}	C_{5v}	C_{4v}	C_{3v}	C_{2v}	C_6	C_5	C_4	C_3	C_2	C_s
a_1	a_1	a_1	a_1	a_1	a_1	a	a	a	a	a	a'
e_1	e_1	e_1	e	e	b_1+b_2	e_1	e_1	e	e	$2b$	$a'+a''$

Homonuclear case $D_{\infty h}$

$D_{\infty h}$	D_{6h}	D_{5h}	D_{4h}	D_{3h}	D_{2h}	D_{3d}	D_{2d}	S_6	S_4
a_{1g}	a_{1g}	a'_1	a_{1g}	a'_1	a_g	a_{1g}	a_1	a_g	a
a_{2u}	a_{2u}	a''_2	a_{2u}	a''_2	b_{1u}	a_{2u}	b_2	a_u	b
e_{1u}	e_{1u}	e'_1	e_u	e'	$b_{2u}+b_{3u}$	e_u	e	e_u	e
e_{1g}	e_{1g}	e''_1	e_g	e''	$b_{2g}+b_{3g}$	e_g	e	e_g	e

$D_{\infty h}$	D_6	D_5	D_4	D_3	D_2	C_{6h}	C_{5h}	C_{4h}	C_{3h}	C_{2h}
a_{1g}	a_1	a_1	a_1	a_1	a	a_g	a'	a_g	a'	a_g
a_{2u}	a_2	a_2	a_2	a_2	b_1	a_u	a''	a_u	a''	a_u or b_u
e_{1u}	e_1	e_1	e	e	b_2+b_3	e_{1u}	e'_1	e_u	e'	$2b_u$ or a_u+b_u
e_{1g}	e_1	e_1	e	e	b_2+b_3	e_{1g}	e''_1	e_g	e''	$2b_g$ or a_g+b_g

$D_{\infty h}$	C_{6v}	C_{5v}	C_{4v}	C_{3v}	C_{2v}	C_6	C_5	C_4	C_3	C_2	C_s	C_i
a_{1g}	a_1	a_1	a_1	a_1	a_1	a	a	a	a	a	a'	a_g
a_{2u}	a_1	a_1	a_1	a_1	a_1 or b_2	a	a	a	a	a or b	a'' or a'_2	a_u
e_{1u}	e_1	e_1	e	e	a_1+b_1 or b_1+b_2	e_1	e_1	e	e	$2b$ or $a+b$	$2a'$ or $a'+a''$	$2a_u$
e_{1g}	e_1	e_1	e	e	a_2+b_2 or b_1+b_2	e_1	e_1	e	e	$2b$ or $a+b$	$2a''$ or $a'+a''$	$2a_g$

The $C_{\infty v}$ table was worked from first principles as were the D_{6h}, D_{5h}, and D_{4h} components of the $D_{\infty h}$ table. The remainder of the latter table was constructed from the correlation tables of Ref. [4] via the D_{6h}, D_{5h}, and D_{4h} components. The choices which arise in the $D_{\infty h}$ table arise from different selections of axes and the correct choice will be obvious from context in a given problem.

m.o.s are

$$S^x\phi_{bjs} = \sum_{t=1}^{d_j} B_j(S^x)_{tr}\phi_{bjt} \qquad F\phi_{bjs} = e_{jb}\phi_{bjs} \tag{6}$$

together with the analogue of Eq. (4).

Some relevant examples are given in Table 2. In working with the molecule group and its subgroups, we will need the correlation tables between a group and its subgroups. These are available in the standard texts [4] apart from those for C_{ri} and D_{rh} which are given in Table 3.

2. The l.m.o.s and the Molecule Group

The l.m.o.s are now given three labels. The first (k) is a serial label denoting the position of the bond in the molecule, the second (w) being a distinguishing label between the equivalent bonds of one set and the third (p) distinguishing between the members of a degenerate set. An example is the molecule of Fig. 2a.

The l.m.o.s are related to the canonical m.o.s by an orthogonal transform given by

$$\mu = \phi A \qquad \phi = \mu A^{-1} = \mu \tilde{A} \tag{7}$$

where μ is the row vector of the l.m.o.s, ϕ is the row vector of the canonical m.o.s and A is an orthogonal (more generally, unitary) $n \times n$ matrix. In components, we have

$$\mu_{kwp} = \sum_{bjs} \phi_{bjs} A_{bjs}^{kwp} \qquad \phi_{bjs} = \sum_{kwp} \mu_{kwp} A_{kwp}^{bjs}. \tag{8}$$

It is well known that this transformation does not change the total wave function of the molecule [1, 3].

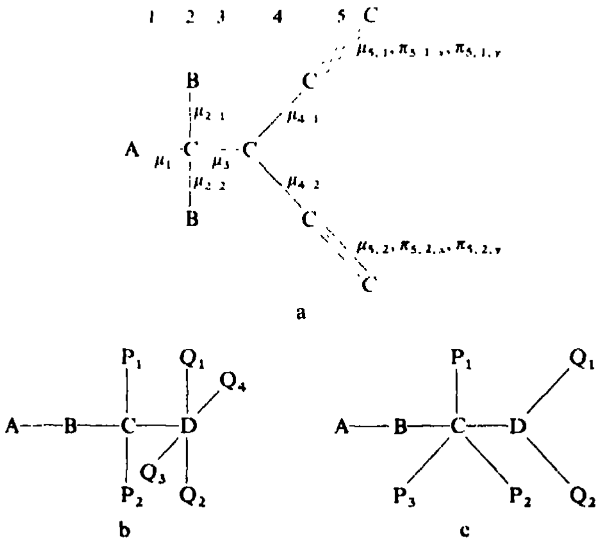

Fig. 2

The type of symmetry which occurs with the l.m.o.s is different from that of the canonical m.o.s. The former is a generalised type of permutational symmetry which is based on the physical assumption that equivalent bonds have l.m.o.s which are equivalent. By "equivalent" is meant differing only on their positions in space and not in the essentials of their functional form.

This type of permutational symmetry (more correctly perhaps pseudo-permutational symmetry) is important in the development of this work. In these permutational matrices, unity occurs once in each row and once in each column. Such matrices are orthogonal matrices. It is generally true that not all possible permutations between equivalent bonds are physically possible under the usual symmetry operations (e.g., the six C–H bonds of benzene) although exceptionally the molecule group and the permutation group are isomorphous (methane, T_d, is the permutation group on four objects). It follows that we are not concerned with the permutation groups themselves.

These matrices are block diagonal, each block clearly corresponding to a set of equivalent bonds in the molecule. An important property of such matrices is that one may strike out certain rows and columns in such a way as to remove the entire block and still have a permutational matrix. It is *not* generally possible to strike out the *same* rows and columns from all the matrices and still have a set of permutational matrices when dealing with the molecule group.

The above remarks apply to single bonds. If two dimensional π bonds are involved, the theory is readily extended to deal with such an example.

We may now write

$$R\mu_{kwp} = \sum_{w'p'} C^{kwp}_{kw'p'}\mu_{kw'p'} \tag{9}$$

where $C^{kwp}_{kw'p'}$ is the matrix element. Notice that we cannot assume $p = p'$ as a few simple examples show.

3. The l.m.o.s and the Bond-Molecule Group

Suppose that we are concerned with the bond μ_1. We select from the g matrices of the molecule group those matrices which correspond to the operations S^1 of the bond-molecule group H^1. There will be h^1 such matrices which form a representation of the bond-molecule group. The l.m.o.s form a basis for this representation in the usual way. The h^1 matrices differ from the entire set of g matrices in that the matrix element corresponding to the bond μ_1 is particularly simple. If μ_1 is a σ bond, then the top left element of the permutation matrices is $+1$ for *all* the matrices of the bond-molecule group. That is, all the h^1 matrices have the partial structure

$$S^1(\mu_1 \ldots \mu_n) = (\mu_1 \ldots \mu_n)\begin{bmatrix} +1 & 0 & 0\ldots \\ 0 & & \\ 0 & & \\ \ldots & \ldots & \end{bmatrix}. \tag{10}$$

This result is only true for the bond-molecule group and not for the molecule group.

It follows that the l.m.o. μ_1 belongs to an irreducible representation of the bond-molecule group H^1. We have then

$$S^1 \mu_{1js} = \sum_{t=1}^{d_j} B_j(S^1)_{jt} \mu_{1jt} \,. \tag{11}$$

Equations such as (10) and (11) will clearly hold for all the bonds in the molecule. If a doubly degenerate π bond is being dealt with, then the theory is extended in a straightforward way. Notice that all the functions $\mu_1 \ldots \mu_n$ will occur in each case but that different selections of the set of g matrices will be needed for the different bonds and bond-molecule groups.

Now we focus attention on the bond μ_1 again. The h^1 matrices of Eq. (10) are already partly reduced but we may if we wish reduce them completely. It is convenient to do this in two steps. First, we reduce each block under the "block group" which consists of μ_1 plus the block under discussion. Thus in the example of Fig. 2b, we have C_{2v} and C_{4v} block groups present. If we reduce the blocks in this way, we must of course replace the set of functions spanning each block with symmetrised functions as usual. That is, we replace the set of functions μ_{kwp} with the set of functions ϱ_{kjs} where now the second and third labels denote the s^{th} row of the j^{th} irreducible of the block group. Second, we reduce *all* the blocks under the *one* bond-molecule group. This bond-molecule group will clearly be the block group of lowest order or, in some cases, a group of lower order than any of the block groups. As an example of these two steps, we take the molecule of Fig. 2b and first reduce the P block under C_{2v} and the Q block under C_{4v}. Then both are classified under the bond-molecule group C_{2v}. A contrasting example is the molecule of Fig. 2c where we have both a C_{2v} and a C_{3v} block group while the bond-molecule group is C_s.

4. The Transformation between the l.m.o.s and the Canonical m.o.s

At this point we settle the question of the extent to which the matrix elements of the A matrix are determined by symmetry alone. We consider the reverse transformation between $\boldsymbol{\mu}$ and $\boldsymbol{\phi}$ of Eq. (7)

$$\boldsymbol{\phi} = \boldsymbol{\mu} \boldsymbol{A} \,. \tag{7}$$

Suppose that we are given the $\boldsymbol{\mu}$ and we then reduce this set of functions under the molecule group in the usual way to generate a set of functions v_{air}. That is

$$\boldsymbol{v} = \boldsymbol{\mu} \boldsymbol{B} \tag{12}$$

where $\boldsymbol{v}$ is the n dimensional row of the symmetry adapted functions v_{air}. The matrix $\boldsymbol{B}$ is determined by symmetry alone. To convert the $\boldsymbol{v}$ to the $\boldsymbol{\phi}$ requires the solution of the secular equation and we think of this as a transformation with the orthogonal matrix $\boldsymbol{C}$ where

$$\boldsymbol{\phi} = \boldsymbol{v} \boldsymbol{C} \tag{13}$$

and

$$C^{air}_{bjs} = \delta_{ij} \delta_{rs} C^{air}_{bir} \tag{14}$$

and the elements of $\boldsymbol{C}$ are otherwise arbitrary as far as symmetry is concerned.

The complete transformation is then

$$\phi = \mu BC \qquad \mu = \phi \tilde{C}\tilde{B}. \tag{15}$$

As an example of this process, consider the methyl chloride molecule with the four l.m.o.s written as μ_{CCl}, μ_{CH}, $\mu_{\mathrm{CH'}}$, $\mu_{\mathrm{CH''}}$. The $\boldsymbol{B}$ and $\boldsymbol{C}$ matrices are then

$$\boldsymbol{B} = \begin{bmatrix} 1 & 0 & 0 & 0 \\ 0 & 1/3 & 0 & 2/3 \\ 0 & 1/3 & 1/2 & -1/6 \\ 0 & 1/3 & -1/2 & -1/6 \end{bmatrix} \qquad \boldsymbol{C} = \begin{bmatrix} c & s & & \\ -s & c & & \\ & & 1 & \\ & & & 1 \end{bmatrix} \tag{16}$$

where $c = \cos(\gamma)$ and $s = \sin(\gamma)$ and γ is arbitrary.

5. l.m.o.s of the Truncated Molecule and the Bond Groups

The formal theory of the symmetry of the l.m.o.s which has been developed so far is complete in itself but it must be taken further is symmetry is to be of practical value in computing l.m.o.s. In particular, we must be able to truncate the secular equations and the secular determinant of Sect. 1 in ways suggested by chemical experience. We know, for example, that the properties of a given bond in a large molecule will be affected only slightly by the nature of a remote bond or group of atoms.

Suppose that we are again concerned with the bond whose l.m.o. is μ_1. We truncate the molecule by removing an atom or atoms and we clearly remove the atomic orbitals which are centred on the deleted atoms from the basis set of orbitals. In general, the symmetry of the bond-molecule group will change when atoms are deleted although cases do arise in which there is no such change in symmetry. Indeed, to change the symmetry an atom must be removed from an off-axis position as in the case of atom P in examples such as the molecule of Fig. 3a. If there is a set of several off-axis atoms which are equivalent, it is clear

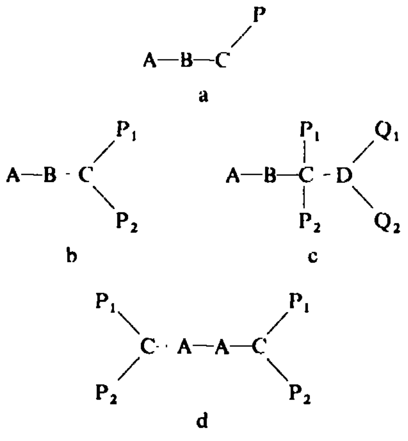

Fig. 3

that we must remove all of them at the same time. A simple example of an increase of symmetry resulting from the removal of a set of atoms is the removal of atoms P_1 and P_2 from the molecule of Fig. 3b.

As the symmetry of the molecule is increased by truncation of the molecule, operations must be added to the bond-molecule group. If the bond is $C_{\infty v}$, then as we truncate the molecule we can add only rotations (C_n) and reflections in a place which contains the bond axis (σ_v). If the bond is $D_{\infty h}$, we may add the same operations as before plus two fold rotations about the axis perpendicular to the bond axis together with σ_h, the inversion i and the rotary reflections (S_n). Some of these operations are interconnected and they cannot be added in arbitrary sets.

We now have the extended bond group. The matrices which we had before the truncation are dealt with by striking out the appropriate rows and columns. We strike out the appropriate functions from the row of l.m.o.s together with the contributions of the deleted atoms' atomic orbitals to the remaining l.m.o.s. We also write down by inspection the new matrices for the new operations which are now present in the extended bond group. We now have a set of permutation matrices which represent the extended bond group and all of these matrices have the partial structure

$$\begin{bmatrix} +1 & 0 & 0 & 0 \\ 0 & 0 \ldots\ldots\ldots & & \\ 0 \ldots\ldots\ldots\ldots\ldots & & & \\ \ldots\ldots\ldots\ldots\ldots\ldots & & & \end{bmatrix}.$$

The extension of this process to such cases as the molecules of Figs. 3c and 3d is straightforward.

Table 4. Matrices of the irreducible representations of the bond groups

Heteronuclear bond $C_{\infty v}$

Bond		E	$2C_\alpha$	σ_v
σ or σ^*	a_1	1	1	1
π or π^*	e_1	$\begin{bmatrix} 1 & 0 \\ 0 & 1 \end{bmatrix}$	$\begin{bmatrix} c_\alpha & -s_\alpha \\ s_\alpha & c_\alpha \end{bmatrix}$	$\begin{bmatrix} c_{2\alpha} & s_{2\alpha} \\ s_{2\alpha} & -c_{2\alpha} \end{bmatrix}$

Homonuclear bond $D_{\infty h}$

Bond		E	$2C_\alpha$	σ_v	i	S_α	C_2'
σ	a_{1g}	1	1	1	1	1	1
σ^*	a_{2u}	1	1	1	-1	-1	-1
π	e_{1u}	$\begin{bmatrix} 1 & 0 \\ 0 & 1 \end{bmatrix}$	$\begin{bmatrix} c_\alpha & -s_\alpha \\ s_\alpha & c_\alpha \end{bmatrix}$	$\begin{bmatrix} c_{2\alpha} & s_{2\alpha} \\ s_{2\alpha} & -c_{2\alpha} \end{bmatrix}$	$\begin{bmatrix} -1 & 0 \\ 0 & -1 \end{bmatrix}$	$\begin{bmatrix} c_\alpha & -s_\alpha \\ s_\alpha & c_\alpha \end{bmatrix}$	$\begin{bmatrix} -c_{2\alpha} & -s_{2\alpha} \\ -s_{2\alpha} & c_{2\alpha} \end{bmatrix}$
π^*	e_{1g}	$\begin{bmatrix} 1 & 0 \\ 0 & 1 \end{bmatrix}$	$\begin{bmatrix} c_\alpha & -s_\alpha \\ s_\alpha & c_\alpha \end{bmatrix}$	$\begin{bmatrix} c_{2\alpha} & s_{2\alpha} \\ s_{2\alpha} & -c_{2\alpha} \end{bmatrix}$	$\begin{bmatrix} 1 & 0 \\ 0 & 1 \end{bmatrix}$	$\begin{bmatrix} -c_\alpha & s_\alpha \\ -s_\alpha & -c_\alpha \end{bmatrix}$	$\begin{bmatrix} c_{2\alpha} & s_{2\alpha} \\ s_{2\alpha} & -c_{2\alpha} \end{bmatrix}$

The symbols c_α and s_α denote cosine(α) and sine(α) respectively.

Returning now to the truncation of the molecule, we continue this until there remains only the bond in question and its two nuclei. The bond group is thus $C_{\infty v}$ or $D_{\infty h}$. Throughout the truncation we deal with a chain of subgroups each of which is contained in a larger group. The chain begins with the bond-molecule group and ends with the bond group $C_{\infty v}$ or $D_{\infty h}$. When we have only the two nuclei of the bond μ_1 remaining then we have only one function left in the row of l.m.o.s. The corresponding matrices will be 1×1. They correspond to a row of the $C_{\infty v}$ or $D_{\infty h}$ character tables (Table 4). If a two dimensional π bond is being discussed, then the theory is extended in a natural way.

As an example of this truncation process, consider the methyl chloride molecule again. Taking the C–Cl bond as μ_1, the bond-molecule group is C_{3v} and the bond group $C_{\infty v}$. We must use the top line of the $C_{\infty v}$ character table. Or, were we interested in the π bond of methyl acetylene, we must end the truncation with the e_{1u} matrices of the $D_{\infty h}$ table.

6. Solution of the Secular Equations

We now show how symmetry simplifies the solution of the secular equation of the l.m.o.s. Before symmetry is considered, the matrix of Fig. 1 contains no zeros although matrix elements between functions which are far apart in space will clearly be small. It is convenient to divide this section into three subsections. In the first subsection, we examine the solution of the 2×2 secular determinant where the bond is perfectly localised and the operators which make up the F operator are confined to the two atoms forming the bond. In the second subsection, we expand the F operator until the entire molecule is represented in this operator while at the same time the secular determinant remains a 2×2 one. This is the stage in which the chemical ideas of polarisation and induction are incorporated into the theory and given a rigorous definition. In the third subsection, we allow the delocalisation of the bond μ_1 say over the entire molecule. This is the quantitative formulation of the chemical idea of hyperconjugation.

a) Operator and Orbital Localised

Here we suppose that we are solving a 2×2 secular determinant with a fully symmetrical operator. There are some questions about the detailed formulation of this operator but we leave these aside for the moment. If we are concerned with a σ bond, the matrix of the F operator over the basis functions u_1 and u_1^* is then [3]

$$\begin{bmatrix} F_{1,1} & F_{1,1^*} \\ F_{1,1^*} & F_{1^*,1^*} \end{bmatrix} \qquad F_{1,1} = \langle u_1 | F | u_1 \rangle \text{ etc.} \tag{17}$$

We naturally choose the two basis functions to transform under $C_{\infty v}$ or $D_{\infty h}$ just as we would in dealing with a diatomic molecule. We will emerge at the end with the a_1 or e_1 m.o.s of the $C_{\infty v}$ case or with the a_{1g}, a_{1u}, e_{1u} or e_{1g} m.o.s of the $D_{\infty h}$ case.

b) Extended Operator, Localised Function

At the end of the previous section, we were left with a diagonalised 2 × 2 matrix. We now allow the F operator to expand until it encompasses the entire molecule. Physically, this means that the two electrons of the bond μ_1 can see the attraction and repulsion of all the nuclei and electrons of distant atoms. The F operator now has the symmetry of the extended molecule but the electron is confined to the vicinity of the chosen bond μ_1 and this situation is just that of an external static electric field with the symmetry of the F operator. All we require is that the l.m.o. μ_1 transforms as the irreducible representation of the bond molecule group H^1. This may require the use of an extended basis set for the two atoms of the bond μ_1.

c) Extended Operator and Extended Orbital

In this section we consider the extension of the secular determinant until finally the complete μ_1 is reached. We begin with the two atoms of the bond and then add atoms to the molecule and add functions to the row of functions in Eq. (10) at the same time as we add the new μ^* to the basis of the secular equation. We also increase the size of the matrices while reducing the number of them. For convenience, we may replace the μ^* with the set of symmetry adapted functions ϱ^* each of which transforms as the s^{th} row of the j^{th} irreducible representation of the extended group. Then we may use the familiar theorem that the matrix elements of the F operator will vanish unless both functions belong to the same irreducible representation and to the same row of this representation. That is

$$\langle \varrho^*_{kjs} | \boldsymbol{F} | \varrho^*_{k'j's'} \rangle = \delta_{ss'} \delta_{jj'} \langle \varrho^*_{kjs} | \boldsymbol{F} | \varrho^*_{k'js} \rangle . \tag{18}$$

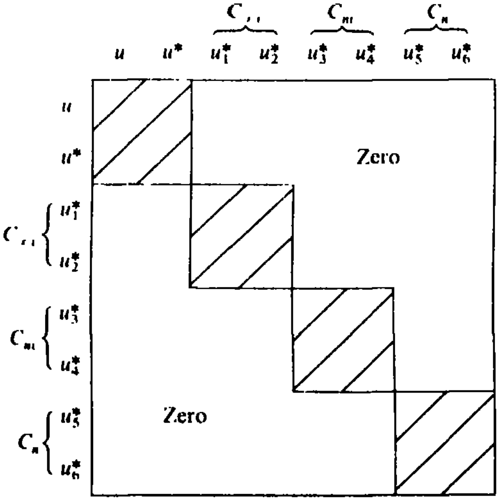

Fig. 4. An example of the F matrix over the l.m.o. after the use of symmetry (AB case)

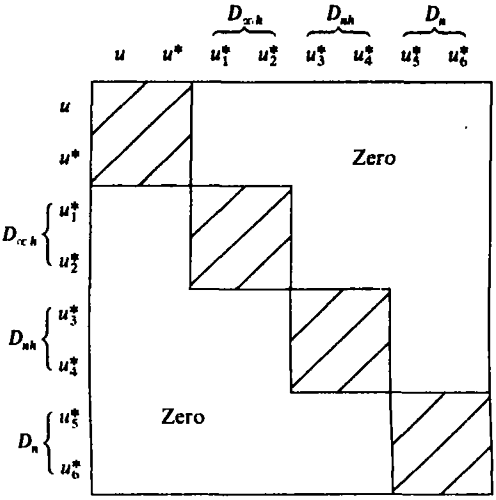

Fig. 5. An example of the F matrix over the l.m.o. after the use of symmetry (AA case)

This result will reduce the dimension of the secular determinant in nearly all cases. In the general case, the F matrix will take the form shown in Fig. 4 for a $C_{\infty v}$ bond and that shown in Fig. 5 for a $D_{\infty h}$ bond. The ordering of the blocks is the natural order for $C_{\infty v}$ but is somewhat arbitrary in the $D_{\infty h}$ case.

7. Summary and Comments

To summarise this work, we may say that the following points have been established:

1. The nature of the various symmetry groups with which we are concerned in dealing with the l.m.o.s is established (Table 5).

Table 5. Summary of the different groups involved with the bonds of a molecule

Molecule group	Bond-molecule groups	Bond groups
1) One group, G, order g, operations R	n groups, H^α, order h^α operations S^α	n groups, all $C_{\infty v}$ or $D_{\infty h}$
2) n occupied m.o.s, either localised or canonical	n m.o.s for each bond-molecule group	one or three m.o.s for each bond
3) Number of matrices is g	Number of matrices h^α for each bond	Number of matrices is infinite
4) All matrices may appear in permutational or reduced form	All matrices may appear in permutational or reduced form	All matrices fixed once and for all
5) Example of methyl chloride C_{3v}, 6th order, operations are E, C_3, and σ_v	Four groups, C_{3v} and C_s (three times)	$C_{\infty v}$ for all four bonds

2. The nature of the relevant reducible and irreducible representations of these groups is established.

3. The nature of the basis functions of these representations is clarified.

4. The order of the secular determinant is reduced.

Taken in conjunction with the theory of l.m.o.s reported earlier [3] this work and some other results to be reported later on perturbation methods establish a complete theory of the l.m.o. at the restricted Hartree-Fock level of approximation.

Extension of this work to deal with subsystems consisting of three or more atoms is quite feasible and can be made by inspection given the earlier work. Typical situations which will require this extension are the hydrogen bonding problem and the general chemical reactivity problem.

Finally, it should be noted that symmetry is of much greater use in l.m.o. theory where it is almost always useful for all bonds and not for just a small proportion of cases as is true of the theory of symmetry and canonical m.o.s.

References

1. Ruedenberg, K.: In: Modern quantum theory, Vol. 1, Chapter 4. New York: Academic Press Inc.
Hall, G. G.: Proc. Roy. Soc. (London) **202** A, 336 (1950).
Peters, D: J. chem. Soc **1963**, 2003, 2015, 4017; **1964**, 2901, 2908, 2916; **1965**, 3026; **1966**, 644, 652, 665.
2. Schonland, D. S.: Molecular symmetry. Chapter 9. London: Van Nostrand Ltd. 1965.
3. Peters, D.: J. chem. Physics **51**, 1559, 1566 (1969).
4 Wilson, E. B., Decius, J. C., Cross, P. C.: Molecular vibrations, p. 333. New York: McGraw-Hill 1955.

Dr. David Peters
Royal Holloway College
University of London
Englefield Green, Surrey, England

Theoret. chim. Acta (Berl.) 24, 29-34 (1972)
© by Springer-Verlag 1972

Gombás Pseudopotential SCF Calculations for Atoms*

W. H. EUGEN SCHWARZ

Lehrstuhl für Theoretische Chemie der Universität Bonn, Wegeler Straße 12, D-5300 Bonn, Germany

Received September 9, 1971

The "Simplified SCF Method" of Gombás, in which the orbital orthogonality conditions are replaced by statistical pseudopotentials, has been tested for the first time by accurate numerical calculations without any further approximation. Whereas the original version of the method leads to characteristic error trends, a correction factor recently introduced by Gombás into the pseudopotential expression, produces surprisingly good results.

Das sog. „Vereinfachte SCF-Verfahren“ von Gombás, bei welchem die Orthogonalitätsbedingungen der Orbitale durch statistische Pseudopotentiale ersetzt werden, wird erstmalig durch saubere numerische Rechnungen getestet. Während die unkorrigierte Version der Methode Resultate mit charakteristischen Fehlern liefert, führt der kürzlich von Gombás abgeleitete Korrekturfaktor im Besetzungsverbotpotential zu überraschend guten Ergebnissen.

La «méthode SCF simplifiée» de Gombás, où les conditions d'orthogonalité des orbitales sont remplacées par des pseudo potentiels statistiques, a été pour la première fois éprouvée avec des calculs numériques précis sans aucune autre approximation. Alors que la version originale de la méthode conduit à des tendances d'erreurs caractéristiques, un facteur de correction récemment introduit par Gombás dans l'expression du pseudo-potential, produit des résultats remarquablement bons.

Introduction

In order to make allowence for the Pauli exclusion principle in Hartree SCF theory, one has to impose the condition on the one-electron orbitals that they have definite numbers of nodal surfaces. In Hartree-Fock theory, in order to get a similar and simple formalism, the orbitals are assumed to be orthogonal. Consequently in both cases the higher orbitals show a pronounced short wavelength oscillatory behaviour near the nuclei. This causes a severe complication in valence-electrons calculations, as it necessitates the use of rather large basis sets (in expansion methods) or rather narrow grids (in numerical methods).

Therefore, Hellmann [1] and Gombás [2] developped the concept of pseudopotentials: no atomic orbital must have inner radial nodes; the kinetic energy associated with these nodes is taken into account instead by a statistical "occupation exclusion" pseudopotential.

In the so-called "Simplified SCF-Method for Atoms" of Gombás [3] one tarts with the energy expression

$$E = T_{\mathrm{rad}} + T_{\mathrm{ang}} + V + E_{\mathrm{ex}} . \tag{1}$$

V is the potential energy of the atom,

$$V = \sum_{i}^{\mathrm{occ.}} \left\langle i \left| -\frac{Z}{r} \right| i \right\rangle + \sum_{i>j}^{\mathrm{occ.}} \left\langle ij \left| \frac{1}{r_{12}} \right| ij \right\rangle . \tag{2}$$

---

* Dedicated to the memory of Professor Paul Gombás.

E_{ex} is the exchange energy correction. The angular kinetic energy is given by

$$T_{ang} = \sum_i^{occ} \left\langle i \left| \frac{l_i(l_i+1)}{2r^2} \right| i \right\rangle \tag{3}$$

and the radial kinetic energy by

$$T_{rad} = \sum_i^{occ} \left\langle i \left| -\frac{\Delta_r}{2} + \bar{G}_i \right| i \right\rangle . \tag{4}$$

Here the pseudopotential $\bar{G}_i$, acting on the electron in the spin-orbital i with radial function $P_{n_i l_i}(r)$ ($\int P^2\, dr = 1$) is given by

$$\bar{G}_i = \frac{\pi^2}{2}(D_i^2 + D_i \cdot P^2_{n_i l_i}) + \frac{1}{8r^2} \tag{5}$$

with

$$D_i = \sum_{n=l_i+1}^{n_i-1} P^2_{nl_i} . \tag{6}$$

The corresponding SCF-equations [3], obtained by energy variation, differ from the usual Hartree-Fock-Slater equations only by the additional pseudopotential term g_i in the Fock operator,

$$g_i = \frac{\pi^2}{2}(D_i^2 + 2D_i \cdot P^2_{n_i l_i}) + \frac{1}{8r^2} \tag{7}$$

but there are no orthogonality or nodal conditions.

They have been solved by Gombás and coworkers [3, 4]. The results are rather satisfactory. However, several approximations had been made in these calculations, the two most important ones being the following:

1. all orbitals within a shell of principal quantum number n are assumed to be identical (compare, however, Figs. 1 and 2);

2. each orbital is represented by a single (ν, ζ)-optimized STO $r^\nu \cdot \exp(-\zeta r)$ only.

On the other hand, the g-pseudopotential (7) has been used in valence electron calculations without these approximations [5]. There it showed up, that the calculated energies are lower than the experimental ones, or in other words that the pseudopotentials are somewhat too small.

There upon Gombás [6] deduced a correction factor for the D-values (6) in the pseudopotentials (5), (7):

$$D_i^{corr} = \left| 1 + \frac{1}{4}\left(1 + \frac{1}{n_i - l_i - 1}\right)\right| \cdot D_i , \tag{8}$$

which seemed to improve the results [5, 6].

Calculations and Results

The "Simplified SCF Equations" of Gombás have now been solved without any further approximation by numerical integration for a lot of atoms from all over the periodic table. A few results, with and without the correction of Eq. (8)[1],

---

[1] The SCF equations with correction (8) show a much better convergence behaviour than the uncorrected ones.

Table 1. SCF calculations on the Kr atom. Orbital parameters ε and orbital expectation values $\langle r^2 \rangle$ and $\langle 1/r \rangle$ in a.u.

		Hartree-Fock HF	Hartree-Fock-Slater HFS	Corrected[a] Gombás CG	Simple[a] Gombás SG
$-\varepsilon$	1s	1040	1020	1028	1018
	2s	140	132	133	161
	2p	126	120	123	115
	3s	21.7	18.5	19.6	29.8
	3p	16.7	14.0	13.9	16.6
	3d	7.7	6.0	6.1	2.7
	4s	2.3	1.5	1.7	3.2
	4p	1.05	0.60	0.58	0.63
$\langle r^2 \rangle$	1s	0.00241	0.00242	0.00241	0.00241
	2s	0.0413	0.0416	0.0413	0.0307
	2p	0.0320	0.0321	0.0314	0.0321
	3s	0.332	0.339	0.325	0.193
	3p	0.344	0.349	0.354	0.255
	3d	0.371	0.379	0.365	0.492
	4s	3.04	2.96	2.64	1.32
	4p	4.46	4.60	4.48	3.16
$\langle 1/r \rangle$	1s	35.50	35.45	35.50	35.50
	2s	7.92	7.88	6.09	7.37
	2p	7.89	7.87	7.94	7.87
	3s	2.64	2.62	2.05	2.74
	3p	2.52	2.51	2.02	2.50
	3d	2.28	2.27	2.32	2.09
	4s	0.80	0.83	0.73	1.05
	4p	0.67	0.68	0.59	0.74

[a] With Dirac-Gáspár exchange potential, see Ref. [7].

Table 2 Gombás SCF results on several atoms. Deviation of total atomic energy E and expectation values $\langle r^2 \rangle$ and $\langle 1/r \rangle$ from Hartree-Fock-Slater[a] results in %

Z	Atom	E		$\langle r^2 \rangle$		$\langle 1/r \rangle$	
		SG	CG	SG	CG	SG	CG
4	Be	−0.8	−0.00	−20	−1	+0.1	−2
10	Ne	−1.1	+0.00	− 2.5	−0.1	−0.7	−2
12	Mg	−1.2	+0.03	−35	−6	−0.3	−2
18	Ar	−1.9	−0.02	−16	−2	−0.5	−3
20	Ca	−2.1	−0.04	−40	−9	−0.4	−3
26	Fe	−2.4	−0.02	−22	−8	−1.1	−4
36	Kr	−2.7	−0.02	−29	−4	−1.0	−4
54	Xe	−3.4	−0.02	−34	−4	−1.2	−6
86	Rn	−3.9	+0.05	−38	−4	−1.7	−6

[a] With Dirac-Gáspár exchange potential, see Ref. [7].

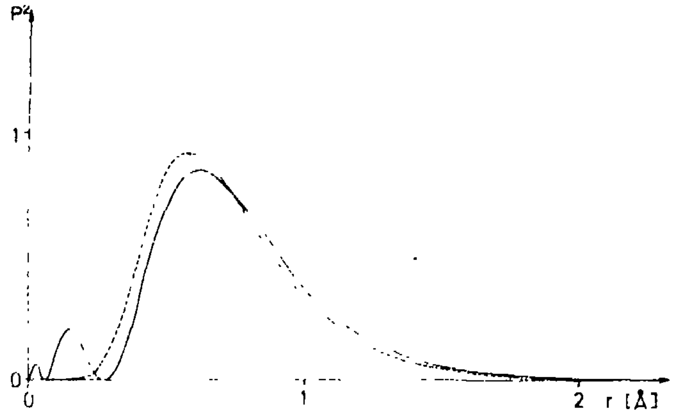

Fig. 1. Radial density $P^2(r)$ of the Ar-3s-orbital HFS results; CG results; ·· SG results

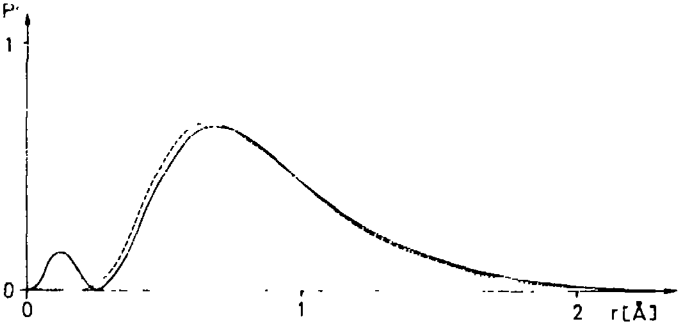

Fig. 2. Radial density $P^2(r)$ of the Ar-3p-orbital. HFS results; -- CG results; ······· SG results

are shown in Tables 1-2 and Figs. 1-2. These results have been obtained with the so-called Kohn-Sham-exchange potential of Dirac and Gáspár [7], and are compared with values from the corresponding version of a Hartree-Fock-Slater (HFS) program [9]. Results obtained with other exchange potentials [7, 8] are very similar to these and are therefore not reproduced here. Results on other atoms than those of the Tables show quite similar trends.

Discussion

In Table 1 orbital parameters and expectation values are given for the Kr atom. The *ε-values* of the corrected Gombás SCF method (CG) compare very nicely with ordinary HFS values, the differences not exceeding a few percent. The simple Gombás version (SG) on the other hand exhibits drastic deviations. *s*-type orbitals (except the lowest one, on which no pseudopotential acts) are much too low, whereas orbitals with $l \geq 2$ come out much too high. As a consequence the 4*s* orbital lies below the 3*d* one. Corresponding inversions of the sequence of the SG orbitals too occur in other atoms, e.g. in Radon

$$\varepsilon_{5s} < \varepsilon_{5p} < \varepsilon_{4f} < \varepsilon_{6s} < \varepsilon_{5d} \quad \text{instead of} \quad \varepsilon_{4f} < \varepsilon_{5s} < \varepsilon_{5p} < \varepsilon_{5d} < \varepsilon_{6s} \,.$$

That the corrected Gombás orbital parameters, just as the Hartree-Fock-Slater ones, exceed the exact SCF ε-values (especially in the case of the higher orbitals), is not a serious drawback: a) In statistical theories ε corresponds to $\frac{dE}{dN}$ (N = number of electrons), whereas in the usual SCF theory according to Koopmans' theorem $\varepsilon \approx \frac{\Delta E}{\Delta N = 1}$. Slater [11] has shown how to get ionisation potentials from statistical orbital parameters. b) Furthermore the asymptotic behaviour of the orbitals is determined by ε. However the discussion of Handy *et al.* [12] has shown that it is quite questionable wether the long range behaviour of SCF-orbitals is of real physical significance.

The same trends as in the ε-values show up in the $\langle r^2 \rangle$*-values:* HFS and CG values differ by not more than a few percent. In the SG method, however, orbitals with large values of $n-l$, especially the higher s-type ones; are contracted by up to or more than 50%, whereas d (and f) orbitals are too diffuse.

These findings indicate that the simple Gombás pseudopotential (7) is too weak and that the correction factor of Eq. (8), despite its very crude nature [6], is quite sufficient. The pseudopotential - usually of greatest importance to s-type orbitals - in its uncorrected form, is not large enough to prevent the higher s-typ *orbitals* from strongly penetrating into the already occupied regions near the nucleus. This can also be seen from Fig. 1. With p orbitals the situation is similar but less pronounced (see Fig. 2). As a consequence of this contraction of the s and p electrons, the d and f orbitals are then dilated because of the better shielded nucleus. Summarizing the CG method reproduces the main density maxima fairly well, whereas the SG method does not.

The inner density oscillations of the orbitals are by definition not obtained in pseudopotential theory. Therefore expectation values which are strongly dependent on them such as the $\langle 1/r \rangle$*-values* should not directly be compared with normal SCF results. Nevertheless we mention that the differences are not very marked and that the SG values agree somewhat better with the HF or HFS values than the CG results do.

Total atomic expectation values are given in Table 2. The corrected Gombás $\langle r^2 \rangle$ and $\langle 1/r \rangle$ values are in error by only a few percent whereas the simple Gombás $\langle r^2 \rangle$ results are rather useless. But most impressive are the total atomic energy values calculated by Eq. (1). While the simple pseudopotential leads to energies which are definitely too low – especially for heavier atoms, although statistical methods should usually give better results for systems with more electrons – the correction Eq. (8) results in an unexpectedly good agreement with HFS energies for all atoms of the periodic table, far better than 1‰.

Concluding, these results encourage one to use the corrected Gombás statistical pseudopotential in cases where it is impossible to construct the usually preferable semiempirical pseudo- or model-potentials [10].

This work has been stimulated by discussions with Prof. P. Gombás. Computer time on the IBM 7090 of the GMD at Bonn is gratefully acknowledged.

References

1. Hellmann, H.: J. chem. Physics **3**, 61 (1935).
2. Gombás, P.: Z. Physik **94**, 473 (1935).
3. — Theoret. chim. Acta (Berl.) **5**, 112 (1966).
4. Szondy, T. Lösungen des vereinfachten Self-Consistent Field für alle Atome. Budapest: Akadémiai Kiado 1970.
5. Schwarz, W. H. E.: Acta phys. Acad. Sci. Hung. **27**, 391 (1969).
6. Gombás, P.: Theoret. chim. Acta (Berl.) **11**, 210 (1968).
7. Schwarz, W. H. E.: Z. Physik **214**, 149 (1968); **239**, 162 (1970).
8. — Theoret. chim. Acta (Berl.) **23**, 21 (1971).
9. Herman, F., Skillman, S.: Atomic structure calculations. Englewood Cliffs (N.J.): Prentice Hall 1963.
10. Schwarz, W. H. E.: Theoret. chim. Acta (Berl.) **23**, 147 (1971).
11. Slater, J. C.: Int. J. quant. Chemistry **4**, S3 (1971).
12. Handy, N. C., Marron, M. T., Silverstone, H. J.: Physic. Rev. **180**, 45 (1969).

Dr. W. H. Eugen Schwarz
Lehrstuhl für Theoretische Chemie
der Universität
D-5300 Bonn, Wegeler Str. 12, Germany

Theoret. chim. Acta (Berl.) 24, 35—41 (1972)
© by Springer-Verlag 1972

Molecular Orbital Study of the Conformational Properties of Phenothiazines

J. L. COUBEILS and B. PULLMAN

Institut de Biologie Physico-chimique, Laboratoire de Biochimie Théorique associé au C.N.R.S.,
13, rue P. et M. Curie, Paris 5è

Received September 22, 1971

The conformation of the side-chain attached to N_{10} of the phenothiazine ring system is investigated by the molecular orbital PCILO method. It is shown that this conformation depends on the folding of the ring along the S–N central axis. The theoretical results are in very satisfactory agreement with the available X-ray crystallographic data on chlorpromazine, thiethylperazine, diethazine and mopazine.

La conformation de la chaîne latérale partant du N_{10} du noyau phenothiazinique est étudiée par la méthode PCILO. Les résultats montrent que cette conformation dépend notablement du degré de pliage de la molécule le long de l'axe S N central. Les prédictions théoriques sont en excellent accord avec les données expérimentales provenant de l'étude cristallographique de la chlorpromazine, la thiethylperazine, la diethazine et la mopazine.

Die Konformation der Seitenkette am N_{10} des Phenothiazinringsystems wird mit der PCILO-Methode untersucht. Es wird gezeigt, daß diese Konformation von der Stellung des Rings entlang der zentralen S N Achse abhängt. Die theoretischen Ergebnisse stimmen sehr gut mit den vorhandenen kristallographischen Daten von Chlorpromazin, Thiethylperazin, Diethazin und Mipazin überein.

Introduction

Phenothiazine derivatives have numerous pharmacological activities, the best known being their action as tranquilizers [1]. Quantum-mechanical calculations have contributed to the knowledge of the electronic properties of these compounds [2] and have, in particular, attracted attention to their electron-donor properties and their ability to participate in charge-transfer complexes [3, 4]. In fact, a theory was proposed [5] linking the tranquilizing activity of phenothiazines to their ability to act as electron donors. As might have been expected, it is not universally adopted (see e.g. the discussion after Ref. [2], at the 2nd International Symposium on "The Action Mechanism and Metabolism of Phychoactive Drugs Derived from Phenothiazine and Structurally Related Compounds", hold in Paris in October 1967).

Whatever the significance of the electronic properties of the phenothiazine ring for the pharmacological activity of phenothiazine drugs, it has long been realized that this activity depends also on the geometrical and conformational properties of these compounds. In a previous publication [6] we have studied quantum-mechanically one aspect of these properties namely the folding of the phenothiazine ring system along the central S–N axis. The present paper is devoted to the study of another, at least as and possibly more important aspect *of these properties namely the conformational arrangement of the side chain attached to the N atom with respect to the folded ring. The mutual interlationship* of these two properties is also investigated to some extent.

The Method

This paper forms a part of a general investigation of conformational properties of pharmacological drugs and in particular of drugs composed of side chains attached to aromatic rings. The method utilized is the PCILO (Perturbative Configurational Interaction using Localized Orbitals) method [7], which is a refined all-valence electrons procedure going beyond the self-consistent field approximation by incorporating an appreciable part of correlation energy. It has been used succesfully for a large study of the conformational properties of the constituents of proteins (see e.g. [8, 9]) and nucleic acids [10, 11] and of a series of pharmacological drugs: acetylcholine and its agonists [12], serotonine [13], histamine [14], phenylethylamines [15], barbiturates [16], monoaminooxidase inhibitors [17] etc.

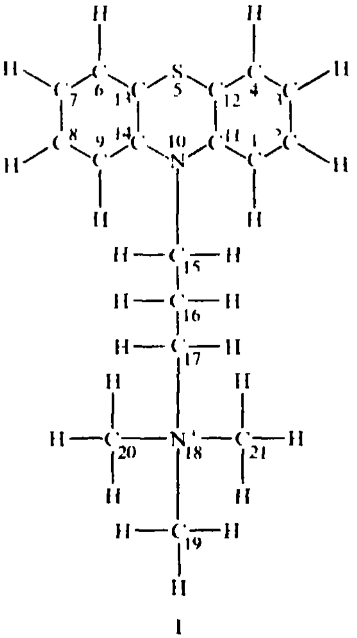

I

The calculations have been carried out on the model compound *I*, composed of the phenothiazine ring and the typical dimethylaminopropyl side chain, which, however, for reasons of computational simplification, was taken in the cationic $-N^{+}(CH_3)_3$ form. The geometrical input data (bond length and angles) were taken following the crystallographic indications of [18].

The calculations on the conformation of the side chain with respect to the ng were carried out for two preselected values of the angle of folding φ of the ng system along the S-N central axis: $\varphi = 140°$, a popular value derived ready a long time ago on the basis of dipole moment measurements [19] and observed recently in X-rays studies of a number of phenothiazines (*vide infra*) and $\varphi = 160°$ corresponding to a flattened ring found recently in one such study (*vide infra*).

The essential torsion angles to be investigated are $\tau_1(S_5{-}N_{10}{-}C_{15}{-}C_{16})$, $\tau_2(N_{10}{-}C_{15}{-}C_{16}{-}C_{17})$ and $\tau_3(C_{15}{-}C_{16}{-}C_{17}{-}N_{18})$. (We remind that the torsion angle τ of the atoms A–B–C–D is the angle between the planes ABC and BCD. Viewed from the direction of A, τ is positive for clockwise and negative for anticlockwise rotations. The value $\tau = 0°$ corresponds to the planar-*cis* arrangement of the bonds AB and CD. Usually the definition is applied to a series of bonded atoms. It is enlarged here to involve the non bonded S, N atoms.) The $N^+(CH_3)_3$ group was fixed in a staggered position following previous results [12-14].

The rotations about the torsion angles τ_1 and τ_2 were carried out with 30° increments. For τ_3, two preselected values of 180° and 60° were utilized. The calculations indicate that for both values of $\varphi = 140°$ and $\varphi = 160°$, the global minimum of the map obtained with $\tau_3 = 180°$ is about 30 kcal/mole lower than that of the map obtained with $\tau_3 = 60°$. Consequently, only the maps corresponding to $\tau_3 = 180°$ will be reproduced in this paper[1].

Results and Discussion

Fig. 1 represents the conformational energy map for compound *I* corresponding to the preselected values $\varphi = 140°$, $\tau_3 = 180°$. The map shows two practically equivalent global minima at:

$$\tau_1 = 30°, \quad \tau_2 = -60°,$$

and

$$\tau_1 = 30°, \quad \tau_2 = 180°.$$

In both conformations the β-CH_2 group leans towards one of the lateral benzene rings of the phenothiazine system. The two conformations differ, however, by the orientation of the further part of the side chain which points respectively toward and away from the ring system.

Fig. 2 represents the conformational energy map for the same compound *I*, corresponding to the preselected values $\varphi = 160°$, $\tau_3 = 180°$. This map shows three practically equivalent minima. To the previous minima at:

$$\tau_1 = 30°, \quad \tau_2 = -60°,$$

and

$$\tau_1 = 30°, \quad \tau_2 = 180°,$$

---

[1] The conformational energy maps corresponding to $\tau_3 = 60°$ show also a very restricted permissible conformational zone, with global minima always at $\tau_2 = 150°$ and $\tau_1 = \pm 30°$ for $\varphi = 140°$ and $\tau_1 = 180°$ for $\varphi = 160°$. There is also a local minimum at $\tau_2 = 150°$, $\tau_1 = 180°$ for $\varphi = 140°$ and at $\tau_2 = 150°$, $\tau_1 = \pm 30°$ for $\varphi = 160°$.

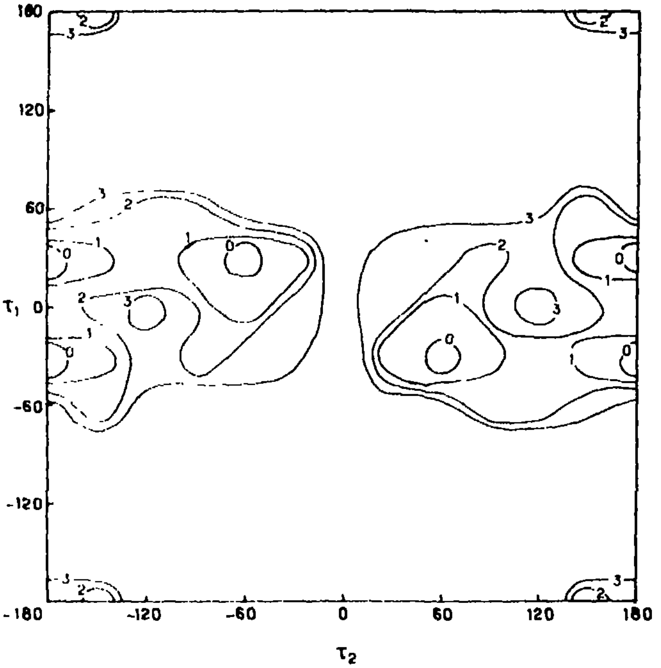

Fig. 1. Conformational energy map of phenothiazine I for $\varphi = 140°$, $\tau_3 = 180°$. Isoenergy curves in kcal/mole with respect to the global minimum taken as energy zero

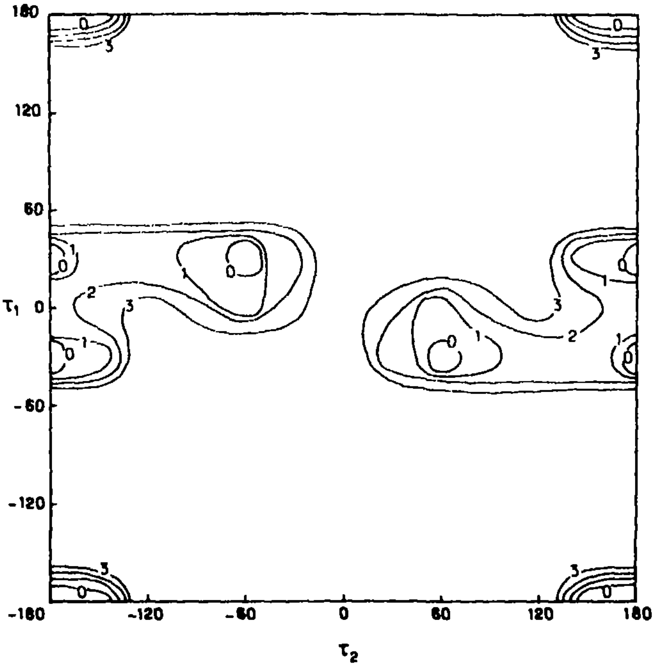

Fig. 2. Conformational energy map of phenothiazine I for $\varphi = 160°$, $\tau_3 = 180°$. Isoenergy curves in kcal/mole with respect to the global minimum taken as energy zero

is now added a third minimum at:

$$\tau_1 = 180^\circ, \quad \tau_2 = 180^\circ.$$

The flattening of the ring has therefore the effect of producing a new stability zone corresponding to an *all-trans* arrangement of the side chain with respect to the ring.

It must be stressed that the calculations indicate that, fundamentally, the conformation with $\varphi = 160^\circ$ is about 30 kcal/mole less stable than the conformation with $\varphi = 140^\circ$. Although the results refer, of course, only to the model compound and moreover *in vacuum*, this difference is sufficiently pronounced to justify the expectation that phenothiazines should exist preferentially with $\varphi = 140^\circ$, in which case they should adopt the overall conformations predicted for this form. Nevertheless, should the ring system be induced for some reasons (other substituents at the ring susceptible to interact with the side-chain, crystal packing forces, solvent effects, etc.) to adopt a more flattened shape, around $\varphi = 160^\circ$, a third overall conformation appears possible.

We may now turn to the few available experimental data in order to compare them with the theoretical results. These data come from recent X-ray crystallographic studies on some simple phenothiazine derivatives: chlorpromazine (II) [18, 20], thiethylperazine (III) [21], diethazine (IV) [22] and mopazine (V) [18]. The experimental values of the angles φ, τ_1 and τ_2 in these compounds are shown in Table 1.

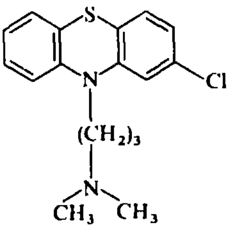

II

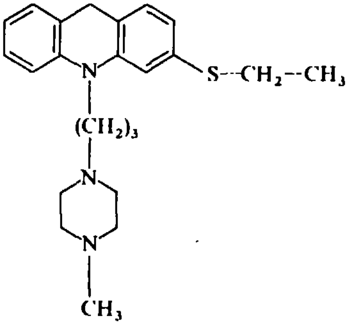

III

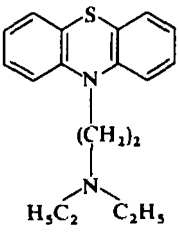

IV

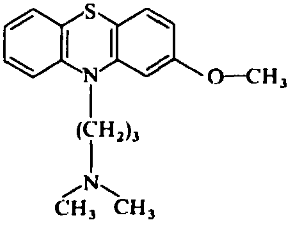

V

Table 1. X-ray crystallographic results

Molecule	φ	τ_1	τ_2	Ref.
Chlorpromazine	139.4	-34.5	−160	[20]
Chlorpromazine	139.5	34.6	164	[18]
Thiethylperazine	139	−32	175	[21]
Diethazine	138	38	171	[22]
Mopazine	157.7	178.8	175.5	[18]

The agreement between the theoretical results and the experimental data is extremely striking. Three of the four compounds studied have their angle of folding φ in the vicinity of 140 and the three of them exhibit a conformation of their side chain very close to the theoretical global minimum predicted for $\tau_1 = 30$, $\tau_2 = 180$. This correspondance is even observed for diethazine (IV) whose side chain only contains two CH_2 groups indicating thus that the principal conformational features of the side chain do not seem to depend too drastically on the length of the chain. On the other hand one compound, mopazine, investigated experimentally in the form of mopazine maleate with therefore environmental factors of prominent importance, presents a folding angle close to the value of 160. It is particularly striking that this compound, and this compound alone, shows a conformation of the side chain near $\tau_1 = \tau_2 = 180$ corresponding thus to the third, new global minimum specific for the higher value of φ. This situation clearly indicates the important influence of the degree of folding of the ring system upon the conformation of the side chain.

Conclusion

The results indicate once more the reliability of the PCILO method for the evaluation of molecular conformations. They indicate a far reaching selectivity in the overall conformations susceptible to be adopted by phenothiazine drugs and the interrelation of the conformations of the side chain with the magnitude of folding of the phenothiazine ring system.

Acknowledgement. The authors wish to thank Dr. Marsau from the Crystallography Laboratory of the University of Bordeaux for communication of data prior to publication.

References

1. See e.g. Bodea, C., Silberg, I.: Advances in heterocyclic chemistry 9, 321 (1968).
2. Pullman, B.: Agressologie 9, 1 (1968).
3. Pullman, A.: Biochim. biophysica Acta 35, 535 (1959).
4. - Quantum-biochemistry. New York: Academic Press 1963.
5. Karreman, G., Isenberg, I., Szent-Gyorgyi, A.: Science 130, 1191 (1959).
6. Malrieu, J. P., Pullman, B.: Theoret. chim. Acta (Berl.) 2, 293 (1964).
7. Diner, S., Malrieu, J. P., Jordan, F., Gilbert, M.: Theoret. chim. Acta (Berl.) 15, 100 (1969) and the references indicated therein.
8. Pullman, B.: In: Aspects de la chimie quantique contemporaine (R. Daudel and A. Pullman eds.). Colloques Internationaux du C.N.R.S., Paris 1971, p. 261 and the references indicated therein.

9. Pullman, B.: Intern. J. Quant. Chem. **4**, 319 (1971).
10. Berthod, H., Pullman, B.: Biochim. biophysica Acta **232**, 595 (1971).
11. — — In: The purines: Theory and experiment. Proc. of the 4th Jerusalem Symposium (E. D. Bergmann and B. Pullman eds.). New York: Academic Press, in press.
12. Pullman, B., Courrière, Ph., Coubeils, J. L.: Molecular Pharmacol. 7; 397 (1971).
13. Courrière, Ph., Coubeils, J. L., Pullman, B.: Compt. Rend. Acad. Sci. Paris **272**, 1697 (1971).
14. Coubeils, J. L., Courrière, Ph., Pullman, B.: Compt. Rend. Acad. Sci. Paris **272**, 1813 (1971).
15. Pullman, B., Coubeils, J. L., Courrière, Ph., Gervois, J. P.: J. med. Chem., in press.
16. — J. theoret. Biol., in press.
17. Coubeils, J. L., Pullman, B.: Compt. Rend. Acad. Sci. Paris **273**, 1164 (1971).
18. Marsau, P.: Private communication.
19. See e.g. Pullman, B., Pullman, A.: Les Théories Electroniques de la Chimie Organique, Masson Ed. Paris 1952.
20. McDowell, J. J. H.: Acta crystallogr. B **25**, 2175 (1969).
21. — Acta crystallogr. B **26**, 954 (1970).
22. Marsau, P.: Acta crystallogr. B **27**, 42 (1971).

Prof. Dr. B. Pullman
Institut de Biologie Physico-chimique
Laboratoire de Biochimie Théorique
associé au C.N.R.S.
13, rue P. et M. Curie
Paris 5è (France)

[illegible]
38962
Date 29.4.82

Theoret. chim. Acta (Berl.) 24, 42–50 (1972)
© by Springer-Verlag 1972

Contracted and Uncontracted Oscillator Orbitals in CI Calculations on Two Electron Systems

GIULIANO ALAGONA and JACOPO TOMASI

Laboratorio di Chimica Quantistica ed Energetica Molecolare del C.N.R.
Via Risorgimento 35, 56100 Pisa, Italy

Received July 29, 1971

Oscillator orbitals as expansion functions for the correlation holes have been checked by using them in two simple two electron systems, H_2 and Li^+.

A contraction of the oscillators has been introduced and proved useful to ameliorate energy and convergence rate.

Oszillatororbitale als Entwicklungsfunktion zur Darstellung des Korrelationsloches werden durch Anwendung bei zwei einfachen Zweielektronensystemen H_2 und Li^+ geprüft. Eine Kontraktion der Oszillatoren wird eingeführt, welche die Energie und die Konvergenzgeschwindigkeit verbessert.

Essai d'orbitales oscillantes comme fonctions de base pour les trous de corrélation dans deux systèmes biélectroniques simples: H_2 et Li^+.

L'introduction d'une contraction des ces orbitales s'est avérée utile pour améliorer l'énergie et la vitesse de convergence.

1. Introduction

Several considerations support the convenience of using in MO CI calculations a basis of localized orbitals (LO) rather than delocalized one.

Suffice it to recall here that the heuristic value of the CI calculations is actually greatly emphasized because one is allowed to get a quantum-mechanical counterpart (electronic correlation included) of the intuitive "chemical" model of the bonding, which possibly might take into account the bond transferability, the inductive effect along the bonds, the short range forces arising from localized (e.g. reactive) perturbations, etc. The final goal of such a type of calculations should presently be to get semiempirical recipes to be used on molecular systems of large dimensions.

The first step in this direction is to define a suitable set of localized virtual orbitals, connected with SCF LO's which can be obtained from the canonical ones by means of an appropriate orthogonal transformation.

The pioneer work in this field is due, as far as we know, to Foster and Boys [1]: they introduced a new type of localized orbitals (exclusive orbitals) of fairly simple determination and defined, for each LO, a set of virtual localized orbitals (oscillator orbitals) with a view to building up additional Slater determinants for the CI process. This sort of virtual orbitals has however some deficiencies; the actual calculations made in the original paper [1] (on the formaldehyde molecule) are too limited to evidence them, therefore, as a matter of convenience, we will make reference to later results of our Laboratory [2] related to a type of virtual orbitals somewhat different from Foster and Boys's, both of them having however the characterizing feature of being obtained through an orthogonal transformation from the set of virtual SCF MO's. The results of Ref. [2] show that it was not possible to obtain, for each exclusive orbital, more than two or three satisfactory virtual LO's, the other ones being completely delocalized and ineffective as regards the corresponding energy improvement. This is a consequence of the well known fact that the virtual SCF orbitals are not suitable to expand the correlation hole in the regions of higher electron density. Such an inconvenience is not overcome by enlarging the basis set; computational problems and storage facilities of the computer quickly become the limiting factors.

Another proposal made by Boys aims to avoiding this inconvenience [3]. For each SCF LO a set of adjustment functions is defined; these functions, after a suitable orthonormalization process, performed in two stages, become the oscillator orbitals. These adjustment functions are not defined in terms of the virtual SCF orbitals, but directly originate in the SCF LO's according to a genealogical procedure. This is the peculiar feature of the oscillator orbitals (new version); this paper is devoted to a control of how such a set works.

2. Definition of Oscillator Orbitals and Some Results for the H_2 Molecule

Let us suppose to have, for a given molecule, a set of LO's obtained from a previous SCF calculation. Let us pick up one among them, φ_a, which describes, for example, a bond between the atoms A and B. The correlation between the electron pair belonging to this bond may be described, in a first approximation, by including the configurations arising from substitutions of φ_a with polarized orbitals which cause the electrons to avoid each other, like $\varphi_a x_c$, $\varphi_a y_c$, $\varphi_a z_c$. The subscript c emphasizes that the most suitable origin of the polarization function lies in the charge center of the distribution $\varphi_a^* \varphi_a$ with axes parallel to the principal axes of the inertia tensor of such a charge distribution.

This statement is intuitively acceptable because such a procedure corresponds to expand at first the most important part of the correlation hole. An empirical verification may be found e.g. in Ref. [2].

Boys [3] extends this idea and defines accordingly a system of adjustment functions:

$$\overline{\varphi}_{apqs} = \varphi_a x_c^p y_c^q z_c^s \, .$$

From them one can obtain the oscillator orbitals φ_{apqs}, after a suitable orthonormalization process (see Ref. [3] for a detailed description) which preserves any symmetry present among the φ_{apqs}, maximizes the overlap between the oscillator orbital and the original adjustment function and retains $\varphi_{a000} = \varphi_a$. The virtual SCF space is therefore completely discarded. The adjustment functions are sufficiently general (no limitations are imposed on the integers p, q, s) to consider the set as complete.

The practical use of the oscillator orbitals requires a systematization of the computing machinery going beyond the limits of a simple investigation as the present one. It may be recalled here that a promising suggestion was made by Boys himself in another paper [4]. The numerical results reported in this paper were obtained by means of an exact expansion of the oscillator orbitals into Slater-type atomic orbitals (STO's).

Table 1. *Some results for H_2 molecule*[a]

SCF wavefunction				Oscillator orbital CI wavefunction	
Center	STO	ζ	Coeff.	Orbital	Coeff.
1	1s	1.14	0.58685	φ_a	0.99332
1	$2p_a$	1.77	0.03196	$\varphi_a z_r$	−0.09206
2	1s	1.83	−0.01777	$\varphi_a x_r$	−0.04914
2	2s	1.83	−0.02673	$\varphi_a y_r$	−0.04914
2	$2p_a$	1.83	0.00000		
2	3s	1.83	−0.06351		
3	1s	1.14	0.58685		
3	$2p_a$	1.77	0.03196		
Energy	1.13345			Energy: −1.15061	

Geometry

Center	x	y	z
1	0.0	0.0	0.7004
2	0.0	0.0	0.0
3	0.0	0.0	0.7004

[a] Energies and distances in a. u.

A first test has been performed on the hydrogen molecule, using as a starting point a good SCF wavefunction [5] whose basis set is characterized by having STO's centered also on the molecular midpoint (see Table 1). The corresponding SCF energy (− 1.13345 a.u.) is sufficiently near the Hartree-Fock limit (the latter being − 1.133629 a.u.) to consider any further energy improvement as being due to correlation. Inclusion of the first three oscillator orbitals, having all $p+q+s=1$, in the CI process leads to an energy of − 1.15061 a.u., with an improvement over the SCF value of − 0.01716 a.u., corresponding to 41% of the correlation energy.

The SCF basis set being quite extended, it is obvious to forecast that the conventional CI method works in this case as much as possible. In fact, if one uses the SCF basis set implemented by some π virtual orbitals (STO's $2p_x$ and $2p_y$ having the same orbital exponent as the $2p_z$ STO's already present in the set) one obtains $E = 1.17102$ a.u., i.e. $\cong 92\%$ of the correlation energy. Confining ourselves to the three best configurations ($1\sigma_u$, 1π and $1\bar{\pi}$) we get a total energy of − 1.15945 a.u., which corresponds to an energy improvement over the SCF value of − 0.026002 a.u., (64% of the correlation energy) decidedly better than that obtained using oscillator orbitals.

A closer analysis shows that the main differences are in the σ part. In fact a CI calculation with the first excited σ configuration leads to $\Delta E = -0.015748$ a.u. and the corresponding one with $\varphi_a z_r$ leads to $\Delta E = -0.010077$, whereas the conventional method with configurations $1\pi_u^2$ and $1\bar{\pi}_u^2$ leads to $\Delta E = -0.011287$ a.u., to be compared with $\Delta E = -0.007663$ obtained with $\varphi_a x_r$ and $\varphi_a y_r$.

For other comparisons the reader is deferred to other CI results available in the literature, e.g. to the paper of Weiss, McLean and Yoshimine [6].

Such comparisons may result more favourable to the oscillator orbitals than the present ones, but we are here especially interested in pointing out that even the oscillator orbitals show some deficiencies in the expansion of the correlation. The main reason for such a poor behaviour seems to lie in the fact that the multiplication of the localized orbital by positive powers of the coordinates, though giving the correct shape to the adjustment functions, excessively spreads out the charge distribution. The fact may be easily verified in the preceding example if one compares the spatial density distribution of the σ_u natural orbital with that arising from the $\varphi_a z_c$ function.

It would be of some interest to look for a correction in this sense to all the oscillator orbitals. The simplest way to obtain it is the introduction in the oscillator orbitals of a sort of contracting factor.

In the next section are reported some results obtained with an exponential contraction factor.

3. Contracted Oscillator Orbitals

For the contraction factor we have tentatively adopted the form $\exp(-kr_c)$, with k positive, r_c being the distance from the orbital charge center.

Such a choice was suggested by practical reasons: budget restrictions have not allowed us to extend the calculations on polycentric systems to oscillators having a degree (i.e. sum of the exponents p, q, s) higher than one, which are necessary to test how a contraction factor works. As a consequence we considered the simpler case of an atomic system, and in this case the form chosen is the most suitable for expanding oscillator orbitals in terms of STO's.

When one deals with a monocentric system, it is convenient to re-state the adjustment functions in spherical coordinates. The expression:

$$\bar{\varphi}_{anlmk} = \varphi_a r_c^n Y_l^m(\vartheta, \varphi) \exp(-kr_c),$$

where $Y_l^m(\vartheta, \varphi)$ is a real spherical harmonic, has the advantage of taking directly into account the radial correlation. Terms like $\bar{\varphi}_{an000}$ do not actually appear in the original definition. Of course this definition contains also the older: for example $\bar{\varphi}_{a1100} = \varphi_a r_c Y_1^0$ corresponds to $\bar{\varphi}_{a001} = \varphi_a z_c$, etc. The orthonormalization process (Boys' one may be conserved, with minor modifications) will lead to oscillators having the correct nodal surfaces.

For a numerical test we have chosen the Li^+ ion. The SCF wavefunction, reported in Table 2, was taken from an early work of our Laboratory [7] and the corresponding energy is, again, very close to the H–F limit (-7.2364135 a.u. [8]).

A first set of calculations was made without contraction factor ($k = 0$). To evidence the convergence rate different cases are reported in Table 3. Column 2 reports the oscillator orbitals considered in each case, the notation should be evident: the symbols 3(2*p*) and 5(3*d*) respectively indicate the sets of three *p*-type oscillators φ_{a11m} and of five *d*-type oscillators φ_{a22m}. Column 3 reports the energy increment with respect to the SCF value, obtained by complete diagonalization of the corresponding secular matrix.

Table 2. SCF *wavefunction for* Li^+

Basis orbitals				Coefficients
n	l	m	ζ	
1	0	0	2.448	0.88935561
1	0	0	4.58	0.12546063
2	0	0	5.00	0.00011982
$E = -7.236412$				

Table 3. CI *results for* Li^+ *with some sets of oscillator orbitals*

Wave function	Oscillator set	Without contraction	With contraction	
		ΔE	k	ΔE
1	r	−0.013113	0.26	−0.01390
2	r, r^2	−0.014632	1.23	−0.01561
3	r, r^2, r^3	−0.015126	1.23	−0.01582
4	$3(2p)$	−0.013799	1.26	−0.02154
5	$r, 3(2p)$	−0.026449	0.6	−0.03170
6	$r, r^2, 3(2p)$	−0.027864	1.2	−0.03631
7	$r, r^2, r^3, 3(2p)$	−0.028432	1.4	−0.03652
8	$3(2p), 5(3d)$	−0.014212	1.5	−0.02344
9	$r, 3(2p), 5(3d)$	−0.026817	0.65	−0.03300
10	$r, r^2, 3(2p), 5(3d)$	−0.028235	1.34	−0.03833
11	$r, r^2, r^3, 3(2p), 5(3d)$	−0.028767	1.46	−0.03842

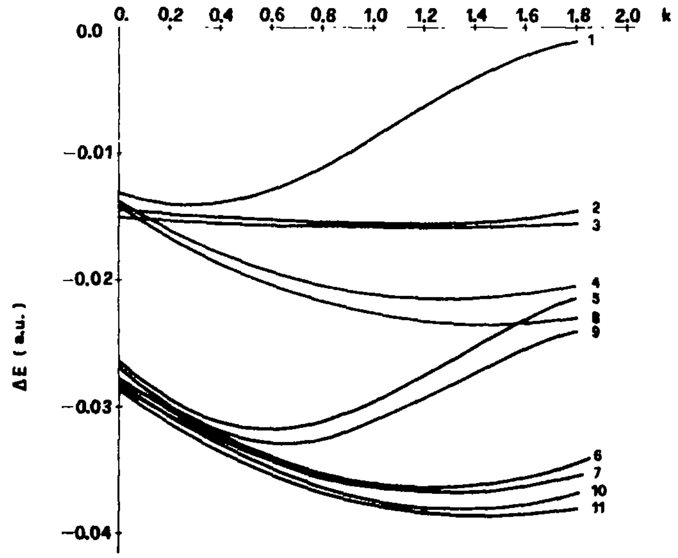

Fig. 1. ΔE dependence on the contraction factor k for all the Li^+ wavefunctions listed in Table 3

The first three wavefunctions contain only radial terms. Wavefunction 4 contains Boys' oscillators of the first degree and wavefunction 7 those of the first and second degree. Energies for wavefunctions 3, 7 and 11 are the approximations, within the set here employed, of the S, P and D limits for the Li^+ ion; a comparison with accurate results is performed in Table 4.

As a further step, in each of the wavefunctions of Table 3 a contraction factor was introduced, equal for all the oscillator orbitals included in the wavefunction. Results are graphically reported in Fig. 1. Each curve refers to a different wavefunction (the reference numbers are the same as in Table 3) and shows how energy changes when contraction factor increases. The optimal values of k and the corresponding energy improvements are reported in the last two columns of Table 3.

When only the first radial oscillator is included in the calculation, the optimum value of the contraction factor is low (wavefunction 1), whereas by enlarging the number of radial oscillators the wavefunction becomes more and more insensitive to the contraction factor (wavefunctions 2 and 3). Contraction factors for the first angular oscillators are larger than for radial oscillators (wavefunctions 4 and 8). The optimum k values for more complete wavefunctions are easily rationalized in comparison with the values of the simpler aforementioned cases. The energy improvement due to the contraction factor is sensible especially when a larger number of oscillators is employed.

Table 4. *Comparison of energies for* Li^+ (a.u.)

	Accurate results		This paper			
		%[d]	$k=0$	%[d]	k best	%[d]
HF	−7.236413[a]	0	−7.236412	0	−7.236412	0
HF + S	−7.25242[b]	37.3	−7.25153	35.2	−7.25221	36.8
HF + S + P	−7.27575[b]	91.7	−7.26484	66.3	−7.27301	85.3
HF + S + P + D	−7.27845[b]	98.0	−7.26512	66.9	−7.27481	89.5
Exper.	−7.2798[c]		—		--	

[a] Ref. [8].

[b] Ref. [9].

[c] Ref. [10].

[d] % of the correlation energy (with allowance for relativistic energy).

A comparison with accurate results is made in Table 4. With three radial oscillators, 98% of the corresponding correlation energy is accounted for. Going to superior limits, 88% of the S + P correlation energy is reproduced and 74.5% of the S + P + D value. Such results are favourably compared with limited CI performed on large basis sets.

On wavefunction 6, which seems to us to be an acceptable compromise between accuracy and simplicity, the contraction factors of the radial oscillators and those of the angular ones were allowed to vary independently. As one could expect, on the basis of the results of Fig. 1, the new values do not noticeably differ from the previous ones: $k(\text{rad}) = 1.1$ and $k(\text{ang}) = 1.3$. Also the energy does not change appreciably: 0.03640 against 0.03636 a.u.

The quite limited checks on oscillator orbitals here reported may give an answer only to a part of the question about the convenience of using oscillators in actual molecular calculations. The whole orthonormalization procedure for systems having more than two electrons must be checked carefully and appropriate integration techniques for calculating secular matrix elements are necessary. In any case the introduction of some sort of contraction factor, which at least for inner shells may be chosen equal for all the pertinent oscillators, can improve the energy and even the convergence rate.

Appendix

On Second Order CI Calculations

When one tries to improve a SCF wavefunction by means of a CI treatment, one is strongly exposed to the temptation of confining the calculation to the second order only. Two reasons may be alleged for: the calculations are far simpler, a quite limited number of the secular matrix elements being necessary, and the results are easily interpreted in terms of effects on a single SCF orbital. The goal mentioned in the introduction, to get semiempirical recipes useful to deal with large molecules, could be in this way facilitated.

The application of a perturbative treatment to an oscillator interaction problem requires some manipulations on the zeroth-order hamiltonian (see Ref. [11]). In fact the usual perturbative treatment is not possible because we have not expansion functions which are eigenfunctions with known eigenvector of H_0. A way of circumventing this difficulty is to define a new imperturbed hamiltonian

$$H'_0 = H_{\mathrm{HF}} + \sum_i \langle i|V|i\rangle\, |i\rangle\langle i|$$

and a new perturbation

$$V' = V - \sum_i \langle i|V|i\rangle\, |i\rangle\langle i| \,.$$

Here the set $|i\rangle$, formed by the oscillators together with the exclusive orbital $|0\rangle$, is considered orthonormal and complete; i.e.

$$\langle i|j\rangle = \delta_{ij}, \quad \sum_i |i\rangle\langle i| = 1 \,.$$

With such a partition of the complete hamiltonian, the second order energy, in the Rayleigh-Schrödinger treatment is written as:

$$E^{(2)} = \sum_{i \neq 0} (\langle 0|H|0\rangle - \langle i|H|i\rangle)^{-1} \langle 0|V|k\rangle^2 \,. \tag{1}$$

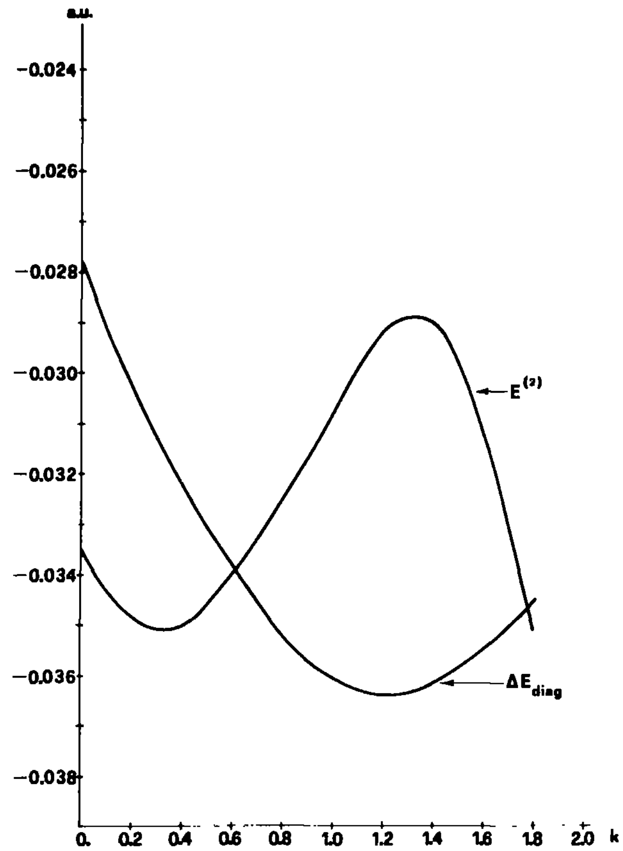

Fig. 2. Comparison of exact and second order energy improvement for wavefunction 6 of Table 3

Such an expression is frequently employed, even with the conventional virtual orbitals.

In this appendix we wish to point out, using a numerical example taken from the preceding calculations, that such a formula may give sometimes a very poor approximation. Fig. 2 reports the energy changes for wavefunction 6 of Li^+ varying the contraction factor calculated either exactly (curve ΔE_{diag}, the same as in Fig. 1) or according to Eq. (1). Similar trends have been found also for the other wavefunctions considered in Fig. 1.

References

1. Foster, J. M., Boys, S. F.: Rev. mod. Physics 32, 300 (1960).
2. Bonaccorsi, R., Petrongolo, C., Scrocco, E., Tomasi, J.: Theoret. chim. Acta (Berl.) 15, 332 (1969).
3. Boys, S. F.: Quantum theory of atoms, molecules and the solid state. ed. by P. O. Löwdin, p. 253, New York: Academic Press 1966.
4. Rajagopal, P.: Adv. in quantum chem., vol. 2, p. 1, New York: Academic Press 1965.
5. Bonaccorsi, R., Salvetti, O., Scrocco, E., Tomasi, J.: J. chem. Physics 44, 4361 (1966).
6. McLean, A. D., Weiss, A., Yoshimine, M.: Rev. mod. Physics 32, 211 (1960).

7. Arrighini, G. P., Guidotti, C., Tomasi, J.: Theoret. chim. Acta (Berl.) **18**, 329 (1970).
8. Clementi, E.: Supplement to IBM Journal of Research Development **9**, 2 (1965).
9. Weiss, A. W.: Physic. Rev. **122**, 1826 (1961).
10. Cade, P., Huo, W.: J. chem. Physics **47**, 614 (1967).
11. Diner, S. J., Malrieu, J. P., Claverie, P.: Theoret. chim. Acta (Berl.) **8**, 390 (1967).

Dr. J. Tomasi
Laboratorio di Chimica Quantistica
ed Energetica Molecolare del C.N.R.
Via Risorgimento 35
I-56100 Pisa, Italia

Theoret. chim. Acta (Berl.) 24, 51–60 (1972)
© by Springer-Verlag 1972

The Molecular Electrostatic Potentials for the Nucleic Acid Bases: Adenine, Thymine, and Cytosine

R. Bonaccorsi

Laboratorio di Chimica Quantistica ed Energetica Molecolare des C.N.R.,
Via Risorgimento, 35, 56100 Pisa, Italy

A. Pullman

Institut de Biologie Physico-Chimique, 13, rue P. et M. Curie, Paris Vè, France

E. Scrocco and J. Tomasi

Istituto di Chimica Fisica dell' Università, 56100 Pisa, Italy

Received April 29, 1971

The electrostatic potentials arising from *ab initio* MO LCAO GTO SCF wave functions for adenine, thymine and cytosine are given and discussed.

Well defined characteristic regions of immediate chemical significance are found. The analysis of such results aims at comparing different protonation sites in the same molecule as well as in different ones. Differences among the proton affinities of the nitrogen atoms (pyridine-like, amine and imine) are evidenced, as well as the distinction between oxygen and nitrogen atoms.

Les potentiels electrostatiques moléculaires calculés à partir de fonctions d'onde *ab initio* MO SCF LCAO GTO sont donnés et discutés pour l'adénine, la thymine et la cytosine.

Des régions bien définies sont obtenues dont la signification chimique apparait clairement. L'analyse de l'ensemble des résultats permet la comparaison des differents sites de protonation dans une même molécule ainsi que dans differentes molécules, ainsi que la distinction entre oxygene et azote d'une part, azotes de differents types d'autre part.

Die mit Hilfe von *ab initio* MO LCAO GTO SCF Wellenfunktionen berechneten elektrostatischen Potentiale von Adenin, Thymin und Cytosin werden angegeben und diskutiert.

Man findet genau bestimmte charakteristische Zonen von klarer chemischer Bedeutung. Durch die Analyse solcher Resultate können verschiedene Protonierungsplätze sowohl in ein und demselben Molekül als auch in verschiedenen Molekülen verglichen werden. Deutlich zeigen sich Unterschiede der Protonenaffinitäten der unterschiedlich chemisch gebundenen Stickstoffatome (pyridinartiger, Amin- und Iminstickstoff) und der Unterschied zwischen Stickstoff- und Sauerstoffatomen.

Introduction

It has been suggested recently [1, 2], that the information enclosed in a molecular wave function can be used in the form of the electrostatic potential created in the neighbouring space by the nuclear charges and the electronic distribution. For a given wave function with the corresponding first order density function ϱ (1) the average value of such a potential $V(r_i)$ at a given point i of space is [2]:

$$V(r_i) = -\int \frac{\varrho(1)}{r_{1i}} d\tau_1 + \sum_{\alpha}^{\text{nucl}} \frac{Z_\alpha}{r_{\alpha i}}, \qquad (1)$$

where Z_α is the nuclear charge of nucleus α.

This quantity, like the electron density distribution, is directly obtainable from the wave function and thus does not suffer from the drawbacks inherent to the classical population analysis. Moreover, its very definition seems to make it an appropriate index for the study of chemical reactivity at least in the early phase of approach of a given reagent for reactions with an ionic mechanism. In particular, the interaction energy between the molecular distribution (considered unperturbed) and an external point charge q placed at point i is $qV(r_i)$. It may be worth pointing out that $qV(r_i)$ is rigorously the first order perturbation energy of the molecule in the field of the charge q.

Maps of electrostatic interaction energies with a unit positive charge have already been drawn for the molecules of cyclopropane, aziridine, oxirane, thiirane, diazirine and cyclopropene [2], for oxaziridine and diaziridine [3] as well as for N_2, NOF, NH_3, H_2O and H_2S [4] using *ab initio* SCF molecular wave functions of "Slater minimal basis set" accuracy. In the present paper we report on similar curves drawn for adenine, I, cytosine, II, and thymine, III, using the *ab initio* SCF molecular wave functions obtained previously [5] in a small gaussian basis set. We have not treated guanine because its wave function was not available in the same basis set.

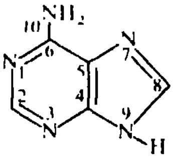

I

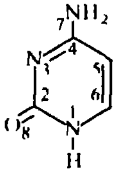

II

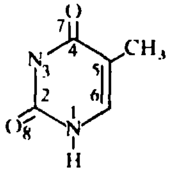

III

The particular interest of this type of molecules for this kind of study lies in the fact that each of them presents more than one potential site for protonation or electrophilic attack, thus providing a good test as to the possibilities of isopotential curves to distinguish among different positions of attack, or among different molecules. The basicity of such heterocycles has been essentially dealt with, in the past, in the π-electron approximation where it was shown that the sole consideration of the local charge of the atoms involved was not sufficient to distinguish among the different sites [6]. We shall come back in the discussion to this point and to the comparison of the isopotential results with other indices.

Computation Details

Within the LCAO MO framework, the potential $V(r_i)$ can be expressed in terms of the P_{rs} elements of the charge-bond order matrix relating to the atomic orbitals χ_r and χ_s as:

$$V(r_i) = -\sum_{r,s} P_{rs} \int \frac{\chi_r(1)\chi_s(1)}{r_{i1}}\, d\tau_1 + \sum_{\alpha} \frac{Z_\alpha}{r_{\alpha i}}. \tag{2}$$

A new version of the program for calculating $V(r_i)$, which had been previously written [2] for Slater orbitals, has been coded for Gaussian basis functions. This new version uses only the MO coefficients as input and relies on the calculation of nuclear attraction type integrals. The interaction energy with a hypothetical positive charge was calculated at regular intervals in the outer molecular space for the three molecules and iso-energy curves have been drawn accordingly.

Results and Discussion

Isopotential curves drawn in the molecular plane for the three molecules considered are given in Figs. 1, 2, and 3. Isopotential maps in selected planes perpendicular to the molecular one are reported in Figs. 4 and 5 for adenine, Fig. 6 for cytosine and Fig. 7 for thymine.

Adenine: In the molecular plane three regions of attraction appear towards the three pyridine-like nitrogens with distinct minima of -78.3 (N_3), -77.0 (N_1), and -69.4 (N_7) kcal/mole respectively. The regions around N_1 and N_3 are very similar in shape and depth, whereas the N_7-region is narrower and less deep. These regions clearly correspond to the lone pairs of the nitrogens which were apparent in the isodensity diagrams obtained from the molecular wave function [7]. They are similar to those found for the nitrogens of diazirine [2] (the numerical values are not to be strictly compared on account of the differences in the atomic basis sets).

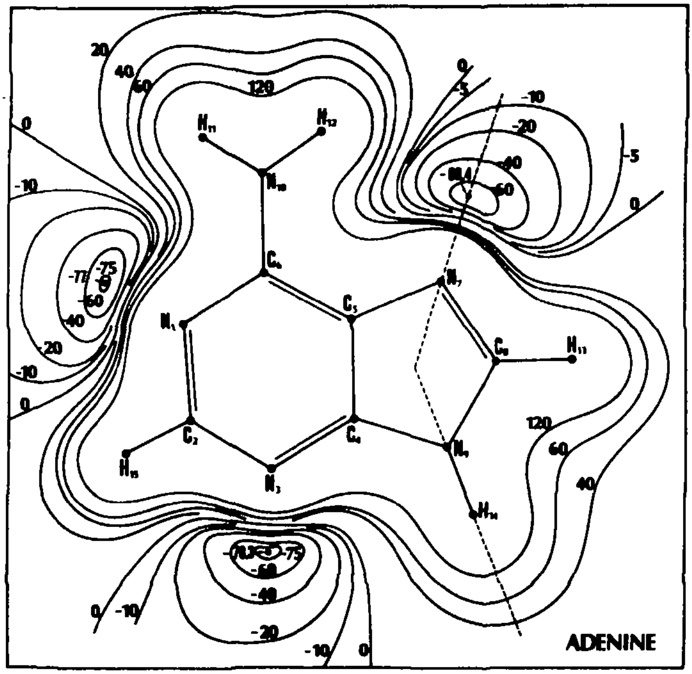

Fig. 1. Electrostatic molecular potential-energy map for adenine in the ring plane. The energies are expressed in kcal/mole

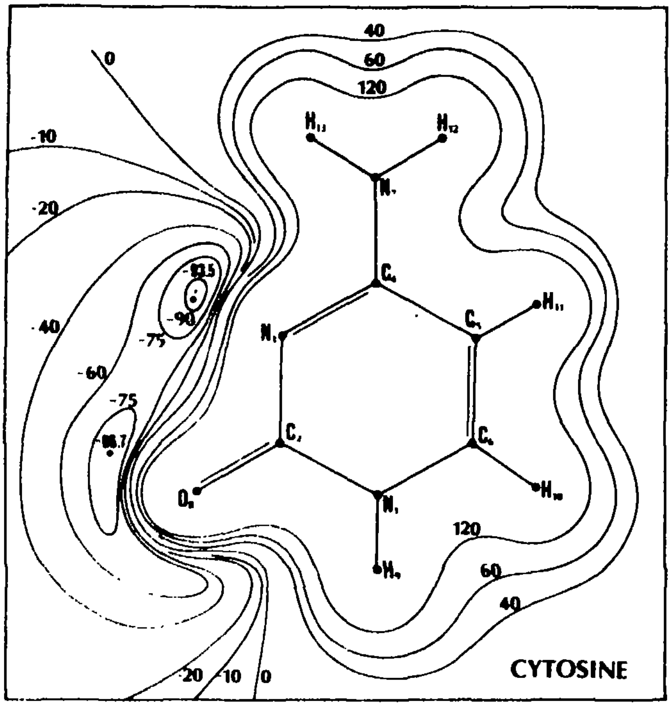

Fig. 2. Electrostatic molecular potential-energy map for cytosine in the ring plane

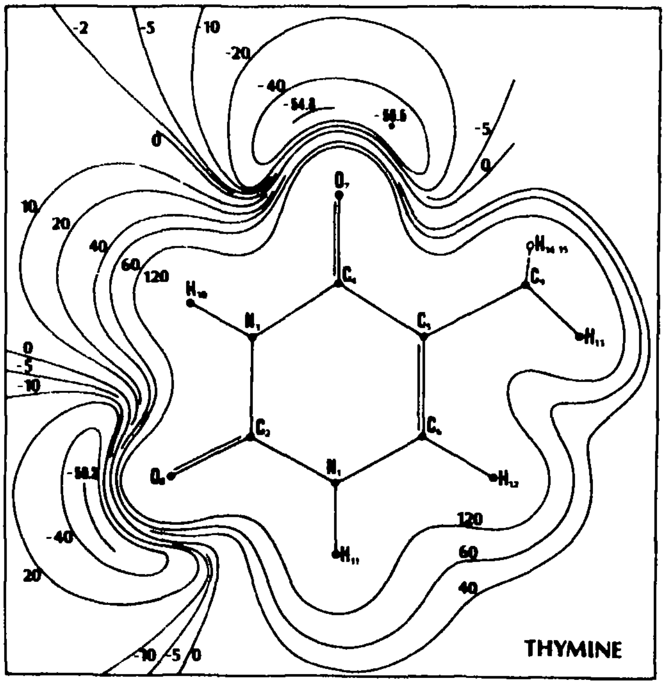

Fig. 3. Electrostatic molecular potential-energy map for thymine in the ring plane

The NH and CH regions as well as the neighbourhood of the amino group appear repulsive. Fig. 4 is instructive in this connection: it shows the potential energy above the plane of the molecule in a perpendicular section through N_{10}, C_6, and N_3. A secondary minimum of −24.8 kcal/mole is located above the amino nitrogen. Worth noting is the fact that a wide attractive area covers the whole $N_{10}C_6N_3$ region until a rather small distance. The shape of this attractive region and the relative depths of the minima around N_{10} and N_3 indicate clearly that the basicity (or nucleophilic character) of a pyridine-like nitrogen is larger than that of an NH_2-group, when the two are present, a conclusion in very good agreement with well-known experimental facts [8, 9]. Fig. 5 refers to a section

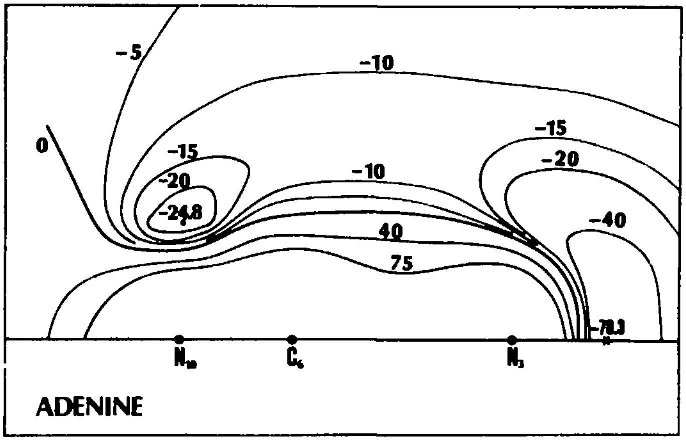

Fig. 4. Potential-energy map for adenine in the plane perpendicular to the ring plane and passing through N_{10}, C_6, and N_3 atoms

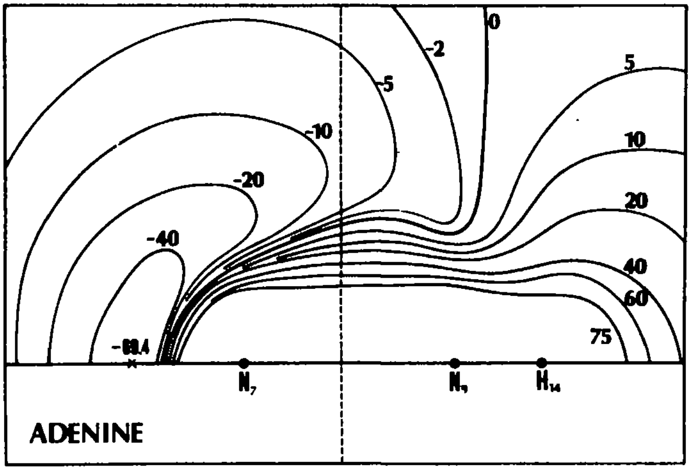

Fig. 5. Potential-energy map for adenine in a section perpendicular to the ring plane, containing N_7, N_9, and H_{14} atoms, and having as intersection the dotted line shown in Fig. 1

perpendicular to the molecular plane, containing atoms H_{14}, N_9, and N_7, and having as intersection with the molecular plane the dotted line shown in Fig. 1. A wide negative area which reaches the N_7 atom probably spreads out from the N_7 lone pair region (as in the case of N_3 in Fig. 4), but it reaches only the vertical of N_9, clearly showing the difference between amino and imino nitrogens.

As to the comparison of the present theoretical results with experimental data concerning electrophilic attack on adenine itself, one may mention that protonation, as well as alkylation, involves the ring nitrogens. Among them, the preferred regions of attack are definitely N_1 and N_3, the distinction among the two positions being difficult: results on the base itself indicate N_1 as the first protonation site [10, 11] but N_3 was found more reactive than N_1 towards alkylating agents [12].

In nucleotides, nucleosides, and in the nucleic acids, N_1 seems to be the first protonation site [13], alkylation occurring at both N_1 and N_3 [14]. In RNA, N_1 is the principal minor site of alkylation (the major site is N_7 of guanine) while this site shifts to N_3 in DNA (where N_1 is involved in hydrogen-bonding) [15].

Cytosine: The in-plane diagram of cytosine (Fig. 2) presents a new situation due to the presence of a carbonyl group adjacent to a pyridine-like nitrogen: a wide attractive region for electrophilic agents appears on this side of the molecule, with two deep minima, one located in the direction of the molecule, with two deep minima, one located in the direction of the nitrogen lone-pair, the other at an angle of 55° from the C=O bond. This last location is quite interesting in view of the fact that the *global* isodensity curves show no directional properties around the carbonyls [7]. In fact there is a slight anisotropy of the electron density hidden inside the roughly spherical cloud of oxygen, the SCF canonical orbitals comprising one nearly pure oxygen *p* atomic orbital perpendicular to the CO bond, and another (roughly *sp*) hybrid along the CO bond, each occupied by a pair of electrons [5]. If one transforms this canonical set into a set of localized orbitals according to the criterion of Foster and Boys [16], one obtains two oxygen lone-pair orbitals pointing approximately at 120° from each other on each side of the CO bond [17]. In the molecules previously studied [1, 2, 4], the minima of the potentials were located approximately in the direction of the localized lone-pair orbitals: in the present case the lone-pair directionality around the carbonyl oxygen is clearly overwhelmed by the effect of the neighbouring groups, the strong attractive character of the neighbour nitrogen enhancing the oxygen minimum on one side, the repulsive character of the NH group being strongly felt on the other side. The strong effect of the environment appears also in the diagram of thymine (*vide infra*).

An intermediate situation may be found in the CH_2NHO molecule [3] where two minima on the oxygen site are still present but noticeably influenced by the attractive character of the nitrogen lone-pair and by the repulsive effect of the NH bond.

A rather remarkable feature concerning cytosine is the fact that the potential well is deeper for N_3 than for O_8. Note also that the minimum for N_3 is deeper than for either nitrogen in adenine.

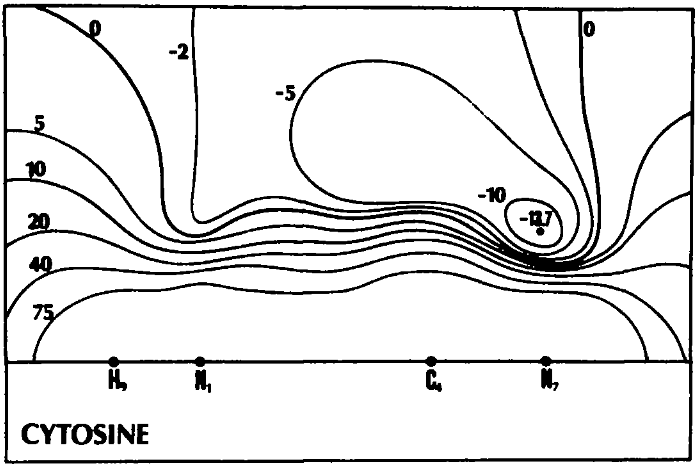

Fig. 6. Potential-energy map for cytosine in the plane perpendicular to the ring plane and passing through H_9, N_1, C_4, and N_7

The amino nitrogen N_7 has two equivalent minima of -13.7 kcal/mole above and below the molecular plane while the electrostatic potential around the imino nitrogen N_1 is very similar to the one found in the corresponding N_9H zone of adenine (see Fig. 6).

From the experimental point of view, protonation of cytosine, its nucleoside and nucleotide, occurs on N_3 [10, 18], and so does alkylation [19, 15], both reactions being easier in cytosine than in adenine. The basic pK's are 4.6 and 4.2 respectively [9, 18, 11]. In DNA, where the N_3 position is involved in hydrogen-bonding the reactivity of cytosine towards methylation is much reduced or even suppressed depending on the reagent [15]. A protonation of the oxygen of cytosine in DNA with no disruption of hydrogen bonding has been reported [20].

All these experimental facts are in very satisfactory agreement with the conclusions that can be drawn from the potential energy curves.

Thymine: The in-plane isopotential curves of thymine are given in Fig. 3. This molecule has no-pyridine-like nitrogens, but has two carbonyl oxygens one of which is adjacent to one NH group on each side, the other has one NH neighbour and one CCH_3 on the other side. The shape of the potentials shows two regions of attraction towards the two oxygen atoms, the rest of the molecule being repulsive. As noted in the case of cytosine, the directionality of the attraction is strongly influenced by the environment: the oxygen O_8 which has two NH neighbours presents one symmetrical potential well, whereas two minima appear near O_7, one being clearly pushed away from the NH region.

The isopotential curves in the perpendicular plane passing through H_{11}, N_1, C_4, and O_7 (Fig. 7) show that the imino group is surrounded in this molecule by a repulsive area, although immediately above the N atom a decrease of the $V(r_i)$ values may be evidenced.

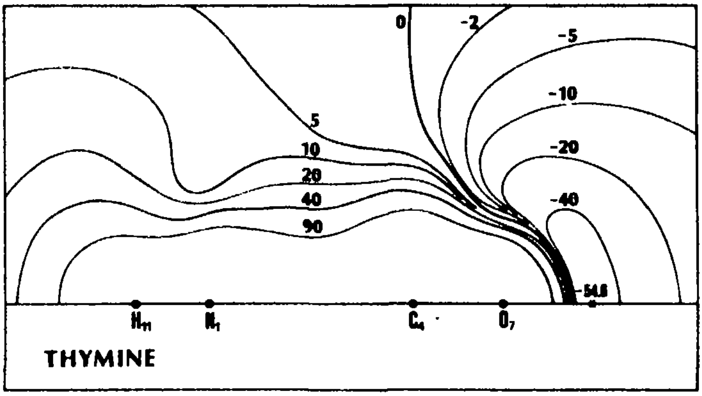

Fig. 7. Potential-energy map for thymine in the plane perpendicular to the ring plane and passing through H_{11}, N_1, C_4, and O_7

The depth of the minima in thymine is much smaller than that of the corresponding wells in cytosine, in complete agreement with the fact that thymine and thymidine are much less basic than cytosine and cytidine [15] and that neutral thymine does not undergo alkylation in the conditions under which the other bases react [11, 12]; the same is true in the nucleic acids [15, 17].

General Remarks and Conclusion

The present extension of the study of isopotential curves to large heterocycles clearly confirms the interest and usefulness of this technique for extracting from a wave function the information it encloses in a form which appears suitable for the investigation of problems of chemical reactivity.

Clear-cut differences appear between the different zones of complex molecules and the positions and depths of the potential wells are undoubtedly connected with the ease of electrophilic attack. Even though the electrostatic energy considered here is but a fraction of the total energy of interaction of the molecule with an approaching proton, it clearly appears as a determining element. Although polarization and charge transfer effects are neglected in this representation, it seems – in the case studied – as if they had their maxima in the same directions as those given by the consideration of the electrostatic energy alone.

Quite interesting is the fact that the present technique allows a neat discrimination between the different possible sites of protonation on a same molecular skeleton, an achievement which is not possible on simple inspection of the isodensity contours. The reason for this is that potential energies are very sensitive to small differences in electron densities, differences which are not perceptible in the global density contours generally utilized[1].

---

[1] It is perhaps not superfluous to remark that a variation in density of $6 \cdot 10^{-3}$ electron per $(a_0)^3$ is sufficient to produce a variation of 1 kcal/mole in the interaction energy with a unit positive charge situated at a distance of 4 atomic units.

Another advantage of the isopotential curves is the possibility of comparing potential protonation sites of different kinds (oxygen with nitrogen, pyridine-like nitrogen with amino nitrogens, etc. ...) and also sites on different molecules. A noticeable result of the present study is the fact that doubly-bonded oxygen atoms appear less basic than doubly-bonded nitrogens. This is probably related to the greater directionality of the charge cloud around the nitrogens.

If we consider the nitrogen atoms, we can remark that

a) pyridine-like atoms have the greatest proton affinity; the region of negative potential extends above and below the molecular plane but the minimum is in the plane.

b) The amino nitrogens have a remarkable proton affinity in the regions outside the molecular plane (corresponding to potential minima of -24 kcal/mole for adenine and -13.7 kcal/mole for cytosine).

c) Finally, the imino atoms seem to have the lowest proton affinity; the isopotential maps do not show minima directly related to this type of atoms, although from Figs. 5, 6, and 7 one is allowed to infer a small negative contribution due to their π electrons.

Finally, one seemingly important effect appears in the study of the electrostatic potential seen by an approaching proton, namely the repulsive role of the peripheral hydrogen atoms attached to the molecule. These hydrogens are always more or less discharged with respect to a neutral atom (especially when bound to nitrogen in an amino group or in NH), so that the effect of the nuclei overbalances the attraction of the electronic density. This creates large repulsive regions which should help directing the approaching proton into the corridors leading to the strongly attractive zones. This effect of the peripheral hydrogens has never been taken into account in studies of basicities, and might well be quite important. The effect is perhaps exaggerated in the present results where the wave functions utilized correspond to a rather strong depopulation of the hydrogen atoms. But in any event, the qualitative effect would remain (similar effects can be observed in the small molecules of Ref. [2] and [3]).

In conclusion, we think that pursuing the study of reactivity along these lines is worth further efforts. The use of *ab initio* wave functions (and if possible even of higher accuracy than the present ones) is of course of prime importance at the beginning, but recent investigations using the CNDO-method have proven extremely encouraging [21] and a close parallel study with *ab initio* results will probably lead to a satisfactory calibration of semi-empirical procedures.

References

1. Bonaccorsi, R., Petrongolo, C., Scrocco, E., Tomasi, J.: In: Quantum aspects of heterocyclic compounds in chemistry and biochemistry, Jerusalem Symposia Vol. II, 181 (1970).
2. Scrocco, E., Tomasi, J.: J. chem. Physics **52**, 5270 (1970).
3. — — Theoret. chim. Acta (Berl.) **21**, 17 (1971).
4. — — Theoretical section progress report, Laboratorio di Chimica quantistica del C.N.R. e Istituto di Chimica Fisica dell'Università, p. 35. Pisa 1969-1970.
5. Mély, B., Pullman, A.: Theoret. chim. Acta (Berl.) **13**, 278 (1969).
6. Nakajima, T., Pullman, A.: J. Chim. physique **55**, 793 (1958).

7. Pullman,A., Dreyfus,M., Mély,B.: Theoret. chim. Acta (Berl.) **16**, 85 (1970).
8. Pullman,B.: Les Théories électroniques de la Chimie Organique, Masson (1952), for numerous examples.
9. Albert,A.: In: Physical methods in heterocyclic chemistry, ed. by A. R. Katritzky. New York: Academic Press 1963.
10. Cavalieri,L.F., Rosenberg,B.H.: J. Amer. chem. Soc. **79**, 5352 (1957).
Zubay,G.: Bioph. Bioch. Acta **28**, 644 (1958).
11. Christensen,J.J., Rytting,J.H., Izatt,R.M.: Biochemistry **9**, 4907 (1970).
12. Pal,B.C.: Biochemistry **1**, 558 (1962).
13. Bryan,R.F., Tomita,K.: Acta crystallogr. **15**, 1179 (1962).
14. Brookes,P., Lawley,P.D.: J. chem. Soc. (London) **1960**, 539.
Jones,J.W., Robins,R.K.: J. Amer. chem. Soc. **85**, 193 (1963).
Lawley,P.D., Brookes,P.: Biochem. J. **92**, 19C (1964); **89**, 127 (1963).
15. Progress in nucleic acid research **5**, 89 (1966).
16. Foster,J.M., Boys,S F.: Rev. mod. Physics **32**, 300 (1960).
17. Pullman,A., Berthod,H.: Unpublished results.
18. Christensen,J.J., Rytting,J.H., Izatt,R.M.: J. physic. Chem. **91**, 2700 (1967).
19. Brookes,P., Lawley,P D.: J. chem Soc. (London) **1962**, 1348; Bioph. Bioch. Acta **26**, 450 (1957).
20. Dove,N F., Wallace,F.A., Davidson,N.: Bioch. Bioph Res Comm. **1**, 312 (1959).
21. Giessner-Prettre,C., Pullman,A : Comp. Rend. Ac Sci Paris **272**C, 750 (1971).

Dr. R. Bonaccorsi
Laboratorio di Chimica Quantistica
ed Energetica Molecolare del C.N.R.
Via Risorgimento 35
I-56100 Pisa, Italia

Theoret. chim. Acta (Berl.) 24, 61 70 (1972)
© by Springer-Verlag 1972

Configuration Analysis and Electronic States Properties

I. Four- and Six-π-Electron Systems

G. FAVINI and G. BUEMI
Istituto di Chimica Fisica dell'Università, Viale A. Doria 8, Catania, Italy

Received June 11, 1971

The excited-states electronic properties of unsaturated small-ring hydrocarbons with four- and six-π-electrons have been studied by the "Molecules in Molecules" method and compared with experimental data and PPP results interpreted through a "configuration analysis" procedure. The results show that the MIM method is applicable with good reliability.

Die elektronischen Eigenschaften der angeregten Zustände von ungesättigten kleinen Kohlenwasserstoffringen mit vier und sechs π-Elektronen wurden mit Hilfe der „Molekül- im-Molekül"-Methode untersucht und die Ergebnisse mit experimentellen Daten und PPP Resultaten, die durch eine „Konfigurationsanalyse" interpretiert wurden, verglichen. Die Ergebnisse zeigen, daß die MIM-Methode mit großer Zuverlässigkeit anwendbar ist.

1. Introduction

The semiempirical PPP method [1] has been applied with remarkable success to a large number of organic molecules. One may point out, however, that the wavefunctions finally obtained by this method for electronic states of a molecule are not immediately understandable when an extended configuration interaction is included.

A procedure, tentatively called "configuration analysis", has been developed by Baba, Suzuki and Takemura [2] to interpret the results of PPP calculations directly in terms of the localized orbital model [3] in which the excited states are classified as locally excited or as charge-transfer states. This procedure enables one to compare the results of the PPP method with those of the MIM calculations.

By this correlation it should be possible to obtain informations on the validity of the choise of the reference orbitals used in MIM calculations, on the reliability of the results when an incomplete configuration interaction treatment is adopted, and finally on the effectiveness of the comparison between the electronic transition energies obtained in PPP and MIM calculations.

Aim of the present investigation was to apply this procedure to a series of non-benzenoid hydrocarbons as a mean for the discussion of their spectroscopic properties.

The ground- and excited-states electronic properties of these derivatives were already studied in the PPP approximation [4], by means of a refined ω-technique [5] and by the VESCF method [6].

2. Method

The details of the configuration analysis procedure have been described in the original paper [2], where also the symbols used were defined.

In MIM calculations ethylene and *cis*-butadiene are considered as component systems; a small conjugation between the components is predicted across the "long" bonds in the composite systems.

The SCF MO and the experimental transition energies of the component molecules are given in Table 1; the values and the data of the cyclopentadiene were adopted for the *cis*-butadiene molecule.

Table 1. SCF MO's, experimental transition energies (in eV) of the component molecules, and configurations to which they are assigned

Molecule	SCF MO's	Configuration	E_{exp}	Refs.
Ethylene	$\varphi_1 = 1/\sqrt{2}(\chi_1 + \chi_2)$	$\varphi_1\,{}^1\varphi_2$	6.94[a]	[7, 8]
	$\varphi_2 = 1/\sqrt{2}(\chi_1 - \chi_2)$		6.60[b]	
			6.63[c]	
cis-butadiene[d]	$\varphi_1 = a(\chi_1 + \chi_4) + b(\chi_2 + \chi_3)$	$A_1 = \varphi_2\,{}^1\varphi_3$	5.18	[9, 10]
$a = 0.4361$	$\varphi_2 = b(\chi_1 - \chi_4) + a(\chi_2 - \chi_3)$	$A_2 = 1/\sqrt{2}(\varphi_1\,{}^1\varphi_3 - \varphi_2\,{}^1\varphi_4)$	6.20	[11]
$b = 0.5566$	$\varphi_3 = b(\chi_1 + \chi_4) - a(\chi_2 + \chi_3)$	$A_3 = 1/\sqrt{2}(\varphi_1\,{}^1\varphi_3 + \varphi_2\,{}^1\varphi_4)$	7.90	[11]
	$\varphi_4 = a(\chi_1 - \chi_4) - b(\chi_2 - \chi_3)$	$A_4 = \varphi_1\,{}^1\varphi_4$	8.53[e]	

[a] For ethylene 1,2-disubstituted

[b] For ethylene 1,1-disubstituted.

[c] For ethylene tetrasubstituted.

[d] Geometry of cyclopentadiene (*cfr*. Ref. [12]).

[e] Evaluated from E_{1_1} plus the energy differences between SCF-MO's $\varphi_4 - \varphi_3$ and $\varphi_2 - \varphi_1$.

First ionization potentials and electron affinities of the component systems are taken from the literature [13]; for butadiene the electron affinity (−0.60 eV) was calculated through the Briegleb's relationship [14]. Second ionization potential (8.58 eV) and electron affinity (−2.55 eV) for butadiene were obtained from the above values minus the energy difference between the relevant SCF orbitals.

Coulomb integrals $\gamma_{\mu\nu}$ were calculated by the previously given formula [15] and the resonance integrals $\beta_{\mu\nu}$ by the Kon's relationship [16].

3. Results

The topology of the molecules studied is shown in Fig. 1.

Triafulvene (Methylenecyclopropene) (I)

The results of PPP method in Ref. [17] were subjected to configuration analysis and compared with our standard MIM calculations (columns A in Table 2); those of PPP method in Ref. [4], after application of the configuration

Fig. 1

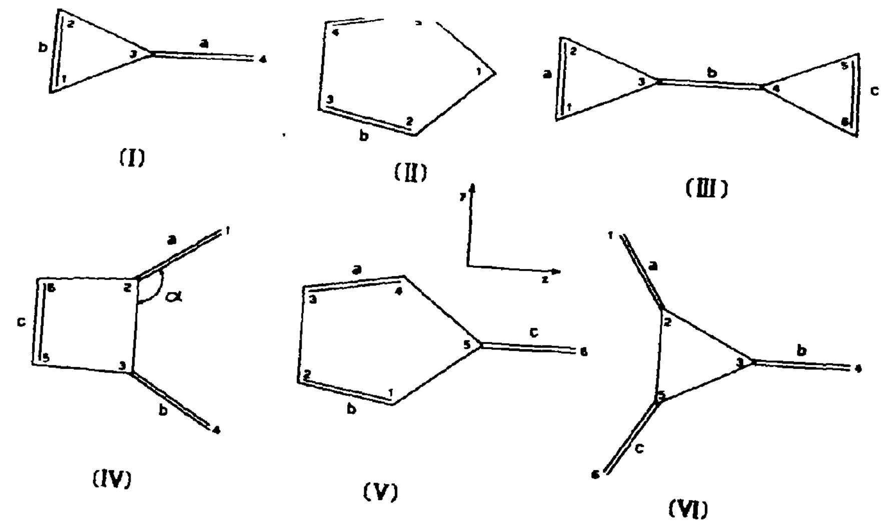

Table 2. Excited singlet states of triafulvene (weights of states: transition energies, oscillator strengths and polarizations)

States	$^1B_2$				$^1A_1$				$^1B_2$				$^1A_1$			
	MIM		PPP		MIM		PPP		MIM		PPP		MIM		PPP	
	A	B	A	B	A	B	A	B	A	B	A	B	A	B	A	B
Γ	—	—	—	—	0.08	0.13	0.07	0.08	—	—	—	—	0.04	0.06	0.01	0.08
A_a	—	—	—	—	0.54	0.57	0.23	0.62	—	—	—	—	0.46	0.42	0.72	0.29
A_b	0.38	0.40	0.63	0.29	—	—	—	—	0.62	0.60	0.33	0.63	—	—	—	—
T_b^*	—	—	—	—	0.38	0.30	0.63	0.18	—	—	—	—	0.50	0.52	0.22	0.51
T_a^*	0.62	0.60	0.32	0.59	—	—	—	—	0.38	0.40	0.60	0.25	—	—	—	—
Total weight (%)	100	100	95.1	87.8	100	100	92.6	88.1	100	100	92.8	87.6	100	100	95.4	88.0
ΔE (eV)	4.83	4.19	5.48	4.33	5.38	5.16	6.37	6.15	8.23	8.77	9.49	9.10	8.50	9.27	9.61	10.34
f	0.13	0.10	0.27	0.10	0.50	0.49	0.41	0.74	0.36	0.32	0.25	0.44	0.02	<0.01	0.23	0.02
Polar.	y	y	y	y	z	z	z	z	y	y	y	y	z	z	z	z

analysis treatment, were compared with the results of a MIM procedure carried with the same parameters as in Ref. [4] (columns B in Table 2). In this table are given the weights of the individual locally excited states (A_n) or charge transfer states (T_m^k), together with the total weight of the V_σ^0 and the data on the electronic transitions; the ground state is indicated by the symbol Γ.

Cyclopentadiene (II)

The structure of the molecule has been recently discussed [12, 18] and a planar configuration with C_{2v} symmetry has been confirmed. The π-electronic states were obtained by the PPP method starting from the SCF–MO's of Table 1 and using the standard parameters: the configuration analysis was applied to the results of the above calculation and a comparison with the results of the MIM procedure is shown in Table 3.

Table 3. Excited singlet states of cyclopentadiene

States	$^1B_2$		$^1A_1$		$^1A_1$		$^1B_2$	
	MIM	PPP	MIM	PPP	MIM	PPP	MIM	PPP
Γ			0.06	0.06			-	
$A_a(A_b)$	0.25	0.295			0.50	0.485	0.25	0.19
$T_b^a(T_a^b)$	0.25	0.19	0.47	0.43			0.25	0.295
Total weight (%)	100	97	100	92	100	97	100	97
ΔE (eV)	4.44	5.85	6.62	7.65	7.69	8.55	7.91	9.20
f	0.16	0.21	0	0	1.01	1.13	<0.01	<0.01
Polar.	y	y		-	z	z	y	y

Triafulvalene (Bis-Cyclopropenylidene) (III)

The results of the PPP method in Ref. [4], after application of the configuration analysis treatment, were compared with the results of MIM calculations; the same geometry was adopted and the resonance integrals were evaluated by the Kon's formula [16] (columns A in Table 4) or by the exponential formula of Ref. [4] (columns B in Table 4).

Dimethylenecyclobutene (IV)

The results of the PPP method in Ref. [19] were subjected to configuration analysis and compared in Table 5 with the MIM calculations obtained for the observed geometry [20] (columns B) by considering three ethylene fragments; columns A relate to a procedure in which the same parameters and geometry as

Table 4. Excited singlet states of triafulvalene (allowed transitions)

States	$^1B_{1u}$			$^1B_{2u}$			$^1B_{2u}$			$^1B_{1u}$			$^1B_{2u}$		
	MIM/A	MIM/B	PPP	MIM/A	MIM/B	PPP	MIM/A	MIM/B	PPP	MIM/A	MIM/B	PPP	MIM/A	MIM/B	PPP
$1/\sqrt{2}(A_a + A_c)$	—	—	—	0.25	0.26	0.17	0.63	0.61	0.64	—	—	—	0.12	0.14	0.01
$1/\sqrt{2}(T_b^a + T_b^c)$	—	—	—	0.64	0.63	0.48	0.08	0.06	0.09	—	—	—	0.28	0.31	0.20
$1/\sqrt{2}(T_a^c + T_c^a)$	—	—	—	0.11	0.11	0.12	0.29	0.33	0.12	—	—	—	0.60	0.55	0.59
$1/\sqrt{2}(T_a^b + T_c^b)$	0.55	0.55	0.38	—	—	—	—	—	—	0.45	0.45	0.50	—	—	—
A_b	0.45	0.45	0.50	—	—	—	—	—	—	0.55	0.55	0.38	—	—	—
Total weight (%)	100	100	87.8	100	100	77.1	100	100	85.1	100	100	87.8	100	100	79.7
ΔE (eV)	3.58	3.20	5.58	4.04	3.68	3.55	7.80	7.84	8.93	9.09	9.46	11.09	10.12	10.45	11.53
f	0.45	0.43	0.85	0.12	0.11	0.13	0.60	0.56	0.92	<0.01	<0.01	0.02	0.15	0.17	0.05
Polar.	z	z	z	y	y	y	y	y	y	z	z	z	y	y	y

Table 5. First excited singlet states of dimethylenecyclobutene (three ethylenes as component systems)

States	$^1B_2$			$^1A_1$			$^1A_1$			$^1B_2$		
	MIM/A	MIM/B	PPP	MIM/A	MIM/B	PPP	MIM/A	MIM/B	PPP	MIM/A	MIM/B	PPP
Γ	—	—	—	—	—	0.01	0.02	0.03	0.04	—	—	—
$1/\sqrt{2}(A_a + A_b)$	—	—	—	0.25	0.32	0.24	—	—	~0	—	—	—
$1/\sqrt{2}(T_c^a + T_c^b)$	—	—	—	0.37	0.34	0.31	0.27	0.26	0.13	—	—	—
$1/\sqrt{2}(T_a^c - T_b^c)$	—	—	—	0.37	0.34	0.26	0.27	0.26	0.31	—	—	—
$1/\sqrt{2}(T_a^b + T_b^a)$	—	—	—	—	—	0.01	0.44	0.45	0.32	—	—	—
$1/\sqrt{2}(A_a - A_b)$	0.02	0.30	0.01	—	—	—	—	—	—	0.62	0.35	0.55
A_c	0.30	0.19	0.21	—	—	—	—	—	—	0.08	0.23	~0
$1/\sqrt{2}(T_c^a - T_c^b)$	0.18	0.05	0.12	—	—	—	—	—	—	0.06	0.20	0.04
$1/\sqrt{2}(T_a^c + T_b^c)$	0.18	0.05	0.21	—	—	—	—	—	—	0.06	0.20	0.10
$1/\sqrt{2}(T_a^b - T_b^a)$	0.31	0.41	0.26	—	—	—	—	—	—	0.18	0.02	0.16
Total weight (%)	100	100	81.5	100	100	83.3	100	100	80.1	100	100	85.5
ΔE (eV)	5.01	4.29	4.68	5.00	4.43	6.02	5.08	4.77	4.77	4.63	4.99	6.31
f	0.06	0.02	0.12	0.41	0.45	0.77	0	0	0.01	0.64	0.72	0.89
Polar.	y	y	y	z	z	z	—	—	z	y	y	y

Table 6. First excited singlet states of dimethylenecyclobutene (ethylene(E) and *cis*-butadiene(B) as component systems)

States	$^1B_2$		$^1A_1$		$^1A_1$		$^1B_2$	
	MIM/B	PPP	MIM/B	PPP	MIM/B	PPP	MIM/B	PPP
I			0.04	0.12	0.05	0.02		
$(A_2)_B$			0.11	0.26	0.35	0.01		
$(A_3)_B$			0.09	0.01	0.05	0.24		
T_E^{3B}			0.06	0.11	0.55	0.33		
T_{2B}^E			0.70	0.28	~0	0.27		
A_E	0.31	0.24					~0	~0
$(A_1)_B$	0.01	0.19					0.98	0.66
$(A_4)_B$	0.13	0.09					~0	0.07
T_{1B}^E	0.35	0.22					0.01	0.11
T_E^{4B}	0.20	0.13					~0	0.04
Total weight (%)	100	87.3	100	77.3	100	87.4	100	88.2
ΔE (eV)	4.17	4.68	4.50	4.77	4.98	6.02	5.18	6.31
f	0.25	0.12	0.27	0.01	0.13	0.77	0.45	0.89
Polar	y	y	z	z	z	z	y	y

$(A_n)_B$. locally excited states of *cis*-butadiene.

T_E^{nB} and T_{nB}^E: charge transfer configuration from ethylene to *cis*-butadiene and from *cis*-butadiene to ethylene respectively

in Ref. [19] were applied. Finally in Table 6 are shown the results obtained when ethylene and *cis*-butadiene are considered as component systems.

Fulvene (V)

The electronic system of fulvene has been the subject of a large number of studies by various methods [21]. In MIM calculations we used the molecular geometry based upon the crystallographic data on dimethylfulvene [22]. The coplanarity of the carbon skeleton has been recently confirmed by electron diffraction study and nearly equal geometrical parameters were found [23]. The resonance integrals were evaluated by the Kon's formula or by the exponential formula of Ref. [4] (columns A and B respectively in Tables 7 and 8). The configuration analysis procedure was applied to the results of the PPP method [4] by considering as component systems three molecules of ethylene or, alternatively, one molecule of ethylene and one molecule of *cis*-butadiene; a comparison with the MIM results is shown in Tables 7 and 8 respectively.

Trimethylenecyclopropane (*[3]-Radialene*) (VI)

Standard parameters and observed geometry [24] were used in the calculations; the results of the configuration analysis treatment for the first three excited states are compared with those of the MIM procedure in Table 9.

	$^1B_2$			$^1A_1$			$^1A_1$			$^1B_2$		
	MIM A	MIM B	PPP	MIM A	MIM B	PPP	MIM A	MIM B	PPP	MIM A	MIM/B	PPP
Γ	—	—	—	0.04	0.04	0.10	~0	~0	0.01	—	—	—
$1/\sqrt{2}(A_a + A_b)$	—	—	—	0.08	0.09	0.02	~0	~0	0.01	—	—	—
A_c	—	—	—	0.29	0.29	0.22	0.08	0.08	0.21	—	—	—
$1/\sqrt{2}(T_a^c + T_b^c)$	—	—	—	0.21	0.22	0.12	0.11	0.11	0.05	—	—	—
$1/\sqrt{2}(T_c^a + T_c^b)$	—	—	—	0.30	0.29	0.18	0.14	0.14	0.07	—	—	—
$1/\sqrt{2}(T_a^b + T_b^a)$	—	—	—	0.08	0.07	0.11	0.67	0.67	0.41	—	—	—
$1/\sqrt{2}(A_a - A_b)$	0.36	0.36	0.25	—	—	—	—	—	—	0.01	0.06	0.04
$1/\sqrt{2}(T_a^c - T_b^c)$	0.27	0.27	0.34	—	—	—	—	—	—	0.36	0.14	0.07
$1/\sqrt{2}(T_c^a - T_c^b)$	~0	~0	~0	—	—	—	—	—	—	0.30	0.48	0.29
$1/\sqrt{2}(T_a^b - T_b^a)$	0.37	0.37	0.19	—	—	—	—	—	—	0.33	0.32	0.42
Total weight (%)	100	100	77.5	100	100	75.0	100	100	75.9	100	100	82.1
ΔE (eV)	3.29	2.93	3.27	3.95	3.64	5.05	6.28	6.28	6.98	6.45	6.45	8.21
f	0.06	0.05	0.05	0.57	0.55	0.67	0.12	0.12	0.31	0.13	0.12	0.29
Polar.	y	y	y	z	z	z	z	z	z	y	y	y

Table 8. First excited singlet states of fulvene (ethylene(E) and *cis*-butadiene(B) as component systems)

States	$^1B_2$		$^1A_1$		$^1A_1$		$^1B_2$	
	MIM/A	PPP	MIM/A	PPP	MIM/A	PPP	MIM/A	PPP
Γ	—	—	0.02	0.05	0.01	0.01	—	—
$(A_2)_B$	—	—	0.14	0.19	0.69	0.49	—	—
$(A_3)_B$	—	—	0.06	0.02	0.01	0.01	—	—
A_E	—	—	0.23	0.25	0.22	0.24	—	—
T_{1B}^E	—	—	0.21	0.12	0.02	0.04	—	—
T_E^{3B}	—	—	0.34	0.23	0.05	0.06	—	—
$(A_1)_B$	0.39	0.38	—	—	—	—	0.61	0.31
$(A_4)_B$	—	~0	—	—	—	—	—	0.11
T_{2B}^E	0.61	0.47	—	—	—	—	0.39	0.36
T_E^{4B}	—	~0	—	—	—	—	—	0.07
Total weight (%)	100	85.4	100	85.8	100	84.9	100	85.0
ΔE (eV)	3.26	3.27	3.55	5.05	6.23	6.98	6.44	7.26
f	0.02	0.05	0.51	0.67	0.16	0.31	0.18	0.11
Polar.	y	y	z	z	z	z	y	y

Table 9. First excited singlet states of [3]-radialene (three ethylenes as component systems)

States	${}^1E'_1$		${}^1E'_1$		${}^1A'_1$	
	MIM	PPP	MIM	PPP	MIM	PPP
$1/\sqrt{2}(A_a - A_c)$	0.44	0.45	0.31	0.27	—	—
$1/\sqrt{2}(T_b^a - T_b^c)$	~0	~0	0.27	0.22	—	-
$1/\sqrt{2}(T_a^c - T_c^a)$	0.29	0.24	0.02	0.02	--	—
$1/\sqrt{2}(T_a^b - T_c^b)$	0.27	0.22	0.40	0.37	--	—
$1/\sqrt{6}(T_a^b + T_b^c + T_c^a - T_b^a - T_c^b - T_a^c)$	-	-		--	1.00	0.88
Total weight (%)	100	91	100	88	100	88
ΔE	3.86	5.89	6.70	7.98	6.97	8.38
f	0.46	0.81	0.15	0.17	0	0
Polar.	y, z	y, z	y, z	y, z	--	—
	(degenerate transition)		(degenerate transition)			

4. Discussion

For the triafulvene, in which strong bond fixation exists, the calculated results for both the ground state and the excited states are sensitive to the dependence of the resonance integrals on bond length and to the choice of empirical values for the repulsion integrals. The results in Table 2 reveal clearly that the dependence is more remarkable in PPP calculations than in MIM calculations. Unfortunately, the triafulvene spectrum is not available for a direct comparison between theory and experiment; however, by the configuration analysis treatment a better agreement between the theoretical results is found for the case B in Table 2. In the first transition ${}^1B_2 \leftarrow {}^1A_1$ the effect of a charge transfer from ethylene *a* to ethylene *b* is remarkable and it determines a spectral shift of about 2 eV respect to the component molecules.

For the cyclopentadiene the results of the configuration analysis and of the MIM technique are similar in the excited state composition, in spite of the differences in transition energies. The first absorption band observed at 5.18 eV [9, 10] is intermediate between the values calculated for the ${}^1B_2 \leftarrow {}^1A_1$ transition, in the two procedures. The second band of moderate intensity observed at 6.20 eV corresponds to the ${}^1A_1 \leftarrow {}^1A_1$ transition found at 6.62 eV in MIM calculation (forbidden in the π-approximation). The very strong band at 7.90 eV is assigned to the next ${}^1A_1 \leftarrow {}^1A_1$ transition ($\Delta E = 7.69$ eV and $f = 1.01$ in MIM calculations). These results are congruent with the values obtained by the CNDO treatment of the molecule [11].

In the case of triafulvalene a remarkable difference in energy is found for the first ${}^1B_{1u} \leftarrow {}^1A_{1g}$ transition which should be appear as charge transfer band in the longest wave-length region (about 350 nm) if the MIM results are reliable and as ethylenic band at about 220 nm if one look at PPP calculations. Unfortunately a choice is not possible since experimental data are lacking.

The results obtained for the dimethylenecyclobutene are rather contradictory. A comparison between PPP and MIM states is possible; however, in PPP calculations two electronic transitions with different polarization and low intensity are found at about 4.7 eV and other two transitions with different polarization and high intensity are found at about 6 eV, whilst in MIM calculations the four corresponding transitions range from 4.2 to 5.2 eV with different sequence according to the component systems considered and the parameters chosen.

The interpretation of the UV spectra of this compound by the simple method applied to other derivatives is not acceptable; it is necessary probably to include the doubly excited configurations in the CI treatment and the core resonance integral between the opposite carbon atoms in the ring which are only about 2.0 Å apart [6].

The electronic absorption spectrum of fulvene in the gas phase has been recently investigated [25] and four electronic transitions have been identified. The lowest energy (3.42 eV) transition of weak intensity ($f = 0.008$) is assigned to a ${}^1B_2 \leftarrow {}^1A_1$ transition in which a remarkable charge transfer occurs from butadiene to exocyclic ethylene. The second transition is strong ($f = 0.34$) and extends from 267 to 205 nm with a maximum at 235 nm (5.28 eV); it is assigned to a ${}^1A_1 \leftarrow {}^1A_1$ transition and the PPP transition energy agrees with the maximum frequency, whilst the MIM transition energy results lower than the observed 0 – 0 frequency (4.65 eV); the excited states composition shows an overestimation in MIM calculations of the contribution of the charge transfer configuration from ethylene to butadiene responsible of the bathochromic shift of the ethylenic band. The third and fourth bands observed at 201.7 nm (6.15 eV) and at 178 nm (6.95 eV) are assigned on the basis of our MIM calculation to an ${}^1A_1 \leftarrow {}^1A_1$ transition at 6.23–6.28 eV and to a ${}^1B_2 \leftarrow {}^1A_1$ transition at 6.44–6.45 eV. It is interesting to remark that the molecule behaves both like a weakly coupled *cis*-butadiene plus ethylene entity and like three ethylene entities as suggested by Heilbronner and coworkers [26].

The trimethylenecyclopropane spectrum [24] is well interpreted by the results of MIM calculation. The first (4.20 eV) and the second (6.70 eV) absorption bands are assigned to allowed degenerate transitions ${}^1E_1' \leftarrow {}^1A_1'$ at 3.86 and 6.70 eV respectively. The energies of these transitions can not be reproduced by simple PPP calculations including only single excited configurations, also when the composition of the two excited states, as results by configuration analysis, is in agreement with that obtained in MIM calculations.

The results obtained for the above four- and six-π-electron systems of unsaturated small-ring hydrocarbons seem to suggest these general conclusions:

a) it is confirmed the validity of the MIM method for compounds in which alternanting single and double bonds occur, also by different choice of the component systems when allowed by molecular symmetry;

b) the additional informations drawn from the results of the calculations of the PPP type through the configuration analysis treatment justify, except for the dimethylenecyclobutene, the inclusion of only single excited configurations in MIM calculations of electronic transition energies;

c) remarkable differences in transition energies related to same electronic excited states may occur in PPP and MIM calculations with the same parameters; MIM energies should be the most reliable.

Financial aid from the Italian C.N.R. is gratefully acknowledged.

References

1. Parr, R.G.: The quantum theory of molecular electronic structure. New York: W. A. Benjamin 1963.
2. Baba, H., Suzuki, S., Takemura, T.: J. chem. Physics **50**, 2078 (1969).
3. Longuet-Higgins, H.C., Murrell, J.N.: Proc. physic. Soc. A **68**, 601 (1955).
4. Yamaguchi, H., Nakajima, T.: Theoret. chim. Acta (Berl.) **12**, 349 (1968).
5. Dorko, E.A., Nielsen, H.P., Bahr, W.C.: Theoret. chim. Acta (Berl.) **14**, 357 (1969).
6. Brown, R.D., Burden, F.R., Williams, G.R.: Austral. J. Chem. **21**, 1939 (1968).
7. Roos, B.: Acta chem. scand. **21**, 2318 (1967).
8. Allinger, N.L., Tai, J.C., Stuart, T.W.: Theoret. chim. Acta (Berl.) **8**, 101 (1967).
9. Trombetti, A., Zauli, C.: Ann. Chim. **53**, 797 (1963).
10. Miller Layton, E., Jr.: J. molecular Spectroscopy **5**, 181 (1960).
11. Del Bene, J., Jaffé, H.H.: J. chem. Physics **48**, 4050 (1968).
12. Scharpen, L.H., Laurie, V.W.: J. chem. Physics **43**, 2765 (1965).
13. Vedeneyev, V.I., Gurvich, L.V., Kondrat'Yev, V.N., Medvedev, V.A., Frankenich, Ye.L.: Bond energies, ionization potentials and electron affinities. London: Edward Arnold 1966.
14. Briegleb, G.: Angew. Chem., Intern. Ed. (Engl.) **3**, 617 (1964).
15. Favini, G., Vandoni, I., Simonetta, M.: Theoret. chim. Acta (Berl.) **3**, 45 (1965).
16. Kon, H.: Bull. chem. Soc. Japan **28**, 275 (1955).
17. Watanabe, A., Yamaguchi, H., Amako, Y., Azumi, H.: Bull. chem. Soc. Japan **41**, 2196 (1968).
18. O'Sullivan, P.S., Hameka, H.F.: Chem. Physics Letters **4**, 123 (1969).
19. Skancke, A., Skancke, P.N.: Acta chem. scand. **22**, 175 (1968).
20. — Acta chem. scand. **22**, 3239 (1968).
21. Tinland, B.: J. molecular Structure **3**, 429 (1969) and references therein cited.
22. Norman, N., Post, B.: Acta crystallogr. **14**, 503 (1961).
23. Chiang, J.F., Bauer, S.H.: J. Amer. chem. Soc. **92**, 261 (1970).
24. Dorko, E.A., Hencher, J.L., Bauer, S.H.: Tetrahedron **24**, 2425 (1968).
25. Brown, R.D., Domaille, P.J., Kent, J.E.: Austral. J. Chem. **23**, 1707 (1970).
26. Straub, P.A., Meuche, D., Heilbronner, E.: Helv. chim. Acta **49**, 517 (1966).

Prof. G. Favini
Istituto Chimica Fisica
Università di Milano
Via Saldini 50
Milano, Italia

Theoret. chim. Acta (Berl.) 24, 71 – 77 (1972)
© by Springer-Verlag 1972

Electron Spin-Spin Contact Interaction in Many-Electron Atoms*

B. W. N. Lo, K. M. S. Saxena, and S. Fraga

Division of Theoretical Chemistry, Department of Chemistry, University of Alberta,
Edmonton 7, Alberta, Canada

Received May 24, 1971

A general formulation has been developed for the evaluation of the total electron spin-spin contact interaction in many-electron atoms, including both the intra- and inter-shell contributions. Calculations have been carried out, using existing analytical Hartree-Fock functions, for the positive ions, neutral systems, and negative ions for all the atoms from He to Kr.

Es wird ein allgemeiner Formalismus zur Berechnung der gesamten Elektronen-Spin-Spin-Kontakt-Wechselwirkung in Vielelektronen-Atomen angegeben, der sowohl die Anteile der Wechselwirkung innerhalb einer Schale als auch zwischen einzelnen Schalen berücksichtigt. Berechnungen wurden unter Benutzung vorhandener analytischer Hartree-Fock-Funktionen für die positiven Ionen, die neutralen Systeme und die negativen Ionen aller Atome von He bis Kr durchgeführt.

Introduction

The electron spin-spin contact interaction has received little attention in the past by comparison with the better known fine and hyperfine interactions.

The formulation for the intrashell contribution to this interaction has been developed by Sessler and Foley [22] (s^n configurations), Fraga and Thorhallsson [13] (p^n configurations), and Armstrong [1, 2] (d^n and f^n configurations). Numerical values have been determined for the highest occupied shell of the positive ions, neutral systems, and negative ions from He to Kr by Fraga, Thorhallsson, and Fisk [14] and for a large number of lanthanide ions by Saxena, Lo, and Fraga [21].

It is now intended to present the complete theoretical formulation and use it for the evaluation of the total electron spin-spin contact interaction in the positive ions, neutral systems, and negative ions for all the atoms from He to Kr.

Theoretical Formulation

The electron spin-spin contact hamiltonian operator is (Armstrong [1] and Fontana and Meath [12])

$$\begin{aligned} H_{\text{ssc}} &= -(32\pi/3)\mu_B^2 \sum_{i<j} (\boldsymbol{s}_i \cdot \boldsymbol{s}_j)\, \delta(\boldsymbol{r}_i - \boldsymbol{r}_j) \\ &= -(8\pi/3)\alpha^2 \sum_{i<j} (\boldsymbol{s}_i \cdot \boldsymbol{s}_j)\, \delta(\boldsymbol{r}_i - \boldsymbol{r}_j), \end{aligned}$$

---

* This work has been supported in part by the National Research Council of Canada.

the last expression being given in a.u. The position and spin angular momentum vector operators are denoted by $\boldsymbol{r}$ and $\boldsymbol{s}$, $\delta(\boldsymbol{r}_i - \boldsymbol{r}_j)$ represents the three-dimensional delta function, and the summation extends over all the pairs of electrons in the system; μ_B denotes the Bohr magneton and α is the fine structure constant.

The total electron spin-spin contact interaction may be written as

$$E_{\mathrm{ssc}} = \langle \Psi | H_{\mathrm{ssc}} | \Psi \rangle = \sum_{a} E_{\mathrm{ssc,aa}} + \sum_{a<b} E_{\mathrm{ssc,ab}},$$

where distinction is made between the intra- and inter-shell contributions; the summations extend over all the occupied shells. The total, antisymmetric function, Ψ, may be written in a given coupling scheme, using the notation of Innes and Ufford [15], as

$$\Psi = |l_1^{n_1}\gamma_1\Gamma_1, l_2^{n_2}\gamma_2\Gamma_2, l_3^{n_3}\gamma_3\Gamma_3, \ldots, l_g^{n_g}\gamma_g\Gamma_t\rangle,$$

where γ_i denotes the total quantum numbers for the shell l_i, occupied by n_i electrons. Γ_i is obtained by coupling of γ_i with Γ_{i-1}, and so on; Γ_1 is identical to γ_1 and Γ_t represents the quantum numbers for the state under consideration, standing in the present work for τLS, where τ denotes whatever additional quantum numbers are required to completely determine the state.

Using the general coefficients of fractional parentage (CFP) (Chisholm *et al.* [5]), the two types of contributions mentioned above may be expressed as linear combinations of matrix elements over antisymmetrized two-electron states. (In this connection see the work of Armstrong [3, 4], de-Shalit and Talmi [7], Donlan [8], Doyle [10], Fano [11], Innes and Ufford [15] and Shore [23].) One obtains

$$\begin{aligned} E_{\mathrm{ssc,aa}} = {} & \frac{1}{2}\, n_a(n_a - 1) \\ & \cdot \Sigma\, [l_a^2\Gamma; l_1^{n_1}\gamma_1\Gamma_1 \ldots l_a^{n_a-2}\gamma_a''\Gamma_a'' \ldots l_g^{n_g}\gamma_g\Gamma_t'' \,|\,\}\, l_1^{n_1}\gamma_1\Gamma_1 \ldots l_a^{n_a}\gamma_a\Gamma_a \ldots l_g^{n_g}\gamma_g\Gamma_t] \\ & \cdot [l_a^2\bar{\Gamma}; l_1^{n_1}\gamma_1\Gamma_1 \ldots l_a^{n_a-2}\gamma_a''\Gamma_a'' \ldots l_g^{n_g}\gamma_g\Gamma_t'' \,|\,\}\, l_1^{n_1}\gamma_1\Gamma_1 \ldots l_a^{n_a}\gamma_a\Gamma_a \ldots l_g^{n_g}\gamma_g\Gamma_t] \\ & \cdot \langle l_a^2\Gamma | A^{\dagger}\boldsymbol{h}_{\mathrm{ssc}} A | l_a^2\bar{\Gamma}\rangle, \end{aligned}$$

$$\begin{aligned} E_{\mathrm{ssc,ab}} = {} & n_a n_b\, \Sigma\, [l_a l_b \Gamma; l_1^{n_1}\gamma_1\Gamma_1 \ldots l_a^{n_a-1}\gamma_a'\Gamma_a' \ldots l_b^{n_b\;\;1}\gamma_b'\Gamma_b'' \ldots l_g^{n_g}\gamma_g\Gamma_t'' \\ & \cdot |\,\}\, l_1^{n_1}\gamma_1\Gamma_1 \ldots l_a^{n_a}\gamma_a\Gamma_a \ldots l_b^{n_b}\gamma_b\Gamma_b \ldots l_g^{n_g}\gamma_g\Gamma_t] \\ & \cdot [l_a l_b \bar{\Gamma}; l_1^{n_1}\gamma_1\Gamma_1 \ldots l_a^{n_a-1}\gamma_a'\Gamma_a' \ldots l_b^{n_b-1}\gamma_b'\Gamma_b'' \ldots l_g^{n_g}\gamma_g\Gamma_t'' \\ & \cdot |\,\}\, l_1^{n_1}\gamma_1\Gamma_1 \ldots l_a^{n_a}\gamma_a\Gamma_a \ldots l_b^{n_b}\gamma_b\Gamma_b \ldots l_g^{n_g}\gamma_g\Gamma_t] \\ & \cdot \langle l_a l_b \Gamma | A^{\dagger}\boldsymbol{h}_{\mathrm{ssc}} A | l_a l_b \bar{\Gamma}\rangle, \end{aligned}$$

where the summations extend over all the coparent (Γ and $\bar{\Gamma}$) and preparent (Γ_t'') states; the primes and double primes indicate the loss of one and two electrons, respectively, and the expressions in brackets denote the corresponding CFP. $\boldsymbol{h}_{\mathrm{ssc}}$ represents the spin-spin contact interaction operator for two electrons.

The two-electron matrix elements may be written as

$$\begin{aligned}\langle l_a^2\Gamma|A^\dagger h_{\mathrm{ssc}}A|l_a^2\bar{\Gamma}\rangle &= \langle l_a^2 SM_SLM_L|h_{\mathrm{ssc}}|l_a^2\bar{S}\bar{M}_S\bar{L}\bar{M}_L\rangle\\ &= \frac{\alpha^2}{3}\left[\frac{3}{2}-S(S+1)\right]R_2(a,a)\left\{\sum_k(2k+1)f_k(l_al_aL)\right\}\\ &\quad\cdot\delta(S,\bar{S})\,\delta(M_S,\bar{M}_S)\,\delta(L,\bar{L})\,\delta(M_L,\bar{M}_L),\end{aligned}$$

$$\begin{aligned}\langle l_al_b\Gamma|A^\dagger h_{\mathrm{ssc}}A|l_al_b\bar{\Gamma}\rangle &= \langle l_al_bSM_SLM_L|h_{\mathrm{ssc}}|l_al_b\bar{S}\bar{M}_S\bar{L}\bar{M}_L\rangle\\ &\quad+(-1)^{l_a+l_b+S-L}\langle l_bl_aSM_SLM_L|h_{\mathrm{ssc}}|l_al_b\bar{S}\bar{M}_S\bar{L}\bar{M}_L\rangle\\ &= \frac{\alpha^2}{3}\left[\frac{3}{2}-S(S+1)\right]R_2(a,b)\\ &\quad\cdot\left\{\sum_k(2k+1)\left[f_k(l_al_bL)+(-1)^S g_k(l_al_bL)\right]\right\}\\ &\quad\cdot\delta(S,\bar{S})\,\delta(M_S,\bar{M}_S)\,\delta(L,\bar{L})\,\delta(M_L,\bar{M}_L),\end{aligned}$$

with

$$f_k(l_al_bL)=(-1)^{L+l_a+l_b}\begin{Bmatrix}L & l_b & l_a\\ k & l_a & l_b\end{Bmatrix}\langle l_a\|C^{(k)}\|l_a\rangle\,\langle l_b\|C^{(k)}\|l_b\rangle,$$

$$g_k(l_al_bL)=(-1)^{l_a+l_b+k}\begin{Bmatrix}L & l_a & l_b\\ k & l_a & l_b\end{Bmatrix}\langle l_a\|C^{(k)}\|l_b\rangle^2,$$

in terms of $6-j$ symbols and double-barred matrix elements[1] of the spherical harmonics tensor operators; f_k and g_k represent the direct and exchange contributions, respectively. The radial integrals, $R_2(a,b)$, are defined by

$$R_2(a,b)=\int_0^\infty P_a^2(r)\,P_b^2(r)r^{-2}dr,$$

with the radial function, $P_a(r)$, being normalized according to

$$\int_0^\infty P_a^2(r)dr=1.$$

The values of the CFP have been determined by Chisholm et al. [5] for configurations containing up to three shells of non-equivalent electrons. For more complex configurations the generalized CFP may be calculated from the single- and/or two-particle CFP, tabulated by Nielson and Koster [18], Karaziya *et al.* [16], and Donlan [9].

The above expressions[2] may be simplified in the case of electronic configurations with only one open shell. The formulas for the intra-shell contribution reduce

---

[1] For the definition of the double-barred matrix elements, see the work (pp. 288–294) of Shore and Menzel [24].

[2] It should be mentioned that a different formulation has been given by Rudzikas and co-workers [19, 20].

then to those given by Sessler and Foley [22], Fraga and Thorhallsson [13], and Armstrong [2]. The inter-shell contribution, when at least one of the two shells is fully occupied, becomes (see de-Shalit and Talmi [7])

$$E_{\mathrm{ssc},ab} = \frac{1}{4} n_a n_b \Sigma \left[(2S+1)(2\bar{S}+1)(2L+1)(2\bar{L}+1)\right]^{\frac{1}{2}}$$

$$\cdot \left[(2l_a+1)(2l_b+1)\right]^{-1} \langle l_a l_b S L | A^{+} h_{\mathrm{ssc}} A | l_a l_b \bar{S} \bar{L} \rangle$$

where the summation extends over L, $\bar{L}$, S, and $\bar{S}$, and $\bar{S}$. This expression can be rewritten as

$$E_{\mathrm{ssc},ab} = \frac{\alpha^2}{3} n_a n_b R_2(a,b) \sum_k (2k+1) \left[f_k(l_a l_b) + g_k(l_a l_b)\right]$$

with

$$f_k(l_a l_b) = \left[4(2l_a+1)(2l_b+1)\right]^{-1} \langle l_a \| C^{(k)} \| l_a \rangle \langle l_b \| C^{(k)} \| l_b \rangle$$

$$\cdot \sum_L (-1)^{l_a+l_b+L} (2L+1) \begin{Bmatrix} L & l_b & l_a \\ k & l_a & l_b \end{Bmatrix}$$

$$\cdot \sum_S (2S+1) \left[\frac{3}{2} - S(S+1)\right],$$

$$g_k(l_a l_b) = (-1)^{l_a+l_b+k} \left[4(2l_a+1)(2l_b+1)\right]^{-1} \langle l_a \| C^{(k)} \| l_b \rangle^2$$

$$\cdot \sum_L (-1)^{2L} (2L+1) \begin{Bmatrix} L & l_a & l_b \\ k & l_a & l_b \end{Bmatrix} \sum_S (-1)^S (2S+1) \left[\frac{3}{2} - S(S+1)\right].$$

Taking into account that these expressions reduce to

$$f_k(l_a l_b) = 0,$$

$$g_k(l_a l_b) = \frac{3}{4} (-1)^{l_a+l_b+k} \left[(2l_a+1)(2l_b+1)\right]^{-1} \langle l_a \| C^{(k)} \| l_b \rangle^2,$$

one finally obtains, after carrying out the k-summation (see, e.g., Shore and Menzel [24]),

$$E_{\mathrm{ssc},ab} = \frac{\alpha^2}{4} n_a n_b R_2(a,b).$$

Results and Discussion

The radial integrals, R_2, have been evaluated from the analytical Hartree-Fock functions of Clementi [6] and Malli [17]. Table 1 collects the values of the total electron spin-spin contact interaction for the positive ions, neutral systems, and negative ions for all the atoms from He to Kr; the relative weights of the intra- and inter-shell contributions are exemplified in Table 2 for Br.

This interaction, as expected, is not negligible; a value of about 1 a.u. is predicted for Kr. It must be concluded that, when considering the absolute magnitude of the relativistic corrections, this interaction should be included.

The difference observed in the values for the various states arising from a given configuration is very small. On the other hand, however, the energies of other excited states relative to the groundstate may be affected considerably by consideration of this interaction, depending on what shell the electron(s) has (have) been excited from.

Table 1. Total electron spin-spin contact interaction (in cm^{-1}) for positive ions, neutral atoms and negative ions

Configuration^a	State	Positive ions		Neutral atoms		Negative ions	
		System	E_{ssc}	System	E_{ssc}	System	E_{ssc}
$1s^2$	^1S	Li	57	He	14		
$2s^1$	^2S	Be	151	Li	58		
$2s^2$	^1S	B	325	Be	154	Li	58
$2p^1$	^2P	C	587	B	322		
$2p^2$	^3P	N	965	C	582	B	320
	^1D		970		584		321
	^1S		976		587		321
$2p^3$	^4S	O	1484	N	959	C	579
	^2D		1495		965		581
	^2P		1502		968		582
$2p^4$	^3P	F	2196	O	1491	N	961
	^1D		2206		1496		963
	^1S		2221		1504		966
$2p^5$	^2P	Ne	3120	F	2201	O	1491
$2p^6$	^1S	Na	4292	Ne	3124	F	2199
$3s^1$	^2S	Mg	5745	Na	4295		
$3s^2$	^1S	Al	7515	Mg	5750	Na	4296
$3p^1$	^2P	Si	9617	Al	7511		
$3p^2$	^3P	P	12094	Si	9612	Al	7509
	^1D		12096		9613		7509
	^1S		12096		9613		7510
$3p^3$	^4S	S	14981	P	12089	Si	9609
	^2D		14983		12090		9611
	^2P		14983		12091		9611
$3p^4$	^3P	Cl	18316	S	14977	P	12087
	^1D		18317		14978		12088
	^1S		18320		14979		12088
$3p^5$	^2P	A	22136	Cl	18313	S	14975
$3p^6$	^1S	K	26476	A	22133	Cl	18310
$4s^1$	^2S	Ca	31384	K	26482		
$4s^2$	^1S			Ca	31391	K	26481
$3d^1$	^2D			Sc	36831		
$3d^2$	^3F	Sc	36775	Ti	42873	Sc	36794
$3d^3$	^4F	Ti	42808	V	49548	Ti	42825
$3d^4$	^5D	V	49478	Cr	56896	V	49496
$3d^5$	^6S	Cr	56812	Mn	64947	Cr	56863
$3d^6$	^5D	Mn	64886	Fe	73792	Mn	64909
$3d^7$	^4F	Fe	73718	Co	83428	Fe	73743
$3d^8$	^3F	Co	83342	Ni	93881	Co	83375
$3d^9$	^2D	Ni	93782	Cu	105214		

Table 1 (continued)

Configuration[a]	State	Positive ions		Neutral atoms		Negative ions	
		System	E_{ssc}	System	E_{ssc}	System	E_{ssc}
$3d^{10}$	^1S	Cu	105105				
$4s^1$	^2S	Zn	117419	Cu	105134	Ni	93947
$4s^2$	^1S	Ga	130741	Zn	117451	Cu	105136
$4p^1$	^2P	Ge	145001	Ga	130739		
$4p^2$	^3P	As	160405	Ge	145040	Ga	130732
	^1D		160408		145042		130733
	^1S		160409				
$4p^3$	^4S	Se	176885	As	160404	Ge	145036
	^2D		176881		160402		145034
	^2P		176880		160405		145036
$4p^4$	^3P	Br	194503	Se	176882	As	160400
	^1D		194504		176879		160398
	^1S		194507		176884		160397
$4p^5$	^2P	Kr	213321	Br	194507	Se	176873
$4p^6$	^1S			Kr	213316	Br	194497

[a] The positive ions of the transition elements (from Sc through Cu) have configurations $4s^0 3d^n$.

Table 2. Inter- and intra-shell contributions (in cm^{-1}) to the electron spin-spin contact interaction in Br

	$1s$	$2s$	$3s$	$4s$	$2p$	$3p$	$4p$	$3d$
$1s$	119993							
$2s$	18926	1634						
$3s$	2925	422	63					
$4s$	274	39	10	2				
$2p$	16813	6217	763	70	14260			
$3p$	2509	540	270	20	2958	461		
$4p$	138	29	11	5	158	41	5	
$3d$	68	700	337	26	1821	997	44	959

References

1. Armstrong, Jr., L.: J. math. Physics **7**, 1891 (1966).
2. - Physic. Rev **170**, 122 (1968).
3. -- Physic. Rev. **172**, 12 (1968).
4. -- Physic. Rev. **172**, 18 (1968).
5. Chisholm, C. D. H., Dalgarno, A., Innes, F. R.: Advanc. atom. molec. Physics **5**, 297 (1969).
6. Clementi, E.: Tables of atomic functions. San Jose: IBM 1965.
7. De-Shalit, A., Talmi, I.: Nuclear shell theory. New York: Academic Press 1963.
8. Donlan, V. L.: J. chem. Physics **52**, 3431 (1970).
9. -- Tables of two-particle fractional parentage coefficients for the p^n, d^n and f^n configurations. Technical Report AFML-TR-70-249, Air Force Material Laboratory, Wright-Patterson Air Force Base, Dayton, Ohio, 1970.
10. Doyle, H. T.: Advanc. atom. molec. Physics **5**, 337 (1969).
11. Fano, U.: Physic. Rev. **140**, A 67 (1965).
12. Fontana, P. R., Meath, W. J.: J. math. Physics **9**, 1357 (1968).
13. Fraga, S., Thorhallsson, J.: Physic. Rev. **178**, 70 (1969).
14. — — Fisk, C.: Can. J. Physics **47**, 1415 (1969).

15. Innes, F. R., Ufford, C. W.: Physic. Rev. **111**, 194 (1958).
16. Karaziya, R. I., Vizbaraite, Ya. I., Rudzikas, Z. B., Yutsis, A. P.: Tables for calculating matrix elements of operators for atomic quantities. Computation Center, The Academy of Sciences, Moscow, USSR., 1967.
17. Malli, G.: Canad. J. Physics **44**, 3121 (1966).
18. Nielson, C. W., Koster, G. F.: Spectroscopic coefficients for the p^n, d^n and f^n configurations. Cambridge: MIT Press 1963.
19. Rudzikas, Z.: Liet. Fiz. Rinkinys **9**, 707 (1969).
20. — Karaziya, R. I.: Liet. Fiz. Rinkinys **10**, 13 (1970).
21. Saxena, K. M. S., Lo, B. W. N., Fraga, S.: Canad. J. Physics **49**, 2031 (1971).
22. Sessler, A. M., Foley, H. M.: Physic. Rev. **92**, 1321 (1953).
23. Shore, B. W.: Physic. Rev. **139**, A 1042 (1965).
24. - Menzel, D. H.: Prinziples of atomic spectra. New York: John Wiley & Sons 1968.

Dr. S. Fraga
Division of Theoretical Chemistry
Department of Chemistry
University of Alberta
Edmonton 7, Alberta, Canada

Theoret. chim. Acta (Berl.) 24, 78–88 (1972)
© by Springer-Verlag 1972

Electronic Structures and MCD Spectra of Trigonal CR(III)S_6 Systems[*]

P. J. HAUSER[**], A. F. SCHREINER, J. D. GUNTER, W. J. MITCHELL
and M. K. DEARMOND

Department of Chemistry, North Carolina State University, Raleigh, North Carolina 27607

Received June 29, 1971

MCD, electronic absorption, external heavy atom, and crystal field data are presented for the low energy region (^2E_g, $^2T_{1g}$, $^4T_{2g}$) and high energy region ($^2T_{2g}$, $^4T_{1g}$) of Cr(dtp)$_3$, Cr(dtc)$_3$, and Cr(exan)$_3$. At low energy, MCD intensities of $^2E(^2E_g)$ and $^2E(^2T_{1g})$ are as large or larger than "$^4T_{2g}$", and the MCD technique is advantageous over electronic absorption in this respect. The MCD positions of "^2E_g" and "$^2T_{1g}$" are nearly the same for these molecules (~ 13 kK and ~ 13.6 kK) · $^4T_{2g}$ of this region appears trigonally split ($\sim 500\ \text{cm}^{-1}$) in the MCD of dtp but to a smaller extent than in the electronic crystal spectrum of Lebedda and Palmer ($\sim 600\ \text{cm}^{-1}$). MCD did not resolve such components for exan and dtc. The higher energy region includes $^2T_{2g}$ and $^4T_{1g}$, and the combined MCD and electronic absorption *data* of the three compounds taken together lead us to conclude the ordering $^2A_1(^2T_{2g}) < {^2E}(^2T_{2g}) < {^4E}(^4T_{1g})$. The potentially useful external heavy atom affect on the solution-observed electronic ^2E and ^4E bands of Cr(dtp)$_3$ did not shed additional light on this order of E states. Finally, it is concluded that the order of $^4T_{1g}$ and $^2T_{2g}$ cannot be decided from O_h crystal field *calculations* because of experimental uncertainties about choosing centers of gravity. In addition, "$^4T_{1g}$" and "$^2T_{2g}$" are close together so that ordering $^2E < {^4E}$ does not guarantee $^2T_{2g} < {^4T_{1g}}$. However, it can be concluded that the ratio $C/B \simeq 4$ is not correct, whereas the larger $7 < (C/B) < 8$ is consistent with the data of all three molecules because of small B parameters (~ 0.4). Locating $O \rightarrow O$ transitions may somewhat decrease C/B and Dq.

In der vorliegenden Arbeit werden folgende Meßergebnisse mitgeteilt; MCD, elektronische Absorption, Einfluß eines äußeren schweren Atoms sowie Kristallfelddaten für den Bereich niedriger Energie (^2E_g, $^2T_{1g}$, $^4T_{2g}$) und den Bereich hoher Energie ($^2T_{2g}$, $^4T_{1g}$) von Cr(dtp)$_3$, Cr(dtc)$_3$ und Cr(exan). Bei niedriger Energie sind die MCD-Intensitäten von $^2E(^2E_g)$ und $^2E(^2T_{1g})$ genau so groß, oder größer als „$^4T_{2g}$", und die MCD-Technik bietet Vorteile gegenüber der elektronischen Absorptionsmethode. Die MCD-Werte von „^2E_g" und „$^2T_{1g}$" sind für die genannten Moleküle etwa gleich (~ 13 kK und $\sim 13{,}6$ kK). $^4T_{2g}$ dieses Gebietes erscheint trigonal aufgespalten ($\sim 500\ \text{cm}^{-1}$) bei MCD von dtp, aber in einem geringeren Maß als im elektronischen Kristallspektrum von Lebedda und Palmer ($\sim 600\ \text{cm}^{-1}$) MCD löste solche Komponenten bei exan und dtc nicht auf. Der Bereich höherer Energie enthält $^2T_{2g}$ und $^4T_{1g}$, und aus der Kombination von Daten der MCD-Methode sowie der elektronischen Absorption schlossen wir auf die Anordnung $^2A_{1g}(^2T_{2g}) < {^2E}(^2T_{2g}) < {^4E}(^4T_{1g})$. Der möglicherweise nützliche Effekt eines äußeren schweren Atoms auf die in Lösung beobachteten elektronischen ^2E- und ^4E-Banden von Cr(dtp)$_3$ brachte bezüglich dieser Anordnung der E-Zustände nichts Neues. Weiterhin wird gefolgert, daß die Ordnung von $^4T_{1g}$ und $^2T_{2g}$ nicht aus O_h-Kristallfeldberechnungen entschieden werden kann, da experimentelle Unsicherheiten bezüglich der Wahl von Schwerpunkten bestehen. Außerdem liegen „$^4T_{1g}$" und „$^2T_{2g}$" nahe zusammen, sodaß aus der Anordnung $^2E < {^4E}$ nicht notwendig $^2T_{2g} < {^4T_{1g}}$ folgt. Es kann jedoch gefolgert werden, daß das Verhältnis $C/B \cong 4$ nicht korrekt ist, während $7 < (C/B) < 8$ konsistent mit den Daten aller drei Moleküle ist, da die B-parameter klein sind ($\sim 0{,}4$). Die Vokalisierung der $O \rightarrow O$-Übergänge könnten C/B und Dq etwas erniedrigen.

---

[*] Presented in part at the 161st American Chemical Society National Meeting, Los Angeles, California, March-April, 1971.

[**] NDEA Pre-Doctoral Fellow.

Introduction

The electronic spectroscopic work of Kida and Yoneda [1] and Jorgensen [2] is among the early definitive studies of transition metal sulfur chelates [3]. Jorgensen's papers have been most responsible for initiating more recent studies of this area of chemistry [4–8, 14]. As a coordinating atom within ligands, sulfur has the interesting spectral property of exhibiting a large nephelauxetic effect, i.e., perhaps in the vicinity of iodine, even though it is an element of the third period, whereas its position in the spectrochemical series is not at all in close proximity to the iodide ion but between Cl^- and H_2O [2]. Thus far magnetic circular dichroism (MCD) studies of trigonal chromium(III) chelate compounds have been restricted to CrO_6 and CrN_6 chelate systems such as $Cr(ox)_3^{3-}$ and $Cren_3^{3+}$ [9]. This communication concerns itself with the MCD spectra of the chromium(III) sulfur chelates of diethyldithiophosphate (dtp^-), diethyldithiocarbamate (dtc^-), and ethylxanthate ($exan^-$), i.e., $Cr(dtp)_3$, $Cr(dtc)_3$, and $Cr(exan)_3$[1]. It was of interest to first of all determine effects on the MCD dispersions of coordinated atoms known to have a higher one-electron spin-orbit coupling constant, especially the effect on the intensities of spin forbidden transitions. Furthermore, the intramolecular ring size is now four, 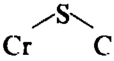 and 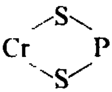, rather than five as in the trigonal oxalato and ethylenediamine molecule-ions. This also constitutes the first report of MCD measurements on CrS_6 systems. Finally, the conclusions of this study also relate to the order of excited state assignments for these compounds on the basis of these MCD data, octahedral crystal field calculations, external heavy atom effect observations, and an earlier report [7a] of crystal spectra of one of the compounds, $Cr(dtp)_3$.

Experimental

The compounds were prepared by methods described in the literature [10]. Spectra were obtained in methylenechloride solutions of the complexes. The heavy atom solvents ethylbromide and ethyliodide, impure due to the presence of halogens, were purified by passing each through alumina columns.

The magnetic field for MCD measurements were generated using a Nb/Ti superconducting coil wound by Westinghouse and built into a 300° K 80° K 4° K dewar system. Fields of ca. 42 kGauss were employed and were measured to within 1% accuracy using a rotating coil gaussmeter. The latter was calibrated against a more accurate Magnion G-502, and the magnetic field and light directions were made to parallel each other. The circularly dichroic light of the Durrum JASCO model ORD/UV/CD-5 was used, and the xenon source was found not to require shielding in fields used here. However, the end-on photomultiplier tube was removed, shielded, and housed outside the instrument. The instrument is still usable for absorption optical measurements, since the chopper drive cable was lengthened and repositioned by us. The instrument MCD calibration is checked against the spectrum of $K_3[Fe(CN)_6] \cdot 3\,H_2O$ [11]. Wavelength calibrations are made by comparing JASCO and Cary 14 optical absorption spectra of aqueous solutions of the rare earth salts $Nd(NO_3)_3 \cdot 5\,H_2O$ and $UO_2(NO_3)_2 \cdot 6\,H_2O$, and of silicate glasses of holmium oxide and neodymium oxide. The MCD band maxima recorded in Tables 1–3 are such corrected values, but the spectra of Fig. 2 are direct tracings of the JASCO spectra.

---

[1] $dtp^- = [S_2P(OC_2H_5)_2]^-$; $dtc^- = [S_2CN(C_2H_5)_2]^-$; $exan^- = [S_2COC_2H_5]^-$.

Calculations were done on an IBM 360/75 system.

Results and Discussion

Octahedral (O_h) and trigonal (D_3) $d-d$ state diagrams for a d^3 metal ion are shown in Fig. 1. The ordering of several excited states was decided on the basis of MCD, external heavy atom effect, and crystal field data to be discussed here, and in part it is based on polarized crystal data [7] of the two optically intense regions of one of the complexes, $Cr(dtp)_3$. The solution MCD and electronic absorption spectra in the $d-d$ region of the representative sulfur chelate $Cr(dtp)_3$ are shown in Fig. 2, and higher energy $d-d$ bands in the ${}^4T_{1g}$, ${}^2T_{2g}$ region are shown in Fig. 3. The MCD spectra of the $Cr(S_2)_3$ will be considered next in two parts, viz., the low energy portion containing components a, b, c, and d, and the higher energy portion containing extrema e, f, and g (Figs. 2 and 3 and Tables 1–3).

The lower energy region of the MCD spectra will arise from transitions to the four D_3 states ${}^2E({}^2E_g)$, ${}^2E({}^2T_{1g})$, ${}^4E({}^4T_{2g})$ and ${}^4A_1({}^4T_{2g})$ (Fig. 1) according to spatial MCD and formal electric dipole selection rules. Since the spin doublets arise from "t_{2g}^3" intraconfigurational transitions, they are expected to be narrow and of very low dipole strengths. Consequently, ${}^2E({}^2E_g)$ and ${}^2E({}^2T_{1g})$ are only barely discernible in electronic absorption spectra of $Cr(dtp)_3$ [7, 8], $Cr(dtc)_3$ and $Cr(exan)_3$ even at low temperature [8]. Also, this problem arises in large part because these ${}^2\Gamma$ are located under the relatively very intense ${}^4T_{2g}$ band. Quite on the contrary, the two doublets are very clearly seen in the MCD spectra

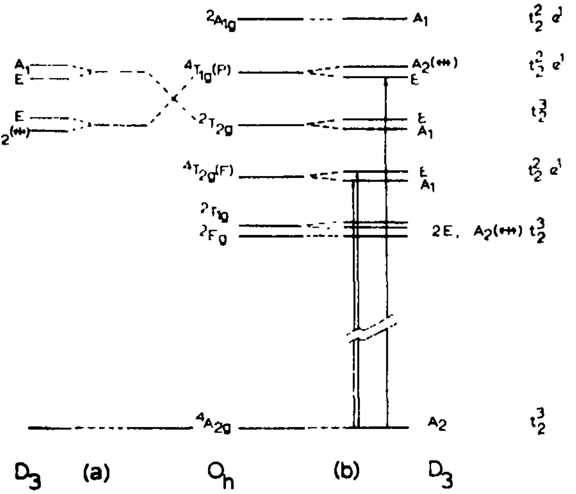

Fig. 1. Several O_h and D_3 states of Cr(III) $d-d$ transitions (see text)

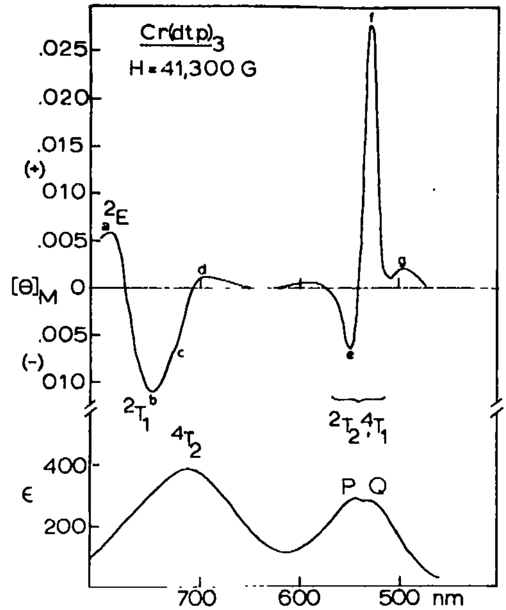

Fig. 2. MCD and electronic absorption spectra of $Cr(dtp)_3$ in CH_2Cl_2 solution. $[\theta]_M$ = molar ellipticity/Gauss = deg-cm^2 – dmole^{-1} – Gauss^{-1}, or deg-dl-dm^{-1} – mole^{-1} – Gauss^{-1}

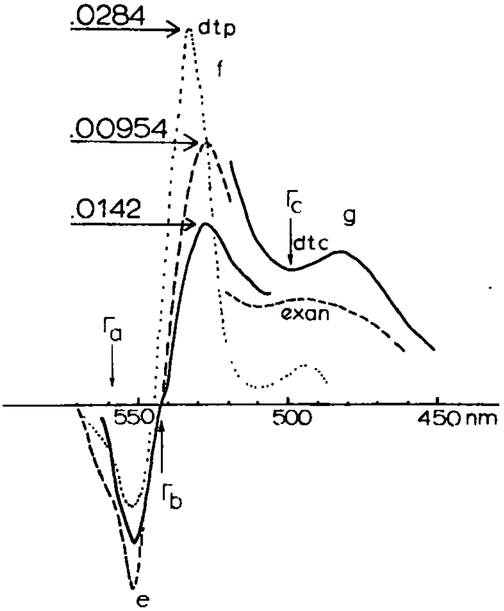

Fig. 3. MCD spectra of $Cr(dtp)_3$, $Cr(dtc)_3$ and $Cr(exan)_3$ (in CH_2Cl_2) between 600 nm and 450 nm (Molar ellipticity values per Gauss of several band maxima appear above arrows)

Table 1. Band extrema of $Cr(dtp)_3$[a]

Bands	O_h	D_3	MCD[b]	Electronic			Crystal field predictions				
				Present work[c]	Jorgensen[d]	Lebedda[f] and Palmer		I[e]	II[f]	III[g]	IV[h]
g	$^4T_{1g}$; $^2T_{2g}$	$(^4A_2)$, ^4E; ^2E, $^2A_1$	20.38				$^2A_{1g}$	21.0	25.8	25.83	24.84
f			19.05	19.2	18.8 ("$^4T_{1g}$")	19.25 ($^2T_{2g}$)	$^2T_{2g}$	12.83	19.25	19.62	19.39
e			18.45	18.69	18.6 19.1 ("$^2T_{2g}$")	18.75 ($^4T_{1g}$)	$^4T_{1g}$	18.77	18.7	18.72	19.67
			(~ 17)			17					
d	$^4T_{2g}$	^4E	14.43	14.3	14.3 ("$^4T_{2g}$")	14.5	$^4T_{2g}$	14.3	14.5	14.25	13.8
c		$^4A_1$	13.95			13.86					
b	$^2T_{1g}$	^2E	13.59		13.6	13.6	$^2T_{1g}$	8.58	13.1	13.44	13.57
a	^2E_g	^2E	13.04		13.1	13.1	^2E_g	8.23	12.8	13.14	13.04
							$Dq =$	1.43	1.45	1.425	1.38
							$B =$	0.42	0.389	0.42	0.60
							$C =$	1.68	3.26	3.30	2.88
							$C/B =$	4.0	8.38	7.86	4.8

---

[a] Positions and crystal field parameters in units of kK.

[b] Recorded on JASCO but positions corrected as described in experimental section.

[c] Cary 14.

[d] Ref. [4].

[e] Present calculation using Jorgensen's parameter [4].

[f] Ref. [7b].

[g-h] This work (see text).

Bands	O_h	D_3	MCD^b	Electronic		Crystal field predictions					
				Present work^c	Jorgensen^d		I^e	II^f	III^g	IV^h	V^i
g	$^4T_{1g}$; $^2T_{2g}$	$(^4A_2)$, ^4E; ^2E, $^2A_1$	21.01			$^2A_{1g}$	22.38	27.20	27.40	27.60	26.80
f			19.21	20.2	20.4 ("$^4T_{1g}$")	$^2T_{2g}$	13.22	20.03	20.06	20.09	18.87
e			18.45	(18.55)		$^4T_{1g}$	20.11	19.73	19.94	20.14	20.25
			18.18	(18.2)							
c, d	$^4T_{2g}$	^4E, $^4A_1$	15.50	15.6	15.5 ("$^4T_{2g}$")	$^4T_{2g}$	15.50	15.40	15.60	15.80	15.90
b	$^2T_{1g}$	^2E	13.61			$^2T_{1g}$	8.80	13.59	13.60	13.60	12.70
a	^2E_g	^2E	12.93			^2E_g	8.44	13.33	13.33	13.34	12.43
						Dq =	1.55	1.54	1.56	1.58	1.59
						B =	0.430	0.400	0.400	0.400	0.40
						C =	1.720	3.400	3.400	3.400	3.10
						C/B =	4.00	8.500	8.500	8.500	7.75

[a–e] See footnotes of Table 1. [f–i] This work (see text).

Table 3. Band extrema of Cr(exan)$_3$[a]

Bands	O_h	D_3	MCD^b	Electronic		Crystal field predictions					
				Present work^c	Jorgensen^d		I^e	II^f	III^g	IV^h	V^i
g	$^4T_{1g}$; $^2T_{2g}$	$(^4A_2)$, ^4E; ^2E, $^2A_1$	20.6–21.0			$^2A_{1g}$	22.24	26.51	27.40	27.84	26.80
f			19.25	20.3	20.26 ("$^4T_{1g}$")	$^2T_{2g}$	12.16	18.48	19.69	20.13	18.87
e			18.45	(18.65)		$^4T_{1g}$	20.26	20.69	20.25	19.86	20.25
			(18.03)	(18.3)							
c, d	$^4T_{2g}$		15.82	16.1	16.0 ("$^4T_{2g}$")	$^4T_{2g}$	16.0	16.0	15.9	15.9	15.90
b	$^2T_{1g}$		13.83			$^2T_{1g}$	8.0	12.45	13.3	13.57	12.70
a	^2E_g		12.95			^2E_g	7.7	12.14	13.04	13.36	12.49
						Dq =	1.6	1.6	1.59	1.59	1.59
						B =	0.390	0.436	0.40	0.36	0.40
						C =	1.56	2.921	3.30	3.50	3.10
						C/B =	4.00	6.70	8.25	9.7	7.75

[a–e] See footnotes of Table 1. [f] This work, using Witzke's [5] parameters. [g–i] This work (see text).

of all three compounds[2] as they are of relatively large intensity, e.g., bands *a* and *b* of Fig. 2 are ${}^2E({}^2E_g)$ and ${}^2E({}^2T_{1g})$ of Cr(dtp)$_3$. The separation of their band maxima is about 550 cm^{-1}. The locations of these band maxima and those reported by others [4, 7b] are shown in Table 1 and are in good agreement.

The two trigonal components of ${}^4T_{2g}$ are also apparent in the Cr(dtp)$_3$ MCD spectrum as bands *c* and *d* of Fig. 2, and the higher energy component of ${}^4T_{2g}$ is known to have E symmetry [7] (Fig. 1). While the MCD band locations do not infer that ${}^4E({}^4T_{2g})$ has a dominating A-term, a small A contribution compared to the intensity contribution from $(B + C/kT)$ cannot be ruled out. The trigonal splitting of ${}^4T_{2g}$ (MCD bands at 13.95 kK and 14.43 kK) derived from these data is ca. 500 cm^{-1} compared to 600 cm^{-1} obtained from the polarized absorption data [7]. The solution electronic absorption spectrum does not show this trigonal splitting [2, 4]. The ability to locate these *spin-forbidden* transitions is the major advantage of the MCD spectrum over all previously reported electronic absorption results [2, 7a, 8]. This and other reported results for ${}^4T_{2g}$ of Cr(dtp)$_3$ are also given in Table 1, i.e., Jorgensen [2, 4] observed only one component ("${}^4T_{2g}$"), but Lebedda and Palmer [7] observed components at 13.86 kK and 14.50 kK.

The comparison of band positions in the low energy portion of MCD spectra for Cr(dtp)$_3$, Cr(dtc)$_3$, and Cr(exan)$_3$ are summarized in Tables 1–3. One important feature to be noted is that the positions of MCD band maxima *a* and *b* remain almost constant for the three compounds. This behavior is indeed expected of ${}^2E({}^2E_g)$ and ${}^2E({}^2T_{1g})$ to good approximation [12]. On the other hand the MCD position of "${}^4T_{2g}$" showed significant dependence on the ligand, viz., transition energies to ${}^4T_{2g}$ increased in the order Cr(exan)$_3$ > Cr(dtc)$_3$ > Cr(dtp)$_3$, and the MCD based order follows the previously found [4] spectrochemical series, $\ldots \mathrm{Cl}^- < \mathrm{dtp}^- < \mathrm{F}^- < \mathrm{dtc}^- < \mathrm{exan}^- < \mathrm{H_2O} \ldots$. The locations of ${}^2E_g$ and ${}^2T_{1g}$ were not reported for Cr(dtc)$_3$ and Cr(exan)$_3$ by Jorgensen [4]. On the other hand, he reports "${}^4T_{2g}$" as a single component for dtc and exan. These electronic band positions agree well with our own, and ${}^4T_{2g}$ also appears unsplit in the MCD of these two compounds. However, the intraconfigurational spin doublets are nicely located again and are given in Tables 2 and 3. Crystal field predictions (*vide infra*) agree with the above order ${}^2E_g < {}^2T_{1g} < {}^4T_{2g}$.

We now turn to the higher energy region of each MCD spectrum which includes ${}^2E({}^2T_{2g})$, ${}^2A_1({}^2T_{2g})$ and ${}^4E({}^4T_{1g})$, and perhaps ${}^2A_1({}^2A_{1g})$ (Fig. 1), using D_3 spatial selection rules again. This region is not as simple to analyze due to the close proximity of ${}^4T_{1g}$ and ${}^2T_{2g}$ in the region 18 kK – 20 kK, i.e., several pieces of data support the assignment ${}^2T_{2g} < {}^4T_{1g}$, whereas other data seem to indicate ${}^2T_{2g} > {}^4T_{1g}$. Cr(dtp)$_3$ data will be considered by itself and with those of exan and dtc in an attempt to resolve the ambiguity.

First, bands P and Q of Cr(dtp)$_3$ are known to be E states [7]. However, it has not as yet been unambiguously ascertained [7b] whether band P (or Q) is ${}^2E({}^2T_2)$ or ${}^4E({}^4T_1)$. For example, regardless of whether *octahedral* crystal field calculations (Tables 1–3) predict ${}^2T_{2g} > {}^4T_{1g}$ or ${}^2T_{2g} < {}^4T_{1g}$, either D_3 order ${}^2E < {}^4E$ or ${}^2E > {}^4E$ is possible (Fig. 4), especially in the light of Cr(dtp)$_3$ data

---

[2] It was recognized by McCaffery *et al.* [9] that ${}^4A_2 \rightarrow {}^2\Gamma$ positions are advantageously located for Cr(III)L$_6$ (L = N, O) chromophores by means of MCD.

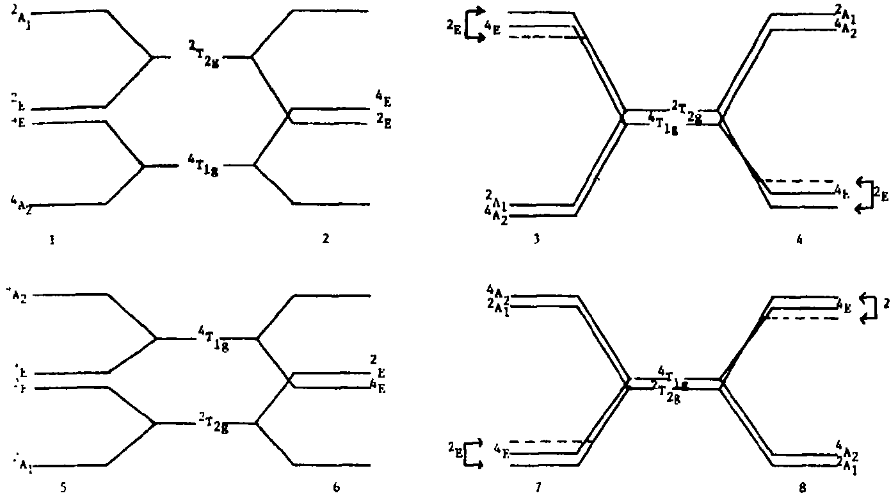

Fig. 4. Possible orders of D_3 components for $^4T_{1g} > {}^2T_{2g}$ and $^4T_{1g} < {}^2T_{2g}$

above, because the bands are close to each other. The following information supports $^2E < {}^4E$. First, we note that a transition to $^2E(^2T_{2g})$ is t_2^3 intraconfigurational and will essentially be independent of ligand field strength within the strong field approximation of the energy matrix constructed with strong field functions [12]. However $^4E(T_1)$ will be dependent. We discuss dtc first.

In Fig. 3 we indicate by arrows (Γ_a, Γ_b, Γ_c) the positions of electronic absorption band maxima of Cr(dtc)$_3$, which can be observed at 80° K in glassy media as well as in the 4° K unpolarized crystal spectrum. Since Γ_a and Γ_b have extremely small dipole strengths with $\varepsilon \leqq 1$ they correspond to $^2A_1$ and ^2E of $^2T_2$. Thus, dispersion e–f is an apparent A-term. However, since we estimate that A/D is an order of magnitude too large for e–f to be a true A-term, it must be assigned to the sum of two $(B + C/kT)$ bands having opposite signs (probably Kramer's $2\bar{A}$ and $\bar{E}_a$ of ^2E). Γ_c is the location of $^4E(T_1)$, and its MCD activity is region g of Figs. 2 and 3.

We conclude that the state ordering in the high energy region of Cr(dtc)$_3$ is $^2A_1 < {}^2E < {}^4E$, and probably $^2T_2 < {}^4T_1$, which is the order of Fig. 1(b). Our reasons, then, for this order are as follows. First, the content of the above paragraph based on intensities. Second, the two $^2T_2$ components (Γ_a, Γ_b) are unshifted in exan and dtc, as expected of t_2^3 spin doublets. Also, Γ_b of dtp is also unshifted, whereas Γ_a is only slightly so. Third, MCD band g corresponding to ^4E in these compounds shifts qualitatively in the direction expected on the basis of the spectrochemical series [4] of the ligands. Fourth, prominent MCD extrema e, f, and g are extremely similar in the three compounds. (By the way, the lower energy 18.2–18.3 kK components of exan and dtc appear as red MCD shoulders on the more intense band e.) These data taken together lead us to conclude $^2T_{2g} < {}^4T_{1g}$ for each of the three molecules is probably the correct order. Certainly one knows $^2A_1, {}^2E < {}^4E$, or $^2T_{2g} < {}^4E$, whereas the location of $^4A_2(T_1)$ is unknown.

The alternative order of these two bands (Γ_b and Γ_c) is $^4E(^4T_{1g}) < {}^2E(^2T_{2g})$. However, the trigonal splitting of $^2T_{2g}$ (energy of Γ_c minus energies of red shoulders on band *e*) would take on unprecedented, exceedingly high values, i.e., $> 2000\,\mathrm{cm}^{-1}$. Furthermore, this would be inconsistent with observed electronic absorption intensities.

The external heavy-atom solvent effect [13] of ethylbromide and ethyliodide on the electronic absorption intensity and structure of the $^4T_{1g}$, $^2T_{2g}$ region of Cr(dtp)$_3$ was measured, since the two bands of the compound are clearly resolved in solution. It was considered possible that the experiment might give additional support to our assignment $^2E(^2T_{2g}) < {}^4E(^4T_{1g})$. The measurements are summarized in Table 4. It can be seen that; while the intensity of this $^4T_{1g}$, $^2T_{2g}$ region increases in the order $C_2H_5I > C_2H_5Br$, both bands increase by about an equal amount. Furthermore, the $^4T_{2g}$ region was effected in the same way. This experiment is not considered to be definitive for our purposes, therefore.

Table 4 External heavy atom effect on molar extinction coefficients of Cr(dtp)$_3$

Solvant	$^4T_{2g}$ $\varepsilon_{703\,\mathrm{nm}}$	($^2T_{2g}$, $^4T_{1g}$) $\varepsilon_{535\,\mathrm{nm}}$	$\varepsilon_{525\,\mathrm{nm}}$	$\varepsilon_{535}/\varepsilon_{703}$	$\varepsilon_{535}/\varepsilon_{525}$
Cyclohexane	355	248	248	0.697	1.000
Methylenechloride	373	268	265	0.718	1.011
Ethylbromide	361	256	255	0.709	1.004
Ethyliodide	393	276.5	275	0.703	1.0055

We initially considered the Γ_c (MCD band *g*) as "$^2A_{1g}$"$(t_{2g}^2e_g^1)$, but any choice of crystal field parameters from a reasonable range rules out this possibility (Tables 1–3). Thus using Griffith's strong field two-electron matrix elements [12], and allowing all states of t_{2g}^3 and t_{2g}^2e of the same spin-space identity to interact, the calculation appears to successfully account for the approximate locations of ^2E_g, $^2T_{1g}$, $^4T_{2g}$, $^2T_{2g}$, and $^4T_{1g}$ of these configurations to within a few hundred wavenumbers (Tables 1–3). Therefore, it is reasonable to expect that it will predict the location of $^2A_{1g}(t_{2g}^2e_g^1)$ equally well. Since the prediction for $^4A_{2g} \rightarrow {}^2A_{1g}$ is 25 kK to 26 kK, we discount the possibility that our 20.4 kK MCD band *g* is $^2A_{1g}$.

The following additional comments need be made regarding the usefullness of the crystal field calculations. The results for Cr(dtp)$_3$ are shown in Table 1. The previously published parameters [4] used in our calculation I (Table 1) are ruled out because of ~ 5 kK deviations between calculated and observed positions of the two low energy doublets. However, the set of parameters from Lebedda and Palmer are in close agreement with ours (calculations II and III). Yet, since the center of gravity of $^4T_{1g}$ is not known and $10\,Dq$ may be chosen between ~ 14.5 kK and ~ 13.9 kK, the order of *octahedral* parents $^4T_{1g}$ and $^2T_{2g}$ can be reversed (compare predictions IV with II and III, Table 1) and a reasonable fit maintained. Computationally $^2T_{2g} > {}^4T_{1g}$ is favored only *if* $^2T_2 \sim 19.2$ kK, but either $^4T_{1g} > {}^2T_{2g}$ or $^4T_{1g} < {}^2T_{2g}$ can permit $^4E < {}^2E$ or

$^4E > {}^2E$ (Fig. 4). But, work in progress now indicates $^2T_2 \sim 18$ kK and $^4E(T_1) \sim 19.2$ kK.

It was also necessary to exercise caution when the crystal field calculations were carried out for the dtc and exan compounds. Considering $Cr(dtc)_3$ first (Table 2), we rule out the parameters [4] of our calculation I, e.g., $C/B = 4.0$, because the predicted energies of ^2E_g and $^2T_{1g}$ are about 4.5 kK too low. The search for our parameters was constrained by our observation of approximate band locations of "^2E_g", "$^2T_{1g}$", and the two intense electronic absorption band maxima of "$^4T_{2g}$" and "$^4T_{1g}$" at, respectively ~ 13 kK, ~ 13.6 kK, ~ 15.6 kK, and ~ 20 kK. However, again it is difficult to decide upon centers of gravity for $^2T_{1g}$, $^4T_{2g}$, and $^4T_{1g}$. For this reason only approximate parameters $Dq \cong 1.6$, $B \cong 0.4$, $C \cong 3$ - 3.3 can be given. The low energy region can be fitted nicely (^2E_g, $^2T_{1g}$, $^4T_{2g}$), but the order of $^4T_{1g}$ and $^2T_{2g}$ cannot unambiguously be decided, since several similar sets of parameters produce cross-overs of these two states (calculations II-V, Table 2). However, we definitely rule out the 21 kK MCD band as $^2A_{1g}$. Furthermore, $^4T_{1g}$ and $^2T_{2g}$ are predicted to be very close to each other, so that their D_3 components are expected to interact severely upon spin-orbit coupling.

The crystal field predictions and experimental situation for $Cr(exan)_3$ resemble those of $Cr(dtc)_3$, and are summarized in Table 3. Again, the parameters [4] of calculation I do not predict the bands of the low energy region. Second, while Witzke's [5] Racah parameters (calculation II: $B = 0.436$ kK, $C = 2.921$ kK), derived when the low energy spin doublets were not observed yet, are much better than Jorgensen's [4] (calculation I: $B = 0.39$ kK, $C = 1.56$ kK), the first two calculated spin doublets ^2E_g and $^2T_{1g}$ are still underestimated. Improved parameters are $Dq = 1.59$ kK, $B \cong 0.40$ kK and $C \cong 3.1$ kK. While this particular set of parameters predicts $^4T_{1g} > {}^2T_{2g}$ (calculation V), a quite similar set (calculation IV) has $^4T_{1g} < {}^2T_{2g}$ but the high energy region is not fitted well.

We are in the process of broadly extending this MCD work in order to determine effects of ring size[3]; of inductive effects of R of the ligand; of replacing S with Se; and of variations of temperature on MCD intensities and mechanisms. We defer trigonal crystal field and molecular orbital interpretations until these and our polarized crystal spectral data are completed.

References

1. Kida, S., Yoneda, H.: Nippon Kagaku Zasshi **76**, 1059 (1955).
2. Jorgensen, C. K.: J. inorg. nuclear Chem. **24**, 1571 (1962).
3. Schäffer, C. E., Jorgensen, C. K.: Molecular Physics **9**, 401 (1965); and much of the cited literature of Ref. [4].
4. Jorgensen, C. K.: Inorg. chim. Acta Rev. **2**, 65 (1968).
5. Witzke, H.: Theoret. chim. Acta (Berl.) **20**, 171 (1971).
6. (a) Furlani, C., Porta, P., Sgamellotti, A., Tomlinson, A. A. G.: J. chem. Soc. D, 1046 (1969).
   (b) Hidaka, J., Douglas, B. E.: Inorg. Chem. **3**, 1724 (1964).
7. (a) Lebedda, J. D., Palmer, R. A.: 160th American Chemical Society National Meeting, Chicago, Illinois, September 1970.
   (b) Work to be published.

---

[3] This will be necessary because both ring size and types of coordinating atoms were changed simultaneously in going from $Crox_3^{3-}$ of Ref. [9] to Cr(III)S_6 of this study.

8. Mitchell, W. J., DeArmond, K.: (To be published, including low temperature results).
9. McCaffery, A. J., Stephens, P. J., Schatz, P. N.: Inorg. Chem. **6**, 1614 (1967).
10. Galsbol, F., Schäffer, C. E.: Inorg. Syntheses **10**, 42 (1967).
11. Schatz, P. N., McCaffery, A. J., Süetaka, W., Henning, G. N., Ritchie, A. B.: J. chem. Physics **45**, 722 (1966).
12. Griffith, J. S.: The theory of transition-metal ions. Cambridge, Great Britain: Cambridge University Press 1961.
13. McGlynn, S. P., Azumi, T., Kinoshita, M.: Molecular Spectroscopy and the Triplet State. Englewood Cliffs, New Jersey: Prentice-Hall 1969.
14. Wasson, J. R., Wasson, S. J., Woltermann, G. M.: Inorg. Chem. **9**, 1576 (1970).

Prof. Dr. A. F. Schreiner
Department of Chemistry
North Carolina State University
Ralegh, North Carolina 27607, USA

Theoret. chim. Acta (Berl.) 24, 89–98 (1972)
© by Springer-Verlag 1972

SCC–EH–MO Calculations on the Bonding and Electric Field Gradient in Oxyhaemoglobin and Other Haem Derivatives

MARGARET P. HALTON

Chemistry Department, Victoria University of Wellington, New Zealand

Received September 27, 1971

SCC–EH–MO theory satisfactorily accounts for the sign and relative magnitude of the electric field gradient at the nucleus in several haem derivatives. The bonding in oxyhaemoglobin and some iron(III) porphyrins is discussed and a theory for the stability of oxyhaemoglobin is examined.

Die SCC–EH–MO Theorie gibt für einige Häm-Derivate zufriedenstellend die Verhältnisse bezüglich Vorzeichen und relativer Stärke des elektrischen Feldgradienten beim Kern wieder. Die Bindungsverhältnisse in Oxyhämoglobin und einigen Eisen(III)porphyrinen werden diskutiert, und eine Theorie für die Stabilität von Oxyhämoglobin wird geprüft.

Introduction

Bonding in iron porphyrins continues to be a subject of much interest because of their well known biological significance. A variety of theoretical methods have been employed but several experimental features have not yet been explained. In particular, for haemoglobin derivatives, the Mössbauer spectra have not been fully accounted for, while the unusual stability of the oxygen binding in oxyhaemoglobin has been well characterised [1] but not completely understood. We report now the application of a model system, based on SCC–EH MO's (Self Consistent Charge Extended Hückel Molecular Orbitals), to examine the quadrupole splitting in the Mössbauer spectrum and the nature of the bonding in a number of iron porphyrin (haem) derivatives.

Method

The formalism of Extended Hückel theory (EHT) is well known [2], and only the important features included in this paper. Diagonal elements, H_{ii}, of the $\boldsymbol{H}$ matrix were taken from valence state ionisation energies (VSIE's) which have been obtained from spectral data. Zerner and Gouterman's values [3] were used for the iron, and Hinze and Jaffé's [4] for all other atoms. The off-diagonal terms, H_{ij}, were constructed from the Wolfsberg-Helmholtz relation [5].

a) The Model

An all valence orbital calculation of the complete iron porphyrin system (Fig. 1) involves more than 125 orbitals, and the computing facilities available to us could not handle such a large basis set. Group theoretical methods could not

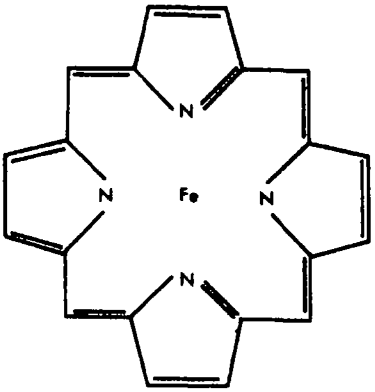

Fig. 1. Iron porphyrin

Table 1. Systems studied

System	Simulated species[a]	Spin	Sixth ligand	Ligand orbitals	Details
1	Hb	2			
2	HbO_2	0	O_2	all 2*s*, 2*p*	$A, a = 0°$
3	HbO_2	0	O_2	all 2*s*, 2*p*	$A, a = 60°$
4	HbO_2	0	O_2	all 2*s*, 2*p*	$B, b = 0°$
5	HbO_2	0	O_2	all 2*s*, 2*p*	$B, b = 60°$
6	HiH_2O	5/2	H_2O	2*s*, 2*p*, 1*s*	acid form
7	HiOH	5/2	O^-	2*s*	basic form
8	HiOH	3/2	O	2*s*	basic form
9	HiOH	1/2	O	2*s*	basic form low temperature
10	HiCl	5/2	Cl	3*s*	in pyridine solution
11	HbCO	0	C	(*sp*)	

[a] Hb denotes iron(II) haemoglobin; Hi denotes iron(III) haemoglobin.

be used because we are interested in some asymmetric geometries of the oxygenated system. Furthermore, since computing time increases rapidly with the size of the basis set, we required a model system which minimised the matrix order but which still effectively simulated the iron in the porphyrin environment.

Because the electron distribution around the iron itself is of prime interest in this work, all valence orbitals ($3d, 4s, 4p$) of the iron were included, but only the nitrogen orbitals of the porphyrin ring. Each porphyrin nitrogen was represented by a pi orbital in the z direction and a trigonal hybrid (sp^2) orbital in the xy plane (plane of the porphyrin). An sp^2 orbital was used so that the geometry of the porphyrin sigma system was imposed upon the model. Recent workers have shown [6] that sp^2 hybridisation is an adequate picture of the nitrogen orbital in an analogous copper complex. The fifth ligand was represented by a single neutral nitrogen sp^2 hybrid orbital, since the protein of haemoglobin co-ordinates to the iron through an imidazole [7]. The orbitals employed for the sixth ligand are given in Table 1. The overlap integrals of Ohno *et al.* [8] were used for the iron-nitrogen bonds and all other overlap integrals were calculated from Slater atomic orbitals [9]. Zerner *et al.* [10] have examined the effects of non-planar metal porphyrin and their results showed little difference in orbital populations between planar and non-planar systems. Consequently we assumed the iron to lie in the porphyrin plane. Errors arising from the use of a limited basis set are constant for all haem systems studied and therefore a significant discussion of experimental trends and bonding of the iron itself can be made.

Iterative EH calculations were performed using the self consistent charge (SCC) procedure of Zerner and Gouterman [3]. Because EHT does not include electron repulsion terms, the number of unpaired electrons was imposed upon the calculation. All computations were performed on an Elliott 503 computer, using modifications of Bailey's programs [11].

b) Choice of Systems

Haem derivatives were selected for study which had available Mössbauer data and these systems are listed in Table 1. The bonding in oxyhaemoglobin has been the subject of much controversy but two main cases have been proposed, the Pauling [12] and Griffith [13] models (see Fig. 2, $A, a = 60°$ and $B, b = 0°$ respectively). A systematic study of several geometrical arrangements has been made [14] and two were calculated to be particularly stable (in Fig. 2, $A, a = 60°$ and $B, b = 60°$). These two geometries were studied using the SCC model reported here, together with the extreme cases ($A, a = 0°$ and $B, b = 0°$). The bond lengths used were: iron-oxygen = 2.1 Å, oxygen-oxygen = 1.48 Å [14]. Reduced haemoglobin has no ligand in the sixth position [7] and was simulated by system 1 (see Table 1). The acid form of iron(III) haemoglobin contains water in the fifth position and is high-spin [15], but the basic form, with hydroxide in the sixth position, has unusual spin behaviour. At low temperatures, $S = 1/2$ appears to be correct [16] but at room temperature the magnetic moment corresponds to a spin of 3/2 and has been ascribed to an equilibrium of the high-spin ($S = 5/2$) and low-spin forms [17]. Therefore, we examined the three possible spin states ($S = 1/2, 3/2, 5/2$). System 10, in Table 1, was assumed to simulate chloro-iron(III) protoporphyrin IX in pyridine solution, since a nitrogen sp^2 orbital was used in the fifth position for every system studied. Since the iron itself is of prime interest for systems 5–11, a limited set of basis orbitals was used for several of these systems in order to minimise computing time. Because the Mössbauer results were found to be successful, this assumption was not modified. Whenever a single orbital was employed for the axial ligands, a fixed charge for that ligand was assumed in the iterative procedure.

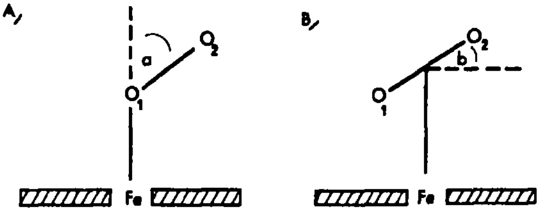

Fig. 2. Geometries of oxygenated iron porphyrin

c) Calculation of Electric Field Gradient

Mössbauer data are particularly useful in testing the theoretical model of this work since EHT is suitable only for ground state properties and the Mössbauer spectrum pertains to ground state iron alone. The electric field gradient, EFG, at the nucleus is determined from the MO coefficients [18]:

$$V_{zz} = -e\Sigma\langle\psi_i|3\cos^2\theta_i - 1|\psi_i\rangle N_i\langle r^{-3}\rangle \qquad (1)$$

and

$$V_{xx} - V_{yy} = -e\Sigma\langle\psi_i|3(x_i^2 - y_i^2)/r_i^2|\psi_i\rangle N_i\langle r^{-3}\rangle \qquad (2)$$

where N_i is the number of electrons in MO ψ_i, and $(-e)$ the electron charge. (The cross terms of the EFG tensor V are neglected). The observed quadrupole splitting ΔE_Q is proportional to the EFG, such that

$$\Delta E_Q \propto V_{zz}(1+\eta^2/3)^{\frac{1}{2}} \qquad (3)$$

where

$$\eta = (V_{xx} - V_{yy})/V_{zz}\,.$$

For convenience, Eqs. (1)–(3) were simplified by introducing a parameter B which was directly proportional to ΔE_Q, and the constants e and $\langle r^{-3}\rangle$ incorporated into the proportionality constant. The sign of B was then the predicted sign of the EFG, and the sign convention adopted was such that a positive EFG implied that the nuclear excited 3/2 state was higher in energy than the nuclear excited 1/2 state. Thus, for zero η B is given by:

$$B = [N_{x^2-y^2} + N_{xy} - (N_{xz} + N_{yz})/2 - N_{z^2}]\,4/7 + [N_x + N_y - 2N_z]\,2/5 \qquad (4)$$

where N_j is the gross atomic population for basis orbital j, and j covers all $3d$ and $4p$ iron orbitals. The expression for B when $\eta \neq 0$ follows readily. There are two major assumptions in this formulation of B; first that $\langle r^{-3}\rangle$ is the same for both $3d$ and $4p$ orbitals, and second, that the use of GAP values, which are appropriate for $3d$, are also appropriate for $4p$. However, errors arising from these assumptions were found to cancel for the systems studied here [19].

Results and Discussion

In the following discussions, the MO's are often referred to as a particular atomic orbital, for convenience. This implies that the MO is predominantly that atomic orbital in character and not necessarily pure atomic orbital. In fact, only the $3d_{xy}$ iron orbital is ever found to be a pure atomic orbital in these systems. Only those results pertinent to the discussion are recorded, and these in the appropriate sections below.

a) Electric Field Gradient

The gross atomic populations (GAP) for the iron orbitals in each of the systems 1–11 are listed in Table 2, and the consequent B values are given in Table 3. The experimental sign of the EFG is known for the molecules simulated by systems 1–6 and 10, and in each case experiment and theory agree. Because of this agreement for all known cases, we assumed that the sign of B

Table 2. Iron orbital populations

System	1	2	3	4	5	6	7	8	9	10	11
$4s$	0.330	0.312	0.346	0.258	0.367	0.317	0.404	0.448	0.473	0.434	0.323
$4p_x$	0.071	0.104	0.108	0.091	0.108	0.077	0.076	0.094	0.106	0.078	0.073
$4p_y$	0.071	0.104	0.102	0.105	0.106	0.089	0.076	0.094	0.106	0.078	0.073
$4p_z$	0.221	0.253	0.326	0.148	0.319	0.267	0.255	0.307	0.303	0.281	0.215
$3d_{xy}$	2.000	2.000	2.000	2.000	2.000	2.000	2.000	2.000	2.000	2.000	2.000
$3d_{yz}$	1.433	2.000	2.000	2.000	1.876	1.531	1.500	1.708	1.896	1.502	2.000
$3d_{xz}$	1.433	2.000	1.988	1.933	1.958	1.520	1.500	1.708	1.896	1.502	2.000
$3d_{z^2}$	0.917	0.452	0.796	0.297	0.938	0.950	1.023	1.069	0.381	1.056	0.312
$3d_{x^2-y^2}$	1.117	0.289	0.306	0.255	0.304	1.131	1.124	0.303	0.341	1.127	0.241
Fe chge	0.407+	0.486+	0.028+	0.913+	0.024+	0.120+	0.042+	0.269+	0.498+	0.058−	0.763+

Table 3. Theoretical and experimental EFG

System	Molecule	B	ΔE_Q mm/sec	Ref.
1	Hb	+0.318	+2.40	[20]
2	HbO_2	−0.212	−2.25	[21]
3	HbO_2	−0.455	−2.25	[21]
4	HbO_2	−0.015	−2.25	[21]
5	HbO_2	−0.486	−2.25	[21]
6	HiH_2O	+0.228	+2.00	[21]
7	HiOH	+0.220	1.57	[21]
8	HiOH	−0.441	1.90	[21]
9	HiOH	0.196	0.98	[20]
10	HiCl	+0.163	+0.78	[20]
11	HbCO	−0.155	0.36	[21]

corresponded to the sign of the EFG in every system. We plotted the experimental quadrupole splitting (see Table 3) against B for the systems 1, 6, 9–11 and obtained an excellent linear correlation (Fig. 3). Only the low-spin case for HiOH ($S = 1/2$) was included in this plot since the higher spin states correspond

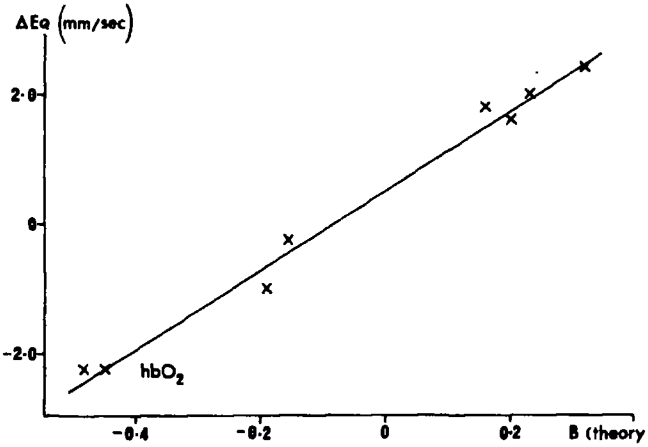

Fig. 3. Plot of experimental quadrupole splitting against theoretical electric field gradient parameter, B

to higher temperatures and MO calculations are most pertinent at very low temperatures. This species is discussed further below. Fig. 3 also shows the position of systems 3 and 5 but the oxygenated cases are discussed separately.

The satisfactory correlation demonstrates the success of our model in spite of its approximations and the inherent assumptions of SCC–EHT. Hence, our consequent deductions about the systems studied are justified, provided the limitations of the model are remembered. Our correlation plot is much better than that achieved by other workers [22] who used similar calculations, and reasons for this will become clear in the following discussions.

b) High-Spin Iron(III) Porphyrins

The two high-spin iron(III) derivatives studied, systems 6 and 11, have led to the first successful prediction of the sign of their EFG. Several workers [22, 23] have examined these species using the MO calculations of Zerner *et al.* [10] but all have predicted negative EFG values, contrary to experiment [23]. The successful prediction in our work arises from the assumption of a new ground state. We found, as have other workers [10], that the relative energies of the highest occupied MO's are:

$$xy < a_1 < xz \sim yz < z^2 < x^2 - y^2$$

where a_1 denotes the highest occupied MO of porphyrin pi orbitals, assuming C_{2v} symmetry. This ordering of the energy levels leads to the $^6A_2(d^6)$ configuration:

$$(xy)^2 (a_1)^1 (xz)^1 (yz)^1 (z^2)^1 (x^2 - y^2)^1$$

which we adopted in the SCC procedure but Zerner *et al.* [10] insisted upon the $^6A_1(d^5)$ configuration

$$(xy)^1 (a_1)^2 (xz)^1 (yz)^1 (z^2)^1 (x^2 - y^2)^1$$

in their calculations. The multiplicity of both configurations correspond to the magnetic susceptibility data [15] but since the Mössbauer spectrum pertains to the iron itself, not the entire system, the EFG is a more appropriate experimental quantity to use to distinguish between the alternative configurations. The $^6A_1$ state leads to a negative EFG [22] contrary to experiment [23], while the $^6A_2$ state not only predicts correctly a positive EFG but also accounts for the unusually large observed value of the quadrupole splitting. Furthermore, esr data for these derivatives have been explained by assuming a large asymmetry in the iron environment [24]. Such asymmetry is unusual for high-spin d^5 species but characteristic of high-spin d^6. Our calculations refer to low temperatures and a thermal equilibrium between the $^6A_1$ and $^6A_2$ states may exist at room temperature. Experimental properties such as isomer shifts and absorption spectra cannot be examined with SCC–EHT because of the inherent approximations. However, a detailed theoretical study of these properties will be necessary before the proposed $^6A_2$ ground state can be confirmed.

c) Iron(III) Haemoglobin Hydroxide

The spin state of the hydroxide derivative has not been well established. However, at room temperature the magnetic susceptibility corresponds to a spin of 3/2 [17] while at 5° K esr data indicates a spin of 1/2 [16]. Mössbauer spectra have been observed [21] at 4° K, 77° K, and 195° K, and if Blume's [25] arguments are followed, the EFG is negative at 4° K but positive at 77° K and 195° K. We predict a negative EFG for the $S = 1/2$ case (system 9), positive EFG for $S = 5/2$ (system 7), and negative EFG for $S = 3/2$ (system 8). The magnitude of the calculated EFG parameter, B, follows the correlation curve in Fig. 3 for all three systems, and hence only the sign of the EFG for the $S = 3/2$ case is unexplained. A detailed experimental study of magnetic susceptibilities over a wide temperature range and a careful examination of the 3/2 state and possible equilibria between 5/2 and 1/2 will be required before the hydroxide case is fully understood.

d) Oxyhaemoglobin

Considerable difficulty was encountered with systems 2–5 (the oxygenated species) in positioning the $3d$ orbitals and achieving satisfactory convergence. This arose because the oxygen $2p$ orbitals were lower in energy than the iron $3d$ orbitals, so that electrons were assigned to the oxygen orbitals at the expense of those of the iron. In effect the MO calculations were predicting that oxidation would occur, and this is observed generally for iron(II) porphyrins. These theoretical difficulties were overcome by adding two electrons to the system; because oxyhaemoglobin is diamagnetic [15] any extra electrons must be added in pairs. Our theoretical model can be compared with that of Zerner *et al.* [10]. These workers examined two geometries only, corresponding to $A, a = 0°$ and $B, b = 0°$ in Fig. 2, and did not add two extra electrons. For the linear case $(A, a = 0°)$ they found that the oxygen $2p$ orbitals were much lower in energy than the iron $3d$, as we found, and concluded that oxidation would occur. Their case corresponding to $B, b = 0°$, converged satisfactorily but, because all of the porphyrin valence orbitals had been included, the porphyrin was able to compensate for the electron loss to the oxygen orbitals. Of all the systems studied by Zerner *et al.*, only this case led to a positive charge on the porphyrin nitrogens. Furthermore, Zerner *et al.*'s MO's lead to a positive EFG [22], contrary to experiment [21]. Our MO's determined with the two extra electrons, lead to a negative EFG, in agreement with experiment (see Table 3).

In view of these results, and the demonstrated success of our theoretical model, a theory which accounts for the unusual stability of oxyhaemoglobin, and oxymyoglobin, has been proposed [19]: oxidation of iron(II) porphyrin will occur unless two electrons are added to the oxygenated iron. Since haemoglobin is an oxygen carrier and not part of an enzyme system, the protein is presumed to provide the electrons through the fifth ligand and the delocalised pi orbitals of the porphyrin. Indirect experimental evidence is available from studies of oxygen binding in some cobalt complexes and reconstituted haems and haemoglobins. Caughey *et al.* [26] have shown that an increase in the pi electron donation to the metal enhances oxygen binding and this can be understood from our pro-

Table 4. Results for oxygenated systems

System[a]	2	3	4	5
Chge O^1	−0.830	−0.618	−0.901	−0.688
Chge O^2	−0.930	−0.751	−0.934	−0.816
Chge $O^1 + O^2$	−1.760	−1.369	−1.835	−1.504
NOP O^1	0.261	0.294	0.185	0.280
NOP O^2	0.142	0.157	0.182	0.159
NOP $O^1 + O^2$	0.403	0.451	0.367	0.439

[a] O^1 refers to oxygen closest to the iron, O^2 to distal oxygen.

posed theory: the electrons lost to the oxygen are from the metal d_π orbitals so that any factor which increases the pi electron donation will increase the stability of the metal-oxygen system. Several workers [27] have established that an increase in the basicity of the fifth ligand in model systems leads to an increased oxygen affinity, and this correlates with our proposed requirement of electron transfer to the iron to compensate for the loss to the oxygen.

There are two main features of this theory of two electron transfer: first, the iron exists as a d^6 species in oxyhaemoglobin, and second, the oxygen molecule exists as an oxyanion (see Table 4). These features can be compared with the suggestions of other workers. Weiss [28] proposed that the electron distribution in oxyhaemoglobin corresponds to Fe(III).O_2^-. We have calculated a large negative charge on the oxygen (Table 4) but deduced the electron transfer to be compensated by a transfer from the protein to the iron. Pauling has suggested a charge separation within the oxygen molecule of one electron [12], i.e. Fe(II) O^+ O^-, while our calculations predict a significant, but much smaller separation (Table 4).

Support for Weiss' configuration (Fe(III).O_2) has been claimed by analogy with the model cobalt complexes [29]. The cobalt oxygen adducts can be represented formally by Co(III).O_2 because ESR studies have established that the single unpaired electron is mostly associated with the oxygen. However, our calculations show that this does not necessarily infer the corresponding Fe(III).O_2 in oxyhaemoglobin. The z^2 orbital (unoccupied in oxyhaemoglobin) is thoroughly mixed with the oxygen 2_{p_z} orbital for most metal-oxygen geometries [19]. In the cobalt adducts this z^2 orbital is singly occupied so that unpaired electron character is associated with the oxygen. Specific calculations on some cobalt-oxygen adducts are in progress in our laboratory.

Now, the particular geometry of the iron-oxygen system is of interest. The relative strengths of the iron-oxygen bond can be estimated from the calculated overlap populations [30]. Each atom is assigned a net overlap population, NOP, which is due to that atom's bonding with neighbouring atoms, and we assumed that the system which predicts the largest total NOP for the oxygen molecule, corresponds to the bonding in oxyhaemoglobin. The NOP values are listed in Table 4. Although these NOP values are sensitive to the assumed bond lengths, consistent variation of bond lengths affects the magnitude of the NOP's but not the relative values, and any comparison of bond strengths, as a function of geometry, can only be made for fixed bond distances.

Both asymmetric systems (3 and 5) predict a stronger oxygen binding than the extreme cases (2 and 4), with the Pauling model (system 3) predicting the strongest of all. These conclusions agree well with our earlier results [14] from other models.

The Mössbauer data can be used for an independent prediction of the best simulation. When the plot of Fig. 3 is extrapolated to the observed quadrupole splitting of oxyhaemoglobin, only systems 3 and 5 lie near the line and the Pauling model (3) is the better fit. The asymmetric contribution, η, to the B values is small (0.001 for systems 3 and 5), in agreement with experimental analyses [21], and therefore is not the cause of the unusually large quadrupole splitting in oxyhaemoglobin. We consider this unusual magnitude to be due to covalent effects and the proposed donation of two electrons from the protein.

Conclusion

We have applied a theoretical model to a number of iron porphyrin derivatives and have found a good correlation between theoretical and experimental EFG values. Although the porphyrin ring has been grossly approximated, the consequent errors were constant for all systems studied and the model was appropriate for a discussion of ground state properties of the iron itself. A new description of the ground state in some high-spin iron(III) porphyrins has led to the first correct prediction of a positive EFG, while the proposed two electron transfer to the iron-oxygen system in haemoglobin (or myoglobin) accounts for not only the stability of the oxygen adduct but also the observed sign of the EFG.

Acknowledgements. I wish to thank Prof. J. F. Duncan for many discussions and financial support from U.S.A.F. Grant No. A.F.O.S.R. 1236-69 is gratefully acknowledged.

References

1. Antonini, E.: Physiol. Rev. **45**, 123 (1965).
2. Jug, K.: Theoret. chim. Acta (Berl.) **14**, 91 (1969).
3. Zerner, M., Gouterman, M.: Theoret. chim. Acta (Berl.) **4**, 44 (1966).
4. Hinze, J., Jaffé, H. H.: J. Amer. chem. Soc. **84**, 540 (1962).
5. Wolfsberg, M., Helmholz, L.: J. chem. Physics **20**, 837 (1952).
6. Guzy, C. M., Raynor, J. B., Symons, M. C. R.: J. chem. Soc. A 2299 (1969).
7. Perutz, M. F.: Proc. Roy. Soc. B **173**, 113 (1969).
8. Ohno, K., Tanabe, Y., Sasaki, F.: Theoret. chim. Acta (Berl.) **1**, 378 (1963).
9. Slater, J. C.: Physic. Rev. **36**, 57 (1930).
10. Zerner, M., Gouterman, M., Kobayashi, H.: Theoret. chim. Acta (Berl.) **6**, 363 (1966).
11. Bailey, J. P. M.: Report No. CD2091, DSIR, New Zealand (1967).
12. Pauling, L.: Nature **203**, 182 (1964).
13. Griffith, J. S.: Proc. Roy. Soc. A **235**, 23 (1956).
14. Halton, M. P.: Theoret. chim. Acta (Berl.), in press.
15. Pauling, L., Coryell, C. D.: Proc. Natl. Acad. Sci. **22**, 159 (1936); ibid. **22**, 210 (1936).
16. Gibson, J. F., Ingram, D. J., Schonland, D.: Discuss. Faraday Soc. **26**, 72 (1958).
17. George, P., Beetlestone, J., Griffith, J. S.: Rev. mod. Physics, 441 (1964).
18. Cotton, F. A., Harris, C. G.: Proc. Natl. Acad. Sci. **56**, 12 (1966).
19. Halton, M. P.: Ph. D. Thesis, Victoria University of Wellington, New Zealend (1971).
20. Gonser, U., Grant, R. W.: Biophys. J. **5**, 823 (1965).
21. Lang, G., Marshall, W.: Proc. physic. Soc. **87**, 3 (1966).

22. Weissbluth, M., Maling, J. E.: J. chem. Physics **47**, 4166 (1967).
23. Moss, T. H., Bearden, A. J., Caughey, W. S.: J. chem. Physics **51**, 2624 (1969).
Han, P. S., Das, T. P., Rettig, M. F.: Theoret. chim. Acta (Berl.) **12**, 178 (1968).
24. Kotani, M.: Ann. N.Y. Acad. Sci. **158**, 20 (1969).
25. Blume, M.: Physic. Rev. Letters **14**, 96 (1965).
26. Caughey, W. S., Alben, J. O., Beaudreau, C. A.: In: Oxidases and Related Redox Systems, ed. King, T. E., Mason, H. S., Morrison, M., p. 97. London: Wiley 1964.
27. Caughey, W. S., Eberspaecher, H., Fuchsman, W. H., McCoy, S.: Ann. N.Y. Acad. Sci. **153** (3), 722 (1969). Crumbliss, A. L., Basolo, F.: J. Amer. chem. Soc. **92** (1), 55 (1970).
28. Weiss, J. J.: Nature **202**, 83 (1964).
29. Schrauzer, G. N., Lian Pin Lee: J. Amer. chem. Soc. **92** (6), 1551 (1970).
Walker, F. A.: J. Amer. chem. Soc. **92** (14), 4235 (1970).
Nan-Loh Yang, Oster, G.: J. Amer. chem. Soc. **92** (17), 5265 (1970).
30. Mulliken, R. S.: J. chem. Physics **23**, 1833 (1955).

Dr. M. P. Halton
Chemistry Department
Victoria University of Wellington, New Zealand

Theoret. chim. Acta (Berl.) 24, 99--101 (1972)
© by Springer-Verlag 1972

Relationes

Hyperconjugation in the 2-Butyl Cation

J. J. DANNENBERG and T. D. BERKE

Department of Chemistry, Hunter College of the City University of New York
695 Park Ave., New York, N.Y. 10021

Received June 29, 1971

A comparison of the optimized geometries of the hydrogen-bridged ethyl and 2-butyl cations suggest the contribution of hyperconjugation to the stability of the latter to be ≥ 10 kcal/mole. An examination of the barrier to rotation of a methyl group is in accord with the phenomenon of hyperconjugation.

As part of an investigation of the energy surfaces of various carbonium ions [1], we have optimized the geometries of both the open and hydrogen-bridged structures of the ethyl and 2-butyl cations using the INDO approximation of molecular orbital theory [2]. A comparison of the optimized hydrogen-bridged structures of these ions provides an interesting example of the contribution of hyperconjugation to the stability such ions.

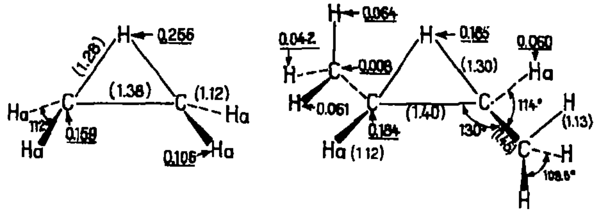

Fig. 1. Optimized geometries for the ethyl and 2-butyl cation. Charge densities are underlined, bond lengths are in parentheses. For the ethyl cation, the C–H_a bonds make an angle of 3.5° with the plane that contains the two carbons and is perpendicular to the 3-membered ring. For the 2-butyl cation, all four carbons and both H_a's are coplanar

The optimized structures of the two ions are described in Fig. 1. In the ethyl cation, the four H_a's are not coplanar with the two carbon atoms (they are bent 3.5° below the plane). In the case of the 2-butyl cation, however, the two H_a's are coplanar with the four carbons. If one considers the bridged ethyl cation as arising from the protonation of an ethylene molecule, one would expect the H_a's to move out of the ethylene plane in the opposite direction from the incoming proton. Such a distortion would be expected from the increasing sp^3 character of the carbon orbitals in the C–H_a bonds and from the tendency to minimize the repulsions between the bridged proton and the H_a's. In principle,

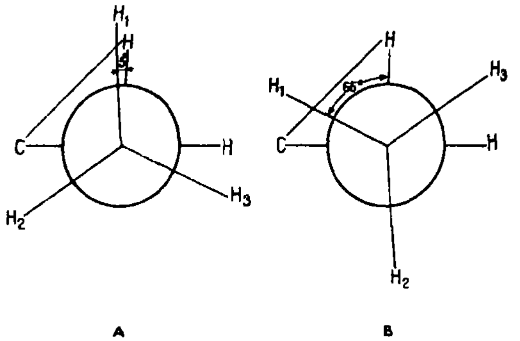

Fig. 2. Rotation of a methyl group in the bridged 2-butyl cation. a) Minimum energy and b) maximum energy configurations

one should expect an analogous distorsion from planarity if one considers the protonation of *trans*-2-butene to form the bridged *trans*-2-butyl cation. The observation that no such distortion is predicted by the calculations suggests that there exists a hyperconjugative interaction between the two methyl groups and the protonated π-system. Furthermore, the maximization of this hyperconjugative interaction must contribute more to the stability of the ion then would the displacement of the two methyl carbons and two H_a's out of the plane, as in the ethyl cation.

To obtain an approximate estimate of the stabilization due to hyperconjugation, the energy of an ethyl cation of the same geometry as in Fig. 1, except that the H_a's were made coplanar with the carbons, was calculated. This energy was found to be 10 kcal/mole higher than that of the optimized geometry. Reasoning that, in the absence of hyperconjugation, the bridged 2-butyl cation would have to overcome a similar barrier to attain its calculated structure, the stabilization due to hyperconjugation must be $\geqq 10$ kcal/mole[1]. This estimate seems in reasonable accord with the work of Baird [4], who estimated the hyperconjugative stabilization of carbonium ions by comparing separate CNDO calculations of the same ions, with the interaction of the methyl hydrogen and the adjacent carbon either included or neglected.

The threefold rotational barrier of a methyl group around the axis of the C_1–C_2 bond is also instructive. The magnitude of this barrier is calculated to be 5.0 kcal/mole. The energy minimum corresponds to a structure with a methyl hydrogen slightly distorted (ca. 5°) from the position eclipsing the bridging hydrogen (see Fig. 2), whereas the energy minimum corresponds to a structure that is more or less skew. Thus, maximization of the electronic interactions seems more important to the stability of the ion then does minimization of the H–H repulsions. Furthermore, the minimum energy conformation has a distortion from the eclipsed geometry in the direction that maximizes the interaction of the C–H_2 bond (Fig. 2) with the π-system as it rotates this bond away from the node of the π-system. (Since H_2 is nearer to the center of the π-system then is H_3, a rotation in this direction should be more beneficial than a rotation in the opposite direction.)

---

[1] It should be noted that the CNDO method (therefore presumably the INDO method) favors small ring structures over open chain isomers [3]. This may very well be due to the neglect of 3 and 4 centered repulsive interactions in the method. Nevertheless, a comparison between two analogous cyclic structures is less likely to encounter problems of this nature.

The total energies of the various geometries of the ions studied were calculated using the INDO method of Pople, Beveridge, and Dobosh [2]. The calculations were judged to be self-consistent when the energies of two successive approximations differed by less than 10^{-7} atomic units. The geometries of Fig. 1 were optimized for all bond lengths and all bond angles. The rotational barrier was calculated by rotating the methyl group in steps of 5° and calculating the energy of each rotational isomer. A plot of total energy versus rotation angle exhibits one minimum, one maximum and is continuous.

Acknowledgment. The authors would like to thank Dr. D. L. Beveridge for a copy of his INDO program. J. J. Dannenberg also thanks Drs. R. Daudel and O. Chalvet for their hospitality at the Centre de Mécanique Ondulatoire Appliquée in June 1971.

References

1. Dannenberg, J. J., Berke, T. D.: 158th National American Chemical Society Meeting, New York, September, 1969: Abstract Phys. 163 and unpublished results.
2. Pople, J. A., Beveridge, D. L., Dobosh, P. A.: J. chem. Physics **47**, 2026 (1967).
3. Snyder, E. I.: J. Amer. chem. Soc. **92**, 7529 (1970).
   Sustmann, R., Williams, J. E., Dewar, M. J. S., Allen, L. C., von Schleyer, P. R.: J. Amer. chem. Soc. **91**, 5350 (1969).
4. Baird, N. C.: Theoret. chim Acta (Berl.) **16**, 239 (1970).

Dr. J. J. Dannenberg
Department of Chemistry
Hunter College of the City University of New York
695 Park Avenue
New York, N.Y. 10021, USA

Theoret. chim. Acta (Berl.) 24, 102 – 106 (1972)
© by Springer-Verlag 1972

An SCF Study of P_4O_6 and P_4O_{10}

B. J. McAloon and P. G. Perkins

Department of Pure and Applied Chemistry, University of Strathclyde, Glasgow, C. 1, Scotland

Received March 18, 1971

The electronic structures of the oxides P_4O_6 and P_4O_{10} are calculated by the self-consistent molecular orbital method including all valence electrons and the 3*d* orbitals on phosphorus. It is found that the former molecule appears to be virtually non-polar whilst in the latter, the P–O (terminal) bonds are highly polar. The bond order matrix shows that the internal P P bonding in the P_4 unit is not marked.

Introduction

An interesting feature of molecules which contain second-row atoms is the extent to which the formally empty 3*d* orbitals participate in the bonding scheme. This problem is particularly cogent in the case of phosphorus compounds and in order to throw light on the area, a number of *ab initio* calculations have been performed [3, 4, 8].

The *ab initio* approach, however, becomes computationally infeasible for large molecules because of the size of basis set required for accuracy: in this respect *minimum* basis set *ab initio* calculations may well be less accurate than semi-empirical ones. This point has yet to be fully investigated.

In the present paper a rationale of the bonding in the phosphorus oxides P_4O_6 and P_4O_{10} is attempted in terms of the LCAO SCF CNDO formalism [6, 9]. The calculational scheme employed was essentially similar to that of our previous calculations on phosphorus compounds [1].

As stated above, because of the size and complexity of *ab initio* calculations, it is clear that semi-empirical treatments of molecules of chemical interest will be required for some time to come. However, it is important that comparisons between *ab initio* and CNDO type calculations be made for molecules containing second-row atoms in order to establish the degree of reliability of the latter method. Hence, we carried out calculations on phosphine and phosphine oxide, both of which have been studied using Gaussian-type orbitals [3, 4, 8]. All the details of these calculations are to be found in Ref. [1b]. For P_4O_6 and P_4O_{10}, bond distances and angles were abstracted from standard compilations [5]. Burns' orbitals were chosen as the basis set and, for the 3*d* group, an exponent corresponding to a "diffuse" orbital was employed: this choice was made in order that our calculated results would be directly comparable to those for the P_4 tetrahedron [1]. This is important, since both P_4O_6 and P_4O_{10} are based structurally on the P_4 tetrahedron. In any case, diffuse *d* orbitals should be more appropriate, since in P_4 itself their radial extension is such that they are able to overlap with orbitals defined in the opposite faces of the tetrahedron [1]. All calculations were performed on the Strathclyde University ICL 1905 computer, using a symmetry based SCF programme.

Results and Discussion

An abstract of the principal results for PH_3 and PH_3O is given in Table 1 together with data from the *ab initio* calculations. No detailed discussion need be given here but it is at once clear that, for these two systems, our results are in substantial agreement with those of the more sophisticated treatments. This result encourages the belief that a CNDO-based method can be a reliable tool for calculating valence electronic structures for phosphorus compounds.

The results of the calculations on P_4O_6 and P_4O_{10} are now discussed under three heads

Table 1. *Calculated data for phosphine and phosphine oxide*

Atomic populations	PH_3				PH_3O		
	Present work[f]	Previous work			Present work[f]	Previous work	
		[a]	[b]	[c]		[d]	[e]
P 3*s*	1.57	1.64	1.566	1.54	1.51	1.20	–
3*p*	3.27	3.48	3.173	3.23	2.76	2.36	– –
3*d*	0.14	0.26	0.188	0.09	0.37	0.36	-
Nett charge on P	+0.02	−0.32	+0.073	+0.14	+0.36	+1.08	+0.245
Nett charge on H	−0.00	+0.11	−0.024	−0.04	−0.01	−0.12	+0.250
O 2*s*	—	– –		—	1.61	1.84	—
2*p*	—	-	-	—	4.71	4.84	—
Nett charge on O		—	– –	—	−0.32	−0.72	−0.334
Energy of highest bonding orbital (eV)	−11.7	−10.02	– –	– –	−10.6	—	−10.3

[a] Ref. [4].
[b] Lehn, J. M., Munsch, B.: Chem. Comm. 1970, 1321.
[c] Ref. [8].
[d] Ref. [3].
[e] Ref. [8]; the data in this paper are not analysed as separate *s*, *p*, and *d* orbital populations.
[f] "contracted" *d* orbitals were included on phosphorus (see Ref. [1b]).

a) Charge Distribution

A population analysis performed on the molecules with and without inclusion of 3*d* orbitals in the basis set yielded the charge distribution over the atomic skeleton shown in Fig. 1. The axis system illustrated here determines the orientations of the orbitals on all the atoms. First of all, the results show clearly that 3*d* orbital participation in phosphorus bonding is influential and that one of the effects of this participation is to even out the relative charges on the phosphorus and oxygen atoms and so to make the electronic picture more realistic. This seems to be a general effect in P–O compounds [1, 7]. The actual extent of the *d*

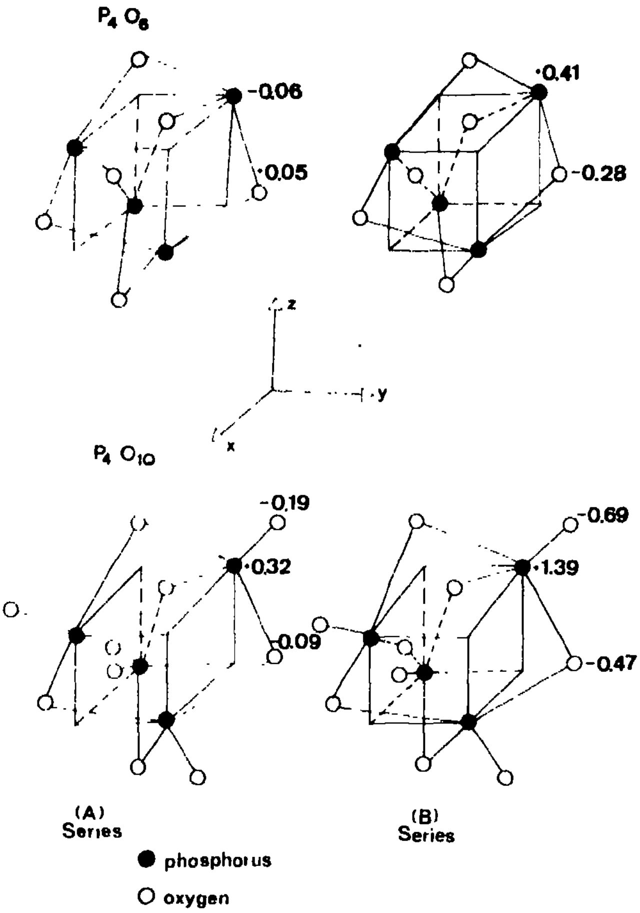

Fig. 1. Charge distribution in P_4O_6 and P_6O_{10}. Series A; 3*d* orbitals included; Series B; 3*d* orbitals neglected

Table 2. *Orbital occupation in* P_4O_6 *and* P_4O_{10}

	P_4O_6		P_4O_{10}	
	Without *d* orbitals	With *d* orbitals	Without *d* orbitals	With *d* orbitals
P 3*s*	1.273	1.046	0.951	0.780
3*p*	3.312	2.745	2.660	2.225
3*d*		1.275		1.672
Nett charge on P	+0.415	−0.066	+1.389	+0.323
O (bridge) 2*s*	1.113	1.089	1.155	1.102
2*p*	5.163	4.866	5.311	4.995
Nett charge on O (bridge)	−0.276	+0.045	−0.466	−0.097
O (term) 2*s*	—	—	1.232	1.230
2*p*	-		5.458	4.955
Nett charge on O (term)	—	—	−0.690	−0.185

orbital participation is reflected in the calculated orbital charge densities (Table 1) and is seen to be substantial. It is striking that the *d* orbital population is so large and, moreover, it is noteworthy that the *d* electron density increases with the greater number of oxygens in the molecule, i. e., it is greater in P_4O_{10} than in P_4O_6. This, however, is consistent with early ideas on the mode of *d* orbital participation [2], in which it was suggested that electronegative groups around phosphorus would help contract the 3*d* orbitals and mix them in to a greater extent.

In P_4O_6 the charge distribution over the PO_3 units is very similar to that in the hypothetical trihydroxyphosphine [1] an isomer of phosphorous acid; thus, P_4O_6 appears to be virtually electronically neutral. The polarity and multiplicity of the P–O bond in these oxides and, indeed, in P–O compounds in general, is a matter of some importance, since these are the properties which can help rationalise the chemical behaviour of the compounds. It is of considerable significance that the charge separation across the P–O (terminal) bond in P_4O_{10} is marked even after attenuation by the 3*d* orbitals. An examination of the results for other P–O compounds or ions which have been studied (the phosphate series [7], Me_3PO, PH_3O [1, 3, 8]) reveals that the degree of charge separation in P_4O_{10} is only matched by that of the P–O bond in PH_3O. It is significant that the latter compound has not yet been prepared, possibly for this very reason; it would lead to great lability. The high reactivity of P_4O_{10}, especially its avidity for polar hydroxy compounds, is hardly surprising in view of this highly polar charge distribution. This finding is consistent with the supposed mode of reaction of P_4O_{10} with alcohols and water [10], i. e.,

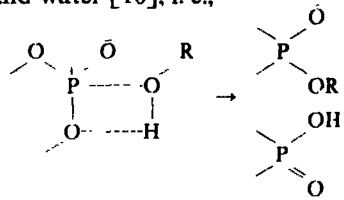

The interesting point here is that the reaction mechanism depends on the attachment of the acidic hydrogen atom to a bridging oxygen which is the *least* negative of the two types. This may reflect the relationship of the electronic properties of the P_4 unit in the oxides to that of P_4 itself, since the edges and faces of the latter basic unit are regions in which charge density is highly concentrated [1].

b) Bond Orders

Because of the relationship of both molecules to the P_4 tetrahedron, it is first of interest to examine the changes brought about in the bonding of the latter by addition of oxygens at corners and along edges of this unit. In P_4 the stability of the molecule is enhanced by strong $3p_\pi 3p_\pi$ bonding along the tetrahedron edges, accompanied by 3-centre φ bonding on the trigonal faces; the latter is strengthened by interaction with 3*d* orbitals centred on corresponding atoms, i. e., opposite the faces.

When we pass to P_4O_6 and P_4O_{10} the essential P_4 unit is retained, although it is somewhat enlarged in these systems, the P–P distance increasing from 0.221 *nm* to nearly 0.3 *nm* [5]. In forming P_4O_6 from P_4 the edge oxygen atoms appear to add across the edge $p_\pi p_\pi$ bonds of P_4 and so weaken them. This means that the expansion of the tetrahedron is energetically favoured, since repulsive forces will assume more importance when bonding is diminished. Moreover, in P_4O_{10}, involvement of the phosphorus orbitals in bonding to the external oxygens will remove electron density from inside the tetrahedron where it appears to be concentrated in P_4. This will decrease the nuclear shielding between the four phosphorus atoms and this, in turn, can be relieved by cage expansion. The bond orders calculated bear out this interpretation: the $p_\pi p_\pi$ edge bonds of P_4 are virtually nonexistent in the oxides whilst the *d* orbitals cease to interact markedly with the opposite face orbitals: P–P bond orders in general are much reduced.

The P_4 tetrahedron with P–P = 0.221 *nm* could, in principle, be retained with narrow POP bridging bond angles: (they would have to be ~86°). Obviously, nuclear repulsion between oxygens would be increased in this situation and it seems that this factor militates against the retention of the small P_4 unit, especially as it must lose P P edge bonding through linking to oxygen.

The P O (terminal) bonds are multiple in nature and have a considerable π component resolved from the *p* and *d* orbitals on phosphorus. This is consistent with the observed shortness of this bond in P_4O_{10} (1.39 Å [5]).

c) Energies

Both systems retain full tetrahedral symmetry and so the eigenvalues fall into both doubly and triply degenerate sets. In P_4O_6 the highest bonding and lowest antibonding orbitals are of *t* and *e* symmetry respectively and have energies −6.6 and 9.3 eV. In P_4O_{10} the corresponding energy levels are *t* and *a*, with energies −9.7 and 11.2 eV.

With regard to the total energies the *d* orbitals lower the energy of P_4O_6 by 6.6% and of P_4O_{10} by 6.0%. This is rather less than that calculated for P_4 (11%).

Acknowledgement. We are grateful to Albright and Wilson Ltd. for a Maintenance Grant (to B. J. McA.) and other support for this work and we thank Mr. J. J. Stewart for help with the use of the programme.

References

1a. Archibald, R. M., Perkins, P. G.: Chem. Comm. **1970**, 569.
1b. Rev. Roum. Chim., submitted for publication
2. Craig, D. P., Zauli, C.: J. chem. Physics **37**, 601 (1962).
3. Demuynck, J., Veillard, A.: Chem. Comm. **1970**, 873.
4. Hillier, I. H., Saunders, V. R.: Chem. Comm. **1970**, 316.
5. Interatomic distances in molecules and ions, Chem. Soc. Special Publ., No. 11, London 1958.
6. Levison, K. A., Perkins, P. G.: Theoret. chim. Acta (Berl.) **14**, 206 (1969).
7. McAloon, B. J., Perkins, P. G.: Theoret. chim. Acta (Berl.) **22**, 304 (1971).
8. Marsmann, H., Groenweghe, L. C. D., Schaad, L. J., Van Wazer, J. R.. J. Amer. chem. Soc. **92**, 6107 (1970).
9. Pople, J. A., Santry, D. P., Segal, G. A.: J. chem. Physics **43**, S129 (1965).
10. Van Wazer, J. R.: Phosphorus and its compounds, Vol. 1, New York-London: Interscience 1958.

Prof. P. G. Perkins
Dept. of Pure and Applied Chemistry
University of Strathclyde
Glasgow, C. 1, Scotland

Theoret. chim. Acta (Berl.) 24, 107—110 (1972)
© by Springer-Verlag 1972

Freie Elektronenpaare in lokalisierten CNDO/2-Wellenfunktionen der Stickstoffverbindungen

R. Polák und P. Rosmus*

Institut für Physikalische Chemie, Tschechoslowakische Akademie der Wissenschaften
Praha, Tschechoslowakei

Eingegangen am 24. Februar 1971

Free Electron Pairs in Localized CNDO/2 *Wave Functions of Nitrogen Compounds*

The method for constructing hybrid orbitals described earlier is now used for the analysis of CNDO/2 wave functions of molecules containing nitrogen atoms in order to get information on the type of hybridization of nitrogen "lone pair" orbitals in various compounds.

1. Einleitung

Eine kürzlich beschriebene Methode der „lokalisierten natürlichen Orbitale" [1, 2] gestattet eine einfache Konstruktion der optimalen streng lokalisierten Orbitale in der Basis der Hybridorbitale.

Dieses Verfahren wird in der vorliegenden Arbeit zur Lokalisierung der leicht zugänglichen CNDO/2-Wellenfunktionen angewandt, um die Eigenschaften dieser Funktionen bei der Lokalisierung zu testen (vgl. [3, 4]), und Aussagen über die Hybridisierung am Stickstoffatom in verschiedenen Stickstoffverbindungen zu gewinnen.

2. Rechenverfahren

Die Bedingung für die Konstruktion der optimalen streng lokalisierten Orbitale [1, 2] ist durch die maximale Projektion in den durch die besetzten kanonischen CNDO/2-Molekülorbitale definierten Raum gegeben

$$n = \max\,[\mu^{+} \varrho \mu]\,,$$

wobei μ die lokalisierten Funktionen, ϱ die spinlosen Dichtematrizen 1. Ordnung und n die Besetzungszahlen der entsprechenden lokalisierten Funktionen sind. Die Methode gehört zu den sog. allgemeinen externen Methoden [5], denn die Bestimmung der optimalen Hybridorbitale hängt von der Wahl der am streng lokalisierten Orbital beteiligten Atomorbitale ab. Die Konstruktion der lokalisierten Orbitale ist im Gegensatz zu der in [3, 4] verwendeten semiempirisch modifizierten Edmiston-Ruedenberg-Methode [6] nicht an die Verwendung der CNDO-Zweiteilchenintegrale gebunden.

Die für die Konstruktion der spinlosen Dichtematrix verwendeten kanonischen Molekülorbitale wurden mit der CNDO/2-Methode [7] in ihrer ursprünglichen Parametrisierung gewonnen. Für die in den Tabellen aufgeführten

---

* Jetzige Adresse: Institut und Zentrum für Theoretische Chemie der Universität Frankfurt am Main, Robert-Mayer-Str. 11, D-6000 Frankfurt am Main, Deutschland.

Moleküle mit der Bezeichnung *E* wurden die genauen experimentellen Geometrien [8], für die Moleküle mit der Bezeichnung *I* die idealisierten Geometrien verwendet. Im letzteren Fall wurden $r_{NH} = 1$ Å, $r_{N=N} = 1{,}25$ Å, $r_{C=N} = 1{,}29$ Å, $r_{C-H} = 1{,}09$ Å, $r_{C=O} = 1{,}25$ Å, $r_{C-N} = 1{,}30$ Å, $r_{OH} = 0{,}96$ Å und alle Winkel bei der klassischen sp^2-Hybridisierung zu 120° gewählt. In Pyridin betrug $r_{C-N} = r_{C-C} = 1{,}39$ Å, in HNC $r_{NC} = 1{,}18$ Å, in CN^- $r_{CN} = 1{,}15$ Å, in H_2NNO_2 $r_{NN} = 1{,}4$ Å und $r_{NO} = 1{,}18$ Å, wobei die NH_2-Gruppe aus N_2H_4 übernommen wurde. In HOCN betrug der HOC-Winkel 110°.

3. Ergebnisse und Diskussion

Zur Charakterisierung der streng lokalisierten freien Elektronenpaare liefert das angewandte Verfahren zwei Kenngrößen: Den mit der höchsten Besetzungszahl verknüpften Spaltenvektor (Hybridorbital) der Matrix μ, und die entsprechende Besetzungszahl des streng lokalisierten Orbitals. Diese Besetzungszahl stellt gleichzeitig einen Maßstab dafür dar, inwieweit eine strenge Lokalisierung im vorgeschriebenen Sinne möglich ist. Die streng lokalisierten Funktionen der freien Elektronenpaare unterscheiden sich von den früher definierten optimalen Hybridorbitalen [2] dadurch, daß die Orthogonalitätsbedingung für die an einem Atom lokalisierten Hybridorbitale nicht in Betracht gezogen wurde. Bei der Konstruktion aller an einem Atom lokalisierten Hybridorbitale wäre allgemein eine zusätzliche Annahme [9] notwendig, um Schwierigkeiten mit der möglichen Entartung der höchsten Besetzungszahl zu umgehen (vgl. [2]).

Ausgehend von der klassischen Hybridvorstellung sind die Ergebnisse in den Tabellen 1, 2 und 3 zusammengestellt. Auch bei den streng lokalisierten Funktionen kann in den meisten Fällen zwischen den einzelnen Hybridtypen unterschieden werden. Der *s*-Charakter, mit Ausnahme der fluorsubstituierten Verbindungen, liegt allerdings um 10–20% höher, als es der klassischen Hybridisierung entsprechen würde.

Wie aus den Besetzungszahlen hervorgeht, lassen sich die freien Elektronenpaare in einigen Verbindungen nicht genau lokalisieren, wie z.B. in HNCO, wo nach diesen Berechnungen am Stickstoffatom kaum ein freies Elektronenpaar formuliert werden kann. In *trans*-Verbindungen sind die freien Elektronenpaare besser definierbar als in *cis*-Verbindungen, wobei dieser Effekt mit einer Erniedrigung des *s*-Charakters in *trans*-Verbindungen begleitet wird.

Tabelle 1. Charakter der freien Elektronenpaare in Stickstoffverbindungen des sp^3-Typs

Verbindung		% *s*-Charakter	Besetzungszahl	Ladungsdichte am N-Atom (in 10^{-3} AE)
E NH_3	(C_{3v})	38,14	2,0000	–234
E NF_3	(C_{3v})	72,08	2,0000	373
E H_2NNH_2	(90°, C_2)	29,71	1,9894	–155
I H_2NNO_2	(C_s)	37,47	1,9959	–211
E H_2NOH	(C_s) *cis*	41,74	1,9958	–102
E H_2NOH	(C_s) *trans*	40,65	1,9992	–115

Tabelle 2. Charakter der freien Elektronenpaare in Stickstoffverbindungen des sp^2-Typs

erbindung			%s-Charakter	Besetzungszahl	Ladungsdichte am N-Atom (in 10^{-3} AE)
NO_2^-	(C_{2v})		57,37	2,0000	84
HNCO	(C_s)		45,79	1,8278	−370
H_2CNH	(C_s)		44,54	1,9690	−171
HNNH	(C_{2v}) *cis*		54,85	1,9815	− 55
HNNH	(C_{2h}) *trans*		51,58	1,9936	− 71
FNNF	(C_{2v}) *cis*		64,42	1,9758	131
FNNF	(C_{2h}) *trans*		60,45	1,9898	122
Pyridin	(C_{2v})		45,95	1,9751	−150
$HCONH_2$	(C_s)		0	1,7821	−265
NH_2CONH_2	(C_{2v})		0	1,8195	−312
${}^{a}NH_2CNHNH_2$	(C_s)	N_1	0	1,8433	−304
		N_2	48,21	1,9658	−451
		N_3	0	1,8397	−308

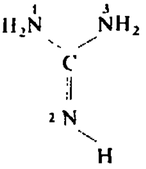

Tabelle 3. Charakter der freien Elektronenpaare in Stickstoffverbindungen des sp-Typs

Verbindung			%s-Charakter	Besetzungszahl	Ladungsdichte am N- bzw. C-Atom (in 10^{-3} AE)
E N_2	$(D_{\infty h})$		68,56	2,0000	
I CN^-	$(C_{\infty v})$	N	60,22	2,0000	−588
		C	68,08	2,0000	−412
E HCN	$(C_{\infty v})$		65,16	1,9916	−101
I HNC	$(C_{\infty v})$	N	0	1,3385	− 62
		C	73,65	1,9887	− 87
E NCCN	$(D_{\infty h})$		64,83	1,9952	− 98
E CH_3CN	(C_{3v})		66,24	1,9911	−262
E H_2NCN	(C_{2v})	N_1	0	1,8845	−229
		N_2	67,91	1,9923	−227
I HOCN	(C_s)		67,73	1,9887	−186
E FCN	$(C_{\infty v})$		68,74	1,9859	−165
E H_2CN_2	(C_{2v})	C	0	1,4830	−248
		N_1	84,29	1,3302	298
		N_2	74,34	1,9967	131
E N_3^-	$(D_{\infty h})$		75,64	1,9968	−723
E N_2O	$(C_{\infty v})$		75,60	1,9960	− 55

Ein Vergleich des Substituenteneinflusses zeigt in den meisten Fällen, daß die s-Charaktere der lokalisierten freien Elektronenpaare qualitativ der von Bent aufgestellten Regel [11] entsprechen (vgl. [3, 4, 10]). Der Hybridcharakter wird überwiegend durch die Topologie des Moleküls und durch die Eigenschaften der unmittelbar benachbarten Atome bestimmt. Am stärksten macht sich in den lokalisierten CNDO-Wellenfunktionen der Einfluß der elektronegativen Fluor- und Sauerstoffatome bemerkbar.

Bei Verbindungen des XCN-Typs sinkt zwar die negative Ladungsdichte am Stickstoffatom in der Reihenfolge $CH_3 > NH_2 > OH > F$, der *s*-Charakter der freien Elektronenpaare aber bleibt ziemlich konstant. Die Unvollständigkeit der Lokalisierung gestattet hier allerdings keine genauere Abstufung der *s*-Charaktere.

Literatur

1. Polák, R.: Theoret. chim. Acta (Berl.) **14**, 163 (1969).
2. — Int. J. quantum Chem. **4**, 271 (1970).
3. Trindle, C., Sinanoğlu, O.: J. Amer. chem. Soc. **91**, 853 (1969).
4. England, W., Gordon, M. S.: J. Amer. chem. Soc. **91**, 6864 (1969).
5. Ruedenberg, K.: Modern quantum chemistry, Vol. 1, S. 85. Ed. Sinanoğlu, O.; New York: Academic Press Inc. 1965.
6. Edmiston, C., Ruedenberg, K.: Rev. mod. Physics **35**, 457 (1963).
7. Pople, J. A., Segal, G. A.: J. chem. Physics **44**, 3289 (1966)
8. Tables of interatomic Distances. London: The Chemical Society 1958.
9. Polák, R.: In Vorbereitung
10. Magnasco, V., Perico, A.: J. chem. Physics **47**, 971 (1967).
11. Bent, H. A.: Chem. Rev. **61**, 275 (1961).
12. Trindle, C., Sinanoğlu, O.: Sigma molecular orbital theory, S. 209. Ed. Sinanoğlu, O., Wiberg, K. B., New Haven and London: Yale University Press 1970.

Dr. Rudolf Polák
Institut für Physikalische Chemie
Tschechoslowakische Akademie
der Wissenschaften
Praha 2, Máchova 7, Tschechoslowakei

Theoret. chim. Acta (Berl.) 24, 111—116 (1972)
© by Springer-Verlag 1972

Excited State Wave Functions

I. Comparison of the Messmer and Rayleigh-Ritz Variational Methods in the Case of Hydrogen

A. C. Brett and T. W. Dingle
Department of Chemistry, University of Victoria, Victoria, B. C., Canada

Received August 23, 1971

Wave functions and energies were calculated for the $2s$, $3p_0$, and $4d_0$ states of the hydrogen atom using the Messmer and Rayleigh-Ritz variational methods with minimization of the second eigenvalue. The wave functions were linear expansions of Gaussian functions and both linear and exponential parameters were varied. Except for the two term expansions, calculated values of the energies and expectation values, $\langle r^{-1}\rangle$, $\langle r\rangle$ and $\langle r^2\rangle$ were within two percent of the true values for both methods.

1. Introduction

A variational method for obtaining the wave functions of excited states has been proposed recently by Messmer [1, 2]. He has stated that this method is free from the restriction that the excited state wave function must be orthogonal to all the true wave functions of states of the same symmetry and of lower energy. The basis of the method is a minimization of the quantity ε^2/Δ where $\varepsilon = E - W$ and $\Delta = \langle\Phi|(H-E)^2|\Phi\rangle$. $E = \langle\Phi|H|\Phi\rangle$ where H denotes the true Hamiltonian, W the true energy, and Φ an approximate wave function for the excited state.

Messmer has argued that minimization of ε^2/Δ produces a wave function which is the best approximation to the true wave function for the system over the whole of configuration space, i. e., that the overlap between the true and approximate wave function is maximized. He has also suggested that a possible criterion for testing the validity of this contention is comparison of the values of the quantities $\langle r^{-1}\rangle$, $\langle r\rangle$ and $\langle r^2\rangle$, computed from the approximate wave function, with known values for these quantities.

The purpose of the work described here was to investigate the Messmer method as applied to a simple system. We chose to work with the hydrogen atom, using Gaussian-type functions of the form:

$$\Phi_{l,m} = \sum_i c_i r^l \exp(-\eta_i r^2)\, Y_{l,m}(\theta, \phi) \qquad (1)$$

to approximate the $2s$, $3p_0$ and $4d_0$ states. The hydrogen atom seemed to be a reasonable system to study since it is simple and exact values for W, $\langle r^{-1}\rangle$, $\langle r\rangle$ and $\langle r^2\rangle$ are known. Moreover, there is at present, considerable interest in the use of Gaussian-type functions to approximate molecular wave functions.

2. Application of the Messmer Method

Since the approximate wave functions (1) are not normalized, E and Δ must be defined so as to include the overlap integral. Therefore,

$$E = \langle H\rangle / \langle S\rangle$$

and (2)

$$\Delta = \langle H^2\rangle / \langle S\rangle - E^2 ,$$

where $\langle H\rangle = \langle \Phi_{l,m} | H | \Phi_{l,m}\rangle$, $\langle H^2\rangle = \langle \Phi_{l,m} | H^2 | \Phi_{l,m}\rangle$ and $\langle S\rangle = \langle \Phi_{l,m} | \Phi_{l,m}\rangle$. The condition that ε^2/Δ be minimal, *viz.*, $\delta(\varepsilon^2/\Delta) = 0$, gives

$$2\delta\varepsilon - (\varepsilon/\Delta)\,\delta\Delta = 0 . \tag{3}$$

Now

$$\varepsilon = \langle H\rangle / \langle S\rangle - W$$

and

$$\Delta = \langle H^2\rangle / \langle S\rangle - (\langle H\rangle / \langle S\rangle)^2 ,$$

therefore, for a given W we have

$$\delta\varepsilon = \delta\langle H\rangle / \langle S\rangle - (\langle H\rangle / \langle S\rangle^2)\,\delta\langle S\rangle \tag{4}$$

and

$$\begin{aligned}\delta\Delta = {} & \delta\langle H^2\rangle / \langle S\rangle - (\langle H^2\rangle / \langle S\rangle^2)\,\delta\langle S\rangle - 2(\langle H\rangle / \langle S\rangle^2)\,\delta\langle H\rangle \\ & + 2(\langle H\rangle^2 / \langle S\rangle^3)\,\delta\langle S\rangle .\end{aligned} \tag{5}$$

Substitution of (4) and (5) into (3) gives

$$2\delta\langle H\rangle - (E+W)\,\delta\langle S\rangle - (\varepsilon/\Delta)\,(\delta\langle H^2\rangle - 2E\delta\langle H\rangle + E^2\delta\langle S\rangle) = 0 \tag{6}$$

after rearrangement.

To find the trial function which satisfies Eq. (6), the exponential parameters, η_i, and the linear coefficients, c_i, are varied in a nested fashion. The exponential parameters are varied by a direct (pattern) search technique [3]. For each set of values given for the η_i by the search routine, ε^2/Δ is minimized with respect to the c_i. This latter process yields in each case, a set of linear equations of which the following is the i^{th} member:

$$\begin{aligned}\sum_j c_j \{ & 2H_{ij} + 2H_{ji} - (E+W)(S_{ij} + S_{ji}) \\ & - (\varepsilon/\Delta)\,[H^2_{ij} + H^2_{ji} - 2E(H_{ij} + H_{ji}) + E^2(S_{ij} + S_{ji})]\} = 0 ,\end{aligned} \tag{7}$$

where

$$H_{ij} = \langle \phi^i_{l,m} | H | \phi^j_{l,m}\rangle , \quad H^2_{ij} = \langle \phi^i_{l,m} | H^2 | \phi^j_{l,m}\rangle ,$$

$S_{ij} = \langle \phi^i_{l,m} | \phi^j_{l,m}\rangle$ and $\phi^i_{l,m}$ denotes the i^{th} term in (1). If E were known, then the equations represented by (7) could be solved immediately as an eigenvalue problem of the form $(\boldsymbol{A} - (\varepsilon/\Delta)\,\boldsymbol{B})\,\boldsymbol{C} = 0$, or

$$(\boldsymbol{B}^{-1}\boldsymbol{A} - (\varepsilon/\Delta)\,\boldsymbol{I})\,\boldsymbol{C} = 0 , \tag{8}$$

where the elements of the arrays $\boldsymbol{A}$ and $\boldsymbol{B}$ have the form

$$A_{ij} = 2H_{ij} + 2H_{ji} - (E+W)(S_{ij} + S_{ji}) ,$$

$$B_{ij} = H^2_{ij} + H^2_{ji} - 2E(H_{ij} + H_{ji}) + E^2(S_{ij} + S_{ji})$$

and where $\boldsymbol{C}$ denotes the array of linear coefficients.

Since E is not known *a priori*, an iterative calculating procedure must be employed. For an initial trial E, (8) is solved for (ε/Δ) and the array of coefficients $\boldsymbol{C}$. The vector of coefficients corresponding to the *second* lowest eigenvalue (ε/Δ) is selected from $\boldsymbol{C}$. These coefficients are used to compute another value for E according to Eq. (2). This new E is then used to solve (8) again. The procedure just described is repeated until the trial E and the next calculated value of E are consistent. ε^2/Δ is then calculated. The exponential parameters are changed by the search routine and the iterative procedure is repeated. This nested variation of the linear and non-linear parameters is continued until ε^2/Δ attains a stationary value.

Table 1. Results obtained with the Messmer method

	E	$\langle r^{-1}\rangle$	$\langle r\rangle$	$\langle r^2\rangle$
$2s$ orbital				
2 terms	−0.1164	0.2451	6.141	44.68
3 terms	−0.1236	0.2493	5.993	41.73
4 terms	−0.1246	0.2502	5.966	41.19
true	−0.1250	0.2500	6.000	42.00
$3p_0$ orbital				
2 terms	−0.05367	0.1094	12.59	183.9
3 terms	−0.05533	0.1108	12.46	177.9
4 terms	−0.05546	0.1111	12.43	176.6
true	−0.05556	0.1111	12.50	180.0
$4d_0$ orbital				
2 terms	−0.03058	0.06162	21.09	510.3
3 terms	−0.03118	0.06240	20.92	497.5
4 terms	−0.03121	0.06244	20.90	496.3
true	−0.03125	0.06250	21.00	504.0

The proceeding procedure was carried out using 2, 3 and 4 term expansions of the type given by Eq. (1) to describe each of the $2s$, $3p_0$ and $4d_0$ states of the hydrogen atom. The appropriate known true value for W was used in each case. The functions thus determined were used to calculate values for $\langle r^{-1}\rangle$, $\langle r\rangle$ and $\langle r^2\rangle$. The results are given in Table 1.

The reason for choosing the second eigenvalue was to ensure that the approximate wave function approached the true wave function for the excited state under consideration as ε^2/Δ approached zero. Messmer points out that both ε^2 and Δ must approach zero as ε^2/Δ approaches zero if the approximate wave function is to be reasonably close to the true wave function. Some calculations were done using the vector of coefficients associated with the lowest eigenvalue and these gave very poor wave functions. In this case ε^2 can be made equal to zero, but Δ is not approaching zero in any reasonable manner; hence, the above criteria are not satisfied. These results emphasize the need for choosing the appropriate eigenvalue.

3. Application of the Rayleigh-Ritz Method

The results obtained with the Messmer method as outlined above, were compared with wave functions of the form (1), calculated from a modification of the Rayleigh-Ritz variational method. Variation of the linear and non-linear (exponential) parameters was again carried out in a nested fashion. For each set of the exponential parameters given by the direct search routine, secular equations of the form

$$(S^{-1}H - EI)C = 0 \tag{9}$$

were solved for the eigenvalues, E, and the eigenvectors, C (H, S and I denote the Hamiltonian, Gram and identity matrices respectively). The exponential parameters were varied and Eq. (9) was solved for each variation until a minimal second lowest eigenvalue was achieved. The vector of coefficients corresponding to the second eigenvalue was selected from C. The wave function thus determined was used to compute values for $\langle r^{-1}\rangle$, $\langle r\rangle$ and $\langle r^2\rangle$ which are reported in Table 2. The energy values obtained for the 2s state are identical to those reported by Reeves [4] using a similar method and very similar expansions.

Table 2. Results obtained with the Rayleigh-Ritz method

	E	$\langle r^{-1}\rangle$	$\langle r\rangle$	$\langle r^2\rangle$
2s orbital				
2 terms	−0.1168	0.2340	6.355	47.68
3 terms	−0.1237	0.2479	6.016	42.04
4 terms	−0.1246	0.2491	5.982	41.41
true	−0.1250	0.2500	6.000	42.00
$3p_0$ orbital				
2 terms	−0.05369	0.1074	12.82	190.8
3 terms	−0.05533	0.1104	12.49	178.6
4 terms	−0.05547	0.1108	12.45	177.1
true	−0.05556	0.1111	12.50	180.0
$4d_0$ orbital				
2 terms	0.03059	0.06116	21.29	520.4
3 terms	−0.03118	0.06236	20.94	498.6
4 terms	−0.03121	0.06242	20.92	496.9
true	−0.03125	0.06250	21.00	504.0

4. Discussion and Conclusions

The percentage deviation of the calculated value from the true value was determined in each case for $\langle r^{-1}\rangle$, $\langle r\rangle$ and $\langle r^2\rangle$. These values are recorded in Table 3. Examination of this table shows that the Messmer method, as described in Section 2, gives better results for the calculated quantities with the two term expansions than does the Rayleigh-Ritz method. Moreover, it yields better results for $\langle r^{-1}\rangle$ with the three and four term expansions. However, on the whole the Rayleigh-Ritz method gives better results for $\langle r\rangle$ and $\langle r^2\rangle$. Thus it would seem that the Messmer method yields wave functions which are better in the vicinity of the nucleus. This conclusion was confirmed by calculating the root mean square

Table 3. Percentage deviation of calculated values of $\langle r^{-1}\rangle$, $\langle r\rangle$ and $\langle r^2\rangle$ from the true values using the Messmer and Rayleigh-Ritz wave functions

	$\langle r^{-1}\rangle$		$\langle r\rangle$		$\langle r^2\rangle$	
	Messmer	Rayleigh-Ritz	Messmer	Rayleigh-Ritz	Messmer	Rayleigh-Ritz
$2s$ orbital						
2 terms	−1.96	−6.40	2.35	5.92	6.38	13.5
3 terms	−0.28	−0.84	−0.12	0.27	−0.64	0.10
4 terms	0.08	−0.36	−0.57	−0.30	−1.93	−1.40
$3p_0$ orbital						
2 terms	−1.53	−3.33	0.72	2.56	2.17	6.00
3 terms	−0.27	−0.63	−0.32	−0.08	−1.17	−0.78
4 terms	0.00	−0.27	−0.56	−0.40	−1.89	−1.61
$4d_0$ orbital						
2 terms	−1.41	−2.14	0.43	1.38	1.25	3.25
3 terms	−0.16	−0.22	−0.38	−0.28	−1.29	−1.07
4 terms	−0.10	−0.13	−0.48	−0.38	−1.53	−1.41

Table 4. Overlap of approximate with true wave function

	Rayleigh-Ritz Method	Messmer Method
$2s$ orbital		
2 terms	0.992152	0.994997
3 terms	0.999287	0.999324
4 terms	0.999339	0.999322
$3p_0$ orbital		
2 terms	0.994861	0.996927
3 terms	0.999256	0.999255
4 terms	0.999174	0.999159
$4d_0$ orbital		
2 terms	0.995887	0.997130
3 terms	0.999196	0.999180
4 terms	0.999117	0.999105

deviation of the wave function from the true wave function in the vicinity of the nucleus. Again the Messmer method yielded a better wave function, indicating that the Messmer functions fit the true wave function better in the least squares sense in this region.

Another criterion for assessing the goodness of the approximate wave functions is to calculate the overlap between the approximate and the true wave function. The results of such calculations are shown in Table 4. They show that the Messmer method gives significantly better wave functions only for the two term expansion.

Except for the results obtained with the two term expansion, the Messmer method as we have applied it, does not seem to give significantly better wave functions compared to those obtained with the Rayleigh-Ritz method. In view of the much greater amount of effort required in using the Messmer method, as measured in terms of computer time and preliminary mathematical manipulation, there is some question in our minds as to its superiority over some modification of the established variational method.

One possible approach is suggested by the method we used to obtain the excited states within the context of the Rayleigh-Ritz method. If a wave function is approximated by a linear combination of functions, then substitution of this approximation into the expression for the energy, followed by minimization of the energy with respect to the linear parameters, leads to the familiar secular equation. If there are N linear terms, then there will be N solutions to the secular equation. It can be shown [5] that the k^{th} lowest eigenvalue is an upper bound to the k^{th} lowest state of the symmetry under consideration. Usually, the non-linear (exponential) parameters are varied so as to give the lowest possible value for the lowest eigenvalue. This leads to the best possible basis set of the given mathematical form for the lowest state. However, it is unlikely that this will be a good basis set to represent the excited states. If the appropriate eigenvalue is minimized with respect to the non-linear parameters, then it should produce the best basis set to represent the excited state.

Our calculations show that this is true for the hydrogen atom. Hylleraas [6] has carried out variational calculations of this type on the helium atom and obtained reasonable energies for the excited state. Recently, Bishop *et al.* [7, 8] have done calculations on some excited states of H_2O and NH_3 using one-center multiconfigurational wave functions containing orthogonalized Slater type functions. They have minimized the appropriate eigenvalue with respect to the exponential parameters for each state. They obtained the correct order for the states and the energy differences between the states were quite reasonable. Moreover, the predicted nuclear geometries were consistent with the known experimental data. Some unpublished data of ours on the He atom indicate that the energies for the excited states are better than for the ground state to the same level of approximation. We are continuing to explore this method of obtaining excited states.

Acknowledgements. Financial assistance from the National Research Council of Canada is gratefully acknowledged.

References

1. Messmer, R.: Theoret. chim. Acta (Berl.) **14**, 319 (1969).
2. Choi, J. H., Lebeda, C. F., Messmer, R. P.: Chem. Physics Letters **5**, 503 (1970).
3. Hooke, R., Jeeves, T. A.: J. Ass. Comp. Mach. **8**, 212 (1961); Ludwig, O. G.: Ph. D. Thesis, Carnegie Institute of Technology, Pittsburgh, Pennsylvania, USA, 1962.
4. Reeves, C. M.: J. chem. Physics **39**, 1 (1963).
5. Gould, S. H.: Variational methods for eigenvalue problems, 2nd ed., p. 75–79. Oxford: University Press 1966; see also MacDonald, J. K. L.: Physic. Rev. **43**, 8310 (1933).
6. Hylleraas, E. A.: Z. Physik **65**, 759 (1930).
7. Bishop, D. M., Wu, A. A.: J. chem. Physics **54**, 2917 (1971).
8. LeClerc, J.-C., Takahata, Y.: J. molecular Spectroscopy **39**, 79 (1971).

Prof. Thomas Dingle
University of Victoria
Department of Chemistry
Victoria, British Columbia, Canada

Instructions to Authors

1. *Manuscripts* should be submitted in duplicate, typed in double-line spacing on one side of the paper only; they will not be returned to the authors. Form and contents should be carefully checked to exclude the need for corrections in proof. A charge will be made for changes introduced after the manuscript has been set in type.

Formulae should be typewritten whenever possible, special attention being given to the placing of indices and exponents so that they are recognizable as such even though there is no difference in size. Formulae should preferably be written in a "linear" form (e.g. $\exp(-\varepsilon/kT)$ instead of $e^{-\frac{\varepsilon}{kT}}$). Special typefaces (Greek, Script) should be shown by underlining in color. To avoid confusing the printer, please use red for Greek and green for Script, and underline in brown for bold face. Characters which are easily confused, e. g. 0 (zero) and capital O (letter) or 1 (figure one) and small l (letter), should have some special distinguishing mark. When formulae are inserted by hand, small letters should be underlined once and capital letters twice.

2. *Illustration copies* (graphs and structural formulae) should be drawn in Indian ink in clean uniform lines and sent in on separate sheets. Captions, which should be brief, should be typed separately and attached to the manuscript.

3. Original papers should be preceded by a *summary* (not more than 100 words) in English, German and French. (The editorial staff is willing to translate English summaries if asked.) Short notes need only an English summary. Papers not written in English should have an *English title* for use by such journals as Current Contents.

4. *Literature references* should be numbered and listed at the end of the paper. They should be cited as follows: journal papers — initials and names of all authors, journal in the accepted abbreviation, volume and page number, year; books — names of authors, full title, edition, place, publisher and year. References should be cited in the text by number.

5. 75 *offprints* of each paper will be supplied free of charge; additional copies may be ordered at cost price.

6. *Editorial enquiries* should be addressed to:

Prof. Dr. Hermann Hartmann, Theoretica Chimica Acta, Institut für physikalische Chemie der Universität, Robert-Mayer-Straße 11, D-6000 Frankfurt am Main 1

Manuscripts should be sent to the Editor or to one of the Co-editors:

Prof. Dr. Carl J. Ballhausen, Chemical Laboratory IV, H. C. Ørstedinstitutet Universitetsparken 5, København Ø, Danmark,

Prof. Dr. Ronald D. Brown, Monash University, Department of Chemistry, P. O. Box 92, Clayton, Victoria, Australia 3168,

Prof. Dr. Edgar Heilbronner, Physikalisch-Chemisches Institut der Universität Basel, CH-4000 Basel, Klingelbergstraße 80,

Prof. Dr. Jan A. A. Ketelaar, Laboratory for Electrochemistry, Plantage Muidergracht 14, Amsterdam-C, Nederland,

Prof. Dr. Masao Kotani, 36-3 Sanno 3 chome, Ota-ku, Tokyo, Japan,

Prof. Dr. Jaroslav Koutecký, Československá Akademie Věd. Ústav Fyzikální Chemie, Praha 2-Vinohrady, Máchova 7, ČSSR,

Prof. Dr. Jack W. Linnett, Department of Physical Chemistry, Lensfield Road, Cambridge, England,

Prof. Dr. E. E. Nikitin, Institute of Chemical Physics, Academy of Sciences, Vorobyevskoye Chaussée 2b, Moskwa V-334, USSR,

Prof. Dr. Ralph G. Pearson, Department of Chemistry, Northwestern University, Evanston, Illinois 60201, USA,

Prof. Dr. Bernard Pullman, Université de Paris, Institut de Biologie physicochimique, 13, rue Pierre Curie, Paris V, France,

Prof. Dr. Klaus Ruedenberg, Department of Chemistry, Iowa State University of Science and Technology, Ames, Iowa 50010, USA,

Prof. Dr. Camille Sandorfy, Université de Montréal, Case Postale 6128, Montréal, Canada,

Prof. Dr. Massimo Simonetta, Istituto di Chimica Fisica dell'Università di Milano, Via Saldini, 50, Milano, Italia,

Prof. Dr. Oktay Sinanoğlu, Department of Chemistry, Yale University, 225 Prospect Street, New Haven, Conn. 06520, USA.

7. All *business communications* should be sent to:

Springer-Verlag, D-6900 Heidelberg 1, Postfach 1780, Tel. (06221) 49101, Telex 04-61723

Hinweise für die Autoren

1. *Manuskripte* werden mit einer Kopie, auf einseitig beschriebenen Blättern mit doppeltem Zeilenabstand erbeten; sie werden nicht mehr an die Verfasser zurückgesandt. Die Manuskripte müssen formal wie inhaltlich so durchgearbeitet sein, daß Änderungen in den Korrekturfahnen unnötig sind. Nachträgliche (vom Manuskript abweichende) Korrekturen müssen den Autoren in Rechnung gestellt werden.

Alle Formeln sind möglichst mit der Maschine zu schreiben. Dabei ist darauf zu achten, daß Indices und Exponenten trotz des fehlenden Größenunterschiedes genau als solche zu erkennen sind. Besondere Lettern (griechische, Script) sind durch farbige Unterstreichungen zu kennzeichnen. Zur Vereinfachung für den Setzer wird gebeten, griechische Buchstaben rot, Scripttypen grün und Halbfette braun zu unterstreichen. Auch einander ähnliche Zeichen, z. B. 0 (Null) und O (Buchstabe) oder 1 (Eins) und l (Buchstabe) sind besonders zu kennzeichnen. Bei handgeschriebenen Formeln ist bei allen vorkommenden Alphabeten zwischen Groß- und Kleinbuchstaben (durch doppeltes bzw. einfaches Unterstreichen) zu unterscheiden.

2. *Abbildungsvorlagen* werden als Tuschezeichnungen mit tiefschwarzem einheitlichen Strich auf besonderen Blättern erbeten. Kurze Abbildungsunterschriften sollen getrennt davon am Schluß des Manuskripts beigefügt werden.

3. Bei Originalarbeiten wird um je eine *Zusammenfassung* (nicht über 100 Wörter) in Englisch, Deutsch und Französisch, bei Kurzmitteilungen um eine in Englisch gebeten. (Übersetzung ins Französische kann in der Redaktion vorgenommen werden.) Nichtenglischen Arbeiten soll außerdem eine englische Titelübersetzung beigefügt werden.

4. *Literaturangaben* sind am Schluß der Arbeit zusammenzustellen und zu numerieren. Sie enthalten Initialen und Namen aller Autoren, den nach den internationalen Regeln gekürzten Zeitschriftentitel, Band-, Seiten- und Jahreszahl; bei Büchern Autorennamen, vollen Titel, Auflage. Ort, Verlag und Jahr. Zitierung im Text erfolgt mit Nummer.

5. Von jeder Arbeit werden 75 *Sonderdrucke* kostenlos zur Verfügung gestellt. Weitere Separata können von den Autoren zum Selbstkostenpreis bezogen werden.

6. *Redaktionelle Anfragen* sind zu richten an:

Theoretica Chimica Acta, Prof. Dr. Hermann Hartmann.

Manuskripte können an alle Mitherausgeber eingesandt werden. Adressen umstehend.

7. Alle die Zeitschrift betreffenden *geschäftlichen Mitteilungen* werden erbeten an den Springer-Verlag, D-6900 Heidelberg 1, Postfach 1780, Tel. (06221) 49101, Fernschr. 04-61723.

Indications pour les auteurs

1. *Les manuscrits* seront envoyés en deux exemplaires dactylographiés au recto seulement. Ils ne seront plus renvoyés aux auteurs. Tant la forme extérieure que le contenu doivent avoir leur aspect définitif, afin que des corrections sur les épreuves ne soient plus nécessaires. Toute correction s'écartant du manuscrit original sera facturée aux auteurs. Dans la mesure du possible les formules doivent être tapées à la machine. On veillera à ce que les indices et les exposants soint facilement reconnaissables lorsqu'ils ne sont pas différenciés par leur taille. Sinon, ils devront être inscrits à la main. Les lettres spéciales (grecques, script) doivent être soulignées en couleur. Pour simplifier le travail du typographe on recommande de souligner en rouge les lettres grecques et en vert les script. Les lettres grasses seront soulignées en brun. Dans la mesure où des caractères manuscrits sont utilisés on distinguera (même pour les caractères latins) les majuscules, qu'on soulignera deux fois, des minuscules, soulignées une fois. Des difficultés spéciales naissent du fait que les machines à écrire ne font pas, en général, de différence entre 0 (zéro) et O (lettre) ainsi qu'entre 1 (un) et l (lettre). Dans ce cas, des signes distinctifs sont absolument indispensables.

2. Des *graphiques* et des formules développées doivent être tracés en lignes noires à l'encre de Chine. Les légendes sont part du texte et sont demandées sur des feuilles séparées à la fin de l'article.

3. Les travaux originaux doivent comporter de brefs *résumés* (100 mots maximum), rédigés dans les 3 langues: anglais, français et allemand. Le résumé des communications brèves doit être rédigé en anglais. (Sur demande, le résumé original peut être traduit par la rédaction, en allemand). Pour faciliter la documantation un titre anglais doit être ajouté à chaque article n'étant pas écrit en anglais.

Les *références* bibliographiques seront numérotées et rassemblées à la fin du texte. Les citations se présenteront comme suit: initiales et noms de tous les auteurs, titre du journal abrégé selon les règles internationales, tome, numéros des pages et année. Les livres seront cités précédés du nom de l'auteur, titre complet, édition, lieu de publication, éditeur et date de parution. Les références dans le texte doivent être indiquées par des numéros.

5. 75 *tirés à part* de chaque article seront remis gratuitement aux auteurs. Pour les exemplaires supplémentaires le prix de revient sera facturé aux auteurs.

6. *Les demandes au rédacteur* doivent être adressées à

Theoretica Chimica Acta, Prof. Dr. Hermann Hartmann.

Les *manuscrits* peuvent être envoyés à tous les co-éditeurs (adresses susmentionnées)

7. Toutes *les communications d'affaires* doivent être adressées à:

Springer-Verlag, D-6900 Heidelberg 1, Postfach 1780, Tel. (06221) 49101, Téléx 04-61723

Theoret. chim. Acta (Berl.) 24, 117—131 (1972)
© by Springer-Verlag 1972

Commentationes

The Shape of Molecules

LELAND CULLEN ALLEN
Department of Chemistry, Princeton University, Princeton, New Jersey 08540, USA

Received August 30, 1971

The two most important molecular shape models are the Valence-Shell-Electron-Pair-Repulsion scheme and the Walsh-Mulliken Diagrams. These models, with illustrative examples, are described and a rigorous quantum mechanical definition of each is stated. A physical-mathematical proof ot their equivalence and of their origin is given along with an analysis of the failures to be expected. The theoretical prediction of bond angles is contrasted with the corresponding prediction of bond lengths, and the low information content inherent to the specification of bond angles shows their determination to be considerably easier than bond lengths.

Die beiden wichtigsten Modelle zur Molekülgeometrie sind das Modell der Valenzelektronen-Paar-Abstoßung und das Walsh-Mulliken-Diagramm. Beide Modelle werden anhand illustrativer Beispiele vorgestellt, eine quantenchemische Definition beider wird gegeben. Ihre physikalische Äquivalenz wird bewiesen; diese Analyse zeigt auch die Grenzen der Modelle. Die theoretische Voraussage von Winkeln wird der von Bindungslängen gegenübergestellt. Da der Informationsgehalt der Winkelspezifikation niedriger ist, ist diese Angabe wesentlich leichter als die der Bindungslängen.

Les deux modèles de forme moléculaire les plus importants sont le schéma de répulsion électronique des paires d'électrons des couches de valence et les diagrammes de Walsh-Mulliken. Ces modèles sont décrits, avec des examples illustratifs, et l'on donne une définition quantique rigoureuse de chacun d'entre eux. Une preuve physicomathématique de leur équivalence et de leur origine est fournie avec une analyse des échecs à attendre. La prédiction théorique des angles de valence est opposée aux prédictions théoriques des longueurs de liaison; le faible contenu informationnel inhérent à la spécification des angles de liaison montre que leur détermination est considérablement plus aisée que celle des longueurs de liaison.

Karl Heinz Hansen

Karl Hansen first attracted my attention in 1963 through his articles on group theory in the ligand field problem and on spin valence theory in the first volume of *Theoretica Chimica Acta.* Hansen's work on spin valence theory showed a fresh and creative approach to electronic structure theory. It marked him as the possessor of a superior intellect and demonstrated his mastery of mathematical technique. It was with keen interest that I followed the great variety and mathematical ingenuity displayed in his theoretical work during the succeeding half-dozen years. As a tribute to Karl, I have chosen to write on the geometry of molecules because our research came closest together on this subject.

I will always recall with pleasure his visit to Princeton in 1966 and the opportunity we had for scientific interchange. At this time I became acquainted with the man himself, and I was fascinated by his character and the nature of his ideas.

Much of his thought had clearly been influenced by the war. Although on opposing sides, the common experiences of low-ranking enlisted men quickly establish a cord of understanding, and I could well sense his terror and excitement in service with his antiaircraft battery. Very much on his mind during his Princeton visit was the planning, anxiety, and frustration attendant to finding a permanent academic position in the reemerging German university establishment. I also learned about the exhilaration Karl felt when driving a car at high speed and about the fatalism which pervaded his thoughts.

In 1967 my visit to Frankfurt was arranged in style by Karl. We had a number of meals together and again the chance to share a wide range of experiences and thoughts. Again I found him a stimulating colleague, and I retain many happy memories of this occasion.

More recently, I had been delighted to learn of Karl's appointment at Bonn. In this period he also undertook close collaboration with experimenters, and this was one promising new aspect in his career development. I was shocked indeed when I received notice of his untimely death. Karl Hansen made unique contributions to theoretical chemistry he would have generated many more had time been allowed him.

Background

Two of the most successful models in all of chemistry are the valence-shell electron-pair repulsion model identified with Sidgwick and Powell [1] and Gillespie and Nyholm [2] and the orbital energy versus angle diagrams associated with Walsh [3] and Mulliken [4]. These two models have dominated the systematization and rationalization of non-transition metal inorganic chemistry and spectroscopy. Even though far more rigorous and accurate quantum mechanical solutions now have been obtained for many polyatomic molecules, these simple models continue to provide the conceptual framework for understanding molecular shape.

Although it has been known for some time that these two models generally provide similar predictions, they appear, at least superficially, to operate on entirely different principles: The valence-shell electron-pair repulsion (VSEPR) model utilizing classical electrostatics, the Walsh diagrams being a manifestation of atomic orbital hybridization with complete neglect of the nuclei and electron-electron interactions.

It is the purpose of this article to demonstrate the physical and mathematical equivalence of these two models and to derive their properties from Schrödinger's equation. Beyond the satisfaction of knowing that these two models are basically similar, the analysis brings out the conditions under which these models fail.

Valence-Shell Electron-Pair Repulsion Model

The original article by Sidgwick and Powell [1] related the angular arrangement of electrons around a central atom to the number of electrons in its outer shell plus the valence of the attached atoms. The resultant number of electron pairs (irrespective of whether lone pairs or bond pairs) was put in one-to-one correspondence with molecular shape: two pairs linear, three pairs a planar triangle, four pairs tetrahedral, five pairs a trigonal bipyramid, six pairs octahedral. These same results derive from the even simpler model of point charges on a spherical surface interacting through the force law $1/(r_{ij})^n$, irrespective of the value of n [5]. Seven particles is an exception [6]. However, both in the models and in nature itself, seven coordination is rare and special, and it is not appropriate for further discussion here because it obscures the central features of the model. The ultimate simplicity of the charges-on-a-sphere model as much as anything else has fixed in people's minds the idea of electrostatic repulsion as the basic origin of inorganic stereochemistry.

Gillespie and Nyholm [2] significantly enhanced the original Sidgwick and Powell model by recognizing a distinction between lone pairs and bond pairs. Lone pairs are closer to nuclear centers than bonds and occupy more space thereby leading them to the additional rule for interaction energies: lone pair – lone pair > lone pair – bond pair > bond pair – bond pair. This greatly increased the precision and scope of the model. By bringing together most all of the existing experimental data and by further refining the model, Gillespie [7] has been able to encompass and bring into systemization a larger body of structural knowledge than has been accomplished ever before. As examples we consider shape predictions for four simple cases. BH_2^+ has four valence electrons, two bond pairs, and therefore a linear configuration. BH_2^- has six valence electrons, two bond pairs plus a boron lone pair. Since lone pair – bond pair interaction energy > bond pair – bond pair interaction energy, the ion is strongly bent. XeF_2 obtains eight electrons from xenon, plus one from each fluorine, yielding three lone pairs and two bond pairs. The arrangement with the lowest electrostatic repulsion energy is the trigonal bipyramid with three lone pairs in a plane perpendicular to the linear F–Xe–F bond axis. The six electron pairs of XeF_4 divide into four bond pairs and two lone pairs. Electrostatic energy is minimized by keeping the lone pairs as far apart as possible, thereby producing a square planar arrangement of fluorines with lone pairs protruding above and below the plane.

A mathematically and physically rigorous definition of the VSEPR model exists, and in order to clearly state this definition, it is worthwhile recalling three of the well-established approximations of electronic structure theory. First is the non-relativistic assumption, second is the complete separation of electronic and vibrational motion (Born-Oppenheimer clamped nuclei). Third is the claim that a single determinant composed of one-electron spin orbitals is a satisfactory approximate solution to Schrödinger equation for predicting molecular geometry with an error of only a few percent. The validity of this assumption stands on consistent numerical results obtained from over a thousand polyatomic *ab initio* wavefunctions constructed during the last dozen years. The invariance of such single-determinant wavefunctions to an arbitrary unitary transformation has long been recognized, and over twenty years ago Lennard-Jones [8] proposed orbitals whose shapes would correspond to the elementary picture of a localized electron-pair bond. More recently Edmiston and Ruedenberg [9] have given a precise prescription for constructing these orbitals and worked out a number of examples [10]. Schematically the total molecular energy may be partitioned into the following components:

$$E_T = KE + V_{ne} + V_{nn} + V_{\mathrm{Coulomb}} - V_{\mathrm{exchange}} .$$

The energy localized orbitals of Edmiston and Ruedenberg are defined by minimizing the V_{exchange} *between different bond orbitals.* In physical terms this makes the quantum mechanical description behave as closely as possible to a classical electrostatic interaction between electron pairs. The numerical calculations they carried out for LiH, BH, NH, FH, Li_2, B_2, Be_2, N_2, F_2, CO, BF, LiF, H_2O, NH_3, C_2H_6, and CH_4 display just the sort of lone-pair and bond-pair charge lobes prescribed by the VSEPR model, and a rigorous, *ab initio* basis for this model is thereby established.

Walsh-Mulliken Diagrams

In his classic set of papers [3] Walsh deduced orbital energy versus bond angle diagrams for a series of generic species: AH_2, AH_3, AB_2, AB_3, HAB, A_3, HAAH, HAB_2 and H_2AB. A and B represent atoms such as C, N and O. His AH_2 diagram is illustrated by the dashed lines of Fig. 1. Only valence electrons are considered. To construct his diagrams, Walsh employed known results on molecular shape, observed molecular excitation energies and simple arguments concerning the mixing and relative weighting of atomic orbitals. These diagrams may be used to predict molecular shape by filling up the energy levels with pairs of valence electrons, summing the energies, and finding the bond angle that yields the smallest sum. For the four valence electrons of BH_2^+ only the lowest two states are occupied and a linear ion results. In BH_2^- the $3a_1$ is also occupied producing a sharply bent ion. An additional two valence electrons are present in H_2O, but they reside in the flat $1b_1$ level and again the molecule is strongly bent. Examples like these im-

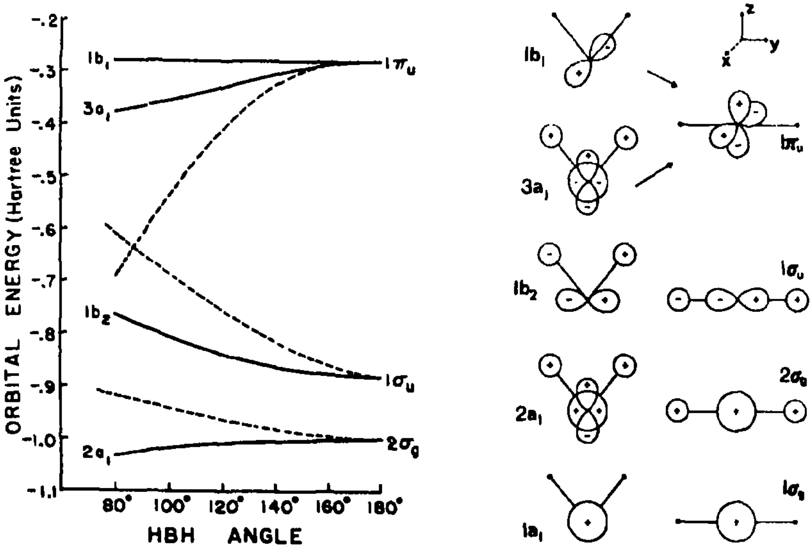

Fig. 1. Walsh-Mulliken Diagram for AH_2 molecules (dashed lines). *Ab initio* one-electron molecular orbital energies for BH_2^+ (solid lines). Right side: atomic orbital mixing for bent and linear AH_2

mediately demonstrate that molecular shape – a bent or linear AH_2 species in our example – is determined solely by the *number* of valence electrons.

In a manner parallel to that described for the VSEPR model, Walsh-Mulliken diagrams can be generated directly from *ab initio*, single-determinant wavefunctions. The one-electron molecular spin orbitals which make up the determinant are expressed as a linear combination of the atomic-like functions mounted on the various nuclear centers:

$$\varphi_i^{\text{Mol.}}(1) = \sum_j C_{ij}\eta_j^{\text{Atom}}(1).$$

The linear coefficients, C_{ij}, are varied to minimize the energy with the molecular orbitals and corresponding orbital energies (ε_i) expressed in canonical (diagonal) eigenvalue form:

$$\mathscr{H}\varphi_i^{\text{Mol.}}(1) = \varepsilon_i\varphi_i^{\text{Mol.}}(1).$$

The solid lines of Fig. 1 result from an *ab initio* calculation of BH_2^+ [11], and *ab initio* Walsh-Mulliken diagrams now exist for over fifty polyatomic molecules [12]. In each case they closely resemble Walsh's original constructs, and they preserve their generic form for sequences of A and B atoms. The atomic orbital mixing combinations allowed by symmetry, along with their irreducible representation labels, are displayed schematically in both linear and bent configurations on the right-hand side of Fig. 1. From the schematics it is obvious that there is an intimate mixture of $2s$ and $2p$ orbitals in $2a_1$ and $3a_1$. Actual calculations reveal that around 90° $2s$ dominates $2a_1$, and correspondingly $2p$ dominates $3a_1$ in this angular range. As noted by Mulliken long ago [13], Walsh neglected a $2s$ contribution from $3a_1$ in the 90° region leading to incorrect slopes for these two molecular orbitals, but fortunately, Walsh's error was not so severe as to vitiate his qualitative conclusions.

There is another way of obtaining bond angles from the molecular orbitals generated by the diagonal eigenvalue equation stated above. This is *via* the second-order ("pseudo") Jahn-Teller perturbation theory [14] and, although entirely equivalent to the Walsh diagram approach, it sometimes provides a useful viewpoint. Bartell has applied it to shape prediction [15], and I note it here for completeness. The scheme starts with a high-symmetry reference configuration-linear for AH_2 systems. Standard perturbation theory arguments then show that the sign of the coefficient of the square of the appropriate normal mode vibration coordinate, S_i, determines whether or not the high-symmetry reference configuration will deform:

$$\left\langle \psi_0 \left| \frac{\partial^2 H}{\partial S_i^2} \right| \psi_0 \right\rangle - 2\sum_n \frac{\left| \left\langle \psi_n \left| \frac{\partial H}{\partial S_i} \right| \psi_0 \right\rangle \right|^2}{E_n - E_0}.$$

The possibility of energy lowering under deformation is controlled by the summation because this term comes in with a negative sign. Thus a bent molecule results when the first excited states are sufficiently low and their symmetry such as to produce non-vanishing matrix elements of the force operator.

In discussing the VSEPR scheme, we noted that the extreme simplicity of the charges-on-a-sphere model appeared to reveal the underlying operating principle through which molecular shape was determined. Several simple semi-empirical and parametric electronic structure schemes have been shown capable of generating Walsh-Mulliken diagrams, and they similarly claim to shed light on the origin of these diagrams. Thus Schmidtke and Preuss [16] were able to reproduce AH_2 and AH_3 diagrams using a Hamiltonian that only contained the one-electron terms: kinetic energy and electron-nuclear attraction. Bingle [17] produced correct AH_2 and AH_3 diagrams from a united atom perturbation theory approach that omits most of the influence of the nuclear framework potential. Reasonable AH_2 and AH_3 diagrams were obtained by Leclerc and Lorquet [18] with extended Hückel theory which employs an attractive bond-forming interaction, but omits explicit expressions for kinetic energy, nuclear framework potential, and electron-electron interactions. A paper by Allen and Russell [19] showed the remarkable degree of parallelism between diagrams generated by extended Hückel and *ab initio* methods, and a series of articles by Gimarc [20] has verified the qualitative capability of extended Hückel theory to produce all nine types of Walsh-Mulliken diagrams.

Equivalence of VSEPR and Walsh-Mulliken Diagrams

In all three sections above we have pointed out the similar shape predictions generally given by VSEPR and Walsh-Mulliken, and this provides circumstantial evidence for the equivalence of these two models. But we seem to be faced with a severe dichotomy when the two models are examined in detail. The electron repulsions which appear to dominate VSEPR can be omitted entirely from theories which satisfactorily construct Walsh-Mulliken diagrams while the details of atomic orbital hybridization that are central to the Walsh-Mulliken diagrams are nowhere put into VSEPR. In spite of these contradictions the two models *are* equivalent and the physical-mathematical proof is given below.

Pauli Principle. In Gillespie's later writings he has stated his belief that it is primarily the workings of the Pauli principle rather than electrostatic repulsion which provides the driving force for VSEPR. This is certainly correct. Two electrons of opposite spin in the same orbital act toward a nearby similar pair as two helium atoms. Their effective repulsion can be represented by an inverse power of r. Opposite spin pairs (in the same orbital) moving on the surface of a sphere will obviously produce the same geometries as the charges-on-a-sphere model. The difference between lone-pairs and bond-pairs is mainly manifest through size and shape rather than charge density, thus the rule:

lone pair – lone pair > lone pair – bond pair > bond pair – bond pair

is a size-Pauli exclusion principle result. This reasoning in no way denies the existence of electrostatic repulsion between bond pairs and lone pairs, but rather shows that shape does not follow directly from simple electrostatics.

Trace Invariance. Unitary transformations of a single determinant wavefunction preserve the trace of the canonical Hamiltonian matrix. That is, the sum of ε_i's over occupied orbitals in the molecular orbital determining eigenvalue equation given in the previous section is unchanged when a transformation to Edmiston-Ruedenberg localized orbitals is made. It is $\sum_i^{\text{val.}} \varepsilon_i$ which is the shape criteria of the Walsh-Mulliken diagrams, and we have already noted that a single determinant *ab initio* wavefunction is adequate to yield both these diagrams and the VSEPR-like localized lone pairs and bond pairs. In fact the localized orbital pictures computed by Edmiston and Ruedenberg [10] were obtained by transforming solutions of the canonical eigenvalue equation, and solutions to this equation have been shown by direct construction capable of generating Walsh-Mulliken diagrams.

Another way to check the equivalence of VSEPR and Walsh-Mulliken is by investigating the symmetry properties of the transformation that takes orbitals from one model to the other. A simple and effective way of doing this for seven of Walsh's generic types has been carried out by Thompson [21]. Assuming a particular point group, he constructs a mechanical ball-and-stick model representing localized bond pairs and lone pairs. Following Gillespie, a lone pair is assumed to preempt more solid angle around a nucleus than a bond pair, and, where ambiguity exists, lone pairs are oriented to match the molecular framework symmetry. Linear combinations of bond pairs and of lone pairs that transform as irreducible representations can generally be made up by inspection or formally by employing character projection operators. Thompson then finds a one-to-one correspondence between the number and symmetry type of molecular symmetry orbitals constructed in this manner and the corresponding number and type found in Walsh's original diagrams. For AH_3 and AB_3 types Thompson also works out molecular symmetry orbitals for the now well-established T-shaped molecules, such as ClF_3 and BrF_3. Walsh did not include this possibility, and Thompson suggests that these species may be outside the Walsh systemization scheme. This problem can be stated and resolved as follows: Walsh AH_3 and AB_3 systems transform from C_{3v} to D_{3h} by change of a single angle, but there is no single angle that transforms the T point group, C_{2v}, to C_{3v} or D_{3h}. Therefore there are basically two classes of AH_3 and AB_3 molecules, and the one that is realized can only be determined by computing which structure has the lowest total energy [22]. The appropriate Walsh-Mulliken abscissa for T-shaped molecules is the in-plane angle Θ which converts a Y-shaped molecule into T shape for $\Theta = 180°$. For $\Theta = 120°$ the symmetry is D_{3h} and therefore a common point between the two classes of AH_3 and AB_3 molecules. The series of extended Hückel generated Walsh-Mulliken diagrams computrd by Gimarc [20] contains a $Y - T$ diagram for AH_3 and results for LiH_3^+ (Y-shaped). Qualitative slopes and energy ordering for the first few levels of the $Y - T$ diagram from 120° to 180° can be directly inferred from the AH_2 diagram because both reflection planes of C_{2v} pass through the added bond in a $Y - T$ molecule. Thus the first four valence molecular orbitals will be $2a_1$, $1b_2$, $3a_1$, and $1b_1$ - just as in AH_2. Thompson's analysis and Gimarc's diagrams are both compatible with this simple reasoning. It is also worth noting that in this case as well as others, d-orbitals are not required as they are in the valence bond hybridization scheme of Kimball [23].

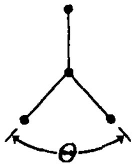

There is still another line of argument which brings out the equivalence of the two models, and this concerns cases where both models fail. It has frequently been pointed out that VSEPR fails for bonds which are highly ionic [7, 15]. The same is true for Walsh's rules. Li_2O is the simplest example. According to VSEPR there are two bond pairs and two lone pairs leading to a bent molecule. Assigning eight electrons to the AH_2 Walsh-Mulliken diagram also leads to a bent molecule – just like H_2O. Actually, of course, Li_2O is almost $Li^+O^=Li^+$ and definitely linear. Both models fail for lack of a Madelung potential term. When the Edmiston-Ruedenberg transformation is applied to a high-accuracy *ab initio* calculation of Li_2O, the charge lobes arrange themselves in an approximately tetrahedral fashion around oxygen – none of them pointing toward the lithium nuclei [24]. This result is indicative of the faithful representation of VSEPR provided by the Edmiston-Ruedenberg localized orbital definition.

An important observation arising from the large amount of research done on molecular shape is that almost any model or computational scheme yields reasonable bond angle predictions, and this suggests a low information content inherent to the specification of molecular shape. The most dramatic and elegant *manifestation of this observation* is Karl Hansen's development of spin valence theory and the results he obtained from it [25, 26, 27]. Using only the *ab initio* determinantal formalism for constructing wavefunctions, group theory, and the assumption of maximum multiplicity on the central atom, Hansen was able to determine the electronic ground state configuration and shape (point group) for AH_2 and AH_3 species without numerical computations. He made 24 predictions – all in complete accord with Walsh-Mulliken diagram results.

The Origin of Walsh's Rules

Having demonstrated the equivalence of VSEPR and Walsh-Mulliken, it remains to elucidate their basic origin. Because of their quantitative association with molecular orbital theory, Walsh-Mulliken diagrams are much easier to treat theoretically. Although schemes for computing these diagrams have been available for many years now, the progress toward understanding the physical-mathematical principles behind them has been slower to evolve. In particular there was a long period of uncertainty over the precise definition of Walsh's "orbital energies". An important paper by Coulson and Neilson [28] concluded that these were the "partitioned energies", $e_i = \frac{1}{2}[\varepsilon_i + (i\,|\,\text{one-electron terms in the Hamiltonian}\,|\,i)]$, whose sum equals the total energy. Bingel used the one-electron eigenvalue of his total energy united atom Hamiltonian, and this quantity is different from either ε_i or e_i, but, in practice, it behaves much like e_i. Schmidtke and Preuss employed the eigenvalues of a secular equation over a one-electron Hamiltonian composed of kinetic and electron-nuclear potential terms with an effective nuclear charge for the central atom. Their energies also have an angular dependence very similar to e_i. Coulson and Neilson's H_2O, Bingel's AH_2 and AH_3, and Schmidtke and Preuss's AH_2 and AH_3 all yielded diagrams in qualitative agreement with Walsh. On the other hand Bingel's A_3 and AB_3 and Schmidtke's AB_2 yield curves that all fall off very strongly at small angles and are essentially identical to the e_i curves for F_2O [29]. None of these resemble the corresponding Walsh diagrams.

As displayed above, e_i differs from ε_i by the addition of the one-electron terms in the Hamiltonian, and at small angles electrons of one ligand atom are attracted to the nucleus of a nearby "non-bonded" ligand atom, and this pulls down the e_i curves. For a light ligand atom like hydrogen, this effect is relatively small, and therefore qualitatively acceptable results were obtained for the hydrides. Another approach to the origin of Walsh's rules was proposed by Peters [30]. He equated the orbital energies with the *change* in ionization potential of the molecular orbital upon molecule formation. All of these previous hypotheses are incorrect, and they reflect the fact that an adequate supply of accurate *ab initio* computational results was unavailable to these authors. It has been numerical reproduction of Walsh-Mulliken diagrams for many individual cases that has clearly focused on ε_i, the eigenvalue in the canonical molecular orbital determining equation, as the correct definition of "orbital energy". As everyone knows, ε_i enjoys the great advantage of being identified with experimentally determined ionization potentials via Koopmans' theorem. When the Edmiston-Ruedenberg transformation is applied to canonical molecular orbitals, off-diagonal ε_{ij}'s are introduced, and the problem of physically interpreting or experimentally determining these quantities is the principal reason why it is difficult to carry out a detailed and complete analysis of VSEPR.

Central to the origin of Walsh's rules is a mathematical and computational justification of how a minimum in $\sum_i^{\text{val.}} \varepsilon_i$ can determine bond angles when it is well known that this sum has a grossly different value from the total energy, E_T:

$$E_T = \sum_i^{\text{val.}} \varepsilon_i + \left[\sum_i^{\text{core}} \varepsilon_i - V_{ee} + V_{nn}\right].$$

The key is to consider the derivative of E_T with respect to Θ rather than E_T itself, because it is an extremum in the derivative which governs the angle. Thus if

$$\frac{\dfrac{\partial}{\partial\Theta}\left[\sum_i^{\text{val.}} \varepsilon_i\right]}{\dfrac{\partial}{\partial\Theta}\left[\sum_i^{\text{core}} \varepsilon_i - V_{ee} + V_{nn}\right]} > 0$$

or if

$$\left|\frac{\partial}{\partial\Theta}\left[\sum_i^{\text{val.}} \varepsilon_i\right]\right| > \left|\frac{\partial}{\partial\Theta}\left[\sum_i^{\text{core}} \varepsilon_i - V_{ee} + V_{nn}\right]\right|.$$

$\dfrac{\partial}{\partial\Theta}\left[\sum_i^{\text{val.}} \varepsilon_i\right]$ will have the same sign as $\dfrac{\partial}{\partial\Theta}[E_T]$ and the minimum in $\sum_i^{\text{val.}} \varepsilon_i$ will occur at the same angle as the E_T minimum [31]. Physically, the inequalities will be satisfied if there is little charge transfer from one atom to another because then the effective screening potential, V_{ee}, will shield V_{nn} and changing bond angle will be like moving neutral bonds. Numerical proof of the inequalities has been obtained for a number of cases, two of which (BH_2^- and F_2O) are shown in Fig. 2 $\left(E_T\right.$, solid lines, compared to $\sum_i^{\text{val.}} \varepsilon_i$, dashed lines, from the same *ab initio* calculation$\left.\right)$.

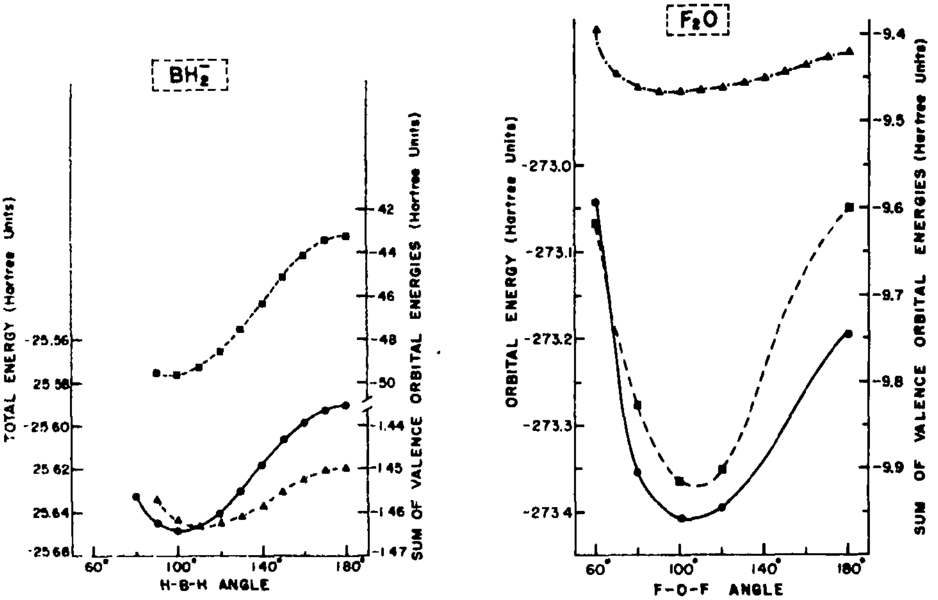

Fig. 2 Numerical proof of inequalities for covalent molecules. *Ab initio* E_T (solid lines), *ab initio* $\sum^{\text{val}} \varepsilon$ (dashed lines), extended Hückel $\sum^{\text{val}} \varepsilon$ (staggered lines)

It is a remarkable fact (already noted in a section above) that the simplest of all electronic structure models, extended Hückel theory, is able to generate reasonable Walsh-Mulliken diagrams. I have discussed the origin of this model at length elsewhere [32], here the most important point is demonstration that $\sum_i^{\text{val.}} \varepsilon_i$ from extended Hückel theory maintains the same sign of derivative versus angle as *ab initio* E_T and *ab initio* $\sum_i^{\text{val.}} \varepsilon_i$. Fig. 2 (staggered lines) shows that it does. The rather large differences in detail between extended Hückel $\sum_i^{\text{val.}} \varepsilon_i$ and *ab initio* $\sum_i^{\text{val.}} \varepsilon_i$ is one measure of the crudity of extended Hückel theory, but because of the low information content inherent to angle specification, extended Hückel angle predictions can be quantitatively useful.

The origin of the Walsh rule breakdown for highly ionic bonds is nicely brought out in the inequalities. Changes with angle of $\sum_i^{\text{core}} \varepsilon_i - V_{ee}$ no longer cancel changes with angle of V_{nn}, and the resultant Coulomb term destroys the inequality. This is illustrated in Fig. 3 by *ab initio* calculations on Li$_2$O $\left(E_T \text{ solid line, } \sum_i^{\text{val.}} \varepsilon_i \text{ dashed lines}\right)$. The sign of $\partial/\partial\Theta \left[\sum_i^{\text{val.}} \varepsilon_i\right]$ for extended Hückel theory is also opposite to that of $\partial/\partial\Theta(E_T)$. For extended Hückel theory the failure in $\sum_i^{\text{val.}} \varepsilon_i$ is paralleled by large

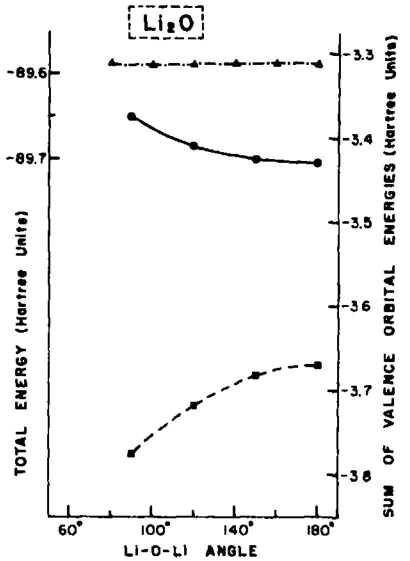

Fig. 3. Break of Walsh's rules for ionic molecules. *Ab initio* E_T (solid line), *ab initio* $\sum^{\text{val.}} \varepsilon$ (dashed line), extended Hückel $\sum^{\text{val.}} \varepsilon$ (staggered line)

inaccuracies in ε_i and in the molecular orbital coefficients. Since these quantities are the sole output of extended Hückel theory, it is clear that this model is only valid when Walsh's rules hold, and from a chemical viewpoint this implies small bond dipoles and a relatively smooth charge distribution.

Bond Lengths

In its simplest form, VSEPR does not address itself to bond length predictions, but some elaborations by Gillespie [7] have enabled him to account for trends in sequences of compounds. These additional postulates are: (a) Successive addition of electronegative ligands increases the effective electronegativity of the central atom and decreases bond lengths. (b) Different ligands have different environments, therefore different bond lengths. For example, five electron pairs lead to a trigonal-bipyramid with two axial positions and three equatorial ones. Results from the charges-on-a-sphere model (for $n \geq 4$ in $1/r_{ij}^n$) show a greater force at the axial position than equatorial, and this gives qualitative rationalization to the 10–20% longer axial bond observed for AX_5, AX_4E, and AX_3E_2 species. Application of both these additional rules to noble gas compounds has led to a useful systematization of bond length trends in these molecules [33].

Walsh-Mulliken diagrams likewise do not address themselves to bond lengths, but it is informative to apply the same analytical techniques to bond lengths as proved successful for bond angles. We carried this out in my laboratory [34] and found that $\sum_i^{\text{val.}} \varepsilon_i$ provides no guide at all to bond length, and the corresponding inequalities do not hold.

There are four other model schemes that are used for estimating and rationalizing bond lengths, and a review of them sheds light on the further analysis to be given below. The oldest, simplest and most used is tabulation of atomic and ionic radii. Pauling [35] has been principally responsible for developing this scheme. Mulliken [36] proposed that bond length trends be related to change in the occupancy of bonding and antibonding orbitals along a sequence of neutral or ionic species. The correctness of this hypothesis has been proved many times, but no general quantification of this model has yet arisen. Pauling's and Mulliken's models apply to any molecule but lack precision. If attention is restricted to hydrocarbons, much higher accuracy can be obtained, and two model theories have been widely employed: "molecular mechanics" [37] and the bond-order versus bond-length diagrams originated by Coulson [38]. The latter have been mostly applied to bond-length changes arising from changes in the number of π-electrons, and π-orbital Hückel theory has proved adequate for generating bond orders. Coulson's model may be thought of as a special case of Mulliken's general orbital occupancy concept. A review of molecular mechanics is beyond the scope of this article, but Bartell [15] has given examples and pointed out inherent difficulties in the method that are relevant to our discussion here. Overall, one can say that the precision achieved for hydrocarbon bond-length trends by molecular mechanics and bond-orders is to be viewed as the result of a sophisticated interpolation scheme rather than due to an intrinsically accurate description of the basic force laws involved.

Beyond the six models discussed so far in this section, there are the quantum mechanical calculational methods. The method with the highest level of reliability which is still able to handle large enough systems to be of practical interest to many inorganic and organic chemists is the single determinant, self-consistent field molecular orbital method. We have displayed the canonical orbital determining equation for this method, and even when a relatively crude basis set is used to expand the molecular orbitals, generally correct trends are found and absolute errors are 1-10%. Fortunately, the efficiency of this *ab initio* method is rapidly improving, and molecules composed of twenty atoms and sixty electrons are practical at this time. Extended Hückel theory with its high computation speed and low *a priori* reliability for predicting bond lengths is at the opposite end of the scale. Detailed examination shows [32] that extended Hückel theory generates its bond lengths by a physically incorrect process and this scheme is essentially useless for their prediction. There exist a number of methods that are intermediate in all respects to these extremes. A great deal of everyday chemical utility has been achieved through their use and the absolute error in bond lengths does not generally exceed 12%. However, the trends through a chemical sequence are often incorrectly ordered.

Two quite general results from theoretical chemistry suggest why the precise determination of bond lengths is so difficult. First is the well-known united atom – separated atom energy level correlation diagram [39]. Examination of the numerous cases given by Herzberg shows that the pattern of level spacings is vastly different between the two sides of these diagrams. The actual levels manifest by the molecule may be close to one side or to the other or somewhere near the middle. Second is the plot of average kinetic energy and average potential energy versus internuclear separation found in several textbooks [40]. These show that around the equilibrium separation both average kinetic and average potential energies are changing very rapidly in opposite directions while the total energy has a very much slower change. These rapid opposing changes cannot cancel because, of course, their sum is the total energy curve. Bond lengths are clearly a delicate balance between electron-nuclear attraction, screening, and nuclear repulsions as well as between the total potential and kinetic energies, and a considerable amount of detailed information is required about these terms to specify bond lengths.

Summary and Conclusions

Because of its name, the fact that repelling charges on a sphere can produce its results, and because the relative repulsion of bond pairs and lone pairs successfully rationalizes their observed positions, the origin of the VSEPR model has been popularly associated with electron-electron repulsion. Walsh-Mulliken diagrams, on the other hand, are associated with molecular ionization potentials and omit electron-electron and nuclear-nuclear repulsions. That these two models are, in fact, equivalent follows from four considerations: (a) The same single determinant *ab initio* wavefunction can produce all of the directly identifiable features of both models. (b) The trace of the Hamiltonian matrix for this wavefunction is invariant under transformation from a localized (VSEPR) representation to a delocalized (Walsh-Mulliken) representation. (c) Size and Pauli exclusion principle repulsion of closed shells replaces electron-electron repulsion as the true driving force in VSEPR. (d) Both models fail simultaneously when bonds become sufficiently ionic that a significant Madelung term is introduced.

Many early papers misinterpreted the dependent variable in Walsh-Mulliken diagrams, and it has only been relatively recently that "orbital energy" has been unequivocally established as the Koopman-theorem related ε. The basic mathematical-physical origin of Walsh's rules resides in the dominance of $\partial/\partial\Theta\left[\sum_i^{\text{val.}}\varepsilon_i\right]$ over other terms in the total energy expression, and this holds only when the molecular charge distribution is rather smooth and no significant between-atom charge transfer occurs. Because only sign information concerning $\partial/\partial\Theta\left[\sum_i^{\text{val.}}\varepsilon_i\right]$ is required, many highly approximate quantum mechanical schemes, such as extended Hückel theory, are able to yield useful predictions.

In sharp contrast to angles, bond lengths are difficult to predict with precision. This is due to the delicate balance of energy components that occurs around equilibrium bond separations. Model schemes, such as sum of radii or number of occupied bonding and anti-bonding orbitals, are not adequately quantitative, while some schemes only apply to special classes of hydrocarbons. At present, *ab initio* calculation is the only method that yields reliable *a priori* bond length predictions.

Acknowledgement. I wish to acknowledge stimulating and informative conversations with Karl Hansen and Klaus Ruedenberg.

References

1. Sidgwick, N. V., Powell, H. M.: Proc. Roy. Soc. A **176**, 153 (1940).
2. Gillespie, R. J., Nyholm, R. S.: Quart. Rev. (Lond.) **11**, 339 (1957).
3. Walsh, A. D.: J. chem. Soc. (Lond.) 2260, 2266, 2288, 2296, 2301 (1953); Prog. Stereochem. **1**, 1 (1954).
4. Mulliken, R. S.: Rev. mod. Physics **14**, 204 (1942); J. Amer. chem. Soc. **11**, 887 (1955).
5. Shütte, K., Van der Waerden, B. L.: Math. Ann. **123**, 96 (1951); Gillespie, R. J.: Canad. J. Chem. **38**, 818 (1960).
6. Claxton, T. A., Benson, G. C.: Canad. J. Chem. **44**, 157 (1966); Thompson, H. B., Bartell, L. S.: Inorg. Chem. **7**, 488 (1968).
7. Gillespie, R. J.: Angew. Chem. **6**, 819 (1967); J. chem. Educat. **47**, 18 (1970).
8. Lennard-Jones, J. E.: Proc. Roy. Soc. A **198**, 1, 14 (1949); Lennard-Jones, J. E., Pople, J. A.: Proc. Roy. Soc. A **202**, 166 (1950).
9. Edmiston, C., Ruedenberg, K.: Rev. mod. Physics **35**, 457 (1963); Ruedenberg, K.: Modern quantum chemistry **1**, 85, Ed. by O. Sinanoğlu. New York: Academic Press 1965.
10. — J. chem. Physics **43**, 597 (1965); Quantum theory of atoms, molecules and the solid state, p. 263, Ed. by P. O. Löwdin. New York: Academic Press 1966.
11. Peyerimhoff, S. D., Buenker, R. J., Allen, L. C.: J. chem. Physics **45**, 734 (1966).
12. Results obtained in my laboratory at Princeton are: Peyerimhoff, S. D., Buenker, R. J., Allen, L. C.: J. chem. Physics **45**, 734 (1966) [BH_2, BH_2, NH_2^+, BeH_2, BH_3, CH_3^+, BeH_3]; Buenker, R. J., Peyerimhoff, S. D., Whitten, J. L., Allen, L. C.: J. chem. Physics **45**, 2835 (1966) [B_2H_6 and C_2H_6]; Buenker, R. J., Peyerimhoff, S. D.: J. chem. Physics **45**, 3682 (1966) [F_2O, Li_2O, FOH, LiOH]; Peyerimhoff, S. D., Buenker, R. J.: J. chem. Physics **47**, 1953 (1967) [O_3 and N_3]; Peyerimhoff, S. D., Buenker, R. J.: Theoret. chim. Acta (Berl.) **9**, 103 (1967) [FNO]; Peyerimhoff, S. D., Buenker, R. J.: J. chem. Physics **49**, 2473 (1968) [N_2O]; Pfeiffer, G. V., Allen, L. C.: J. chem. Physics **51**, 190 (1969) [NO_2^+ and NO_2]; Pan, D. C., Allen, L. C.: J. chem. Physics **46**, 1797 (1967) [HCN]; Pan, D. C., Fink, W. H., Allen, L. C.: J. chem. Physics **52**, 6291 (1970) [N_2H_2]; Rauk, A., Clementi, E., Allen, L. C.: J. chem. Physics **52**, 4133 (1970) [NH_3].
13. Mulliken, R. S.: J. Amer. chem. Soc. **11**, 887 (1955).
14. Longuet-Higgens, H. C.: Proc. Roy. Soc. (London) A **235**, 537 (1956); Opik, U., Pryce, M. H. L.: Proc. Roy. Soc. (London) A **238**, 425 (1957); Den Boer, D. M. W., Longuet-Higgins, H. C.: Molecular Physics **5**, 387 (1962); Nicholson, B. J., Longuet-Higgins, H. C.: Molecular Physics **9**, 461 (1965); Bader, R. F. W.: Molecular Physics **3**, 137 (1960).
15. Bartell, L. S.: J. chem. Educat. **45**, 754 (1968).
16. Schmidtke, H. H., Preuss, H.: Z. Naturforsch. **16a**, 790 (1961); Schmidtke, H. H.: Z. Naturforsch. **17a**, 121 (1962); **18a**, 496 (1963).
17. Bingle, W. A.: An explanation of Walsh's rules using united atom molecular orbitals. In: Molecular orbitals in chemistry, physics, and biology, p. 191. Ed. by P.-O. Löwdin and B. Pullman. New York: Academic Press 1964.
18. Leclerc, J. C., Lorquet, J. C.: Theoret. chim. Acta (Berl.) **6**, 91 (1966).
19. Allen, L. C., Russell, J. D.: J. chem. Physics **46**, 1029 (1967).
20. Gimarc, B. M.: J. Amer. chem. Soc. **92**, 266 (1970); **93**, 593, 815 (1971).
21. Thompson, H. B.: Inorg. Chem. **7**, 604 (1968).
22. This situation would also occur in distinguishing the isomers of H_2AB and HABH and other molecules with more than three atoms.
23. Kimball, G. E.: J. chem. Physics **8**, 188 (1940).
24. Unpublished calculations by J. F. Liebman and L. C. Allen.
25. Hansen, K. H.: Theoret. chim. Acta (Berl.) **1**, 353 (1963).
26. — Theoret. chim. Acta (Berl.) **3**, 31 (1965).
27. — Theoret. chim. Acta (Berl.) **6**, 437 (1966).
28. Coulson, C. A., Neilson, A. H.: Discuss. Faraday Soc. **35**, 71 (1963).
29. Buenker, R. J., Peyerimhoff, S. D.: J. chem. Physics **45**, 3682 (1966).
30. Peters, D.: Trans. Faraday Soc. **62**, 1353 (1966).
31. As noted previously, a great many *ab initio* numerical experiments have established that the E_T minimum predicts experimentally observed angles quite accurately.
32. Allen, L. C.: Why three-dimensional Hückel theory works and where it breaks down. In: Sigma molecular orbital theory, p. 227. Ed. by O. Sinanoglu and K. B. Wiberg. Yale University Press 1970.

33. Gillespie, R. J.: The noble-gas fluorides, oxyfluorides, and oxides, predictions of molecular shapes and bond lengths. In: Noble gas compounds, p. 333. Ed. by H. H. Hyman. University of Chicago Press 1963.
34. Peyerimhoff, S. D., Buenker, R. J., Whitten, J. L.: J. chem. Physics **46**, 1707 (1967).
35. Pauling, L.: The nature of the chemical bond. 3rd Ed. Cornell University Press 1960.
36. Mulliken, R. S.: Rev. mod. Physics **14**, 204 (1942).
37. Allinger, N. L., Tribble, M. T., Miller, M. A., Wertz, D. H.: J. Amer. chem. Soc. (in press); Boyd, R. H.: J. chem. Physics **49**, 2574 (1968).
38. Coulson, C. A.: Valence, 2nd Ed. Oxford University Press 1961.
39. Hund, F.: Z. Physik **40**, 742 (1927); **42**, 93 (1927); **51**, 759 (1928); Mulliken, R.S.: Physic. Rev. **32**, 186 (1928); Rev. mod. Physics **4**, 1 (1932); Eyring, H., Walter, J., Kimball, G. E.: Quantum chemistry, Chapter XI. New York: Wiley 1944; Herzberg, G.: Molecular spectra and molecular structure. I. Spectra of diatomic molecules. Princeton: Van Nostrand 1950; and III. Electronic spectra and electronic structure of polyatomic molecules. Princeton: Van Nostrand 1966.
40. For example: Slater, J. C.: Quantum theory of molecules and solids, Vol. 1, p. 56. New York: McGraw Hill 1963.

Prof. L. C. Allen
Department of Chemistry
Princeton University
Princeton, New Jersey 08540, USA

Theoret. chim. Acta (Berl.) 24, 132 - 146 (1972)
© by Springer-Verlag 1972

Extension of Walsh's Rules to More General Systems*

ROBERT J. BUENKER
Department of Chemistry, University of Nebraska, Lincoln, Nebraska 68508, USA

SIGRID D. PEYERIMHOFF
Institut für Physikalische Chemie, Johannes Gutenberg-Universität 6500 Mainz, Germany

Received July 1, 1971

It is demonstrated that location of hydrogen atoms within bonding distance of a simple triatomic molecule can alter the order of energy levels relative to that of the parent system without significantly changing the behavior of the orbital energies under geometrical variation. As a result the ground state electronic configurations of H_nAB_2 systems often differ from those of triatomics with the same number of electrons and this fact is shown to be directly responsible for the existence of such distinctive geometrical structures as those possessed by cyclopropane, cyclopropyl and allyl cations and cyclopropene. Thus the familiar prescription of Walsh's rules which states that isoelectronic molecules possess identical geometries is seen to be valid only if the systems in question possess the same electronic configuration; in reality it may be an excited state of one system which has the same geometry as the ground state of another and *vice versa*. It is concluded that the methodology of Walsh's rules can be extended to a much larger class of systems than heretofore assumed simply by taking explicit account of the predictable effects of hydrogen addition upon the electronic configuration and hence on the skeletal arrangement of the heavy nuclei.

Es wird gezeigt, daß in Bindungsnähe eines dreiatomigen Moleküls befindliche Wasserstoffatome die Reihenfolge der ursprünglichen Energieniveaus im System ändern können, ohne dabei das Verhalten der Orbitalenergien hinsichtlich geometrischer Veränderungen erheblich zu beeinflussen. Als Folge davon unterscheidet sich die Grundzustands-Elektronenkonfiguration eines H_nAB_2 Systems oft von der entsprechenden der dreiatomigen Moleküle mit gleicher Elektronenzahl, und es läßt sich zeigen, daß diese Tatsache für das Auftreten der besonderen geometrischen Strukturen von Cyclopropan, Cyclopropyl- und Allyl-Kation oder Cyclopropen unmittelbar verantwortlich ist. Die übliche Anwendungsweise der Walshschen Regeln, nach der iso-elektronische Moleküle gleiche Geometrien haben, ist also nur gültig, wenn die entsprechenden Systeme in der gleichen Elektronenkonfiguration auftreten; in Wirklichkeit kann es vorkommen, daß der angeregte Zustand eines Systems die gleiche Geometrie hat wie der Grundzustand eines anderen und umgekehrt. Es zeigt sich dann, daß das Verfahren der Walshschen Regeln auf eine viel größere Klasse von Systemen ausgedehnt werden kann als bisher angenommen wurde, wenn man die vorhersagbaren Wirkungen, welche die Wasserstoffanlagerung auf die Elektronenkonfiguration und damit auf das Kerngerüst der schwereren Atome hat, direkt berücksichtigt.

1. Introduction

The basis for the MO description of molecular geometry is embodied in a series of principles known collectively as Walsh's rules [1, 2]. Although often more complicated to apply in a specific case than the methodology of valence bond theory, these empirical prescriptions have the distinct advantage of being equally applicable to both ground and excited states of molecules. The basic unit in this theory is the correlation diagram, essentially a plot of valence orbital energies as a function of some geometrical variable; the implicit assumption is made that the same diagram is applicable to all systems within a given class, which is to say: a) that the shapes of corresponding orbital energy curves are identical and b) that the stability ordering is also unchanged from one system to another within this class[1]. Originally the details of the various correlation diagrams were worked out by Mulliken [1] and Walsh [2] on the basis of empirical data and certain conclusions relative to the bonding or antibonding character of MO's derivable from symmetry considerations. In the meantime it has been demonstrated that these correlation diagrams can in principle be calculated using self-consistent field theory [3–5].

---

* Dedicated to the memory of Prof. K. H. Hansen.

Irrespective of the method with which the necessary data are obtained, however, the most serious drawback to this general theory, aside from the relatively complicated manner in which it is applied, is the fact that apparently the families of molecules describable in terms of a given correlation diagram are relatively small and at present confined to fairly simple types of systems such as AH_2, AB_2 and HAB species, for example. Obviously enlarging the class of systems to which a given correlation diagram is applicable and thereby extending the scope of the original theory is a quite desirable objective and it is therefore the purpose of the present paper to consider how this possibility can be realized.

2. Possible Extensions of Walsh's Rules

One possible way in which the class of molecules described by a particular correlation diagram could be expanded would be to allow for the addition of an arbitrary number of hydrogen atoms to any member of the original family. For example, one might ask whether all H_nAB_2 systems can be treated on the same footing as AB_2 molecules (where A and B are heavier nuclei than H), whose general correlation diagram is well established. This question can be rephrased in a somewhat different (and not necessarily equivalent) form: do all H_nAB_2 systems which are isoelectronic with a given triatomic species possess the same (or nearly the same) internuclear angle in their respective ground state equilibrium nuclear configuration?

Inspection of a number of typical examples contained in Table 1 shows that there is good reason to look for such a generalization. On the other hand, it is well known, of course, that not every H_nAB_2 system with 22 electrons is linear (as Walsh's rules predict for simple triatomics with a like number of electrons), with cyclopropene (51°), cyclopropyl- ($\approx 80°$) and allyl-cation (120°) obvious counterexamples; nor does every 24-electron species possess a BAB angle in the neighborhood of 120° (for example, cyclopropane, ethylene oxide and ethyleneimine all have much smaller angles of close to 60°). It will therefore clearly be necessary to determine whether the aforementioned counterexamples merely

---

[1] Actually use of the same correlation diagram for two systems implies more than the two relationships given above, namely point for point equality, but it may easily be shown that the results of applying Walsh's rules are unchanged by removing the restriction of equal spacing among the orbital energy curves as long as assumptions a) and b) are valid.

Table 1. Experimental[a] equilibrium angles for various systems with a triatomic skeleton (exclusive of hydrogen atoms); N is the total number of electrons

Molecule		N	Angle	(Degrees)
Dioxyfluoride	F_2O	26	FOF	103.8
Difluoromethane	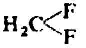 $H_2C{<}^{F}_{F}$	26	FCF	108.5
Dimethyl ether	$H_3C-O-CH_3$	26	COC	111.5
Dimethylamine	$H_3C-NH-CH_3$	26	CNC	108 ± 4
Ethylamine	$H_3C-CH_2-NH_2$	26	CCN	110 ± 3
Propane	$H_3C-CH_2-CH_3$	26	CCC	111.5
Ozone	O_3	24	OOO	116.8
Nitrite ion	NO_2	24	ONO	116
Formyl fluoride	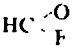 $HC{}^{O}_{F}$	24	FCO	121.1
Acetaldehyde	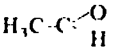 $H_3C-C{}^{O}_{H}$	24	CCO	123.9
Formamide	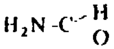 $H_2N-C{}^{H}_{O}$	24	NCO	123.6
Formic acid	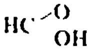 $HC{}^{O}_{OH}$	24	OCO	124.3
Propylene (propene)	$H_3C-CH-CH_2$	24	CCC	124.8
Vinyl fluoride	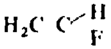 $H_2C-C{}^{H}_{F}$	24	CCF	121
Carbon dioxide	CO_2	22	OCO	180
Nitrous oxide	N_2O	22	NNO	180
Hydrogen azide (ion)	$HN_3(N_3^-)$	22	NNN	180
Cyanamide	H_2N-C-N	22	NCN	180
Diazomethyne	H_2C-N-N	22	CNN	180
Allene	$H_2C-C-CH_2$	22	CCC	180
Methylacetylene	$HC-C-CH_3$	22	CCC	180
Ketene	H_2C-C-O	22	CCO	180
Methyl cyanide	H_3C-C-N	22	CCN	180
Methyl isocyanide	H_3C-N-C	22	CNC	180
Borine carbonyl	H_3B-C-O	22	BCO	180
Hydrogen isocyanate	$HN-C-O$	22	NCO	180

[a] *Tables of interatomic distances and configurations in molecules and ions* (The Chemical Society, London). Spec. Publ. No. 11 (1958) and No. 18 (1965).

represent unusually large numerical discrepancies in the theoretical method or if instead there is a logical extension of the underlying theory which will allow inclusion of these cases in a systematic fashion.

In order to investigate these questions it is necessary to take a closer look at the assumptions, either implicit or explicit, in the application of Walsh's rules in general. In particular it will be helpful to determine how the calculated correlation diagrams of the exceptional systems differ from the more conventional sets of orbital energy curves of apparent general validity for the parent AB_2 molecules.

3. Basis for Walsh's Rules

The underlying basis for Walsh's rules can be summarized in a series of three principles: 1) the valence orbital energies weighted according to occupation are to a good approximation the sole geometry determining factor responsible for the shapes of molecules; 2) altering the nuclear charge of the various atomic centers does not result in any significant changes in the shapes of the valence orbital energy curves in the parent correlation diagram; and 3) such redistribution of the nuclear charge also does not change the order of the various orbital energies. An important corollary of the third point is that the electronic configuration of the molecular ground state is independent of the distribution of nuclear charge.

The first of these principles is generally recognized as the most tenuous even for the simpler systems. The results of non-empirical SCF calculations [3–5] have been used previously to examine the validity of this statement in specific examples and it has been shown that in a few cases other contributions to the total energy such as nuclear and electronic repulsion can significantly influence the shape of the potential surface; this situation arises for triatomic molecules such as Li_2O and LiOH, for example [4], which have strong local centers of positive and negative charge. Nevertheless, none of the H_nAB_2 counterexamples mentioned above would seem to fall into this category any more than do the conventional examples included in Table 1, and thus it seems clear that something more than the effect of other terms in the total energy expression is responsible for the distinctive value of ∢ BAB for these systems.

The question of possible differences between the shapes of corresponding orbital energy curves for AB_2 and H_nAB_2 systems can be answered in a straight-

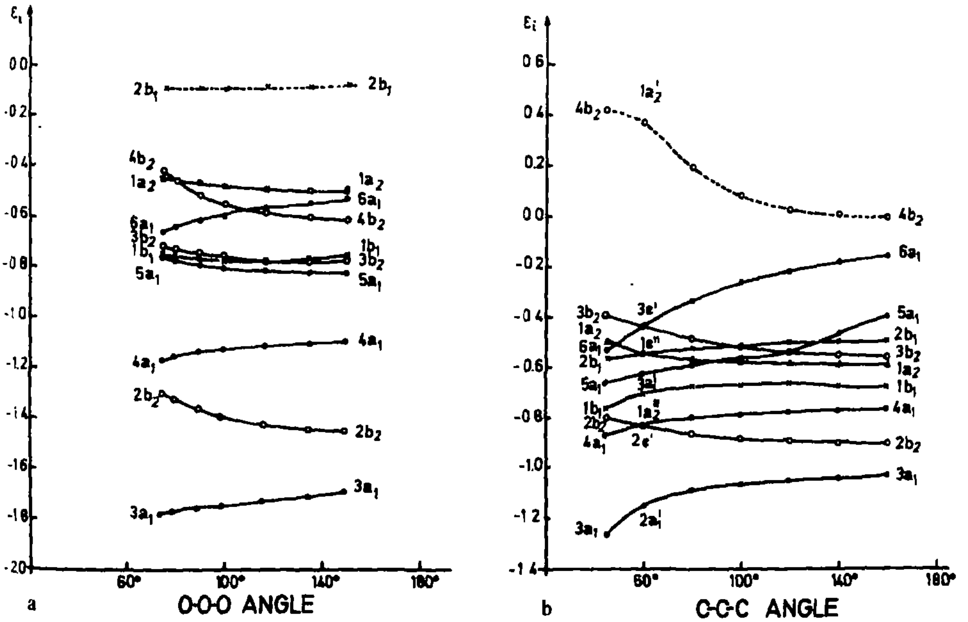

Fig. 1. Correlation diagram for (a) the ground state of ozone and (b) the ground state of cyclopropane. (Energy values are in hartree units)

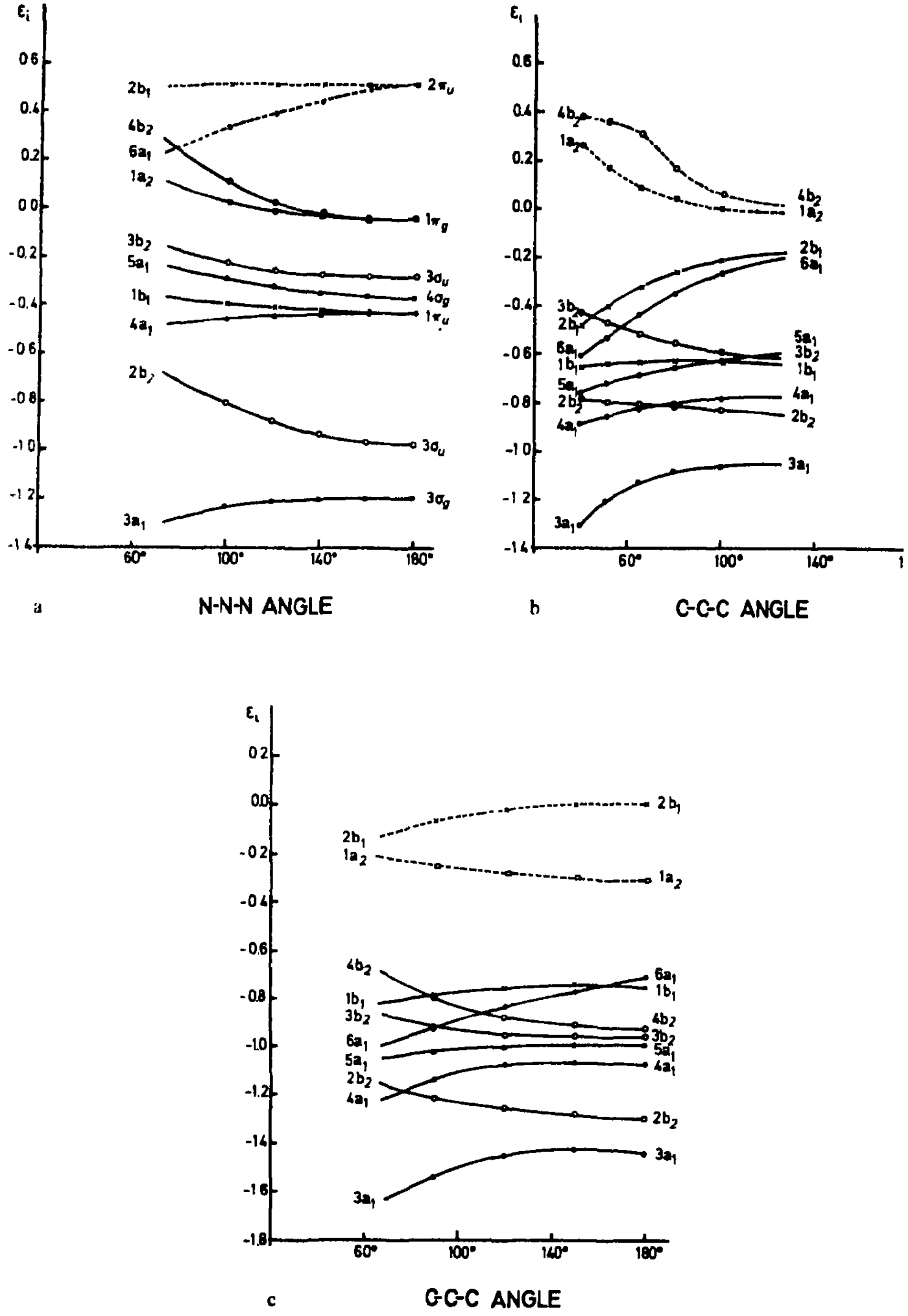

Fig. 2. Correlation diagram for (a) the ground state of N_3^-, (b) the ground state of cyclopropene and (c) the ground state of allyl cation. (Energy values are in hartree units)

forward manner by carrying out SCF calculations for molecules with both typical and unusual geometries from the point of view of Walsh's rules. Comparison of the resulting correlation diagrams for the 24-electron systems ozone [5] and cyclopropane [6] (Figs. 1a, b) shows clearly that with only minor exceptions the variation of orbital energies with ∡OOO and ∡CCC respectively follow very much the same pattern; this second principle is seen to be particularly valid for the important upper valence orbital species, $6a_1$, $4b_2$, $1a_2$ and $2b_1$.

Yet the same figures show even more clearly that the third of the aforementioned underlying principles is unquestionably violated in this comparison; in the O_3 ground state configuration the $2b_1$ MO is the least stable of the upper valence orbitals and is thus unoccupied whereas in cyclopropane the highest energy species in this category is the $4b_2$ and is thus left vacant. Similar findings result from SCF calculations for the 22-electron systems azide ion [5] N_3^- (180° equilibrium angle), cyclopropene [7] (51°) and the allyl cation [8] $C_3H_5^+$ (120°), for which only two of the four upper valence species are occupied in their respective ground state electronic configurations. The calculated diagrams for these systems given in Figs. 2a–c show that the two orbitals occupied in each case are: $4b_2$ and $1a_2$ for N_3^-, $6a_1$ and $2b_1$ for cyclopropene, and $6a_1$ and $4b_2$ for

Table 2. Ground state electronic configuration of several hydrocarbons deduced from a group theoretical analysis of their respective valence bond structures

	VB-Description	Occupied MO's			
		a_1	b_2	b_1	a_2
Cyclopropane	3 × 1*s*	2	1		
	3 × CC-bond	2	1		
	2 × CH-bond (central)	1		1	
	4 × CH-bond (terminal)	1	1	1	1
	Total	6	3	2	1
Cyclopropene	3 × 1*s*	2	1		
	3 × CC single bond	2	1		
	π-bond			1	
	2 × CH-bond (central)	1		1	
	2 × CH-bond (terminal)	1	1		
	Total	6	3	2	0
Allyl cation	3 × 1*s*	2	1		
	2 × CC-bond	1	1		
	1 × CN-bond (central)	1			
	4 × CH-bond (terminal)	2	2		
	π-bond			1	
	Total	6	4	1	0
Cyclopropyl cation	3 × 1*s*	2	1		
	3 × CC-bond	2	1		
	1 × CH-bond (central)	1			
	4 × CH-bond (terminal)	1	1	1	1
	Total	6	3	1	1

the allyl cation. In addition one can point to the cyclopropyl cation as a 22-electron system which occupies yet a different pair of upper valence MO's in its ground state, namely the $6a_1$ and $1a_2$ species. Furthermore, an elementary analysis using group theoretical techniques of the VB structures of the various counterexample molecules demonstrates that the calculated MO electronic configurations for these systems are wholly consistent with their valence bond descriptions and in fact easily derivable therefrom without the aid of explicit calculation (Table 2).

The fact remains, however, that the shapes of corresponding orbital energy curves in each of Figs. 1a, b and 2a–c, particularly those of the critical upper valence MO's, are satisfactorily similar, in agreement with the second underlying principle of Walsh's rules. The question thus arises whether the distinctive geometries of systems such as cyclopropane and cyclopropene can be explained consistently in terms of the MO theory simply by modifying the aforementioned third principle to take account of the fact that changes in electronic configuration generally imply alteration of the equilibrium nuclear geometry.

4. Relation between Electronic Configuration and Equilibrium Geometry

If the difference in electronic configuration between an H_nAB_2 molecule possessing an unusual geometry (at least from the standpoint of Walsh's rules) and an isoelectronic member of the parent triatomic family is responsible for the distinction in equilibrium geometry, it should be possible to demonstrate this relationship by carrying out calculations in which one system is forced into the ground state electronic configuration of the *other* and *vice versa*. In order to conveniently discuss the results of these calculations the following notation is introduced: a given electronic configuration is denoted by a quartet (i, j, k, l) where i, j, k and l are the numbers of a_1, b_2, b_1 and a_2 MO's respectively which are *doubly* occupied in this case. If attention is restricted, as will be useful, to those configurations in which only the $6a_1$, $4b_2$, $2b_1$ and $1a_2$ MO's are allowed variable occupation, a total of $\binom{4}{3} = 4$ possible 24-electron configurations and $\binom{4}{2} = 6$

Table 3. Notation for various electronic configurations of 22 and 24 electron molecules, showing respectively the number of doubly occupied a_1, b_2, b_1 and a_2 MO's in each case. The simple integer labels are used to identify these configurations in Figs. 3 and 4

	Label	Electronic configuration
24 electron system	1	(6,4,1,1)
	2	(5,4,2,1)
	3	(6,3,2,1)
	4	(6,4,2,0)
22 electron system	1	(5,4,1,1)
	2	(6,4,1,0)
	3	(5,3,2,1)
	4	(6,3,1,1)
	5	(5,4,2,0)
	6	(6,3,2,0)

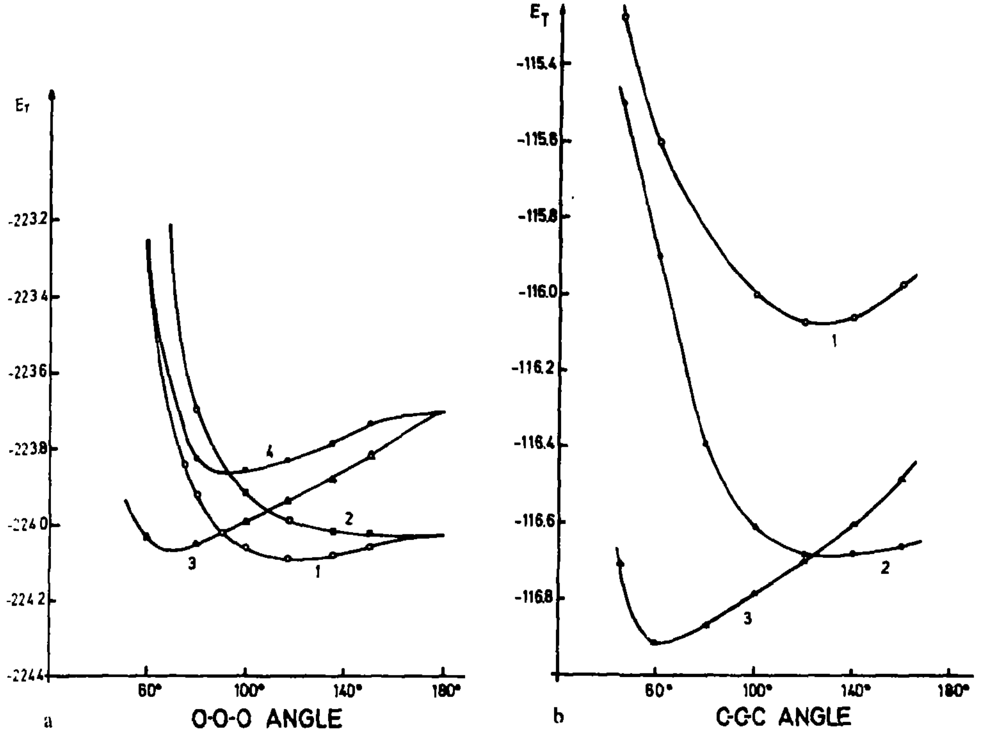

Fig. 3. Angular potential curves for several states of ozone (Fig. a) and cyclopropene (Fig. b). The integer labels for the curves correspond to the electronic configurations given in Table 3. (Energy values are in hartree units)

twentytwo-electron species can be distinguished; the notation used throughout this paper for each of these configurations is given in Table 3.

According to this notation the ground state electronic configuration of ozone is (6,4,1,1) while that of cyclopropane is (6,3,2,1). Potential curves for these and the other two configurations listed in Table 3 are given in Fig. 3a for ozone and from this figure the degree to which electronic configuration determines nuclear geometry is quite apparent; in particular it can be seen that the (6,3,2,1) configuration in ozone is associated with a very small internuclear angle, just as it is in cyclopropane. In other words, what is the ground state electronic configuration of one system corresponds to an excited state of the other; interestingly enough the energy minimum for the "cyclopropane" state of O_3 is calculated to lie only 0.02 hartree (12 kcal/mole) above the absolute potential minimum of its ground state configuration.

Only three of the possible four potential curves of cyclopropane have been obtained (Fig. 3b) but from these results it is clear that the relationship between corresponding states of O_3 and cyclopropane is reciprocal in nature. The ozone ground state configuration (1) corresponds to a very highly excited state of the hydrocarbon, but it still leads to a potential minimum at roughly 120°, the conventional value. The similarity between the potential curves of configuration 2

(Table 3) for each system clearly substantiates the conclusion that the equilibrium geometry of a system is determined to a very large extent by its electronic configuration.

In a completely analogous manner the (6,4,1,0), (6,3,1,1) and (6,3,2,0) excited configurations of N_3^- are seen to correspond to the ground states of the allyl and cyclopropyl cations and cyclopropene respectively; calculated N_3^- potential curves for these SCF states lead to equilibrium angles of 115°, 85° and less than 60° respectively (Fig. 4a), all of which being clearly compatible with the aforementioned ground state equilibrium CCC angles of the hydrocarbons in question. Potential curves for these 22-electron H_nAB_2 molecules (Fig. 4b) further demonstrate the close connection between equilibrium geometry and electronic configuration.

It can therefore be concluded that the conventional AB_2 correlation diagram employed in the application of Walsh's rules can also be used to predict the skeletal geometries of related H_nAB_2 systems as long as it is recognized that the order of orbital energy levels can be altered by the addition of hydrogen atoms; thus it can no longer be simply assumed that isoelectronic molecules possess the same geometries unless they are known to have the same electronic configuration. For simple triatomics it is of course known that the absolute stabilities of the various MO's change upon redistribution of protons among the three centers

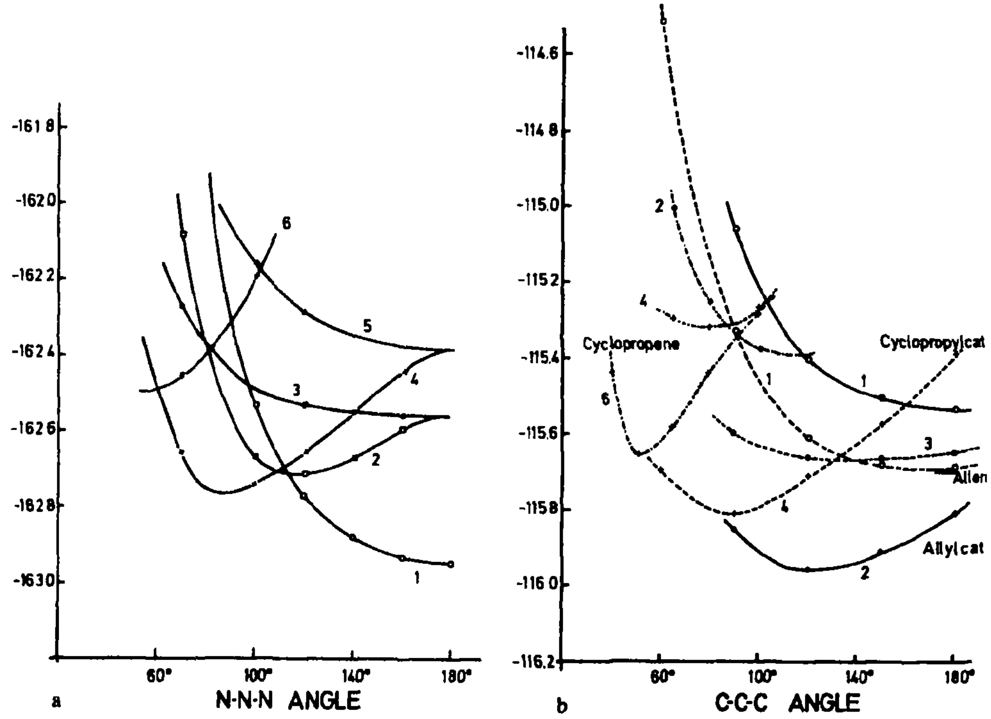

Fig. 4. Angular potential curves for several states of N_3^- (Fig. a) and 22-electron hydrocarbons (Fig. b). The integer labels for the curves correspond to the electronic configurations given in Table 3. (Energy values are in hartree units; dashed lines correspond to cyclopropyl cation states, dotted-dashed lines to cyclopropene and the two solid curves to allyl cation states)

Table 4. Characterization of the uppermost valence orbitals in an AB_2 system

MO		Geometrical trend	Orientation	Charge density maximum[a]
π_u	$6a_1$	Strongly bent	In-plane	Central
	$2b_1$	Bent	Perpendicular	Central
π_g	$1a_2$	Linear	Perpendicular	Terminal
	$4b_2$	Strongly linear	In-plane	Terminal

[a] For typical charge density contour diagrams for these orbitals see for example Ref. [4].

[4, 5, 9] but the subsequent reordering (if any) apparently never leads to a change in the ground state electronic configuration. Nevertheless it is not difficult to understand how such changes in the relative spacing of the energy levels result in substantial differences in the absolute magnitude of corresponding spectral transition energies for isoelectronic species. For example, in ozone the $4b_2$ and $2b_1$ MO's are nearly isoenergetic and this fact leads to the aforementioned proximity of the potential minima for the (6,4,1,1) ground and (6,3,2,1) excited states of this system; increasing the nuclear charge of the end atoms at the expense of the central to give CF_2, however, causes the $4b_2$ to become significantly more stable than the $2b_1$, thereby producing a much larger separation between the corresponding potential minima in this system. This behavior can easily be understood from Table 4, which characterizes the four upper valence MO's according to the location of their respective charge density maxima; increasing the nuclear charge of the terminal atoms obviously adds to the stability of the $4b_2$ while decreasing the charge at the central nucleus has the opposite effect on the $2b_1$.

If the redistribution of protons takes the form of attaching hydrogen atoms to a triatomic skeleton, the changes effected on the various orbital energies can be quite selective. For example, if a pair of hydrogen atoms is situated in the same plane as that containing the three heavy atoms, subsequent mixing of the hydrogen AO's with the orbital of the triatomic parent is understandably more effective for those species whose charge density maxima lie in this plane ($6a_1$ and $4b_2$) than for those which do not (Table 4); similarly the $1a_2$ and $2b_1$ MO's are expected to be selectively stabilized if the hydrogens are located above and below this plane respectively. With these guidelines then it is generally a simple matter to predict the order of the upper valence orbital energies in a given H_nAB_2 molecule, at least to a sufficient degree to ascertain the ground state electronic configuration and thereby, upon subsequent application of Walsh's method, the approximate equilibrium geometry of the system.

5. Application of the Extended Method to C_3H_n Systems

Consideration of various C_3H_n hydrocarbons will be useful in demonstrating the extension of Walsh's rules to general H_nAB_2 systems and should hopefully indicate how the scope of the former theory may be enlarged to deal with molecules formed by the addition of hydrogen atoms to other types of parent species.

a) C_3H_6 *Isomers: Cyclopropane, Trimethylene and Propylene*

If six hydrogens are distributed equally among three carbons two isomers are possible, one with all perpendicular CH_2 groups (cyclopropane) and one with only the central methylene group so oriented (trimethylene). With all the hydrogen atoms out of the CCC plane it is the π type upper valence MO's ($1a_2$ and $2b_1$, see Table 4) which are most susceptible to mixing with the H AO's. The degree of mixing can be judged from the combined charge density contours of these species for 60° cyclopropane shown in Fig. 5; this figure in turn is wholly similar to that representing the contours of the $1b_{3g}$ CH bonding orbital in ethylene [10]. Thus in contrast to the situation for simple triatomic systems the orbital energies of the $1a_2$ and $2b_1$ MO's in cyclopropane lie considerably lower than those of the $6a_1$ and $4b_2$ in-plane species (compare Figs. 1a, b). Consequently it is energetically favorable to occupy the $2b_1$ instead of the $4b_2$ MO in this C_3H_6 isomer; it is of course well known that substitution of the $4b_2$, with its minimum orbital energy occurring for linear geometry, by the $2b_1$ (possessing the opposite geometrical trend) leads to a substantial decrease in internuclear angle, thereby producing in the present case the familiar equilateral triangle arrangement of cyclopropane.

Choosing the other in-plane orbital ($6a_1$), with its strong trend toward bent geometry, for substitution by the $2b_1$ leads to the (5,4,2,1) state, which has a much larger equilibrium CCC angle, but just as in ozone the energy minimum of this configuration (Fig. 3b) is considerably higher than that of the (6,3,2,1) species. In general it can be said that since the ground state electronic configuration of this molecule is associated with the smallest equilibrium angle possible for any of the 24-electron states of triatomics, any type of electronic excitation will lead to at least a partial opening of its CCC ring.

Location of all the terminal hydrogens in the CCC plane naturally has the opposite effect on the upper valence MO's, causing the in-plane $4b_2$ and $6a_1$ species to be considerably more stable than the $1a_2 - 2b_1$ out-of-plane pair.

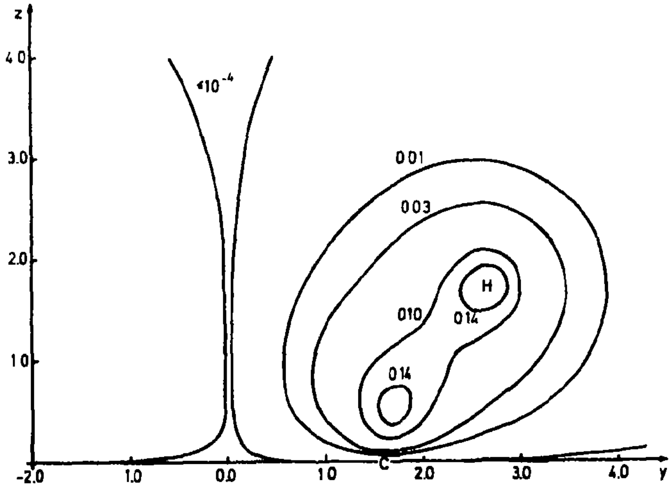

Fig. 5. Charge density contours for the $1e''$ MO of cyclopropane ($\measuredangle$ CCC = 60°)

A complicating factor for the description of trimethylene, however, is the fact that in the region of 120° ∢ CCC the $1a_2$ and $2b_1$ MO's are nearly isoenergetic, with the $2b_1$ the more stable at smaller angles, the $1a_2$ more stable at larger values. The situation is different from that in a simple triatomic (Fig. 1a) for the reason that the $2b_1$ in trimethylene is much more localized on the termini and therefore much less antibonding[2]. As a result the most stable configuration in this case is open-shell, with partial occupation of both the $2b_1$ and $1a_2$ MO's, and in agreement with Walsh's rules the equilibrium angle possessed by trimethylene [11] is believed to be in the neighborhood of 120°.

The third and most stable C_3H_6 isomer propylene has three hydrogens on one of the terminal carbons, two on the other and one on the central carbon; this system thus does not possess the vertical symmetry plane of all the other AB_2 and H_nAB_2 molecules discussed to this point, so that conclusions drawn for this system are necessarily somewhat less rigorous. Nevertheless with most of the hydrogens in the CCC plane, as is the case at equilibrium, it is once again clear that the in-plane $6a_1$ and $4b_2$ MO's (or their counterparts in the decreased symmetry of propylene) are relatively more stable than the out-of-plane pair. Since all out-of-plane hydrogens are on a terminal carbon, the normal stability ordering (with $1a_2$ below $2b_1$) is expected (Table 4) and therefore the ozone ground state configuration (with $2b_1$ unoccupied) is preferred for propylene and its observed equilibrium CCC angle (Table 1) is thus normal from the standpoint of Walsh's rules[3].

b) Hydrocarbons with 22 Electrons

According to Walsh's rules the normal ground state geometry of triatomics with 22 electrons is linear; the preferred electronic configuration is (5,4,1,1), i.e. the $6a_1$ and $2b_1$ MO's ($2\pi_u$ in linear symmetry) are not occupied. The C_3H_4 isomers allene and methylacetylene have all of their attached hydrogens on the terminal carbons, thus favoring the $4b_2$ and $1a_2$ MO's at the expense of the $6a_1$ and $2b_1$ species (see Table 4). Consequently both of these systems favor a linear arrangement of carbons, in conformity with the general rule.

To obtain a different nuclear arrangement at equilibrium for a 22-electron hydrocarbon it is necessary to attach some hydrogens to the central heavy atom and thereby stabilize either or both of the $6a_1$- and $2b_1$-type MO's. In the first example to be considered, allyl cation $C_3H_5^+$, one hydrogen atom is attached to the central carbon and located in the CCC plane, thereby selectively stabilizing the $6a_1$ species; at the same time rotation of the terminal methylene groups into the plane of the carbons causes an increase in the orbital energy of the out-of-plane $1a_2$-type MO compared to its value in allene. As a result the $6a_1$, with its strong preference for bent geometry, is occupied instead of the $1a_2$, producing the (6,4,1,0) ground state electronic configuration of allyl cation; both the predictions of Walsh's rules and the calculated potential curves of N_3^- (Fig. 4a) are consistent with the observed equilibrium angle for this system of approximately 120° (Fig. 4b). In addition the theory predicts that the addition of two electrons to this system to give the allyl anion results in the occupation of the $1a_2$ MO and in an accompanying slight increase in CCC angle; the anion, of course, is yet another example of a 24-electron system preferring the normal (6,4,1,1) electronic configuration predicted by the original theory.

---

[2] Because of CH bonding the $1b_1$ of trimethylene has its charge density maximum at the central heavy atom, also in contrast to the situation in simple triatomics.

[3] That the preferred angle is somewhat larger than that of ozone could indicate a partial mixing of the $2b_1$ and $1a_2$ species (now allowed in the reduced symmetry), although there is really little reason for expecting the theory to be capable of such discrimination under the circumstances.

Rotating the CH_2 groups of the allyl cation out of the CCC plane to give cyclopropyl cation has the effect of inverting the stability order of the MO's with charge density maxima at the terminal carbons, thereby favoring occupation of the out-of-plane $1a_2$ over the in-plane $4b_2$ species. This change in configuration should be accompanied by a substantial decrease in internuclear angle, as is demonstrated by the calculated potential curves for these systems given in Fig. 4b.

Placing two hydrogens at the central carbon atom further aids those orbitals with substantial central atom character, namely the $6a_1$ and $2b_1$ MO's, so much so that in cyclopropene it becomes energetically favorable to substitute these orbitals for the $4b_2$ and $1a_2$ species occupied in the conventional linear 22-electron systems. The resulting (6,3,2,0) electronic configuration is characterized by the smallest known internuclear angle observed for H_nAB_2 molecules.

c) Other Systems

Just as with simple triatomics the sum of 26 electrons represents the point of complete occupation or saturation of all the possible valence MO's of H_nAB_2 systems. It is not at all surprising then that no particularly novel structures are known for 26-electron members of this family (see Table 1). The well-known tetrahedral angle purported by valence bond theory to characterize all unsaturated bonding situations is thus seen to result according to Walsh's rules from the exhaustion of all available valence MO's; in good analogy with the geometry of F_2O, the corresponding skeletal internuclear angles invariably are found to lie in the neighborhood of 105–110°.

The theory of course is not restricted to systems with an even number of electrons; the allyl radical represents an example of an odd-electron system which is particularly worth noting. Even though this system is isoelectronic with nitrogen dioxide NO_2, its equilibrium CCC angle (120°) is found to be significantly smaller than that of the simple triatomic ($\sphericalangle$ ONO = 135°). This difference is again understandable and indeed predictable from consideration of Walsh's rules because of the fact that the two systems in question differ in ground state electronic configuration. The corresponding anions NO_2^- and $C_3H_5^-$ do possess the same configuration, identical to that of ozone, and approximately the same internuclear angle but ionization of these systems to give the respective free radicals occurs from orbitals of different symmetry, notably the $6a_1$ in NO_2 and (as has already been suggested in the discussion of the allyl cation) the $1a_2$ in C_3H_5. The qualitative theory unambiguously predicts that ionization of a $6a_1$ electron from an ozone configuration will cause a decided increase in internuclear angle but that loss of an electron from the $1a_2$ MO will be followed by a slight decrease in angle in good agreement with what is found.

Thus far the discussion has centered around H_nAB_2 systems with a symmetric BAB skeleton. Inspection of Table 1, however, indicates at least empirically that the present extension of Walsh's rules is equally valid for more general hydride systems with a non-symmetric ABC skeleton. In the case of simple triatomics this similarity between the geometries of symmetric and non-symmetric species has been justified, at least partially, on the basis of non-empirical calculations for NNO [9], from which it can be seen that a definite similarity exists between corresponding MO's of both types of systems (see, for example, Figs. 4–6 of Ref. [9] for a comparison of analogous MO's for symmetric NON and non-symmetric NNO), at least in the range of 180° to 110°. In particular it is found that the correlation diagrams calculated for non-symmetric triatomics are quite similar to those of BAB type in the latter range of internuclear angle.

6. Conclusion

Addition of hydrogen atoms to a triatomic molecule alters the relative stability ordering of the molecular orbitals of the parent system but does not significantly change the behavior of the orbital energies upon bending of the triatomic skeleton. As a result it is possible to predict the equilibrium angles of H_nAB_2 systems on the basis of Walsh's rules simply by allowing for the fact that the ground state electronic configuration of such molecules may differ from that of simple triatomic species with the same number of electrons. Thus the identical arguments used to predict the equilibrium geometries of the excited states of N_3^- and O_3 can be used to ascertain the *ground state* structures of all known H_nAB_2 systems with 22 and 24 electrons respectively, including such distinctive species as cyclopropane and cyclopropene.

The theory is thus seen to be capable of treating large numbers of molecules, inorganic and organic alike, on the basis of a single correlation diagram, albeit one with the added flexibility of allowing the energy levels to be shifted with respect to one another. Although only systems with a triatomic skeleton have been given explicit consideration in the foregoing discussion, the utility of the general theory is by no means restricted to molecules of this type; applications for systems with four heavy atoms, for example, have already been considered in connection with calculations for cyclobutadiene [12] C_4H_4. In addition the theory has the obvious advantage of being equally applicable to ground and excited states, thereby affording the prediction of details of electronic spectra which are otherwise all but inaccessable. It should therefore be possible on the basis of the aforementioned modified H_nAB_2 correlation diagrams to predict the structures of such systems in their excited states in much the same manner as Mulliken and Walsh have been able to do for the parent molecules not containing hydrogens.

Acknowledgement. The authors gratefully acknowledge the financial support of the Deutsche Forschungsgemeinschaft for this work.

References

1. Mulliken, R. S.: Rev. mod. Physics 14, 204 (1942).
2. Walsh, A. D.: J. chem. Soc. (London) 1953, 2260.
3. Peyerimhoff, S. D., Buenker, R. J., Allen, L. C.: J. chem. Physics 45, 734 (1966).
4. Buenker, R. J., Peyerimhoff, S. D.: J. chem. Physics 45, 3682 (1966).

5. Peyerimhoff, S. D., Buenker, R. J.: J. chem. Physics **47**, 1953 (1967).
6. Buenker, R. J., Peyerimhoff, S. D.: J. physic. Chem. **73**, 1299 (1969).
7. Peyerimhoff, S. D., Buenker, R. J.: Theoret. chim. Acta (Berl.) **14**, 305 (1969).
8. – – J. chem. Physics **51**, 2528 (1969).
9. – – J. chem. Physics **49**, 2473 (1968).
10. Buenker, R. J., Peyerimhoff, S. D., Whitten, J. L.: J. chem. Physics **46**, 2029 (1967); see Fig. 7.
11. Hoffmann, R.: J. Amer. chem. Soc. **90**, 1475 (1968).
12. Buenker, R. J., Peyerimhoff, S. D.: J. chem. Physics **48**, 354 (1968), Sect. VI.

Prof. Robert J. Buenker
Department of Chemistry
University of Nebraska
Lincoln, Nebraska 68508, USA

Prof. Sigrid D. Peyerimhoff
Institut für Physikalische Chemie
Johannes Gutenberg-Universität
D-6500 Mainz, Germany

Theoret. chim. Acta (Berl.) 24, 147--151 (1972)
© by Springer-Verlag 1972

On the Rules of Scheibe*, **

KARL JUG*** and ROBERT G. PARR
Department of Chemistry, The Johns Hopkins University, Baltimore, Maryland 21218

Received August 12, 1971

Scheibe's rules state that ionization potentials of first and higher excited states in molecules are approximately constant and hydrogen-atom-like. A simple explanation is given emphasizing the atomic nature of this effect. The analysis is based on a partitioning of space into nonoverlapping regions and the diffuse character of local charge distributions in singly-occupied antibonding MO's. The existence of bonding MO's in small molecules like H_2 is briefly discussed.

Die Scheibeschen Regeln sagen aus, daß die Ionisierungsenergien angeregter Zustände in Molekülen konstant und wasserstoffatomähnlich sind. Wir geben eine einfache Erklärung, die die atomare Natur dieses Effektes betont. Die Ableitung basiert auf Raumaufteilung in nichtüberlappende Gebiete und diffusem Charakter der lokalen Ladungsverteilung in einfach besetzten antibindenden MO's. Auf das Vorkommen bindender MO's in kleinen Molekülen wie H_2 wird kurz eingegangen.

Les règles de Scheibe affirment que les potentiels d'ionisation du premier état excité et des états excités plus élevés des molécules sont approximativement constants et semblables à ceux de l'atome d'hydrogène. On fournit une explication simple en insistant sur la nature atomique de cet effet. L'analyse est fondée sur une division de l'espace en régions disjointes et sur le caractère diffus des distributions de charge locale dans les orbitales moléculaires antiliantes simplement occupées. L'existence d'orbitales moléculaires liantes dans des petites molécules comme H_2 est brièvement discutée.

1. Introduction

Almost twenty years ago, Scheibe and coworkers [1] discovered in an investigation of a large number of molecules that the difference between first-excited state energy and ionization limit is approximately constant. The effect was also studied for second-, third- and some fourth-excited states. Scheibe tentatively assigned them as $2p\pi, 3p\pi, 4p\pi$, etc., and compared their relative energies with the excited states of the hydrogen atom.

A theoretical discussion in terms of Hückel theory was given by Hartmann [2]. He found that an admixture of $3p\pi$ atomic orbitals to the usual $2p\pi$ orbitals could explain Scheibe's findings. Later Kollaard and Colpa [3] suggested that an explanation based solely on $2p\pi$ orbitals was possible.

Both of these explanations were embedded in concepts of the old semiempirical methods, with Slater exponents for AO's and a common basis set for both ground and excited states. The following explanation, involving a new concept of antibonding orbitals, may be more realistic.

---

* Dedicated to the memory of Prof. K. H. Hansen.

** Aided by research grant to The Johns Hopkins University from the National Institutes of Health.

*** Permanent address: Department of Chemistry, Saint Louis University, Saint Louis, Missouri 63156, USA.

2. Derivation

For convenience we study the effect in a simple hydrocarbon which is representative for π-electron systems: ethylene. In the π-electron approximation [4], the ground state is represented by a doubly-occupied bonding MO ϕ_0, the first-excited state by a singly-occupied MO ϕ_0 and a singly-occupied antibonding MO ϕ_1, and the ionized state by a singly-occupied MO ϕ_0. Contrary to previous approaches, we shall compare first-excited state and ionized state directly, i.e., without direct reference to the ground state.

The total wavefunctions of the two states are

$$\begin{aligned} {}^{1,3}\Psi &= \tfrac{1}{2}\{(\phi_0\bar{\phi}_1) \mp (\bar{\phi}_0\phi_1)\} \\ {}^{2}\Psi &= \phi_0 \end{aligned} \tag{1}$$

and their energies are

$$\begin{aligned} {}^{1,3}E &= {}^{1,3}\varepsilon_0^{\mathrm{core}} + {}^{1,3}V_{\mathrm{nuc}} + {}^{1,3}\varepsilon_1 \\ {}^{2}E &= {}^{2}\varepsilon_0^{\mathrm{core}} + {}^{2}V_{\mathrm{nuc}} \,. \end{aligned} \tag{2}$$

$\varepsilon_0^{\mathrm{core}}$ is the core energy of the electron in the bonding orbital, V_{nuc} is the interaction energy of the framework and ε_1 is the SCF energy of the electron in the antibonding orbital. It is reasonable to assume that the removal of an electron from a singly-occupied antibonding orbital does not change very much the sum of core attraction and framework interaction of the remaining electrons. Thus the energy difference ΔE between first-excited and ionized state is equal to the SCF energy of the electron in the antibonding orbital.

$$\Delta E = \varepsilon_1 \,. \tag{3}$$

This means that we assume Koopman's theorem to be valid for excited states.

Let us now proceed to some more specific considerations. The MO's ϕ may be represented by a sum of cut-off AO's [5, 6] defined in three nonoverlapping

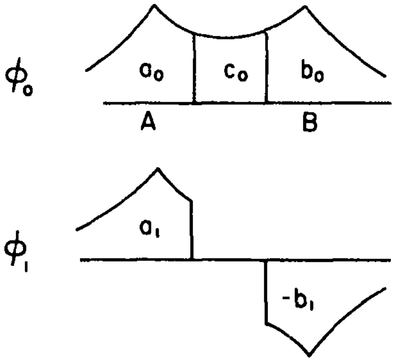

Fig. 1. Partitioning of bonding orbital ϕ_0 and antibonding orbital ϕ_1 in three nonoverlapping parts a, b, c for 1*s* orbitals

regions of space: two atomic and one bonding region.

$$\begin{aligned}\phi_0 &= (2+\langle c_0|c_0\rangle)^{-1/2}(a_0+b_0+c_0)\\ \phi_1 &= 2^{-1/2}(a_1-b_1)\,.\end{aligned}\tag{4}$$

For $1s$ orbitals these functions are schematically presented in Fig. 1; a and b are renormalized and represent the atomic regions, c_0 is continuous with a_0 and b_0 on the boundary surfaces and represents the bonding region. Questions concerning the discontinuity in ϕ_1 are discussed elsewhere [6]. With these assumptions and a partitioning of the SCF energy into core attraction and electron interaction, the energy difference ΔE becomes

$$\begin{aligned}\Delta E &= {}^{1,3}E-{}^{2}E\\ &= \varepsilon_1^{\text{core}}+J\pm K\\ &= \langle\phi_1|T-\frac{Z_{\text{eff}}}{r_a}-\frac{Z_{\text{eff}}}{r_b}|\phi_1\rangle\\ &\quad+\langle\phi_0\phi_0|\phi_1\phi_1\rangle\pm\langle\phi_0\phi_1|\phi_0\phi_1\rangle\\ &= \langle a_1|T-\frac{Z_{\text{eff}}}{r_a}-\frac{Z_{\text{eff}}}{r_b}|a_1\rangle\\ &\quad+\langle\phi_0\phi_0|a_1a_1\rangle\pm\langle\phi_0a_1|\phi_0a_1\rangle\mp\langle\phi_0a_1|\phi_0b_1\rangle\,.\end{aligned}\tag{5}$$

If the dimensions of the charge cloud of the antibonding orbital become large compared to the internuclear distance, the effective charge Z_{eff} will approach unity. The difference of exchange integrals $\langle\phi_0a_1|\phi_0a_1\rangle$ and $\langle\phi_0a_1|\phi_0b_1\rangle$ will become negligibly small and the Coulomb repulsion integral $\langle\phi_0\phi_0|a_1a_1\rangle$ will approximately cancel the nuclear attraction term $\langle a_1|-\frac{Z_{\text{eff}}}{r_b}|a_1\rangle$. The final expression for ΔE then takes the form

$$\Delta E=\langle a_1|T-\frac{1}{r_a}|a_1\rangle\,.\tag{6}$$

This formula is of course approximate, but it should describe the situation fairly accurately.

Because of its cut-off character, a_1 cannot be an exact eigenfunction of the hydrogen atom Hamiltonian. But since it is normalized, the integral (6) should come close to a hydrogen atom energy if a proper type of orbital with a hydrogen atom exponent is chosen. This would be in the case of ethylene a $2p\pi$ orbital with $\zeta=1/2$. This is exactly what Scheibe found in his investigation. Hence we expect from experiment that an atomic exponent of 0.5 in antibonding $2p\pi$ orbitals would be more appropriate than Slater exponents which are about three times larger. This conclusion is in agreement with a calculation by Huzinaga [7], who found $\zeta=0.4$ most appropriate for the antibonding orbital in ethylene. His grid of $\Delta\zeta=0.2$ was too coarse for greater accuracy.

Scheibe also collected data for several molecules, e.g., H_2 and Li_2, in which the situation is completely different from ethylene. In the case of H_2, the first excited Π state is obtained by the promotion of an electron from a bonding σ MO to a bonding π MO. It is the second excited Π state which contains an antibonding π MO. These two states labeled Π_u and Π_g have been extensively studied by Jug *et al.* [8]. It was found that in the LCAO description the π_u orbital is described mainly by a linear combination of $2p\pi$ AO's with exponents $\zeta = 0.442$ for $^1\Pi_u$ and $\zeta = 0.562$ for $^3\Pi_u$ at 2 Bohr. The SCF energy of the former state is slightly higher and of the latter slightly lower than the energy of the first-excited state of the hydrogen atom. Most remarkable is the Π_g state, where the π_g orbital at 2 Bohr is a linear combination of 99% of $2p\pi$ orbitals with exponents $\zeta = 0.245$ and 1% of $3d\pi$ orbitals. The SCF energy equals the $3d$-energy of the hydrogen atom to three figures. The singlet-triplet splitting is negligibly small. Here Scheibe's rule describes the situation better than in the Π_u states.

There are some questions which are still unanswered. One concerns the practical definition of the bonding region, the other the explicit form of the atomic basis functions. Some discussion can be found elsewhere [6]. However, the mathematical evaluation offers difficulty and the consequences of truncation and discontinuous functions are not yet completely explored.

3. Conclusion

We have seen that Scheibe's rules can be explained on the basis of atomic considerations. Two different situations exist in molecules, which are distinguished by the bonding and antibonding character of the highest singly occupied MO. The two cases are typified by H_2 and ethylene. In both cases the expection values of the charge distribution of the π orbital perpendicular to the molecular axis is large compared to the internuclear distance. For example, in H_2 it yields (at an internuclear distance of 2 Bohr) for $^1\Pi_u$, $\langle \varrho_\pi^2 \rangle^{1/2} = 5.6$ Bohr and for $^1\Pi_g$, $\langle \varrho_\pi^2 \rangle^{1/2} = 8.8$ Bohr. This allows us to characterize the situation as nearly atomic. It is the expansion of the main LCAO orbitals rather than the admixture of higher AO's which is responsible for the effect. For larger polyatomic molecules, we expect the situation to be ethylene-like, i.e., characterized by local antibonding expansions upon excitation.

Here we have invoked a picture where the basis functions entering the antibonding orbitals are atomic orbitals which are separated by a nonbonding region. We promote the idea that antibonding orbitals are almost nonbonding. A calculation on the antibonding orbital of $^1\Pi_g$ in H_2 substantiates this [9]. We point out that this view of the antibonding orbital has consequences for the parametrization of semi-empirical methods. The energy difference between bonding and antibonding orbitals should be set equal to β rather than 2β.

Finally, Scheibe's measurements do not appear to show any manifestations of the fact that there is a degeneracy in the hydrogen atom: for example, there should be two states close together in molecules which correspond to the $3p\pi$ and $3d\pi$ hydrogen states. Perhaps Scheibe's resolution was not good enough to separate them.

Acknowledgement. We thank Professor H. Hartmann for stimulating our interest in this subject at the Konstanz Summer Institute in 1963.

References

1. Scheibe, G., Brück, D., Dörr, F.: Chem. Ber. **85**, 867 (1952).
2. Hartmann, H.: Z. Naturforsch. **15a**, 993 (1960).
3. Kollaard, U.H., Colpa, J.P.: Molecular Physics **8**, 295 (1964).
4. Lykos, P.G., Parr, R.G.: J. chem. Physics **24**, 116; **25**, 1301 (1956).
5. Weare, J.H., Parr, R.G.: Chem. Physics Letters **1**, 349 (1967).
6. Stuebing, E.W.: Discontinuous approximate wavefunctions. Ph. D. Thesis, The Johns Hopkins University, 1970.
7. Huzinaga, S.: J. chem. Physics **36**, 453 (1962).
8. Jug, K., Lykos, P.G., McLean, A.D.: Optimal double-configuration study of the lowest excited Π states of H_2, I. Theoret. Chim. Acta (Berl.) (in press).
9. — — — Optimal double configuration study of the lowest excited Π states of H_2, II. Theoret. Chim. Acta (Berl.) (in press).

Prof. Karl Jug
Institut für Theoretische Chemie
der Universität Stuttgart
D-7 Stuttgart 1
Germany

Theoret. chim. Acta (Berl.) 24, 152–169 (1972)
© by Springer-Verlag 1972

The Direct Determination of Brueckner Orbitals with Application to the H_2 Molecule*

VOLKER STAEMMLER
Institut für Physikalische Chemie und Elektrochemie, Abteilung Theoretische Chemie,
D-75 Karlsruhe, Kaiserstraße 12, Germany

MARTIN JUNGEN
Physikalisch-Chemisches Institut der Universität Basel,
Klingelbergstraße 80, CH-4056 Basel, Switzerland

Received June 16, 1971

An iterative procedure is presented which allows for the direct determination of approximate Brueckner orbitals for small atomic and molecular systems. Starting from the Hartree-Fock determinant one first determines pair natural orbitals (PNOs) of independent electron pairs in the HF-field of the remaining electrons. The use of the generalized Brillouin-theorem then leads to an approximate Brueckner orbital for each electron pair. This procedure must be repeated up to self-consistency which is reached generally after 4–5 macroiterations. Applications to the ground state of H_2 show how important the use of Brueckner orbitals is to get good expectation values of one-electron operators and the correct asymptotic behaviour of the potential energy curve for large internuclear distances.

Es wird eine Iterationsmethode beschrieben, die eine direkte Bestimmung genäherter Brueckner-orbitale für kleine atomare und molekulare Systeme gestattet. Ausgehend von der Hartree-Fock-Determinante bestimmt man zunächst Paar-NOs (PNOs) der unabhängigen Elektronenpaare im HF-Feld der übrigen Elektronen des Systems. Mit Hilfe des verallgemeinerten Brillouin-Theorems erhält man dann ein genähertes Bruecknerorbital für jedes Elektronenpaar. Dies Verfahren muß bis zur Selbstkonsistenz wiederholt werden, die man im allgemeinen nach 4–5 solcher Makroiterationen erreicht. Anwendung auf den Grundzustand des H_2-Moleküls zeigt, wie wichtig die Benutzung von Bruecknerorbitalen ist, wenn man gute Erwartungswerte von Einelektronenoperatoren und das richtige asymptotische Verhalten der Potentialkurve bei großen Abständen erhalten will.

On propose un schéma itératif qui permet le calcul direct des orbitales de Brueckner approchées pour les atomes et les petites molécules. Partant du déterminant Hartree-Fock on calcule d'abord les PNO (pair natural orbitals) des paires indépendantes d'électrons dans le champ effectif des autres électrons dans l'approximation Hartree-Fock. Ensuite le théorème de Brillouin généralisé permet de calculer les orbitales de Brueckner approchées pour chaque paire d'electrons. On recommence le calcul des PNO, la "self-consistance" de cette méthode itérative s'établit en général au bout de 4 ou 5 macroitérations. Les applications à la molécule H_2 démontrent que l'utilisation d'orbitales de Brueckner s'impose si l'on s'intéresse à des bonnes valeurs moyennes d'opérateurs monoélectroniques ou au comportement asymptotique correct des courbes de potentiel aux grandes distances.

1. Introduction

The convenient starting point for a configuration interaction (CI) treatment of the electronic correlation in atoms and small molecules is a conventional restricted Hartree-Fock (HF) calculation, yielding the HF-determinant as a reasonable leading configuration and an orthonormal set of occupied and virtual orbitals from which excited configurations – in the following we shall prefer the term "substituted configurations" – can be constructed.

---

* Dedicated to the memory of Prof. K. H. Hansen.

The reason to choose this starting point for the CI-expansion is that the HF-determinant in many cases is already a good approximation to the wavefunction of the state under consideration. Only doubly substituted configurations (in the following abbreviated as DSC's) contribute largely to the correlation energy, since because of the Brillouin-theorem [1, 2] the energy contributions of the singly, triply, and higher substituted configurations vanish in first order. But the choice of the HF-determinant is unfavourable in two respects:

1. The coefficients of the singly substituted configurations (SSC's) do not vanish exactly, so that the HF-determinant despite of being the energetically best one-determinantal wavefunction has neither the best overlap with the true wavefunction of the system nor the best expectation values of one-electron operators obtainable with a one-determinantal wavefunction.

2. The HF-wavefunction is a rather poor approximation of the true one whenever it is degenerate or nearly degenerate with other configurations of the same symmetry, i.e. whenever the CI-expansion coefficients of one or more of the DSC's are comparable – in absolute value – to that of the HF-determinant. This happens, for instance, in many molecular systems at large internuclear distances; we only mention the well known example of H_2.

These deficiencies of the HF-determinant can be corrected by the inclusion of SSC's into the CI-expansion. Equivalently, one can start from the "best-overlap"- or "Brueckner"-determinant, constructed from the socalled "best-overlap" or "Brueckner-orbitals" (BO's) [3–8]. This choice of the leading configuration guarantees that the coefficients of the SSC's vanish identically [9], so that they need not to be included into the CI-expansion.

More familiar to quantum chemists are the "natural orbitals" (NO's) first introduced by Löwdin [10], which diagonalize the first order density matrix of the system. It has been noted that the BO's coincide with the first NO's in the case of two electrons [11, 12], but this holds only approximately for systems with more than two electrons [12, 13]. Whenever we are dealing with two electrons we shall use the terms "Brueckner orbitals" and "first NO's" synonymously.

Unfortunately, the determination of BO's and first NO's is much more complicated than the determination of the HF-orbitals. The reason is that because of the Brillouin-theorem [1, 2] the matrix elements of the Hamiltonian between the HF-determinant and the SSC's vanish. Therefore, the SSC's interact with the HF-determinant only indirectly via the DSC's, thus an expansion including SSC's and DSC's is necessary to determine the BO's.

The procedures proposed in the literature to construct BO's for atoms and molecules can be divided in two classes:

1. If very accurate wavefunctions of the state under consideration are known the BO's can be obtained according to the condition that the Brueckner-determinant has maximum overlap with the true wavefunction. But this method obviously is limited to systems for which sufficiently accurate wavefunctions are available and has been applied only to two-electron systems [11, 14–18] and to the Li-atom [12].

2. For the determination of BO's without knowledge of a very accurate wavefunction the conventional CI-expansions or MCSCF procedures are adequate provided that SSC's and DSC's are included simultaneously or that the leading configuration is reoptimized in the field of the DSC's. Of the latter type are the "extended Hartree-Fock" calculations of the Das and Wahl [19–21] yielding very good potential energy curves for H_2, Li_2, and F_2. Ahlrichs, Kutzelnigg, and Bingel [22] have calculated the first NO for the He-atom using a "macroiteration" scheme in which the "correlation potential" leading to the BO is taken into account iteratively. The same technique has been applied later by Kutzelnigg and Gélus [23] to calculate the valence shell correlation energy of Li_2 at large internuclear distances, but these authors run into difficulties with non-diagonal Lagrange multipliers if they want to include higher NO's of the same symmetry as the BO.

In this paper we present an alternative method for the direct determination of BO's avoiding this difficulty. The BO for a two-electron system is calculated in a macroiteration procedure using the generalized Brillouin-theorem [24] for MCSCF-wavefunctions. Each macroiteration cycle contains several microiterations to determine the higher NO's and the BO as described in Sect. 2a. For systems with more than two electrons we use the "independent electron pair approach" (IEPA) with step-by-step determination of "pair-NO's" or "pseudo-NO's" [25] for each individual pair in the HF-field of the remaining electrons as described by Ahlrichs and Kutzelnigg [26]. In this approximation we obtain a BO for each pair which should be called "pair-BO" or "pseudo-BO", analogously to the higher NO's. This procedure is similar to the one recently proposed by Larsson [18].

In Sect. 3 applications to the calculation of one-electron properties of H_2 at the equilibrium distance of 1.4 a_0 are presented. The errors of expectation values of some one-electron operators with the HF-determinant, Brueckner-determinant, and different CI-expansions are compared to the very accurate results of Kolos and Wolniewicz [27].

Sect. 4 contains results of the calculation of the potential energy curve of H_2 at large internuclear distances. A two-configuration wavefunction yields the correct asymptotic behaviour only if the first determinant is the Brueckner-determinant.

2. The Macroiteration Scheme to Determine Brueckner-Orbitals

a) The Ground State of a Two-Electron System

Let us first consider a two-electron system in its singlet ground state. Let φ_α, $\alpha = 1, 2 \ldots$, be a fixed set of orthonormal orbitals where φ_1 is the doubly occupied HF-orbital or an approximation to it.

The normalized wavefunction $\Psi(1,2)$ of the system can be expanded into a series of Slaterdeterminants

$$\Psi(1,2) = c_1 \Phi_1 + \sum_{\alpha>1} c_\alpha \Phi_\alpha + \sum_{\alpha \geq \beta > 1} c_{\alpha\beta} \Phi_{\alpha\beta} \tag{1}$$

where Φ_1 is the HF-determinant and Φ_α and $\Phi_{\alpha\beta}$ are singly and doubly substituted configurations (SSC's and DSC's, respectively):

$$\Phi_1 = |\varphi_1\bar{\varphi}_1|\,, \tag{2a}$$

$$\Phi_\alpha = \frac{1}{\sqrt{2}}\{|\varphi_1\bar{\varphi}_\alpha| + |\varphi_\alpha\bar{\varphi}_1|\}\,, \tag{2b}$$

$$\Phi_{\alpha\beta} = \frac{1}{\sqrt{2}}\{|\varphi_\alpha\bar{\varphi}_\beta| + |\varphi_\beta\bar{\varphi}_\alpha|\}\,. \tag{2c}$$

We shall assume for simplicity that the c_α, $c_{\alpha\beta}$ are real. The expectation value of an arbitrary operator O with respect to $\Psi(1,2)$ is then given by

$$\begin{aligned}(\Psi|O|\Psi) = {} & c_1^2(\Phi_1|O|\Phi_1) + 2c_1\sum_\alpha c_\alpha(\Phi_1|O|\Phi_\alpha)\\ & + 2c_1\sum_{\alpha\gtrless\beta} c_{\alpha\beta}(\Phi_1|O|\Phi_{\alpha\beta}) + \sum_\alpha\sum_\gamma c_\alpha c_\gamma(\Phi_\alpha|O|\Phi_\gamma)\\ & + \sum_{\alpha\gtrless\beta}\sum_{\gamma\gtrless\delta} c_{\alpha\beta}c_{\gamma\delta}(\Phi_{\alpha\beta}|O|\Phi_{\gamma\delta})\\ & + 2\sum_\alpha\sum_{\gamma\gtrless\delta} c_\alpha c_{\gamma\delta}(\Phi_\alpha|O|\Phi_{\gamma\delta})\,.\end{aligned} \tag{3}$$

If O is a one-electron operator A, the terms $(\Phi_1|A|\Phi_{\alpha\beta})$ vanish. Further, if φ_1 is the HF-orbital and φ_α, $\alpha > 1$, orthogonal to it, as we have assumed, the Brillouin-theorem [1, 2] states that

$$(\Phi_1|H|\Phi_\alpha) = 0 \quad \text{for all } \Phi_\alpha \tag{4}$$

and in most cases the coefficients c in (1) fulfill the relations

$$c_1 \approx 1\,; \qquad c_\alpha, c_{\alpha\beta} \ll 1\,.$$

Actually, c_1, $c_{\alpha\beta}$ and c_α are of zeroth, first and second order, respectively, but here we are not concerned with a thorough discussion of the relative orders of magnitude of the terms appearing in (3), which has been given by Grimaldi [28].

With these simplifications the expectation values of A and H become

$$(\Psi|A|\Psi) = c_1^2(\Phi_1|A|\Phi_1) + 2c_1\sum_\alpha c_\alpha(\Phi_1|A|\Phi_\alpha) + \cdots\,, \tag{5a}$$

$$(\Psi|H|\Psi) = c_1^2(\Phi_1|H|\Phi_1) + 2c_1\sum_{\alpha\gtrless\beta} c_{\alpha\beta}(\Phi_1|H|\Phi_{\alpha\beta}) + \cdots\,. \tag{5b}$$

The terms represented by dots are identical to the last three terms in (3). Their overall contributions to the total expectation values are comparable to those of the terms linear in c_1.

The expressions (5a) and (5b) can be further simplified. If we know the coefficients c_α of the SSC's Φ_α, we can perform a linear transformation

$$\chi_1' = \mathcal{N}\left\{\varphi_1 + \frac{1}{\sqrt{2}c_1}\sum_\alpha c_\alpha\varphi_\alpha\right\} \tag{6}$$

where $\mathcal{N}$ is the normalization constant for the new orbital χ_1'. The Slater-determinant

$$\Phi_1' = |\chi_1'\bar{\chi}_1'| = \frac{\mathcal{N}^2}{c_1}\left\{c_1\Phi_1 + \sum_{\alpha} c_\alpha\Phi_\alpha + \frac{1}{\sqrt{2}c_1}\sum_{\alpha\geq\beta} c_\alpha c_\beta\Phi_{\alpha\beta}\right\} \tag{7}$$

coincides with Ψ as far as Φ_1 and the SSC's are concerned. Φ_1' differs from Ψ only in the DSC's. This means, that on replacing Φ_1 by Φ_1' we get rid of the SSC's, or, stated differently, the choice of Φ_1' instead of Φ_1 makes the coefficients of the SSC's vanish. The wavefunction $\Psi(1,2)$ can now be written as

$$\begin{aligned}\Psi(1,2) &= \frac{c_1}{\mathcal{N}^2}\Phi_1' + \sum_{\alpha\geq\beta}\left(c_{\alpha\beta} - \frac{c_\alpha c_\beta}{\sqrt{2}c_1}\right)\Phi_{\alpha\beta} \\ &= c_1'\Phi_1' + \sum_{\alpha\geq\beta} c'_{\alpha\beta}\Phi_{\alpha\beta}\,.\end{aligned} \tag{8}$$

According to (6) the orbital χ_1' is not orthogonal to the φ_α, $\alpha>1$, therefore the $\Phi_{\alpha\beta}$ in (8) are not orthogonal to Φ_1' and the expressions for the expectation values of A and H become more complicated. If we replace the virtual orbitals φ_α, $\alpha>1$, by a new set φ_α', $\alpha>1$, orthogonal to χ_1' and express the $\Phi_{\alpha\beta}$ in terms of these φ_α' we find still remaining SSC's

$$\Phi_\alpha' = \frac{1}{\sqrt{2}}\{|\chi_1'\bar{\varphi}_\alpha'| + |\varphi_\alpha'\bar{\chi}_1'|\}$$

with coefficients c_α' roughly proportional to $\sum_\beta c_{\alpha\beta}c_\beta$, i.e. generally much smaller than the original c_α.

Therefore, to construct the correct Brueckner orbital (BO) [3–8] χ_1 satisfying the Brueckner condition [9]

$$d_\alpha = \left(\Psi\,\middle|\,\frac{1}{\sqrt{2}}\{|\chi_1\bar{\chi}_\alpha| + |\chi_\alpha\bar{\chi}_1|\}\right) = 0 \quad \text{for all} \quad \alpha>1 \tag{9}$$

(with the χ_α, $\alpha>1$, orthogonal to χ_1) an iteration scheme is necessary:

Starting with φ_1, φ_α we determine χ_1' according to (6) and a set φ_α' orthogonal to χ_1'. Then we have to determine the new c_α' to perform the transformation (6) again and so forth.

In quite the same way – i.e. by changing the weakly occupied orbitals φ_α analogously to (6) – we can get rid of the "non-diagonal" coefficients $c_{\alpha\beta}$ with $\alpha\neq\beta$ and end up with the diagonal expansion

$$\Psi = d_1\Psi_1 + \sum_\alpha d_{\alpha\alpha}\Psi_{\alpha\alpha} = d_1|\chi_1\bar{\chi}_1| + \sum_\alpha d_{\alpha\alpha}|\chi_\alpha\bar{\chi}_\alpha|\,. \tag{10}$$

It is the well-known "natural expansion" of the wavefunction [29, 11], the orbitals χ_α are called "natural orbitals" (NO's) [10]. For the two-electron system the first NO χ_1 is identical to the Brueckner-orbital [11]. Wavefunctions of type (10) are nowadays often used in accurate ab-initio calculations because of their simplicity and rapid convergency.

The expectation values of A and H now read

$$(\Psi|A|\Psi) = d_1^2(\Psi_1|A|\Psi_1) + \sum_\alpha d_{\alpha\alpha}^2(\Psi_{\alpha\alpha}|A|\Psi_{\alpha\alpha}), \tag{11a}$$

$$\begin{aligned}(\Psi|H|\Psi) &= d_1^2(\Psi_1|H|\Psi_1) + 2\sum_\alpha d_1 d_{\alpha\alpha}(\Psi_1|H|\Psi_{\alpha\alpha}) \\ &\quad + 2\sum_\alpha\sum_\beta d_{\alpha\alpha}d_{\beta\beta}(\Psi_{\alpha\alpha}|H|\Psi_{\beta\beta}).\end{aligned} \tag{11b}$$

Ψ_1 is the one-determinantal wavefunction giving the maximum overlap with Ψ and in most cases the best expectation values of one-electron operators (compare Sect. 3, [18]), but in view of the definition of the HF-orbital φ_1 it yields a poorer energy than Φ_1.

Now our problem is to calculate the coefficients c_α for a fixed set of orbitals φ_α in order to perform the transformation (6) from the MF-orbital to the first NO. This can be done with some different procedures, the conventional ones are:

a) Carry out a full configuration interaction with all SSC's Φ_α and all DSC's $\Phi_{\alpha\beta}$. Because of the Brillouin-theorem the SSC's do not contribute directly to the energy, thus, unfortunately, it is necessary to include all the DSC's, too.

b) Apply second order perturbation theory. Because of the Brillouin-theorem the first non-vanishing contribution to c_α is given by an expression like

$$c_\alpha = \sum_{\beta\gamma} \frac{(\Phi_1|H|\Phi_{\beta\gamma})(\Phi_{\beta\gamma}|H|\Phi_1)}{(E_1 - E_{\beta\gamma})(E_1 - E_\alpha)}. \tag{12}$$

E_1, E_α and $E_{\beta\gamma}$ are the energy expectation values of Φ_1, Φ_α and $\Phi_{\beta\gamma}$, respectively.

Both these methods are straightforward, but rather tedious, so we looked for a simpler, alternative procedure. The easiest way seems to use the generalized Brillouin-theorem [24] in connection with the NO-expansion (10). We shall describe this method in the following.

Again we start with a HF- or a near HF-solution φ_1. In the first step we calculate approximate NO's χ'_α, $\alpha > 1$, using the approximation $\chi_1 = \varphi_1$. We obtain an expansion

$$\Psi' = c_1|\varphi_1\bar{\varphi}_1| + \sum_\alpha d'_{\alpha\alpha}|\chi'_\alpha\bar{\chi}'_\alpha| \tag{13}$$

analogous to (10), but φ_1 still being the HF-orbital and χ'_α only approximate NO's. This first step is described explicitly by Ahlrichs and Kutzelnigg [26, 30], where one can find all the equations and formulae necessary for the calculation of the χ'_α and $d'_{\alpha\alpha}$.

The remaining error of the expansion (13) – provided that enough terms $|\chi'_\alpha\bar{\chi}'_\alpha|$ are included – comes from the approximation $\chi_1 = \varphi_1$. It can be corrected by the addition of SSC's. Let us for instance consider the SSC

$$\Phi_\lambda = \frac{1}{\sqrt{2}}\{|\varphi_1\bar{\varphi}_\lambda| + |\varphi_\lambda\bar{\varphi}_1|\} \tag{14}$$

with a trial orbital φ_λ, which is chosen to minimize the energy expectation value of the wavefunction

$$\Psi'' = c_1|\varphi_1\bar{\varphi}_1| + \sum_\alpha d'_{\alpha\alpha}|\chi'_\alpha\,\bar{\chi}'_\alpha| + c_\lambda\Phi_\lambda = \Psi' + c_\lambda\Phi_\lambda. \tag{15}$$

Obviously the addition of one single SSC Φ_λ is sufficient, because $c_\lambda \varphi_\lambda$ with optimized c_λ and φ_λ is completely equivalent to the sum $\sum_\alpha c_\alpha \varphi_\alpha$ with fixed φ_α entering into (6).

This is a variation problem for both c_λ and φ_λ, whereas c_1, $d'_{\alpha\alpha}$, φ_1, χ'_α remain fixed. The only constraint for the variation of φ_λ is that it must be orthogonal to φ_1. This problem is very similar to the HF-problem, and the easiest way to derive the variational equation for φ_λ is to use the generalized Brillouin-theorem [24]. It states – analogously to the common Brillouin-theorem in (4) – that the "optimal" orbital φ_λ fulfills the equation

$$(\Psi''|H|\Psi''(\lambda \to \mu)) = 0 \tag{16}$$

for every φ_μ orthogonal to φ_1 and φ_λ.

In (16) $\Psi''(\lambda \to \mu)$ is the function derived from Ψ'' (15) by replacing φ_λ by φ_μ and dropping all determinants not containing φ_λ. Written explicitly the condition for φ_λ is

$$\begin{aligned} 0 &= (\Psi''|H|\Psi''(\lambda \to \mu)) \\ &= \sqrt{2}c_1(h_{1\mu} + J^1_{1\mu}) + \sqrt{2}\sum_\alpha d'_{\alpha\alpha}(h_{1\alpha}S_{\alpha\mu} + K^\alpha_{1\mu}) \\ &\quad + c_\lambda(h_{\lambda\mu} + J^1_{\lambda\mu} + K^1_{\lambda\mu}) \\ &= (\varphi_\mu \,|\, \sqrt{2}c_1(\boldsymbol{h} + \boldsymbol{J}^1)\,\varphi_1 + \sqrt{2}\sum_\alpha d'_{\alpha\alpha}(\boldsymbol{K}^\alpha \varphi_1 + h_{\alpha 1}\boldsymbol{S}\chi'_\alpha) \\ &\quad + c_\lambda(\boldsymbol{h} + \boldsymbol{J}^1 + \boldsymbol{K}^1)\varphi_\lambda) \end{aligned} \tag{17}$$

where $\boldsymbol{h}$ is the one-electron part of the Hamilton-operator, $\boldsymbol{S}$ the overlap matrix, $\boldsymbol{J}^i$ and $\boldsymbol{K}^i$ the Coulomb- and exchange operators of the orbital i, respectively. This condition can be fulfilled for any φ_μ only when φ_λ satisfies the following relation

$$\begin{aligned} &\sqrt{2}\left\{c_1(\boldsymbol{h} + \boldsymbol{J}^1)\,\varphi_1 + \sum_\alpha d'_{\alpha\alpha}[\boldsymbol{K}^\alpha \varphi_1 + h_{\alpha 1}\boldsymbol{S}\chi'_\alpha]\right\} \\ &\qquad + c_\lambda(\boldsymbol{h} + \boldsymbol{J}^1 + \boldsymbol{K}^1)\varphi_\lambda = \mu_\lambda \varphi_\lambda\,. \end{aligned} \tag{18}$$

This equation is very similar to the equation for the higher NO's χ'_α, but contains an inhomogeneous part not depending on φ_λ itself. For the solution of such inhomogeneous eigenvalue equations we use the method of Gabel [31], the explicit appearance of c_λ in (18) makes an iterative procedure necessary which is completely analogous to the iterative procedure for the construction of the approximate NO's themselves [26]. We shall call this type of iterations *microiterations.*

With the so determined c_λ and φ_λ we can perform the transformation

$$\chi'_1 = \mathcal{N}\left\{\varphi_1 + \frac{1}{\sqrt{2}c_1}c_\lambda \varphi_\lambda\right\} \tag{19}$$

from φ_1 to χ'_1 which is equivalent to (6). But according to the discussion following Eq. (8) this χ'_1 is not yet the correct BO. Similarly, the χ'_α are not yet the correct higher NO's, since they are determined with the approximation $\chi_1 = \varphi_1$. Therefore, we have to use a *macroiteration* procedure: We start with $\chi_1^{(0)} = \varphi_1$, calculate the

$\chi_\alpha^{(0)}$ and $\varphi_\lambda^{(0)}$, perform the transformation (19) to construct a first approximation $\chi_1^{(1)}$ as described above. This $\chi_1^{(1)}$ is used to calculate better approximations $\chi_\alpha^{(1)}$ and $\varphi_\lambda^{(1)}$ for the higher NO's and so on. To reach self-consistency about 2–5 macroiterations are sufficient in our applications.

It is easy to see that our microiteration procedure for the determination of φ_λ and c_λ corresponds to an optimized fourth order perturbation method. Let us consider the typical fourth order energy contribution

$$E_\lambda^{(4)} = \sum_{\beta\gamma}\sum_{\delta\varepsilon} \frac{(\Phi_1|H|\Phi_{\beta\gamma})(\Phi_{\beta\gamma}|H|\Phi_\lambda)(\Phi_\lambda|H|\Phi_{\delta\varepsilon})(\Phi_{\delta\varepsilon}|H|\Phi_1)}{(E_1-E_{\beta\gamma})(E_1-E_\lambda)(E_1-E_{\delta\varepsilon})} \tag{20}$$

and vary the orbital φ_λ occurring in the SSC Φ_λ to make $|E_\lambda^{(4)}|$ as large as possible. Using the abbreviations

$$c_{\beta\gamma} = \frac{(\Phi_1|H|\Phi_{\beta\gamma})}{E_1 - E_{\beta\gamma}}, \quad c_{\delta\varepsilon} = \frac{(\Phi_1|H|\Phi_{\delta\varepsilon})}{E_1 - E_{\delta\varepsilon}} \tag{21}$$

for the terms in (20) not depending on φ_λ and noting that the orbital φ_λ as a linear combination of all the φ_α, $\alpha > 1$, cannot be orthogonal to the φ_α we get after some manipulations exactly formula (18) for the determination of φ_λ with the only trivial difference, that now also nondiagonal $c_{\beta\gamma}$ are occurring.

Our procedure can be summarized by the following floating diagram

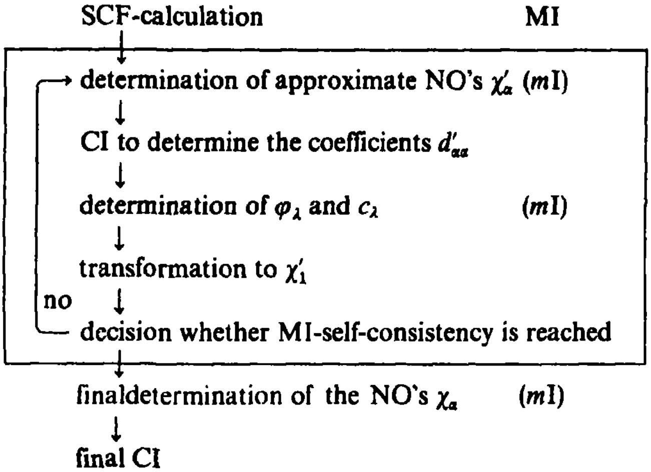
SCF-calculation
MI
determination of approximate NO's χ'_α (*m*I)
CI to determine the coefficients $d'_{\alpha\alpha}$
determination of φ_λ and c_λ (*m*I)
transformation to χ'_1
no
decision whether MI-self-consistency is reached
finaldetermination of the NO's χ_α (*m*I)
final CI

*m*I means that for this step *micro*iterations are necessary while MI denotes the whole *macro*iteration block.

The advantage of this method seems to be that it is sufficient to determine only one single optimized function φ_λ instead of calculating all the c_α or instead of including all the SSC's into the CI in each MI-step. The determination of φ_λ and c_λ is very fast compared with the calculation of the matrix elements for the CI. In some cases it is possible to simplify the procedure in order to save computation time:

1. If all the $d'_{\alpha\alpha}$ in (13) are small compared with c_1 it is sufficient to determine φ_λ only once from (18), and to estimate c_λ and the energy contribution of Φ_λ per-

turbationally by

$$c_\lambda \approx \frac{(\Psi'|H|\Phi_\lambda)}{E(\Psi')-E_\lambda}, \tag{22a}$$

$$\Delta E_\lambda \approx (\Psi'|H|\Phi_\lambda)c_\lambda . \tag{22b}$$

The recalculation of better χ'_α, $d'_{\alpha\alpha}$ etc. does not change the results appreciably in that case (see, for instance, the equilibrium distance of H_2, Sect. 3).

2. Sometimes one can use a reduced basis throughout the whole MI-block. For instance, in H_2 at large internuclear separations only the second NO, which is of σ_u-type, has a large coefficient and must be included in the MI-procedure (Sect. 4). Therefore, we can limit ourselves to σ-type basis functions in the MI-block, the π-basis is necessary only for the final determination of all the NO's.

b) Closed Shell Systems with More than Two Electrons

Within the framework of the IEPA our procedure to construct first natural orbitals can be applied to closed shell systems with more than two electrons with slight modifications. Starting from the HF-determinant

$$\Phi_1 = |\varphi_1\bar{\varphi}_1 \cdots \varphi_n\bar{\varphi}_n| \tag{23}$$

for a $2n$-electron system we pick out a pair of electrons occupying the same spatial orbital, say i. This pair can be treated completely analogous to the two-electron system in Sect. 2a, the only difference is that it now moves in the HF-field of the remaining electrons.

We shall not repeat all the details of the procedure, we only describe briefly the new points of view. Using the appropriate antisymmetrizer $\mathscr{A}$ we can split Φ_1 in the following way

$$\Phi_1 = \mathscr{A}|\varphi_i\bar{\varphi}_i| \cdot |\varphi_1\bar{\varphi}_1 \cdots \bar{\varphi}_{i-1}\varphi_{i+1} \cdots \varphi_n\bar{\varphi}_n| \tag{24}$$

and replace the pair $|\varphi_i\bar{\varphi}_i|$ by an expansion of type (13)

$$|\varphi_i\bar{\varphi}_i| \rightarrow c_1^i\,|\varphi_i\bar{\varphi}_i| + \sum_\alpha d_{\alpha\alpha}^i|\chi_\alpha^i\bar{\chi}_\alpha^i| \tag{25}$$

the index i indicates that we are dealing with pair i. All the other pairs remain unchanged. The equation that determines the optimal φ_λ^i in the SSC

$$\Phi_\lambda^i = \frac{1}{\sqrt{2}}\,\{|\varphi_i\bar{\varphi}_\lambda^i| + |\varphi_\lambda^i\bar{\varphi}_i|\} \tag{26}$$

now reads

$$\begin{aligned}\sqrt{2}\left\{c_1^i(F_i+J^i)\varphi_i + \sum_\alpha d_{\alpha\alpha}^i[K^\alpha\varphi_i + (\chi_\alpha^i|F_i|\varphi_i)S\chi_\alpha^i]\right\}& \\ + c_\lambda^i(F_i+J^i+K^i)\varphi_\lambda^i = \mu_i\varphi_\lambda^i&\end{aligned} \tag{27}$$

with

$$F_i = h + \sum_{j=1,n}^{j\neq i}(2J^j - K^j)\,. \tag{28}$$

This is completely analogous to (18), the only difference is the replacement of h by the effective one-electron potential F_i. The solution of (27) involving micro- and macroiterations follows exactly the scheme described above for the solution of (18).

It must be noted that the NO's χ_α^i in (25) – including the first NO χ_1^i – are NO's of the pair i, but not of the whole system. That means, they only diagonalize the first order density matrix originating from the pair i in the HF-field of the remaining electrons of the system, but they do not diagonalize the total first order density matrix. These "pair-NO's" sometimes are called "pseudo-NO's" [25] or "quasi-NO's" [32]. In the same sense the χ_1^i are not the correct Brueckner-orbitals of the system, but "pair-Brueckner-orbitals", making vanish only that part of the SSC-coefficients c_α^i originating from DSC's in the same pair i. We are quite sure that this is the largest part of the c_α^i, but a thorough discussion of this question must be postponed and can be answered only in connection with the question of the additivity of pair-correlation energies in the IEPA. As we are dealing with an effective two-electron system, the "pair-Brueckner-orbitals" coincide with the first pair-NO's. Though this does not hold for the true orbitals [7], there is numerical evidence that they actually deviate very little from one-another [12].

This whole procedure can be carried through for each individual pair $i = 1, \ldots, n$. But here one more step is necessary: One has to take into account that after the transformation from φ_i to χ_1^i the field in which the remaining electrons are moving has changed, too. To reach self-consistency we therefore need a still higher level of macroiterations: One starts, for instance, with the construction of χ_1^1 in the HF-field of all the other pairs, continues with the construction of χ_1^2 in the field of $\chi_1^1, \varphi_3, \ldots, \varphi_n$, and so on to χ_1^n. Then one corrects χ_1^1, now in the field of the just determined $\chi_1^2, \ldots, \chi_1^n$, and so on up to self-consistency.

3. Expectation Values of One-Electron Operators. The Quadrupole Moment and Field Gradient of H_2

As a first example of the application of our macroiteration procedure we have calculated the energy and the expectation values of some one-electron operators for the H_2-molecule at its equilibrium distance.

We start from a wavefunction as described in (13), i.e. from a CI-function containing the SCF-determinant Φ_1 and all the DSC's (or a sufficiently large number of them), but which does not include the SSC's. According to Sect. 2 functions of this type generally give good expectation values for the Hamiltonian, since the SSC's neglected in (13) have a priori vanishing matrix elements with Φ_1. But this does not hold for other operators.

Therefore, to get as accurate results for the expectation values of one-electron operators as for the Hamiltonian we must include the SSC's or, equivalently, use the full diagonal expansion (10). Such a wavefunction will give a slightly better value for the energy, too, for now the matrix elements of the type (SSC|H|DSC) are also taken into account. How to construct the full diagonal expansion was shown in Sect. 2.

For the calculation of H_2 at its equilibrium distance we used an extended Hoyland-type basis [33] of 45 Gaussian lobe functions contracted to 23 groups (11σ-type, 5π-type and one δ-type for both components). This medium-sized basis

Table 1. CI-function for H_2 before and after the MI treatment (equilibrium distance)

No.	Configurations	Before MI Coefficient	 Energy contribution	After MI Coefficient	 Energy contribution
1	$\sigma_g\bar{\sigma}_g$	0.99086	-1.133095^a	0.99086	-1.132977^a
2	$\sigma_u\bar{\sigma}_u$	−0.10076	−0.016717	−0.10164	−0.017043
3	$\sigma_g\bar{\sigma}_g$	−0.05533	−0.007429	−0.05474	−0.007355
4, 5	$\pi_u\bar{\pi}_u$	−0.04666	−0.005310	−0.04645	−0.005289
6	$\sigma_u\bar{\sigma}_u$	−0.01039	−0.000763	−0.01047	−0.000776
7	$\sigma_u\bar{\sigma}_g$	−0.00974	−0.000720	−0.00983	−0.000733
8, 9	$\pi_g\bar{\pi}_g$	−0.00842	−0.000499	−0.00844	−0.000504
0.11	$\delta_g\bar{\delta}_g$	−0.00646	−0.000299	−0.00642	−0.000296
12	$\sigma_g\bar{\sigma}_g$	−0.00645	−0.000338	−0.00641	−0.000335
13, 14	$\pi_u\bar{\pi}_u$	−0.00606	−0.000290	−0.00604	−0.000289
15	Φ_λ	0.00959	−0.000112	0.00000_5	0.000000
E_{total}			−1.171970		−1.171973

[a] All energies in atomic units (a.u.).

should allow for rather good results. Thus, our SCF-energy is about 0.0005 a.u., our correlation energy about 0.0019 a.u. poorer than the very accurate results of Kolos and Roothaan [34].

In Table 1 the results of the calculation of the total energy are summarized. For each configuration we tabulated the expansion coefficient and the energy contribution obtained 1) with the wavefunction (13) augmented by one optimized configuration Φ_λ and 2) after the complete MI-procedure (3 macroiterations were necessary to reach self-consistency to 7 figures in energy). The first configuration is the SCF-determinant (after MI of course the Brueckner-determinant), the last configuration the optimized SSC Φ_λ, which does not contribute to the energy after the MI-procedure.

The very small differences between the results before and after the MI show that it is sufficient in this case just to consider the wavefunction (13) as long as one is interested only in energies. The contribution of Φ_λ – equivalent to *all* the SSC's – is about 3‰ of the total correlation energy, an order of magnitude less than the errors arising from the deficiencies of our basis. And the recalculation of the higher NO's, i.e. the MI process itself, has almost no effect, it leads to an energy decrease of about 0.000003 a.u.

This behaviour is independent of the basis, it is merely the consequence of the smallness of the coefficients $d_{\alpha\alpha}$ for $\alpha > 1$, and cannot be expected if one of the $d_{\alpha\alpha}$ is comparable in its absolute value with d_1.

To study the influence of the SSC's on expectation values of one-electron operators we considered the operators x^2 (x being the molecular axis), y^2, r^2, $Q = 3x^2 - r^2$ (quadrupole moment of the electron charge distribution) and $F = r^{-5}(3x^2 - r^2)$ (field gradient of the electron charge distribution, calculated at the position of the nuclei). We can compare our results for E, $\langle x^2 \rangle$, $\langle y^2 \rangle$, $\langle Q \rangle$ with the very accurate results of Kolos and Wolniewicz [27]; comparison with experimental data is less valuable because the molecular vibrations are neglected in our calculations. Also for $\langle F \rangle$ Kolos-Roothaan-type calculations have been done [35], but the result seems not to be accessible to our knowledge. Very accurate calculations of $\langle F \rangle$ are necessary to determine the nuclear quadrupole moment of deuterium by nuclear quadrupole resonance [36].

The first thing we noticed was that our results depend significantly on the number of DSC's in the wavefunction. So we have tabulated in Table 2 the expectation values of the above operators calculated with MI-functions of the increasing size (1–14 determinants, 3 macroiterations) to test their convergency properties. The largest relative differences and the relative differences in the last step (from 9–14 determinants) are also given together with the results of Kolos and Wolniewicz [27]. Table 2 shows that all quantities seem to converge to the corresponding Kolos-Wolniewicz-values in more or less the same way as the energy itself, despite of the fact that only E varies monotonously.

Table 2. Macroiterated CI wavefunctions for H_2 ($R = 1.4a_0$) with different numbers of configurations. Convergency test for the energy and some one-electron operators

Number of configurations	E (a.u.)	$\langle x^2 \rangle$	$\langle y^2 \rangle$	$\langle r^2 \rangle$	$\langle Q \rangle$	$\langle F \rangle$
1 (SCF)	−1.133095	2.0507	1.5508	5.1522	0.9999	0.3782
2	−1.151543	2.0621	1.5112	5.0844	1.1019	0.3799
3	−1.158925	2.0823	1.5347	5.1516	1.0953	0.3865
5	−1.169147	2.0624	1.5325	5.1274	1.0597	0.3793
9	−1.170885	2.0591	1.5284	5.1159	1.0615	0.3799
14	−1.171973	2.0554	1.5262	5.1079	1.0585	0.3802
Maximum relative differences (in ‰)	34	15	26	13	91	22
Relative differences in the last step (in ‰)	1	2	1	1	3	1
Values of Kolos and Wolniewicz [27]	−1.174470	2.0459	1.5234	5.0927	1.0451	

Table 3. Expectation values of some one-electron operators, calculated with the different wavefunctions. In parentheses: Differences with respect to the SCF-expectation value

Wavefunction	E (a.u.)	$\langle x^2 \rangle$	$\langle y^2 \rangle$	$\langle r^2 \rangle$	$\langle Q \rangle$	$\langle F \rangle$
(1) SCF-determinant	−1.133095	2.0507	1.5508	5.1522	0.9999	0.3782
(2) SCF-determinant + 13 DSC's	−1.171858	2.0667 (+0.0160)	1.5521 (+0.0013)	5.1710 (+0.0188)	1.0291 (+0.0292)	0.3752 (−0.0030)
(3) SCF-determinant + Brueckner term		2.0391 (−0.0116)	1.5253 (−0.0255)	5.0897 (−0.0625)	1.0277 (+0.0278)	0.3834 (+0.0052)
(4) SCF-determinant + 13 DSC's + Brueckner term	−1.171970	2.0562 (+0.0055)	1.5278 (−0.0230)	5.1118 (−0.0404)	1.0569 (+0.0570)	0.3801 (+0.0019)
(5) Contributions of (2) and (3) added to (1)		2.0551 (+0.0044)	1.5266 (−0.0242)	5.1085 (−0.0437)	1.0569 (+0.0570)	0.3804 (+0.0022)
(6) 14 determinant function after macroiteration	−1.171973	2.0554 (+0.0047)	1.5262 (−0.0246)	5.1079 (−0.0443)	1.0585 (+0.0586)	0.3802 (+0.0020)

Table 3 contains the expectation values of the same operators as above, in different stages of perfection to show the relative order of magnitude of the different contributions. The wavefunctions are

(1) SCF-determinant,

(2) SCF-determinant and DSC's,

(3) SCF-determinant and optimized SSC Φ_λ (Brueckner correction),

(4) wavefunction of Table 1 without MI, i.e. CI with SCF-determinant, DSC's and Φ_λ,

(5) contributions of (2) and (3) simply added to the SCF-result,

(6) full MI-wavefunction of Table 1.

The results of Table 3 show that the MI-treatment does not improve the values of (4) considerably - the same holds for the energy - , and further that the changes caused by admixing the DSC's and the Brueckner correction are to a good degree additive.

To answer the question whether the SCF- or the Brueckner-determinant yields better expectation values of one-electron operators we have to distinguish two cases:

(a) The contributions of the DSC's and of the Brueckner correction Φ_λ to the expectation value have more or less the same magnitude, but different signs (or they are both small). In this case the two corrections add up to about zero and the SCF-determinant gives already a good result. Examples in Table 3: $\langle x^2 \rangle, \langle F \rangle$.

(b) The two corrections have the same sign or they have different signs and rather different magnitude. Here the SCF-function is no longer a good approximation for calculating expectation values. Examples: $\langle y^2 \rangle, \langle r^2 \rangle, \langle Q \rangle$.

As can also be seen in Table 3 generally neither the correction due to the DSC's nor the Brueckner correction can be neglected; they contribute both up to 3% to the expectation values. Since different operators can behave differently and one does not know signs and magnitudes of the corrections in advance, one has to calculate (or to estimate) both to ensure that the SCF-values are good not only by chance.

In agreement with Larsson [18] we can conclude by stating that generally the Brueckner-determinant yields more accurate expectation values of one-electron operators than the SCF-determinant. This can be hidden if the corrections due to the DSC's and to Φ_λ are accidentally of the same magnitude and of different sign, but such a behaviour cannot be expected in advance.

4. The H_2 Molecule at Large Internuclear Separations

It is well known that the SCF-method fails to describe the behaviour of the H_2 potential energy curve at large internuclear distances, since the system of two H-atoms changes from a closed-shell state at equilibrium distance $R = R_0 = 1.4\, a_0$ to an open-shell one for $R \to \infty$. For $R = R_0$ the one-determinantal SCF-wavefunction $\Phi_1 = |1\sigma_g \overline{1\sigma_g}|$ is a good approximation of the exact wavefunction Ψ and a good starting point for the CI. For $R \to \infty$ this configuration becomes degenerate with $\Phi_2 = |1\sigma_u \overline{1\sigma_u}|$, therefore a wavefunction containing at least these two determinants is necessary to get the correct behaviour of the potential energy curve for large distances.

Since the coefficient of Φ_2 changes from about -0.1 at R_0 (see Sect. 3) to $-1/\sqrt{2}$ at $R \to \infty$, its influence backwards on Φ_1 increases and it becomes more and more necessary to change from the SCF-orbital to the first NO. This behaviour is typical for non-dynamical or degeneracy-type correlation [13]; other examples are Li_2 at large internuclear separations [20, 23] or CH_2 *in its lowest* $^1A_1$ state for nearly linear geometry [37, 38].

With our MI-treatment it is very easy to account for this behaviour. From the numerical point of view the situation for large distances becomes even more favourable than for small ones (see Sect. 3), because all higher NO's – except for $1\sigma_g$ and $1\sigma_u$ – become more and more unimportant, so we can go through all the MI-block with only the two configurations Φ_1 and Φ_2. These two contain only σ-type orbitals, so we can limit our basis for the MI-part of the calculation to σ-type basis functions.

We calculated the potential energy curve for H_2 in the range from $R = 1.4\,a_0$ to $R = 10.0\,a_0$ with a Gaussian basis set containing for each atom a 6*s*-Huzinaga basis [39] (contracted to 4 groups) augmented by three *p*-groups (exponents 1., 0.28, 0.08) in all three directions. The p_σ-group with the exponent 0.28 was uncoupled, so that our complete basis consisted of 48 Gaussian lobe functions contracted to 16σ, $6\pi_y$ and $6\pi_z$ groups. For $R = R_0$ this basis is poorer than the one used in Sect. 3, for large R it becomes rather good, the energy of two independent H-atoms calculated with this basis is -0.999881 a.u. [39].

Before we present the whole potential energy curve we pick out two of its points to show how differently the MI-procedure works in the two limiting cases where

a) $c_1 \approx 1$, all $|c_\alpha|$, $\alpha > 1$, very small, i.e. for $R \approx R_0$,

b) $|c_1| \approx |c_2| \approx 1/\sqrt{2}$, all $|c_\alpha|$, $\alpha > 2$, very small, i.e. for large R.

We have chosen the points $R = R_0 = 1.4 a_0$ and $R = 5.0 a_0$ and summarize some results in Table 4. In both calculations only the $|1\sigma_u \overline{1\sigma_u}|$ configuration is

Table 4. MI-procedure for H_2 at $R = 1.4\,a_0$ and $R = 5.0\,a_0$

		$R = 1.4$	$R = 5.0$
Without MI	$E_1 = E_{SCF}$	-1.133135	-0.859051
	E_2	-1.151390	-0.987635
	E_{13}	-1.170842	-0.988826
First MI	ΔE_λ	-0.000282	-0.013534
	c_λ	0.015337	0.146339
	E_1	-1.132842	-0.847547
	E_2	-1.151667	-1.001515
	Number of MI	2	5
Last MI	E_1	-1.132851	-0.836534
	E_2	-1.151667	-1.002728
After MI	E_{13}	-1.170950	-1.003387
	c_1	0.990987	0.793303
	c_2	-0.100458	-0.608349

All energies in a.u.

included in the MI-treatment which is completely sufficient for $R = 5.0 a_0$, but leads to a small error for $R = R_0$, as will be shown later.

Because of this simplification of the MI-treatment the results for $R = R_0$ do not agree completely with those of our former calculation (Sect. 3). ΔE_λ, c_λ, the increase in E_1 and decrease in E_2 are much larger in Table 4 than in Table 1. But all these quantities are very small, the gain in the total energy E_{13} after MI is about 0.0001 a.u. in both calculations and can be neglected in comparison with the still remaining error of 0.0035 a.u. For $R = 5.0 a_0$ the situation is completely different: ΔE_λ and c_λ are large, the decrease in E_2 and E_{13} cannot be neglected. Most of the energy is gained in the first MI, to reach self-consistency to six figures in the energy five macroiterations are necessary. But because the full basis – including the π-orbitals – is needed only for E_{13} and not in the SCF- and MI-steps, the computer time necessary for the MI-step is quite small. (For our basis we needed 10 sec for the evaluation of the integrals, 6 sec for the SCF-calculation, 3 sec for each MI, and 35 sec for the final determination of the higher NO's and the CI to calculate E_{13}, all for an IBM 360/85.)

Table 5 contains our results for the potential energy curve of H_2. For nine values of R from $R = R_0$ to $R = 10.0 a_0$ we have tabulated the energies E_1, E_2, and E_{13}, calculated in three steps of increasing accuracy, namely:

a) standard CI with doubly substituted NO-configurations, using the approximation $\chi_1 = \varphi_1$ (first NO = SCF-orbital), i.e. without MI-step;

b) after determination of the first NO χ_1, i.e. after MI-step, only one DSC is incorporated in the MI-block;

c) after determination of χ_1, but the four most important DSC's incorporated in the MI-block.

To enable comparison we have included in Table 5 the results of the "double configuration SCF" (DCSCF) calculation of Bowman, Hirschfelder, and Wahl [21] which must be compared with our E_2 of calculation b), and the nearly exact potential energy curve of Kolos and Wolniewicz [27].

Comparing these different calculations we come to the following conclusions:

1. Neither E_{SCF} nor E_{13} of calculation a) approaches the correct limit of two separate H atoms in their ground states (in our basis -0.999881 a.u.) for $R \to \infty$. Thus, the incorrect asymptotic behaviour of the SCF-energy is not fully balanced by the CI with only DSC's and the approximation $\chi_1 = \varphi_1$.

2. After the determination of the first NO (MI-block in b) and c)) the correct behaviour of E_2 and E_{13} for large R is obtained. For $R \to \infty$ the difference between our calculations and those of Kolos and Wolniewicz [27] or Bowman, Hirschfelder and Wahl [21] are only due to the deficiency of our Gaussian basis. For small R our results are poorer, because we did not optimize our basis to give a good description of the bonding region.

3. For large R the difference between E_{13} and E_2 should be equal to the London dispersion energy [40]. Its leading term is $-6.5 R^{-6}$ a.u. [41, 42], while we got -0.000007 a.u. for $R = 10.0 a_0$.

4. The differences in E_2 and E_{13} between the two calculations b) and c) are rather small, but noticeable for $R = R_0$, they become smaller for increasing R, and are less than 0.000001 a.u. for $R \geq 6.0 a_0$. (Therefore we did not perform the much more time consuming calculation c) for $R \geq 6.0 a_0$.) That is due to the fact that the

Table 5. Potential energy curve of H_2 (all energy values are negative)

R	$1.4\,a_0$	$1.6\,a_0$	$2.0\,a_0$	$3.0\,a_0$	$4.0\,a_0$	$5.0\,a_0$	$6.0\,a_0$	$8.0\,a_0$	$10.0\,a_0$
a) E_{SCF}	1.133135	1.126001	1.091374	0.989186	0.911505	0.859051	0.824326	0.785618	0.766951
E_2	1.151390	1.147266	1.119834	1.044436	1.003452	0.987635	0.982312	0.980752	0.981815
E_{13}	1.170842	1.165126	1.134139	1.052096	1.006544	0.988826	0.982899	0.981038	0.982018
b) E_1	1.132851	1.125578	1.090491	0.984823	0.898614	0.836534	0.795992	0.755630	0.738548
E_2	1.151667	1.147675	1.120677	1.048180	1.013025	1.002728	1.000437	0.999899	0.999882
E_{13}	1.170950	1.165329	1.134714	1.055243	1.015417	1.003387	1.000622	0.999927	0.999889
c) E_1	1.133030	1.125808	1.090878	0.985669	0.899773	0.837399			
E_2	1.151621	1.147629	1.120618	1.048139	1.013004	1.002721			
E_{13}	1.170975	1.165354	1.134724	1.055264	1.015429	1.003390			
E(DCSCF)	1.152148	1.147992	1.120896	1.048092	1.013088	1.002847	1.000555	1.000018	1.000000_5
$E(K-W)$	1.174474	1.168580	1.138131	1.057312	1.016369	1.003763	1.000815	1.000053	1.000009_1

a), b), c) description see text, all energies in a.u.

coefficients c_3, c_4, c_5 of the configurations Φ_3, Φ_4, and Φ_5 – being about -0.05 at $R = R_0$ (compare Table 1) – decrease very rapidly with increasing R, whereas c_2 increases from about -0.1 at $R = R_0$ to $-1/\sqrt{2}$ for $R \to \infty$.

Thus, we can conclude by stating that our MI-treatment to determine the first NO enables us to get rather good results even in unfavourable cases, when the CI-coefficients of one or more excited configurations are large. Especially, the behaviour of potential energy curves can be obtained correctly. This is of special importance for the interaction of atoms or molecules at large internuclear distances.

Acknowledgements. We are indebted to Dr. W. Kutzelnigg, Dr. R. Ahlrichs (Karlsruhe) and Dr. M. Gélus (Grenoble) for their interest in this work and numerous discussions on this subject. This work is part of the project Nr. SR 2.120.69 of the „Schweizerischer Nationalfond" and has been supported in part by the „Deutsche Forschungsgemeinschaft".

We thank the computation centers of the "Sandoz AG, Basel" and the „Gesellschaft für Kernforschung mbH, Karlsruhe" for their kind assistance in the numerical computations and the Sandoz AG for a grant of computation time.

References

1 Brillouin, L.: Actualites Sci. et Ind. No 71 (1933); Nos. 159, 160 (1934).
2. Møller, C., Plesset, M. S.: Physic Rev. **46**, 618 (1934).
3. Brueckner, K. A., Levinson, C. A.: Physic. Rev. **97**, 1344 (1955)
4. Wada, W.: Physic. Rev. **103**, 1008 (1956).
5 Brenig, W.: Nuclear Physics **4**, 633 (1957).
6 Primas, H.: In: Modern quantum chemistry, Vol. 2, p. 45. Ed. by O. Sinanoglu. New York: Academic Press 1965.
7 Kutzelnigg, W., Smith, V. H., Jr.: J. chem. Physics **41**, 896 (1964).
8 Smith, V. H., Jr., Kutzelnigg, W.: Ark. Fysik **38**, 309 (1968).
9. Nesbet, R. K.: Physic. Rev. **109**, 1632 (1958).
10. Löwdin, P. O.: Physic. Rev. **97**, 1474 (1955).
11. - Shull, H.: Physic. Rev. **101**, 1730 (1956).
12. Larsson, S., Smith, V. H.: Physic. Rev. **178**, 137 (1969).
13. Sinanoglu, O., Tuan, D. F. T.: J. chem. Physics **38**, 1740 (1963).
14. Shull, H., Löwdin, P. O.: J. chem. Physics **30**, 617 (1959).
15 – J. chem. Physics **30**, 1405 (1959).
16. Davidson, E. R., Jones, L. L.: J. chem. Physics **37**, 2966 (1962).
17. J. chem. Physics **39**, 875 (1963).
18. Larsson, S.: Chem. Physics Letters **7**, 165 (1970).
19. Das, G., Wahl, A. C.: J. chem. Physics **44**, 87 (1966).
20. J. chem. Physics **46**, 1568 (1967).
21. Bowman, J. D., Jr., Hirschfelder, J. O., Wahl, A. C.: J. chem. Physics **53**, 2743 (1970).
22. Ahlrichs, R., Kutzelnigg, W., Bingel, W. A.: Theoret. chim. Acta (Berl.) **5**, 289 (1966).
23. Kutzelnigg, W., Gélus, M.: Chem. Physics Letters **7**, 296 (1970).
24. Levy, B., Berthier, G.: Int. J. quant. Chemistry **2**, 307 (1968).
25. Edminston, C., Kraus, M.: J. chem. Physics **45**, 1833 (1966).
26. Ahlrichs, R., Kutzelnigg, W.: J. chem. Physics **48**, 1819 (1968).
27. Kolos, W., Wolniewicz, L.: J. chem. Physics **43**, 2429 (1965).
28. Grimaldi, F.: Advances chem. Physics, Vol. **14**, p. 341. London: Interscience 1969.
29. Hurley, A. C., Lennard-Jones, J., Pople, J. A.: Proc. Roy. Soc. (London), A **220**, 446 (1953).
30. Kutzelnigg, W.: Theoret. chim. Acta (Berl.) **1**, 327, 343 (1963).
31. Gabel, B.: Diplomarbeit (thesis), University of Göttingen, 1970 (unpublished).
32. Jungen, M., Ahlrichs, R.: Theoret. chim. Acta (Berl.) **17**, 339 (1970).
33. Hoyland, J. R.: J. chem. Physics **40**, 3540 (1964).
34. Kolos, W., Roothaan, C. C. J.: Rev. mod. Physics **32**, 219 (1960).

35. Auffray, J. P.: Physic. Rev. Letters 6, 120 (1961).
36. Newell, G. F.: Physic. Rev. 78, 711 (1950).
37. Harrison, J. F., Allen, L. C.: J. Amer. chem. Soc. 91, 807 (1969).
38. O'Neil, S. V., Schäfer III, H. F., Bender, C. F.: To be published.
39. Huzinaga, S.: J. chem. Physics 42, 1293 (1965).
40. Eisenschitz, R., London, F.: Z. Physik 60, 491 (1930).
41. Hirschfelder, J. O., Löwdin, P. O.: Molecular Physics 2, 229 (1959).
42. Dalgarno, A., Davidson, W. D.: Advances in atomic and molecular physics, Vol. 2, p. 1. New York: Academic Press 1966.

Dr. Martin Jungen
Physikalisch-Chemisches Institut
Universität Basel
Klingelbergstraße 80
CH-4050 Basel, Switzerland

Dr. Volker Staemmler
Institut für Physikalische Chemie und Elektrochemie
Abteilung Theoretische Chemie
D-75 Karlsruhe, Kaiserstr. 12
Germany

Theoret. chim. Acta (Berl.) 24, 170 – 190 (1972)
© by Springer-Verlag 1972

Berechnung der Bandstruktur vom Vanadiumcarbid VC*

A. NECKEL, P. RASTL, P. WEINBERGER und RENATE MECHTLER
Institut für Physikalische Chemie der Universität, Wien IX., Währingerstr. 42, Österreich

Eingegangen am 27. August 1971

Calculation of the Band Structure of Vanadium Carbide VC

The energy band structure of stoichiometric VC has been calculated by the quasi-self-consistent APW method. For the exchange potential a parametrized Slater-free-electron approximation has been used. The energy eigenvalues have been calculated for 256 *k*-points in the first Brillouin zone. Further energy values (for a total number of 16384 *k*-points) have been obtained by the LCAO interpolation method of Slater and Koster. From these energy values the density-of-states histogram has been calculated. The partial LCAO-densities-of-states are largely in agreement with the APW-character-densities. Both quantities give information about the *l*-character of the energy bands. The charges in the APW-spheres indicate a charge transfer from vanadium to carbon.

Die Bandstruktur von stöchiometrischem Vanadiumcarbid VC wird mit Hilfe der quasi-selbstkonsistenten APW-Methode ermittelt. Als Austauschpotential wird ein parametrisiertes Slatersches Austauschpotential verwendet. Die Energie-Eigenwerte werden für 256 *k*-Punkte in der 1. Brillouin-Zone berechnet. Zur Berechnung der Zustandsdichte werden weitere Energiewerte (für insgesamt 16384 *k*-Punkte) nach der LCAO-Interpolationsmethode von Slater und Koster bestimmt und mit diesen die Zustandsdichte ermittelt. Die partiellen LCAO-Zustandsdichten zeigen weitgehende Übereinstimmung mit den APW-Charakterdichten und geben Aufschluß über den *l*-Charakter der Energiebänder. Die Ladungsverteilung im Kristall weist auf eine Ladungsüberführung vom Vanadium zum Kohlenstoff und damit auf eine gewisse Ionizität der Verbindung VC hin.

La structure des bandes énergétiques du VC de composition stoichiométrique a été calculée par la méthode APW quasiautoconsistante. On s'est servi d'un potentiel d'échange paramétrisé selon Slater. Les eigen-valeurs d'énergie sont déterminées pour 256 points *k* dans la premiere zone de Brillouin. Pour dériver la densité d'états énergétiques ainsi que les densités d'états partielles (densités d'états du caractère 2*s*, 2*p* et 3*d*) des valeurs d'énergie pour d'autres points *k* (en somme 16384) sont trouvées avec l'aide de la méthode d'interpolation LCAO de Slater et Koster. Il n'y a pas des différences significantes entre ces quantités et les densités des caractères *l* calculées directement par la méthode APW. Des densités d'états partielles on peut dériver le caractère *l* des bandes énergétiques.
De la distribution des charges dans le cristal résulte un transfer de charge du vanadium au carbon ce qui signifie que le VC possède une certaine ionicité.

1. Einführung

Berechnungen der Bandstruktur der metallischen Hartstoffe sollen einen Beitrag zum Verständnis der Eigenschaften und einen Einblick in den Bindungscharakter dieser überaus interessanten Substanzklasse liefern. Im folgenden wird über die Berechnung der Bandstruktur von Vanadiumcarbid VC nach der "Augmented Plane Wave" (APW) Methode [1] berichtet, die bereits auf eine Reihe anderer Vertreter der metallischen Hartstoffe oder verwandter Verbindungen, wie z.B. auf ScC [2], ScN [2, 3], ScO [4], TiC [5–7], TiN [5],

---

* Dem Gedenken an Herrn Prof. Dr. K. H. Hansen gewidmet.

TiO [5, 8], VO [9], VN [9] und NbN [10] mit Erfolg angewendet worden ist. Allen genannten Verbindungen ist gemeinsam, daß sie in der NaCl-Struktur kristallisieren und mehr oder weniger große Abweichungen von der stöchiometrischen Zusammensetzung zeigen. Die Nicht-Stöchiometrie wurde bei den Bandstruktur-Rechnungen, mit Ausnahme der Untersuchungen von Schoen und Denker [8] an TiO, nicht berücksichtigt. Vanadiumcarbid besitzt einen Kohlenstoffdefekt und ist in einem Homogenitätsbereich von $VC_{0,75}$ bis $VC_{0,88}$ existent [11]. Die stöchiometrische Verbindung VC ist nicht bekannt und ist offenbar instabil gegenüber Zerfall in $VC_{0,88}$ und C.

2. Berechnungsmethode

Der Verlauf einer quasi-selbstkonsistenten Bandstruktur-Rechnung nach der APW-Methode ist bereits mehrfach beschrieben worden [3, 12].

Wie üblich, wird für Kristallpotential und Ladungsdichte das "muffin-tin"-Modell angenommen.

a) Wahl des Austauschpotentials

Das für Bandstruktur-Rechnungen zu verwendende Austauschpotential steht zur Zeit noch zur Diskussion [13–27]. Slater [28] hat vorgeschlagen, den Austauschanteil des Hartree-Fock (HF) Potentials für Atome und Festkörper durch den lokalen, für ein freies Elektronengas geltenden Ausdruck

$$V_{XS}(r) = -6\left[\frac{3}{8\pi}\varrho(r)\right]^{1/3} \tag{1}$$

($\varrho(r)$: Elektronendichte im Punkte r) zu ersetzen. Später haben unabhängig voneinander Gáspár [13] und Kohn und Sham [17] die Variationsmethode auf das statistische Atommodell von Thomas und Fermi angewandt und einen Ausdruck abgeleitet, der sich von dem Slaterschen Austauschpotential nur durch den Faktor 2/3 unterscheidet. Keines dieser beiden Austauschpotentiale führt jedoch zu Ergebnissen, die in vollkommener Übereinstimmung mit einer selbstkonsistenten Hartree-Fock-Rechnung oder mit dem Experiment stehen. In den letzten Jahren wurden daher in einer Reihe von Arbeiten Parameter für das Slatersche Austauschpotential diskutiert. Dabei sind sowohl einparametrige Ausdrücke, als auch zweiparametrige Formen [21, 25] beschrieben worden. Die einparametrige Form (2)

$$V_{X\alpha}(r) = -6\alpha\left[\frac{3}{8\pi}\varrho(r)\right]^{1/3} \tag{2}$$

dürfte vor allem wegen ihrer einfachen Handhabung für die Verwendung in Festkörper-Rechnungen besonders geeignet sein.

Zur Bestimmung des Faktors α bieten sich im wesentlichen folgende drei Methoden an:

1. Berechnung des Erwartungswertes für die HF-Gesamtenergie unter Verwendung von $X\alpha$-Orbitalen und Aufsuchen jenes Wertes von α, der zu einem Minimum der Gesamtenergie führt [16, 26].

2. Berechnet man den Virialkoeffizienten

$$\eta = -\frac{\langle V\rangle}{2\langle T\rangle} \tag{3}$$

($\langle V\rangle$, $\langle T\rangle$: Erwartungswert des HF-Operators für die potentielle bzw. kinetische Energie) unter Verwendung von HF-Orbitalen, so ist das Virialtheorem automatisch erfüllt [15]. Verwendet man hingegen $X\alpha$-Orbitale, so hängt α näherungsweise linear von η ab. Durch die Bedingung $\eta = 1$ kann α festgelegt werden [23, 27].

3. Die (statistische) Gesamtenergie im $X\alpha$-Formalismus ist näherungsweise eine lineare Funktion von α. Man wählt nun α so, daß die statistische Gesamtenergie gleich der HF-Gesamtenergie wird [27].

Über den Einfluß des Austauschpotentials auf die Energiebandstruktur und Zustandsdichte sowie über die Überprüfung von Rechnungen mit verschiedenen Austauschpotentialen durch das Experiment liegen unseres Wissens nur wenige Arbeiten vor. So haben einige Autoren [29–32] über die Verwendung des Gáspár-Kohn-Sham-Faktors ($\alpha = 2/3$) berichtet. Snow [33, 34] verglich in seinen Arbeiten über Kupfer und Silber die mit $\alpha = 1$ und $\alpha = 5/6$ berechneten Zustandsdichten mit experimentell ermittelten Werten. Bemerkenswert hierbei ist, daß die mit $\alpha = 5/6$ bestimmte Zustandsdichte in wesentlich besserer Übereinstimmung mit dem Experiment steht als jene, die mit $\alpha = 1$ erhalten wurde. Schwarz und Conklin [7] haben schließlich am Beispiel von Titancarbid den Einfluß verschiedener Austauschpotentiale untersucht, wobei auch nach dem Virialtheorem parametrisierte Austauschpotentiale verwendet wurden.

b) Abhängigkeit der Energiebandstruktur vom Gitterparameter

Von den Untersuchungen über den Einfluß des Gitterparameters auf die Bandstruktur seien hier die mit Hilfe der APW-Methode durchgeführten Rechnungen erwähnt.

Von Rudge [35] wurden selbstkonsistente Bandstrukturen für verschiedene Gitterkonstanten – unter Einbeziehung einer praktisch unendlichen Gitterkonstante, die einer Separation des Gitters in Atome entspricht – zur Berechnung der Gesamtenergie von Lithium in Abhängigkeit vom Gitterparameter verwendet. Daraus wurden die Gleichgewichtsgitterkonstante sowie die Kohäsionsenergie abgeleitet. Alle Berechnungen wurden sowohl für den Austauschparameter $\alpha = 1$ als auch für $\alpha = 2/3$ durchgeführt. Für NbN wurden von Schwarz [10] für zwei verschiedene Gitterparameter selbstkonsistente Energiebandstrukturen angegeben. Die von Schwarz verwendeten Austauschpotentiale waren nach dem Virialtheorem parametrisiert worden. Ross und Johnson [36] haben die Bandstruktur von Aluminium unter Verwendung des Austauschpotentialfaktors $\alpha = 2/3$ für verschiedene Gitterparameter berechnet.

c) Parameter der Bandstruktur-Rechnung

In der vorliegenden Arbeit wird die Energiebandstruktur für vier verschiedene Gitterkonstanten berechnet. Diese Berechnungen sollen die Grundlage für die in Vorbereitung befindliche Behandlung nichtstöchiometrischer Phasen bilden.

Tabelle 1. Gitterkonstanten a, Atomsphärenradien R_p, konstantes Potential V_c zwischen den Atomsphären und Austauschparameter α

a		R_V	R_C	$-V_c$	α
at. E.	Å	at. E.	at. E.	Ryd	
7,80656	4,131	2,04316	1,86012	0,0301	≠ 1
7,83869	4,148	2,05144	1,86790	0,0269	≠ 1
7,87176	4,165	2,05998	1,87590	0,0224	≠ 1
7,90256	4,182	2,08073	1,87051	0,0253	≠ 1
7,90256	4,182	2,08763	1,86362	0,3510	= 1

Nimmt man näherungsweise eine lineare Abhängigkeit der Gitterkonstante der Phase VC_{1-x} vom Kohlenstoffgehalt an, so entspricht die kleinste Gitterkonstante der Zusammensetzung $VC_{0,75}$, während die größte Gitterkonstante etwa der hypothetischen Verbindung VC entsprechen würde [11, 37].

Das Kristallpotential wird im 1. Iterationsschritt durch Überlagerung der selbstkonsistenten parametrisierten Hartree-Fock-Slater-(HFS)Potentiale der freien Atome in ihren Grundzuständen gebildet. Der Schnittpunkt der Potentialkurven bestimmt die Atomsphärenradien, die während des Iterationsprozesses konstant gehalten werden.

Gitterkonstanten a, Atomsphärenradien R_p, sowie die selbstkonsistenten Potentiale V_c zwischen den Atomsphären sind in Tab. 1 angeführt.

Für sämtliche Energiebandstrukturen werden innerhalb der Atomsphären die nach dem Virialtheorem parametrisierten Austauschpotentiale der freien Atome [27] verwendet. Innerhalb der Vanadiumsphäre wird der Faktor $\alpha = 0,7150$, innerhalb der Kohlenstoffsphäre der Faktor $\alpha = 0,7581$ benutzt. Die gleichen Faktoren werden auch der Berechnung der HFS-Potentiale der freien Atome zugrunde gelegt. Da zwischen den Atomsphären eine konstante Ladungsdichte angenommen wird, die dem Modell des freien Elektronengases entspricht, wird für diesen Bereich der Faktor $\alpha = 2/3$ verwendet. Kohn und Sham [17] haben nämlich darauf hingewiesen, daß für den Fall eines homogenen Elektronengases eine Variationsrechnung zu dem Faktor $\alpha = 2/3$ führt, der eine bessere Näherung darstellt als $\alpha = 1$.

Um den Einfluß des Austauschpotentials auf die Bandstruktur zu untersuchen, wird für eine Gitterkonstante ($a = 7,90250$ at. E.) zusätzlich eine selbstkonsistente Bandstruktur-Rechnung mit dem vollen Slaterschen Austauschpotential ($\alpha = 1$) durchgeführt.

Zur Bestimmung des Kristallpotentials werden zwar in jedem Iterationsschritt die Semirumpfbänder[1], nicht jedoch die Rumpfzustände ($C:(1s)^2$ und $V:(1s)^2\,(2s)^2\,(2p)^6$) in die APW-Rechnung mit einbezogen. Die Rechnungen werden für 256 k-Punkte (19 nichtäquivalente Punkte) in der 1. Brillouin-Zone (B. Z.) durchgeführt. In der Entwicklung der Wellenfunktionen wird als obere Schranke für den Wellenvektor $|k| = \frac{\pi}{a}\sqrt{80}$ verwendet [2].

---

[1] Unter den Semirumpfbändern werden jene Bänder verstanden, die den atomaren $3s$- und $3p$-Zuständen entsprechen.

d) *Konvergenz*

Im Gegensatz zu anderen selbstkonsistenten APW-Rechnungen für refraktäre Phasen, wie etwa für ScN, ScO, TiC oder NbN ist für VC die Selbstkonsistenz wesentlich schwerer zu erreichen. Ursache hierfür ist, daß in der unmittelbaren Nähe der Fermienergie, die ja sehr wesentlich in die Bestimmung eines Iterationspotentiales eingeht, mehrere Energie-Eigenwerte zu liegen kommen, die in verschiedenen Iterationsschritten in verschiedener Weise besetzt werden. Die abwechselnde Besetzung bzw. Nichtbesetzung dieser Energiezustände führt zu starken Schwankungen des Kristallpotentials, wodurch die Konvergenz des Iterationsprozesses beeinträchtigt wird.

In Tab. 2 sind für die verwendeten Gitterkonstanten die maximalen und mittleren Abweichungen der Energie-Eigenwerte in den beiden letzten Iterationsschritten zusammengefaßt.

Tabelle 2. Konvergenzkriterien für Valenzbänder (Angaben in Rydberg)
(Differenz zwischen den beiden letzten Iterationen)

Kriterium		Gitterparameter [at. E.]			
		7,80656	7,83869	7,87176	7,90256
maximale Differenz	der Energie-Eigenwerte $E_\mu(k)$	0,011	0,003	0,003	0,001
mittlere Differenz		0,007	0,002	0,002	0,0007

3. Ergebnisse

a) *Energie-Eigenwerte und selbstkonsistentes Potential*

Die Energie-Eigenwerte $E_\mu(k)$ für die vier Gitterkonstanten sind in Tab. 3 zusammengefaßt. Für die Gitterkonstante $a = 7{,}9025$ at. E. sind sowohl die Energie-Eigenwerte, die mit dem parametrisierten Austauschpotential, als auch jene, die mit dem vollen Austauschpotential $\alpha = 1$ erhalten wurden, angegeben.

Tabelle 3. Energie-Eigenwerte $E_\mu(k)$ in Ryd. (Der Wellenvektor k ist in Einheiten von $\pi/2a$ angegeben)

Gitterkonstante		7,8066 ($\alpha \neq 1$)	7,8387 ($\alpha \neq 1$)	7,8718 ($\alpha \neq 1$)	7,9025 ($\alpha \neq 1$)	7,9025 ($\alpha = 1$)
k	irreduzible Darstellung	$E_\mu(k)$				
000	Gamma 1	−3,8782	−3,8909	−3,8966	−3,9173	−4,4678
		−0,2454	−0,2466	−0,2515	−0,2605	−0,6400
	Gamma 12	0,7882	0,7767	0,7696	0,7489	0,3309
	Gamma 25′	0,7083	0,6989	0,6930	0,6738	0,2684
	Gamma 15	−2,0281	−2,0410	−2,0477	−2,0687	−2,5940
		0,8448	0,8390	0,8271	0,8141	0,4196

Tabelle 3 (Fortsetzung)

Gitterkonstante		7,8066 ($\alpha \neq 1$)	7,8387 ($\alpha \neq 1$)	7,8718 ($\alpha \neq 1$)	7,9025 ($\alpha \neq 1$)	7,9025 ($\alpha = 1$)
k	irreduzible Darstellung	$E_n(k)$				
010	Delta 1	−3,8770	−3,8898	−3,8957	−3,9163	−4,4671
		−2,0327	−2,0454	−2,0517	−2,0723	−2,5968
		−0,2099	−0,2116	−0,2170	−0,2265	−0,6081
		0,5920	0,5862	0,5793	0,5649	0,1713
		1,0260	1,0137	1,0009	0,9806	0,5583
	Delta 2	0,7990	0,7874	0,7801	0,7591	0,3398
	Delta 2′	0,6798	0,6712	0,6659	0,6472	0,2471
	Delta 5	−2,0295	−2,0423	−2,0489	−2,0698	−2,5949
		0,6767	0,6690	0,6623	0,6454	0,2469
		0,9009	0,8924	0,8808	0,8645	0,4576
020	Delta 1	−3,8743	−3,8873	−3,8933	−3,9139	−4,4650
		−2,0431	−2,0555	−2,0615	−2,0819	−2,6045
		−0,1263	−0,1289	−0,1354	−0,1454	−0,5328
		0,4310	0,4274	0,4217	0,4095	0,0284
		1,1457	1,1294	1,1147	1,0904	0,6494
	Delta 2	0,8217	0,8097	0,8019	0,7805	0,3578
	Delta 2′	0,6161	0,6089	0,6045	0,5874	0,1971
	Delta 5	−2,0337	−2,0462	−2,0525	−2,0732	−2,5977
		0,6573	0,6507	0,6429	0,6279	0,2341
		0,9550	0,9433	0,9319	0,9121	0,4899
030	Delta 1	−3,8716	−3,8849	−3,8909	−3,9117	−4,4634
		−2,0535	−2,0654	−2,0711	−2,0907	−2,6114
		−0,0636	−0,0659	−0,0724	−0,0825	−0,4741
		0,3931	0,3892	0,3828	0,3710	−0,0038
		1,1470	1,1290	1,1144	1,0884	0,6352
	Delta 2	0,8456	0,8328	0,8249	0,8029	0,3767
	Delta 2′	0,5599	0,5540	0,5502	0,5344	0,1512
	Delta 5	−2,0375	−2,0503	−2,0564	−2,0769	−2,6006
		0,6804	0,6743	0,6649	0,6510	0,2598
		0,9340	0,9206	0,9106	0,8886	0,4588
040	X 1	−3,8705	−3,8839	−3,8899	−3,9108	−4,4627
		−0,0521	−0,0540	−0,0599	−0,0697	−0,4614
		1,1007	1,0827	1,0686	1,0428	0,5885
	X 2	0,8558	0,8427	0,8347	0,8125	0,3847
	X 3	0,5387	0,5330	0,5296	0,5140	0,1334
	X 5	0,8993	0,8853	0,8766	0,8533	0,4192
	X 4′	−2,0582	−2,0695	−2,0751	−2,0949	−2,6146
		0,4214	0,4168	0,4091	0,3972	0,0234
	X 5′	−2,0392	−2,0519	−2,0581	−2,0785	−2,6018
		0,7071	0,7013	0,6906	0,6777	0,2908
110	Sigma 1	−3,8761	−3,8889	−3,8949	−3,9155	−4,4664
		−2,0385	−2,0512	−2,0573	−2,0777	−2,6011
		−0,1755	−0,1776	−0,1836	−0,1933	−0,5771
		0,5514	0,5462	0,5393	0,5254	0,1370
		0,8015	0,7899	0,7826	0,7615	0,3430
		0,9660	0,9538	0,9420	0,9216	0,5004
	Sigma 2	0,7397	0,7297	0,7233	0,7033	0,2938
	Sigma 3	−2,0315	−2,0443	−2,0506	−2,0714	−2,5961
		0,5945	0,5884	0,5826	0,5672	0,1785
		0,9233	0,9143	0,9025	0,8858	0,4763

Tabelle 3 (Fortsetzung)

Gitterkonstante		7,8066 ($\alpha \neq 1$)	7,8387 ($\alpha \neq 1$)	7,8718 ($\alpha \neq 1$)	7,9025 ($\alpha \neq 1$)	7,902 ($\alpha = 1$
k	irreduzible Darstellung	$E_\mu(k)$				
110	Sigma 4	2,0283	−2,0412	−2,0479	−2,0689	−2,5941
		0,5830	0,5774	0,5709	0,5566	0,1623
		1,1171	1,1043	1,0906	1,0702	0,6425
120	Even	−3,8736	−3,8866	−3,8926	−3,9133	−4,4645
		−2,0467	−2,0586	−2,0647	−2,0846	−2,6066
		−2,0303	−2,0433	−2,0497	−2,0706	−2,5954
		−0,0948	−0,0978	−0,1046	−0,1151	−0,5047
		0,4161	0,4126	0,4070	0,3947	0,0153
		0,5600	0,5548	0,5481	0,5343	0,1434
		0,8585	0,8455	0,8374	0,8149	0,3880
		1,0057	0,9921	0,9799	0,9579	0,5298
		1,2093	1,1931	1,1787	1,1548	0,7135
	Odd	−2,0359	−2,0485	−2,0547	−2,0755	−2,5995
		0,5342	0,5289	0,5235	0,5093	0,1273
		0,7459	0,7365	0,7295	0,7104	0,3022
		0,9603	0,9489	0,9372	0,9178	0,4965
130	Even	3,8712	−3,8845	−3,8905	−3,9113	−4,4631
		2,0515	−2,0635	−2,0692	−2,0891	−2,6100
		2,0348	2,0478	−2,0539	−2,0748	−2,5989
		0,0375	−0,0403	0,0472	−0,0578	−0,4518
		0,3881	0,3844	0,3782	0,3666	−0,0072
		0,5730	0,5676	0,5601	0,5464	0,1565
		0,8972	0,8835	0,8746	0,8514	0,4195
		0,9926	0,9789	0,9676	0,9451	0,5167
		1,1656	1,1482	1,1337	1,1088	0,6600
	Odd	2,0398	−2,0522	−2,0587	−2,0791	−2,6022
		0,5010	0,4965	0,4911	0,4774	0,0992
		0,7608	0,7523	0,7437	0,7260	0,3216
		0,9381	0,9268	0,9147	0,8929	0,4644
140	Z 1	−3,8705	−3,8839	−3,8899	−3,9108	−4,4627
		−2,0394	−2,0521	−2,0583	2,0788	−2,6020
		0,0306	−0,0329	−0,0394	−0,0495	−0,4435
		0,5749	0,5695	0,5617	0,5482	0,1598
		0,9681	0,9543	0,9433	0,9213	0,4922
		1,0932	1,0758	1,0622	1,0368	0,5894
	Z 2	0,8996	0,8856	0,8768	0,8535	0,4194
	Z 3	−2,0553	−2,0668	−2,0726	−2,0923	−2,6127
		0,4228	0,4183	0,4111	0,3991	0,0252
		0,9025	0,8890	0,8798	0,8572	0,4264
	Z 4	−2,0418	−2,0544	−2,0605	−2,0809	−2,6037
		0,4893	0,4847	0,4797	0,4662	0,0895
		0,7830	0,7750	0,7651	0,7492	0,3507
220	Sigma 1	−3,8724	−3,8856	−3,8916	−3,9123	−4,4638
		−2,0513	−2,0634	−2,0690	−2,0890	−2,6099
		−0,0265	−0,0303	−0,0382	−0,0493	−0,4449
		0,3573	0,3543	0,3491	0,3375	−0,0357
		0,8823	0,8688	0,8600	0,8375	0,4069
		1,0402	1,0250	1,0123	0,9890	0,5559

Tabelle 3 (Fortsetzung)

Gitterkonstante		7,8066 ($\alpha \neq 1$)	7,8387 ($\alpha \neq 1$)	7,8718 ($\alpha \neq 1$)	7,9025 ($\alpha \neq 1$)	7,9025 ($\alpha = 1$)
$\bar{k}$	irreduzible Darstellung	$E_n(\bar{k})$				
220	Sigma 2	0,8091	0,7974	0,7900	0,7686	0,3492
	Sigma 3	−2,0409	−2,0535	−2,0597	−2,0801	−2,6030
		0,4727	0,4683	0,4626	0,4497	0,0724
		0,9723	0,9602	0,9485	0,9282	0,5031
	Sigma 4	−2,0313	−2,0441	−2,0505	−2,0712	−2,5960
		0,4919	0,4876	0,4820	0,4689	0,0807
		1,2679	1,2517	1,2363	1,2130	0,7668
230	Even	−3,8709	−3,8842	−3,8902	−3,9111	−4,4629
		−2,0497	−2,0618	−2,0675	−2,0879	−2,6089
		−2,0347	−2,0470	−2,0531	−2,0741	−2,5984
		0,0023	−0,0012	−0,0089	−0,0199	−0,4183
		0,3698	0,3666	0,3612	0,3495	−0,0212
		0,5082	0,5036	0,4975	0,4844	0,0968
		0,8754	0,8631	0,8539	0,8321	0,4081
		1,0567	1,0410	1,0282	1,0037	0,5656
		1,1706	1,1544	1,1407	1,1163	0,6781
	Odd	−2,0466	−2,0585	−2,0644	−2,0846	−2,6068
		0,4461	0,4418	0,4358	0,4233	0,0481
		0,8410	0,8289	0,8208	0,7993	0,3767
		0,9460	0,9327	0,9222	0,9005	0,4716
240	W 1	−2,0395	−2,0522	−2,0584	−2,0789	−2,6020
		−0,0054	0,0083	−0,0154	−0,0260	−0,4229
		1,0474	1,0305	1,0176	0,9925	0,5430
	W 2	0,8983	0,8843	0,8756	0,8524	0,4183
	W 2′	−3,8705	−3,8839	−3,8899	−3,9108	−4,4627
		0,4887	0,4844	0,4779	0,4652	0,0819
		1,0669	1,0521	1,0395	1,0163	0,5904
	W 3	−2,0488	−2,0608	−2,0665	−2,0870	−2,6084
		0,4395	0,4352	0,4290	0,4167	0,0421
		0,8756	0,8642	0,8545	0,8345	0,4161
330	K 1	−3,8706	−3,8840	−3,8900	−3,9109	−4,4628
		−2,0467	−2,0586	−2,0644	−2,0846	−2,6068
		−0,0114	−0,0143	−0,0213	−0,0318	−0,4280
		0,4187	0,4149	0,4096	0,3972	0,0247
		0,7872	0,7777	0,7689	0,7506	0,3447
		1,0837	1,0669	1,0534	1,0281	0,5831
	K 2	0,8750	0,8615	0,8532	0,8305	0,4005
	K 3	−2,0524	−2,0644	−2,0701	−2,0898	−2,6107
		0,4258	0,4214	0,4146	0,4026	0,0284
		0,9340	0,9201	0,9103	0,8876	0,4550
	K 4	−2,0364	−2,0491	−2,0552	−2,0759	−2,5999
		0,5590	0,5539	0,5468	0,5333	0,1424
		1,0805	1,0664	1,0536	1,0315	0,6007
111	Lambda 1	−3,8753	−3,8882	−3,8942	−3,9148	−4,4658
		−2,0449	−2,0570	−2,0629	−2,0833	−2,6056
		−0,1422	−0,1447	−0,1510	−0,1611	−0,5470
		0,4822	0,4776	0,4712	0,4580	0,0773
		0,8969	0,8861	0,8752	0,8559	0,4417

Tabelle 3 (Fortsetzung)

Gitterkonstante		7,8066 ($\alpha \neq 1$)	7,8387 ($\alpha \neq 1$)	7,8718 ($\alpha \neq 1$)	7,9025 ($\alpha \neq 1$)	7,9025 ($\alpha = 1$)
k	irreduzible Darstellung	$E_\mu(k)$				
111	Lambda 3	−2,0297	−2,0425	−2,0491	−2,0700	−2,5951
		0,5559	0,5507	0,5446	0,5305	0,1390
		0,7856	0,7743	0,7673	0,7467	0,3304
		1,1249	1,1118	1,0979	1,0773	0,6481
121	Even	−3,8729	−3,8860	−3,8920	−3,9127	−4,4640
		−2,0492	−2,0608	−2,0664	−2,0870	−2,6080
		−2,0302	−2,0430	−2,0493	−2,0703	−2,5951
		−0,0639	−0,0672	−0,0747	−0,0853	−0,4773
		0,3781	0,3747	0,3692	0,3572	−0,0175
		0,4977	0,4933	0,4877	0,4743	0,0899
		0,7890	0,7783	0,7709	0,7503	0,3364
		0,9492	0,9363	0,9254	0,9033	0,4784
		1,2320	1,2157	1,2007	1,1772	0,7341
	Odd	−2,0327	−2,0454	−2,0517	−2,0724	−2,5969
		0,5349	0,5297	0,5238	0,5101	0,1205
		0,8503	0,8374	0,8294	0,8072	0,3807
		1,1241	1,1104	1,0966	1,0753	0,6442
131	Even	−3,8711	−3,8844	−3,8904	−3,9113	−4,4630
		2,0530	−2,0646	−2,0700	−2,0900	−2,6106
		−2,0379	−2,0507	−2,0564	−2,0772	−2,6007
		−0,0135	−0,0168	−0,0244	−0,0352	−0,4317
		0,3584	0,3551	0,3495	0,3378	−0,0323
		0,4667	0,4624	0,4566	0,4437	0,0648
		0,7866	0,7766	0,7684	0,7492	0,3392
		0,9492	0,9353	0,9250	0,9018	0,4717
		1,1701	1,1529	1,1384	1,1132	0,6666
	Odd	−2,0355	−2,0481	−2,0543	−2,0751	−2,5993
		0,5455	0,5404	0,5339	0,5202	0,1301
		0,8767	0,8632	0,8548	0,8321	0,4013
		1,0949	1,0809	1,0678	1,0459	0,6155
221	Even	−3,8721	−3,8853	−3,8913	−3,9121	−4,4636
		−2,0558	−2,0671	−2,0730	−2,0927	−2,6127
		−2,0335	−2,0460	−2,0521	−2,0730	−2,5974
		0,0006	−0,0036	−0,0121	−0,0236	−0,4219
		0,3003	0,2977	0,2928	0,2817	−0,0861
		0,4785	0,4742	0,4686	0,4557	0,0723
		0,8718	0,8587	0,8502	0,8274	0,3990
		0,9605	0,9470	0,9359	0,9136	0,4863
		1,1802	1,1647	1,1503	1,1269	0,6883
	Odd	−2,0315	−2,0443	−2,0507	−2,0714	−2,5962
		0,4769	0,4728	0,4674	0,4545	0,0674
		0,8356	0,8232	0,8154	0,7935	0,3694
		1,2760	1,2597	1,2442	1,2210	0,7751
231	Q 1	−2,0557	−2,0671	−2,0730	−2,0927	−2,6128
		−2,0338	−2,0464	−2,0525	−2,0734	−2,5979
		0,0158	0,0118	0,0034	−0,0080	−0,4083
		0,4550	0,4509	0,4450	0,4324	0,0526
		0,8524	0,8400	0,8315	0,8099	0,3854
		1,1565	1,1400	1,1258	1,1015	0,6584

Tabelle 3 (Fortsetzung)

Gitterkonstante		7,8066 ($\alpha \neq 1$)	7,8387 ($\alpha \neq 1$)	7,8718 ($\alpha \neq 1$)	7,9025 ($\alpha \neq 1$)	7,9025 ($\alpha = 1$)
k	irreduzible Darstellung	$E_n(k)$				
231	Q 2	−3,8714	−3,8846	−3,8907	−3,9115	−4,4632
		−2,0393	−2,0520	−2,0582	−2,0787	−2,6018
		0,3153	0,3124	0,3075	0,2963	−0,0700
		0,4980	0,4935	0,4877	0,4746	0,0870
		0,8562	0,8436	0,8354	0,8132	0,3872
		0,9449	0,9313	0,9210	0,8985	0,4707
		1,1882	1,1728	1,1585	1,1356	0,6987
222	L 1	−2,0615	−2,0728	−2,0782	−2,0976	−2,6167
		0,0377	0,0325	0,0228	0,0106	−0,3932
	L 3	−2,0313	−2,0441	−2,0505	−2,0712	−2,5960
	L 2′	−3,8724	−3,8856	−3,8916	−3,9123	−4,4638
		0,2390	0,2371	0,2331	0,2227	−0,1392
		0,9661	0,9520	0,9410	0,9185	0,4884
	L 3′	0,4646	0,4606	0,4556	0,4427	0,0565
		0,8619	0,8488	0,8406	0,8181	0,3895
		1,2878	1,2716	1,2558	1,2321	0,7873

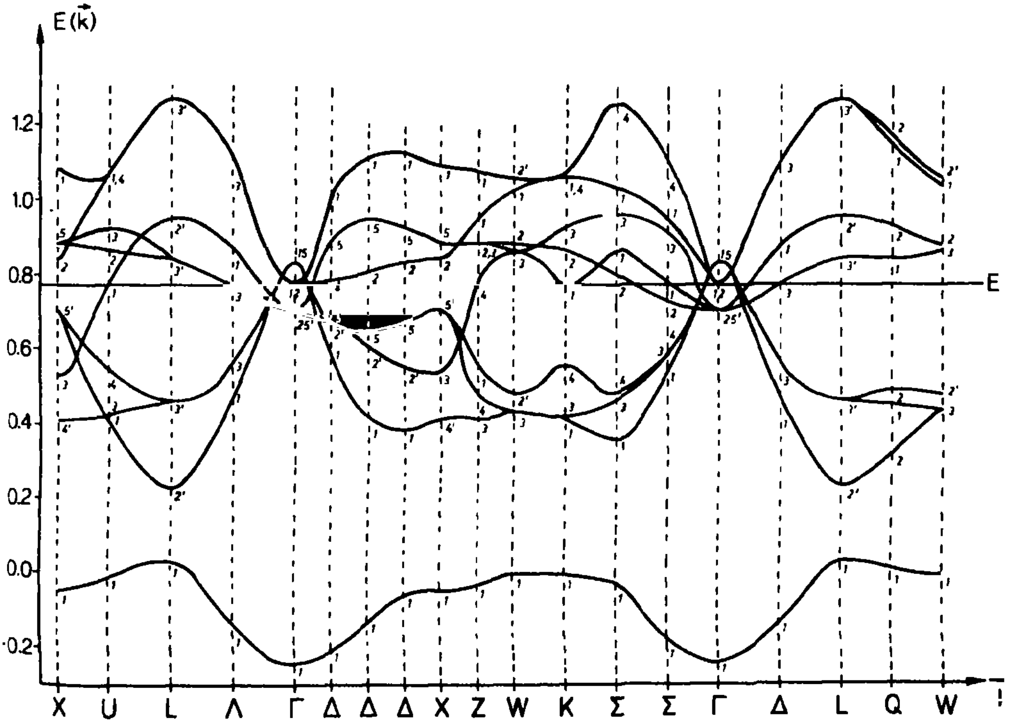

Fig. 1. Bandstruktur von VC für die Gitterkonstante $a = 7{,}87176$ at. E. (Energie in Rydberg)

In Fig. 1 ist für die Gitterkonstante $a = 7,87176$ at. E. die selbstkonsistente Bandstruktur entlang eines Streckenzuges in der 1. B.Z. wiedergegeben.

Um den Einfluß der Gitterkonstante auf die Bandstruktur überblicken zu können, sind in Tab. 4 einige charakteristische Bandbreiten sowie der Bandabstand zwischen dem $2s$- und dem $2p$-Band (energetischer Abstand der Punkte L'_2 und L_1) in Abhängigkeit von der Gitterkonstante angegeben. Wie zu erwarten, nimmt mit zunehmender Gitterkonstante die Breite des $2s$-Bandes sowie die Breite der überlappenden $2p/3d$-Bänder ab. Ebenso nimmt die Breite des besetzten Bereiches der $2p/3d$-Bänder mit zunehmendem Gitterparameter ab, die Bandlücke zwischen dem $2s$- und dem $2p$-Band wird größer.

Das selbstkonsistente Potential $V(r)$ für die Gitterkonstante $a = 7,8387$ at. E. ist in der Form $r\,V(r)$ in Tab. 5 angegeben.

Tabelle 4 Bandbreiten und Bandabstände in Abhängigkeit von Gitterparameter (Angaben in Rydberg)

Energetischer		Gitterparameter [at. E.]					Bemerkung
Abstand		7,80656	7,83869	7,87176	7,90256	7,90256*	
L_1	Γ_1	0,2831	0,2791	0,2743	0,2711	0,2468	Breite des 2s-Bandes
L'_2	L_1	0,2013	0,2046	0,2103	0,2121	0,2540	Abstand zwischen dem 2s- und 2p-Band
Γ'_1	L'_2	1,0488	1,0345	1,0227	1,0094	0,9265	Breite der überlappenden 2p/3d-Bänder
E_F	L'_2	0,5501	0,5416	0,5377	0,5276	0,4783	Breite des besetzten Bereiches der 2p/3d-Bänder

* Volles Slatersches Austauschpotential.

Tabelle 5 Selbstkonsistentes Potential $V(r)$ [Ryd] als Funktion des Abstandes r [at. E.] vom Mittelpunkt der jeweiligen Atomsphäre ($a = 7,8387$ at. E.)

r	$-rV(r)$	r	$-rV(r)$	r	$-rV(r)$
		Kohlenstoff-Sphäre			
0,00244	11,9523	0,25336	7,6795	1,54937	1,1475
0,00487	11,8042	0,26310	7,5622	1,58834	1,0847
0,00731	11,8557	0,27284	7,4474	1,62732	1,0272
0,00974	11,8067	0,28259	7,3350	1,66630	0,9751
0,01218	11,7574	0,29233	7,2248	1,70528	0,9282
0,01462	11,7078	0,30208	7,1168	1,74426	0,8867
0,01705	11,6580	0,31182	7,0108	1,78323	0,8503
0,01949	11,6079	0,32157	6,9067	1,82221	0,8192
0,02193	11,5577	0,33131	6,8045	1,86119	0,7933
0,02436	11,5073	0,34106	6,7041	1,90017	0,7726
0,02680	11,4568	0,36054	6,5085	1,93914	0,7573
0,02923	11,4062	0,38003	6,3193	1,97812	0,7474
0,03167	11,3556	0,39952	6,1364	2,01710	0,7430
0,03411	11,3049	0,41901	5,9595	2,05608	0,7443
0,03654	11,2543	0,43850	5,7885	2,09506	0,7515
0,03898	11,2036	0,45799	5,6233	2,13403	0,7647
0,04141	11,1530	0,47748	5,4638	2,17301	0,7843
0,04385	11,1025	0,49697	5,3101	2,21199	0,8106
0,04629	11,0520	0,51646	5,1620		
0,04872	11,0017	0,53594	5,0195		
0,05359	10,9014	0,55543	4,8822		

Tabelle 5 (Fortsetzung)

r	$-rV(r)$	r	$-rV(r)$	r	$-rV(r)$
0,05847	10,8017	0,57492	4,7501		
0,06334	10,7027	0,59441	4,6228		
0,06821	10,6045	0,61390	4,5000		
0,07308	10,5073	0,63339	4,3814		
0,07796	10,4110	0,65288	4,2668		
0,08283	10,3157	0,67237	4,1557		
0,08770	10,2216	0,69186	4,0480		
0,09257	10,1285	0,71134	3,9432		
0,09744	10,0366	0,73083	3,8413		
0,10232	9,9459	0,76981	3,6450		
0,10719	9,8564	0,80879	3,4578		
0,11206	9,7681	0,84777	3,2786		
0,11693	9,6810	0,88674	3,1068		
0,12181	9,5951	0,92572	2,9419		
0,12668	9,5104	0,96470	2,7837		
0,13155	9,4270	1,00368	2,6320		
0,13642	9,3447	1,04265	2,4867		
0,14129	9,2636	1,08163	2,3476		
0,14617	9,1837	1,12061	2,2147		
0,15591	9,0274	1,15959	2,0880		
0,16566	8,8755	1,19857	1,9674		
0,17540	8,7279	1,23754	1,8529		
0,18514	8,5845	1,27652	1,7443		
0,19489	8,4450	1,31550	1,6418		
0,20463	8,3092	1,35448	1,5451		
0,21438	8,1769	1,39346	1,4542		
0,22412	8,0480	1,43243	1,3691		
0,23387	7,9222	1,47141	1,2897		
0,24361	7,7994	1,51039	1,2158		

Vanadium-Sphäre

0,00156	45,7599	0,16188	28,4164	1,01489	6,3579
0,00311	45,5175	0,16811	27,9881	1,06470	5,8676
0,00467	45,2735	0,17434	27,5706	1,11451	5,4146
0,00623	45,0286	0,18056	27,1637	1,16432	4,9953
0,00778	44,7832	0,18679	26,7670	1,21413	4,6065
0,00934	44,5379	0,19302	26,3803	1,26394	4,2452
0,01090	44,2932	0,19924	26,0031	1,31375	3,9089
0,01245	44,0493	0,20547	25,6353	1,36356	3,5952
0,01401	43,8065	0,21170	25,2766	1,41338	3,3024
0,01557	43,5652	0,21792	24,9267	1,46319	3,0288
0,01712	43,3254	0,23037	24,2524	1,51300	2,7730
0,01868	43,0874	0,24283	23,6099	1.56281	2,5341
0,02024	42,8514	0,25528	22,9971	1,61262	2,3112
0,02179	42,6175	0,26773	22,4117	1,66243	2,1035
0,02335	42,3856	0,28018	21,8515	1,71224	1,9103
0,02491	42,1560	0,29264	21,3145	1,76205	1,7313
0,02646	41,9287	0,30509	20,7989	1,81186	1,5659
0,02802	41,7037	0,31754	20,3027	1,86167	1,4136
0,02958	41,4810	0,33000	19,8246	1,91148	1,2740
0,03113	41,2606	0,34245	19,3630	1,96129	1,1467
0,03424	40,8269	0,35490	18,9168	2,01110	1,0313

Tabelle 5 (Fortsetzung)

r	$-rV(r)$	r	$-rV(r)$	r	$-rV(r)$
0,03736	40,4024	0,36735	18,4849	2,06091	0,9273
0,04047	39,9868	0,37981	18,0665	2,11072	0,8345
0,04358	39,5799	0,39226	17,6609	2,16053	0,7524
0,04670	39,1813	0,40471	17,2675	2,21035	0,6809
0,04981	38,7907	0,41716	16,8859	2,26016	0,6198
0,05292	38,4079	0,42962	16,5157	2,30997	0,5689
0,05604	38,0324	0,44207	16,1566	2,35978	0,5281
0,05915	37,6639	0,45452	15,8083	2,40959	0,4976
0,06226	37,3022	0,46697	15,4704	2,45940	0,4774
0,06538	36,9472	0,49188	14,8252		
0,06849	36,5984	0,51678	14,2172		
0,07160	36,2558	0,54169	13,6429		
0,07472	35,9191	0,56660	13,0984		
0,07783	35,5882	0,59150	12,5803		
0,08094	35,2630	0,61641	12,0854		
0,08406	34,9435	0,64131	11,6114		
0,08717	34,6293	0,66622	11,1565		
0,09028	34,3205	0,69112	10,7192		
0,09339	34,0169	0,71603	10,2987		
0,09962	33,4251	0,74093	9,8941		
0,10585	32,8528	0,76584	9,5048		
0,11207	32,2990	0,79074	9,1305		
0,11830	31,7626	0,81565	8,7706		
0,12453	31,2426	0,84055	8,4246		
0,13075	30,7380	0,86546	8,0922		
0,13698	30,2478	0,89036	7,7730		
0,14321	29,7712	0,91527	7,4664		
0,14943	29,3075	0,94018	7,1720		
0,15566	28,8561	0,96508	6,8893		

b) Zustandsdichte

Berechnet man die Zustandsdichte aufgrund der APW-Energie-Eigenwerte für 256 *k*-Punkte in der 1. B.Z. nach einer Histogramm-Technik, so wird man nur ein rohes Abbild der tatsächlichen Zustandsdichte erhalten. Erfahrungsgemäß hängt die so berechnete Zustandsdichte von der Breite des gewählten Energieintervalls ΔE und von der Wahl des Nullpunktes des Energiebereiches ab. Üblicherweise wählt man ΔE so, daß die Zustandsdichte möglichst wenig mit der Intervallbreite variiert. Die Güte der Zustandsdichte kann dadurch wesentlich verbessert werden, daß man den Raster der *k*-Punkte verfeinert. Aus rechentechnischen Gründen ist es jedoch nicht zweckmäßig, die Energiewerte für den feineren Raster der *k*-Punkte nach der APW-Methode zu berechnen. Statt dessen erweist es sich als günstiger, eine LCAO-Interpolation nach Slater und Koster [38] vorzunehmen. Ausgehend von den 2*s*- und 2*p*-Funktionen des Kohlenstoff-Atoms und den 3*d*-Funktionen des Vanadium-Atoms werden formal Löwdin-Orbitale [39] konstruiert und aus diesen Blochsummen gebildet. Die sich bei Durchführung der Tight-Binding-Methode ergebenden Wechselwirkungsintegrale werden nun als Parameter betrachtet, die durch eine nichtlineare kleinste Fehler-

Tabelle 6. Angepaßte LCAO-Wechselwirkungsintegrale in Rydberg für die Gitterkonstante $a = 7{,}87176$ at. E. (Bezeichnungsweise nach Slater u. Koster [38], Koordinaten in Vielfachen von $a/2$)

$E_{XY,XY}(000)$	0,73718	$E_{S,3Z^2-R^2}(012)$	−0,00262
$E_{XY,XY}(110)$	−0,03364	$E_{S,3Z^2-R^2}(021)$	0,00122
$E_{XY,XY}(011)$	0,01028	$E_{X,XY}(210)$	−0,00076
$E_{3Z^2-R^2,3Z^2-R^2}(000)$	0,92007	$E_{X,XY}(120)$	−0,00230
$E_{3Z^2-R^2,3Z^2-R^2}(110)$	−0,00013	$E_{Z,3Z^2-R^2}(012)$	0,00136
$E_{X^2-Y^2,X^2-Y^2}(110)$	−0,01401	$E_{Z,3Z^2-R^2}(201)$	−0,00150
$E_{X,X}(000)$	0,66862	$E_{Z,X^2-Y^2}(201)$	−0,00024
$E_{X,X}(011)$	−0,00803	$E_{Z,X^2-Y^2}(012)$	0,00598
$E_{X,X}(110)$	0,02613	$E_{X,XY}(012)$	0,00050
$E_{X,XY}(010)$	0,08702	$E_{X,XY}(021)$	0,00090
$E_{Z,3Z^2-R^2}(001)$	0,13292		
$E_{XY,XZ}(011)$	0,01254		
$E_{XY,3Z^2-R^2}(110)$	−0,00484		
$E_{X,Y}(110)$	0,02038		
$E_{X,XY}(111)$	−0,00398		
$E_{X,X^2-Y^2}(111)$	0,00170		
$E_{X,YZ}(111)$	−0,00030		
$E_{S,S}(000)$	0,00190		
$E_{S,S}(110)$	−0,02035		
$E_{S,3Z^2-R^2}(001)$	−0,08640		
$E_{S,X}(110)$	0,01870		
$E_{S,XY}(111)$	0,00196		
$E_{S,S}(200)$	−0,00243		
$E_{Y,X}(200)$	0,01421		
$E_{Y,Y}(200)$	−0,01214		
$E_{XY,XY}(200)$	0,00134		
$E_{XY,XY}(002)$	−0,00091		
$E_{3Z^2-R^2,3Z^2-R^2}(002)$	−0,01954		
$E_{X^2-Y^2,X^2-Y^2}(002)$	−0,00263		
$E_{S,XY}(120)$	0,00332		

quadrat-Rechnung so optimiert werden, daß die nach der LCAO-Tight-Binding Methode berechneten Energiewerte möglichst gut mit den APW-Energie-Eigenwerten übereinstimmen. Für die vorliegende Rechnung wurden alle Wechselwirkungsintegrale einschließlich jener, die den fünftnächsten Nachbarn entsprechen, berücksichtigt. Insgesamt ergeben sich somit 40 Parameter für den Ausgleich. Zur Durchführung des LCAO-Interpolations-Verfahrens wurde ein Rechenprogramm von Connolly [40] benützt, das in entsprechender Weise modifiziert und erweitert worden ist, um die erhöhte Zahl von Parametern und die hier vorliegenden Funktionen behandeln zu können. Die optimierten Wechselwirkungsintegrale für $a = 7{,}87176$ at. E. sind in Tab. 6 wiedergegeben.

Um die Güte der Anpassung beurteilen zu können, sind in Tab. 7 die Wurzel aus dem mittleren Fehlerquadrat, die maximale Abweichung der berechneten LCAO-Energien von den APW-Energie-Eigenwerten und die maximale Energie-Abweichung unterhalb des Fermi-Niveaus angegeben. Bei Erhöhung der Zahl der Parameter von 22 (drittnächste Nachbarn) auf 40 (fünftnächste Nachbarn) sinken sowohl die Wurzel aus dem mittleren Fehlerquadrat als auch die maximale Abweichung etwa auf die Hälfte.

Tabelle 7. Vergleich der LCAO-Energiewerte mit APW-Energie-Eigenwerten (Angaben in Rydberg)

Gitterparameter [at. E.]	Wurzel aus dem mittleren Fehlerquadrat	maximale Abweichung	maximale Abweichung für $E \leq E_F$
7,80656	0,0054	0,026	0,018
7,83869	0,0053	0,026	0,017
7,87176	0,0052	0,025	0,017
7,90256	0,0052	0,025	0,016

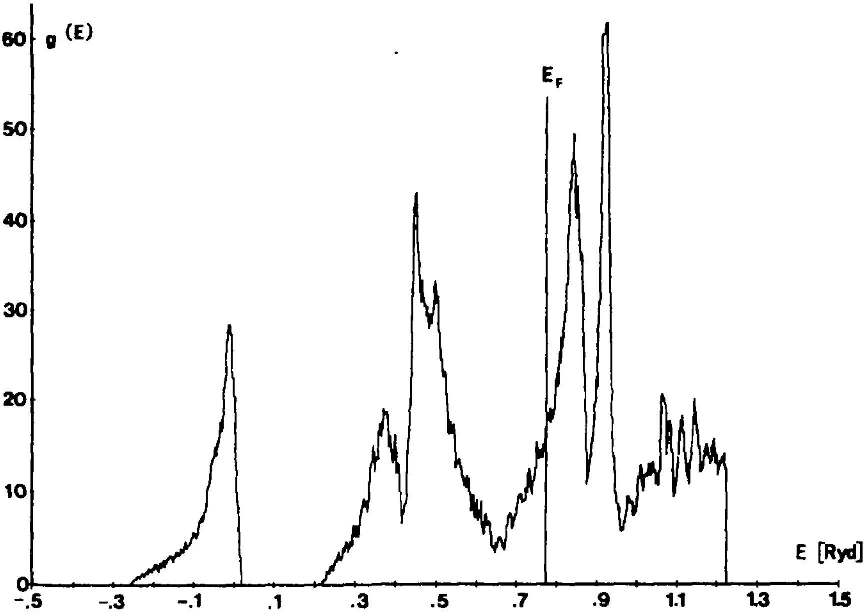

Fig. 2. LCAO-Zustandsdichte $g(E)$ für die Gitterkonstante $a = 7{,}87176$ at. E. $g(E)$ [Zahl der Zustände (Spin inbegriffen) pro primitiver Elementarzelle × Rydberg]

Mit Hilfe der optimierten Wechselwirkungsintegrale wurden nun die LCAO-Energien für 16384 k-Punkte in der 1. B.Z. berechnet. Unter Verwendung der so berechneten Energiewerte wurde nach einer Histogrammtechnik mit einem Energieintervall von $\Delta E = 0{,}002$ Ryd die Zustandsdichte ermittelt. Fig. 2 zeigt die Zustandsdichte für die Gitterkonstante $a = 7{,}87176$ at. E. Die Zustandsdichten für die anderen Gitterkonstanten unterscheiden sich, abgesehen von den bei der Besprechung der Bandstrukturen erwähnten Änderungen der Bandbreiten, nur unwesentlich. Durch Integration der Zustandsdichten wurden die Fermi-Energien ermittelt, die in Tab. 8 angegeben sind.

Um den Einfluß des Austauschpotentials auf die Zustandsdichte zu untersuchen, wurde für die Gitterkonstante $a = 7{,}90256$ at. E. die Zustandsdichte sowohl aus den Energie-Eigenwerten, die mit dem parametrisierten Austauschpotential ($\alpha \neq 1$), als auch aus den Energie-Eigenwerten, die mit dem vollen Slaterschen Austauschpotential ($\alpha = 1$) erhalten wurden, berechnet. Als Energie-

Tabelle 8. Fermienergien (Angaben in Rydberg)

Gitterparameter [at. E.]	Fermienergie
7,80656	0,7891
7,83869	0,7787
7,87176	0,7708
7,90256	0,7503

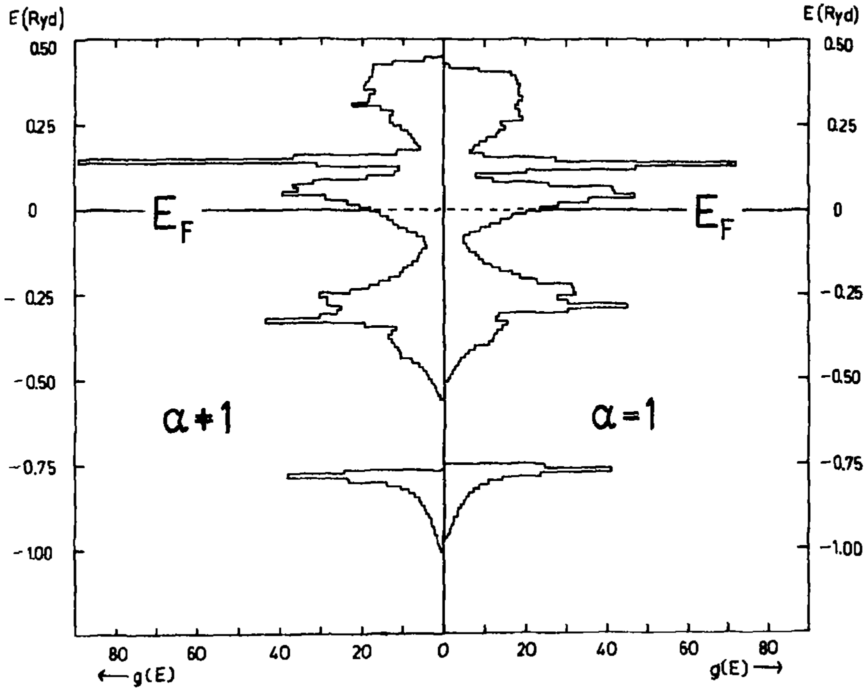

Fig. 3. Einfluß des Austauschpotentials auf die Zustandsdichte $g(E)$ [Zahl der Zustände (Spin inbegriffen) pro primitiver Elementarzelle × Rydberg]. ($\Delta E = 0{,}012$ Ryd)

intervall wurde in diesem Falle $\Delta E = 0{,}012$ Ryd verwendet. Die beiden Zustandsdichten sind in Fig. 3 so dargestellt, daß sie in der Fermi-Energie übereinstimmen. Wie zu erwarten, führt die Verringerung des Austauschpotentials ($\alpha \neq 1$) zu einer Verbreiterung der Bänder. Man beobachtet eine Vergrößerung des energetischen Abstandes zwischen Valenz- und Leitfähigkeitsbändern von etwa 0,05 Ryd. Diese Verschiebungen bedingen aber keine wesentlichen Änderungen in der Bandstruktur. Auch der l-Charakter (s. unten) wird durch das Austauschpotential nur wenig beeinflußt. Die Schlüsse über die Bindungsverhältnisse in VC sind daher von der Art des gewählten Austauschpotentials weitgehend unabhängig. Empfindlich beeinflußt wird jedoch die Fermi-Oberfläche und alle von dieser Größe abhängenden Eigenschaften. Auch die Kohäsionsenergie wird vermutlich sehr stark vom Austauschpotential abhängen.

c) APW-*Charakterdichten und partielle* LCAO-*Zustandsdichten*

Die APW-Methode gestattet die Ermittlung einer Charakterdichte $\chi_l(E)$, welche die Zahl der Elektronen mit einem bestimmten l-Charakter innerhalb der Atomsphären im Einheitsintervall der Energie angibt [2]. In analoger Weise kann man aus den nach der LCAO-Tight-Binding Methode erhaltenen Kristallwellenfunktionen eine partielle Zustandsdichte mit bestimmtem l-Charakter berechnen. Die so gewonnenen partiellen Zustandsdichten werden sich zweifellos von den APW-Charakterdichten unterscheiden, und zwar aus folgenden Gründen:

a) Die APW-Charakterdichten beziehen sich nur auf den Bereich innerhalb der Atomsphären, während die partiellen LCAO-Zustandsdichten die gesamte Elementarzelle berücksichtigen.

b) Entsprechend den für das LCAO-Interpolationsverfahren verwendeten Basisfunktionen treten im vorliegenden Falle nur eine 2*s*-, 2*p*- und eine 3*d*-Zustandsdichte auf, während aus den APW-Funktionen Charakterdichten für die l-Werte $l = 0$ bis $l = 12$ gebildet werden können. (In der vorliegenden Rechnung wird nämlich zur Entwicklung der APW-Kristallwellenfunktion der Wertesatz $l = 0$ bis $l = 12$ verwendet.)

Ferner ist zu beachten, daß für die APW-Charakterdichten ein relativ großes Energieintervall ($\Delta E = 0{,}05$ Ryd) verwendet werden muß, da die Charakterdichten auf den Energie-Eigenwerten von nur 256 *k*-Punkten in der 1. B. Z. beruhen.

Aus den angeführten Gründen kann man daher nur eine begrenzte Übereinstimmung zwischen diesen beiden Größen erwarten [10].

Einen Vergleich der APW-Charakterdichten mit den partiellen LCAO-Zustandsdichten erlauben die Fig. 4, 5 und 6. Man erkennt, daß diese beiden

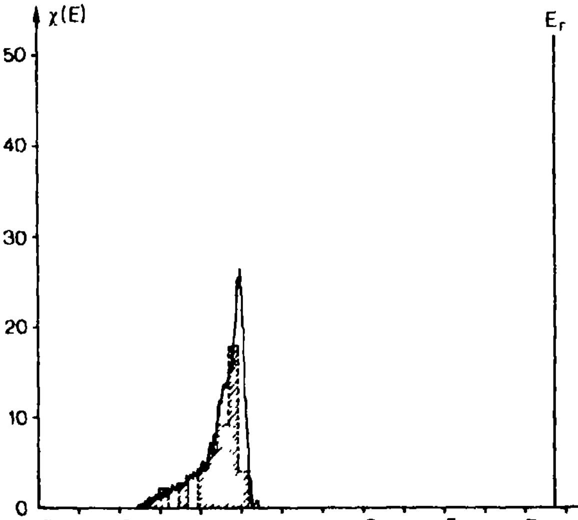

Fig. 4. Vergleich der LCAO 2*s*-Zustandsdichte [Zahl der 2*s*-Zustände (Spin inbegriffen) pro primitiver Elementarzelle × Rydberg] (ausgezogene Kurve) mit der APW 2*s*-Charakterdichte [Zahl der 2*s*-Elektronen (Spin inbegriffen) innerhalb der Atomsphären pro primitiver Elementarzelle × Rydberg] (strichlierte Kurve) für die Gitterkonstante $a = 7{,}83869$ at. E.

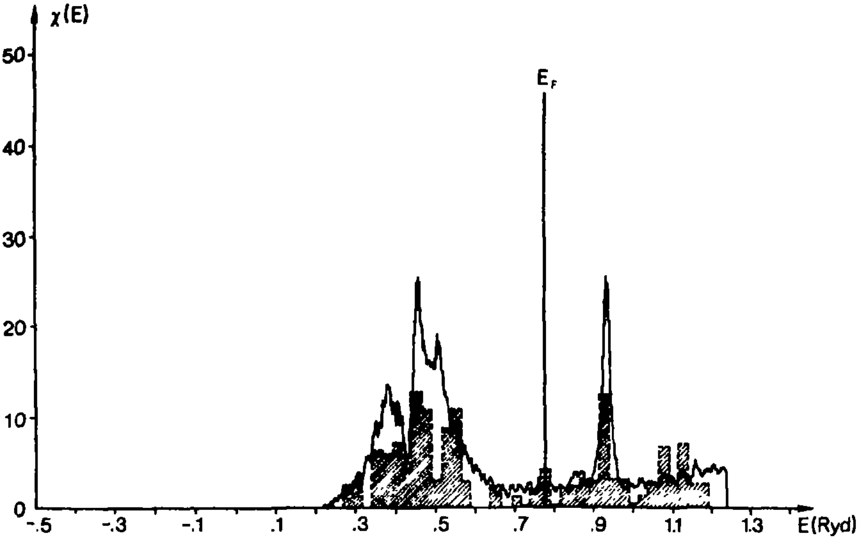

Fig. 5. Vergleich der LCAO $2p$-Zustandsdichte [Zahl der $2p$-Zustände (Spin inbegriffen) pro primitiver Elementarzelle × Rydberg] (ausgezogene Kurve) mit der APW $2p$-Charakterdichte [Zahl der $2p$-Elektronen (Spin inbegriffen) innerhalb der Atomsphären pro primitiver Elementarzelle × Rydberg] (strichlierte Kurve) für die Gitterkonstante $a = 7{,}83869$ at. E.

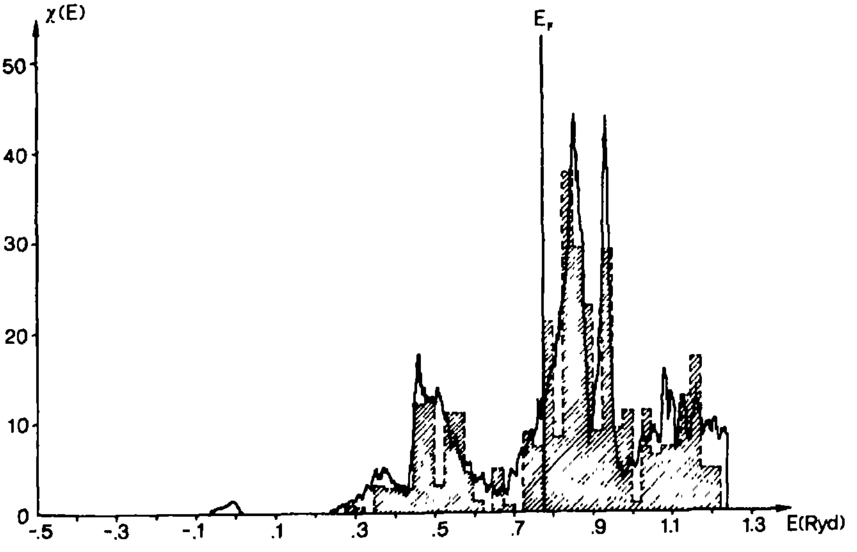

Fig. 6. Vergleich der LCAO $3d$-Zustandsdichte [Zahl der $3d$-Zustände (Spin inbegriffen) pro primitiver Elementarzelle × Rydberg] (ausgezogene Kurve) mit der APW $3d$-Charakterdichte [Zahl der $3d$-Elektronen (Spin inbegriffen) innerhalb der Atomsphären pro primitiver Elementarzelle × Rydberg] (strichlierte Kurve) für die Gitterkonstante $a = 7{,}83869$ at. E.

Größen einen weitgehend ähnlichen Verlauf zeigen. Inwieweit jedoch die Feinheiten der partiellen Zustandsdichten physikalisch bedeutungsvoll sind, kann auf Grund dieses Vergleiches nicht beurteilt werden.

Beide Analysen zeigen jedoch übereinstimmend, daß das energetisch tiefstliegende Valenzband fast ausschließlich $2s$-Charakter mit einer geringfügigen Zumischung von $3d$-Zuständen besitzt (Fig. 4). Die nach einer Energielücke von 0,2 Ryd im Energiebereich von 0,2 bis 0,7 Ryd (vgl. die Fig. 2, 5 und 6) folgenden überlappenden Bänder stellen eine Mischung von $2p$- und $3d$-Zuständen dar. Eine Abschätzung aufgrund der APW-Charakterdichten führt zu einem Anteil von etwa 45% $3d$-Zuständen. Die nach Durchlaufen des Minimums der Zustandsdichten folgenden Bänder besitzen vornehmlich $3d$-Charakter mit einem beträchtlichen Anteil von $2p$-Zuständen. Die Zustandsdichte am Fermi-Niveau besitzt etwa 85% $3d$-Charakter. Die hier diskutierten Befunde sind im untersuchten Bereich praktisch unabhängig von der Gitterkonstante.

d) Ladungsverteilung

Wie bereits früher beschrieben [2, 5], erlaubt die APW-Methode die Bestimmung der Einzelladungen mit einem bestimmten l-Charakter innerhalb einer Atomsphäre. Um die bei der Verbindungsbildung auftretende Ladungsverschiebung abschätzen zu können, wurden die Ladungen berechnet, die in den Atomsphären auftreten würden, wenn das Gitter aus neutralen Atomen aufgebaut wäre. Zu diesem Zwecke wurden die Elektronendichten der neutralen Atome nach der α-Expansions-Methode von Löwdin [41] überlagert und durch Integration die Ladung innerhalb einer Atomsphäre ermittelt. In Tab. 9 sind für die Gitterkonstante $a = 7{,}87176$ at. E. die Einzel- und Gesamtladungen in den Atomsphären im Kristall angegeben und den Gesamtladungen, die sich durch Überlagerung der atomaren Ladungsdichten ergeben, gegenübergestellt.

Tabelle 9. Ladungsaufteilung in VC für $a = 7{,}87176$ at. E. (Angaben in Elektronenladungen)

Zustand		Kristall	überlagerte atomare Ladung
		Vanadium-Sphäre	
Rumpf		10,0000	10,0000
Semi-Rumpf	$3s$	1,9805	
	$3p$	5,8433	
Valenz	$3d$	2,6781	
	$4s$	0,1384	
	$4p$	0,2467	
	höhere Zustände	0,0309	
Gesamt		20,9179	21,2426
		Kohlenstoff-Sphäre	
Rumpf		2,0000	2,0000
Valenz	$2s$	1,2935	
	$2p$	2,2875	
	$3d$	0,0599	
	höhere Zustände	0,0147	
Gesamt		5,6556	5,1927

Ladung zwischen den Atomsphären im Kristall: 2,4263

Man erkennt, daß die Wellenfunktionen der Semi-Rumpfzustände (3*s*- und 3*p*-Zustand von V) aus der V-Sphäre hinausreichen und daß sich beispielsweise 2,6% der Ladung des 3*p*-Zustandes außerhalb der V-Sphäre befinden. Dieses Verhalten zeigt, daß die Semi-Rumpfzustände durch ein Bändermodell beschrieben werden sollten [3].

Die Gesamtladung in der V-Sphäre hat im Kristall gegenüber den überlagerten Ladungsdichten um etwa 0,32 Elektronen abgenommen, während die Ladung in der C-Sphäre um etwa 0,46 Elektronen zugenommen hat. Dieser Befund weist auf eine gewisse Ionizität der Verbindung VC hin. Die Ladungsverteilung ändert sich im untersuchten Bereich mit der Gitterkonstante um einige Hundertstel Elektronenladungen. Diese Änderungen sind aber vor allem auf Änderungen in der Größe der Atomsphären zurückzuführen. Die charakteristischen Merkmale der Ladungsverteilung bleiben jedoch erhalten.

Eine Berechnung oder Abschätzung physikalischer Eigenschaften aufgrund der ermittelten Bandstruktur wird in dieser Arbeit nicht vorgenommen. Ein derartiger Vergleich soll erst nach Vorliegen der in Vorbereitung befindlichen Bandstruktur-Rechnungen für nichtstöchiometrische Phasen angestellt werden.

Dem Jubiläumsfonds der österreichischen Nationalbank sind wir für die gewährte finanzielle Unterstützung zu großem Dank verpflichtet. Herrn Prof. Dr. H. Nowotny danken wir für die Förderung, die er dieser Arbeitsrichtung angedeihen läßt. Die große Hilfe von Herrn Dr. K. Schwarz, University of Florida, Gainesville, wird dankbar anerkannt.

Literatur

1. Slater, J. C: Physic. Rev. **51**, 846 (1937).
2. Schwarz, K., Weinberger, P., Neckel, A.: Theoret. chim. Acta (Berl.) **15**, 149 (1969).
3. Weinberger, P., Schwarz, K., Neckel, A.: Int. J. phys. and chem. Solids **32**, 2063 (1971).
4. — Rastl, P., Mechtler, R., Neckel, A.: (In Vorbereitung).
5. Ern, V., Switendick, A. C.: Physic. Rev. **137 A**, 1927 (1965).
6. Conklin, J. B., Silversmith, D. J.: Int. J. quant. Chemistry II, 243 (1968).
7. Schwarz, K., Conklin, J. B.: Physic. Rev. (in Vorbereitung).
8. Schoen, J. M., Denker, S. P.: Physic. Rev. **184**, 864 (1969).
9. Neckel, A., Rastl, P., Weinberger, P., Mechtler, R.: (In Vorbereitung).
10. Schwarz, K.: Mh. Chem. **102**, 1400 (1971).
11. Storms, R. K.: The refractory carbides. New York: Acad. Press 1967.
12. Mattheiss, L. F., Wood, J. H., Switendick, A. C.: Methods in computational physics, Vol. 8, p. 63. New York: Acad. Press 1968.
13. Gáspár, R.: Acta physica hung. **3**, 263 (1954).
14. Latter, R.: Physic. Rev. **99**, 510 (1955).
15. Löwdin, P. O.: J. molecular Spectroscopy **3**, 46 (1959).
16. Lindgren, I.: Physic. Rev. Letters **19**, 382 (1965).
17. Kohn, W., Sham, L. J.: Physic. Rev. **140 A**, 1133 (1965).
18. Sham, L. J., Kohn, W.: Physic. Rev. **145**, 561 (1966).
19. Payne, H.: Physic. Rev. **157**, 515 (1967).
20. Liberman, D.: Physic. Rev. **171**, 1 (1968).
21. Rosén, A., Lindgren, I.: Physic. Rev. **176**, 114 (1968).
22. Gáspár, R.: Int. J. quant. Chemistry III, 723 (1969).
23. Berrondo, M., Goscinski, O.: Physic. Rev. **184**, 10 (1969).
24. Slater, J. C., Wilson, T. M., Wood, J. H.: Physic. Rev. **179**, 28 (1969).
25. Herman, F., Dyke, J. P., Ortenburger, I. B.: Physic. Rev. Letters **22**, 807 (1969).

26. Kmetko, E. A.: Physic. Rev. **1** A, 37 (1970).
27. Schwarz, K.: Physic. Rev. (im Druck).
28. Slater, J. C.: Physic. Rev. **81**, 385 (1951).
29. Connolly, J. W. D.. PP 94, Quant. Theory Project, Fla 1968.
30. — Physic. Rev. **159**, 415 (1967).
31. Snow, E. C., Waber, J. T.: Physic. Rev. **157**, 570 (1967).
32. Rudge, W. E.: Physic. Rev. **181**, 1024 (1969).
33. Snow, E. C.: Physic. Rev. **171**, 785 (1968).
34. - Physic. Rev. **172**, 708 (1968).
35. Rudge, W. E.: Physic. Rev. **181**, 1033 (1969).
36. Ross, M., Johnson, K. W.: Physic. Rev. B **2**, 4709 (1970).
37. Storms, E. K., McNeal, R. J.: J. physic. Chem. **66**, 1401 (1962).
38. Slater, J. C., Koster, F. G.: Physic. Rev. **94**, 1498 (1954).
39. Löwdin, P. O.: J. chem. Physics **18**, 365 (1950).
40. Connolly, J. W. D.: 3. I.M.R. Symposium; Electronic density of states, N.B.S. Spec. Publ. 323 (im Druck).
41. Löwdin, P. O.: Advances in Physics **5**, 96 (1956).

Dr. A. Neckel
Institut für Physikalische Chemie
der Universität
Wien 9, Währingerstr. 42
Österreich

Theoret. chim. Acta (Berl.) 24, 191 -200 (1972)
© by Springer-Verlag 1972

Modellrechnungen zur Solvatation einatomiger Ionen* (LCAO–MO-Untersuchungen von Molekülstrukturen VIII**)

P. RUSSEGGER, H. LISCHKA und P. SCHUSTER
Institut für Theoretische Chemie der Universität, Wien, Währinger Str. 38, Österreich

Eingegangen am 6. August 1971

Model Calculations of the Solvation of Oneatomic Ions (LCAO–MO-Investigations of Molecular Structures VIII)

Hydrates of the ions Li^+, Na^+, Be^{2+}, F^- and Cl^- with coordination numbers 1, 2, 4, 6 and 8 and up to three shells of water molecules were calculated with the CNDO/2 method. The strength of the hydrogen bond in the outer shells is determined largely by the charge transfer from the central ion to the ligands. In the third hydration shell of the F^- ion the average binding energy is almost the same as in pure water clusters. In the case of Li^+ the influence of the ion reaches one shell further. For both ions the coordination number 6 is the most favourable one.

Hydrate der Ionen Li^+, Na^+, Be^{2+}, F^- und Cl^- mit den Koordinationszahlen 1, 2, 4, 6 und 8 sowie bis zu drei Hydrathüllen wurden mit Hilfe des CNDO/2-Verfahren berechnet. Die Stärke der Wasserstoffbrücken in den äußeren Sphären wird durch die Ladungsübertragung vom Zentralion zu den Liganden stark beeinflußt. Bei F^- unterscheidet sich die mittlere Bindungsenergie in der dritten Sphäre kaum mehr vom reinen Wasser; bei Li^+ reicht der Einfluß um eine Wasserhülle weiter. Für beide Ionen wird 6 als günstigste Koordinationszahl erhalten.

Calcul par la méthode CNDO/2 des hydrates des ions Li^+, Na^+, Be^{2+}, F^- et Cl^-, à nombres de coordinence 1, 2, 4, 6 et 8, avec jusqu'à trois couches de molécules d'eau. La force de la liaison hydrogène dans les couches externes est largement déterminée par le transfert de charge à partir de l'ion central vers les ligands. Dans la troisième couche d'hydratation de l'ion F^- l'énergie de liaison moeyenne est presque la meme que dans les essaims d'eau pure. Dans le cas de Li^+ l'influence de l'ion atteint une couche supplèmentaire. Pour ces deux ions le nombre de coordinence 6 s'avère le plus favorable.

Einleitung

Seit etwa drei Jahren werden *ab initio*- und semi-empirische LCAO-MO-SCF-Methoden mit Erfolg zur Berechnung von Strukturen mit Wasserstoffbrücken angewendet (z.B. [1–5]). Obwohl die Wechselwirkung in den Hydraten kleiner Ionen von ähnlicher Art sein sollte, wurden nur ganz wenige LCAO-MO-Rechnungen über derartige Strukturen ausgeführt [5–9]. Der Grund dafür ist wohl darin zu suchen, daß ein großer Teil der Wechselwirkungsenergie durch den reinen elektrostatischen Beitrag verursacht wird, welcher sehr einfach abgeschätzt werden kann. Dementsprechend gibt es auch zahlreiche elektrostatische Modelle, mit deren Hilfe Hydratisierungsenergien und freie Hydratisierungsenthalpien berechnet werden können. Alle derartigen Modelle weisen jedoch auch eine ganze Reihe von Nachteilen auf: Da alle „nicht elektrostatischen“ Beiträge zur Wechselwirkungsenergie vernachlässigt werden, muß jene Geometrie, welche durch die Ion-Dipol-Wechselwirkung bestimmt wird, als energetisch günstigste Anordnung vorausgesetzt werden (**1**, **2a**). Bei den Hydratkomplexen von Anionen werden hingegen mehr oder weniger starke Wasserstoffbrücken ausgebildet, welche in der linearen Anordnung von X^-, H und O (**2b**) am stärksten sind. Die elektrostatischen Modelle können keine Auskunft über die Elektronenverteilung in den Solvaten geben, weil sie jede Ladungsübertragung vom Zentralion zu den Molekülen der Solvathülle ausschließen. Außerdem benötigen die elektrostatischen Modelle noch eine Reihe von empirischen Parametern, wie z. B. Ionenradien und lokale Dielektrizitätskonstanten, welche vor allem die Berechnung von nicht wäßrigen Solvathüllen, für die viel weniger experimentelles Datenmaterial als im Fall von Wasser vorliegt, stark erschweren (vgl. z. B. [10, 11]). Es erschien daher angezeigt, auch den alternativen Versuch von LCAO-MO-Beschreibungen der solvatisierten Ionen zu unternehmen.

---

* Dem Andenken an Herrn Prof. Dr. K. H. Hansen gewidmet.

** 7. Mitt.: Schuster, P., Preuss, H.-W.: Chem. Physics Letters 11, 35 (1971).

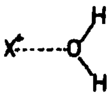

1

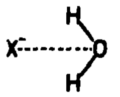

2a

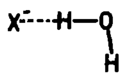

2b

In der vorliegenden Arbeit werden LCAO-MO-Rechnungen an den Hydratkomplexen von Li^+, Na^+, Be^{2+}, F^- und Cl^- mit verschiedenen Koordinationszahlen und mehreren Solvathüllen beschrieben. Da die betrachteten Strukturen für *ab initio*-Rechnungen mit ausreichenden Basissätzen zu groß sind, wurde die semiempirische LCAO-MO-SCF-Methode von Pople, Segal und Santry (CNDO) [12–14] angewendet, welche sich als gut geeignet zur Beschreibung von Strukturen mit Wasserstoffbrücken erwiesen hatte.

Rechenmethode

Alle hier beschriebenen Ergebnisse wurde mit der CNDO/2-Methode in ihrer ursprünglichen Parametrisierung [14] erhalten. Die numerischen Rechnungen wurden mit einer modifizierten Version des Computerprogrammes QCPE 141[1] durchgeführt, welche die Gesamtenergie bezüglich einer Dimension selbsttätig minimalisiert. Als Rechenmaschine stand uns die IBM 360/44-Anlage des Instituts für Statistik der Universität Wien zur Verfügung.

Ergebnisse

1. Hydrathülle

Die wichtigsten Rechenergebnisse – ΔE, R_{OX}, R_{OH} und die Ladungsübertragung vom Zentralion auf die Wassermoleküle – sind in den Tabellen 1–5 für verschiedene Koordinationszahlen in der 1. Hydrathülle angegeben. Die Stabilisierungsenergie der Komplexionen (ΔE) wurde als Differenz der Gesamtenergien berechnet.

$$\Delta E\,[X(H_2O)_n] = E\,[X(H_2O)_n] - \{E\,(X) + n\,E\,(H_2O)\}$$

---

[1] Quantum Chemistry Program Exchange, Bloomington, Indiana, USA.

Tabelle 1. Rechenergebnisse von Li^+-Komplexionen mit einer Hydrathülle

n	R_{OLi}	ΔE	$\Delta E/n$	q_{Li}	q_{H_2O}
	(Å)	(kcal/mol)			
1	2,35	45,7	45,7	+ 0,836	+ 0,163
2	2,37	87,9	44,0	+ 0,688	+ 0,156
4	2,41	164,3	41,1	+ 0,444	+ 0,139
6	2,48	217,7	36,2	+ 0,311	+ 0,114
8	2,55	257,9	32,2	+ 0,245	+ 0,095

Tabelle 2. Rechenergebnisse von Na^+-Komplexionen mit einer Hydrathülle

n	R_{ONa}	ΔE	$\Delta E/n$	q_{Na}	q_{H_2O}
	(Å)	(kcal/mol)			
1	2,92	32,9	32,9	+ 0,827	+ 0,173
2	2,92	64,7	32,4	+ 0,775	+ 0,112
4	2,93	125,9	31,5	+ 0,564	+ 0,109
6	2,95	181,1	30,2	+ 0,381	+ 0,103
8	2,98	229,6	28,7	+ 0,253	+ 0,093

Tabelle 3. Rechenergebnisse von Be^{2+}-Komplexionen mit einer Hydrathülle

n	R_{OBe}	ΔE	$\Delta E/n$	q_{Be}	q_{H_2O}
	(Å)	(kcal/mol)			
1	1,70 (R_{OH} = 1,03)	217,6	217,6	+ 1,475	+ 0,524
2	1,71	411,8	205,9	+ 1,007	+ 0,496
4	1,80	682,9	170,7	+ 0,562	+ 0,359
6	1,89	821,4	136,9	+ 0,496	+ 0,250
8	1,99	891,2	111,4	+ 0,529	+ 0,184
1	1,70 (R_{OH} = 1,05)	218,4	218,4		

Tabelle 4. Rechenergebnisse von F^--Komplexionen mit einer Hydrathülle

n	R_{OF}	R_{OH}	ΔE	$\Delta E/n$	q_F	q_{H_2O}
	(Å)	(Å)	(kcal/mol)			
1	2,22	1,12	79,8	79,8	—0,656	—0,344
2	2,28	1,09	118,3	59,2	—0,590	—0,205
4	2,36	1,06	164,0	41,0	—0,549	—0,113
6	2,43	1,05	189,3	31,6	—0,560	—0,073
8	2,51	1,04	168,7	21,1	—0,582	—0,052

Tabelle 5. Rechenergebnisse von Cl^--Komplexionen mit einer Hydrathülle

n	R_{OCl}	R_{OH}	ΔE	$\Delta E/n$	q_{Cl}	q_{H_2O}
	(Å)	(Å)	(kcal/mol)			
1	2,74	1,06	23,6	23,6	—0,905	—0,095
2	2,75	1,05	45,6	22,8	—0,854	—0,073
4	2,79	1,05	79,8	19,9	—0,788	—0,053
6	2,81	1,04	108,3	18,1	—0,756	—0,042
8	2,84	1,04	98,2	12,3	—0,738	—0,033

In Übereinstimmung mit *ab initio*-Rechnungen [6, 9] wurden die Orientierungen **1** und **2b** für die Wassermoleküle angesetzt[2]. Bei der Koordinationszahl $n = 2$ wurden die Liganden linear, bei $n = 4, 6$ oder 8 an den Eckpunkten eines regulären Tetraeders, Oktaeders bzw. archimedischen Antiprismas angeordnet. Bei den hydratisierten Kationen wurde nur der Abstand R_{OX} variiert. Die Wassermoleküle beließen wir in der CNDO/2-Minimumsgeometrie ($R_{OH} = 1{,}03$ Å, $< HOH = 107{,}1°$). Anhand des stärksten Komplexes – $Be(OH_2)^{2+}$ – wurde gezeigt, daß eine Variation des OH-Abstandes die Gesamtenergie nur wenig erniedrigt (Tab. 3). Bei den hydratisierten Anionen wurden sowohl der Abstand R_{OX} als auch die Lage des Protons in der Wasserstoffbrücke variiert. Die Länge der zweiten OH-Bindung und der Bindungswinkel blieb in allen Rechnungen konstant.

2. *Hydrathülle*

In den folgenden Beispielen näherten wir den optimalisierten Komplexionen mit einer Hydrathülle weitere Wassermoleküle. Bei konstanter Geometrie der inneren Hydrathülle wurden die OO-Abstände zwischen den Wassermolekülen der ersten und zweiten Sphäre (R_{OO}) variiert. Die Wechselwirkungsenergien ΔE^{II} beziehen sich nun auf den Anbau der Wassermolekülen in der zweiten Sphäre:

$$\Delta E^{II}[X(H_2O)_{m+n}] = E[X(H_2O)_{m+n}] - \{E[X(H_2O)_n] + mE(H_2O)\}$$

Zur Untersuchung des Anteils der Wechselwirkung zwischen den einzelnen Wassermolekülen der zweiten Sphäre, welcher durch die elektronische Rückkopplung verursacht wird, wurden einige zweidimensionale Li^+-Komplexe – **3** ($n = 1$) und **4** ($n = 2$) – berechnet, bei welchen sterische Effekte keine entscheidende Rolle spielen (Tab. 6).

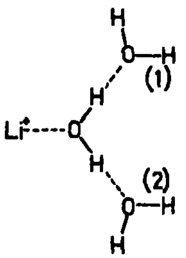

3

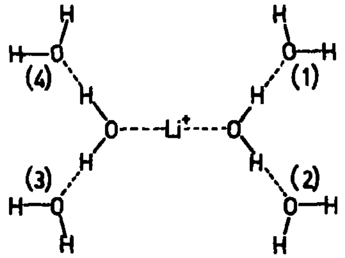

4

In den dreidimensionalen Strukturen ($n = 4$, 6 oder 8) gingen wir von der tetraedrischen Anordnung der Wasserstoffbrücken im Eis I aus. An die drei freien Koordinationsstellen der Wassermoleküle der ersten Sphäre können in der zweiten Sphäre weitere Wassermoleküle angebaut werden. Als Folge der Ladungsübertragung vom Zentralion auf die inneren Wassermoleküle unter-

---

[2] Bei $F(H_2O)^-$ stimmen die *Minimumsgeometrien* von *ab inito*– und CNDO/2-Rechnungen gut überein [6, 8]. Widersprüche treten hingegen beim Komplex $Li(H_2O)^+$ auf, dessen günstigste Geometrie im Rahmen der CNDO/2-Methode als Pyramide, mit anderen semiempirischen (z. B. INDO) oder *ab initio* Methoden hingegen planar [9] berechnet wird.

Tabelle 6. Bindungsenergien und Abstände zwischen den Wassermolekülen in Li^+-Komplexionen mit zwei Hydrathüllen (Koordinationszahl $n = 1, 2$)

n	Struktur	2. Sphäre bereits gebundene H₂O-Moleküle	2. Sphäre neu angebaute H₂O-Moleküle	R_{OO} (Å)	ΔE (kcal/mol)	$\Delta E/m$ (kcal/mol)
1	**3**	—	1	$2{,}42_2$	21,6	21,6
		—	1, 2	$2{,}45_8$	39,0	19,5
2	**4**	—	1	$2{,}43_3$	20,3	20,3
		—	1, 2	$2{,}46_3$	36,6	18,3
		1, 2	3	$2{,}45_6$	19,7	19,7
		1, 2	3, 4	$2{,}46_8$	36,0	18,0

Tabelle 7. Ladungsverschiebung in tetraedrisch koordinierten hydratisierten Ionen $[X(H_2O)_4]$

X	Δq_X	Δq_O	Δq_{H_1}[a]	Δq_{H2}
Li^+	−0,556	+0,014	+0,062	+0,062
Be^{2+}	−1,438	+0,037	+0,161	+0,161
Na^+	−0,436	+0,009	+0,050	+0,050
F^-	0,451	−0,149	+0,122	−0,087
Cl^-	0,212	−0,085	+0,092	−0,060

[a] In den Hydraten der Anionen ist H_1 das in der Wasserstoffbrücke befindliche Proton.

Tabelle 8. Bindung von Wassermolekülen an verschiedenen Stellen der tetrakoordinierten Ionen Li^+ und F^-

Zentralion	Struktur	neu angebaute H₂O-Moleküle	R_{OO} (Å)	ΔE^{II} (kcal/mol)	$\Delta E^{II}/m$ (kcal/mol)
Li^+	**5**	*a*	2,56	9,6	9,6
		b + *b*	2,49	33,8	16,9
		a + *b* + *b*	2,50	45,6	15,2
F^-	**6**	*a*	2,65	0,9	0,9
		b + *b*	2,49	29,6	14,8
		a + *b* + *b*	2,50	34,8	11,6

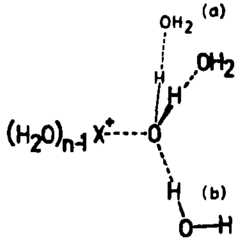

5

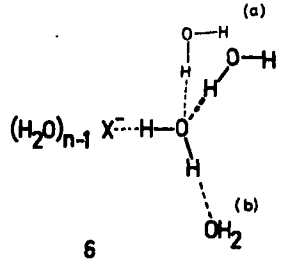

6

scheiden sich die Elektronendichten von den entsprechenden Werten in reinen Wasserclustern (Tab. 7). Dadurch erhalten wir unterschiedliche ΔE^{II}-Werte, je nachdem, ob wir die Wasserstoffbrücken mit dem H-Atom oder mit dem O-Atom des Wassers knüpfen (**a** bzw. **b** in **5** oder **6**, vgl. Tab. 8).

Tabelle 9. Mittlere Bindungsenergien und Gesamtladungen der Wassermoleküle in der zweiten Hydrathülle

Zentralion	n	q_{H_2O}	$\overline{\Delta E}^{II}/m$ (kcal/mol)
Li^+	4	+0,027	15,2
	6	+0,023	13,9
	8	+0,020	13,3
Be^{2+}	4	+0,052	22,0
	6	+0,037	18,8
	8	+0,028	18,3
F^-	4	−0,033	11,6
	6	−0,028	11,2
	8	−0,026	9,9

In den Li^+ und F^- Komplexionen mit den Koordinationszahlen 4, 6 und 8 wurden zur Berechnung der mittleren Wechselwirkungsenergien an ein Wassermolekül der ersten Sphäre drei Wassermoleküle in der zweiten Sphäre angebaut (**5** und **6**). Die mittleren Energiewerte und die Gesamtladungen der H_2O-Moleküle sind in Tab. 9 zusammengefaßt.

3. *Hydrathülle*

Genauso wie bei dem vorhin beschriebenen Modell für die zweite Sphäre wurden als Modell für die dritte Sphäre an ein Wassermolekül der zweiten Sphäre drei weitere Wassermoleküle angebaut. Für diesen Anbau gibt es im

Tabelle 10. Mittlere Bindungsenergien und Gesamtladungen der Wassermoleküle in der 3. Hydrathülle

Zentralion	n	$\bar{q}_{H_2O}$	$\overline{\Delta E}^{III}/m$ (kcal/mol)
Li^+	4	+0,005	11,2
	6	+0,005	11,3
	8	+0,005	11,1
Be^{2+}	4	+0,009	11,5
	6	+0,009	12,0
	8	+0,009	11,8

Tabelle 11. Abgeschätzte Hydratisierungsenergien in kcal/mol

Ion	n	$\Delta E_{Hydr.}$					ΔH (exp)	
		1. Sphäre	2. Sphäre	1. + 2. Sphäre	3. Sphäre	1. + 2. + 3. Sphäre	[10]	[15]
Li	4	126	67	193	58	251	128	130
	6	160	77	238	31	268		
	8	181	59	240	24	264		
Be^{2+}	4	644	149	793	68	862		608
	6	764	166	930	43	973		
	8	814	139	953	35	989		
F^-	4	126	24	150	–	150	120	98
	6	132	29	161	–	161		
	8	92	5	97	–	97		

Prinzip zwei Möglichkeiten, da wir in der zweiten Sphäre zwei Typen von Wassermolekülen unterscheiden können. Die Berechnung ergab jedoch kaum merkbare Unterschiede bezüglich der mittleren Wasserstoffbrückenenergien und der mittleren Ladungsübertragung in den vollständigen Tetraedern der dritten Sphäre. Die Zahlenwerte für Li^+ und Be^{2+} sind in Tab. 10 zusammengestellt. Bei F^- erhielten wir in der dritten Sphäre fast die gleichen Wechselwirkungsenergien für die Wasserstoffbrücken wie im reinen Wassercluster ($\Delta\bar{E} \sim 9.6$ kcal/mol).

Diskussion

Die Ergebnisse für die 1. Hydrathülle mit den Koordinationszahlen $n = 1$, 2, 4 und 6 wurden bereits an anderer Stelle diskutiert [7, 8], weshalb sie hier nur kurz zusammengefaßt werden sollen. Je mehr Wassermoleküle an das Zentralion gebunden werden, um so geringer wird die Bindungsenergie pro Wassermolekül. Bei allen berechneten Kationen, Li^+, Na^+ und Be^{2+} führt das Hinzufügen weiterer Wassermoleküle in unseren Rechnungen ($n \leqq 8$) zu einer Energieerniedrigung (Tab. 1, 2 und 3). Die ΔE-Werte der Hydratkomplexe der Anionen F^- und Cl^- hingegen weisen ein Minimum bei $n = 6$ auf, d.h. der Anbau von weiteren Wassermolekülen an das oktaedrische Komplexion führt zu einer Energiezunahme (Tab. 4 und 5). Hand in Hand mit der Verringerung der Wechselwirkungsenergie geht eine Verlängerung der Abstände R_{OX} mit steigendem n. Die vom Zentralion auf das einzelne Wassermolekül übertragene Ladung nimmt in allen untersuchten Komplexionen monoton mit n ab. Die Änderung der Nettoladung am Zentralion verläuft nur in jenen Fällen monoton, bei denen der Abstand R_{OX} mit steigender Koordinationszahl nicht zu stark zunimmt – Li^+, Na^+, Cl^-. Bei den verschiedenen Hydraten von Be^{2+} und F^- treten hingegen sehr starke relative Abstandsänderungen auf und die Elektronendichte am Zentralion durchläuft bei bestimmten Koordinationszahlen einen Extremwert.

Die Wechselwirkungsenergien und damit auch das Ausmaß der Ladungsübertragung werden im Rahmen der CNDO/2-Methode wesentlich zu groß berechnet [3]. Besonders ausgeprägt ist diese Übertreibung bei den Hydraten von F^-. Von den semiempirischen Rechnungen dürfen wir uns daher nur ein qualitatives Bild von den Bindungsverhältnissen in den hydratisierten Ionen erwarten.

Die Rechnungen an den zweidimensionalen Modellen der zweiten Hydrathülle von Li^+-Komplexen ($n = 1$ und 2) geben uns eine Antwort auf die Frage wie weit sich die Wassermoleküle innerhalb der zweiten Sphäre gegenseitig beeinflussen. Da in den betrachteten Strukturen (3 und 4) die einzelnen Wassermoleküle genügend weit voneinander entfernt sind, geben die Ergebnisse die elektronische Kopplung zwischen den Liganden ohne sterische Beiträge wieder. Die berechneten Bindungsenergien für die einzelnen Wassermoleküle der zweiten Sphäre sind deutlich geringer als in der ersten Sphäre, aber immer noch bedeutend höher als die Energie der Wasserstoffbrücken in reinen Wasserclustern ($[H_2O]_{11}$:$\Delta E = 9.6$ kcal/mol). Ganz allgemein nehmen auch in der zweiten Sphäre die mittleren Bindungsenergien – $\Delta E^{II}/m$ – ab, wenn die Zahl der Wassermoleküle (*m*) erhöht wird. Wird das neu hinzutretende Wassermolekül am selben Wassermolekül der ersten Sphäre gebunden, so tritt eine Abnahme der mittleren Bindungsenergien von bis zu 10% auf. Wassermoleküle, welche an verschiedenen Molekülen der ersten Hydrathülle gebunden werden, beeinflussen sich hingegen nur wenig; im Modellbeispiel unterscheiden sich die Bindungsenergien nur um 2–3%.

Das vorhin beschriebene Ergebnis rechtfertigt das verwendete Modell für die 2. und 3. Hydrathülle der Ionen, in welchem stets nur an einem Wassermolekül ein Tetraeder der nächsten Sphäre angebaut wurde. Dabei vernachlässigten wir die elektronische Wechselwirkung zwischen den Wassermolekülen, welche durch mehr als ein dazwischenliegendes Molekül getrennt sind.

Die Rechenergebnisse von vierfach koordiniertem Li^+- und F^--Ion zeigen deutlich, daß wir in der zweiten Hydrathülle zwei Typen von Wassermolekülen unterscheiden können, welche ungleich fest gebunden sind. Im hydratisierten Kation wird Elektronendichte vom Wasser auf das Zentralion übertragen, welche sowohl von den H-Atomen als auch vom O-Atom stammt (Tab. 7). Dadurch werden die H-Atome acider und können stärkere Wasserstoffbrücken ausbilden als nicht an Kationen gebundenes Wasser. Das zweite einsame Elektronenpaar des O-Atoms wird jedoch durch die Ladungsübertragung weniger basisch und bildet eine schwächere Brücke aus (Tab. 7).

Bei den Anionen wird Elektronendichte in umgekehrter Richtung, vom Zentralion zu den Liganden übertragen. Dadurch nimmt die Elektronendichte am O-Atom und an dem nicht in der Wasserstoffbrücke gefunden Proton (H_2) zu. Durch analoge Überlegungen wie oben können wir verstehen, daß die von den einsamen Elektronenpaaren des O-Atoms ausgehenden Wasserstoffbrücken stärker als im nicht koordinativ gebundenen Wasser sind. Die dritte Wasserstoffbrücke aber wird wegen der geringeren Acidität des Protons stark geschwächt. Infolge der durch die CNDO/2-Parametrisierung übertriebenen Ladungsübertragung von F^- auf die Wassermoleküle sind auch die Unterschiede in den Energien der Wasserstoffbrücken dieses Ions besonders groß.

Auf die Wassermoleküle der dritten Hydrathülle wird nur mehr sehr wenig Ladung übertragen ($\Delta q < 0{,}01$). Die Energien der Wasserstoffbrücken sind auch nur mehr bei den Kationen nennenswert größer als in reinen Wasserclustern. In diesem Bereich ist daher zu erwarten, daß die elektronischen Effekte gegenüber der Raumerfüllung der Moleküle stark in den Hintergrund treten. Die wesentlichen Beiträge aus der dritten Hydrathülle stammen daher von den unterschiedlichen sterischen Verhältnissen bei den Koordinationszahlen 4, 6 oder 8.

Hydratisierungsenergien

Von besonderem Interesse erschien der Versuch einer Abschätzung von Hydratisierungsenergien und Koordinationszahlen mit Hilfe unserer Ergebnisse. Da nur wenig experimentelle Daten über die Struktur von flüssigem Wasser vorliegen, erweist es sich auch als ziemlich schwierig, ein realistisches Modell für den Hydratisierungsprozeß zu finden. Das einfachste Modell besteht darin, daß wir in einem Wassercluster von genügender Größe das im Zentrum befindliche Wassermolekül durch das entsprechende Ion ersetzen. Die Reaktionsenergie des Prozesses

$$X + (H_2O)_{N+1} \leftrightharpoons X(H_2O)_N + H_2O ,$$

$\Delta E_{\mathrm{Hydr.}}$, betrachten wir dementsprechend als näherungsweises Maß für die Hydratisierungsenergie. In tetraedrischen Hydratkomplexen bereitet dieses Modell keine Schwierigkeiten, da wir durch den sukzessiven Anbau der äußeren Hüllen direkt zu einem Ausschnitt aus einem Eis-I-Kristall kommen.

Bei den hydratisierten Ionen mit höheren Koordinationszahlen – 6 oder 8 – treten vor allem zwei Schwierigkeiten auf: Der Anbau von „Wassertetraedern" an den Eckpunkten führt zu komplizierten Strukturen, welche nicht ohne weiteres in einen Eis-I-Kristall eingebaut werden können. Wie Molekülmodelle zeigen, kommen sich die Wassermoleküle in den höheren Hydrathüllen räumlich zu nahe. Im oktaedrischen Komplexion können wir zwar in der zweiten Sphäre noch je drei Wassermoleküle unterbringen. In der dritten Sphäre ist dann jedoch nur mehr Platz für ein Wasser pro Wassermolekül der zweiten Sphäre. Beim archimedischen Antisprisma ist die sterische Behinderung noch größer: In der zweiten Sphäre können wir nur mehr je zwei Wassermoleküle, in der dritten nur mehr je ein Wassermolekül unterbringen.

Benutzen wir die oben beschriebenen Wassercluster als Referenz, so ergeben sich die in Tab. 11 zusammengefaßten Ergebnisse. Im Vergleich zu den experimentellen Daten sind sämtliche berechneten Hydratisierungsenergien zu groß. Die relative Abstufung stimmt jedoch befriedigend überein. Mit Ausnahme von Be^{2+} stimmen die berechneten Koordinationszahlen – 6 für Li^+ und F^- – mit anderen Abschätzungen überein. Bei den Be^{2+}-Komplexen kommt es offenbar wegen der zu hoch berechneten Wechselwirkungsenergien in der ersten Sphäre zu einer Überbewertung der höheren Koordinationszahlen.

In unserem einfachen Modell wurden die Umordnungsenergien vernachlässigt, welche zu einer zusätzlichen Stabilisierung der Wassercluster nach Austausch des Zentralions durch ein Wassermolekül führen. Diese Umordnungsenergien sind bei den Koordinationszahlen 6 und 8 wesentlich größer als bei den Tetraedern, welche bereits weitgehend die Struktur von Wasserclustern aufweisen. Eine Einbeziehung der genannten Umordnungsenergien würde dementsprechend die berechneten Koordinationszahlen zugunsten kleinerer Werte verschieben.

Darüber hinaus erhebt sich die Frage, wie weit ein statisches Modell überhaupt zur Beschreibung der hydratisierten Ionen geeignet ist. Da in den Alkalimetallionen sogar die Wassermoleküle der innersten Sphäre praktisch diffusionskontrolliert ausgetauscht werden [16], müssen wir damit rechnen, daß schon in der zweiten Sphäre starke Abweichungen von der statisch günstigsten Anordnung auftreten und die dritte Sphäre unter Umständen nicht mehr voll aufgebaut wird.

Schlußbemerkungen

Die beschriebenen Rechenergebnisse geben uns ein qualitatives Bild von den Hydrathüllen kleiner, einatomiger Ionen. Die Ladungsübertragung vom Zentralion zu den Liganden führt zu charakteristischen Unterschieden in den Energien der Wasserstoffbrücken der äußeren Hydrathüllen. In der zweiten

Sphäre können wir zwei Typen von unterschiedlich stark gebundenen Wassermolekülen unterscheiden. Im Rahmen der semiempirischen Modellrechnungen wird zwar das Ausmaß der Ladungsübertragung übertrieben, doch zeigen die *ab initio*-Rechnungen der einfachsten Strukturen [6, 9], daß die Ladungsverschiebungen in etwas reduzierter Form erhalten bleiben. Wie bei Strukturen mit starken Wasserstoffbrücken werden auch hier die Wechselwirkungsenergien zwischen den Wassermolekülen und Ionen infolge der CNDO/2-Parametrisierung zu hoch berechnet. In weiteren Arbeiten wäre es daher wünschenswert durch die Wahl neuer Parameter eine energetisch korrekte Beschreibung dieser Strukturen zu erzielen. Mit solchen Parametern könnte man auch versuchen die Umordnungsenergien für die Wassermoleküle in den einzelnen Sphären zu berechnen und mit der Beschreibung der dynamischen Vorgänge in den Hydrathüllen zu beginnen.

Dem Rechenzentrum des Institutes für Statistik der Universität Wien danken wir für die großzügige Zuteilung von Rechenzeiten an der IBM 360/44 Anlage.

Literatur

1. Murthy, A. S. N., Davies, R. E., Rav, C. N. R.: Theoret. chim. Acta (Berl.) **13**, 81 (1969).
2. Kollman, P. A., Allen, L. C.: J. Amer. chem. Soc. **92**, 753 (1970).
3. Schuster, P.: Theoret. chim. Acta (Berl.) **19**, 212 (1970).
4. Diercksen, G. H. F.: Theoret. chim. Acta (Berl.) **21**, 335 (1971).
5. Hoyland, J. R., Kier, L. B.: Theoret. chim. Acta (Berl.) **15**, 1-11 (1969).
6. Diercksen, G. H. F., Kraemer, W. P.: Chem. Physics Letters **5**, 570 (1970).
7. Burton, R. E., Daly, J.: Trans. Faraday Soc. **66**, 1281 (1970).
8. Lischka, H., Plesser, Th., Schuster, P.: Chem. Physics Letters **6**, 263 (1970).
9. Schuster, P., Preuß, H.-W.: Chem Physics Letters **11**, 35 (1971).
10. Morris, D. F. C.: Ionic radii and enthalpies of hydration of ions, structure and bonding, Vol. 4, p. 63-82. Berlin: Springer 1968.
11. Morf, W. E., Simon, W.: Helv. chim. Acta **54**, 794 (1971).
12. Pople, J. A., Santry, D. P., Segal, G. A.: J. chem. Physics **43**, 129 (1965).
13. Segal, G. A.: J. chem. Physics **43**, 136 (1965).
14. -- J. chem. Physics **44**, 3289 (1966).
15. Noyes, R. M.: J. Amer. chem. Soc. **84**, 513 (1962).
16. Eigen, M.: Pure appl. Chem. **6**, 97 (1963).

Dozent Dr. P. Schuster
Institut für Theoretische Chemie
der Universität
Wien 9, Währinger Straße 38
Österreich

Theoret. chim. Acta (Berl.) 24, 201—206 (1972)
© by Springer-Verlag 1972

Die Bewegung eines Körpers in einem ringförmigen Potentialfeld*

HERMANN HARTMANN

Institut für Physikalische Chemie der Universität, 6000 Frankfurt (Main) 1,
Robert-Mayer-Straße 11, Deutschland

Eingegangen am 31. August 1971

The Motion of a Body in a Ring-Shaped Potential

The quantum mechanical problem of a particle in the torus shaped potential $V \sim 2 \cdot \frac{r_0}{r} - \frac{1}{\sin^2\theta} \cdot \left(\frac{r_0}{r}\right)^2$ is solved.

Es wird das quantenmechanische Problem eines Teilchens in einem ringförmigen Potential der Art $V \sim 2 \cdot \frac{r_0}{r} - \frac{1}{\sin^2\theta} \cdot \left(\frac{r_0}{r}\right)^2$ gelöst.

Solution du problème quantique de la particule dans un potentiel toroïdal: $V \sim 2 \frac{r_0}{r} - \frac{1}{\sin^2\theta} \left(\frac{r_0}{r}\right)^2$.

Bei der Betrachtung ringförmiger Moleküle taucht die Frage auf, ob es einfache Eigenwertprobleme gibt, bei denen es um die Bewegung eines Körpers in einem ringförmigen Potentialfeld geht. Wir wollen zeigen, daß es ein solches Problem gibt und daß die Eigenwerte und Eigenfunktionen dieses Problems in geschlossener Form angegeben werden können.

Die potentielle Energie des Körpers sei in Kugelkoordinaten

$$V = \eta \sigma^2 \left(\frac{2a_0}{r} - \eta \frac{a_0^2}{r^2 \sin^2 \vartheta} \right) \varepsilon_0 . \tag{1}$$

Dabei sollen a_0 den Wasserstoffradius und ε_0 die Energie des Wasserstoffgrundzustandes bedeuten:

$$a_0 = \frac{h^2}{4\pi^2 \mu e^2}, \quad \varepsilon_0 = -\frac{2\pi^2 \mu e^4}{h^2} . \tag{2}$$

η und σ sind positive reine Zahlen. Bei beliebigem und festem r hat V als Funktion von ϑ seinen Minimalwert bei $\vartheta = \pi/2$, also in der Äquatorialebene des Kugelkoordinatensystems. Dort hat es als Funktion von r seinen Minimalwert bei

$$r_0 = \eta a_0 \tag{3}$$

---

* Dem Andenken an meinen Freund Karl Heinz Hansen gewidmet.

und dieser Wert ist

$$V_0 = \sigma^2 \varepsilon_0 \,. \tag{4}$$

Mit diesen Beziehungen läßt sich der Ausdruck für V umformen zu

$$V = \left(\frac{2r_0}{r} - \frac{r_0^2}{r^2 \sin^2 \vartheta} \right) V_0 \,. \tag{5}$$

V ist die potentielle Energie des Körpers in einem ringförmigen Potentialfeld. Die Linie geringster potentieller Energie ist ein Kreis in der Äquatorialebene mit dem durch entsprechende Wahl von η einstellbaren Radius $r_0 = \eta a_0$. Die Tiefe des ringförmigen Potentialfeldes $V_{r\to\infty} - V_0 = -\sigma^2 \varepsilon_0$ kann durch entsprechende Wahl von σ^2 eingestellt werden. Nach Einführung der Koordinaten d und z durch

$$d = r \sin\vartheta \,, \qquad z = r \cos\vartheta \tag{6}$$

erscheint V in der Gestalt

$$V = \eta \sigma^2 \left(\frac{2a_0}{\sqrt{d^2 + z^2}} - \eta \frac{a_0^2}{d^2} \right) \varepsilon_0 \,. \tag{7}$$

Daraus folgt

$$\left(\frac{\partial^2 V}{\partial d^2} \right)_{\substack{d = r_0 \\ z = 0}} = \left(\frac{\partial^2 V}{\partial z^2} \right)_{\substack{d = r_0 \\ z = 0}} = -\frac{2\sigma^2}{\eta^2} \frac{\varepsilon_0}{a_0^2} = -\frac{2V_0}{r_0^2} \,. \tag{8}$$

Die Linien gleicher potentieller Energie in der d-z-Ebene sind also, insofern sie in geringer Entfernung von dem Punkt minimaler potentieller Energie ($d = r_0$, $z = 0$) verlaufen, praktisch Kreise. Die Linien gleicher potentieller Energie, die in größerer Entfernung von dem Punkt minimaler potentieller Energie verlaufen, greifen nach der Seite größerer d-Werte weiter aus als nach der Seite kleinerer d-Werte.

Die Schrödingergleichung des Problems lautet

$$\begin{gathered} \frac{1}{r^2} \frac{\partial}{\partial r} \left(r^2 \frac{\partial \psi}{\partial r} \right) + \frac{1}{r^2 \sin\vartheta} \frac{\partial}{\partial \vartheta} \left(\sin\vartheta \frac{\partial \psi}{\partial \vartheta} \right) + \frac{1}{r^2 \sin^2\vartheta} \frac{\partial^2 \psi}{\partial \varphi^2} \\ + \frac{8\pi^2 \mu}{h^2} \left[E - \left(\frac{2r_0}{r} - \frac{r_0^2}{r^2 \sin^2\vartheta} \right) V_0 \right] \psi = 0 \,. \end{gathered} \tag{9}$$

In dem Produktansatz für die Lösungsfunktionen

$$\psi(r, \vartheta, \varphi) = R(r)\, \Theta(\vartheta)\, \Phi(\varphi) \tag{10}$$

kann, da die potentielle Energie von φ nicht abhängt, sofort

$$\Phi(\varphi) = \frac{1}{\sqrt{2\pi}} e^{im\varphi} \,, \quad m = 0, \pm 1, \pm 2, \ldots \tag{11}$$

gesetzt werden. Die Separation führt zu den Gleichungen

$$\frac{1}{\sin\vartheta}\,\frac{d}{d\vartheta}\left(\sin\langle\,\frac{d\Theta}{d\vartheta}\right)-\left(\frac{M^2}{\sin^2\vartheta}-L(L+1)\right)\Theta=0 \tag{12}$$

und

$$\frac{1}{r^2}\,\frac{d}{dr}\left(r^2\,\frac{dR}{dr}\right)-L(L+1)\,R+\frac{8\pi^2\mu}{h^2}\left(E+\eta\sigma^2\,\frac{e^2}{r}\right)R=0 \tag{13}$$

für die Funktionen Θ und R. Dabei ist M^2 erklärt durch

$$M^2=m^2+\sigma^2\eta^2\,. \tag{14}$$

$L(L+1)$ ist eine Separationskonstante.

Die Θ-Gleichung geht durch die Substitutionen

$$\cos\vartheta=z,\ \Theta(\vartheta)=\mathscr{P}(z)=(1-z^2)^{\frac{|M|}{2}}\,\mathscr{G}(z) \tag{15}$$

in die Gleichung

$$(1-z^2)\frac{d^2\mathscr{G}}{dz^2}-2(|M|+1)\,z\,\frac{d\mathscr{G}}{dz}+[L(L+1)-|M|(|M|+1)]\,\mathscr{G}=0 \tag{16}$$

über. Der Reihenansatz

$$\mathscr{G}=\sum_{\nu}a_\nu z^\nu \tag{17}$$

führt zu der Rekursionsformel

$$a_{\nu+2}=\frac{(\nu+|M|)\,(\nu+|M|+1)-L(L+1)}{(\nu+1)\,(\nu+2)}\,a_\nu\,. \tag{18}$$

Die Reihe $\mathscr{G}$ muß abbrechen, wenn $\mathscr{P}$ eine auch bei $z=\pm 1$ reguläre Funktion sein soll. Der Grad des dann vorliegenden Polynoms $\mathscr{G}$ sei ν'. Dann muß

$$(\nu'+|M|)\,(\nu'+|M|+1)=L(L+1) \tag{19}$$

oder

$$L=\nu'+|M|\,;\quad \nu'=0,1,2,\ldots \tag{20}$$

sein.

Für die Funktionen

$$(1-z^2)^{\frac{|M|}{2}}\,\mathscr{G}_{\nu'}(z)=\mathscr{P}^{|M|}_{|M|+\nu'}(z)=\mathscr{P}^{|M|}_{L}(z) \tag{21}$$

existiert die erzeugende Funktion

$$\sum_{\nu'=0}^{\infty}\mathscr{P}^{|M|}_{|M|+\nu'}(z)\,t^{\nu'}=\frac{\Gamma(2|M|+1)}{2^{|M|}\,\Gamma(|M|+1)}\;\frac{(1-z^2)^{\frac{|M|}{2}}}{(1-2zt+t^2)^{|M|+\frac{1}{2}}}\,. \tag{22}$$

Speziell ist

$$\begin{aligned} \mathscr{P}_{|M|}^{|M|} &= \frac{\Gamma(2|M|+1)}{2^{|M|}\Gamma(|M|+1)}(1-z^2)^{\frac{|M|}{2}} \\ \mathscr{P}_{|M|+1}^{|M|} &= -\frac{\Gamma(2|M|+1)}{2^{|M|}\Gamma(|M|+1)}(2|M|+1)(1-z^2)^{\frac{|M|}{2}} z \\ \mathscr{P}_{|M|+2}^{|M|} &= \frac{\Gamma(2|M|+1)}{2^{|M|}\Gamma(|M|+1)}\,\frac{2|M|+1}{2}(1-z^2)^{\frac{|M|}{2}}\{1-(3+|M|)z^2\}. \end{aligned} \tag{23}$$

Die Funktionen $\mathscr{P}_L^{|M|}$ sind mit den zugeordneten Legendreschen Polynomen $P_l^{|m|}$ verwandt. Sie gehen mit $\sigma\eta\to 0$ in diese über. (Dabei ist unter l die Zahl $\nu' + |m|$ zu verstehen.)

Die R-Gleichung (13) geht durch die Substitutionen

$$\begin{aligned} \alpha^2 &= -\frac{8\pi^2\mu}{h^2}E, & \lambda &= \frac{4\pi^2\mu e^2}{h^2\alpha} - \eta\sigma^2 \\ 2\alpha r &= \varrho, & R(r) &= e^{-\frac{\varrho}{2}}\varrho^L\mathscr{L}(\varrho) \end{aligned} \tag{24}$$

in die Gleichung

$$\varrho\frac{d^2\mathscr{L}}{d\varrho^2} + [2(L+1)-\varrho]\frac{d\mathscr{L}}{d\varrho} + (\lambda - L - 1)\mathscr{L} = 0 \tag{25}$$

über. Der Reihenansatz

$$\mathscr{L} = \sum_{\nu} b_\nu \varrho^\nu \tag{26}$$

führt zu der Rekursionsformel

$$b_{\nu+1} = \frac{L+1+\nu-\lambda}{2(\nu+1)(L+1)+\nu(\nu+1)}b_\nu. \tag{27}$$

Reguläre Lösungen ergeben sich bei negativem E nur dann, wenn die Reihe $\mathscr{L}$ abbricht.

Wenn dann der Grad des Polynoms $\mathscr{L}n'$ sein soll, muß

$$\lambda = L+1+n'\,; \quad n' = 0, 1, 2, \ldots \tag{28}$$

sein. Daraus folgt mit (24) die Beziehung für die Eigenwerte

$$E = \frac{\eta^2\sigma^4}{N^2} - \varepsilon_0 \quad \text{mit} \quad N = L+1+n'. \tag{29}$$

Für die regulären Lösungsfunktionen $\mathscr{L}_{2L+1+n'}^{2L+1} = \mathscr{L}_{N+L}^{2L+1}$ der $\mathscr{L}$-Gleichung existiert die erzeugende Funktion

$$\sum_{n'=0}^{\infty}\frac{\mathscr{L}_{2L+1+n'}^{2L+1}(\varrho)}{\Gamma(2L+2+n')}u^{n'} = (-1)^{2L+1}\frac{e^{-\frac{\varrho u}{1-u}}}{(1-u)^{2L+2}}. \tag{30}$$

Speziell ist

$$\begin{aligned} \mathscr{L}_{2L+1}^{2L+1} &= \Gamma(2L+2)(-1)^{2L+1} \\ \mathscr{L}_{2L+2}^{2L+1} &= \Gamma(2L+3)(-1)^{2L+1}(2+2L-\varrho). \end{aligned} \tag{31}$$

Die Funktionen $\mathscr{L}_{2L+1+n'}^{2L+1} = \mathscr{L}_{N+L}^{2L+1}$ mit $N = L+1+n'$ sind mit den zugeordneten Laguerreschen Polynomen L_{n+l}^{2l+1} verwandt. Sie gehen mit $\sigma\eta \to 0$ in diese über. (Dabei ist unter n die Zahl $l+1+n'$ zu verstehen.)

Jede der von uns bestimmten regulären Lösungen der Schrödinger-Gleichung ist durch die drei Zahlen $|M|$, L, N charakterisiert. Wir führen nun durch

$$l = |m| + v', \qquad n = l+1+n' \tag{32}$$

die Zahlen l und n ein. Zwischen l und dem Drehimpuls besteht bei dem hier behandelten Problem nicht der vom Keplerproblem her bekannte Zusammenhang. Wir können jetzt schreiben:

$$\begin{aligned} |M| &= \sqrt{m^2 + \sigma^2\eta^2} \\ L &= l + \sqrt{m^2 + \sigma^2\eta^2} - |m| \\ N &= n + \sqrt{m^2 + \sigma^2\eta^2} - |m|. \end{aligned} \tag{33}$$

Mit

$$\delta = \sqrt{m^2 + \sigma^2\eta^2} - |m|$$

vereinfachen sich diese Beziehungen zu

$$\begin{aligned} |M| &= |m| + \delta \\ L &= l + \delta \\ N &= n + \delta. \end{aligned} \tag{35}$$

Wenn man für die vom Keplerproblem her bekannten Quantenzahlen n, l, m ihre dort vorkommenden Wertesysteme zuläßt, erhält man gerade alle gebundenen Zustände unseres Problems.

Wenn man sich speziell für den Grundzustand interessiert, hat man zu fragen, welches der kleinstmögliche Wert von N ist. Dieser wird erhalten für $n = 1$ und $m = 0$. Bei $n = 1$ muß außerdem $l = 0$ sein. Für diesen (1s-)Zustand ist nach (29) und (35)

$$E_{1s} = \frac{\eta^2\sigma^4}{(1+\eta\sigma)^2}\,\varepsilon_0. \tag{36}$$

Die zugehörige Eigenfunktion ist verschieden von der 1s-Funktion des Keplerproblems. Sie lautet

$$\psi_{1s} = K(v \sin\vartheta\, e^{-v})^{\eta\sigma} \tag{37}$$

mit

$$v = \frac{\eta\sigma}{1+\eta\sigma}\,\frac{r}{r_0}.$$

Für den Normierungsfaktor K gilt

$$K = \left\{\frac{\Gamma(\frac{3}{2}+\eta\sigma)\,(\eta\sigma)^{\sigma+2\eta\sigma}\,2^{2+2\eta\varrho}}{2\pi\,\Gamma(1+\eta\sigma)\,\Gamma(\frac{1}{2})\,\Gamma(3+2\eta\sigma)\,(1+\eta\sigma)^3\,r_0^3}\right\}^{\frac{1}{2}}. \tag{39}$$

ψ_{1s} hat seinen Maximalwert in der Äquatorialebene ($\vartheta = \pi/2$). In dieser Ebene liegt das Maximum von ψ_{1s} bei

$$r_{\max} = \frac{1+\eta\sigma}{\eta\sigma} r_0 . \tag{40}$$

Die Lösung des behandelten Problems eröffnet die Wege zur Untersuchung einer Reihe von interessanten Fragestellungen.

Der Vollständigkeit halber sei noch darauf hingewiesen, daß sich in dem Falle, daß man über die Lösungen der Hillschen Differentialgleichung verfügt, auch die Eigenwerte und Eigenfunktionen der Schrödingergleichung mit der potentiellen Energie

$$V = -\frac{A}{r} + \frac{B + C\cos\frac{k\varphi}{2\pi}}{r^2 \sin^2\vartheta} \tag{41}$$

angeben lassen.

Prof. Dr. H. Hartmann
Institut für Physikalische Chemie der Universität
D-6000 Frankfurt (Main) 1
Robert-Mayer-Straße 11
Deutschland

Theoret. chim. Acta (Berl.) 24, 207—215 (1972)
© by Springer-Verlag 1972

Polarisierte Kristallspektren einiger Hexaharnstoffkomplexe bei tiefen Temperaturen

Teil I. Absorption

K. H. HANSEN† und H. J. SCHENK*

Lehrstuhl für Theoretische Chemie der Universität Bonn, 5300 Bonn, Wegelerstraße 12, Deutschland

Eingegangen am 5. April/19. Juli 1971

Polarized Crystal Spectra of Some Hexa-Urea Complexes at Low Temperatures

I. Absorption

The present paper deals with the low-temperature polarized absorption spectra of single crystals $Ti^{3+}: Al(ur)_6X_3$ (X: Cl, Br, I), $Cr^{3+}: Al(ur)_6 (ClO_4)_3$ und $Cr(ur)_6I_3$ in the wavelength range from 7500 Å to 3500 Å. The crystal point group is D_{3d}, the metal ions occupy sites of D_3 symmetry. Experimental values of the cubic parameter Dq and the trigonal parameters v and v' are reported. The hexaureatitanium(III)-complexes are strongly Jahn-Teller-distorted in the ^2E excited state. The distortion in the ground state is likely to depend on the anion.

Gegenstand der vorliegenden Untersuchungen sind die polarisierten Absorptionsspektren der Einkristalle $Ti^{3+}: Alha_6X_3$ (X: Cl, Br, J), $Cr^{3+}: Alha_6(ClO_4)_3$ und $Crha_6J_3$ im Wellenlängenbereich von 7500 Å bis 3500 Å zwischen Zimmertemperatur und der Temperatur des flüssigen Heliums. Makroskopisch gehören die Kristalle zur Klasse D_{3d}, das Metallion sitzt auf einem Platz der Mikrosymmetrie D_3. Die aus den Spektren entnommenen Werte für den kubischen Parameter Dq und die trigonalen Parameter v und v' werden (soweit möglich) mitgeteilt. Die $Tiha_6^{3+}$-Komplexe sind im angeregten trigonalen ^2E-Zustand stark Jahn-Teller verzerrt; die Verzerrung im Grundzustand scheint von dem an das Komplexion gebundenen Anion abzuhängen.

Article consacré aux spectres d'absorption polarisée à basse température de monocristaux $Ti^{3+}: Al(Ur)_6X_3$ (X: Cl, Br, I), $Cr^{3+}: Al(Ur)_6(ClO_4)_3$ et $Cr(Ur)_6I_3$ dans le domaine des longueurs d'onde de 7500 Å à 3500 Å. Le groupe ponctuel cristallin est D_{3d} et les ions métalliques occupent les sites de symétrie D_3. On donne les valeurs expérimentales du paramètre cubique Dq et des paramètres trigonaux v et v'. Les complexes hexauréetitane (III) sont fortement déformés par effet Jahn-Teller dans l'état excité ^2E. La déformation à l'état fondamental dépend vraisemblablement de l'anion.

1. Einleitung

Bei allen bekannten oktaedrischen Titan(3)-Komplexen entspricht dem Übergang $^2T_{2g} \rightarrow {}^2E_g$ stets eine Absorptionsbande mit Doppelstruktur, was manchmal auf niedrig symmetrische Kristallfelder, in den meisten Fällen aber auf einen Jahn-Teller-Effekt im angeregten Zustand zurückgeführt wird. Dies gilt insbesondere auch für Hexaharnstoffverbindungen des Titan(3), von denen das reine $Tiha_6J_3$, teils polykristallin [1], teils in Form von Einkristallen [2] schon spektroskopisch untersucht worden ist. Wir haben die Absorptionsmessungen ausgedehnt auf Titan(3)-haltige Einkristalle von $Alha_6X_3$, (X: Cl, Br, J), um den Einfluß des an das Komplexion gebundenen Anions auf die Spektren näher zu untersuchen.

---

* Dem Andenken an Herrn Prof. Dr. K. H. Hansen gewidmet.

Jahn-Teller-Verzerrungen in angeregten Elektronenzuständen von Komplexionen sollten sich auch in der Schwingungsstruktur der entsprechenden Absorptionsbanden bemerkbar machen [3]. Da ein solcher Effekt zum erstenmal beim Chrom(3) beobachtet werden konnte [4], und da Titan(3)-Spektren selbst bei tiefsten Temperaturen keine Schwingungsstruktur zeigen, haben wir auch die polarisierten Absorptionsspektren der Kristalle Cr^{3+} : M $ha_6(ClO_4)_3$, (M : Al, Ga, In), und $Crha_6J_3$ bei tiefen Temperaturen aufgenommen; diese Absorptionsmessungen sind darüberhinaus gedacht als Ergänzung zu Untersuchungen des Lumineszenzverhaltens von Hexaharnstoffverbindungen des Chrom(3), über die bereits früher berichtet wurde [5, 6].

2. Experimentelle Einzelheiten

Einige Hexaharnstoffverbindungen sind in der Literatur beschrieben: $Crha_6J_3$ und $Crha_6(ClO_4)_3$ von Wilke-Dörfurt [7], $Gaha_6(ClO_4)_3$ von Lloyd und Pugh [8], $Tiha_6J_3$ von Hartmann [9]. Sie wurden von uns nach den dort angegebenen Vorschriften hergestellt. Die Darstellung von $Alha_6(ClO_4)_3$ und $Inha_6(ClO_4)_3$ entspricht der von $Gaha_6(ClO_4)_3$. Die Hexaharnstoffhalogenide von Aluminium schließlich erhält man durch Umsetzen von $AlCl_3$ und Harnstoff mit HCl bzw. $CaBr_2 \cdot 2H_2O$, bzw. KJ in wäßriger Lösung. Auf die Darstellung von reinem kristallinem $Tiha_6Cl_3$ und $Tiha_6Br_3$ haben wir verzichtet, da die Titankomplexe ja doch nur in die entsprechenden Aluminiumverbindungen eingebaut werden sollten.

Die Mischkristalle ließen sich nach der Abkühlungsmethode aus wäßriger Lösung züchten; sie enthielten durchschnittlich 2–3 Mol.-% $Crha_6(ClO_4)_3$ bzw. 15 30 Mol.-% $Tiha_6X_3$. Den makroskopischen Symmetrieelementen nach gehören die Kristalle zur Klasse D_{3d}, die Tracht ist eine Kombination von hexagonalem Prisma 2. Stellung und Rhomboeder.

Aus den Kristallen wurden kristallographisch genau orientierte Platten (senkrecht bzw. parallel zur dreizähligen Hauptachse) der Dimension 5 × 5 × 0,5 mm geschnitten und in einem kommerziellen Metallkryostaten auf die jeweilige Meßtemperatur abgekühlt. Zur Aufnahme der Spektren stand ein Cary-14-Spektralphotometer zur Verfügung, dessen Licht mit einem Polarisationsfilter vom Typ KS-W68 (Käsemann-GmbH, Oberaudorf/Inn) linear polarisiert wurde.

3. Ergebnisse

a) Titan

Die polarisierten Spektren von Ti^{3+} : $Alha_6Cl_3$ und Ti^{3+} : $Alha_6J_3$ sind in den Fig. 1 und 2 dargestellt; das Spektrum von Ti^{3+} : $Alha_6Br_3$ entspricht weitgehend dem Chloridspektrum. Lage und Polarisation der Absorptionsmaxima bei Zimmertemperatur und der Temperatur des flüssigen Heliums sind aus Tab. 1 zu ersehen. Beim Abkühlen von Zimmertemperatur auf 4,2° K nimmt in allen drei Fällen die Aufspaltung ab, und die Gesamtintensität der π-Banden zu: Um 15% beim Jodid, um 9% beim Bromid und um 3% beim Chlorid, die Intensität der σ-Banden nimmt geringfügig ab. Während beim Chlorid und Bromid das π- und

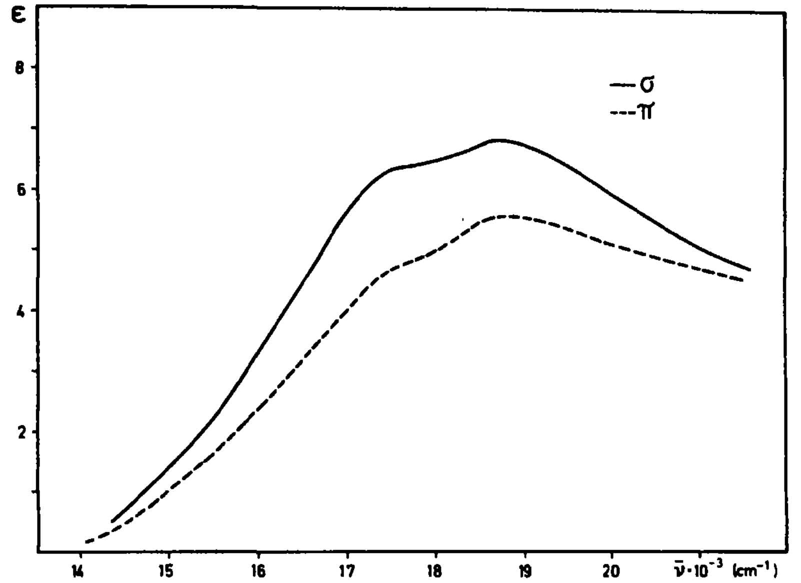

Fig. 1. Polarisierte Spektren von Ti^{3+} : $Alha_6Cl_3$ bei 4,2° K. Das π(σ)-Spektrum wird erhalten mit Licht, dessen elektrischer Vektor parallel (senkrecht) zur dreizähligen Kristallachse schwingt. Beim Erwärmen auf 298° K ändert sich das Spektrum strukturell nicht. ε ist der dekadische molare Extinktionskoeffizient in $l \cdot mol^{-1} \cdot cm^{-1}$

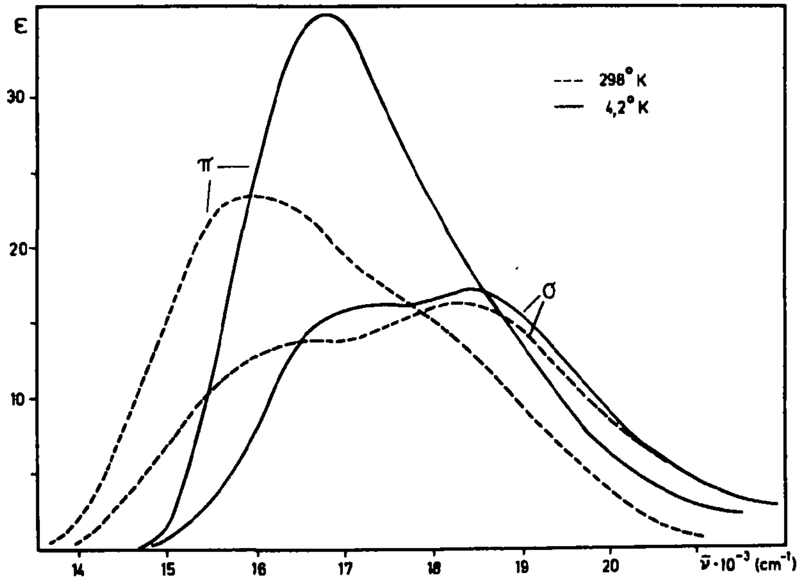

Fig. 2. Polarisierte Spektren von Ti^{3+} : $Alha_6J_3$ bei 298° K und 4,2° K

Tabelle 1. Ti^{3+} : $Alha_6X_3$; Übergang $^2T_{2g} \rightarrow {}^2E_g$; Lage der Absorptionsmaxima (cm^{-1})

Temperatur	Chlorid	Bromid	Jodid
298° K	16950 ($\pi < \sigma$)	16750 ($\pi < \sigma$)	16000 ($\pi > \sigma$)
	18700 ($\pi < \sigma$)	18550 ($\pi < \sigma$)	18300 (π, σ)
4,2° K	17600 ($\pi < \sigma$)	17500 ($\pi < \sigma$)	16800 ($\pi \gg \sigma$)
	18700 ($\pi < \sigma$)	18600 ($\pi < \sigma$)	18400 (σ)

das σ-Spektrum strukturell sehr ähnlich und beide Absorptionsmaxima gleichwertig sind, ist das Jodidspektrum, vor allem bei tiefer Temperatur, ausgesprochen anisotrop: Bei π-Orientierung erscheint nur der langwellige Übergang mit relativ großem Extinktions-Koeffizienten ($\varepsilon \approx 35\, l \cdot mol^{-1} \cdot cm^{-1}$), bei σ-Orientierung haben beide Übergänge etwa gleichen Extinktions-Koeffizienten ($\varepsilon \approx 17\, l \cdot mol^{-1} \cdot cm^{-1}$).

b) Chrom

Fig. 3 zeigt die polarisierten Spektren des Kristalls Cr^{3+} : $Alha_6(ClO_4)_3$ bei 4,2° K. In dem entsprechenden Spektrum bei Zimmertemperatur sind die Liniengruppen bei 14200, 15100 und 21000 cm^{-1} nicht aufgelöst; im übrigen ist das Spektrum unabhängig von der Temperatur. Lage und Polarisation der Banden bzw. Linien sind in Tab. 2 zusammengestellt. Während die beiden Quartett-

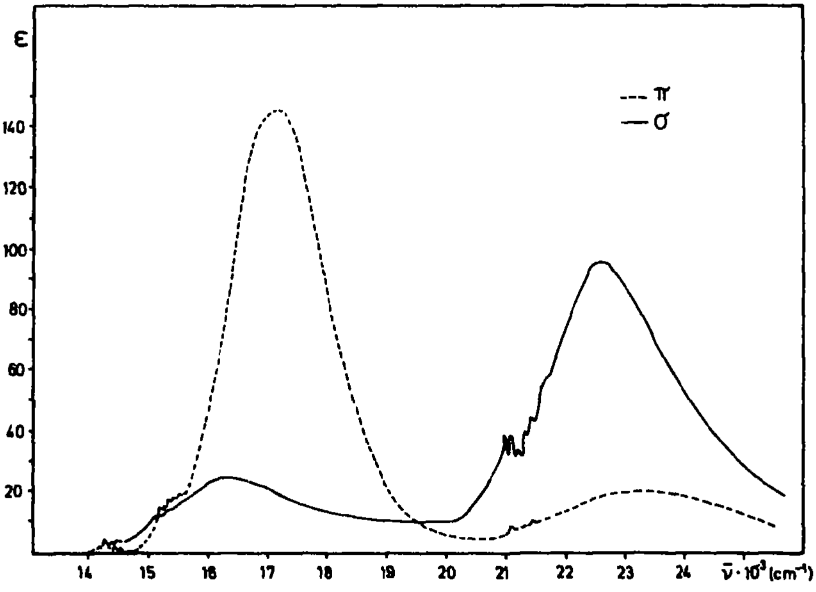

Fig. 3. Polarisierte Spektren von Cr^{3+} : $Alha_6(ClO_4)_3$ bei 4,2° K. Der Übergang $^4A_{2g} \rightarrow {}^4T_{1g}^b$ liegt nicht mehr in dem untersuchten Spektralbereich. Analoge Spektren erhält man bei $Gaha_6(ClO_4)_3$ bzw. $Inha_6(ClO_4)_3$ als Wirtskristall

Tabelle 2. Cr^{3+}: $Alha_6(ClO_4)_3$; Lage der Absorptionsmaxima bei 4,2° K

$\bar{\nu}$ (cm^{-1})	Polarisation	Zuord. bei O_h	Zuord. bei $D_3(D_3')$
14176	π, σ	$^4A_{2g} \rightarrow {}^2E_g$	$^4A_2 \rightarrow E_{1/2}$
14246	$\pi > \sigma$		$^4A_2 \rightarrow E_{3/2}$
14384	$\pi > \sigma$		
14474	$\pi > \sigma$		
15085	π, σ	$^4A_{2g} \rightarrow {}^2T_{1g}$	
15152	$\pi > \sigma$		
15200	$\pi > \sigma$		
15321	$\pi > \sigma$		
15399	π		
15526	π		
16300	σ	$^4A_{2g} \rightarrow {}^4T_{2g}$	$^4A_2 \rightarrow {}^4E$
17100	π		$^4A_2 \rightarrow {}^4A_1$
20973	σ	$^4A_{2g} \rightarrow {}^2T_{2g}$	
21030	$\pi < \sigma$		
21097	σ		
21276	σ		
21345	$\pi < \sigma$		
21589	σ		
22500	σ	$^4A_{2g} \rightarrow {}^4T_{1g}^a$	$^4A_2 \rightarrow {}^4E$
23400	π		$^4A_2 \rightarrow {}^4A_2 \times a_2$

Quartett-Übergänge $^4A_{2g} \rightarrow {}^4T_{2g}$ und $^4A_{2g} \rightarrow {}^4T_{1g}^a$ stark polarisiert sind, ist bei der Liniengruppe um 14200 cm^{-1} keine eindeutige Polarisationsabhängigkeit festzustellen. Wegen des sehr kleinen Extinktionskoeffizienten wird dieser Bereich des Spektrums am Beispiel des reinen $Crha_6J_3$[1] an anderer Stelle [22] gesondert besprochen. Lage und Intensität der beiden breiten Banden sind praktisch unabhängig vom Anion.

In allen Fällen entspricht das axiale Spektrum ganz dem σ-Spektrum; daraus folgt, daß es sich bei allen Banden, bzw. Linien um elektrische Dipolübergänge handelt [21].

4. Diskussion

a) Titan

Die Lichtabsorption oktaedrischer Titan(3)-Komplexe in sichtbarem Spektralbereich ist zurückzuführen auf den Ligandenfeldübergang $^2T_{2g} \rightarrow {}^2E_g$. Bei den von uns untersuchten Mischkristallen ist die für das Spektrum verantwortliche Mikrosymmetrie sicher nicht oktaedrisch: Das reine $Tiha_6J_3$ kristallisiert in der Raumgruppe D_{3d}^6, die Sauerstoffatome der sechs Harnstoffliganden sind trigonal antiprismatisch mit der dreizähligen Achse parallel zur kristallographischen C_3 um das Metallion angeordnet. Die genaue Mikrosymmetrie ist D_3 [11]. Die hier untersuchten Mischkristalle, die makroskopisch dem reinen $Tiha_6J_3$ völlig gleichen, dürften die gleiche Struktur besitzen. Der Übergang $^2T_{2g} \rightarrow {}^2E_g$ ist also in seine trigonalen Komponenten aufzuspalten:

---

[1] Vom reinen $Crha_6(ClO_4)_3$ lassen sich wegen der schlechten Löslichkeit [7] keine größeren Einkristalle züchten.

$$({}^2E, {}^2A_1) \rightarrow {}^2E : {}^2A_1 - (\sigma) \rightarrow {}^2E\,;\ {}^2E - (\pi, \sigma) \rightarrow {}^2E\,.$$

Bei Symmetrie D_3 ist der Übergang $^2A_1 \rightarrow {}^2E$ nur σ-erlaubt, dagegen π-verboten. Da in allen drei Fällen das π- und das σ-Spektrum von durchaus vergleichbarer Intensität sind, ist zu folgern, daß der trigonale Parameter $v > 0$ ist bzw. daß der Term ^2E unter $^2A_1$ liegt, in Analogie zu dem System $Ti^{3+} : Al_2O_3$ [12]. Der genaue Wert von v kann nicht angegeben werden, denn der Übergang $^2E \rightarrow {}^2A_1$ wäre in dem von uns nicht vermessenen fernen IR zu suchen.

Ein Näherungswert für v kann wie folgt aus der Temperaturabhängigkeit der Intensität der π-Banden ermittelt werden: Die Intensität der π-Bande nimmt in allen drei Fällen mit sinkender Temperatur zu, am stärksten beim Jodid (15%), etwas weniger beim Bromid (9%) und am wenigsten beim Chlorid (3%). Da für $E \uparrow\uparrow C_3$ nur der Übergang $^2E \rightarrow {}^2E$, nicht aber der Übergang $^2A_1 \rightarrow {}^2E$ erlaubt ist, kann die Zunahme der Intensität nur bedeuten, daß bei tiefer Temperatur wesentlich mehr Komplexe den Grundterm ^2E besetzen als bei Zimmertemperatur bzw. daß bei Zimmertemperatur ein Teil der Komplexe den $^2A_1$-Term besetzt, was wiederum nur möglich ist, wenn der Abstand v beider Terme von der Größenordnung kT bei Zimmertemperatur ist (etwa 200 cm^{-1}).

Sei n_z der Bruchteil der Komplexe, die bei Zimmertemperatur den Grundterm ^2E besetzen. Dann besetzt der Bruchteil $(1 - n_z)$ bei Zimmertemperatur den Term $^2A_1$. Da v der Abstand beider Terme ist und da ^2E ein doppelt so großes statistisches Gewicht hat wie $^2A_1$, gilt für das Verhältnis der Besetzungszahlen:

$$\frac{n_z}{1 - n_z} = 2x_z\,, \quad \text{mit} \quad x_z = \exp - \frac{v}{k \cdot 298}\,.$$

Entsprechend bei Heliumtemperatur:

$$\frac{n_{\mathrm{He}}}{1 - n_{\mathrm{He}}} = 2 \cdot x_{\mathrm{He}}\,, \quad \text{mit} \quad x_{\mathrm{He}} = \exp - \frac{v}{k \cdot 4{,}2}\,.$$

Hieraus folgt

$$q \equiv \frac{n_z}{n_{\mathrm{He}}} = \frac{1 + \dfrac{1}{2x_{\mathrm{He}}}}{1 + \dfrac{1}{2x_z}}$$

was sich wegen $\dfrac{1}{2x_{\mathrm{He}}} \gg 1$ vereinfachen läßt zu:

$$x_z = \frac{q}{2(1 - q)}$$

bzw.

$$v = k \cdot 298 \ln \frac{q}{2(1 - q)}\,.$$

Wenn man annimmt, daß sich die Besetzungszahlen n_z und n_{He} so verhalten wie die Intensitäten der π-Banden bei den beiden Temperaturen, ergeben sich folgende Werte für den trigonalen Parameter: $v \approx 550\ \mathrm{cm}^{-1}$ (Chlorid), $350\ \mathrm{cm}^{-1}$ (Bromid), $250\ \mathrm{cm}^{-1}$ (Jodid).

Der kubische Parameter 10 Dq entspricht dem gemeinsamen Schwerpunkt der π- und der σ-Bande, vermindert um $\frac{1}{3}v$: $10\,\mathrm{Dq} = 17700\ \mathrm{cm}^{-1}$ (Chlorid), $17500\ \mathrm{cm}^{-1}$ (Bromid), $17000\ \mathrm{cm}^{-1}$ (Jodid). (Diese Werte beziehen sich auf Zimmertemperatur.)

Die Aufspaltung der Absorptionsbanden um etwa $2000\ \mathrm{cm}^{-1}$ kann weder durch das trigonale Kristallfeld (^2E bleibt entartet) noch durch Spin-Bahn-Wechselwirkung erklärt werden (die Spin-Bahn-Kopplungskonstante für das freie Ti^{3+}-Ion beträgt nur $\lambda = 154\ \mathrm{cm}^{-1}$ [13]).

Da einerseits der angeregte Zustand ^2E aus der stark antibindenden oktaedrischen Konfiguration $t_{2g}^0 e_g^1$ resultiert, und da andererseits die Aufspaltung beim Abkühlen von Zimmertemperatur auf 4,2° K beträchtlich abnimmt – von $1800\ \mathrm{cm}^{-1}$ auf $1100\ \mathrm{cm}^{-1}$ beim Chlorid und Bromid bzw. von $2300\ \mathrm{cm}^{-1}$ auf $1600\ \mathrm{cm}^{-1}$ beim Jodid – ist es sehr wahrscheinlich, daß die Tiha_6^{3+}-Komplexe im angeregten Zustand stark Jahn-Teller-verzerrt sind [10, 14].

Die verschiedene Polarisation der Absorptionsmaxima beim Jodid im Vergleich zum Chlorid und Bromid muß mit einer unterschiedlichen Verzerrung der Komplexe im ^2E-Grundzustand zusammenhängen und könnte vielleicht folgendermaßen gedeutet werden: Wenn S_1 und S_2 die beiden für die Verzerrung verantwortlichen Normalkoordinaten der Rasse E von D_3 sind, so wird die Energie des ^2E-Grundzustandes sowohl von $R = \sqrt{S_1^2 + S_2^2}$ als auch vom Polarwinkel Φ in der S_1, S_2-Ebene abhängen, und zwar derart, daß bei den drei Werten von Φ, die der Symmetrie C_2 entsprechen, die Energie besonders tief ist, und daß diese ausgezeichneten Konfigurationen durch Energiesättel getrennt sind. Sind diese drei Potentialschwellen sehr niedrig im Vergleich zu kT, so werden die Komplexe ungehindert schwingen und dabei alle möglichen Verzerrungszustände gleichmäßig durchlaufen; dies sollte der Fall sein beim Chlorid und beim Bromid, denn die beiden Absorptionsmaxima sind einzeln nicht unterschiedlich polarisiert. Sind diese Potentialschwellen dagegen hoch im Vergleich zu kT, so können die Komplexe in einer der bevorzugten Konfigurationen der Symmetrie C_2 eingefangen werden und permanent verzerrt bleiben. Die Übergänge wären dann nach C_2 zu klassifizieren:

$$({}^2A, {}^2B) \rightarrow ({}^2A, {}^2B).$$

Dieser Fall könnte beim Jodid bei tiefer Temperatur vorliegen. Was die Polarisation des Spektrums angeht, so ist allerdings noch zu berücksichtigen, daß es drei gleichwertige zweizählige Achsen gibt und die Komplexe sich gleichmäßig auf die drei möglichen Verzerrungszustände verteilen werden. Deshalb ist das σ-Spektrum in bezug auf die Symmetrie C_2 nicht eindeutig polarisiert, denn wenn für den Lichtvektor E nur gilt: $E \perp C_3$, so wird es genausoviel zweizählige Achsen mit $E \perp C_2$ wie mit $E \uparrow\uparrow C_2$ geben. Das π-Spektrum dagegen ist auch in bezug auf die Symmetrie C_2 eindeutig polarisiert, denn wenn der Lichtvektor parallel zur kristallographischen Hauptachse C_3 schwingt, so schwingt er damit senkrecht zu allen zweizähligen Achsen. Andererseits tritt gerade im π-Spektrum (Fig. 2) der kurzwellige Übergang bei 18400 cm^{-1} mit sinkender Temperatur immer mehr zurück gegenüber dem langwelligen Übergang bei 16800 cm^{-1}. Demnach sollte die monokline Aufspaltung des trigonalen ^2E-Grundzustandes gemäß

$$^2E \rightarrow {}^2A + {}^2B$$

doch groß sein im Vergleich zu kT bei der Temperatur des flüssigen Heliums, denn sonst wäre keine eindeutige Polarisation möglich. Welcher der beiden Spaltterme, ^2A oder ^2B, nun effektiv der C_2-Grundzustand ist, kann nicht entschieden werden. Aufgrund des Spektrums und der für die Gruppe C_2 gültigen Auswahlregeln müßte die Reihenfolge der Spaltterme des angeregten ^2E-Zustandes gerade umgekehrt sein, und es wären folgende beide Fälle möglich:

$$^2A-(\pi)\rightarrow {}^2B\,;\quad {}^2A-(\sigma)\rightarrow {}^2B \quad \text{und} \quad {}^2A$$

oder

$$^2B-(\pi)\rightarrow {}^2A\,;\quad {}^2B-(\sigma)\rightarrow {}^2A \quad \text{und} \quad {}^2B\,.$$

Dies ist nur ein Deutungsversuch; zu klären bliebe nach wie vor die Frage, wieso solche Verzerrungen überhaupt so stark von dem an das Komplexion gebundenen Anion abhängen können.

b) Chrom

Die Mischkristalle Cr^{3+} : Alha$_6$(ClO$_4$)$_3$ gehören zur Klasse D_{3d} und es ist anzunehmen, daß wie beim reinen Crha$_6$(NO$_3$)$_3$ [15] auch hier das Cr^{3+}-Ion auf einem Platz der Mikrosymmetrie D_3 sitzt. Die beiden oktaedrischen Quartett-Quartett-Übergänge spalten dann auf in

$$^4A_{2g}\rightarrow {}^4T_{2g} : {}^4A_2-(\pi)\rightarrow {}^4A_1 \quad \text{und} \quad {}^4A_2-(\sigma)\rightarrow {}^4E$$

bzw.

$$^2A_{2g}\rightarrow {}^4T^a_{1g} : {}^4A_2 \nrightarrow {}^4A_2 \quad \text{und} \quad {}^4A_2-(\sigma)\rightarrow {}^4E\,,$$

und zwar zeigt der Vergleich mit Tab. 2, daß ^4E stets der tiefer liegende Spaltterm ist. Damit wird der trigonale Parameter $v>0$ und aus der Aufspaltung von $^4T_{2g}$ und $^4T^a_{1g}$ folgt [16, 17]: $v/2 = 800$ cm^{-1}, $v' \approx 100$ cm^{-1}. Der Wert für v' ist ungenau, da $^4A_2 \rightarrow {}^4A_2$ rein elektronisch verboten ist und die entsprechende Bande kein scharfes Maximum hat. Der kubische Parameter 10 Dq entspricht der Energie von $^4T_{2g}$ bezogen auf $^4A_{2g}$ [18] und ergibt sich nach dem Schwerpunktsatz aus den Maxima von $^4A_2 \rightarrow {}^4A_1$ und $^4A_2 \rightarrow {}^4E$ zu 10 Dq = 16560 cm^{-1} (4,2 °K). Dem Tanabe-Sugano-Diagramm [18] für ein d^3-Ion kann das Spektrum am besten angepaßt werden bei Dq/B = 2,65, woraus sich der Elektronenwechselwirkungsparameter zu B = 625 cm^{-1} (4,2° K) ergibt. Alle diese Parameter ändern sich nur sehr wenig, wenn man zu Gaha$_6$(ClO$_4$)$_3$ bzw. Inha$_6$(ClO$_4$)$_3$ als Wirtskristall übergeht. Sie sind auch weitgehend unabhängig vom Anion bis auf v und v', die beim Jodid die Werte v = 1400 cm^{-1} und v' = 200 cm^{-1} annehmen.

Wir danken der DFG für eine Sachbeihilfe.

Literatur

1. Schläfer, H. L., Lenz, W., Staab, J.: Z. physik. Chem. N. F. **62**, 290 (1968).
2. Dingle, R.: J. chem. Physics **50**, 545 (1969).
3. Sponer, H., Teller, E.: Rev. mod. Physics **13**, 75 (1941).
4. Ford, R. A., Hill, O. F.: Spectrochim. Acta **16**, 493 (1960).
5. Hansen, K. H., Vierke, G.: Theoret. chim. Acta (Berl.) **6**, 272 (1966).
6. Vierke, G., Hansen, K. H.: Z. physik. Chem. N. F. **59**, 109 (1968).
7. Wilke-Dörfurt, E., Niederer, K.: Z. anorg. allg. Chem. **184**, 145 (1929).
8. Lloyd, D. J., Pugh, W.: J. chem. Soc. **1943**, 76.
9. Hartmann, H., Schläfer, H. L., Hansen, K. H.: Z. anorg. allg. Chem. **289**, 40 (1957).
10. Jones, G. D.: Physic. Rev. **155**, 259 (1967).
11. Linek, A., Šišková, J., Jenšovský, L.: Proc. 9th Intern. Conf. Coord. Chemistry, St. Moritz, Sept. 5–9, 1966.
12. Nelson, E. D., Wong, J. Y., Schawlow, A. L.: Physic. Rev. **156**, 298 (1967).
13. Schläfer, H. L., Gliemann, G.: Einführung in die Ligandenfeldtheorie. Frankfurt (Main): Akad. Verlagsgesellschaft 1967.
14. Liehr, A. D., Ballhausen, C. J.: Ann. Physik (N. Y.) **3**, 304 (1958).
15. Dingle, R.: J. chem. Physics **50**, 1952 (1969).
16. Macfarlane, R. M.: J. chem. Physics **39**, 3118 (1963).
17. Mortensen, O. S.: J. chem. Physics **47**, 4215 (1967).
18. Tanabe, Y., Sugano, S.: J. physic. Soc. Japan **9**, 753 (1954).
19. Sugano, S., Tanabe, Y.: J. physic. Soc. Japan **13**, 880 (1958).
20. Krasser, W.: Persönliche Mitteilung.
21. Sayre, E. V., Sancier, K., Freed, S.: J. chem. Physics **23**, 2060 (1955).
22. Schenk, H. J., Schwarz, W. H. E.: Theoret. chim. Acta (Berl.) **24**, 225 (1972).

Dr. H. J. Schenk
Institut für Radiochemie
Kernforschungsanlage Jülich
D-5170 Jülich, Deutschland

Theoret. chim. Acta (Berl.) 24, 216—224 (1972)
© by Springer-Verlag 1972

Polarisierte Kristallspektren einiger Hexaharnstoffkomplexe bei tiefen Temperaturen

Teil II. Lumineszenz

K. H. HANSEN† und E. KOGLIN*

Lehrstuhl für Theoretische Chemie der Universität Bonn, 5300 Bonn, Wegelerstraße 12

Eingegangen am 5. April/30. August 1971

Polarized Crystal Spectra of Some Hexa-Urea Complexes at Low Temperatures

II. Luminescence

The luminescence spectra of the compounds Cr ur$_6$I$_3$, Cr ur$_6^*$I$_3$ (ur* = deuterated urea), Cr^{3+} : M ur$_6$I$_3$ and Cr^{3+} : M ur$_6$(ClO_4)$_3$ (M : Al; Ga) are studied at temperatures of liquid N_2 and He. *With the He-Ne-laser as excitation source, the $^4T_2$-level will be excited. The splitting of the ^2E-level* will be discussed. It results in two zero-phonon transitions $E_{1/2} \rightarrow {}^4A_2$; $E_{3/2} \rightarrow {}^4A_2$. From isotope effect and a comparison with IR-data, the side bands can be assigned to the excited vibrations of the ground level $^4A_2$. In mixed crystalls Cr^{3+} : Ga ur$_6$I$_3$ an important splitting of the chrom dublett at longer wavelengths would be observed.

Die Lumineszenzspektren der Verbindungen Crha$_6$J$_3$, Crha$_6^*$J$_3$ (ha* = Deuteroharnstoff), Cr^{3+} : Mha$_6$J$_3$ und Cr^{3+} : Mha$_6$(ClO_4)$_3$ (M : Al, Ga) werden bei Stickstofftemperatur und der Temperatur des flüssigen Heliums untersucht. Die Anregung erfolgt über den $^4T_2$-Zustand. Die Aufspaltung des ^2E-Zustandes wird anhand der beiden Null-Null-Übergänge $E_{1/2} \rightarrow {}^4A_2$, $E_{3/2} \rightarrow {}^4A_2$ (Chrom-Dublett) diskutiert. Aus dem Isotopieeffekt und einem Vergleich mit IR-Messungen können die Begleitbanden als angeregte Schwingungen des Grundzustandes $^4A_2$ gedeutet werden. Im Mischkristall Cr^{3+} : Gaha$_6$J$_3$ wird eine deutliche Aufspaltung der längerwelligen Chrom-Dublett-Bande beobachtet.

1. Einleitung

Bei 77 K wird im Lumineszenzspektrum aller bekannten Chromhexaharnstoff-Komplexe eine charakteristische Doppelstruktur des Phosphoreszenzübergangs $^2E \rightarrow {}^4A_2$ beobachtet [1–3]. Die Größe der Aufspaltung dieses Chrom-Dubletts liegt zwischen 70 cm^{-1} und 100 cm^{-1}. Wird die Substanz auf Heliumtemperatur abgekühlt, so nimmt die Intensität der kürzerwelligen Chrom-Dublett-Bande stark ab, und auf der längerwelligen Seite des Dubletts wird eine weitere charakteristische Liniengruppe beobachtet. Als Erklärung für das Auftreten dieser Banden kommen die Aufspaltung des ^2E-Zustandes, vibronische Begleitbanden dieses Zustandes und Cr^{3+}-Cr^{3+}-Wechselwirkungen in Betracht [3]. Der Null-Null-Übergang der Fluoreszenz $^4T_2 \rightarrow {}^4A_2$ ist ebenfalls an dieser Stelle zu vermuten.

Als Beitrag zur Lösung dieser Probleme haben wir unsere Lumineszenzuntersuchungen [4] ausgedehnt:

Der Einfluß des deuterierten Harnstoffliganden auf Änderungen in den Schwingungsfrequenzen und den Intensitäten wird untersucht. Das Cr^{3+}-Ion wird in die Wirtkristalle $Alha_6J_3$, $Gaha_6J_3$, $Alha_6(ClO_4)_3$ und $Gaha_6(ClO_4)_3$ eingebaut. Die Lage des Null-Null-Übergangs der Fluoreszenz soll durch Verwendung anderer Liganden und Anionen bestimmt werden.

---

* Dem Andenken an Herrn Prof. Dr. K. H. Hansen gewidmet.

2. Experimentelles

Die Herstellung der verwendeten Kristalle wurde in Teil I [5] besprochen. Die untersuchten Mischkristalle lagen in folgender Cr^{3+}-Konzentration vor:

$Cr^{3+}:Alha_6J_3$	23 Mol.-%,
$Cr^{3+}:Gaha_6J_3$	11 Mol.-%,
$Cr^{3+}:Alha_6(ClO_4)_3$	2,1 Mol.-%,
$Cr^{3+}:Gaha_6(ClO_4)_3$	2,8 Mol.-%.

Die Kristalle befanden sich in einem He-Kryostaten. Die Anregung der Spektren erfolgte mit dem spektral zerlegten Licht einer Hg-Lampe (HBO-200) bzw. mit einem 5 mW-He-Ne-Laser. Die Lumineszenzspektren wurden photoelektrisch (gekühlter RCA-7102-Multiplier) mit einem 3/4 meter Czerny-Turner Gittermonochromator von Spex aufgenommen.

3. Meßergebnisse

Aus dem Vergleich der Quantenausbeute als Funktion der Anregungswellenlänge hat sich der Anregungsweg $^4A_2 \rightarrow {}^4T_2 \rightarrow {}^2E$ als besonders günstig erwiesen. Die Anregung über die kürzerwelligen Banden ist energetisch weniger günstig.

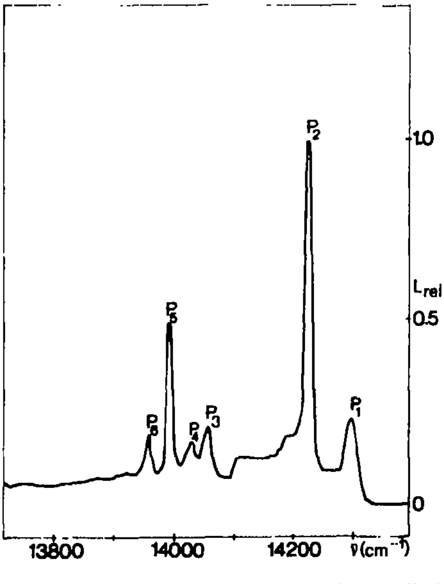

Fig. 1. Phosphoreszenz des $Crha_6J_3$-Kristalls bei 77° K Kristallschliff ↑↑ zu C_3, $\lambda_{\text{Anreg.}} = 6328$ Å – 5 mW-He–Ne-Laser

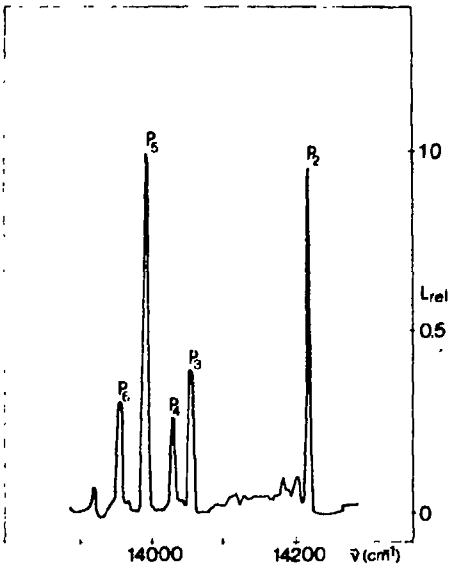

Fig 2

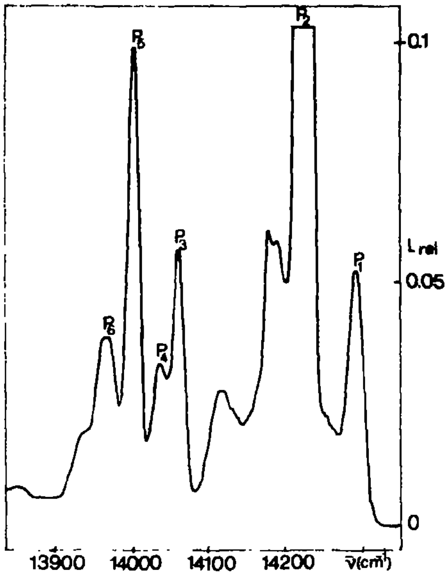

Fig. 3

Fig. 2. Phosphoreszenz des Crha$_6$J$_3$-Kristalls bei 4,2 K Kristallschliff ↑↑ zu C_3,
$\lambda_{\text{Anreg}} = 6328$ Å – 5 mW-He Ne-Laser

Fig. 3 Phosphoreszenz der polykristallinen Chrom(III)-hexadeuteroharnstoff-Verbindung bei 4,2° K
4,2° K

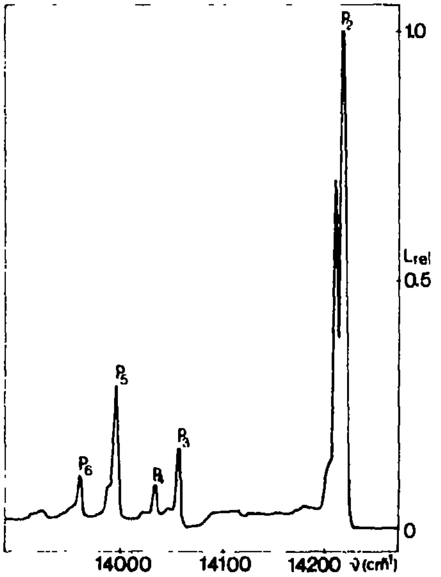

Fig. 4

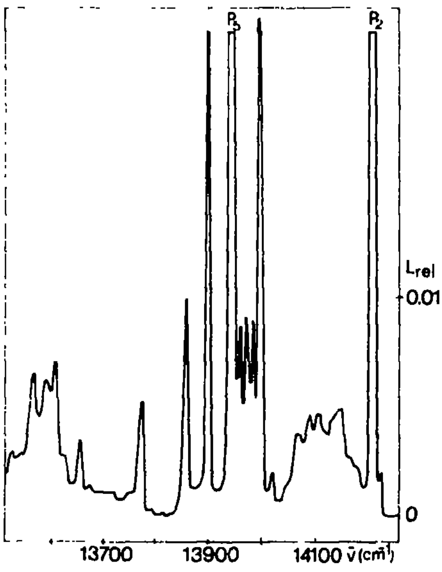

Fig. 5

Fig. 4. Phosphoreszenz des Cr^{3+}: Gaha$_6$J$_3$-Kristalls bei 4,2° K Kristallschliff ⊥ zu C_3

Fig. 5. Phosphoreszenz des Cr^{3+}: Gaha$_6$(ClO$_4$)$_3$-Kristalls bei 4,2° K Kristallschliff ↑↑ zu C_3

Die Fig. 1, 2 und 3 zeigen die Phosphoreszenzspektren des $Crha_6J_3$-Kristalls und der polykristallinen $Crha_6^* J_3$-Verbindung. Im Spektrum des $Crha_6J_3$-Kristalls wird bei 4,2° K die kurzwellige Bande $P_1 = 14299\,cm^{-1}$ nicht mehr beobachtet und die Begleitbande $P_5 = 13994\,cm^{-1}$ ist bei dieser Temperatur die intensivste Phosphoreszenzbande.

In der deuterierten $Crha_6^* J_3$-Verbindung wird das Chrom-Dublett um $9\,cm^{-1}$ zum roten Spektralbereich verschoben. Bei 4,2° K wird die P_1-Bande bei $14290\,cm^{-1}$ nicht gelöscht und die Intensität der Begleitbande $P_5 = 13997\,cm^{-1}$ ist nicht mehr intensiv.

Der sog. Deuteriumeffekt [6] als Zunahme der Phosphoreszenzintensität in der deuterierten Verbindung wird beobachtet. Die relativen Lumineszenzintensitäten betragen bei 4,2° K:

$$\begin{array}{ll} Crha_6J_3 & P_2\text{-Bande bei } 14229\,cm^{-1}: L_{rel} = 6{,}2\;10^{-11} \\ Crha_6^* J_3 & P_2\text{-Bande bei } 14220\,cm^{-1}: L_{rel} = 1{,}1\;10^{-10} \end{array}$$

Fig. 4 zeigt das Phosphoreszenzspektrum des Mischkristalls $Cr^{3+}: Gaha_6J_3$. Hier wird eine Aufspaltung der Chrom-Dublett-Bande P_2 von $7\,cm^{-1}$ beobachtet. Im $Cr^{3+}: Alha_6J_3$-Kristall beträgt diese Aufspaltung $16\,cm^{-1}$. In den Perchloraten kann eine Aufspaltung nicht festgestellt werden. Gegenüber den Jodid-Verbindungen beobachtet man in den Perchloraten eine neue Bande, sie liegt im $Cr^{3+}: Alha_6(ClO_4)_3$-Kristall bei $14015\,cm^{-1}$ und im $Cr^{3+}: Gaha_6(ClO_4)_3$-Kristall bei $14019\,cm^{-1}$ (Fig. 5).

In den Tab. 1 und 2 sind die Wellenzahlen der untersuchten Verbindungen zusammengestellt.

4. Diskussion

a) Das Chrom-Dublett

Der angeregte ^2E-Term spaltet unter Berücksichtigung der trigonalen Symmetrie D_3 und der Spin-Bahn-Wechselwirkung in die Zustände $E_{1/2}$ und $E_{3/2}$ auf. Im Konfigurations-Koordinaten-Modell [7] liegen dann die Minima der drei Potentialkurven $E_{1/2}$, $E_{3/2}$ und $^4A_2$ bei annähernd gleichen Werten der Kernkoordinaten.

Das Chrom-Dublett könnte dann durch die Übergänge

$$P_1: E_{3/2}(n=0) \rightarrow {}^4A_2(m=0)$$
$$P_2: E_{1/2}(n=0) \rightarrow {}^4A_2(m=0)$$

erklärt werden. Da bei 77° K diese beiden Übergänge beobachtet werden (im $Crha_6J_3$-Kristall bei $P_1 = 14299\,cm^{-1}$ und $P_2 = 14229\,cm^{-1}$, Fig. 1) sollte man annehmen, daß die Anregung der Schwingungen im Grundzustand $^4A_2$ von den beiden Niveaus $E_{3/2}$ und $E_{1/2}$ erfolgt:

$$\left.\begin{array}{l} E_m(E_{3/2}) = E(0,0)_1 \quad m\hbar\omega \\ E_m(E_{1/2}) = E(0,0)_2 \quad m\hbar\omega\,. \end{array}\right. \quad m = 0, 1, 2, \ldots$$

Da bei 4,2° K die P_1-Bande verschwindet, müßten dann auch im Spektrum die Schwingungs-Begleitbanden $E_m(E_{3/2})$ mit $m = 1, 2, \ldots$ nicht mehr auftreten. Ein

Tabelle 1. Wellenzahlen (cm^{-1}) der Lumineszenzbanden der Chromhexaharnstoffjodid-Komplexe

Bande	$Crha_6J_3$	$Crha_6^*J_3$	$Cr^{3+}:Alha_6J_3$	$Cr^{3+}:Gaha_6J_3$
1 P_1	*14299*	*14290*	*14306*	*14304*
			14256	14265
2 P_2	*14229*	*14220*	*14230*	*14232*
3	14203		*14214*	*14225*
4	14200	14192		
5	14187			
6	14181	14176	14190	14191
7	14175			
8	14169			
9	14155		14163	14164
10	14148			14157
11	14137			14147
12	14129			14137
13	14126		14134	14121
14	14113	14114	14119	14103
15	14096		14102	
16	14091			
17 P_3	*14058*	*14054*	*14056*	*14058*
18	14044		14042	14047
19 P_4	*14034*	*14033*	*14031*	*14034*
20	14010			
21	14006			
22 P_5	*13994*	*13997*	*13995*	*13994*
				13987
23 P_6	*13957*	*13962*	*13958*	*13957*
24 P_7	*13915*	*13937*	*13920*	*13921*
25	13880		13886	13885
26	13867		13871	
27	13837	13846	13839	13843
28	13830		13831	
29	13817		13818	13819
30	13794		13798	
31	13779		13781	
32	13759		13760	13761
33	13719		13715	13720
34 F_1	*13706*	*13779*	*13706*	*13706*
35	13696	13734	13698	13699
36	13683	13700	13680	13683
37	13641		13639	13644
38 F_2	*13608*	*13650*	*13607*	*13612*
39	13601	13612		13606
40	13478		13473	13481
41 F_3	*13469*	*13473*	*13463*	*13471*
42	13194	13227	13185	13196
43	13069			

Vergleich der Spektren bei 77° K und 4,2° K zeigt, daß bei 4,2° K außer der P_1-Bande keine weiteren Banden verschwinden, d.h. es gibt keine vibronischen Linien von merklicher Intensität des Typs $E_m(E_{3/2}) = E(0,0)_1 - m\hbar\omega$.

Daraus könnte man schließen, daß die Potentialkurven $E_{3/2}$ und $^4A_2$ ihr Minimum bei nahezu gleichen Werten der Kernkoordinaten besitzen. Die im

Tabelle 2. Wellenzahlen (cm^{-1}) der Phosphoreszenzbanden der Chromhexaharnstoffperchlorat-Komplexe

Bande	Cr^{3+} : Alha$_6$(ClO$_4$)$_3$	Cr^{3+} : Gaha$_6$(ClO$_4$)$_3$
1 P_1	*14263*	*14268*
	14204	14197
2 P_2	*14186*	*14184*
3	14160	14156
4		
5	14136	14143
6		
7		
8		14120
9	14094	
10		
11		14089
12		
13		
14		
15	14058	14065
16		14045
O–O	*14015*	*14019*
17 P_3	*13997*	*13998*
18	13988	13986
19 P_4	*13976*	*13974*
20	13964	13966
21		
22 P_5	13948	13950
23 P_6	*13912*	*13909*
24 P_7	*13875*	*13873*

Lumineszenzspektrum beobachteten Schwingungsbanden sollten dann Begleitbanden der Null-Null-Linie $P_2 : E_{1/2} \rightarrow {}^4A_2$ sein. Die im IR gemessene nichttotalsymmetrische Schwingung mit einer Frequenz von 127 cm^{-1} spiegelt sich im Lumineszenzspektrum wieder, wenn man die Wellenzahldifferenzen der folgenden Banden gegen die Phosphoreszenzbande P_2 bildet (Tab. 4).

b) *Isotopie-Effekte*

Eine Betrachtung des Lumineszenzspektrums der deuterierten Crha$_6^*$ J$_3$-Verbindung zeigt, daß alle Banden auf der langwelligen Seite der intensiven P_2-Bande gemäß des Rayleighschen Satzes mit geringerer Frequenz auftreten (Tab. 3). Der Abstand der beiden (0,0)-Banden P_1 und P_2 ist unabhängig von der Deuterierung. Dies deutet darauf hin, daß es sich tatsächlich um die angegebene Aufspaltung des ${}^2E$-Zustandes in die Elektronenübergänge $E_{1/2}$ und $E_{3/2}$ handelt.

Ein Verständnis für die Intensitätszunahme der Phosphoreszenz liefert die Arbeit von Lin [8]. Nach dieser Theorie ist die Übergangswahrscheinlichkeit für einen strahlungslosen Prozeß proportional der Frequenz einer angeregten Schwingung $\omega_i(n)$ des Moleküls. Da $\omega_i(n) = \sqrt{k/m_i}$ ist, wird bei Vergrößerung der Masse im Liganden $\omega_i(n)$ und damit die strahlungslose Übergangswahr-

Tabelle 3. Wellenzahldifferenz $\bar{\nu}_0 - \bar{\nu}_i = \Delta\bar{\nu}$(cm^{-1})

Bande	$\mathrm{Crha_6J_3}$	$\mathrm{Crha_6^* J_3}$	$\mathrm{Cr^{3+}:Alha_6J_3}$	$\mathrm{Cr^{3+}:Gaha_6J_3}$
1	*− 70*	*− 70*	*− 76*	*− 72*
			− 26	− 33
2 P_2	0	0	0	0
3	26		16	8
4	29	28		
5	42			
6	48	44	40	41
7	54			
8	60			
9	74		67	68
10	81			75
11	92			85
12	100			
13	103		96	96
14	116	106	111	112
15	133		128	129
16	138			
17 P_3	*171*	*166*	*174*	*174*
18	185		188	185
19 P_4	*195*	*187*	*199*	*199*
20	219			
21	223			
22 P_5	*235*	*223*	*235*	*238*
				245
23 P_6	*272*	*258*	*272*	*275*
24 P_7	*314*	*283*	*310*	*311*
25	349		344	347
26	362		359	
27	392	374	391	390
28	399		399	
29	412		412	413
30	435		432	
31	450		449	
32	470		470	471
33	510		515	512
34 F_1	*523*	*441*	*524*	*526*
35	533	486	532	533
36	546	520	550	549
37	588		591	588
38 F_2	*621*	*570*	*623*	*621*
39	628	608		626
40	751		757	751
41 F_3	*760*	*747*	*767*	*761*
42	1035	993	1045	1037
43	1160			

scheinlichkeit kleiner. Die bei den Cr(3)-Verbindungen den strahlungslosen Übergang beschreibende Konstante k_6 [9] wird durch den Deuteriumeffekt reduziert. Da die Quantenausbeute der Phosphoreszenz umgekehrt proportional zu dieser Konstante ist [10], bedeutet die Abnahme von k_6 eine Erhöhung der Intensität dieses Übergangs.

Tabelle 4. $\mathrm{Crha_6J_3}$; Bereich von 14300 $\mathrm{cm^{-1}}$ bis 13700 $\mathrm{cm^{-1}}$ (4,2° K)

Bande	$\tilde{\nu}$ ($\mathrm{cm^{-1}}$)	Zuordnung
1 P_1	14299	$(0,0)_1 - E_{3/2} \rightarrow {}^4A_2$
2 P_2	14229	$(0,0)_2 - E_{1/2} \rightarrow {}^4A_2$
14	14113	
15	14096	$(0,0)_2 - 129$
16	14091	
22 P_5	13994	$(0,0)_2 - 2 \times 129 + 27$
25	13880	$(0,0)_2 - 3 \times 129 + 38$
32	13759	$(0,0)_2 - 4 \times 129 + 46$

c) Null-Null-Übergang der Fluoreszenz ${}^4T_2 \rightarrow {}^4A_2$

Da das Potentialminimum des ${}^4T_2$-Terms bei den Verbindungen mit den Jodid-Anion oberhalb des ${}^2E$-Terms liegt [11], kann mit einem Einfluß des (0,0)-Übergangs von ${}^4T_2 \rightarrow {}^4A_2$ auf das Chrom-Dublett nicht gerechnet werden. Der Einfluß des (0,0)-Übergangs kann eine Rolle spielen, wenn der ${}^4T_2$-Term unterhalb des ^{2}E-Terms liegt: z. B. bei der $\mathrm{Crha_6(ClO_4)_3}$-Verbindung. Hier sollte eine zusätzliche Bande im Lumineszenzspektrum beobachtet werden.

In Fig. 5 erkennt man vor der P_3-Bande eine neue schwache Lumineszenzbande. Der Abstand von der P_2-Bande beträgt beim $\mathrm{Cr^{3+}}$: $\mathrm{Alha_6(ClO_4)_3}$-Kristall 171 $\mathrm{cm^{-1}}$ und beim $\mathrm{Cr^{3+}}$: $\mathrm{Gaha_6(ClO_4)_3}$-Kristall 165 $\mathrm{cm^{-1}}$ (Tab. 2). Bei den Chromhexaharnstoff-Komplexen zeigt sich, daß der Fluoreszenzübergang das Chrom-Dublett nicht beeinflußt.

Die von uns untersuchten Chromacetamid-Komplexe zeigen ein entsprechendes Bild. Im Lumineszenzspektrum der von uns weiter untersuchten Chromdimethylsufoxid-Komplexe scheint der Null-Null-Übergang der Fluoreszenz das Chrom-Dublett stark zu beeinflussen. Dies ermöglichte es uns nicht, hier eine eindeutige Angabe über die Lage des Chrom-Dubletts zu geben.

d) $\mathrm{Cr^{3+}}$-$\mathrm{Cr^{3+}}$-*Wechselwirkung*

Forster erwähnte erstmals die Wechselwirkung von $\mathrm{Cr^{3+}}$-Ionen in Molekülverbindungen [12]. In der von ihm untersuchten Verbindung spaltet der Null-Null-Übergang der Phosphoreszenz um 33 $\mathrm{cm^{-1}}$ auf. In den $\mathrm{Cr(Ox)^{3-}}$-Verbindungen wird eine Aufspaltung von 3,1 $\mathrm{cm^{-1}}$ beobachtet [13]. In der von uns untersuchten Cr-Hexaharnstoff-Verbindung kann eine deutliche Aufspaltung von 7 $\mathrm{cm^{-1}}$ im $\mathrm{Cr^{3+}}$: $\mathrm{Gaha_6J_3}$-Kristall beobachtet werden (Fig. 4). Zur langwelligen Seite der P_5-Bande (13994 $\mathrm{cm^{-1}}$) kann eine zusätzliche Begleitbande (13987 $\mathrm{cm^{-1}}$) im Abstand von 7 $\mathrm{cm^{-1}}$ beobachtet werden. Rein phänomenologisch läßt sich dies durch die Aufspaltung des Grundzustandes $2 \times {}^4A_2 \rightarrow {}^4A'_2$ und ${}^4A''_2$ deuten. Es werden die beiden Null-Null-Übergänge $P'_2 : E_{1/2}(n=0) \rightarrow {}^4A'_2(m=0)$ und $P''_2 : E_{1/2}(n=0) \rightarrow {}^4A''_2(m=0)$ beobachtet. Zu jedem dieser Null-Null-Übergänge gibt es eine vibronische Begleitbande in der nichttotalsymmetrischen Schwingung von 127 $\mathrm{cm^{-1}}$. Der P'_2-Bande entspricht die vibronische Begleitbande $P_5 = 13994\ \mathrm{cm^{-1}}$: $E_{1/2}(n=0) \rightarrow {}^4A'_2(m=2)$ der P''_2-Bande die Begleitbande bei 13987 $\mathrm{cm^{-1}}$: $E_{1/2}(n=0) \rightarrow {}^4A''_2(m=2)$.

Eine einfache Übertragung der beim Rubin entwickelten Theorie [14] die Komplexverbindungen ist nicht möglich, da z. B. der Abstand zwischen d Cr^{3+}-Paaren II. Ordnung im Rubin nur 2,8 Å beträgt, der Abstand zwisch den nächsten Cr^{3+}-Nachbarn im $Crha_6J_3$-Kristall beträgt jedoch über 7 Å [1 Forster und Mortensen sind der Ansicht, daß in den Komplex-Verbindungen d Liganden eine Art „Leitung" zwischen den Cr^{3+}-Ionen herstellen. Sie spreche dann von Superaustausch-Wechselwirkung. Um jedoch nähere Angaben üb die Aufspaltung machen zu können, sind Lumineszenzuntersuchungen mit ve schiedenen Cr^{3+}-Konzentrationen erforderlich.

Literatur

1. Porter, G. B., Schläfer, H. L.: Ber. Bunsenges. physik. Chem. **68**, 316 (1964).
2. Vierke, G., Hansen, K. H.: Z. physik. Chem. Neue Folge **59**, 109 (1968).
3. Dingle, R.: J. chem. Physics **50**, 1952 (1969).
4. Koglin, E.: Diplomarbeit Ffm. 1968.
5. Hansen, K. H., Schenk, H. J.: Theoret. chim. Acta (Berl.) (in Druck).
6. Wright, M. R., Frosch, R. P., Robinson, G. W.: J. chem. Physics **33**, 934 (1960).
7. Fowler, W. B.: Physics of COLOR CENTERS. New York: Academic Press 1968.
8. Lin, S. H.: J. chem. Physics **44**, 3759 (1966).
9. Forster, L. S.: Transition Metal Chemistry **5**, 1 (1969).
10. Fleischauer, P. D., Fleischauer, P.: Chem. Reviews **70**, 199 (1970).
11. Hansen, K. H., Vierke, G.: Theoret. chim. Acta (Berl.) **6**, 272 (1966).
12. Forster, L. S., Courtois, M.: J. molecular Spectroscopy **18**, 396 (1965).
13. Mortensen, O. S.: J. chem. Physics **47**, 4215 (1967).
14. Kislink, P., Krupke, W. F.: J. appl. Physics **36**, 1025 (1965).
15. Linek, A., Siskova, J., Jensovsky, L.: Proc. 9th. Intern. Conf. Coord. Chemistry, St. Moritz, Sept. 5 9, 1966.

Dr. E. Koglin
Zentrallabor für Chemische Analyse
Kernforschungsanlage Jülich
D-517 Jülich, Deutschland

Theoret. chim. Acta (Berl.) 24, 225—233 (1972)
© by Springer-Verlag 1972

Spin-Bahn-Wechselwirkung und Jahn-Teller-Effekt. Analyse der ${}^4A_2 \rightarrow {}^2E$-Schwingungsprogression bei $Crha_6J_3$*

H. J. SCHENK und W. H. E. SCHWARZ

Lehrstuhl für Theoretische Chemie der Universität Bonn,
Wegeler Straße 12, D-5300 Bonn, Deutschland

Eingegangen am 30. August 1971

Spin-Orbit Interaction and Jahn-Teller-Effect. Analysis of the ${}^4A_2 \rightarrow {}^2E$-Vibrational Progression of $Crha_6J_3$

The ${}^4A_2 - {}^2E$-transition of $CrUr_6I_3$-single crystals has been measured in absorption with high resolution. Furthermore vibronic spectra have theoretically been calculated under the combined effect of spin-orbit coupling and Teller distortion. Comparison of these results with the experimental spectrum allows the assignement of the band system.

Der ${}^4A_2 - {}^2E$-Übergang in $Crha_6J_3$-Einkristallen wurde mit hoher Auflösung in Absorption gemessen. Weiterhin wurden vibronische Spektren unter gleichzeitiger Berücksichtigung von Spin-Bahn-Wechselwirkung und Teller-Verzerrung theoretisch berechnet. Ein Vergleich des experimentellen Spektrums mit diesen Resultaten ermöglicht eine Zuordnung des Liniensystems.

Mesure haute résolution de l'absorption correspondant à la transition ${}^4A_2 - {}^2E$ dans des monocristaux de $CrUr_6I_3$. Par ailleurs on a calculé théoriquement les spectres vibroniques obtenus sous l'effet combiné du couplage spin-orbite et de la distorsion de Teller. La comparaison de ces résultats avec le spectre expérimental permet l'attribution du système de bandes.

1. Einleitung

Struktur und Spektrum komplex gebundener d^3-Cr(III)-Ionen auf trigonal verzerrten Oktaederplätzen sind sowohl theoretisch wie experimentell intensiv untersucht worden (z. B. [1–7]). Neben oxidischen Verbindungen haben speziell Hexa-Harnstoff-Derivate Interesse gefunden, da von ihnen besonders gute Einkristalle präparativ zugänglich sind und die Spektren fast ausschließlich von lokalen Anregungen herrühren.

Von dem von uns untersuchten $[Crha_6]J_3$ der Makrosymmetrie D_{3d} kann angenommen werden [5], daß das Chrom auf Plätzen der Symmetrie D_3 sitzt, wobei die entsprechende C_3-Achse der Kristallachse parallel ist. Die tiefsten Niveaus des Cr^{3+} im Ligandenfeld, die bei unserer Diskussion eine Rolle spielen werden, liegen wie in Fig. 1. Nach Lit. [1] und [7] sind die Parameter $D \cdot q = 1660\,cm^{-1}$, $v = 1400\,cm^{-1}$, $v' = 200\,cm^{-1}$, $B = 625\,cm^{-1}$, $C = 2900\,cm^{-1}$ (4,2° K).

---

* Dem Andenken an Herrn Prof. Dr. K. H. Hansen gewidmet.

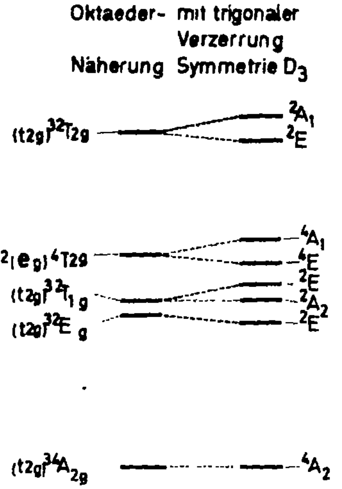

Fig. 1. Schematisches Niveau-Schema vom d^3-Cr^{3+}-Ion im oktaedrisch-trigonalen Ligandenfeld

Während die Übergänge vom $^4A_2$-Grundzustand, der mit ziemlicher Sicherheit praktisch nicht Spin-aufgespalten ist (s. u.), zu den höheren Quartett-Zuständen breite strukturierte Banden liefern, in die die höheren Quartett-Dublett-Übergänge eingebettet sind, gibt der bei 14 kK liegende erste angeregte ^2E-Zustand Anlaß zu einem zwar schwachen, aber gut auflösbaren und interpretierbaren Bandensystem.

In Kap. 2 teilen wir unsere neuen absorptionsspektrometrischen Ergebnisse mit. In Kap. 3 berechnen wir modellmäßig vibronische Spektren unter kombinierter Berücksichtigung von Spin-Bahn-Wechselwirkung und Jahn-Teller-Effekt. In Kap. 4 nutzen wir diese Resultate aus, um das experimentelle Spektrum zu signieren und Angaben über Spin-Bahn-Wechselwirkung und Jahn-Teller-Stabilisierung im $t^3-{}^2E$-Zustand zu machen.

2. Das $Crha_6J_3$-Absorptionsspektrum unterhalb 14650 K

Details über die Präparation der $Crha_6J_3$-Einkristalle und die spektroskopische Technik finden sich in Lit. [4, 6, 7]. Das am besten aufgelöste Spektrum (mit unpolarisiertem Licht bei Helium-Temperatur) ist in Fig. 2 abgebildet. Die Intensitätsverhältnisse bei Durchstrahlung einer parallel zur C_3-Achse geschnittenen Kristallplatte mit polarisiertem Licht bei Stickstoff- und Helium-Temperatur entnimmt man der Tab. 1. Zu höheren Energien schließt sich ein sehr stark ansteigendes strukturiertes Spektrum an, das wir auf den Franck-Condon-verschobenen $^4A_{2g}-{}^4T_{2g}$ sowie den $^4A_{2g}-{}^2T_{1g}$-Übergang zurückführen [7], vgl. auch [5].

Mit Ausnahme der Linie *C* (und der außerordentlich schwachen Linie *D*) lassen sich alle Peaks in zwei genau um 65 cm^{-1} gegeneinander verschobene Progressionen anordnen. Beide Progressionen lassen sich genauer als auf ± 1 cm^{-1}

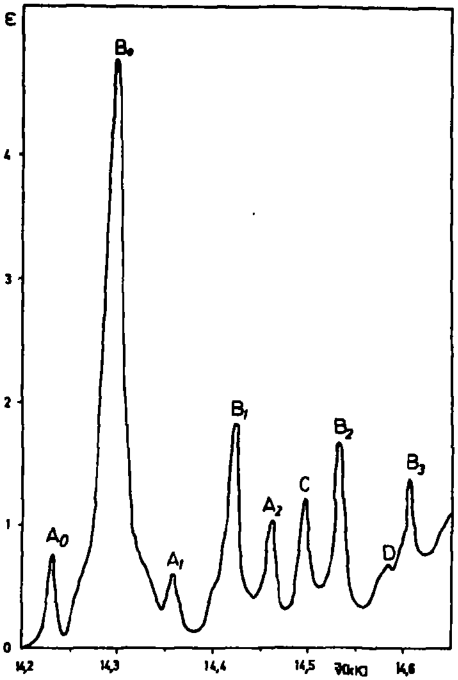

Fig. 2. Unpolarisiertes Absorptionsspektrum von $[Crha_6]J_3$ bei der Temperatur des flüssigen Heliums im Energiebereich unter 14,65 kK

Tabelle 1. Polarisierte Absorptionsspektren unterhalb 14,65 kK einer parallel zur C_3-Achse geschnittenen Kristallplatte von $[Crha_6]J_3$ bei den Temperaturen des flüssigen Stickstoffs und Heliums. Dekadische Extinktionskoeffizienten der Peaks in $[10^3 \cdot cm^2/Mol]$

$\tilde{\nu}$ [K]	N_2-Temp.		He-Temp.		Zuordnung	
	π	σ	π	σ		
14230	2,20	2,69	0,44	0,48	A0	$^4A_2 \to {}^2E_{1/2}$
14295	6,50	2,60	5,08	2,23	B0	$^4A_2 \to {}^2E_{3/2}$
14357	~0,7	~0,4	0,58	0,31	A1	$A0 + \omega$
14422	2,92	1,32	1,46	0,88	B1	$B0 + \omega$
14461	1,68	~0,6	1,04	0,40	A2	$A0 + 2 \times \omega$
14496	1,42	0,97	1,06	0,66	C	$^4A_2 \to {}^4T_2\ (v = 0)$
14526	1,54	1,42	1,36	1,32	B2	$B0 + 2 \times \omega$
14573	~0,2	~0,1	~0,2	~0,1	D	
14603	1,63	1,19	1,36	1,11	B3	$B0 + 3 \times \omega$

durch die Formel

$$139 \cdot v - 12 \cdot v^2\ [cm^{-1}] \qquad v = 0, 1, 2, 3$$

reproduzieren. In diesem Zusammenhang erwähnen wir, daß unsere Kristalle im IR bei 60, 127 und 180 cm^{-1} absorbieren, wobei es sich um lokalisierte $(t_{2g})^3$Cr-Liganden-Schwingungen vom Typ a_2 oder e handeln dürfte. Die 127 K-Linie entspricht übrigens bei einer reduzierten Masse von 50 einer Kraftkonstanten von $\frac{1}{2}\frac{\text{mdyn}}{\text{Å}}$.

Die Intensität der Linien nimmt, grob gesprochen, mit steigendem v ab, wobei allerdings die Linien mit ungeradem v jeweils etwas schwächer sind. Weiterhin ist die π-Absorption insgesamt etwas stärker als die σ-Absorption. Abgesehen von einer beträchtlichen Linienverschärfung fällt bei Temperaturabnahme im wesentlichen die Intensitätsabnahme der A0-Linie auf.

3. Vibronische Niveaus bei Spin-Bahn-Wechselwirkung und Jahn-Teller-Effekt

Wir wollen nun zunächst mit Hilfe des „linearen Modells für nicht-adiabatische Phänomene“ [8] die vibronischen Niveaus eines trigonalen ^2E-Elektronenzustandes berechnen. Hier sind vornehmlich Anregungen von e-Schwingungen von Interesse, da sie Anlaß für den dynamischen Teller-Effekt sind [9].

Wir machen also den Ansatz

$$H\Psi = [T_{X,Y} + h_{el}(X,Y)]\cdot\Psi = E\Psi\,. \tag{1}$$

$T_{X,Y} = -\frac{1}{2}(D_X^2 + D_Y^2)$ ist die kinetische Energie in der entarteten Schwingung mit den beiden Koordinaten X, Y. h_{el}, h_{el}^0 seien der elektronische Born-Oppenheimer-Hamiltonoperator mit bzw. ohne Spin-Bahn-Operator;

$$h_{el}^0\varphi_\pm^0 = \varepsilon_\pm^0\varphi_\pm^0\,. \tag{2}$$

$\varphi_\pm^0$ sind die beiden – in trigonaler Symmetrie ($X = Y = 0$) entarteten – adiabatischen elektronischen Eigenfunktionen. Mit

$$R = \sqrt{X^2 + Y^2}\,,\quad \text{tg}\phi = Y/X \tag{3}$$

läßt sich aus Symmetriegründen

$$\begin{aligned}\varphi_+^0 &= \cos\phi/2\cdot\varphi_1 - \sin\phi/2\cdot\varphi_2\\ \varphi_-^0 &= \sin\phi/2\cdot\varphi_1 + \cos\phi/2\cdot\varphi_2\end{aligned} \tag{4}$$

schreiben, wobei wir in guter Näherung die reellen, orthonormierten *diabatischen* Funktionen $\varphi_{1,2}$ als von R, ϕ unabhängig annehmen können. Weiterhin nehmen wir für die elektronische Energie die harmonische Näherung an:

$$\langle\varphi_\pm^0|h_{el}^0|\varphi_\pm^0\rangle = k/2(R \pm R_0)^2\,. \tag{5}$$

Eine Spin-Bahn-Wechselwirkung macht sich in erster Näherung nur durch ein Nichtdiagonalelement in der Hamiltonmatrix auf adiabatischer Basis bemerkbar. In dieser reellen Basis kann das Matrixelement weiterhin mit guter Näherung als rein imaginäre Konstante angenommen werden:

$$\langle\varphi_+|h_{el}|\varphi_-\rangle = iA\,. \tag{6}$$

Die adiabatischen Potentialkurven ergeben sich dann zu

$$\varepsilon_\pm = k/2(R^2 + R_0^2) \pm \sqrt{(kR_0R)^2 + A^2}\,. \tag{7}$$

Für die weitere Rechnung geeigneter ist die komplexe diabatische Basis

$$\psi^{k}_{1,2} = 1/\sqrt{2}(\psi_1 \pm i\psi_2), \tag{8}$$

die den Spinhamiltonoperator h_{el} im Symmetriepunkt $R=0$ diagonalisiert:

$$[h_{el}] = \begin{pmatrix} k/2(R^2+R_0^2)-A & kR_0Re^{i\phi} \\ kR_0Re^{-i\phi} & k/2(R^2+R_0^2)+A \end{pmatrix}. \tag{9}$$

In Zweizustandsnäherung stellen wir die Gesamtwellenfunktion dar als

$$\Psi = \psi^{k}_{1} \cdot \chi_1(R,\phi) + \psi^{k}_{2} \cdot \chi_2(R,\phi), \tag{10}$$

was auf

$$(T+(k/2)(R^2+R_0^2) \mp A - E) \cdot \chi_{1,2} + kR_0Re^{\pm i\phi} \cdot \chi_{2,1} = 0 \tag{11}$$

führt. Dies gekoppelte Gleichungssystem wurde in der Basis der Eigenfunktionen des zweidimensionalen Oszillators numerisch gelöst. Die Integrale über die verallgemeinerten Laguerre-Funktionen wurden Lit. [10] entnommen.

In Fig. 3 sind vibronische Energieniveaus in Abhängigkeit von Spin-Bahn-Kopplungs-Parameter $\lambda = A/\omega$ und Jahn-Teller-Parameter $q = \sqrt{(k/\omega)} \cdot R_0$ graphisch dargestellt ($\omega = \sqrt{k/\mu}$ ist die harmonische Kreisfrequenz). Und zwar wurden nur diejenigen Niveaus eingetragen, zu denen ein Übergang von einem senkrecht darunterliegenden schwingungslosen A-Zustand möglich ist (vgl. Longuet-Higgins *et al.*, Lit. [11]). Als Energie-Nullpunkt ist jeweils der tiefste vibronische Zustand gewählt. Dessen Stabilisierung durch Jahn-Teller-Effekt und Spin-Bahn-Wechselwirkung wird durch die gestrichelten Kurven wiedergegeben (die elektronische Jahn-Teller-Stabilisierung ohne Spin-Bahn-Effekt ist $(k/2)R_0^2 = (\omega/2)q^2$).

Man erkennt das sehr komplexe Wechselspiel beider Effekte gegeneinander. Wenn sie von vergleichbarer Größenordnung sind, ist das Spektrum sehr kompliziert und das Bild der adiabatischen Potentialkurven völlig unbrauchbar. Ist dagegen einer der beiden Effekte der wesentlich größere, wird der Einfluß des anderen praktisch gänzlich unterdrückt, und man erhält wieder ein harmonisches Niveauschema.

In Fig. 4 sind die Intensitätsverhältnisse (d. h. Franck-Condon-Faktoren) für die $A(v=0) \rightarrow E(v)$-Übergänge dargestellt. Die Resultate für verschwindende Spin-Bahn-Kopplung entsprechen denen von Longuet-Higgins [11]. Die elektronischen Übergangsmomente zu den beiden Komponenten des ^2E-Terms, die als Faktoren in die Absorptionsintensitäten eingehen, sind durch Strichelung bzw. ausgezogene Linien unterschieden.

Die für den reinen Jahn-Teller-Effekt bekannten Intensitätsverhältnisse [9, 11] werden durch die Spin-Bahn-Kopplung folgendermaßen modifiziert: Die aus dem unteren der beiden ^2E-Kramers-Dubletts hervorgehenden vibronischen Niveaus gewinnen Intensität für den 0–0-Übergang; bei der anderen Progression verstärken sich kürzerwellige Übergänge. Bei überwiegender Spin-Bahn-Kopplung bleiben schließlich nur noch zwei Linien übrig, die als 0–0-Übergänge zu den beiden elektronischen Spin-Zuständen bei unterdrücktem Jahn-Teller-Effekt zu deuten sind.

Diese qualitativen Aussagen treffen auch noch für mäßig abgeänderte Modelle zu: Spin-Bahn-Parameter mit reellem bzw. mit R^2-abhängigem Anteil, anharmonischer Term in der Born-Oppenheimer-Energie, quadratischer Teller-Effekt (d. h. Teller-Renner-Effekt).

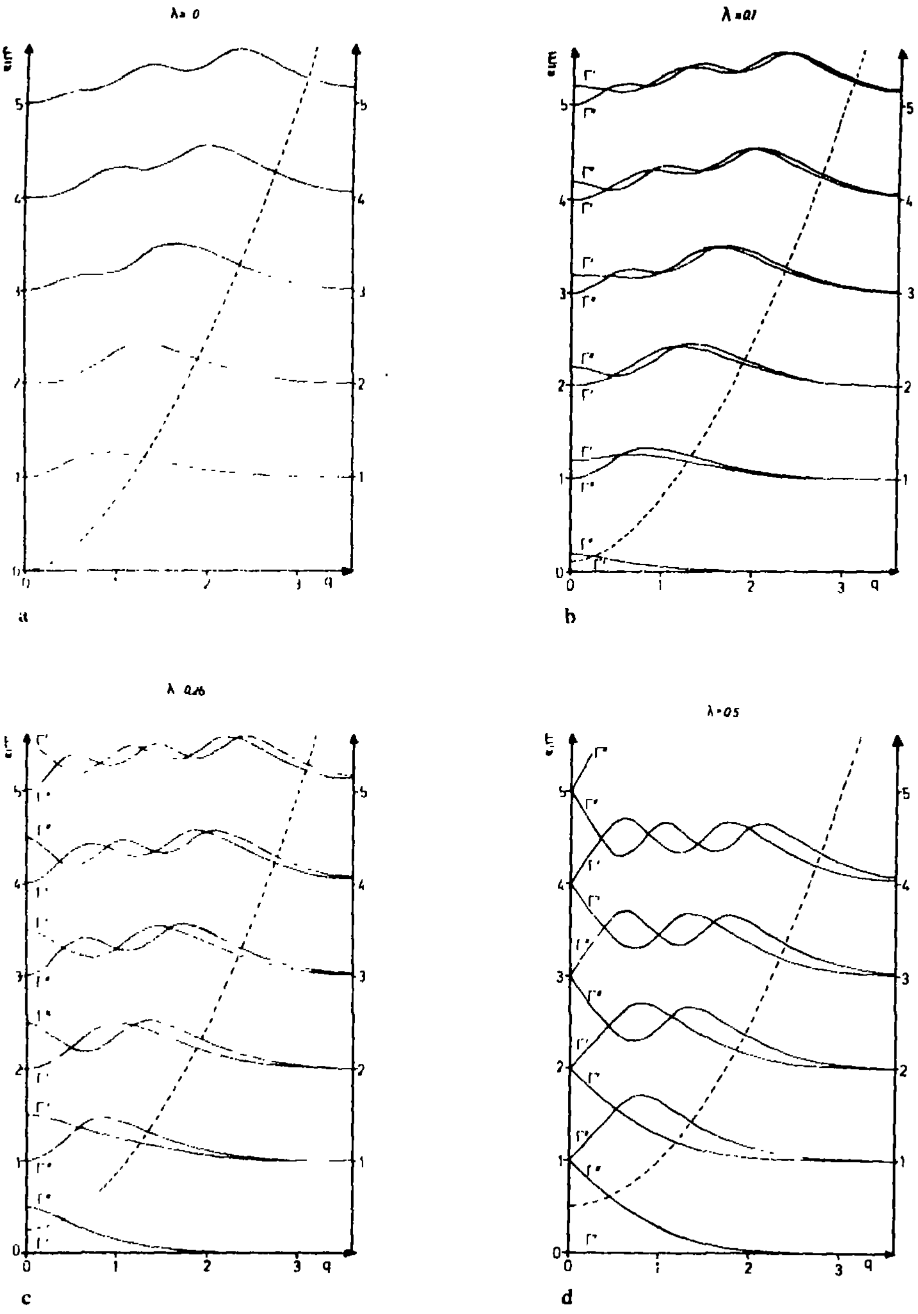

Fig. 3a—d

Fig. 3a–f. Vibronische Energieniveaus eines e-schwingungsangeregten (mit $m = 0$-Anteil) elektronischen trigonalen ^2E-Terms in Abhängigkeit vom Jahn-Teller-Parameter q für verschiedene Spin-Bahn-Wechselwirkungs-Parameter λ (ausgezogene Kurven, Energienullpunkt im untersten Zustand; dessen Stabilisierung wird durch die gestrichelte Linie beschrieben)

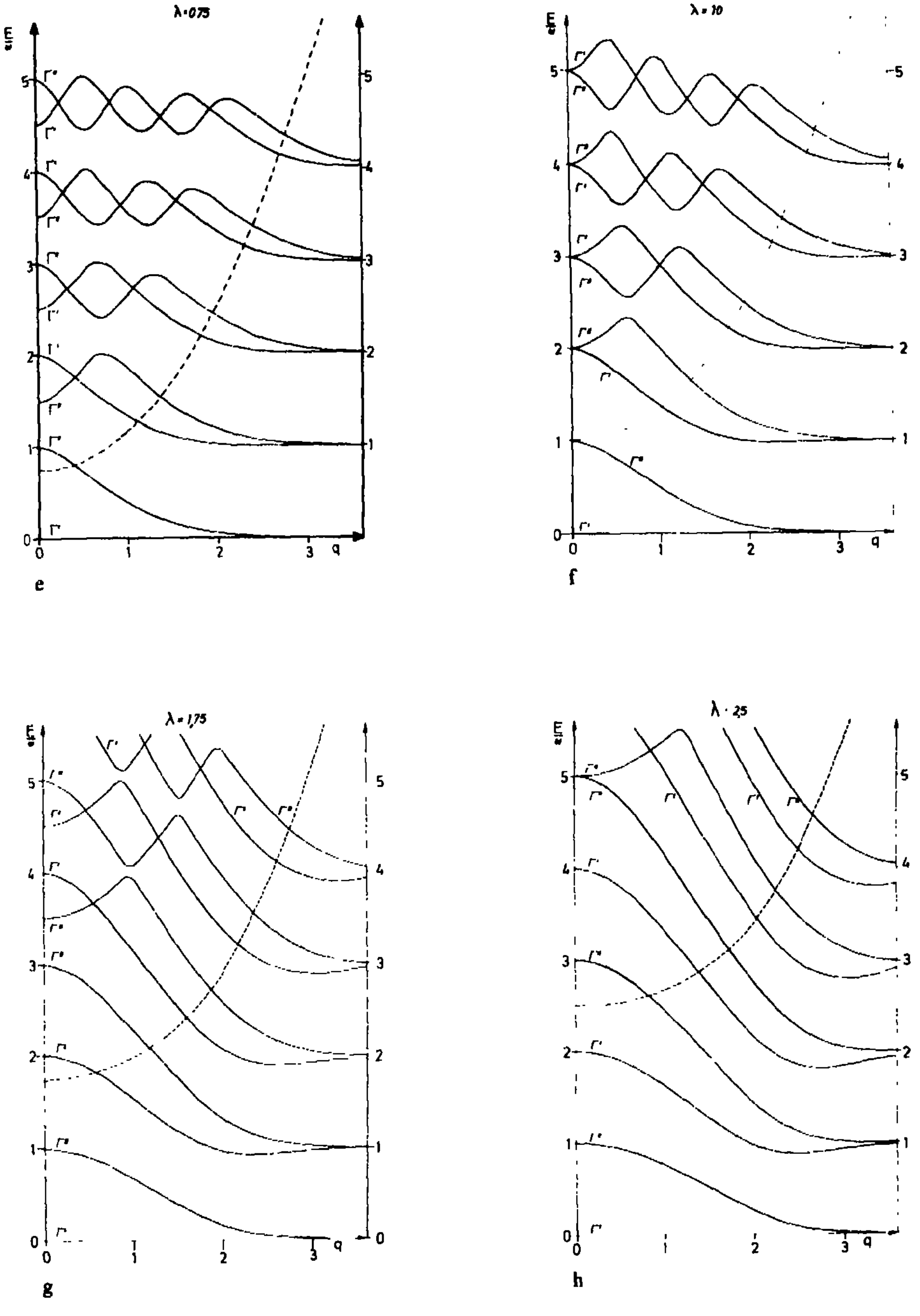

Fig. 3e--f

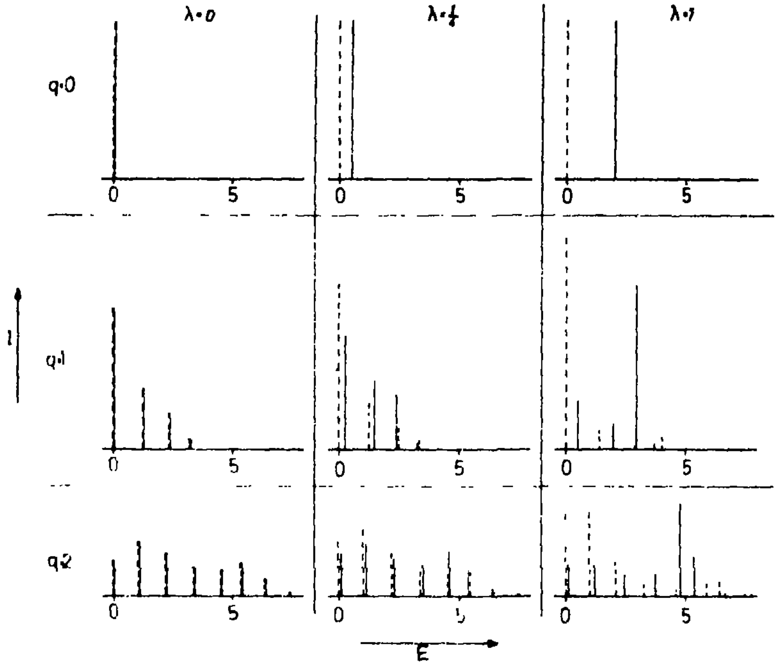

Fig 4. Spektrum und Franck-Condon-Faktoren für den $A(v=0)\to{}^2E$-Übergang bei verschiedener Spin-Bahn-Kopplung λ und Jahn-Teller-Parameter q. Intensitäten, in die das elektronische Übergangsmoment zum unteren bzw. oberen Spin-Zustand eingeht, sind gestrichelt bzw. ausgezogen

4. Diskussion

Die für die beiden Banden A0, B0 vorgeschlagene Zuordnung als 0–0-Übergänge zu den beiden Kramers-Dublett-Komponenten ${}^2E_{1/2}(E)$ und ${}^2E_{3/2}(2A)$ wird durch das Auftreten dieser Linien im Lumineszenzspektrum (bei 14229 bzw. 14299 K), deren Intensitäten-Temperaturabhängigkeit sowie ihrer Isotopie-Unabhängigkeit gestützt [12]. Weiterhin ist nach Sugano und Tanabe [2] die ${}^2E_{1/2}-{}^2E_{3/2}$-Aufspaltung ein Effekt zweiter Ordnung, der näherungsweise durch

$$\Delta E = \frac{4}{3}\,\frac{v\cdot\zeta}{E({}^2T_{2g})-E({}^2E_g)}$$

gegeben ist. Setzt man hier für ζ den um 16% verkleinerten Wert des freien Ions ($\zeta = 275\,\mathrm{cm}^{-1}$) ein sowie die gemessene Termdifferenz $E({}^2T_{2g})-E({}^2E_g)$ von $6700\,\mathrm{cm}^{-1}$ [7], gelangt man gerade zu $\Delta E = 65\,\mathrm{cm}^{-1}$. Die Intensität des ${}^4A_2-{}^2E$-Übergangs stammt vornehmlich vom ${}^4A_2-{}^4T_2$-Übergang [2], welcher stark π-bevorzugt ist [7], was der hier gemessenen stärkeren π-Adsorption entspricht. Weiterhin sollten nach Sugano und Tanabe [2] der ${}^4A_2-{}^2E_{3/2}$-Übergang im π-Spektrum der dreimal intensivere sein, während im σ-Spektrum der ${}^4A-{}^2E_{1/2}$-Übergang etwas bevorzugt sein sollte, wie es bei N_2-Temperatur tatsächlich der Fall ist. Warum bei Abkühlung auf Heliumtemperatur die A0-Bande danach um etwa den Faktor 5 zu schwach wird, können wir nicht erklären. Für eine Sättigung des ${}^2E_{1/2}$-Niveaus jedenfalls reicht die eingestrahlte Intensität nicht aus. Des-gleichen scheidet als Erklärung eine thermische Besetzungsstatistik der Spaltterme des ^4A-Grundzustands aus. Die Nullfeldaufspaltung müßte dann nämlich größenordnungsmäßig 10 K betragen und sollte sich im Spektrum bemerkbar machen, was aber nicht der Fall ist.

Da die übrigen Linien der beiden Progressionen ebenfalls genau den Abstand 65 cm^{-1} haben, kann nur gefolgert werden, daß entweder die Schwingung vom a_2-Typ ist, oder von einem e-Typ, der nur minimale Jahn-Teller-Stabilisierung ermöglicht (nach Fig. 3c müßte $\Delta E_{\mathrm{J.T.}} < 1$ cm^{-1} sein). Zu denken wäre etwa an die Knickschwingung des quasilinearen ha$_3$–Cr–ha$_3$-Systems, welche nur zu einem ^2D-Renner-Effekt Anlaß geben könnte. Da alle Peaks sehr scharf und nicht aufgespalten sind, ist der Zuordnung a_2 der Vorzug zu geben. Außerdem kann daraus gefolgert werden, daß die Nullfeld-Aufspaltung des Grundzustandes unter 1 cm^{-1} liegt. Die Intensitätsverteilung der Schwingungsbanden – insbesondere, daß auf die v = ungerade-Linien etwa 30% der Intensität entfallen – ist qualitativ verständlich bei Berücksichtigung der starken Anharmonizität (die auch von anderer Seite her bekannt ist [12]), einer leichten Dehnung im angeregten Zustand und nichtadiabatischer Kopplungen.

Die C-Linie bei 14230 + 266 cm^{-1} entspricht vermutlich dem $^4A_2 - {}^4E(^4T_{2g})$-0–0-Übergang, der nach Hansen und Vierke [13] 264 cm^{-1} über der A0-Linie liegen sollte. Hinweise auf eine Ion-Ion-Wechselwirkung konnten wir nicht finden.

Wir danken für die auf der IBM 7090 der GMD Bonn bereitgestellte Rechenzeit sowie der DFG für die Gewährung einer Sachbeihilfe.

Literatur

1. Tanabe, Y., Sugano, S.: J. physic. Soc. Japan **9**, 753, 766 (1954).
2. Sugano, S., Tanabe, Y.: J. physic. Soc. Japan **13**, 880 (1958).
3. Macfarlane, R. M.: J. chem. Physics **39**, 3118 (1963).
4. Schenk, H. J.: Diplomarbeit, Universität Frankfurt (1968).
5. Dingle, R.: J. chem. Physics **50**, 1952 (1969).
6. Schenk, H. J.: Dissertation, Universität Bonn (1971).
7. Hansen, K. H., Schenk, H. J.: Theoret. chim. Acta (Berl.) **24**, 207 (1972).
8. Nikitin, E. E.: in Chemische Elementarprozesse, p. 43. Ed. by H. Hartmann. Berlin: Springer 1968.
9. Herzberg, G.: Electronic Spectra and Electronic Structure of Polyatomic Molecules. Princeton: Van Nostrand 1966.
10. Schrödinger, E.: Ann. Physik **80**, 483 (1926).
    Kemble, E. C.: The Fundamental Principles of Quantum Mechanics. New York: McGraw-Hill 1937.
11. Longuet-Higgins, H. C., Öpik, U., Pryce, M. H. L., Sack, R. A.: Proc. Roy. Soc. (London) **244** A, 1 (1958).
12. Hansen, K. H., Koglin, E.: Theoret. chim. Acta (Berl.) **24**, 216 (1972).
13. — Vierke, G.: Theoret. chim. Acta (Berl.) **6**, 272 (1966).

Dr. W. H. Eugen Schwarz
Lehrstuhl für Theoretische Chemie
Universität
D-5300 Bonn, Wegeler Str. 12
Deutschland

Theoret. chim. Acta (Berl.) 24, 234 --240 (1972)
© by Springer-Verlag 1972

The Crystal Field Splittings in the 5f Complexes

*C. J. Ballhausen**

Department of Chemistry, Louisiana State University, Baton Rouge, Louisiana 70803

Received May 3, 1971

The crystal field splittings of some $(5f)^1$ and $(5f)^2$ complexes are investigated. Octahedral coordination leads to crystal field splittings of the same order of magnitude as the spin-orbit coupling parameter ζ. In contrast to this, tetrahedral coordination produces rather small splittings of the atomic levels. The values of the crystal field parameters Θ and Δ are found to be extremely sensitive to small variations is ζ and render any straight-forward least squares analysis of band positions somewhat dubious. The amount of splitting of the $\Gamma_7 \rightarrow \Gamma_8'$ transition provides some insight into the regularity of coordination in $(5f)^1$ compounds. The orders of magnitude for the crystalline field parameters in $(5f)^2$ compounds can distinguish octahedral from tetrahedral coordinations.

Die Kristallfeld-Aufspaltung einiger $5f^1$ und $5f^2$-Komplexe wird untersucht. Oktaedrische Koordination führt zu einer Aufspaltung von etwa der Größenordnung der Spin-Bahn-Kopplungs-Konstanten ζ, während tetraedrische Koordination nur kleine Aufspaltungen der Atomniveaus zur Folge hat. Die Kristallfeldparameter Θ und Δ sind sehr stark von ζ abhängig, weswegen die Adjustierung der drei Parameter an das experimentelle Spektrum recht unsicher wird. Die Aufspaltung des $\Gamma_7 \rightarrow \Gamma_8'$-Übergangs trägt zum Verständnis der Koordination in $5f^1$-Komplexen bei. Auf Grund der Größenordnung der Kristallfeldparameter von $5f^2$-Komplexen kann man zwischen tetra- und hexa-Koordination unterscheiden.

Étude des séparations de champ cristallin de certains complexes $(5f)^1$ et $(5f)^2$. Une coordinence octaédrique provoque des séparations de champ cristallin du même ordre de grandeur que le paramètre ζ de couplage spin-orbite. Au contraire, la coordinence tétraédrique produit des séparations de niveaux atomiques plutôt faibles. Les valeurs des paramètres Θ et Δ du champ cristallin sont extrêmement sensibles à de petites variations de ζ, ce qui rend douteux toute analyse directe des positions de bande par la méthode des moindres carrés. L'importance de la séparation de la transition $\Gamma_7 \rightarrow \Gamma_8$, fournit certains aperçus sur la régularité de la coordinence dans les composés $(5f)^1$. Les ordres de grandeur des paramètres du champ cristallin dans les composés $(5f)^2$ permet de distinguer les coordinences octaédriques et tétraédrique entre elles.

Introduction

Contrary to the situation for $(4f)^n$ complexes of the rare earths it is usually impossible to treat the "crystalline field" acting on complexes of $(5f)^n$ actinides as a small perturbation of atomic levels. In many cases, the spin-orbit coupling parameter ζ and the crystalline field parameters are of comparable magnitude; as a result, the level diagrams for complexes of the actinides containing more than one $5f$ electron are very complicated. On the other hand, there are also some cases where the "crystalline field" appears to be small compared with ζ. We shall show here that these differences result from the coordination geometry and number of the ion: large crystalline fields corresponding to octahedral coordination, small to tetrahedral coordination.

If we conclude that "crystal field splittings" are *not* due to electrostatic perturbations but reflect, instead, the variations of $\varepsilon^{\text{core}}$ values in a Hartree-Fock calculation [1], we must abandon the usual expansion of the crystal field [2] in spherical harmonics. Instead, we must treat the energy separations to be expected from pure symmetry considerations as parameters. Such a treatment focuses attention on the "strong field" point of view that is, with Eisenstein and Pryce [3], the energy matrices will be diagonal in the crystalline field splittings. It is our belief that this approach provides a better understanding of the "crystalline field" than does the eventually equivalent perturbation of the $j-j$ levels [4, 5].

---

* Dedicated to the memory of Professor K. H. Hansen.

In most cases, the actual symmetry of the complex molecule is very low. We shall, however, neglect this feature and treat the systems as if they possessed high symmetry. This will, of course, preclude any "exact" fitting of the energy levels, but will hopefully concentrate the attention on the important features.

Theory

Consider one f-electron in a regular six-coordination of ligands which possesses O_h symmetry. The seven f-orbitals form a basis for the irreducible representations a_{2u}, t_{1u}, and t_{2u} of O_h. The six sigma ligand orbitals and the twelve pi ligand orbitals can form molecular orbitals with $t_{1u}(\sigma,\pi)$ and with $t_{2u}(\pi)$. Consequently, we expect a splitting pattern as in Fig. 1. With $S=\frac{1}{2}$ transforming like Γ_6 in the double group 0^*, the splitting pattern in the strong field case that is with t_{1u}, t_{2u}, and a_{2u} level separations large compared to ζ will be as pictured in Fig. 1 (right). Letting the crystal field go to zero leads to the free ion levels pictured in Fig. 1 (left).

The assumption of a tetrahedral configuration of the ligands changes this splitting pattern drastically. The f-orbitals now transform as a_1 (correlating with a_{2u} in O_h) $t_2(t_{1u}$ in $O_h)$ and $t_1(t_{2u}$ in $O_h)$. The σ ligand orbitals transform as t_2 and a_1, the π ligand orbitals as t_1, t_2, and e. Since the σ group overlap integrals $G(\sigma,a_1)=\frac{2}{3}\sqrt{5}\,S(\sigma,f\sigma)$ and $G(\sigma,t_2)=-\frac{4}{3}\sqrt{3}\,S(\sigma,f\sigma)$, we shall assume $\varepsilon^{\text{core}}(a_1) > \varepsilon^{\text{core}}(t_2) > \varepsilon^{\text{core}}(t_1)$. $S=\frac{1}{2}$ transforms again [6] like Γ_6 and the ensuing splitting pattern is pictured in Fig. 2.

A comparison of Figs. 1 and 2 show that formal reversal of the level order occurs in going from O_h to T_d symmetry. This is, however, a little deceptive; the two t levels are reversed only in name [6].

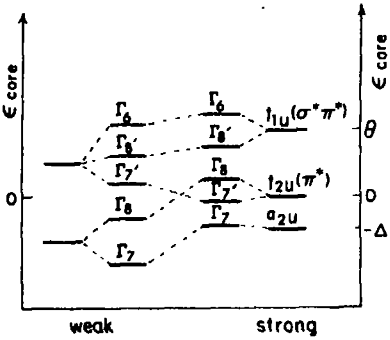

Fig. 1. Crystalline field splitting pattern for fields of O_h symmetry

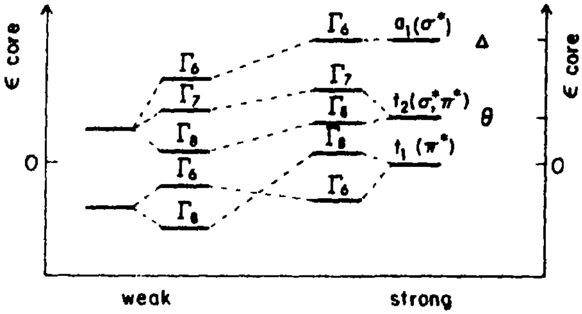

Fig. 2. Crystalline field splitting pattern for fields of T_d symmetry

With Reisfeld and Crosby [5] we shall define $\varepsilon^{\text{core}}(t_{2u}) - \varepsilon^{\text{core}}(a_{2u}) \equiv \Delta$ in O_h symmetry, and similarly $\varepsilon^{\text{core}}(t_1) - \varepsilon^{\text{core}}(a_1) \equiv \Delta$ for T_d symmetry. Notice the similarity of definitions; however, note also that Δ is negative for T_d symmetry and positive for O_h symmetry. We also define $\varepsilon^{\text{core}}(t_{1u}) - \varepsilon^{\text{core}}(t_{2u}) \equiv \Theta$ for O_h symmetry and $\varepsilon^{\text{core}}(t_2) - \varepsilon^{\text{core}}(t_1) = \Theta$ in T_d symmetry. Hence, Θ, as defined here, has the same sign for both tetrahedral and octahedral coordination.

If we adopt the equality $\varepsilon^{\text{core}}(t_{2u}) = \varepsilon^{\text{core}}(t_1) = 0$, we emphasize that the interaction between the levels depends only upon either Θ or Δ. Furthermore, the changes which accompany the transition from octahedral to tetrahedral geometry are easy to visualize.

The octahedral and tetrahedral matrices are then as given by Eisenstein and Pryce [3], but with our change of notation for the crystalline field parameters:

$$\begin{vmatrix} \frac{1}{4}\zeta - \lambda & \frac{3\sqrt{5}}{4}\zeta \\ \frac{3\sqrt{5}}{4}\zeta & \Theta - \frac{3}{4}\zeta - \lambda \end{vmatrix} = 0 \qquad \begin{matrix} O_h: \Gamma_8 \\ T_d: \Gamma_8, \end{matrix}$$

$$\begin{vmatrix} -\Delta - \lambda & \sqrt{3}\zeta \\ \sqrt{3}\zeta & -\frac{1}{2}\zeta - \lambda \end{vmatrix} = 0 \qquad \begin{matrix} O_h: \Gamma_7 \ (\Delta \text{ positive}) \\ T_d: \Gamma_6 \ (\Delta \text{ negative}), \end{matrix}$$

$$\left| \frac{3}{2}\zeta + \Theta - \lambda \right| = 0 \qquad \begin{matrix} O_h: \Gamma_6 \\ T_d: \Gamma_7. \end{matrix}$$

In a strong octahedral field, Γ_7' is the first excited level whereas in the week field, Γ_8 drops below Γ_7'. The cross-over occurs when

$$\zeta\left(4\frac{\Delta}{\Theta} + \frac{15}{4}\frac{\Theta}{\Delta} + \frac{17}{2}\right) = \Theta + \Delta.$$

Assuming $\Theta \simeq 2\Delta$ this expression reduces to $\Delta \simeq 6\zeta$. Evidently the cross-over will take place only at quite strong crystalline fields.

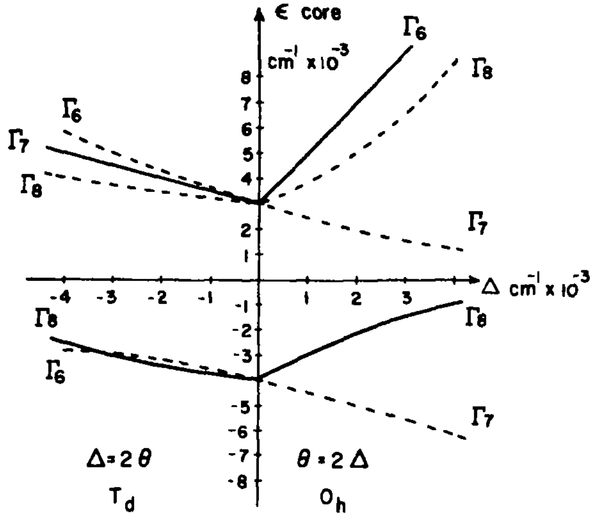

Fig. 3. Quantitative energy diagram for $\varepsilon^{\mathrm{core}}$ in octahedral and tetrahedral fields. Assuming $\zeta = 2000\,\mathrm{cm}^{-1}$ we have in O_h taken $\Theta = 2\Delta$ but in T_d $\Delta = 2\Theta$

Assuming T_d symmetry, the cross-over of Γ_6 and Γ_8 is found when

$$\zeta\left(4\frac{\Delta}{\Theta} + \frac{15}{4}\frac{\Theta}{\Delta} - \frac{17}{2}\right) = \Theta - \Delta\,.$$

For $\Delta \simeq 2\Theta$ this implies $\Theta = \frac{11}{8}\zeta$; the crossing takes place in the "intermediate field" region. Evidently the magnetic properties of tetrahedrally coordinated $5f$ complexes are expected to be very different from those which are octahedrally coordinated.

Assuming $\zeta = 2000\,\mathrm{cm}^{-1}$ and $\Theta = 2\Delta$, the splitting pattern to be expected in O_h symmetry is shown in Fig. 3. The same figure also gives the tetrahedral splittings for $|\Delta| = 2\Theta$. It is clear that quite strong tetrahedral fields provide little alteration of the levels of the "naked" ion. The reason relates to the fact that, in tetrahedral geometry one group of six-fold and another group of eight-fold degenerate levels remain bunched together through the whole range of field strengths. In octahedral geometry the two groups do intermix and, as a result, large splittings are produced. To good approximation, tetrahedral complexes of $(5f)$ ions can therefore be treated as having a small crystalline field in contrast to the octahedral complexes where the splitting must be considered large. Furthermore, eight coordination in the form of a cube should also produce quite small splittings. A distortion of the octahedron towards D_4 will split Γ_8 into two Kramer's doublets – but the overall "strength" of the crystalline field should remain of the octahedral type.

In O_h symmetry the $\Gamma_7 \to \Gamma_7'$ transition is given by

$$\bar{\nu}(\Gamma_7 \to \Gamma_7') = \sqrt{\left(\Delta - \frac{1}{2}\zeta\right)^2 + 12\zeta^2}\,.$$

For $\Delta \leqq \zeta$ we can expand:

$$\bar{\nu}(\Gamma_7 \rightarrow \Gamma_7') \simeq \frac{7}{2}\zeta + \frac{\Delta(\Delta-\zeta)}{7\zeta} \approx \frac{7}{2}\zeta .$$

In other words this transition should occur at $\sim\frac{7}{2}\zeta$ and should be more or less independent of Δ. Taking the experimental value for $\bar{\nu}(\Gamma_7 \rightarrow \Gamma_7')$ as a constant, the permitted variations of Δ and ζ are given by $(2\Delta-\zeta)\,\delta\Delta = (\Delta - \frac{49}{2}\zeta)\,\delta\zeta$. With $\Delta \simeq \zeta$, this reduces to $\delta\Delta = -23.5\,\delta\zeta$. In other words a change in the value of ζ by 40 cm^{-1} will change the value of the parameter Δ by 1000 cm^{-1}. Hence the parameter Δ is very poorly determined and it is extremely sensitive to the value of ζ.

The three experimentally observed transitions in octahedrally coordinated U^{+5} complexes are $\Gamma_7 \rightarrow \Gamma_7'$, $\Gamma_7 \rightarrow \Gamma_8'$ and $\Gamma_7 \rightarrow \Gamma_6$. In principle, it should be possible to evaluate the three parameters Δ, Θ and ζ using a least square analysis. However, the very strong dependence of Δ and Θ upon ζ makes such a procedure dubious. Furthermore, the degeneracy intrinsic to the $\Gamma_7 \rightarrow \Gamma_8'$ transition is usually removed by deviations from the idealized octahedral field. These deviations in turn introduce three additional splitting parameters which must be evaluated simultaneously with Δ, Θ and ζ. It is quite clear that even though an excellent understanding of the spectrum can be generated we cannot expect to extract a unique parametric set which is precisely descriptive of band positions. Such a parameter set is therefore not neccessarily physical meaningful. The parameter values given in Table 2, are therefore not the only possible sets, they are merely representative. In our assignments we follow Selbin *et al.* [11] and Karraker [12] rather than Reisfeld and Crosby [5] who did not recognize the splitting of the $\Gamma_7 \rightarrow \Gamma_8'$ transitions.

Table 1. Values from a Hartree-Fock calculations of ζ_{5f} for some $(5f)^1$ systems [8]

Pa^{+4} : ζ_{5f} = 1584 cm^{-1}
U^{+5} : ζ_{5f} = 2063 cm^{-1}
Np^{+6}: ζ_{5f} = 2553 cm^{-1}

Table 2. Parameter values for some $(5f)^1$ complexes

$PaCl_6$	$\Gamma_7 \rightarrow \Gamma_7'$	$\Gamma_7 \rightarrow \Gamma_8'$	$\Gamma_7 \rightarrow \Gamma_6$
Ref [9]	5215 cm^{-1}	7085 cm^{-1}	8000 cm^{-1}
Parameters	ζ = 1500 cm^{-1}	Δ = 1500 cm^{-1}	Θ = 2000 cm^{-1}
UCl_6	$\Gamma_7 \rightarrow \Gamma_7'$	$\Gamma_7 \rightarrow \Gamma_8'$	$\Gamma_7 \rightarrow \Gamma_6$
Ref. [7]	6800 cm^{-1}	9950 cm^{-1} 10430 cm^{-1}	11470 cm^{-1}
Parameters	ζ = 1940 cm^{-1}	Δ = 1940 cm^{-1}	Θ = 3710 cm^{-1}
NpF_6	$\Gamma_7 \rightarrow \Gamma_8$	$\Gamma_7 \rightarrow \Gamma_7'$	$\Gamma_7 \rightarrow \Gamma_8'$
Ref. [10]	7540 cm^{-1}	9350 cm^{-1}	(24000 cm^{-1})
Parameters[a]	ζ = 2400 cm^{-1}	Δ = 5440 cm^{-1}	Θ = 16800 cm^{-1}

[a] The transitions found around 4000 cm^{-1} cannot be electronic in origin. See also Ref. [3].

Discussion and Conclusions

The $\Gamma_7 \rightarrow \Gamma_8'$ transition is often quite strongly split, and the amount of this splitting serves as indicator for deviations from octahedral symmetry. An illustrative calculation [13] of the effects of the introduction of lower fields indicates that the position of $\Gamma_7 \rightarrow \Gamma_7'$ should remain more or less unaltered, that $\Gamma_7 \rightarrow \Gamma_8'$ and $\Gamma_7' \rightarrow \Gamma_8$ should split significantly and that $\Gamma_7 \rightarrow \Gamma_6$ should tend toward higher energies. These expectations are certainly fulfilled [7, 13].

Of some interest here is the spectrum of the gaseous dimer U_2Cl_{10} reported by Gruen and McBeth [14]. $\Gamma_7 \rightarrow \Gamma_7$ is found at 6660 cm^{-1}, almost as in UCl_6^-, and the components of Γ_8' are split by ~800 cm^{-1}. Since the low energy $\Gamma_7 \rightarrow \Gamma_8$ transition should be strongly split it is reasonable to infer that the band observed at 4500 cm^{-1} corresponds to the upper energy component of Γ_8.

No tetrahedral $(5f)^1$ systems seem to have been characterized. However, when interpreting the spectrum of the $(5f)^2$ compound UCl_4, McLaughlin [15] commented that the spectrum was virtually identical to that expected for the free ion. The structure is known to be an extremely flattened tetrahedron. Later measurements on UCl_4 by Clifton, Gruen and Ron [16] yielded (as recalculated here) $\Delta = -1100$ cm^{-1} and $\Theta = -1130$ cm^{-1}. However, the values of these parameters were obtained by a least-squares fit which assumed a regular tetrahedral coordination and which maintained the values of F_2, F_4, F_6 and ζ_{5f} constant, the last being set equal to 1796 cm^{-1}. Hence all we can safely conclude is that Δ is fairly small and negative. For $UCl_6^=$ in Cs_2UCl_6 where U^{+4} is found at an O_h site, Satten, Schreiber, and Wong [17] found (as recalculated here) $\Delta = 1330$ cm^{-1} and $\Theta = 2370$ cm^{-1}. These values were obtained from a least square fit to 18 observed levels, which provide an evaluation of 6 parameters, including $\zeta_{5f} = 1796$ cm^{-1}.

The spectrum of $CsNpF_6$ was interpreted by Varga *et al.* [8] assuming octahedral coordination. Thirty four observed levels were used in a least-squares refinement of the crystal field parameters. If ζ_{5f} is maintained constant at 2380 cm^{-1} one finds (recalculated here) $\Delta = 375$ cm^{-1} and $\Theta = 1080$ cm^{-1}. If ζ is allowed to vary one finds $\zeta_{5f} = 2230$ cm^{-1}, $\Delta = -210$ cm^{-1} and $\Theta = 610$ cm^{-1}. We must conclude from these parameter values that Np^{+5} is not octahedrally coordinated. We suspect a flattened tetrahedral geometry.

Therefore it would appear possible to infer some structural conclusions from the parametric values necessitated by a formal crystalline field description of the spectra of $(5f)^2$ complexes.

References

1. Dahl, J. P., Ballhausen, C. J.: Advances Quant. Chem. 4, 170 (1968).
2. Wybourne, B. G.: Spectroscopic Properties of Rare Earths. New York: Interscience Publishers, Inc. 1965.
3. Eisenstein, J. C., Pryce, M. H. L.: Proc. Roy. Soc. (London) A 255, 181 (1960).
4. Goodman, G. L., Fred, M.: J. chem. Physics 30, 849 (1959).
5. Reisfeld, M. J., Crosby, G. A.: Inorg. Chem. 4, 65 (1965).
6. Griffith, J. S.: The Theory of Transition Metal Ions. Cambridge: University Press 1961.
7. Ryan, J. L.: J. inorg. nuclear Chem. 33, 153 (1971).

8. Varga, L. P., Brown, J. D., Reisfeld, M. J., Cowan, R. D.: J. chem. Physics **52**, 4233 (1970).
9. Axe, J. D., Stapleton, H. J., Jeffries, C. D.: Physic. Rev. **121**, 1630 (1961).
10. Steindler, M. J., Gerding, T. J.: Spectrochim. Acta **22**, 1197 (1966).
11. Selbin, J., Ortego, J. O., Gritzner, G.: Inorg. Chem. **7**, 976 (1968).
12. Karraker, D G.: Inorg. Chem. **3**, 1618 (1964).
13. Selbin, J., Durrett, D. G., Ballhausen, C. J.: To be published.
14. Gruen, D. M., McBeth, R. L.: Inorg. Chem. **8**, 2625 (1969).
15. McLaughlin, R.: J. chem. Physics **36**, 2699 (1962).
16. Clifton, J. R., Gruen, D. M., Ron, A.: J. chem. Physics **51**, 224 (1969).
17. Satten, R. A., Schreiber, C. L., Wong, E. Y.: J. chem. Physics **42**, 162 (1965).

Prof. C. J. Ballhausen
Dept. of Chemistry
Louisiana State University
Baton Rouge, Louisiana 70803, USA

Theoret. chim. Acta (Berl.) 24, 241–250 (1972)
© by Springer-Verlag 1972

Chemical Effects on Inner Shells Studied by Photo-Electron Spectrometry*

CHRISTIAN KLIXBÜLL JØRGENSEN

Département de Chimie physique, Université de Genève, CH-1211 Genève 4, Switzerland

Received July 12, 1971

Fluorine 2s orbitals with ionization energies *I* about 40 eV still show perceptible inter-ligand chemical effects (in molecules with short *F–F* distances) in agreement with the mutual overlap integral. Other inner shells show only a chemical shift (amounting to 5 or more eV) and adjacent *I* values when the groundstate has positive *S*.

The relativistic separation of the two *I* of 4*f* is measured in 88 compounds of the elements from tantalum to uranium. The behaviour of the rare earths and hafnium is also discussed as well as the large width of 4*d* due to short half-life of the ionized state before a 4*f* electron fills the vacancy. The quantum-mechanical aspects of slowly auto-ionizing states are studied.

In Molekülen mit besonders benachbarten Fluoratomen verursachen die Fluor-2*s*-Orbitale trotz ihrer Energie von ca. 40 eV entsprechend ihren Überlappungen beachtliche chemische Wechselwirkungen. Die Wechselwirkung anderer Orbitale innerer Schalen liefert dagegen nur eine chemische Verschiebung um größenordnungsmäßig 5 eV und eine Aufspaltung der Ionisierungsenergien im Falle eines positiven *S*-Wertes im Grundzustand.

Die Spin-Bahn-Aufspaltung der beiden 4*f*-Ionisierungsenergien in 88 Verbindungen der Elemente Ta bis U wurde gemessen und diskutiert. Auf die große Linienbreite der 4*d*-Ionisierung wird eingegangen.

Les orbitales 2*s* de fluor avec l'énergie d'ionisation *I* autour de 40 eV montrent d'effets chimiques quand les ligandes ont la distance mutuelle courte, et ils sont proportionnels aux intégrales de recouvrement. Les autres couches intérieures montrent seulement un déplacement chimique (de l'ordre de grandeur 5 eV) et des valeurs multiples de *I* quand l'état fondamental a *S* positif. La séparation d'origine relativiste des deux *I* de la couche 4*f* est mesurée dans 88 composés des éléments entre le tantale et l'uranium. Le comportement des terres rares et de l'hafnium est discuté ainsi que la grande largeur du signal 4*d*, où l'état ionisé a une durée très faible parce que la position vacante rapidement est reprise par un électron 4*f*. On étudie les états sujet à l'auto-ionisation lente de point de vue de mécanique ondulatoire.

1. Direct Chemical Bonding between Inner Shells

When the atomic spectroscopists classify energy levels of monatomic systems using electron configurations, the orbitals forming the configurations have a far more objective existence than one would accept from the argument that the anti-symmetrized Slater determinant of a closed-shell system is invariant by a unitary transformation of the orbitals, forming new linear combinations. The weak point of this argument is that the total wave-function Ψ is not exactly an anti-symmetrized Slater determinant (because of correlation effects) and a closer analysis [1] shows that the individual orbitals (which would be the diagonalized eigen-functions of the effective one-electron operator, if such a concept was sharply defined) are those orbitals which are the most appropriate for describing the manifold consisting of the groundstate and the low-lying excited levels, and which form what is called the preponderant electron configuration.

---

* Dedicated to the memory of Prof. K. H. Hansen.

It is not excluded that the preponderant electron configuration may present vacancies in penultimate orbitals (e.g. $1s^2 2s 2p^6 4f$ of a neon atom) and frequently, they correspond to auto-ionizing states like the levels belonging to the configuration [Ar] $3d4d$ of the calcium atom at higher energy than [Ar] $4s$ of Ca^+. It has been realized since the time of Moseley that the X-absorption spectra, and in particular the X-emission lines, are narrow and indicate a quite individual behaviour of the inner shells. There is no intrinsic difference between ultra-violet and X-ray spectra at this point; thus the gaseous potassium atom have excited levels belonging to the configuration [Ne] $3s^2 3p^5 4s^2$ at energies about four times higher than needed to form the groundstate of K^+. According to a proposal by Mulliken, we denote such vacancies by the exponent (-1), such as $(3p)^{-1}$.

In a solid, the lowest ionization energy I relative to vacuo is given by the threshold energy for Einstein photo-electric emission. By the same token, it is relatively easy to determine the lowest I of a gaseous molecule from the lower limit of photon energy needed to maintain a current through the gas. The great progress made possible by photo-electron spectroscopy (either done on gaseous samples with 21.2 or 40.8 eV radiation [2] or on the outermost 50 Å of solid samples with 1253.6 or 1486.6 eV radiation [3] coming from a magnesium or aluminium anti-cathode) is that all the I values for penultimate orbitals and inner shells can be measured up to a higher limit slightly below the energy of the incident photons.

This opens a most valuable opportunity to compare MO calculations with experimentally verifiable quantities and to study regularities by induction from a comparison of many compounds. It is usually argued that the kinetic energy of the emerging photo-electrons is given as the difference between the photon energy (1486.6 eV in our Varian IEE-15 instrument) and the sum of I and the work function of metallic materials. However, in the case of non-conducting samples, it is more appropriate to use an internal standard of reference, and it has been discussed [4] why the I value for the carbon $1s$ orbital in one-sided scotch tape must be close to 290.0 eV. Hence, we define a correction C_{st} as the difference between 290.0 eV and the I^* value recorded by the apparatus for the carbon signal at lowest I. Both in the original instrument in Uppsala and in a home-made instrument in Berkeley [5] magnetic deflection is used, like in the β-ray spectrograph, whereas the commercial instruments generally use electrostatic fields alone.

The photo-electron spectrum of the neon atom [3] shows $(2p)^{-1}$ at $I = 21.6$ eV, $(2s)^{-1}$ at 48.4 and $(1s)^{-1}$ at 870.2 eV. The isoelectronic molecule methane has three degenerate orbitals with $(t_2)^{-1}$ at 14 eV, $(2a_1)^{-1}$ at 24 and $(1a_1)^{-1}$ at 290.8 eV. The water molecule has lower symmetry and correspondingly five distinct I values at 12.6, 14.8, 18.6, 32.2 and 539.7 eV. There is no doubt that the highest I value in CH_4 and H_2O corresponds essentially to $1s$ of the carbon or oxygen atom. The chemist may then ask whether a given I corresponds to $2s$. This is the case, energy-wise, for the 24 eV orbital of methane and the 32.2 eV orbital of water. However, it is expected that the electronic density of these MO is partly delocalized on the hydrogen atoms. In the LCAO approximation, these orbitals are mainly mixtures of H 1*s* and 2*s* of the heavier atom.

It has been realized from the study of electron transfer spectra of transition group complexes [6] that the interactions between the filled *p* shells of adjacent ligands X^- in hexahalide complexes MX_6^{+z-6} are sufficiently strong that the loosest bound MO having many node-planes (four and three) between the ligands are about 1 eV easier to excite than the approximately non-bonding combination. The corresponding effects are stronger [3] in the photo-electron spectrum of CF_4. Thus, the π orbitals have $I = 16.3$, 17.5 and 18.6 eV and the two sets of σ orbitals $I = (22.2$ and $25.1)$ and (40.3 and 43.8 eV). These two sets are, energy-wise, very close to carbon 2*s* and fluorine 2*s*, but the former set is probably fluorine 2*p* to a larger extent. Anyhow, the separations (2.9 and 3.5 eV) between three degenerate σ orbitals of symmetry type t_2 in the point-group T_d and the stronger bound, totally symmetric a_1 orbital must be due to interactions between the four fluoride ligands. A similar effect is observed [3] in SF_6 having the six σ orbitals formed mainly from F2*s* distributed at $(e_g)^{-1}$ 39.3, $(t_{1u})^{-1}$ 41.2 and $(a_{1g})^{-1}$ 44.2 eV.

Normally, the chemist would not expect significant chemical bonding to take place with orbitals having I above 20 eV; it must be remembered that a quite strong single bond with the dissociation energy 115 kcal/mole represents only 5 eV to be distributed among two bonding electrons. What is worse in this respect is that these interactions between equivalent ligands correspond to all the anti-bonding and bonding MO being simultaneously filled what is the standard explanation for the strong repulsion between noble gas atoms brought to a shorter distance than the Van der Waals contact. The photo-electron spectra have demonstrated the presence of a "Underground chemistry" of deep-lying MO, and there is little doubt that the dissociation energy of SF_6 is decreased at least 4 eV by the inter-ligand repulsion of the fluorine 2*s* orbitals.

A direct homo-atomic bond occurs in ethane, and actually, two I values separated by 3.5 eV have replaced the 24 eV value for methane [3]. Again, this is very impressive when comparing with the dissociation energy of the central C-C bond. However, this is probably a rather extreme case of strong interactions between equivalent atoms at a short distance. Thus, we have studied solid GaS having a direct Ga–Ga bond, and found no convincing evidence for a similar effect in the broad signals in the valence region. We found only one Ga 3*d* signal at $I^* = 22.9$ eV and corrected $I = 27.9$ eV to be compared with $I = 22.7$ eV for metallic gallium, 27.6 eV for $Ga_2(SO_4)_3$, 18 H_2O, 27.6 eV for $(NH_4)_3$ GaF_6 and 28.7 eV for Ga_2O_3. This variation is a normal chemical shift dI and is also found for deeper shells, such as I for $2p_{3/2}$ at 1125.2, 1120.6, 1124.9, 1125.0 and 1125.7 eV for the five samples. Also salts of BF_4^-, SiF_6^{-2} show much weaker effects [7] of inter-ligand repulsion than the isoelectronic neutral molecules CF_4 and SF_6.

From a theoretical point of view, one expects a proportionality between the energetic separation and the overlap integral S_{XX} in the homonuclear case [8] whereas the second-order perturbation in the case of weak heteronuclear bonding rather is proportional to the square S_{MX}^2. For our purposes, it is sufficient to consider the model expression for S_{XX} between two hydrogenic 1*s* orbitals with the Slater coefficient μ

$$S_{XX} = \left(1 + \mu R + \frac{1}{3}\mu^2 R^2\right)\exp(-\mu R) \qquad (1)$$

In the case of two adjacent fluorine ligands at a distance 5 bohr units, th approximate value $\mu = 1.2$ produces the overlap integral 0.047. Obviously, th overlap attenuates strongly with distance. Two fluorine atoms in trans-positio in SF_6 are known to have $R = 6$ bohr and hence $S_{XX} = 0.019$ whereas the actua F–F distance in CF_4 is only 4 bohr and $S_{XX} = 0.111$.

In the homonuclear case [8], the proportionality factor in the energetic effects is related to the kinetic energy operator and should be approximately μ^2 hartree for large R. Hence, the order of magnitude expected is 4.4 eV for $R = 4$ bohr, 1.8 eV for $R = 5$ and 0.4 eV for $R = 6$ bohr in agreement with the observations. On the other hand, the inner shells have vanishing energetic effects. Thus, for $R = 4$ bohr, the fluorine 1s shells with $\mu = 8$ produce the overlap integral $5 \cdot 10^{-12}$ and even when multiplied with 64 hartree, the energy separations expected are only 10^{-8} eV. It may be noted that Eq. (1) is 10^{-3} for $\mu R = 10.9$, 10^{-4} for $\mu R = 13.5$ and 10^{-5} for $\mu R = 16.2$.

In the Wolfsberg-Helmholz model, the energetic effect in the homonuclear case is approximately $(K - 1)\, H_X S_{XX}$ producing the same type of result as above. This is less true for the heteronuclear case where the average energy entering in the non-diagonal element is strongly influenced by the orbital having the highest I. But since this model agrees with the considerations of the kinetic energy operator in the bond region [8] in assuming energetic effects proportional to the square of the overlap integral, observable consequences disappear for much smaller values of μR.

2. Ionization Energies of 4*f* in Compounds of Heavy Elements

The probability of ionizing an orbital with small I using photons of 1486.6 eV energy is usually rather low. However, as discussed in the specific case of gold [4] this restriction does not apply to the 4*f* shell. Table 1 gives the I values (obtained from $I^* + C_{st}$) of $4f_{5/2}$ and $4f_{7/2}$ of compounds of elements having the atomic

Table 1 The two ionisation energies I of the 4*f* shell corrected with C_{st} defined in the text to apply relative to vacuo. All values in eV

		C_{st}	$4f_{5/2}$	$4f_{7/2}$	Diff.
Hf:	K_2HfF_6	5.0	(27.5)	26.0	1.5
	$Yb_2Hf_2O_1$	4.7	26.1	24.4	1.7
	$Hf(C_6H_5CHOHCO_2)_4$	5.0	24.9	23.2	1.7
Ta:	K_2TaFy	4.5	37.5	35.7	1.8
	Ta_2O_5	4.9	35.1	33.3	1.8
W:	Na_2WO_4	5.6	44.7	42.9	1.8
	$H_3PW_{12}O_{40}$	4.0	42.95	41.1	1.85
	Cs_2WS_4	5.2	42.7	40.9	1.8
Re:	$CsReO_4$	4.7	56.5	54.3	2.2
	$TlReO_4$	5.1	56.1	53.9	2.2
	$AgReO_4$	4.7	(55.5)	53.4	2.1
	$KReO_4$	3.7	55.1	52.9	2.2
	$As(C_6H_5)_4[ReO_4]$	3.9	53.0	50.6	2.4
	K_2ReCl_6	3.7	51.5	49.15	2.35
	$N(CH_3)_4[ReS_4]$	4.4	(50.8)	48.2	—

Table 1 (continued)

		C_x	$4f_{5/2}$	$4f_{7/2}$	Diff.
Os:	$K_2OsO_2(OH)_4$	4.8	63.2	60.7	2.5
	Cs_2OsCl_6	4.8	62.4	59.8	2.6
	Cs_2OsBr_6	3.8	61.8	59.1	2.7
	K_2OsCl_6	3.8	61.6	58.9	2.7
	Tl_2OsBr_6	6.0	60.7	57.9	2.8
	$Ni_2[Os(CN)_6]$	5.2	60.6	57.9	2.7
Ir:	Cs_2IrCl_6	5.7	73.4	70.7	2.7
	$[Ir(NH_3)_5Cl]Cl_2$	4.4	71.5	68.65	2.85
	$[N(CH_3)_4]_2IrCl_6$	4.4	71.3	68.5	2.8
	$[N(C_4H_9)_4]_3IrCl_6$	4.4	69.8	67.1	2.7
	$Ir[S_2P(OC_3H_7)_2]_3$	4.5	69.8	66.85	2.95
Pt:	K_2PtBr_6	5.0	84.6	81.3	3.3
	$(NH_4)_2PtCl_6$	3.3	84.15	80.9	3.25
	$K_2Pt(SeCN)_6$	4.9	83.9	80.6	3.3
	$K_2Pt(SCN)_6$	4.8	83.1	80.0	3.1
	$[Nien_2]\ [Pt(CN)_4]$	4.0	82.3	79.2	3.1
	K_2PtCl_4	4.0	82.2	79.0	3.2
	Pt	5.7	80.1	76.8	3.3
Au:	$KAuCl_4$	3.2	97.4	93.85	3.55
	$KAu(CN)_2$	4.5	94.85	91.15	3.7
	$AuSCH_2CO_2H$	3.9	94.45	90.8	3.65
	Au	5.4	92.2	88.85	3.65
Hg:	HgO	5.5	112.6	108.55	4.05
	K_2HgI_4	4.6	111.85	107.8	4.05
	$K_2Hg(SCN)_4$	5.0	110.85	106.75	4.1
	$Hg(SCN)_4Co$	4.7	110.6	106.55	4.05
Tl:	TLF	5.2	131.6	127.2	4.4
	$TlReO_4$	5.1	131.45	127.0	4.45
	$TlIO_3$	5.1	131.4	126.95	4.45
	Tl_2SO_4	5.2	131.25	126.8	4.45
	$TlWO_4$	4.8	130.9	126.45	4.45
	Tl_2MoO_4	4.8	130.4	125.95	4.45
	Tl_2CO_3	4.7	130.35	125.9	4.45
	Tl_2CrO_4	4.5	129.95	125.55	4.4
	TlBr	4.6	129.9	125.45	4.45
	$TlB(C_6H_5)_4$	5.0	129.55	125.1	4.45
	TlI	4.85	129.4	125.05	4.35
	Tl_2WS_4	4.5	129.3	124.85	4.45
	$[Co(NH_3)_6]TlCl_6$	3.7	129.0	124.6	4.4
	Tl_2OsBr_6	0.0	128.75	124.4	4.35
	TlBr	3.1	128.75	124.3	4.45
	Tl_2O_3	4.4	127.35	123.0	4.35
Pb:	$Pb(NO_3)_2$	5.3	152.1	147.2	4.9
	PbI_2	5.1	151.7	146.75	4.95
	$PbSO_4$	4.5	150.95	146.1	4.85
	$PbCl_2$	4.6	151.0	146.1	4.9
	$PbBr_2$	4.9	150.85	145.95	4.9
	PbF_2	4.75	150.75	145.9	4.85
	PbS	4.15	149.85	145.0	4.85
	$PbCO_3$	3.2	149.8	145.0	4.8
	$PbSO_4$	3.3	149.75	144.9	4.85
	PbO	3.3	149.0	144.15	4.85
	$PbCrO_4$	3.3	148.6	143.75	4.85

Table (continued)

		C_a	$4f_{5/2}$	$4f_{7/2}$	Diff.
	$Pb[S_2P(OC_2H_5)_2]_2$	4.8	148.2	143.3	4.9
	PbO_2	4.4	147.2	142.4	4.8
Bi:	Bi_2O_3	4.7	172.2	166.85	5.35
	$NaBiO_3$	4.55	171.8	166.5	5.3
	BiI_3	5.0	171.8	166.5	5.3
	$CsBiI_4$	5.0	171.6	166.3	5.3
	$BiOI$	5.05	171.4	166.1	5.3
	$[Co(NH_3)_6]BiCl_6$	3.6	170.2	164.2	5.3
Th:	ThF_4	4.9	354.75	345.4	9.35
	$Th_{0.95}U_{0.05}O_2$	6.4	352.35	343.0	9.35
	ThO_2	4.6	352.0	342.65	9.35
	$Th_{0.6}Ce_{0.2}U_{0.2}O_2$	5.9	351.4	342.1	9.3
	$Th_{0.9}Pr_{0.1}O_2$	5.5	351.1	341.8	9.3
	$Th_{0.5}Eu_{0.5}O_{1.75}$	5.8	351.1	341.75	9.35
U:	$Cu(UO_2)_2(PO_4)_2$	4.6	400.9	390.0	10.9
	$RbUO_2(NO_3)_3$	4.8	400.6	389.7	10.9
	K_2UF_6	4.9	400.4	389.5	10.9
	$Th_{0.95}U_{0.05}O_2$	5.0	400.1	389.2	10.9
	$Th_{0.6}Ce_{0.2}U_{0.2}O_2$	5.9	400.05	382.15	10.9
	$(NH_4)_2U_2O_7$	4.7	399.9	389.05	10.85
	$Ce_{0.5}U_{0.5}O_2$	6.1	399.5	388.8	10.7
	UO_2	3.6	398.1	387.3	10.8
	U_3O_8	4.1	398.0	387.2	10.8
	$[P(C_6H_5)_3H]_2UCl_6$	4.64	396.6	386.0	10.6

number Z above 72. Already in the rare earths, the $4f$ signals are quite perceptible. We find $I = 15.6$ eV for Gd_2O_3, broad structures between 17 and 13 eV in Dy_2O_3, Ho_2O_3 and Tm_2O_3, $I = 13.6$ eV in Yb_2O_3, 13.7 eV in $Yb_2Ti_2O_7$, 14.6 eV in both $Yb_2(SO_4)_3 \cdot 8\,H_2O$ and $YbAsO_4$, 15.0 eV in $Yb_2Hf_2O_7$, 15.1 eV in $Yb_2(WO_4)_3$ and 16.7 eV in YbF_3, all having a weaker signal at 4 eV higher I; and an unresolved (but broadened) signal at 16.0 eV in Lu_2O_3. As will be discussed later with Dr. Christiane Bonnelle and Dr. R. C. Karnatak, these structures are in agreement with the general theory of f^q configurations [1] assuming the parameters $D = 0.8$ eV and $(E - A) = 0.5$ eV. Hedén, Löfgren and Hagström [9] have reported I^* relative to the Fermi level of Lanthanide metals, e.g. $I^* = 7.8$ eV for Gd which is said [10] to have the work function 3.2 eV. The difference in I-values from 15.6 eV for Gd_2O_3 to 11.0 eV for Gd is a quite normal chemical shift dI from the oxide to a metal.

It is well-known from absorption spectra in the near infra-red [11] that the difference $(7\zeta_{4f}/2)$ between $4f_{7/2}$ and $4f_{5/2}$ is 1.3 eV in all ytterbium (III) compounds. HfO_2 shows an unresolved signal at $I = 25.0$ eV. As discussed later with Dr. Lucette Balsenc, metallic hafnium shows $I = 23.7$ eV which may conceivably be due to a superficial suboxide of the type Hf_3O. As seen from Table 1, the compounds starting with tantalum show two distinct $4f$ signals, and the chemical shifts dI between the compounds of the same element achieve values up to 5 eV. Professor Carl Nordling and Dr. Jan Hedman were so kind as o supply I^* values for the oxide-free metals relative to the Fermi level:

$$\begin{array}{llll} \mathrm{Os} & 53.6 & \text{and} & 50.8 \\ \mathrm{Ir} & 64.0 & \text{and} & 61.0 \\ \mathrm{Pt} & 74.4 & \text{and} & 71.0 \\ \mathrm{Au} & 87.5 & \text{and} & 83.8 \end{array} \tag{2}$$

The $5d$ structures of these metals have been studied [12] and it is probable that I s some 4–5 eV larger than the I^* values of Eq. (2). Among the compounds in Table 1, the salts of WS_4^{-2} and ReS_4^- are later going to be discussed with Professor A. Müller and Dr. E. Diemann, the salts of $Os(CN)_6^{-4}$ and $Pt(CN)_4^{-2}$ together with Professor A. Ludi, and the salts of $TlCl_6^{-3}$ and $BiCl_6^{-3}$ were kindly provided by Dr. Peter Day.

Because of the details of the experimental technique, the distance between the two $4f$ relativistic sub-shells should be extremely precisely evaluated, and it is interesting to look for possible chemical effects. The average values found for $(7\,\zeta_{4f}/2)$ are:

$$\begin{array}{cccccccccccc} \mathrm{W} & \mathrm{Re} & \mathrm{Os} & \mathrm{Ir} & \mathrm{Pt} & \mathrm{Au} & \mathrm{Hg} & \mathrm{Tl} & \mathrm{Pb} & \mathrm{Bi} & \mathrm{Th} & \mathrm{U} \\ 1.82 & 2.2 & 2.66 & 2.8 & 3.23 & 3.6 & 4.05 & 4.42 & 4.87 & 5.31 & 9.32 & 10.83 \end{array} \tag{3}$$

Though these values increase with Z, they do not increase in a fully regular fashion. One effect may be an influence from groundstates with positive S. Helmer [13] noted that $2p_{1/2}$ and $2p_{3/2}$ of chromium (VI) in $K_2Cr_2O_7$ have the I^* values 590.8 and 581.6 eV, whereas Cr (III) in Cr_2O_3 has $I^* = 588.9$ and 579.0 eV. The increase of the separation from 9.2 to 9.9 eV cannot be interpreted exclusively as an increase of $(3\,\zeta_{2p}/2)$. Actually, the Cr–3s signal of Cr_2O_3 shows two peaks at $I^* = 81.5$ and 78.2 eV which must be explained by the two excited terms ^3F and ^5F of the electron configuration $[\mathrm{Ne}]3s3p^6 3d^3$, separated by effects of interelectronic repulsion. Hence, the situation is rather similar to the behaviour of high-spin nickel (II) complexes (having $S = 1$ in the groundstate) where the $2p$ region of the photo-electron spectrum shows four signals [4]. The distance between the first and the third peak is 17.7 eV, to be compared with the distance 17.2 eV between the two signals of diamagnetic nickel (II) compounds. The physical origin of these separations is that the probability of ionization is distributed, in a not fully understood fashion, between the 270 states of the ionized configuration containing the two partly filled shells $2p^5$ and $3d^8$. A similar effect of apparently increased relativistic splitting in systems having positive S in the groundstate seems to occur in K_2ReCl_6 $(S = 3/2)$ and in $(P(C_6H_5)_3H)_2UCl_6$ $(S = 1)$.

It is not excluded that the oxides of uranium are superficially oxidized to U (VI). A large number of mixed oxides [14] of thorium (IV) have been measured, also by Dr. W. G. Proctor in Palo Alto and by Dr. W. Bremser and Mr. F. Linnemann in Darmstadt, all showing the $4f$ difference very close to 9.32 eV. The chemical shifts of platinum complexes have been measured [15, 16]. I^* for Pt $4f_{7/2}$ changes from 73.4 eV for L_2PtCl_2 over 71.7 eV for PtL_4 to 71.2 eV for $L_2Pt(CH_3)_2$ where L is $P(C_6H_5)_3$. 5.0 to 5.3 eV have to be added to these values in order to convert them to our I scale. The latter example clearly shows that dI does not indicate the oxidation states Pt(II) and Pt(0) defined [1] on the basis of the preponderant electron configurations $5d^8$ and $5d^{10}$ but rather a quantity related to the fractional charge residing on the central atom [8, 17].

This statement is even more clear-cut in the case of Tl_2O_3 having I distinctly lower than all the 14 thallium(I) compounds in Table 1, and PbO_2 having I below all the 12 lead (II) compounds. However, a residual effect lingers on the limit of the experimental uncertainty. Tl_2O_3 has the $4f$ relativistic separation 0.07 eV below the average value for the other thallium compounds. The same is true for $KAuCl_4$ and Cs_2IrCl_6. These compounds are particularly oxidizing and it cannot be excluded that the inner $4f$ shell is slightly modified by the covalent bonding though it is a little surprising that ζ_{4f} should be decreased by as much as one percent, more than is the case in erbium(III) and ytterbium(III) compounds [1, 14] with I eight times smaller.

3. Conclusions

The persistence of inner shells in compounds [18] has been magnificiently manifested by photo-electron spectra of solid samples. It seems to be exaggeratedly prudent to emphasize the possible delocalization of phosphorus $2p$ orbitals [19] with the exception of the rare compounds (such as H_2PPH_2) having a homo-atomic bond. As a matter of fact, the chemical effects on fluorine $2s$ orbitals seem to be connected with the unusual short F-F distances (well below twice the ionic radius of F^-) in CF_4 and SF_6 and they agree with the expected proportionality with the overlap integral in the homonuclear case. Corresponding heteronuclear effects on inner shells should almost vanish because of the dependence on the (much smaller) square of the overlap integral.

However, one must accept one possible source of chemical effects. The total wave-functions of systems lacking an inner electron cannot be treated variationally. The Hartree-Fock approximation has the additional constraint of a prescribed elec'ron configuration. This is already necessary in the groundstate of certain gaseous anions such as H^- and O^{-2} (in contrast to the isoelectronic F^- and Ne). The latter ion can be stabilized in solid oxides by the Madelung potential but is unstable relative to O^- and an electron at large distance in the gaseous state, and the Hartree-Fock solution only exists in a confined volume or with the superposed condition of six equivalent electrons. Hence, it is not clear whether unexpected effects from the continuum [8] may not influence the I values observed. Manne and Åberg [20] demonstrated that the primary peaks correspond to ionized states where the other electrons have contracted their orbitals, adapting to the more negative central field. The positions of the primary peaks may be influenced by polarizability besides the conventional Madelung potential. As also seen from Table 1, iodides and caesium salts have unexpectedly high I values [4]. The chemical shift dI seems essentially to be an indicator [8, 17] of the variation of the Hartree potential $U(x, y, z)$ including the Madelung potential produced by the surrounding atoms, and if this description is appropriate, the large variation of dI known to have the order of magnitude

5 to 10 eV for most elements does not contribute to the heat of formation of the compound considered, because its contribution cancels when the total energy is evaluated [11].

Another interesting aspect of the auto-ionizing character of our $(n\,l)^{-1}$ systems is the half-width of the photo-electron signals corrected for the background. Under our standard conditions of 100 eV analyzer energy, a normal signal has the sum of $\delta\,(-)$ and $\delta\,(+)$, the half-widths towards smaller and larger I, between 1.9 and 2.0 eV. It is considered evidence for the presence of adjacent signals if this sum exceeds 2.2 eV [4]. However, $\delta\,(-)$ of the $4d_{5/2}$ signal of Lu_2O_3 at $I = 203.9$ eV is 2.1 eV. In the earlier lanthanides, $\delta\,(-)$ is far larger. Thus, 2.0 eV for Tm_2O_3 having $I = 184.5$ eV, 3.0 eV for Ho_2O_3 having $I = 169.4$ eV, and the $4d$ signal expands to a broad hill with $\delta\,(-) = 4.4$ eV in Dy_2O_3 and returns to the normal width 1.1 eV at $I = 98.7$ eV in $BaSO_4$. Fadley and Shirley [21] suggest that the anomalous broadening of the $4d$ signals in Lu(III) is due to a short half-life, transforming rapidly via $4f \to 4d$ transitions. In the earlier lanthanides, an additional source of broadening is the interelectronic repulsion separating the many states belonging to the configuration containing the two partly filled shells $4d^9$ and $4f^q$. On the other hand, our $4f$ signals in elements heavier than hafnium have their normal $\delta\,(-)$ close to 1.0 eV.

The possibility of photo-electron spectrometry with the present technique is based on the moderately good monochromacy of the photons corresponding to the width due to Heisenberg's uncertainty principle, combined with the fortunate fact that the radiative half-life of the $(nl)^{-1}$ systems usually is above 10^{-14} sec with exception of cases such as Lu $4d$.

Acknowledgement. I would like to thank my collaborators, Mr. Hervé Berthou and Dr. Lucette Balsenc, for their careful experimental work, and the authors cited in the text for the gift of rare compounds. The Swiss National Science Foundation provided the grant for the instrument.

References

1. Jørgensen, C. K.: Oxidation numbers and oxidation states. Berlin: Springer Verlag 1969.
2. Turner, D. W., Baker, C., Baker, A. D., Brundle, C. R.: Molecular photoelectron spectroscopy. London: Wiley-Interscience 1970.
3. Siegbahn, K., Nordling, C., Johansson, G., Hedman, J., Hedén, P. F., Hamrin, K., Gelius, U., Bergmark, T., Werme, L. O., Manne, R., Baer, Y.: ESCA applied to free molecules. Amsterdam: North-Holland Publishing Co. 1969.
4. Jørgensen, C. K.: Chimia (Aarau, Schweiz) **25**, 213 (1971).
5. Hollander, J. M., Jolly, W. L.: Accounts Chem. Res. **3**, 193 (1970).
6. Jørgensen, C. K.: Progr. inorg. Chem. **12**, 101 (1970).
7. — Berthou, H., Balsenc, L.: J. Fluorine Chem., in press.
8. — Modern aspects of ligand field theory. Amsterdam: North-Holland Publishing Co. 1971.
9. Hedén, P. O., Löfgren, H., Hagström, S. B. M.: Physic. Rev. Letters **26**, 432 (1971).
10. Eckstein, W., Georg, K. G., Heiland, W., Kirschner, J., Müller, N.: Z. Naturforsch. **25a**, 1981 (1970).
11. Jørgensen, C. K.: Orbitals in atoms and molecules. London: Academic Press 1962.
12. Baer, Y., Hedén, P. F., Hedman, J., Klasson, M., Nordling, C., Siegbahn, K.: Physica Scripta (Stockholm) **1**, 55 (1970).
13. Helmer, J. C.: Report from Varian, Palo Alto (Cf.) 20. July 1970.
14. Jørgensen, C. K., Rittershaus, E.: Mat. fys. Medd. Dan. Vid. Selskab **35**, no. 15 (1967).

15. Cook, C. D., Wan, K. Y., Gelius, U., Hamrin, K., Johansson, G., Olsson, E., Siegbahn, H., Nordling, C., Siegbahn, K.: J. Amer. chem. Soc. 93, 1904 (1971).
16. Clark, D. T., Adams, D. B., Briggs, D.: Chem. Comm. (London) 602 (1971).
17. Jørgensen, C. K.: J. Physique (Colloque CNRS no. 196), in press.
18. – Accounts Chem. Res. 4, 307 (1971).
19. Morgan, W. E., Stec, W. J., Albridge, R. G., Van Wazer, J. R.: Inorg. Chem. 10, 926 (1971).
20. Manne, R., Åberg, T.: Chem. Physics Letters 7, 282 (1970).
21. Fadley, C. S., Shirley, D. A.: Physic. Rev. A2, 1109 (1970).

Prof. Ch. K. Jørgensen
Département de Chimie physique
Université de Genève
CH 1211 Genève 4, Switzerland

Theoret. chim. Acta (Berl.) 24, 251—264 (1972)
© by Springer-Verlag 1972

Eine exakte klassische Behandlung der Schwingungs-Translations-Energieübertragung bei symmetrischen Zentralstößen*

G. H. KOHLMAIER, E. O. SIRÉ UND V. HENSEL

Institut und Zentrum für Theoretische Chemie der Universität
6000 Frankfurt am Main 1, Robert-Mayer-Straße 11, Deutschland

Eingegangen am 2. Juli 1971

An Exact Classical Treatment of the Vibration-Translation Energy Transfer in Symmetrical Central Collision

We discuss an exact classical treatment of an inelastic collision between an assumed structureless atom and a harmonic model molecule in any excited vibrational state (described as a system of uncoupled normal vibrations). The collision process is treated onedimensionally – along one of the symmetry axis of the molecule ("symmetrical central collision"); the interaction of the colliding atom with one of the atoms of the molecule which has its equilibrium position on the symmetry axis is assumed to be a linear repulsive pair potential. The derived exact expressions for the energy transfer processes for all possible initial vibrational states allow a discussion of the possible elementary processes (e.g. deactivation processes, multiple collisions); the results are tabulated according to kinematic and energetic factors.

Es wird eine exakte klassische Behandlung eines unelastischen Stoßvorganges zwischen einem strukturlos gedachten Atom und einem beliebig angeregten vielatomigen Modellmolekül, das als System ungekoppelter Normalschwingungen beschrieben wird, diskutiert. Dabei wird der Stoßvorgang eindimensional – entlang einer Symmetrieachse des Moleküls – behandelt („symmetrischer Zentralstoß"); die Wechselwirkung des einfallenden Atoms mit einem Molekülbaustein, der seine Gleichgewichtslage auf der Symmetrieachse hat, wird als lineares repulsives Paarpotential angesetzt. Die bei beliebigen Anfangs-Schwingungszuständen aus den Rechnungen hergeleiteten exakten Ausdrücke für die Energieübertragung gestatten eine Diskussion der möglichen Elementarprozesse (Desaktivierungs-, Mehrfachstöße usw.); die Ergebnisse werden tabellarisch nach kinematischen und energetischen Gesichtspunkten zusammengestellt.

1. Einleitung

In dieser Arbeit wollen wir uns für Molekülstöße zwischen strukturlosen Atomen und vielatomigen Molekülen interessieren, bei denen beim Stoßvorgang eine Energieübertragung zwischen den Freiheitsgraden der relativen Translation und jenen der Schwingungsanregung erfolgt. Da das vielatomige Molekül in harmonischer Näherung beschrieben werden soll, kann man im Rahmen der Theorie kleiner Schwingungen (bei schwach angeregten Systemen) von der Kopplung zwischen Rotationsfreiheitsgraden und inneren Schwingungen absehen. Außerdem wollen wir solche Zentralstöße betrachten, bei denen der Vektor der Relativgeschwindigkeit zu allen Zeitpunkten die Schwerpunkte der sich begegnenden Systeme enthält. Diese Stöße können bei unserer klassischen

---

* Dem Andenken an Prof. Dr. K. H. Hansen gewidmet.

Betrachtung nur entlang einer der möglichen Symmetrieachsen des symmetrischen Moleküls erfolgen; solche eindimensionalen Stöße definieren wir als symmetrische Zentralstöße (S.Z.-Stöße). Auch bei einem rotierenden Molekül kann man einen S.Z.-Stoß definieren, wenn die Rotationsperiode des Moleküls gegenüber der effektiven Stoßzeit genügend groß ist. Wenn das Molekül vor dem S.Z.-Stoß nicht schwingungsangeregt ist, so wird der Stoßvorgang nur solche Normalschwingungen anregen, die die volle Symmetrie der Stoßkonfiguration besitzen [1]. Auch wenn das Molekül allgemein schwingungsangeregt ist, können wir bei genügend schwacher Wechselwirkung die Kopplung mit den bezüglich der Stoßkonfiguration asymmetrischen Normalschwingungen vernachlässigen; bei Paarwechselwirkung zwischen dem stoßenden Atom und einem Molekülbaustein (dem sog. „Endatom"), das seine Gleichgewichtslage auf der Symmetrieachse hat, ist die Annahme dieser Entkopplung bei kleinen Schwingungsamplituden gerechtfertigt. Für diese Arbeit soll eine derartige Paarwechselwirkung angenommen werden; dabei wird die Menge der S.Z.-Stöße bzw. der symmetrischen Moleküle eingeschränkt.

Vom gruppentheoretischen Standpunkt aus werden nur solche Normalschwingungen des Moleküls in der Stoßdynamik berücksichtigt, die sich nach den irreduziblen Darstellungen der Symmetriegruppe des Stoßkomplexes Atom-Molekül klassifizieren lassen. Wie sprechen von bezüglich eines S.Z.-Stoßes aktiven bzw. inaktiven Normalschwingungen [1]. *Per definitionem* ist die Symmetriegruppe im allgemeinen eine Untergruppe der Punktgruppe des symmetrischen Moleküls, da nach unserer Voraussetzung die Stoßachse mit einer der Symmetrieachsen des Moleküls zusammenfallen soll. Man kann sagen, daß der Stoßvorgang im allgemeinen eine niedrigere Symmetrie induziert.

Man muß beachten, daß bezüglich der Symmetrieachse zwei Stoßrichtungen möglich sind, die zwar in Hinsicht auf die Symmetrie äquivalent sind, aber sich in ihren Wechselwirkungen unterscheiden können. Bei stark anisotroper zwischenmolekularer Wechselwirkung, die z. B. bei polaren Molekülen vorliegt, ist es denkbar, daß die Stoßpartner bei der Begegnung eine bevorzugte Orientierung einnehmen. Dieser Sachverhalt ist für Schwingungsanregung bisher experimentell noch nicht untersucht worden. Eine partielle Präorientierung polarer Moleküle läßt sich heute durch Zustandsselektion mit Hilfe von Kombinationen elektrostatischer Multipolfelder vornehmen [2, 3]. Man hat z. B. bei der Reaktion $K + CH_3I \rightarrow KI + CH_3$ die Streuung von K-Atomen an orientierten CH_3I-Molekülen untersucht [4]. Ähnliche Experimente an vororientierten Molekülen, die zu reiner Schwingungsanregung führen, sind bisher noch nicht durchgeführt worden.

Eine eindimensionale Trajektorienbeschreibung kann auch quantentheoretisch begründet werden, wenn einmal die De Broglie-Wellenlänge gegenüber der charakteristischen Wechselwirkungs-Reichweite genügend klein ist, und außerdem im Schwerpunktsystem eine Rückwärtsstreuung vorliegt (Streuwinkel $\vartheta \approx \pi$) [5]. Schöttler und Toennies [6] haben bei Experimenten zur Schwingungsanregung von H_2-Molekülen mit schnellen Li^+-Ionen Rückwärtsstreuung, bei der Rotationsübergänge ausgeschlossen werden, untersucht. Diese Experimente sind in guter qualitativer Übereinstimmung mit der Theorie von Secrest and Johnson [7], die kollineare Stöße von Atomen an zweiatomigen

Tabelle 1. Klassifikation der Stoßprozesse (1-dim. S.Z.-Stöße, repulsives lineares Potential) nach energetischen und kinematischen Gesichtspunkten

Desaktivierungsfunktion $D(\tau_c)$	$D(\tau_c)$	$-\frac{\beta f(\tau_c)}{2\tau(1+\beta_c)}$	$D(\tau_c)$	$\frac{1}{2}\left[1-\frac{\beta f(\tau)}{2\tau(1+\beta_c)}\right] <$	$D(\tau_c)$	1 <		$D(\tau_c)$
Energetik	Desaktivierung	elastischer Stoß	Aktivierungsprozesse			kein Stoß		Desaktivierung
Absorptionskoeffizient	$a<0$	$a=0$	$0<a<1$	$a=1$	$1>a>0$	$a=0$		$a<0$
Relativer kinematischer Faktor	$q>2$	$q=2$	$2>q>1$	$q=1$	$1>q>0$	$q=0$		$q<0$
Kinematik: v_r „vor" v_r „nach"	$v_r(0)<0$ ← → $v_r(\tau_c)>0$	$v_r(0)<0$ ← → $-v_r(0)=v_r(\tau_c)$	$v_r(0)<0$ ← → $v_r(\tau_c)>0$	$v_r(0)<0$ ← $v_r(\tau_c)=0$	$v_r(0)<0$ ← ← $v_r(\tau_c)<0$	$v_r(0)<0$ ← ← $v_r(0)=v_r(\tau_c=0)$	$v_r(0)>0$ → → $v_r(0)=v_r(\tau_c=0)$	$v_r(0)>0$ → → $v_r(\tau_c)>0$
Mechanismen (Bezeichnungen)	Rückwärtsstreuung			Vollständige Energieaufnahme	Mehrfach-Stöße	Stoß erfolgt nachher	keine Begegnung	Aufholungsmechanismus (bei hoch angeregten Molekülen)
	Energieabgabe im Rückprallmechanismus	totale Reflexion	Einfach-Stöße					

Molekülen mit speziellen Modellpotentialen quantentheoretisch exakt behandelt haben. Eine klassische Behandlung der Schwingungsbewegung des Moleküls, dargestellt als System von entkoppelten Normalschwingungen der Frequenz Ω_j, ist dann gerechtfertigt, wenn die relative kinetische Energie gegenüber der der Schwingungsquanten $\hbar\Omega_j$ genügend groß ist.

2. Die exakte Dynamik bei einem linearen abstoßenden Wechselwirkungspotential

a) Der Energieabsorptionskoeffizient

Für die Diskussion der Energieübertragung ist es bequem, wenn man eine mit der relativen Translationsenergie

$$E_0 = \frac{\mu}{2} v_r^2(0) \tag{1}$$

reduzierte Energieübertragungsgröße, den sog. Energieübertragungskoeffizienten a, einführt:

$$a = \frac{\Delta E}{E_0} = \frac{\mu\{v_r^2(0) - v_r^2(\tau_c)\}}{2E_0} . \tag{2}$$

Dabei ist

$$\mu = \frac{m_0 M_S}{m_0 + M_S} \tag{3}$$

die reduzierte Masse des stoßenden Systems mit m_0, der Atommasse und M_S, der Molekülmasse; ΔE ist die absolut auf das Molekül übertragene Energie, die sich als Differenz der kinetischen Energie der Stoßpartner vor und nach dem Stoß ergibt. Mit $v_r = \dot{X}_r$ bezeichnen wir die Relativgeschwindigkeit des stoßenden Atoms bezüglich der Schwerpunktsbewegung des Moleküls. Die entsprechende Differentialgleichung für die relative Translationsbewegung ist gegeben durch

$$\ddot{X}_r(\tau) = \left(\frac{1}{\beta} + \frac{1}{\gamma}\right)\bar{F}[r(\tau)] \tag{4}$$

mit

$$\beta = \frac{m_0}{m_1} \quad (m_1 = \text{Endatommasse}), \tag{5}$$

$$\gamma = \frac{M_S}{m_1}, \tag{6}$$

und

$$\bar{F}[r(\tau)] = -\frac{1}{k_1}\frac{\partial V}{\partial r}, \tag{7}$$

der mit einer charakteristischen Federkonstante k_1 reduzierten Stoßkraft. r ist der Relativabstand des stoßenden Atoms vom Endatom. Für die Berechnung der übertragenen Energie ist die Kenntnis der reduzierten Stoßzeit

$$\tau_c = t_c\omega\left(\omega = \sqrt{\frac{k_1}{m_1}}\right)$$

notwendig. Diese kann ermittelt werden, wenn man die Gleichung für den Relativabstand $r(\tau)$ zwischen dem stoßenden Atom und dem Endatom des Moleküls kennt. In einer anderen Arbeit [1] wurde die entsprechende Integro-Differentialgleichung hergeleitet:

$$\frac{d^2r}{d\tau^2} = \left(1 + \frac{1}{\beta}\right)\bar{F}[r(\tau)] - \frac{d^2u_1}{d\tau^2} + \int_{\tau_0}^{\tau} \dot{A}_{11}(\tau - \tau')\,\bar{F}[r(\tau')]\,d\tau'. \tag{8}$$

Dabei ist u_1, die freie Verschiebungskoordinate des Endatoms bezüglich des Schwerpunktes, gegeben durch:

$$u_1(\tau) = \sum_{\alpha'=1}^{3N} \{A_{1\alpha'}(\tau - \tau_0)\,X_{\alpha'}(\tau_0) + B_{1\alpha'}(\tau - \tau_0)\,\dot{X}_{\alpha'}(\tau_0)\} \tag{9}$$

(N ist die Anzahl der Molekülbausteine) mit den Matrixelementen

$$A_{1\alpha}(\tau) \equiv \sum_{j=2}^{n} \sqrt{\frac{m_\alpha}{m_1}}\, T_{j1}\, T_{j\alpha} \cos(\lambda_j \tau), \tag{10a}$$

$$B_{1\alpha}(\tau) \equiv \sum_{j=2}^{n} \sqrt{\frac{m_\alpha}{m_1}}\, T_{j1}\, T_{j\alpha} \frac{\sin(\lambda_j \tau)}{\lambda_j}. \tag{10b}$$

Dabei sind X_α die einheitlichen kartesischen Koordinaten der Atome; n ist die Anzahl der vollsymmetrischen Normalschwingungen des Stoßkomplexes, der Index $j = 1$ bezieht sich auf die Molekülschwerpunktsbewegung. Mit $\{T_{j\alpha}\}$ bezeichnen wir den Satz der orthogonalen Transformationselemente für die Diagonalisierung der Hamilton-Funktion des Moleküls; die λ_j sind die mit ω reduzierten Normalschwingungsfrequenzen. die m_α stehen für die Massen der Molekülbausteine ($m_{306-2} = m_{3\alpha-1} = m_{3\alpha}$).

Da die erwähnte Integro-Differentialgleichung (8) im allgemeinen nicht geschlossen lösbar ist, weil bei realistisch angenommenen Wechselwirkungspotentialen diese Gleichung nichtlinear wird, haben wir für die Diskussion ein einfaches, in r lineares Modellpotential angenommen:

$$V[r] = -\bar{F}_0 k_1 r H[-r] \tag{11}$$

($\bar{F}_0$ ist die mit k_1 reduzierte konstante Abstoßungskraft, H die Heaviside-Funktion). Mit den Anfangsbedingungen $r(0) = 0$ und $\dot{r}(0) = \bar{v}_r(0) - \dot{u}_1(0)$ ($\bar{v}_r(0)$ ist die reduzierte Relativgeschwindigkeit vor dem Stoß) ergibt die Integration der Integro-Differentialgleichung die Gleichung für die Relativtrajektorie:

$$r(\tau) = [u_1(0) - u_1(\tau)] + \bar{v}_r(0)\,\tau + \frac{1}{2\beta}\,\bar{F}_0\,\tau\left\{\left(1 + \frac{\beta}{\gamma}\right)\tau + \frac{\beta f(\tau)}{2}\right\} \tag{12}$$

$$(\text{für } \tau_c \geqq \tau \geqq 0).$$

In dieser Gleichung ist $f(\tau)$ eine für die Energieübertragung relevante Funktion, die sog. „Schwingungsfunktion“, sie enthält nur die bezüglich der Stoßkonfigura-

tion aktiven Normalschwingungen und ist durch folgenden Ausdruck gegeben:

$$f(\tau)=2\tau\sum_{j\neq 1}^{n} T_{j1}^{2}\left\{\frac{\sin(\lambda_j\tau/2)}{\lambda_j\tau/2}\right\}^{2}. \tag{13}$$

Die reduzierte Stoßzeit τ_c ist über die Forderung $r(\tau_c)\equiv 0$ definiert; τ_c ist dann die kleinste positive Wurzel der folgenden Gleichung:

$$q\equiv\frac{\bar{v}_r(0)-\bar{v}_r(\tau_c)}{\bar{v}_r(0)}=-\frac{\bar{F}_0\left(1+\frac{\beta}{\gamma}\right)\tau_c}{\beta\bar{v}_r(0)}=\frac{2[1-D(\tau_c)]}{\left[1+\frac{\beta f(\tau_c)}{2(1+\beta/\gamma)\tau_c}\right]}. \tag{14}$$

Dabei sind folgende nützliche Größen eingeführt worden: der relative kinematische Koeffizient q als das Verhältnis der Änderung der Relativgeschwindigkeit zur Relativgeschwindigkeit vor dem Stoß und die Desaktivierungsfunktion $D(\tau_c)$

$$D(\tau_c)\equiv\frac{u_1(\tau_c)-u_1(0)}{\bar{v}_r(0)\,\tau_c}, \tag{15}$$

das Verhältnis der über die Stoßzeit gebildeten mittleren - auf die Molekülschwerpunktsbewegung bezogenen - freien Relativgeschwindigkeit des „Endatoms" zur Anfangs-Relativgeschwindigkeit der beiden Stoßpartner.

Der Wertebereich des Energieabsorptionskoeffizienten a ist nach dieser Definition durch $-\infty<a\leqq 1$ gegeben; dabei betrifft $a>0$ die Aktivierungsprozesse. Mit einigen Umformungen führt das Einsetzen von $\bar{v}_r(\tau_c)$ nach (14) in (2) zu der folgenden Darstellung des Absorptionskoeffizienten:

$$\boxed{a=\frac{4}{\left[1+\frac{\beta f(\tau_c)}{2\tau_c(1+\beta/\gamma)}\right]^{2}}\cdot[1-D(\tau_c)]\left[D(\tau_c)+\frac{\beta f(\tau_c)}{2\tau_c(1+\beta/\gamma)}\right]} \tag{16}$$

Da die Stoßzeit τ_c sich allgemein nicht explizit nach den physikalisch zugängigen Größen $\beta,\gamma,\bar{v}_r(0)$ und $\bar{F}_0$ auflösen läßt, ist der Absorptionskoeffizient a nur implizit über (16) und (14) gegeben.

Bevor wir die allgemeinen Eigenschaften und Grenzfälle des Absorptionskoeffizienten (16) diskutieren, wollen wir zunächst einige wichtige *Eigenschaften der Schwingungsfunktion* (13) zusammenstellen:

1. $f(\tau)\geqq 0,$ (17)

2. $f(\tau)\xrightarrow{\tau\to 0}2\tau(1-1/\gamma),$ (18)

3. $f(\tau)\leqq 2\tau(1-1/\gamma),$ (19)

4. $\lim_{\tau\to\infty} f(\tau)\to 0$ (n endlich), (20)

5. $f(\tau)$ beschränkt für alle n und τ [1]. (21)

b) Adiabatische und diabatische Stöße

Diabatische Stöße

Wenn die Wechselwirkungsdauer eines Stoßvorganges viel kleiner als die mittlere Schwingungsdauer der Normalschwingungen des Moleküls ist, bezeichnet man diesen Stoß als diabatisch (bzw. man spricht dann von einem impulsiven oder harten Stoß, wenn die Repulsivkraft sehr groß ist). Die Kreisfrequenz $\omega_1 = \sqrt{k_1/m_1}$, Parameter unserer Theorie, ist ein Maß für die mittlere Frequenz der Normalschwingungen, so daß die Bedingung für einen diabatischen Stoß durch die Ungleichung

$$\tau_c \equiv t_c \omega_1 \ll 1 \tag{22}$$

ausgedrückt werden kann. Für den Grenzfall $\tau_c \to 0$ nimmt die Stoßzeitgleichung (14) mit (18) die folgende Form an:

$$\tau_c \cong -\frac{2\beta \bar{v}_r(0)}{\bar{F}_0} \cdot \frac{[1-D(0)]}{[1+\beta]} \ll 1 . \tag{23}$$

Dabei ist

$$D(0) = \lim_{\tau_c \to 0} D(\tau_c) = \frac{\dot{u}_1(0)}{\bar{v}_r(0)} . \tag{24}$$

Die Desaktivierungsfunktion ist für diabatische Stöße einfach durch das Verhältnis der Relativgeschwindigkeit des Endatoms, bezogen auf den Schwerpunkt des Moleküls, zur Relativgeschwindigkeit der beiden Stoßpartner vor dem Stoß gegeben. Die reduzierte Stoßzeit wird praktisch unabhängig von $\dot{u}_1(0)$, wenn $|D(0)| \ll 1$ gilt.

Adiabatische Stöße

Adiabatisch ist ein Stoß dann, wenn die Stoßzeit im Vergleich mit der mittleren Normalschwingungsdauer groß ist; d. h., wenn man

$$\tau_c \gg 1$$

annehmen kann. Da die Schwingungsfunktion (13) nach (21) beschränkt ist, außerdem (damit keine Mehrfachstöße auftreten) das Massenverhältnis β eine bestimmte Größe nicht überschreiten darf, ist ein adiabatischer Stoß äquivalent mit der Ungleichung

$$\frac{\beta f(\tau_c)}{2(1+\beta/\gamma)\,\tau_c} \ll 1 \tag{25}$$

definiert. Für die Stoßzeit ergibt sich somit aus (14) folgender impliziter Zusammenhang

$$\tau_c = \frac{-2\beta v_r(0)}{\bar{F}_0(1+\beta/\gamma)} [1-D(\tau_c)] . \tag{26}$$

Bei nicht zu hoher Anregung des Moleküls, also bei

$$|D(\tau_c)| \ll 1 , \tag{27}$$

ergibt sich ein von den Anfangsbedingungen unabhängiger Zusammenhang.

c) Die Klassifikation der Stoßprozesse nach energetischen und kinematischen Gesichtspunkten

Schon mit diesem einfachen Modell der repulsiven linearen Abstoßung lassen sich eine Reihe von interessanten Grenzfällen, z. B. die elastischen und unelastischen (Aktivierungs- und Desaktivierungs-) Stöße, diskutieren; dabei wird eine Unterteilung nach kinematischen Gesichtspunkten vorgenommen.

Elastischer Grenzfall

Notwendige, aber nicht hinreichende Bedingung für elastische Stöße ist das Verschwinden des Absorptionskoeffizienten ($a = 0$); aus der Beziehung (16) folgen zunächst zwei verschiedene Möglichkeiten:

$$D(\tau_c) = 1\,, \tag{28a}$$

$$D(\tau_c) = \frac{-\beta f(\tau_c)}{2(1+\beta/\gamma)\,\tau_c}\,. \tag{28b}$$

Die Bedingung (28a) liefert ein triviales Ergebnis; man sieht mit (14), daß $q = 0$ ist, also daß *kein* Stoß stattfindet. Für den Fall, daß die Relativgeschwindigkeit $\bar{v}_r(0)$ negativ ist (Schwerpunkts-Begegnung), erfolgt notwendigerweise ein Stoß zu einem späteren Zeitpunkt. Die Bedingung für einen elastischen Stoß ist also durch die nichttriviale Beziehung (28b) gegeben: mit (14) sieht man, daß bei diesem Fall $q = 2$ ist, d. h. es folgt $\bar{v}_r(\tau_c) = -\bar{v}_r(0)$. Ein elastischer Stoß kann nur bei Schwerpunktsbegegnung stattfinden, denn – wie man formal aus (14) sieht – wegen $q > 0$ muß $\bar{v}_r(0)$ negativ sein (elastische Rückwärtsstreuung).

Aktivierungsprozesse

Die Bedingung für Energieaufnahme ($a > 0$) ergibt mit (16) die folgende Ungleichung

$$(1 - D(\tau_c))\left(D(\tau_c) + \frac{\beta f(\tau_c)}{2(1+\beta/\gamma)\,\tau_c}\right) > 0\,, \tag{29}$$

d. h., es ergibt sich formal

$$-\frac{\beta f(\tau_c)}{2\tau_c(1+\beta/\gamma)} < D(\tau_c) < 1\,. \tag{30}$$

(30) soll als Aktivierungsbedingung bezeichnet werden. Kinematisch bedeutet Energieaufnahme

$$\left|\frac{\bar{v}_r(\tau_c)}{\bar{v}_r(0)}\right| < 1\,. \tag{31}$$

Da $D(\tau_c) < 1$, muß $0 < q < 2$ gelten, d. h. Aktivierung ist nach (14) nur bei einer Schwerpunktsbegegnung ($\bar{v}_R(0) < 0$) möglich.

α) *Totale Energieabsorption.* Vollständige Energieaufnahme (kein echter Atomeinfang, weil ja das Potential repulsiv ist) ist durch $a = 1$ bzw. $\bar{v}_R(\tau_c) = 0$

charakterisiert. Mit $\bar{v}_R(\tau_c) = 0$ folgt aus (14) $q = 1$ und somit die Bedingung

$$D(\tau_c) = \frac{1}{2}\left\{1 - \frac{\beta f(\tau_c)}{2\tau_c(1+\beta/\gamma)}\right\}. \tag{32}$$

Wenn keine innere Anregung vorliegt, setzt man $D(\tau_c) = 0$ und erhält aus (32)

$$1 = \frac{\beta}{2} \cdot \frac{f(\tau_c)}{\tau_c(1+\beta/\gamma)}. \tag{33}$$

Für diabatische Stöße folgt mit (19) die Bedingung

$$\beta = \frac{\gamma}{\gamma - 2}, \quad \gamma > 2; \tag{34}$$

und für schwere Moleküle ($\gamma \to \infty$) $\beta = 1$.

β) *Einfach-Stöße*. Einfachstöße sind durch Vorzeichenumkehr der Relativgeschwindigkeit definiert:

$$\operatorname{sign}\{\bar{v}_R(\tau_c)\} = -\operatorname{sign}\{\bar{v}_R(0)\}, \tag{35}$$

oder mit (31)

$$0 < -\frac{\bar{v}_r(\tau_c)}{\bar{v}_r(0)} < 1,$$

bzw. mit (14) $1 < q < 2$. Berücksichtigen wir die Beziehung (14), so kann man folgern, daß

$$\frac{-\beta f(\tau_c)}{2\tau_c(1+\beta/\gamma)} < D(\tau_c) < \frac{1}{2}\left[1 - \frac{\beta f(\tau_c)}{2(1+\beta/\gamma)\,\tau_c}\right] \tag{36}$$

gelten muß. Speziell folgt für nichtaktivierte Moleküle ($D(\tau_c) = 0$) die Bedingung für Einfach-Stöße:

$$\frac{\beta f(\tau_c)}{2(1+\beta/\gamma)\,\tau_c} < 1. \tag{37}$$

Für starke Stöße ($\tau_c \to 0$) folgt

$$\beta < \frac{\gamma}{\gamma - 2}, \quad \gamma > 2. \tag{38}$$

γ) *Mehrfach-Stöße*. Mehrfachstöße finden dann statt, wenn sich das Vorzeichen der Relativgeschwindigkeit nach dem ersten Stoß nicht ändert, so daß im allgemeinen noch weitere Stoßprozesse folgen können:

$$\operatorname{sign}\{\bar{v}_R(\tau_c)\} = \operatorname{sign}\{\bar{v}_R(0)\}. \tag{39}$$

Analog zu der vorhergehenden Diskussion zeigt man, daß

$$0 < q < 1$$

gilt; somit ergibt sich mit (14) die allgemeine Bedingung für Mehrfachstöße

$$\frac{1}{2}\left(1 - \frac{\beta f(\tau_c)}{2\tau_c(1+\beta/\gamma)}\right) < D(\tau_c) < 1. \tag{40}$$

Speziell für nichtaktivierte Moleküle ($D = 0$) hat man die Ungleichung

$$1 < \frac{\beta}{2\tau_c} \cdot \frac{f(\tau_c)}{(1+\beta/\gamma)} \,. \tag{41}$$

Für harte Stöße ergibt sich die Ungleichung

$$\beta > \frac{\gamma}{\gamma - 2} \quad (\gamma > 2); \tag{42}$$

und für schwere Moleküle ($\gamma \to \infty$) ist $\beta > 1$.

Desaktivierungsstöße

Energieabgabe ist bei einem Stoß durch $a < 0$ definiert. Formal ergibt sich die Desaktivierungsbedingung aus (16) und (14):

$$D(\tau_c) < -\frac{\beta f(\tau_c)}{2\tau_c(1+\beta/\gamma)} \quad (q > 2), \tag{43}$$

$$D(\tau_c) > 1 \qquad (q < 0). \tag{44}$$

Während im Fall (43) eine Desaktivierung bei einer Schwerpunktsbegegnung ($\dot{r}_R(0) < 0$) stattfindet (Rückprallmechanismus), hat man beim Fall (44) eine Desaktivierung bei einer Entfernung der Schwerpunkte (Aufholmechanismus). Natürlich ist dieser zweite Fall nur bei genügend hoch angeregten Molekülen denkbar. In der folgenden Übersichtstabelle haben wir die möglichen Stoßprozesse nach energetischen und kinematischen Gesichtspunkten klassifiziert.

d) Der Grenzfall der harten Abstoßung

Wenn die Stoßzeit t_c sehr viel kleiner als die mittlere charakteristische Schwingungsdauer der Normalschwingungen ist, so gibt es während des Stoßvorgangs keine nennenswerte Energieabwanderung auf das Restsystem. Der Absorptionskoeffizient ergibt sich in der Grenze adiabatischer Stöße unter Berücksichtigung von (19) zu

$$\boxed{a_{\text{diab.}} = \frac{4(1+\beta/\gamma)^2}{(1+\beta)^2}\,(1 - D(0))\left(D(0) + \frac{\beta(1-1/\gamma)}{(1+\beta/\gamma)}\right)} \tag{45}$$

Für kollineare Stöße an zweiatomigen Molekülen ergibt sich als Spezialfall eine Beziehung, die schon von Benson [8] angegeben wurde. Für nichtaktivierte Moleküle großer Masse ($\gamma \to \infty, D(0) = 0$) ergibt sich aus (45) die klassische Beziehung (46), die schon in der Theorie der Akkomodation bei Festkörpern bekannt ist [9, 10]:

$$a_{\text{diab.}}(\gamma \to \infty, D(0) = 0) = \frac{4\beta}{(1+\beta)^2} \tag{46}$$

e) Desaktivierung beim Vorliegen hochangeregter Moleküle (strong collisions)

Da der Ausdruck $\beta f(\tau_c)/2\tau_c(1+\beta/\gamma)$ höchstens in die Größenordnung von eins kommt (bei nicht zu großen β), ist die Bedingung für einen starken Desaktivierungsstoß nach (16) durch

$$|D(\tau_c)| \gg 1 \cdot (|q| \gg 1) \tag{47}$$

gegeben, d. h. die mittlere (über die Stoßzeit τ_c gemittelte) reduzierte freie Verschiebungsgeschwindigkeit des „Endatoms" ist viel größer als die reduzierte Relativgeschwindigkeit der beiden Stoßpartner. Aus (16), (14) und (47) folgt dann

$$a = -q^2 = -\frac{4D^2(\tau_c)}{\left(1+\dfrac{\beta f(\tau_c)}{2(1+\beta/\gamma)\,\tau_c}\right)^2} \ll 0\,. \tag{48}$$

Der Absorptionskoeffizient für "strong collisions" ist also durch das Quadrat des relativen kinematischen Koeffizienten q (14) bzw. im wesentlichen durch das Quadrat der Desaktivierungsfunktion D gegeben. Die Stoßzeit wird näherungsweise nach (14) bestimmt:

$$\tau_c^2 \cong \frac{2\beta}{(1+\beta/\gamma)} \cdot \frac{u_1(\tau_c)-u_1(0)}{\bar{F}_0}\,. \tag{49}$$

Die Stoßzeit, und somit auch der Absorptionskoeffizient a, ist also *unabhängig* von der Relativgeschwindigkeit $\bar{v}_r(0)$ der Stoßpartner vor dem Stoß. Die Stoßzeit τ_c läßt sich aus (49) numerisch bestimmen.

f) Die Energieübertragung S.Z.-Stöße beim Vorliegen einer mikrokanonischen Schwingungsenergieverteilung des vielatomigen Moleküls

Der allgemeine Ausdruck für den Absorptionskoeffizienten (16) soll über die innere Anfangsverteilung des Moleküls, für ein sog. mikrokanonisches Ensemble, gemittelt werden. Eine wesentliche Annahme bei der Durchführung der Mittlung ist, daß die Stoßzeit, die über (14) definiert ist, praktisch von den Anfangsbedingungen des Moleküls unabhängig ist. Diese Vorstellung ist nur dann sinnvoll, wenn das Molekül schwach angeregt ist; eine Ausnahme ist der Grenzfall diabatischer Stöße (Gl. (45)), bei dem die Mittlung exakt durchführbar ist. Im Bereich adiabatischer Stöße ($\tau_c \gg 1$), der über die Forderung (25) definiert wird, ist eine Mittlung bei nicht zu hoch angeregten Molekülen gerechtfertigt. Eine mikrokanonische Verteilung ist hier über die Gleichungen

$$\langle \dot{Q}_j(0)\rangle = \langle Q_j(0)\rangle = 0\,, \tag{50a}$$

$$\langle Q_j(0)\,Q_{j'}(0)\rangle = \delta_{jj'}\langle Q_j^2(0)\rangle\,, \tag{50b}$$

$$\langle \dot{Q}_j(0)\,\dot{Q}_{j'}(0)\rangle = \delta_{jj'}\langle \dot{Q}_j^2(0)\rangle \tag{50c}$$

und die Beziehung (Gleichverteilungsprinzip):

$$\langle \dot{Q}_j^2(0)\rangle = \lambda_j^2\langle Q_j^2(0)\rangle = \frac{\langle E\rangle}{(3N-6)\,k_1} = \text{const} \tag{50d}$$

für alle Normalschwingungen Q_j ($Q_j = \omega \lambda_j$) des Moleküls definiert. Dabei ist $\langle E \rangle$ als Parameter der mikrokanonischen Verteilung die mittlere innere Energie des Systems. Zur Auswertung von $\langle a \rangle_{\mathrm{M.K.}}$ im Rahmen dieser Voraussetzungen sollen nach (16) nur die Erwartungswerte $\langle D(\tau_c) \rangle$ und $\langle D^2(\tau_c) \rangle$ berechnet werden. Da die Anfangsbedingungen linear in die Desaktivierungsfunktion eingehen, ist $\langle D(\tau_c) \rangle = 0$. Zur Auswertung des Streuungsquadrates der Desaktivierungsfunktion sind die Beziehungen (50a–d) zu berücksichtigen, die innere Koordinate $u_1(\tau)$ läßt sich durch die Normalkoordinaten darstellen:

$$u_1(\tau) = \sum_{j=2}^{n} T_{j1} \left\{ Q_j(0) \cos(\lambda_j \tau) + \dot{Q}_j(0) \frac{\sin(\lambda_j \tau)}{\lambda_j} \right\}. \tag{51}$$

Gehen wir mit (51) in (14) ein, so erhalten wir mit Hilfe der Definition der Schwingungsfunktion (13) die Beziehung

$$\langle D^2(\tau_c) \rangle = \frac{f(\tau_c)}{2 \tau_c} \cdot \frac{\langle Q_j^2(0) \rangle}{\bar{v}_r^2(0)}, \tag{52}$$

oder mit (50d) und (1)

$$\langle D^2(\tau_c) \rangle = \frac{\beta f(\tau_c)}{2(1 + \beta/\gamma)\, \tau_c} \cdot \frac{\langle E \rangle}{2(3N-6)\, E_0}. \tag{53}$$

Setzt man (53) in $\langle a \rangle_{\mathrm{M.K}}$ ein, so erhält man den Ausdruck

$$\langle a \rangle_{\mathrm{M.K.}} = \frac{4}{\left(1 + \frac{\beta f(\tau_c)}{2\tau_c (1 + \beta/\gamma)}\right)^2} \cdot \frac{\beta f(\tau_c)}{2\tau_c \left(1 + \frac{\beta}{\gamma}\right)} \left\{ 1 - \frac{\langle E \rangle}{2(3N-6)\, E_0} \right\}. \tag{54}$$

Wenn man dem Molekül die innere Temperatur T_M zuordnet ($\langle E \rangle = (3N-6) \cdot k_B T_M$) und $E_0 \cong k_B T_0/2$ setzt (T_0 entspricht der Temperatur der relativen kinetischen Energie, der „Badtemperatur"), so wird

$$\langle a \rangle_{\mathrm{M.K.}} \sim \frac{T_0 - T_M}{T_0}. \tag{55}$$

Die Beziehung (54) gilt in der Grenze harter Stöße exakt, nämlich:

$$\langle a \rangle_{\mathrm{M.K.,\,diab.}} = \frac{4\beta \left(1 + \frac{\beta}{\gamma}\right)\left(1 - \frac{1}{\gamma}\right)}{(1+\beta)^2} \cdot \left(1 - \frac{\langle E \rangle}{2(3N-6)\, E_0}\right). \tag{56}$$

Besitzt das Molekül eine Schwingungsüberschußenergie E^*, die man auf das thermische Gleichgewicht bezieht, so ist die innere Energie durch

$$\langle E \rangle = (3N-6)\, k_B T_0 + E^* \tag{57}$$

gegeben (T_0 entspricht dabei der thermodynamischen Gleichgewichtstemperatur). Eine „Aktivierung" des Moleküls, die evtl. zu einem unimolekularen Zerfall führen kann, kann außer über eine Energieübertragung bei unelastischen Stößen auch, z. B., über optische Anregung und chemische Aktivierung stattfinden [11]. Nimmt man an, daß nach einem solchen Anregungsprozeß sich eine statistische Verteilung der inneren Molekülenergie zwischen bestimmten aktiven

Freiheitsgraden relativ schnell einstellt, wobei die anharmonischen Kräfte zwischen Normalschwingungen für die innermolekularen Relaxationen im wesentlichen verantwortlich sind, wie es auch in der statistischen Theorie unimolekularer Reaktionen von Rice, Ramsperger, Kassel und Marcus (RRKM-Theorie [12]) angenommen wird, so könnte man versuchen, die anschließend durch Stoß mit Gasatomen stattfindenden Desaktivierungsprozesse mit Hilfe der Beziehungen (54) bzw. (56) zu beschreiben. Sind nicht alle Normalschwingungen aktiv, d. h. aktiv im innermolekularen Relaxationprozess, so kann man in diesen Beziehungen $(3N-6)$ durch die Anzahl $N_{\text{eff.}}$ der aktiven Normalschwingungen ersetzen, so daß eine effektivere Desaktivierung berechnet wird.

Unsere vereinfachenden Modellüberlegungen eines eindimensionalen S.Z.-Stoßes sollen nun zur Interpretation experimenteller Ergebnisse zur chemischen Aktivierung bzw. von Fluoreszenzausbeutemessungen hochangeregter mehratomiger Moleküle herangezogen werden; die Resultate der übertragenen Energien $|\Delta E|$ (in kcal/Mol) werden einem Übersichtsartikel von Kohlmaier [13] entnommen und sind zusammen mit den theoretischen Werten in der folgenden Tab. 2 zusammengestellt:

Tabelle 2

System	$He_{exp.}$	$Kr_{exp.}$	$He_{Theorie}$	$Kr_{Theorie}$
a)	0.085	0.38	0.05	0.04 kcal/Mol
b)	2–3	3–4	0.43	0.52 kcal/Mol
c)	5	5	1.4	2.2 kcal/Mol

a) 3-Dimethylamino-6-aminophthalimid ($3N-6=72$; $E^* \approx 10$ kcal/Mol).
b) Butylradikalsystem ($3N-6=33$; $E^* \approx 43$ kcal/Mol).
c) Cyclopropan ($3N-6=21$; $E^* \approx 100$ kcal/Mol).

Die erwähnten Moleküle werden für zunächst grobe Interpretationen als homogene Ketten mit gleichen Atombausteinen der Masse des Kohlenstoffs angenommen. Wir haben außerdem die Repulsivkraft F_0 über die Steigung des jeweiligen Lennard-Jones-Paarpotentials am elastischen Umkehrpunkt entnommen [1]. Abschätzungen für die hier betrachteten Systeme ergeben, daß für die Energieübertragungsberechnung der Grenzfall diabatischer Näherung (Gl. (56)) angenommen werden kann. Während die statistische Theorie [14] allgemein zu hohe Energieübertragungswerte liefert, außerdem keine quantitative Unterscheidung der Systeme mit den Stoßpartnern He und Kr liefern kann [13], ergeben die hier angegebenen Schätzwerte der stark vereinfachenden Modellbetrachtungen allgemein zu kleine Werte. Wenn man die Komplexität der realen Systeme bedenkt, außerdem berücksichtigt, daß die gemessenen Energieübertragungswerte statistische Mittelwerte über verschiedene Begegnungsmöglichkeiten (Geometrie, Mehrfach-Wechselwirkungen usw.) darstellen, so sind die Resultate der stark modifizierten vereinfachenden Modellbetrachtung verständlich. Eine Verbesserung der Theorie eindimensionaler Zentralstöße unter Berücksichtigung von mehreren Paarwechselwirkungen realistischer Wechselwirkungspotentiale ist in Vorbereitung. Die wahrscheinlich in Zukunft möglichen unelastischen Molekülstrahlexperimente an gerichteten Molekülen lassen erwarten, daß sich direktere Vergleichsmöglichkeiten zwischen Theorie und Experiment ergeben.

Literatur

1. Siré, E. O.: Dissertation, Frankfurt/Main 1971.
2. Kramer, K. H., Bernstein, R. B.: J. chem. Physics **42**, 767 (1965).
3. Toennies, J. P.: Z. Physik **182**, 257 (1965).
4. Brocks, P. R., Jones, E. M.. J. chem. Physics **45**, 3449 (1966).
5. Wu, T. Y., Ohmura, T.: Quantum theory of scattering. New Jersey: Prentice Hall, Englewood Cliffs 1962
6. Schöttler, J., Toennies, J. P.: Z. Physik **214**, 472 (1968).
7. Secrest, D., Johnson, B. R.. J. chem. Physics **45**, 4556 (1966).
8. Benson, S. W.: The Foundations of Chemical Kinetics. New York: Mc Graw-Hill 1960.
9. Gilbey, D. M.: J. phys. chem. Solids **23**, 1453 (1962).
10. Goodman, F. O.. J. phys. chem. Solids **23**, 1269 (1962).
11. Troe, J.: Ber. Bunsenges. physik. Chemie **72**, 908 (1968).
12. Marcus, R. A. Unimolecular Reaction Rate Theory. In: Chemische Elementarprozesse, Ed. H. Hartmann Berlin. Springer-Verlag 1968.
13. Kohlmaier, G. H.: Zwischenmolekulare Energieübertragung. In: Chemische Elementarprozesse, Ed. H. Hartmann. Berlin: Springer-Verlag 1968.
14. Hoare, M. Molecular Physics **4**, 465 (1961).

Dozent Dr. G. Kohlmaier
Institut und Zentrum für Theoretische Chemie
der Universität
D-6000 Frankfurt (Main) 1, Robert-Mayer-Str. 11
Deutschland

Theoret. chim. Acta (Berl.) 24, 265 –270 (1972)
© by Springer-Verlag 1972

Reversible Energy Transfer

GERALD B. PORTER* **

Centro di Studio sulla Fotochimica e Reattività
degli Stati Eccitati dei Composti di Coordinazione del C.N.R.,
Istituto Chimico dell'Università, Ferrara, Italy

Received August 23, 1971

Analysis of the transient and steady-state kinetics of reversible energy transfer shows that while the interpretation of lifetime measurements is difficult unless the donor and acceptor lifetimes are appreciably different, quantum yield measurements are relatively easy to interpret.

Die Analyse der Kinetik der Übergangszustände und der stationären Zustände der reversiblen Energieübertragung zeigt, daß im Gegensatz zu einer schwierigen Interpretation der Messungen der Lebensdauer – es sei denn die Lebensdauer von Donor und Acceptor sind wesentlich voneinander verschieden – die Messungen der Quantumausbeute verhältnismäßig einfach zu interpretieren sind.

L'analyse de la cinétique de l'état transitoire et de l'état stationnaire du transfert réversible d'énergie montre que, si l'interprétation des mesures de durée de vie est difficile, à moins queles durées de vie du donneur et de l'accepteur soient très différentes, il est par contre relativement facile d'interpréter les mesures de rendement quantique.

Energy transfer has been extensively used to investigate the details of photochemical reactions [1]. The population or depopulation of specific excited electronic states of molecules can give valuable information about the role those states assume in the mechanism. It has been suggested that transfer from one triplet excited state molecule to another, for ground singlet state molecules, is diffusion controlled in fluid solution, provided the donor excited state lies at a higher energy than that of the acceptor.

Bäckström and Sandros [2] and Sandros [3] have described the theoretical and experimental results for systems in which energy transfer is reversible. They found that reverse energy transfer may have to be taken into account when the difference in energy of the donor and acceptor excited states is less than about 2000 cm^{-1}. In an extreme case, Sandros [3] observed back energy transfer from pyrene ($E_T = 16930\,\text{cm}^{-1}$) to the nominal donor, biacetyl ($E_T = 19700\,\text{cm}^{-1}$) even though it is endothermic by almost 3000 cm^{-1} and has a rate constant five orders of magnitude smaller than that for energy transfer from biacetyl to pyrene.

Nordin and Strong [4] have emphasized the importance of the relative donor and acceptor excited state lifetimes on reversible energy transfer. They analyzed the transient kinetics for various lifetimes and energy separations of the excited states in terms of a single donor lifetime, representing the best fit to the calculated decay curves.

The general effect of back energy transfer is to reduce the value of the apparent quenching constant. Nordin and Strong [4] even found negative values under certain conditions. As the quenching constant is an important parameter in the interpretation of energy transfer data, it is essential to understand the conditions under which back energy transfer becomes important as well as the effect it has on rate measurements.

---

* On leave from the Department of Chemistry, University of British Columbia, Vancouver, Canada, 1970–71.

** Dedicated to the memory of Professor K. H. Hansen.

In the following, both the transient and steady-state kinetics of such systems are examined to establish the conditions of lifetimes and energy transfer rate constants in which reversible transfer must be considered. In addition, the effect of reversible energy transfer on the evaluation of rate constants from transient and steady-state data in terms of the normal Stern-Volmer treatment is explored. These problems assume greater importance still when paramagnetic species are used as donors and acceptors, for then spin correlation rules imply that efficient energy transfer may occur from the fluorescent state of one molecule to the phosphorescent state of another as well as the reverse.

General Mechanism

To preserve an element of simplicity, the mechanism can be limited to four steps following excitation:

$$A \xrightarrow[\Phi]{h\nu} A^* \xrightarrow{k_1} A\,, \tag{1}$$

$$A^* + B \xrightarrow{k_{et}} A + B^*\,, \tag{2}$$

$$B^* + A \xrightarrow{k_{ret}} B + A^*\,, \tag{3}$$

$$B^* \xrightarrow{k_2} B\,. \tag{4}$$

Steps 1 and 4 include all unimolecular transformations which depopulate A^* and B^*. Thus k_1 and k_2 represent sums of rate constants, including the radiative rate constants k_r^A and k_r^B for the donor and acceptor, respectively. Normally A^* and B^* are the lowest triplet states for ground singlet state molecules, but may be other multiplicities for paramagnetic molecules. No bimolecular steps involving two excited state molecules have been included in this simple mechanism, but they could be put in without major change [3].

Transient Kinetics

The differential equations for the two species A^* and B^*, following a delta function excitation:

$$\frac{d[A^*]}{dt} = k_{ret}[A]\,[B^*] - (k_1 + k_{et}[B])\,[A^*] \tag{5}$$

$$\frac{d[B^*]}{dt} = k_{et}[B]\,[A^*] - (k_2 + k_{ret}[A])\,[B^*] \tag{6}$$

have the solutions:

$$\begin{aligned}[A^*] = \frac{[A^*]_0}{\lambda_1 - \lambda_2}\,\{&(\lambda_1 - k_2 - k_{ret}[A])\exp(-\lambda_1 t)\\ &+ (k_2 + k_{ret}[A] - \lambda_2)\exp(-\lambda_2 t)\}\,,\end{aligned} \tag{7}$$

$$[B^*] = \frac{k_{et}[A^*]_0\,[B]}{\lambda_1 - \lambda_2}\,\{\exp(-\lambda_2 t) - \exp(-\lambda_1 t)\} \tag{8}$$

in which λ_1 and λ_2 are the roots of:

$$(\lambda - k_2 - k_{\mathrm{ret}}[A])\,(\lambda - k_1 - k_{\mathrm{et}}[B]) = k_{\mathrm{et}}[B]\,k_{\mathrm{ret}}[A]\,. \tag{9}$$

They have therefore the values given by:

$$\begin{aligned} 2\lambda = {} & (k_1 + k_{\mathrm{et}}[B] + k_2 + k_{\mathrm{ret}}[A]) \\ & \pm \{(k_1 + k_{\mathrm{et}}[B] - k_2 - k_{\mathrm{ret}}[A])^2 + 4k_{\mathrm{et}}[B]\,k_{\mathrm{ret}}[A]\}^{1/2}\,. \end{aligned} \tag{10}$$

It will be assumed in the treatment that λ_1 is the larger of the two roots. From Eq. (9), a general relationship may be found

$$\lambda_1 + \lambda_2 = k_1 + k_{\mathrm{et}}[B] + k_2 + k_{\mathrm{ret}}[A] \tag{10}$$

which connects the two lifetimes, $1/\lambda_1$ and $1/\lambda_2$, with the rate constants of the mechanism.

The concentration of the donor excited state, according to Eq. (7), decreases rapidly at first with a lifetime $1/\lambda_1$, then more slowly, eventually with lifetime $1/\lambda_2$. However, only when λ_1 and λ_2 have values of a similar order of magnitude would both parts of the decay be observable; otherwise either the first or the second term dominates the decay. On the other hand, if λ_1 and λ_2 have comparable values, the experimentally measured decay would be difficult to resolve into its two components.

At first, the concentration of the acceptor excited state increases with time, reaches a maximum value at

$$t_{\max} = \frac{\ln(\lambda_1/\lambda_2)}{\lambda_1 - \lambda_2}$$

then decays finally with a lifetime $1/\lambda_2$. Both λ_1 and λ_2 should be measurable from the growth and decay of the acceptor excited state, provided time resolution is adequate.

When both λ_1 and λ_2 can be measured, for example, from the acceptor, together with k_1 and k_2 (which are the reciprocals of the lifetimes of donor and acceptor excited states in the absence of acceptor and donor, respectively), the rate constants for forward and back energy transfer can be evaluated from the following equations, derived from Eqs. (9) and (10):

$$k_{\mathrm{et}}[B] = \frac{(\lambda_1 - k_1)(k_1 - \lambda_2)}{(k_1 - k_2)}\,, \tag{11}$$

$$k_{\mathrm{ret}}[A] = \frac{(\lambda_1 - k_2)(\lambda_2 - k_2)}{(k_1 - k_2)}\,. \tag{12}$$

In the case that $k_1 \gg k_2$ and also $k_1 \gg k_{\mathrm{ret}}[A]$, Eq. (9) reduces to

$$\lambda_1 = k_1 + k_{\mathrm{et}}[B]\,, \tag{13}$$

$$\lambda_2 = k_2 + k_{\mathrm{ret}}[A]\,(k_1/\lambda_1) \tag{14}$$

and the second term of Eq. (7) becomes negligible. Thus, even when there is effective back energy transfer, provided that the donor excited state has a much shorter lifetime than the acceptor excited state, the former decays with a single lifetime $1/\lambda_1$, independent of $[A]$ and thus independent of whether or not back energy transfer in fact occurs. This is so because, while the second term of Eq. (7) may have an appreciable integrated value, its contribution to $[A^*]$ will be orders of magnitude smaller than that of the first term at any one time. The longer lifetime observed for $[B^*]$ after the maximum will, however, be a function of both acceptor and donor concentrations.

For the opposite situation, that the donor excited state is longer lived than the acceptor ($k_2 \gg k_1$ and $k_2 \gg k_{et}[B]$), Eq. (9) becomes:

$$\lambda_1 = k_2 + k_{ret}[A], \tag{15}$$

$$\lambda_2 = k_1 + k_{et}[B]\,(k_2/\lambda_1). \tag{16}$$

Now it is the first term of Eq. (7) that becomes negligible. Except for the initial "grow-in" of B^* with lifetime $1/\lambda_1$, both donor and acceptor excited states decay with the same lifetime, $1/\lambda_2$. This latter lifetime will depend on both donor and acceptor concentrations. Hence a simple Stern-Volmer plot of λ_2 against $[B]$ cannot give the correct energy transfer rate constant, k_{et}, unless it is corrected by the ratio k_2/λ_1.

The situation is more complicated when the lifetimes of donor and acceptor excited states are similar, especially if the forward and reverse energy transfer steps also have similar rates. The behavior of $[A^*]$ and of $[B^*]$ with time, calculated from Eqs. (7) and (8) with $k_1 = 3k_2$, $k_{ret}[A] = k_{et}[B] = 1.5k_2$, is shown in Fig. 1. It is evident that the evaluation of λ_1 and λ_2 from the decay of $[A^*]$ would be difficult unless the data were extremely precise and covered a wide range of $[A^*]$. With limited data, an exponential could be fitted to the decay curve, as shown by the dotted line in Fig. 1, with a lifetime between $1/\lambda_1$ and $1/\lambda_2$. This apparent lifetime is, however, virtually useless. But if $[B^*]$ can be followed, the curve should be resolvable into the two contributions, and both λ_1 and λ_2 can be determined.

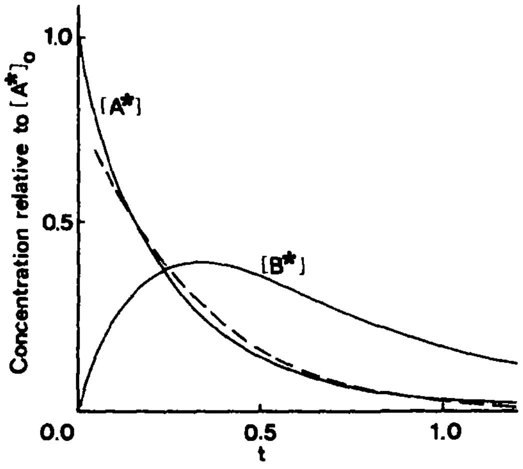

Fig. 1. Decay curves for $[A^*]$ and $[B^*]$ from Eqs. (7) and (8), with the parameters: $k_1 = 3k_2$, $k_{ret}[A] = k_{et}[B] = 1.5k_2$. The dotted line shows a reasonable fit of a single exponential to the curve for $[A^*]$

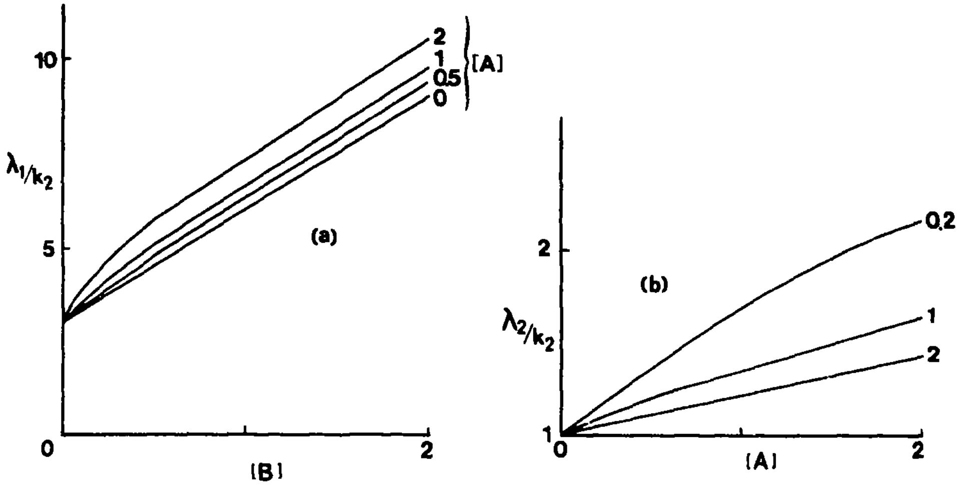

Fig. 2. (a) The dependence of λ_1/k_2 on the concentration of the acceptor species; (b) the dependence of λ_2/k_2 on the donor concentration, calculated from Eq. (10), with $k_1 = 3k_2$, $k_{et} = 3k_2$, and $k_{ret} = k_2$. Concentrations are in arbitrary units

In Fig. 2 are shown the variations of λ_1 and λ_2 with $[A]$ and $[B]$. The normal Stern-Volmer plot of λ_1 against $[B]$ in Fig. 2(a) gives approximately the correct value of k_{et} from its slope at relatively high acceptor concentration, but the curves are displaced upward as $[A]$ increases, and thus as back energy transfer assumes greater importance. The apparent intercepts of the straight portions are no longer equal to $1/k_1$. As can be seen from Fig. 2(b), λ_2 is a strong function of both $[A]$ and $[B]$.

As a rough guide, if $k_1 \geqq 10(k_2 + k_{ret}[A])$, Eq. (13) will hold approximately and the slope of λ_1 against $[B]$ will be within a few percent of the value for k_{et}, and the slope will not depend on $[A]$.

Steady-State Kinetics

The differential equations for the intermediates in Eqs. (1)–(4) on continuous illumination with absorbed intensity I_a are:

$$\frac{d[A^*]}{dt} = \Phi I_a + k_{ret}[A][B^*] - (k_1 + k_{et}[B])[A^*], \tag{17}$$

$$\frac{d[B^*]}{dt} = k_{et}[B][A^*] - (k_2 + k_{ret}[A])[B^*]. \tag{18}$$

With the assumption of a steady-state for both $[A^*]$ and $[B^*]$, the solutions are:

$$[A^*]_{ss} = \frac{\Phi I_a(k_2 + k_{ret}[A])}{k_1(k_2 + k_{ret}[A]) + k_{et}[B]\,k_2}, \tag{19}$$

$$[B^*]_{ss} = \frac{\Phi I_a k_{et}[B]}{k_1(k_2 + k_{ret}[A]) + k_{et}[B]\,k_2}. \tag{20}$$

If these equations are then cast in the form appropriate to a Stern-Volmer treatment, for example, based on quenched emission of A^* and sensitized emission of B^*, the result is:

$$\frac{\Phi_0^A}{\Phi^A} = 1 + \left\{\frac{k_2}{(k_2 + k_{\mathrm{ret}}[A])}\right\}\left\{\frac{k_{\mathrm{et}}}{k_1}\right\}[B] \tag{21}$$

for the donor, and for the acceptor:

$$\frac{1}{\Phi^B} = \frac{1}{k_r^B \Phi}\left\{\frac{k_1(k_2 + k_{\mathrm{ret}}[A])}{k_{\mathrm{et}}[B]} + k_2\right\} \tag{22}$$

Eqs. (21) and (22) show that, unlike the case of lifetime measurements, steady-state quantum yields will have linear Stern-Volmer plots: Φ_0^A/Φ^A against $[B]$ for the donor emission and $1/\Phi^B$ against $1/[B]$ for the acceptor emission. The apparent Stern-Volmer quenching constant, obtained from the slope and the intercept/slope, respectively, for these two plots, will in general be given by:

$$K_{SV} = \left\{\frac{k_2}{(k_2 + k_{\mathrm{ret}}[A])}\right\}\frac{k_{\mathrm{et}}}{k_1}$$

when back energy transfer occurs, rather than the usual k_{et}/k_1.

However, it is then a simple matter to extract the true rate constant ratios: k_1/k_{et} and k_2/k_{ret}, from the data by a plot of the reciprocal of K_{SV} against $[A]$. The intercept of this plot is k_1/k_{et} and the slope/intercept is k_{ret}/k_2.

Conclusion

Reversible energy transfer can be recognized from the results of transient measurements by a dependence of the longer decay lifetime on acceptor concentration, as in Eqs. (14) and (16). In that case, interpretation of the results will be complicated unless the donor lifetime is appreciably shorter than that of the acceptor.

These complications do not arise with steady-state data, although the apparent Stern-Volmer constant will be a function of acceptor concentration if reverse energy transfer occurs to any appreciable extent.

References

1. For a review, see: Lamola, A. A.: In: Technique of organic chemistry, Vol. XIV, Energy transfer and organic photochemistry. Ed. by P. A. Leermakers and A. Weissberger, p. 18 132. New York: Interscience 1969.
2. Bäckström, H. L. J., Sandros, K.: Acta chem. scand. **16**, 958 (1962).
3. Sandros, K.: Acta chem. scand. **18**, 2355 (1964).
4. Nordin, S., Strong, R. L.: Chem. Physics Letters **2**, 429 (1968).

Prof. Gerald B. Porter
Department of Chemistry
University of British Columbia
Vancouver, Canada

Theoret. chim. Acta (Berl.) 24, 271--282 (1972)
© by Springer-Verlag 1972

Constants of Motion for Separable One-Particle Problems with Cylinder Symmetry*

KLAUS HELFRICH
Institute of Theoretical Chemistry, University of Frankfurt, Germany

Received November 12, 1971

For those cylindrically symmetrical one-particle problems which are separable in either prolate spheroidal or parabolic coordinates, a quantum mechanical constant of the motion and its classical analogue are independently derived and compared. The quantum mechanical constant of the motion is a sum of an operator depending only on the coordinate system chosen and possessing a simple physical significance and of a second operator uniquely linked with the special separable potential chosen. The superposition principle for separable potentials also holds for the corresponding operators mentioned before. This constant of the motion does not result from spatial symmetry but from separability. It also must, however, be taken into account for the classification of energy levels depending on a parameter to avoid violations of the non-crossing rule. The formal theory given is applied to several special problems.

Für diejenigen zylindersymmetrischen Einteilchen-Probleme, die sich in elliptischen oder parabolischen Koordinaten separieren lassen, werden eine quantenmechanische Erhaltungsgröße und ihr klassisches Analogon unabhängig voneinander abgeleitet und verglichen. Die quantenmechanische Erhaltungsgröße ist jeweils die Summe eines Operators, der nur vom gewählten Koordinatensystem abhängt und eine einfache physikalische Bedeutung besitzt, und eines zweiten Operators, der eindeutig mit dem gewählten separierbaren Potential verknüpft ist. Das Superpositionsprinzip für separierbare Potentiale überträgt sich auf die zugehörigen, eben genannten Operatoren. Diese Erhaltungsgröße folgt nicht aus der räumlichen Symmetrie. Sie muß jedoch bei der Klassifikation von Energietermen, die von einem Parameter abhängen, mitberücksichtigt werden, um scheinbare Verletzungen der Nichtkreuzungsregel zu vermeiden. Die formale Theorie wird auf mehrere spezielle Probleme angewandt.

Introduction

The problem of classifying the electronic states of atomic and molecular systems with several electrons and of finding the terms resulting from a given electronic configuration has been solved by several authors. The most elegant, group theoretical solution of the latter problem for molecules was certainly given by Hansen [1, 2]. All solutions of this problem are essentially based on the concept of the spatial symmetry group, the largest subgroup of the full rotation-reflection group O_3 consisting of operations which leave the Hamiltonian invariant, and on the properties of its irreducible representations.

This concept of spatial symmetry, however, fails to be efficient for some one-electron problems. "Accidental" degeneracies of energy terms occur for the two- and three-dimensional isotropic harmonic oscillator and for the hydrogen atom; energy levels belonging to different irreducible representations of the spatial symmetry group coincide[1]. In the H_2^+-problem, the energy terms $2s\sigma_g$ and $3d\sigma_g$, belonging to the same irreducible representation σ_g^+ of the *spatial* symmetry group $D_{\infty h}$ do cross in spite of the non-crossing rule. When an expression like $Q/(r_1 \cdot r_2)$ (which preserves separability) is added to the two-centre Coulomb potential $Z_1/r_1 + Z_2/r_2$, the energy levels $2s\sigma_g$ and $3d\sigma_g$ still cross [3]. This last example of degeneracy induced us to study separability, a common feature of all problems mentioned above, in order to try to relate it to a higher symmetry not included in spatial symmetry. Of greatest importance for our aim there proved to be those coordinate systems in which the solutions of the Schrödinger equation separate completely in the spatial variables, but only partially in the separation constants (class B of Morse's classification [5, p. 518]). The most important coordinate systems of this class are the (rotational) prolate spheroidal and the (rotational) parabolic systems.

---

* Dedicated to the memory of Professor K. H. Hansen.

Cylindrically Symmetrical Potentials Separable in Prolate Spheroidal Coordinates

1. Prolate spheroidal coordinates μ, ν, φ are as usually defined by

$$\mu = \frac{r_1 + r_2}{R} \qquad \nu = \frac{r_1 - r_2}{R} \qquad \varphi \tag{1}$$

and are related to cylinder coordinates ϱ, φ, z by

$$\varrho = \sigma \sqrt{(\mu^2 - 1)(1 - \nu^2)} \qquad z = \sigma \mu \nu \qquad \varphi = \varphi \,. \tag{2}$$

The most general cylindrically symmetrical potential energy V for which the Schrödinger equation

$$\left\{ -\frac{\hbar^2}{2M} \Delta + V \right\} \chi = \varepsilon \chi \tag{3}$$

separates in prolate spheroidal coordinates is of the form

$$V(\mu, \nu) = \frac{V_1(\mu) + V_2(\nu)}{\mu^2 - \nu^2} \tag{4}$$

according to Eisenhart [4] or Morse and Feshbach [5, p. 661]. Let us first construct a classical constant of the motion and then return to quantum mechanics.

An easy calculation shows:

Canonical momenta p_μ, p_ν, p_φ which are conjugated to the variables μ, ν, φ are

$$\begin{aligned} p_\mu &= M\sigma^2 \frac{\mu^2 - \nu^2}{\mu^2 - 1} \dot{\mu} \\ p_\nu &= M\sigma^2 \frac{\mu^2 - \nu^2}{1 - \nu^2} \dot{\nu} \\ p_\varphi &= M\sigma^2 (\mu^2 - 1)(1 - \nu^2)\dot{\varphi} \,. \end{aligned} \tag{5}$$

---

[1] H. V. McIntosh gives an excellent survey in his paper "Symmetry and degeneracy" contained in the second volume of "Group theory and its applications", ed. E. M. Loebl, New York: Acad Press 1971.

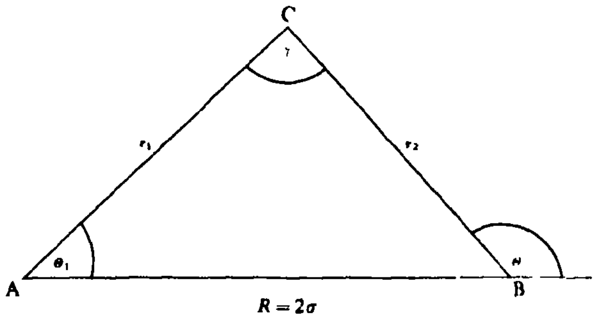

Fig. 1

The Hamiltonian function for a particle with mass M and potential energy V is

$$H(\mu, \nu, \varphi; p_\mu, p_\nu, p_\varphi) = \frac{1}{2M\sigma^2(\mu^2-\nu^2)}\left\{(\mu^2-1)\,p_\mu^2 + (1-\nu^2)\,p_\nu^2 + \left(\frac{1}{\mu^2-1} + \frac{1}{1-\nu^2}\right)p_\varphi^2\right\} + V \tag{6}$$

(see, for instance [6, p. 178]).

As the Schrödinger equation with V given according to Eq. (4) separates, so does the Hamilton-Jacobi Eq. [4a]:

$$H\left(\mu, \nu, \varphi; \frac{\partial S_0}{\partial \mu}, \frac{\partial S_0}{\partial \nu}, \frac{\partial S_0}{\partial \varphi}\right) = E \tag{7}$$

for the characteristic function $S_0(\mu, \nu, \varphi) = S + E \cdot t$. With the ansatz

$$S_0(\mu, \nu, \varphi) = p_\varphi \cdot \varphi + S_1(\mu) + S_2(\nu), \tag{8}$$

where p_φ is a first constant of the motion, we obtain from (7):

$$(\mu^2-1)\left(\frac{dS_1}{d\mu}\right)^2 + \frac{p_\varphi^2}{\mu^2-1} + 2M\sigma^2(V_1(\mu) - E(\mu^2-1)) = \beta \tag{9a}$$

$$(1-\nu^2)\left(\frac{dS_2}{d\nu}\right)^2 + \frac{p_\varphi^2}{1-\nu^2} + 2M\sigma^2(V_2(\nu) - E(1-\nu^2)) = -\beta. \tag{9b}$$

Note that β is not uniquely defined by (4) and (7). Eqs. (9a) and (9b) may be multiplied with a common factor independent of μ, ν, φ, and if a constant independent of μ, ν, φ (but perhaps depending on E and p_φ) is added to β, it cancels when (9a) and (9b) are added to give Eq. (5). In fact, (9a) and (9b) realize a convention frequently used.

We now replace $\partial S_0/\partial\mu = dS_1/d\mu$ by p_μ and $\partial S_0/\partial\nu = dS_2/d\nu$ by p_ν in (9a) and (9b) respectively, then multiply (9a) with $1-\nu^2$ and (9b) with $-(\mu^2-1)$. Adding and thus eliminating E, we finally obtain

$$\beta = \frac{(\mu^2-1)(1-\nu^2)}{\mu^2-\nu^2}(p_\mu^2 - p_\nu^2) + \left(\frac{1}{\mu^2-1} - \frac{1}{1-\nu^2}\right)p_\varphi^2 + 2M\sigma^2\frac{(1-\nu^2)\,V_1(\mu) - (\mu^2-1)\,V_2(\nu)}{\mu^2-\nu^2}. \tag{10}$$

The first two terms of this expression (first line) are independent of the special potential chosen.

Using the relations

$$L^2 = \frac{\mu^2+\nu^2-1}{(\mu^2-1)(1-\nu^2)}\, p_\mu^2 + \frac{(\mu^2-1)(1-\nu^2)}{(\mu^2-\nu^2)^2}(\mu p_\mu - \nu p_\nu)^2\,, \tag{11}$$

$$p_\varrho = M\dot{\varrho} = \frac{(\mu^2-1)(1-\nu^2)}{\sigma(\mu^2-\nu^2)}(\mu p_\mu - \nu p_\nu) \tag{12}$$

for the square of angular momentum $\vec{L} = \vec{r} \times \vec{p}$ and the momentum p_ϱ conjugate to $\varrho = \sqrt{x^2+y^2}$, we finally obtain[2].

$$\begin{aligned} \beta &= -L^2 + \sigma^2\left(p_\varrho^2 + \frac{p_\varphi^2}{\varrho^2}\right) + 2M\sigma^2\,\frac{(1-\nu^2)\,V_1(\mu) - (\mu^2-1)\,V_2(\nu)}{\mu^2-\nu^2} \\ &= -L^2 + \sigma^2(p_x^2+p_y^2) + \beta_{\text{pot}}\,. \end{aligned} \tag{13}$$

The linear combination of two separable potential energies V, V' is again a separable potential V'', so the domain of separable potentials is a function space. As the potential part β_{pot} of β is linear in V_1 and V_2, the process of constructing $\beta_{\text{pot}} = \tilde{V}$ from V is a linear mapping of a function space $\{V\}$ on a second function space $\{\beta_{\text{pot}}\}$:

$$\begin{aligned} \widetilde{cV} &= c\tilde{V} \\ \widetilde{V+V'} &= \tilde{V} + \tilde{V}' \end{aligned} \qquad (c \in \mathbb{R})\,. \tag{14}$$

2. Let us now return to quantum mechanics. The Schrödinger Eq. (4) separates with the ansatz

$$\chi(\mu, \nu, \varphi) = F(\mu)\, G(\nu)\, e^{im\varphi} \tag{15}$$

and gives

$$\left\{h^2\left(-\frac{\partial}{\partial\mu}(\mu^2-1)\frac{\partial}{\partial\mu} + \frac{m^2}{\mu^2-1}\right) + 2M\sigma^2(V_1(\mu) - \varepsilon(\mu^2-1)) - A'\right\}F(\mu) = 0 \tag{16a}$$

$$\left\{h^2\left(-\frac{\partial}{\partial\nu}(1-\nu^2)\frac{\partial}{\partial\nu} + \frac{m^2}{1-\nu^2}\right) + 2M\sigma^2(V_2(\nu) - \varepsilon(1-\nu^2)) + A'\right\}G(\nu) = 0\,. \tag{16b}$$

Note the similarity of (16) with (9).

Now (16a) is multiplied with $(1-\nu^2)\,G(\nu)\,e^{im\varphi}$ and (16b) is multiplied with $-(\mu^2-1)\,F(\mu)\,e^{im\varphi}$. We add the results and thus eliminate ε. Besides we replace $m^2 e^{im\varphi}$ by $-\frac{\partial^2}{\partial\varphi^2}e^{im\varphi}$, use (15) and solve for the separation constant A'.

---

[2] Note that in [6], p. 180, p_ϱ^2 has to be replaced by $p_x^2 + p_y^2$.

The final result has the form

$$\mathbf{A}'\chi = A'\chi \tag{17}$$

where

$$\begin{aligned}\mathbf{A}' = {} & \frac{\hbar^2}{\mu^2-\nu^2}\left\{-(1-\nu^2)\frac{\partial}{\partial\mu}(\mu^2-1)\frac{\partial}{\partial\mu}+(\mu^2-1)\frac{\partial}{\partial\nu}(1-\nu^2)\frac{\partial}{\partial\nu}\right\}\\ & -\hbar^2\left(\frac{1}{\mu^2-1}-\frac{1}{1-\nu^2}\right)\frac{\partial^2}{\partial\varphi^2}+2M\sigma^2\frac{(1-\nu^2)\,V_1(\mu)-(\mu^2-1)\,V_2(\nu)}{\mu^2-\nu^2}.\end{aligned} \tag{18}$$

From the work done by Cordes [7] on separable partial differential equations it follows that the "separation operator" $\mathbf{A}'$, the eigenvalue of which is the separation constant A', commutes with the Hamiltonian $\mathbf{H}$. Therefore, as already Coulson [8] pointed out for a special case, the eigenvalue A' of $\mathbf{A}'$ has to be used as a further classifying property of a one-particle state besides of the corresponding irreducible representation of the spatial symmetry group and the corresponding one-electron energy ε. A complete set of quantum mechanical constants of the motion which commute with each other is provided by $\mathbf{L}_z$, $\mathbf{A}'$, and (of course) $\mathbf{H}$.

A somewhat tedious calculation – which has, in fact, already been performed by Erikson and Hill [9] for the special case of the two-centre Coulomb potential – gives the final result that

$$\begin{aligned}\mathbf{A}' &= -\mathbf{L}^2-\hbar^2\sigma^2\left(\frac{\partial^2}{\partial x^2}+\frac{\partial^2}{\partial y^2}\right)+2M\sigma^2\frac{(1-\nu^2)\,V_1(\mu)-(\mu^2-1)\,V_2(\nu)}{\mu^2-\nu^2}\\ &= -\mathbf{L}^2-\hbar^2\sigma^2\left(\frac{\partial^2}{\partial x^2}+\frac{\partial^2}{\partial y^2}\right)+\beta_{\mathrm{pot}}\end{aligned} \tag{19}$$

where $\mathbf{L}^2$ is the square of the angular momentum operator $\mathbf{L}$. Note that the classical constant of the motion β (Eq. 13) is the precise classical analogue of the separation operator $\mathbf{A}'$ (Eq. 19). This must be the case as can be already seen by comparing Eqs. (10) and (18).

3. We finally mention some special separable problems and their constants of the motion.

i) The shape of an atomic nucleus may very well be described to be a prolate or oblate spheroid, especially in the case of rare earths [10]. The most simple and widely used one-particle model for nucleons is the spheroidal well model

$$V=\begin{cases}-V_0 & \mu \leqq \mu_0\\ \infty & \mu > \mu_0\end{cases} \tag{20}$$

where $\mu=\mu_0$ is the surface of the nucleus. As a consequence, the Hamiltonian commutes with the separation operator

$$\mathbf{A}' = -\mathbf{L}^2+\sigma^2(\mathbf{p}_x^2+\mathbf{p}_y^2)-2M\sigma^2 V_0 \qquad (\mu \leqq \mu_0)\,. \tag{21}$$

ii) The constant of the motion for the two-centre Coulomb potential

$$V=-Z_1 e^2/r_1 - Z_2 e^2/r_2 \tag{22}$$

Table 1

Prolate spheroidal coordinates

$r_1 = \sigma(\mu + \nu) \quad r_2 = \sigma(\mu - \nu)$

$\varrho = \sigma\sqrt{(\mu^2 - 1)(1 - \nu^2)} \quad z = \sigma\mu\nu$

$r^2 = \sigma^2(\mu^2 + \nu^2 - 1)$

Separable potential energy $V = \frac{V_1(\mu) + V_2(\nu)}{\mu^2 - \nu^2}$	$V_1(\mu)$	$V_2(\nu)$	Contribution to Separation operator $\frac{(1-\nu^2)\,V_1(\mu) - (\mu^2 - 1)\,V_2(\nu)}{\mu^2 - \nu^2}$
$\frac{1}{r_1} = \frac{1}{\sigma(\mu + \nu)}$	$\frac{\mu}{\sigma}$	$-\frac{\nu}{\sigma}$	$\frac{1}{\sigma}\,\frac{z_1}{r_1}$
$\frac{1}{r_2} = \frac{1}{\sigma(\mu - \nu)}$	$\frac{\mu}{\sigma}$	$\frac{\nu}{\sigma}$	$\frac{1}{\sigma}\,\frac{z_2}{r_2}$
$r^2 = \sigma^2(\mu^2 + \nu^2 - 1)$	$\sigma^2\mu^2(\mu^2 - 1)$	$\sigma^2\nu^2(1 - \nu^2)$	ϱ^2
$\frac{1}{r_1 \cdot r_2} = \frac{1}{\sigma^2(\mu^2 - \nu^2)}$	$\frac{1}{2\sigma^2}$	$\frac{1}{2\sigma^2}$	$-\frac{\cos\gamma}{2\sigma^2}$
$\frac{1}{\varrho^2} = \frac{1}{\sigma^2(\mu^2 - 1)(1 - \nu^2)}$	$\frac{1}{\sigma^2(\mu^2 - 1)}$	$\frac{1}{\sigma^2(1 - \nu^2)}$	$\frac{1 - r^2/\sigma^2}{\varrho^2}$

was analyzed by Erikson and Hill [9] and turned out to be

$$A' = -L^2 + \sigma^2(p_x^2 + p_y^2) - 2Me^2\sigma(Z_1\cos\theta_1 - Z_2\cos\theta_2). \tag{23}$$

Later on, Coulson and Joseph [8] superposed the two-centre Coulomb potential and a harmonic oscillator potential kr^2:

$$V = -Z_1e^2/r_1 - Z_2e^2/r_2 + kr^2 \tag{24}$$

The constant of the motion for this case,

$$A' = -L^2 + \sigma^2(p_x^2 + p_y^2) - 2Me^2\sigma(Z_1\cos\theta_1 - Z_2\cos\theta_2) + 2M\sigma^2k\varrho^2 \tag{25}$$

is an outgrowth of the superposition of separable potentials according to Eqs. (13) and (19); details are to be found in Table 1.

iii) The superposition of a two-centre Coulomb potential $-Z_1/r_1 - Z_2/r_2$ and a potential $-Q/(r_1r_2)$

$$V = -\frac{Z_1}{r_1} - \frac{Z_2}{r_2} - \frac{Q}{r_1 \cdot r_2} \tag{26}$$

(atomic units in (26)) has found applications in the natural spin orbital analysis of small diatomic molecules [12]. The resulting constant of the motion is [11]:

$$-A' = L^2 - \sigma^2(p_x^2 + p_y^2) + R(Z_1\cos\theta_1 - Z_2\cos\theta_2) + Q\cos\gamma \tag{27}$$

where the third term comes from the two-centre Coulomb potential and the last one from $Q/(r_1 \cdot r_2)$ (compare Table 1).

iv) Teller [13] recently suggested the use of a separable potential energy of the form

$$V \sim \frac{a_{00} + a_{10}\mu + a_{01}\nu + a_{20}\mu^2 + a_{02}\nu^2}{\mu^2 - \nu^2} \tag{28}$$

in an effective one-electron Schrödinger equation for electrons in a diatomic molecule. It is more general than the potential energy (26) because of the quadratic terms $a_{20}\mu^2$ and $a_{02}\nu^2$. Identifying

$$\begin{aligned} V_1(\mu) &= \tfrac{1}{2}a_{00} + a_{10}\mu + a_{20}\mu^2 \\ V_2(\nu) &= \tfrac{1}{2}a_{00} + a_{01}\nu + a_{02}\nu^2 \end{aligned} \tag{29}$$

we get, according to (19),

$$\begin{aligned} A' = &- L^2 - \hbar^2\sigma^2\left(\frac{\partial^2}{\partial x^2} + \frac{\partial^2}{\partial y^2}\right) \\ &+ 2M\sigma^2 \frac{(1-\nu^2)(a_{00}/2 + a_{10}\mu + a_{20}\mu^2) + (\mu^2 - 1)(a_{00}/2 + a_{01}\nu + a_{02}\nu^2)}{\mu^2 - \nu^2} . \end{aligned} \tag{30}$$

It is, however, difficult to give a simple interpretation of this separation constant.

Cylindrically Symmetrical Potentials Separable in Parabolic Coordinates

1. Parabolic coordinates are as usually defined by

$$\xi = r + z \quad \eta = r - z \quad \varphi \tag{31}$$

and are related to (circular) cylinder coordinates ϱ, φ, z by

$$\varrho = \sqrt{\xi\eta} \quad z = \frac{\xi - \eta}{2} \quad \varphi = \varphi . \tag{32}$$

The most general cylindrically symmetrical potential energy V for which the Schrödinger Eq. (3) separates in parabolic coordinates is of the form

$$V(\xi, \eta) = \frac{V_1(\xi) + V_2(\eta)}{\xi + \eta} \tag{33}$$

according to Eisenhart [4] or Morse and Feshbach [5, p. 660].

Let us first construct a classical constant of the motion before treating the Schrödinger Eq. (3) with the potential energy (33). The canonical momenta are

$$\begin{aligned} p_\xi &= \frac{M}{4\xi}(\xi + \eta)\dot{\xi} = \frac{\partial S_0}{\partial \xi} \\ p_\eta &= \frac{M}{4\eta}(\xi + \eta)\dot{\eta} = \frac{\partial S_0}{\partial \eta} \\ p_\varphi &= M\xi\eta\dot{\varphi} \qquad = \frac{\partial S_0}{\partial \varphi} . \end{aligned} \tag{34}$$

The Hamilton-Jacobi-equation separates with the ansatz

$$S_0 = p_\varphi \cdot \varphi + S_1(\xi) + S_2(\eta) \tag{35}$$

giving (according to Landau and Lifschitz [6, p. 177])

$$\begin{aligned} 2\xi p_\xi^2 + \frac{p_\varphi^2}{2\xi} + M(V_1(\xi) - E\xi) &= \beta \\ 2\eta p_\eta^2 + \frac{p_\varphi^2}{2\eta} + M(V_2(\eta) - E\eta) &= -\beta . \end{aligned} \tag{36}$$

Eliminating E from Eq. (36), we obtain for β:

$$\beta = \frac{2\xi\eta}{\xi+\eta}(p_\xi^2 - p_\eta^2) + \frac{\eta-\xi}{2\xi\eta}p_\varphi^2 + M\frac{\eta V_1(\xi) - \xi V_2(\eta)}{\xi+\eta} . \tag{37}$$

Only the last term of the right side of (37) depends on the potential energy (33).

A short calculation shows that the first sum is equal to minus the z-component of the vector $\vec{p} \times \vec{L}$, where $\vec{L} = (L_x, L_y, L_z)$ is the angular momentum $\vec{r} \times \vec{p}$. We therefore obtain

$$\beta = -(p_x L_y - p_y L_x) + M\frac{\eta V_1(\xi) - \xi V_2(\eta)}{\xi+\eta} . \tag{38}$$

2. The Schrödinger Eq. (3) for the potential energy (33) separates with the ansatz

$$\chi(\xi, \eta, \varphi) = X(\xi)\, Y(\eta) e^{im\varphi} . \tag{39}$$

The separated equations are

$$\begin{aligned} &\left\{-\hbar^2\left(2\frac{\partial}{\partial\xi}\left(\xi\frac{\partial}{\partial\xi}\right) - \frac{m^2}{2\xi}\right) + M(V_1(\xi) - E\xi) - A\right\}X(\xi) = 0 \\ &\left\{-\hbar^2\left(2\frac{\partial}{\partial\eta}\left(\eta\frac{\partial}{\partial\eta}\right) - \frac{m^2}{2\eta}\right) + M(V_2(\eta) - E\eta) + A\right\}Y(\eta) = 0 . \end{aligned} \tag{40}$$

We now repeat the calculation which led from Eqs. (16) to (17) and obtain from (40):

$$A\chi = A\chi , \tag{41}$$

the separation operator A being equal to

$$\begin{aligned} A = \frac{\hbar^2}{\xi+\eta}\left\{-2\eta\frac{\partial}{\partial\xi}\xi\frac{\partial}{\partial\xi} + 2\xi\frac{\partial}{\partial\eta}\eta\frac{\partial}{\partial\eta}\right\} + \hbar^2\frac{\eta-\xi}{2\xi\eta}\frac{\partial^2}{\partial\varphi^2} \\ + M\frac{\eta V_1(\xi) - \xi V_2(\eta)}{\xi+\eta} . \end{aligned} \tag{42}$$

Note that again this separation operator is the quantum mechanical analogue of the separation constant β (Eq. (37)) for the Hamilton-Jacobi equation.

A very tedious calculation (which is omitted) shows that the first term in (42) is equal to the operator

$$\begin{aligned} A_z &= \frac{1}{2}\sum_{j=1}^{3}(L_{3j}p_j - p_j L_{j3}) = \frac{1}{2}(L_{31}p_1 - p_1 L_{13} + L_{32}p_2 - p_2 L_{23}) \\ &= z(p_x^2 + p_y^2) - \frac{1}{2}p_z(p_x x + x p_x + y p_y + p_y y) \end{aligned} \tag{43}$$

where

$$L_{ij} = x_i p_j - x_j p_i$$

is the antimetric tensor operator of angular momentum.

The operator A evidently is the quantum mechanical equivalent of the symmetrized classical expression (38).

We therefore obtain the final result that the separation operator A is equal to

$$A = A_z + M \frac{\eta V_1(\xi) - \xi V_2(\eta)}{\xi + \eta} \tag{44}$$

with A_z defined in Eq. (43).

3. Again we mention some special separable potentials and the resulting constants of the motion.

i) The potential energy

$$V = -\frac{Ze^2}{r} = -\frac{2Ze^2}{\xi + \eta} \tag{45}$$

of a particle with mass M and charge $-e$ in the field of a positive charge Ze (Kepler problem) gives rise to the constant of motion

$$\beta = -(p_x L_y - p_y L_x) + MZe^2 \frac{z}{r} \tag{46}$$

after the identification $V_1(\xi) = V_2(\eta) = -Ze^2$.

This is the z-component of the famous Runge-Lenz vector

$$-(\vec{p} \times \vec{L}) + MZe^2 \frac{\vec{r}}{r} \tag{47}$$

pointing in the direction of the major axis of the Kepler ellipse. From (44) its quantum mechanical analogue is derived and turns out to be

$$A = -\frac{1}{2} \sum_{j=1}^{3} (p_j L_{j3} - L_{3j} p_j) + MZe^2 \frac{z}{r}. \tag{48}$$

This is the z-component of the quantum mechanical Lenz-Pauli-vector. Its eigenvalue in the eigenstate $|STm\rangle$ with parabolic quantum numbers S, T, m is given by

$$A = -\frac{S - T}{S + T + |m| + 1} Ze^2 M \tag{49}$$

according to Landau-Lifschitz [14, p. 133].

ii) If a homogeneous electric field with strength F in the direction of the positive z-axis is superimposed to the field of an atomic nucleus with charge Ze, the resulting potential energy of an electron with charge $-e$ is

$$-\frac{Ze^2}{r} + eFz. \tag{50}$$

The resulting constant of the motion now is

$$\beta = -(p_x L_y - p_y L_x) + MZe^2 \frac{z}{r} + \frac{M}{2} eF\varrho^2 \tag{51}$$

in classical mechanics.

The quantum mechanical separation operator is, according to (44), (50), and Table 2

$$A = -\frac{1}{2}\sum_{j=1}^{3}(p_j L_{j3} - L_{3j}p_j) + MZe^2\frac{z}{r} + \frac{M}{2}eF\varrho^2 . \tag{52}$$

In Fig. 2, energy E and separation constant $-A$ of several excited states of (50) with $Z = 1$ are given as a function of the electric field strength F. The method of calculation used was the reduction of the system of two differential eigenvalue Eqs. (40) to a system of two coupled algebraic eigenvalue equations. This system was subjected to a Newton-Raphson-procedure described in the appendix of [15]

Two features of Fig. 2 are essential.

1) $-A$ is a slowly decreasing, almost linear function of F which is well approximated by the expectation value

$$(STm| -A|STm) = \frac{T-S}{S+T+|m|+1} - \frac{1}{2}F(STm|\varrho^2|STm) \tag{53}$$

calculated with parabolic hydrogenic functions $|STm)$. These functions have recently been given as linear combinations of spherical hydrogenic functions $|nlm)$ [16a, b].

2) The state $|040)$ of type σ^+ ($C_{\infty v}$) crosses the states $|300)$, $|210)$, and $|120)$ of equal type σ^+ ($C_{\infty v}$) with regard to energy. This is no violation of the non crossing rule since the full symmetry $C_{\infty v} \times \{A\}$ of (50) has to be taken into account and a complete classification is given by (γ, A) where γ is an irreducible representation of $C_{\infty v}$ and A the separation constant. The values of the separation constant A for all these states are well separated.

iii) We finally mention the problem

$$\left\{-\frac{\hbar^2}{2M}\Delta - e^2 Z/r + \frac{C}{\varrho^2}\right\}\chi = \varepsilon\chi \qquad (\varrho^2 = x^2 + y^2) \tag{54}$$

recently solved by Hartmann [17].

(54) is separable both in spherical and in parabolic coordinates. Separability in spherical coordinates and spatial cylinder symmetry give rise to the two constants of motion

$$L^2 + \frac{2MC}{\sin^2\vartheta}, \tag{55a}$$

$$L_z = \frac{\hbar}{i}\frac{\partial}{\partial\varphi}. \tag{55b}$$

Separability in parabolic coordinates comes from the fact that

$$\frac{1}{\varrho^2} = \frac{1}{\xi\cdot\eta} = \frac{\frac{1}{\xi}+\frac{1}{\eta}}{\xi+\eta}. \tag{56}$$

---

[3] For another derivation of the Stark-effect generalization of the Lenz-Pauli-vector see: Redmond, P. J.: Physic. Rev. 133 B, 1352 (1964).

Table 2

Separable potential energy $V=\dfrac{V_1(\xi)+V_2(\eta)}{\xi+\eta}$	Circular parabolic coordinates $\xi = r+z \quad \eta = r-z \quad \varphi$ $\varrho^2 = \xi\eta$ $V_1(\xi)$	 $V_2(\eta)$	Contribution to separation operator $\dfrac{\eta V_1(\xi)-\xi V_2(\eta)}{\xi+\eta}$
$\dfrac{1}{r}$	1	1	$-\dfrac{z}{r}$
$\dfrac{z}{r}$	ξ	$-\eta$	$\dfrac{\varrho^2}{r}$
z	$\dfrac{\xi^2}{2}$	$-\dfrac{\eta^2}{2}$	$\dfrac{\varrho^2}{2}$
$\dfrac{1}{\varrho^2}$	$\dfrac{1}{\xi}$	$\dfrac{1}{\eta}$	$-\dfrac{2z}{\varrho^2}$

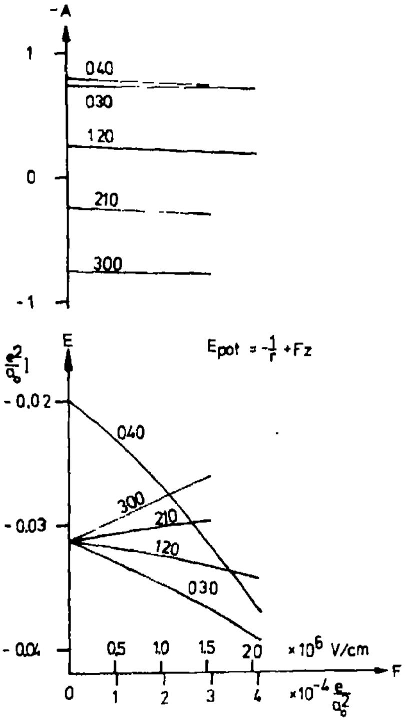

Fig. 2. Energy F and separation constant A as functions of electric field strength F for several electronic states STO of type σ^+ $(m = 0)$. The operator of potential energy is $-\dfrac{1}{r} + Fz$

According to (44) and Table 2, it gives rise to the additional third constant of motion

$$A = -\frac{1}{2}\sum_{j=1}^{3}(p_j L_{j3} - L_{3j} p_j) + MZe^2\frac{z}{r} - MC\frac{2z}{Q^2}. \qquad (55c)$$

So the number of independent constants of the motion is even greater than in the Stark effect problem ii) and equal to the corresponding number in the Zeeman effect problem.

All numerical calculations have been performed on the CD 6600 of Regionales Rechenzentrum Stuttgart and on the TR 440 of Deutsches Rechenzentrum Darmstadt. The author thanks the Deutsche Forschungsgemeinschaft for paying computer time.

References

1. Hansen, K. H.: Theoret. chim. Acta (Berl.) **1**, 159 (1963).
2. Theoret. chim. Acta (Berl.) **1**, 353 (1963).
3. Kehl, S., Helfrich, K., Hartmann, H.: Theoret. chim. Acta (Berl.) **21**, 44 (1971).
4. Eisenhart, L. P.: (a) Ann. Math. **35**, 284 (1934); (b) Physic. Rev. **45**, 427 (1934); (c) Physic. Rev. **74**, 87 (1948).
5. Morse, P. M., Feshbach, H.: Methods of theoretical physics (2 Vol.). New York: McGraw Hill 1953.
6. Landau, L. D., Lifschitz, E. M.: Lehrbuch der theoretischen Physik, Band I, Mechanik. Berlin: Akademie-Verlag 1962.
7. Cordes, H. O.: (a) Math. Ann. **128**, 257 (1954); (b) Math. Ann. **128**, 373 (1955).
8. Coulson, C. A., Joseph, A.: Int. J. quant. Chemistry **1**, 337 (1967).
9. Erikson, H. A., Hill, E. L.: Physic. Rev. **75**, 29 (1949).
10. Rainwater, R.: Physic. Rev. **79**, 432 (1950).
    Feenberg, E., Hammack, K. C.: Physic. Rev. **81**, 285 (1951).
    Baumgärtner, G., Schuh, P.: Kernmodelle. Mannheim: BI 1968.
11. Helfrich, K., Hartmann, H.: Theoret. chim. Acta (Berl.) **16**, 263 (1970).
12. Entwicklung natürlicher Spinorbitale kleiner zweiatomiger Moleküle nach verallgemeinerten Zweizentren-Funktionen. Frankfurt: Habilitationsschrift 1971.
13. Teller, E., Sahlin, H. L.: The hydrogen molecular ion and the general theory of electron structure, in: Physical Chemistry, Vol. 5, H. Eyring, Ed., p. 35. New York: Academic Press 1970.
14. Landau, L. D., Lifschitz, E. M.: Lehrbuch der theoretischen Physik, Band III, Quantenmechanik. Berlin: Akademie-Verlag 1965.
15. Hartmann, H., Helfrich, K.: Theoret. chim. Acta (Berl.) **10**, 406 (1968).
16. a Park, D.: Z. Physik 159, **155**, (1960).
16. b Tarter, C. B.: J. math. Physics **11**, 3192 (1970).
17. Hartmann, H.: Theoret. chim. Acta (Berl.) **24**, 201 (1972).

Dr. Klaus Helfrich
Institut für Theoretische Chemie der Universität
D-6000 Frankfurt a. M.
Robert-Mayer-Str. 11, Germany

Theoret. chim. Acta (Berl.) 24, 283–289 (1972)
© by Springer-Verlag 1972

Commentationes

Über den Kontinuumseinfluß auf die Polarisierbarkeit von Molekülzuständen

K. Jug* und H. Labhart
Physikalisch-Chemisches Institut der Universität Zürich

Eingegangen am 9. September 1971

On the Influence of the Continuum on the Polarizibility of States of Molecules

The influence of the continuum on the polarizibility of long chain molecules is estimated with a model calculation of a square well potential. We differentiate between two contributions: a direct one through transitions from discrete states and an indirect one occuring through energy shift and deformation of the wavefunctions of corresponding states of the box potential. The dependence of this influence on the depth of the well is discussed. For dimensions corresponding to crocetindimethylester, the direct influence is small, whereas the indirect one causes an increase of the polarizibility of about 20%.

Der Kontinuumseinfluß auf die Polarisierbarkeit langgestreckter Moleküle wird anhand einer Modellrechnung an einem eindimensionalen Potentialtopf endlicher Tiefe abgeschätzt. Er läßt sich unterteilen in einen direkten, durch Übergangsmomente aus diskreten Zuständen bedingten Beitrag und einen indirekten Beitrag, der durch die energetische Verschiebung und Verformung der Wellenfunktionen der diskreten Zustände gegenüber den entsprechenden Zuständen im Kasten unendlicher Tiefe bedingt ist. Die Abhängigkeit dieser Einflüsse von der Potentialtopftiefe wird diskutiert. Bei Dimensionen des Potentialtopfes, welche dem Crocetindimethylester entsprechen, ist der direkte Einfluß sehr klein, während der indirekte Einfluß eine Erhöhung der Polarisierbarkeit um rund 20% bewirkt.

1. Einleitung

Wie in einer früheren Publikation [1] bemerkt, wurden bisher zur Berechnung der Polarisierbarkeit von Molekülen ausschließlich beschränkte Sätze von Basisorbitalen verwendet. Diese liefern für Energien oberhalb der Ionisationsenergie kein Kontinuum, sondern eine endliche Zahl diskreter Zustände. Berechnet man die Polarisierbarkeit α_M im Zustand M gemäß der Rayleigh-Schrödingerschen Störungsrechnung zu

$$\alpha_M = 2\sum_N \frac{\langle M|r|N\rangle \langle N|r|M\rangle}{E_N - E_M}, \tag{1}$$

so muß man sich fragen, inwiefern die diskreten Zustände oberhalb der Ionisierungsenergie den wahren Beitrag des Kontinuums ersetzen. Bei Atomen kann der Beitrag des Kontinuums wesentlich sein. Beim H-Atom macht er gemäß Tillieu und Guy [2] ca. 20% der gesamten Polarisierbarkeit aus, während

---

* Daueradresse: Department of Chemistry, Saint Louis University, Saint Louis, Missouri 63156.

Kelly [3] für schwere Atome kleinere Beiträge erhält, für Lithium etwa 1,5%. Die Frage nach dem Beitrag des Kontinuums zur Polarisierbarkeit von Molekülen wurde auch von Banerjee und Salem [4] aufgeworfen. Wir haben keine allgemeine Methode zur Lösung des gestellten Problems gefunden und versuchen es deshalb anhand einer Modellrechnung anzugehen.

2. Ein Modell zur Berechnung der Polarisierbarkeit in Polyenen

Zur Untersuchung der Polarisierbarkeit in Molekülen sind Polyene besonders geeignet, da sie sich modellmäßig eindimensional darstellen lassen [5]. Die Methode des freien Elektronengases in der ursprünglichen Form von Kuhn enthält keine Beschreibung der Kontinuumszustände und muß für unsere Zwecke modifiziert werden. Wir greifen hier auf das Modell des eindimensionalen Potentialtopfes (endlicher Tiefe) zurück. Das effektive Potential soll im Gebiet $|x| \leqq x_0$ den konstanten Wert $V = -V_0$ haben und außerhalb dieses Gebietes $V = 0$ sein. Dies gestattet uns, Eigenfunktionen und Erwartungswerte analytisch anzugeben und die Eigenwerte als Lösungen einfacher transzendenter Gleichungen zu erhalten [6]. Die Parameter x_0 und V_0 werden durch die Länge und Ionisierungsenergie der Polyene festgelegt. Bei der Besetzung der Energieniveaus des Potentialtopfes werden wir uns auf die π-Elektronen beschränken.

Singulettzustände mit geschlossenen Schalen werden durch *eine* Konfiguration, mit offenen Schalen durch zwei oder mehr Konfigurationen von Spin-Orbitalen dargestellt. Die Gesamtpolarisierbarkeit α läßt sich dann als Summe von Orbitalpolarisierbarkeiten α_i von besetzten Spin-Orbitalen angeben

$$\alpha = \sum_i \alpha_i . \tag{2}$$

Außerdem denken wir uns den Hamiltonoperator zu einer Summe von effektiven Einelektronenoperatoren vereinfacht, die die Elektronenwechselwirkung implizit enthalten. Die Orbitale sind Eigenfunktionen des repräsentativen Einelektronenproblems. Die α_i sind durch Orbitalübergangsmomente μ_{ij} und Orbitalenergiedifferenzen $E_j - E_i$ von besetzten Spin-Orbitalen $\varphi_i \omega$ zu unbesetzten Spin-Orbitalen $\varphi_j \omega$ gegeben, wobei ω gleich α oder β ist.

$$\alpha_i = 2 \sum_{j \neq i} \frac{\mu_{ij}^2}{E_j - E_i} , \qquad \mu_{ij} = \langle \varphi_i | x | \varphi_j \rangle \tag{3}$$

φ_i und φ_j sind Eigenfunktionen des Potentialtopfproblems. Die obige Form (3) ist zur Darstellung des Kontinuumbeitrags wenig geeignet. Wir greifen deshalb zu folgendem Hilfsmittel: Wir denken uns die Energiewerte $E > 0$ als Grenzfälle von Eigenwerten eines Potentialkastens mit $V = 0$ und unendlich hohen Wänden, dessen Breite gegen unendlich geht. In diesem Fall wird der Kontinuumbeitrag durch ein Integral dargestellt. Die gesamte Polarisierbarkeit des Orbitals i ergibt sich dann als

$$\alpha_i = 2 \sum_{j \neq i} \frac{\mu_{ij}^2}{E_j - E_i} + \frac{4}{\pi} \int_0^\infty \frac{\mu_i^2(k)}{k^2 + k_i^2} \, dk , \qquad k_i^2 = -2E_i , \qquad k^2 = 2E . \tag{4}$$

In (4) sind zur Berechnung des Übergangsmomentes $\mu_i(k)$ im Gebiet $|x| \geqq x_0$ die Kontinuums-Eigenfunktionen sinkx und coskx mit der Amplitude 1 zu nehmen. Aus den Anschlußbedingungen bei $x = \pm x_0$ läßt sich dann für jedes k die Amplitude im Gebiet $|x| \leqq x_0$ berechnen. Die diskreten Eigenfunktionen wurden aus den in [6] gegebenen transzendenten Gleichungen bestimmt und normiert. Aus den Auswahlregeln für die Übergangsmomente ergibt sich, daß nur Übergänge der Art $g \leftrightarrow u$ erlaubt sind. Da die Berechnung der Energien E_i und der Übergangsmomente kein allzu schwieriges numerisches Problem ist, verzichten wir hier auf weitere Einzelheiten. Im folgenden Abschnitt geben wir einige Resultate für Orbitalpolarisierbarkeiten α_i und Zustandspolarisierbarkeiten α an.

3. Resultate für Orbital- und Zustandspolarisierbarkeiten

Für die Diskussion der Orbitalpolarisierbarkeitsanteile, die durch die Glieder der Summe und das Integral in (4) dargestellt werden, wählen wir einen Potentialtopf mit der halben Breite $x_0 = 6$ a.u., was etwa dem Molekül Butadien entspricht. Fig. 1 zeigt die einzelnen Anteile zur Polarisierbarkeit des untersten Niveaus E_1. Die diskreten Anteile zeigen über den ganzen Bereich $0 \leqq V_0 < \infty$ ähnliche Kurvenform. Die Beiträge verschiedener Orbitale zur Polarisierbarkeit sind in der Größenordnung um Zehnerpotenzen verschieden. Der Hauptbeitrag entsteht durch Übergang zum nächsten Niveau E_2, während die übrigen Beiträge prozentual vernachlässigbar sind. Das aufeinanderfolgende scharfe Abbiegen der Kurven mit kleiner werdenden Werten V_0 erfolgt in der Nähe des Übergangs dieser Niveaus ins Kontinuum. Bekanntlich existieren für jedes endliche Potential V_0 nur endlich viele diskrete Eigenwerte. Beim Übergang ins Kon-

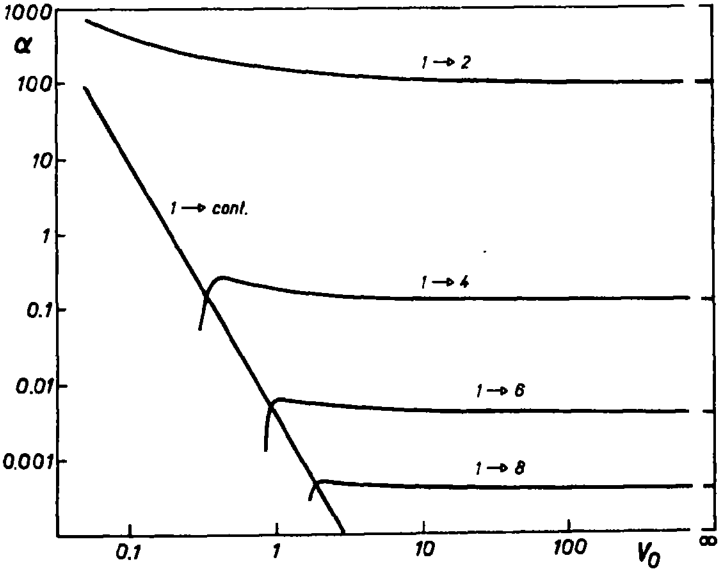

Fig. 1. Orbitalpolarisierbarkeitsanteile zu α_1 (a.u.) durch Übergänge zu den diskreten Orbitalen 2,4, 6,8 und dem Kontinuum in Abhängigkeit von der Potentialtopftiefe V_0 (a.u.) für $x_0 = 6$ a.u.

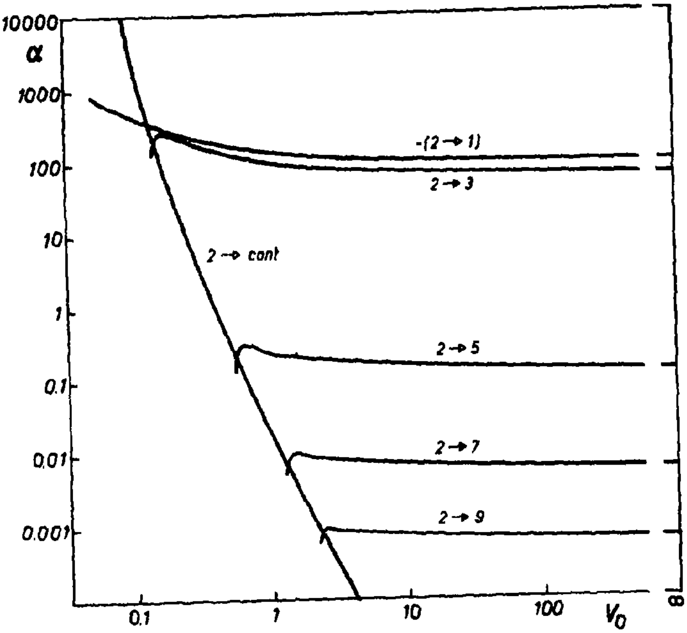

Fig. 2. Entsprechende Anteile zu α_2 (a.u.)

tinuum sinkt der Beitrag eines einzelnen Niveaus zu der Polarisierbarkeit eines diskreten Niveaus, hier E_1, auf Null ab. Ein davon völlig verschiedenes Verhalten zeigt der Beitrag des Kontinuums in Abhängigkeit von V_0. Der Abfall mit wachsendem V_0 ist erheblich stärker als bei jeder Kurve von diskreten Niveaus und so schneidet die Kontinuumskurve die gesamte diskrete Kurvenschar. Der Schnitt mit der Kurve 1→2 ist wegen des kleinen Wertes von V_0 in Fig. 1 nicht dargestellt.

Legt man den Bereich $0{,}1 \leqq V_0 \leqq 1$ a.u. als physikalisch relevant zugrunde, so ersieht man aus Fig. 1, daß der Kontinuumsbeitrag selbst bei $V_0 = 0{,}1$ erst einige Prozent ausmacht und dann schnell abfällt. Vergleicht man den Hauptbeitrag zur Polarisierbarkeit von Niveau E_1 für den Topf mit endlicher Tiefe etwa bei $V_0 = 1$ a.u. und den Kasten mit unendlich hohen Wänden, so ergibt sich ein Verhältnis von 143 zu 90, also eine erhebliche Änderung des Einzelbeitrags.

In Fig. 2 sind die Beiträge zur Polarisierbarkeit des zweiten Niveaus festgehalten. Qualitativ kann man sagen, daß die Folgerungen im wesentlichen die gleichen sind wie für E_1. Unterschiedlich ist, daß ein negativer Beitrag durch den Übergang zum niedrigeren Niveau E_1 entsteht, der alle anderen diskreten Beiträge überwiegt. Die beiden Nachbarniveaus E_1 und E_3 geben einen in der Größenordnung gleichen Beitrag. Der Einfluß des Kontinuums auf die Polarisierbarkeit von E_2 ist naturgemäß größer als auf die von E_1, da E_2 näher an der Kontinuumsgrenze liegt. Quantitativ wächst der Beitrag bei E_2 im Vergleich zu E_1 um einen Faktor 10–300 an, wenn man den genannten Bereich von V_0 zugrunde legt. Bei $V_0 = 0{,}1$ a.u. überwiegt er bereits alle diskreten Beiträge.

Nach diesen Vorbereitungen können wir uns der modellmäßigen Berechnung der Polarisierbarkeit von Grund- und angeregten Zuständen eines langgestreck-

Tabelle 1. Beiträge der einzelnen Orbitalübergänge zur Polarisierbarkeit von Grund- und erstem angeregten Zustand von Crocetindimethylester; $x_0 = 22{,}58$ a.u., α (a.u.) für $V_0 = 0{,}427$ a.u., α' (a.u.) für $V_0 = \infty$

Grundzustand			Erster angeregter Zustand		
Übergang	α[b]	α'	Übergang	α	α'
$9 \to 10$[a]	4611	3636	$10 \to 9$	−4611	−3636
$9 \to 12$[a]	17	13	$10 \to 11$	4266	3306
$9 \to 14$[a]	1	1	$10 \to 13$	16	12
$8 \to 11$[a]	18	14	$9 \to 10$	4611	3636
$8 \to 13$[a]	1	1	$9 \to 12$	17	13
$7 \to 10$[a]	20	16	$9 \to 14$	1	1
$7 \to 12$[a]	1	1	$8 \to 9$	5070	4063
$6 \to 11$[a]	1	1	$8 \to 11$[a]	18	14
$9 \to \infty$[a]	1	0	$8 \to 13$[a]	1	1
$8 \to \infty$[a]	0	0	$7 \to 10$	20	16
			$7 \to 12$[a]	1	1
diskret	9340	7366	$6 \to 9$	22	18
cont	2	0	$6 \to 11$[a]	1	1
total	9342	7366	$10 \to \infty$	3	1[c]
			$9 \to \infty$	1	0
			$8 \to \infty$[a]	0	0
			diskret	9454	7463
			cont	4	1
			total	9458	7464

[a] Doppelt zu rechnen.

[b] 1 a.u. = $0{,}148 \cdot 10^{-24}$ cm^3.

[c] Die Energien der Orbitale $n \geq 15$ liegen oberhalb 0,427 a.u. Die entsprechenden Beiträge zu α' werden deshalb als Ersatz für den Kontinuumsbeitrag im Potentialtopf endlicher Tiefe gerechnet.

ten Polyens zuwenden. Als Prototyp wählen wir Crocetindimethylester, das von Seibold *et al.* [7] experimentell untersucht worden ist. Das System hat 18 π-Elektronen, die wir im Grundzustand durch neun besetzte Niveaus beschreiben. Die Länge des Polyens plus zwei Einfachbindungslängen wählen wir als Breite $2x_0$ des Potentialtopfes, wobei wir Einfachbindungen mit 1,483 Å und Doppelbindungen mit 1,337 Å annehmen [8]. Damit ergibt sich $x_0 = 22{,}58$ a.u. Den Abstand des obersten besetzten Niveaus vom Kontinuum wählen wir gleich der Ionisierungsenergie I des Moleküls. Mit den Tabellen von Kieser [9], die bis zum Dekapentaen gehen, extrapolieren wir $I = 6{,}8$ eV ($= 0{,}25$ a.u.). Zur Adjustierung des neunten Niveaus müssen wir $V_0 = 0{,}427$ a.u. wählen.

Die Gesamtpolarisierbarkeit des Grund- und ersten angeregten Zustandes sowie eine Aufteilung in diskrete und Kontinuumsanteile sind in Tabelle 1 angegeben. Außerdem ist ein Vergleich von Potentialtopf (α) und Potentialkasten (α') angestellt. Allgemein stellt man fest, daß der direkte Einfluß des Kontinuums für beide Zustände vernachlässigbar klein ist. Die Hauptanteile sind durch Nachbarorbitalübergänge gegeben, von denen ein Grundzustand einer und im ersten angeregten Zustand vier vorhanden sind. Zwei davon heben sich gegenseitig auf. Die Gesamtpolarisierbarkeiten sind im Potentialtopfmodell um 20% größer als im Kastenmodell. Dies führt zu einer um etwa 20% größeren Polarisierbarkeitsdifferenz $\Delta\alpha = 116$ a.u. gegenüber $\Delta\alpha' = 98$ a.u. zwischen den beiden Zuständen.

Seibold *et al.* [7] haben die Polarisierbarkeitsänderung in Richtung des Übergangsmomentes zu $\Delta\alpha = 3450$ a.u. gemessen. Dies stimmt mit keinem der beiden Modellwerte überein. Dietrich und Jaenicke [10] hatten die Hauptbeiträge im Kastenmodell abgeschätzt. Ihre gute Übereinstimmung mit der experimentell bestimmten Polarisierbarkeitsänderung läßt sich auf eine fehlerhafte Berechnung der Polarisierbarkeit des Grundzustandes zurückführen. Dieser wurde in [10] um den Faktor 2 zu klein berechnet, da nur der Übergang *eines* der beiden Elektronen aus dem obersten besetzten in das unbesetzte Orbital berücksichtigt wurde. Korrigiert man diesen Fehler, so ergibt sich Übereinstimmung mit unserer Rechnung.

4. Diskussion

Die Analyse der in Abschnitt 3 gegebenen Resultate zeigt, daß die Änderung des berechneten Wertes der Polarisierbarkeit im Potentialtopf endlicher Tiefe gegenüber dem unendlich tiefen Potentialkasten nur zu einem kleinen Teil durch den direkten Beitrag des Kontinuums (Integral in (4)) bedingt ist. Der Hauptanteil rührt von der Veränderung der Eigenfunktionen und Eigenwerte der Energie der diskreten Zustände her.

Man muß sich deshalb fragen, in welchem Maß dieser indirekte Beitrag durch die spezielle Wahl des Modells bedingt ist. Würde man statt der FE-Eigenfunktionen LCAO-MO's verwenden, die wie bei einfachen Verfahren üblich aus einem minimalen Satz wasserstoff-ähnlicher Atomorbitale kombiniert sind, so enthalten diese Funktionen einen exponentiellen Abfall am Kettenende, was bei FE-Funktionen erst bei endlicher Tiefe des Potentialtopfs auftritt. Allerdings ist dieser Abfall für verschiedene MO's derselbe und wird nicht mit wachsender MO-Energie flacher. Dies bedeutet, daß auch in diesem Falle ein indirekter Einfluß des Kontinuums vorhanden sein sollte, der aber wahrscheinlich kleiner ausfällt als bei den FE-Funktionen. Damit erscheinen die von uns anhand des FE-Modells errechneten indirekten Kontinuumseinflüsse als obere Grenze dieses Effektes bei Polarisierbarkeitsberechnungen an Polyenen. Die explizite Berücksichtigung der Elektronenwechselwirkung, insbesondere auch der σ- und π-Elektronen, ist somit wichtiger als die Berücksichtigung der Kontinuumsbeiträge.

Die gefundene große Diskrepanz zwischen experimentellem und berechnetem Wert der Polarisierbarkeitsänderung beim Übergang in den angeregten Zustand ist in Anbetracht des verwendeten groben Modells nicht erstaunlich. Sie kann ihre Ursache haben in der Alternanz der Längen der Doppel- und Einfachbindungen, die ein periodisches Potential bedingen [11] oder auch in der im Grund- und angeregten Zustand verschiedenen Elektronenwechselwirkung.

Wir danken dem Schweizerischen Nationalfonds für die Unterstützung dieser Arbeit.

Literatur

1. Navangul, H., Labhart, H.: Theoret. chim. Acta (Berl.) **17**, 239 (1970).
2. Tillieu, J., Guy, J.: C. R. Acad. Sci. (Paris) **236**, 222 (1953).
3. Kelly, H. P.: Physic. Review **136**, 896 (1964); **152**, 62 (1966).
4. Banerjee, K., Salem, L.: Molecular Physics **11**, 405 (1966).
5. Pilar, F. L.: Elementary quantum chemistry, p. 644ff. New York: McGraw-Hill 1968.
6. Flügge, S.: Rechenmethoden der Quantentheorie, S. 26. Berlin-Heidelberg: Springer 1965.
7. Seibold, K., Navangul, H., Labhart, H.: Chem. Physics Letters **3**, 275 (1969).
8. Schweig, A.: Molecular Physics **14**, 533 (1968).
9. Kieser, R. W.: Tables of ionization potentials. Department of Chemistry, Kansas State University, Manhattan, Kansas 1960.
10. Dietrich, C., Jaenicke, W.: Ber. Bunsenges. physik. Chem. **74**, 24 (1970).
11. Kuhn, H.: J. chem. Physics **17**, 1198 (1949).

Prof. Dr. K. Jug
Institut für Theoretische Chemie
der Universität Stuttgart
D-7000 Stuttgart 1
Relenbergstraße 32
Deutschland

Prof. Dr. H. Labhart
Physikalisch-Chemisches Institut
der Universität Zürich
CH-8001 Zürich, Rämistr. 76, Schweiz

Theoret. chim. Acta (Berl.) 24, 290—299 (1972)
© by Springer-Verlag 1972

Das Kastenmodell als Grundlage für ein *ab initio* Verfahren

II. Berechnung der Integrale

ERNST-ALBRECHT REINSCH

Institut für theoretische Chemie der Johann Wolfgang Goethe-Universität in Frankfurt am Main

Eingegangen am 13. August 1971

The Box Model as a Basis for an ab initio Procedure

II. Evaluation of the Integrals

It is shown how the integrals occurring in the final expressions of part I can be solved.

Es werden Lösungswege für die Integrale, die in den Endausdrücken des ersten Teils dieser Arbeit auftraten, angegeben.

1. Einleitung

Im ersten Teil dieser Reihe [1] wurde ein Verfahren zur Berechnung der Gesamtenergie von Molekülen skizziert, das auf einer Störungsrechnung für freie Teilchen basiert. Unter Verwendung des Formalismus von Brueckner und Goldstone wurden die Ausdrücke für die Terme einschließlich derjenigen dritter Ordnung hergeleitet. In ihnen traten Integrale auf, deren Lösung noch aussteht, wenn man Rechnungen für Probesysteme durchführen will. In diesem zweiten Teil soll gezeigt werden, welche Wege zu ihren Berechnungen eingeschlagen werden können.

Im einzelnen handelt es sich dabei um

a) $$\mathcal{I}_1 = \frac{1}{2} \int \frac{B_1 - B_2}{k_1^2 - k_2^2} \, dk_1 \qquad \text{mit } k_2 = k_1 + n\,, \tag{1}$$

das im Beitrag des Graphen V_K^2 auftritt[1],

b) $$\mathcal{I}_2 = \frac{1}{2} \int \frac{1}{(k_1 - k_4)^2} \, \frac{B_1 - B_2}{k_1^2 - k_2^2} \, \frac{B_3 - B_4}{k_3^2 - k_4^2} \, dk_1 \, dk_4 \tag{2}$$

und

$$\mathcal{I}_2' = \int \frac{B_1 - B_2}{k_1^2 - k_2^2} \, \frac{B_3 - B_4}{k_3^2 - k_4^2} \, dk_1 \, dk_4 \qquad \text{mit } k_2 = k_1 + n \text{ und } k_3 = k_4 + n\,, \tag{3}$$

die beide im Beitrag für $V_K^2 \, V_E(a)$ erscheinen,

c) $$\mathcal{I}_3 = \int \frac{1}{(k_1 - k_2)^2} \, \frac{B_2(B_1 - B_3)}{(k_1^2 - k_3^2)^2} \, dk_1 \, dk_2 \qquad \text{mit } k_3 = k_1 + n \tag{4}$$

---

[1] Die Bedeutung dieser Bezeichnungen findet man in Teil I.

aus dem Ausdruck[2] für $V_K^2 V_E(b)$ und

$$\text{d)}\quad \mathscr{J}_4 = \int \left[\frac{B_1}{(k_2^2-k_1^2)(k_3^2-k_1^2)} + \frac{B_2}{(k_1^2-k_2^2)(k_3^2-k_2^2)} + \frac{B_3}{(k_1^2-k_3^2)(k_2^2-k_3^2)} \right] dk \qquad (5)$$

$$\text{mit } k_1 = k,\ k_2 = k + n_1 \text{ und } k_3 = k + n_2$$

im Beitrag für V_K^3.

Dabei ist n (bzw. n_i) immer Gittervektor im reziproken Gitter und die Integrationsgrenzen sind durch die

$$B_i = \begin{cases} 1 & \text{für } |k_i| \leqq 1 \\ 0 & \text{für } |k_i| > 1 \end{cases}$$

gegeben. Die Faktoren 1/2 in (1) und (2) wurden aus Bequemlichkeit gewählt.

2. Die Integrale $\mathscr{J}_1$ und $\mathscr{J}_2'$

Explizit geschrieben lautet das Integral $\mathscr{J}_1$

$$\mathscr{J}_1(n) = \frac{1}{2} \int\limits_{\substack{|k_1| \leqq 1 \\ |k_1+n| > 1}} \frac{dk_1}{k_1^2-(k_1+n)^2} - \frac{1}{2} \int\limits_{\substack{|k_1+n| \leqq 1 \\ |k_1| > 1}} \frac{dk_1}{k_1^2-(k_1+n)^2}.$$

Substituiert man im zweiten Term $k \to -k-n$, so erkennt man, daß beide Terme bis auf das Vorzeichen gleich sind, und erhält

$$\mathscr{J}_1 = \int\limits_{\substack{|k| \leqq 1 \\ |k+n| > 1}} \frac{dk}{k^2-(k+n)^2}.$$

Der Wert dieses Integrals ist unabhängig von der Richtung des Vektors n. Man legt deshalb das Koordinatensystem am einfachsten so, daß n in Richtung der negativen z-Achse weist. Die Komponenten von k seien x, y und z und die von n, $0, 0, -a$ $(a = |n| > 0)$. Der Integrand lautet dann

$$\frac{1}{a}\,\frac{1}{2z-a}$$

und der Integrationsbereich umfaßt wegen $|k| \leqq 1$ das Innere der Einheitskugel. Ist $a < 2$, so muß daraus noch wegen $|k+n| > 1$ das Innere einer Kugel mit Radius 1, deren Mittelpunkt um a in Richtung der positiven z-Achse verschoben ist, herausgeschnitten werden (Fig. 1).

Der Übergang zu Zylinderkoordinaten und Integration über ϕ liefert, mit $u = r^2$ als neuer Integrationsvariablen,

$$\mathscr{J}_1 = \frac{\pi}{a} \int \frac{du\,dz}{2z-a}.$$

---

[2] Aus Gründen der Zweckmäßigkeit wurde die Benennung der Integrationsvariablen k_1 und k_2 gegenüber Gl. (37) von Teil I vertauscht.

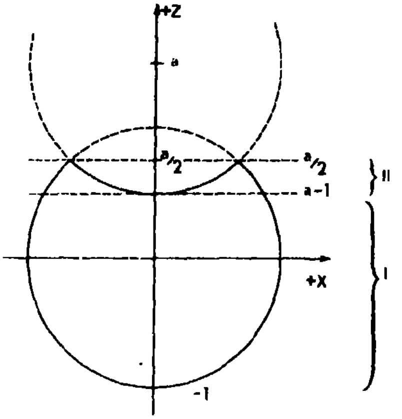

Fig. 1 Integrationsbereich für $y=0$ von $\mathcal{J}_1$ bei $a<2$

Die Integration über u geht im Fall von $a \geqq 2$ von 0 bis $1-z^2$. Im Fall von $a<2$ gilt dies nur für $z \leqq a-1$, während für $z>a-1$ die untere Grenze $1-(z-a)^2$ ist. Die Integration über u ergibt im Fall $a \geqq 2$

$$\frac{\pi}{a} \int_{-1}^{+1} \frac{1-z^2}{2z-a}\, dz$$

und im Fall $a<2$

$$\frac{\pi}{a} \int_{-1}^{a-1} \frac{1-z^2}{2z-a}\, dz - \pi \int_{a-1}^{a/2} dz\,.$$

Das Resultat der Quadratur hat in beiden Fällen die gleiche Form, nämlich

$$\mathcal{J}_1(a) = \frac{\pi}{2a}\left(\frac{4-a^2}{4} \ln \frac{|2-a|}{2+a} - a\right). \tag{6}$$

Das Integral $\mathcal{J}_2'$ läßt sich leicht auf $\mathcal{J}_1$ zurückführen. Es gilt

$$\mathcal{J}_2'(n) = \left\{\int \frac{B_1 - B_2}{k_1^2 - k_2^2}\, dk_1\right\}^2 = 4\mathcal{J}_1^2(n) \qquad (k_2 = k_1 + n)\,. \tag{7}$$

3. Die Integrale $\mathcal{J}_2$ und $\mathcal{J}_3$

Der Lösungsweg ist im Prinzip für beide Integrale der gleiche, so daß sie gemeinsam behandelt werden sollen. $\mathcal{J}_2$ führt auf k-Integrale der Form

$$\pm \int \frac{1}{(k_1-k_4)^2} \frac{1}{k_1^2-(k_1+n)^2} \frac{1}{k_4^2-(k_4+n)^2}\, dk_1\, dk_4\,.$$

Der Integrationsbereich besteht aus vier Zonen:

Zone	$\lvert k_1\rvert$	$\lvert k_1+n\rvert$	$\lvert k_4\rvert$	$\lvert k_4+n\rvert$	Vorzeichen des Integranden
(1)	$\leqq 1$	>1	$\leqq 1$	>1	positiv
(2)	>1	$\leqq 1$	>1	$\leqq 1$	positiv
(3)	$\leqq 1$	>1	>1	$\leqq 1$	negativ
(4)	>1	$\leqq 1$	$\leqq 1$	>1	negativ

Führt man in dem Integral über die Zone (2) die Transformation $k_1 \to -k_1 - n$, $k_4 \to -k_4 - n$ durch, so wird es gleich dem über (1). Transformiert man weiter in (3) mit $k_4 \to -k_4 - n$ und in (4) mit $k_1 \to -k_1 - n$, so ergeben sich ebenfalls zwei gleiche Ausdrücke. Insgesamt wird

$$\mathscr{I}_2(a) = \int\limits_{\substack{|k_1|,\,|k_4| \leqq 1 \\ |k_1+n|,\,|k_4+n| > 1}} \left[\frac{1}{(k_1-k_4)^2} + \frac{1}{(k_1+k_4+n)^2}\right] \frac{dk_1\,dk_4}{[k_1^2-(k_1+n)^2]\,[k_4^2-(k_4+n)^2]}\,. \tag{8}$$

Das Integral $\mathscr{I}_3$ ist von der Form

$$\pm\int \frac{1}{(k_1-k_2)^2}\,\frac{dk_1\,dk_2}{[k_1^2-(k_1+n)^2]^2}$$

mit den Grenzen $|k_1| \leqq 1$, $|k_1+n| > 1$ bei positivem Vorzeichen des Integranden und $|k_1| > 1$, $|k_1+n| \leqq 1$ bei negativem Vorzeichen. Für k_2 gilt in beiden Fällen $|k_2| \leqq 1$. Das Integral über den zweiten Bereich kann durch $k_1 \to -k_1 - n$ in eines über den ersten Bereich transformiert werden; insgesamt ergibt sich

$$\mathscr{I}_3(a) = \int\limits_{\substack{|k_1|,\,|k_2| \leqq 1 \\ |k_1+n| > 1}} \left[\frac{1}{(k_1-k_2)^2} - \frac{1}{(k_1+k_2+n)^2}\right] \frac{dk_1\,dk_2}{[k_1^2-(k_1+n)^2]^2}\,. \tag{9}$$

Wie bei der Berechnung von $\mathscr{I}_1$ kann man das Koordinatensystem so wählen, daß n in die negative z-Richtung weist. Die Komponenten des Vektors k_1 seien x_1, y_1, z_1, die von k_2 bzw k_4 x_2, y_2, z_2 und die von n wie zuvor. Da beide Integrale rotationssymmetrisch sind, geht man auch hier zweckmäßigerweise zu Zylinderkoordinaten über. Die rechten Seiten in Gl. (8) und (9) nehmen dann die Form

$$\int\limits_{\substack{r_1\\z_1}}\int\limits_{\substack{r_2\\z_2}} g(z_1,z_2)\,dr_1 \ldots dz_2 \int\limits_0^{2\pi}\int\limits_0^{2\pi} \frac{d\phi_1\,d\phi_2}{r_1^2+r_2^2 \mp 2r_1r_2\cos(\phi_1-\phi_2)+f(z_1,z_2)}$$

an und ergeben nach Ausführung der ϕ_1, ϕ_2-Integration

$$\int\limits_{\substack{r_1\\z_1}}\int\limits_{\substack{r_2\\z_2}} \frac{4\pi^2 g(z_1,z_2)}{\sqrt{[r_1^2+r_2^2+f(z_1,z_2)]^2-4r_1^2r_2^2}}\,dr_1 \ldots dz_2\,.$$

Man transformiert nun wieder $x = r_1^2$ und $y = r_2^2$ und erhält

a) für das Integral $\mathcal{J}_2$

$$\mathcal{J}_2(a) = \frac{\pi^2}{a^2} \int_{z_1} \int_{z_2} \left\{ \frac{1}{(2z_1 - a)(2z_2 - a)}\, dz_1\, dz_2 \right.$$

$$\left. \cdot \int_x \int_y \left[\frac{1}{\sqrt{[x + y + (z_1 - z_2)^2]^2 - 4xy}} + \frac{1}{\sqrt{[x + y + (z_1 + z_2 - a)^2]^2 - 4xy}} \right] dx\, dy \right\}$$

und

b) für $\mathcal{J}_3$

$$\mathcal{J}_3(a) = \frac{\pi^2}{a^2} \int_{z_1} \int_{z_2} \left\{ \frac{1}{(2z_1 - a)^2}\, dz_1\, dz_2 \right.$$

$$\left. \cdot \int_x \int_y \left[\frac{1}{\sqrt{[x + y + (z_1 - z_2)^2]^2 - 4xy}} - \frac{1}{\sqrt{[x + y + (z_1 + z_2 - a)^2]^2 - 4xy}} \right] dx\, dy \right\}$$

Der Integrationsbereich für k_1 ist der gleiche wie für k in $\mathcal{J}_1$. Dasselbe gilt für k_4 in $\mathcal{J}_2$, während er für k_2 in $\mathcal{J}_3$ einfach das Innere der Einheitskugel ist. Die obere Integrationsgrenze für x ist dann $1 - z_1^2$ und die für y $1 - z_2^2$. Die unteren Grenzen hängen in der gleichen Weise wie diejenigen für u bei $\mathcal{J}_1$ vom Wert des betreffenden z_i und von a ab. Eine Ausnahme gilt für y in $\mathcal{J}_3$: hier ist die untere Grenze stets Null.

Zu lösen ist nun als nächstes das Integral über die Variablen x und y

$$\int_{x = G_1(z_1)}^{1 - z_1^2} \int_{y = G_2(z_2)}^{1 - z_2^2} \frac{dx\, dy}{\sqrt{[x + y + f(z_1, z_2)]^2 - 4xy}}$$

wobei G_i je nachdem 0 oder $1 - (z_i - a)^2$ ist. Das Resultat ist

$$(1 - z_1^2) \ln \frac{f(z_1, z_2) + z_1^2 - z_2^2 + W(1 - z_1^2, 1 - z_2^2)}{f(z_1, z_2) + G_2(z_2) - 1 + z_1^2 + W(1 - z_1^2, G_2(z_2))}$$

$$+ (1 - z_2^2) \ln \frac{f(z_1, z_2) - z_1^2 + z_2^2 + W(1 - z_1^2, 1 - z_2^2)}{f(z_1, z_2) + G_1(z_1) - 1 + z_2^2 + W(G_1(z_1), 1 - z_2^2)}$$

$$+ G_1(z_1) \ln \frac{f(z_1, z_2) + G_2(z_2) - G_1(z_1) + W(G_1, G_2)}{f(z_1, z_2) + 1 - z_2^2 - G_1(z_1) + W(G_1, 1 - z_2^2)}$$

$$+ G_2(z_2) \ln \frac{f(z_1, z_2) - G_2(z_2) + G_1(z_1) + W(G_1, G_2)}{f(z_1, z_2) + 1 - z_1^2 - G_2(z_2) + W(1 - z_1^2, G_2)}$$

$$+ \tfrac{1}{2} [W(1 - z_1^2, 1 - z_2^2) - W(G_1(z_1), 1 - z_2^2) - W(1 - z_1^2, G_2(z_2))$$

$$+ W(G_1(z_1), G_2(z_2))],$$

wobei

$$W(A, B) = \sqrt{f^2(z_1, z_2) + 2f(z_1, z_2) \cdot (A + B) + (A - B)^2}.$$

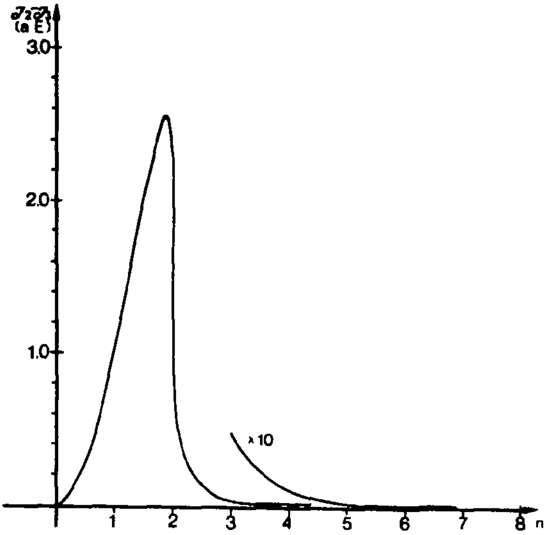

Fig. 2. Ergebnisse der Rechnung für $\mathcal{J}_2 - \mathcal{J}_3$

Die Integrationen über die Variablen z_1 und z_2 sind nur noch numerisch durchzuführen. Sie sind sehr umständlich, weil der Integrand für bestimmte Kurven in dem zweidimensionalen Integrationsbereich logarithmische Unstetigkeiten aufweist und nicht ohne weiteres die Anwendung eines numerischen Verfahrens zuläßt. Man muß vielmehr zunächst geeignete logarithmische Terme abspalten, diese dann analytisch integrieren und das Resultat nach der numerischen Integration des Restes wieder addieren. Dabei werden eine Reihe von langwierigen Grenzübergängen nötig. Die Einzelheiten sind aber in diesem Zusammenhang ohne Interesse und können deshalb hier übergangen werden.

In der Summe der Beiträge für die beiden $V_K^2 V_E$-Graphen tritt nur $\mathcal{J}_2 - \mathcal{J}_3$ auf. Für alle weiteren Zwecke ist daher lediglich die Kenntnis dieser Differenz notwendig. Sie hängt von nur einer Größe, nämlich $u = |n|$ ab und kann deshalb ein für alle Mal berechnet werden. Das Resultat der numerischen Rechnung ist in Fig. 2 enthalten[3].

4. Das Integral $\mathcal{J}_4$

Hier existieren acht Integrationsbereiche, je nachdem, ob der Betrag von k_1, k_2, k_3 größer oder kleiner als 1 ist. Da der Integrand Null wird, wenn alle drei k_i gleichzeitig größer oder kleiner als 1 sind, verbleiben nur sechs Zonen.

Für den Fall $|k_1| \leqq 1$ und $|k_2|$, $|k_3| > 1$ ist nur der erste Summand in Gl. (5) von Null verschieden und es tritt somit das Integral

$$\mathcal{J}_5(n_1, n_2) = \int\limits_{\substack{|k| \leq 1 \\ |k+n_i| > 1}} \frac{dk}{[k^2 - (k+n_1)^2]\,[k^2 - (k+n_2)^2]}$$

---

[3] Es wurde das Integrations-Verfahren von Bulirsch und Stoer [2] angewendet, das nur wenig Stützstellen benötigt und sehr schnell konvergiert.

auf. Für die beiden Fälle – nur $|k_2|$ bzw. $|k_3| \leqq 1$ – führt die Transformation $k \to \mathrm{k} - \mathrm{n}_1$ bzw. $k \to \mathrm{k} - \mathrm{n}_2$ auf

$$\mathcal{J}_5(n_2 - n_1, -n_1) \quad \text{bzw.} \quad \mathcal{J}_5(-n_2, n_1 - n_2).$$

Für den Fall $|k_2| > 1$, $|k_1|, |k_3| \leqq 1$ bleiben im Integranden von $\mathcal{J}_4$ nur der erste und dritte Term stehen; sie können noch zu

$$+\frac{1}{[k^2 - (k + n_1)^2]\,[(k + n_2)^2 - (k + n_1)^2]}$$

zusammengefaßt werden. Das zugehörige Integral lautet nach dem Übergang $k \to k - n_2/2$

$$\mathcal{J}_6(n_1, n_2)$$

$$\int\limits_{\substack{|k+n_1-\frac{n_2}{2}| \le 1 \\ |k+\frac{n_2}{2}| \le 1}} \frac{dk}{\left[\left(k + n_1 - \frac{n_2}{2}\right)^2 - \left(k + \frac{n_2}{2}\right)^2\right]\left[\left(k + n_1 - \frac{n_2}{2}\right)^2 - \left(k - \frac{n_2}{2}\right)^2\right]}.$$

Die zwei noch fehlenden Fälle – jeweils nur $|k_1|$ bzw. $|k_3| > 1$ – lassen sich auf die gleiche Weise wie bei $\mathcal{J}_5$ in

$$\mathcal{J}_6(-n_2, n_1 - n_2) \quad \text{bzw.} \quad \mathcal{J}_6(n_2 - n_1, -n_1)$$

transformieren. Damit wird

$$\begin{aligned}\mathcal{J}_4(n_1, n_2) = \mathcal{J}_5(n_1, n_2) &+ \mathcal{J}_5(n_2 - n_1, -n_1) + \mathcal{J}_5(-n_2, n_1 - n_2) \\ &- \mathcal{J}_6(n_1, n_2) - \mathcal{J}_6(n_2 - n_1, -n_1) - \mathcal{J}_6(-n_2, n_1 - n_2).\end{aligned}$$

Der Beitrag des Graphen V_K^3 [vgl. Gl. (32) in I] ist

$$-\frac{64}{27 m^2 \pi^4 k_F} \sum_{n_1, n_2} S(-n_1)\, S(n_1 - n_2)\, S(n_2)\, \frac{1}{n_1^2}\, \frac{1}{n_2^2}\, \frac{1}{(n_1 - n_2)^2}\, \mathcal{J}_4(n_1, n_2). \quad (10)$$

Man kann nun durch cyclische Vertauschung der Größen $-n_1, n_1 - n_2, n_2$ zeigen, daß die drei $\mathcal{J}_5$-Terme in $\mathcal{J}_4$ jeweils den gleichen Beitrag liefern. Da für die $\mathcal{J}_6$-Terme dasselbe gilt, läßt sich $\mathcal{J}_4$ in Gl. (10) durch

$$3(\mathcal{J}_5 - \mathcal{J}_6)$$

ersetzen.

Zur Berechnung von $\mathcal{J}_5$ und $\mathcal{J}_6$ legt man das Koordinatensystem am besten so, daß n_2 in Richtung der negativen z-Achse weist und n_1 in der xz-Ebene liegt. Diese Vektoren sind dann durch folgende Parameter gegeben: n_1 durch $-b, 0, -c$ und n_2 durch $0, 0, -a$. Mit der Abkürzung $m = \sqrt{b^2 + c^2}$ gilt

$$\mathcal{J}_5(a, b, c) = \frac{1}{a} \int \frac{dx\,dy\,dz}{(2z - a)(2bx + 2cz - m^2)}.$$

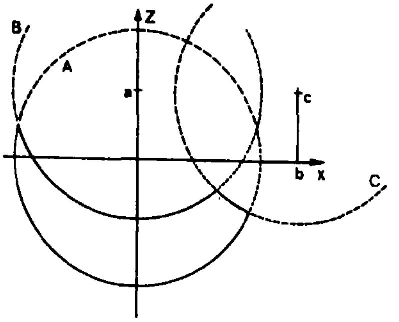

Fig. 3. Beispiel für den Integrationsbereich von $\mathscr{I}_5$ bei $a, m < 2$ (Schnitt in der xz-Ebene)

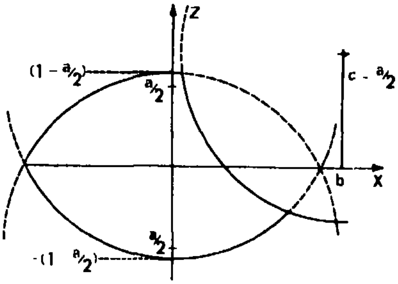

Fig. 4. Beispiel für den Integrationsbereich von $\mathscr{I}_6$ (Schnitt in der xz-Ebene)

Der Integrationsbereich ist das Volumen innerhalb der Einheitskugel um den Nullpunkt (*A* in Fig. 3), aber außerhalb der Einheitskugeln um die Punkte 0, 0, a und b, 0, c (*B* und *C* in Fig. 3).

Für $\mathscr{I}_6$ gilt

$$\mathscr{I}_6(a,b,c) = \int \frac{dx\,dy\,dz}{(2bx+2cz-m^2+ac)\,[2bx+2(c-a)z-m^2+ac]}$$

$$= -\int \frac{1}{2az}\left(\frac{1}{2bx+2cz-m^2+ac} - \frac{1}{2bx+2(c-a)z-m^2+ac}\right) dx\,dy\,dz\,.$$

Hier erstreckt sich die Integration über den Bereich, der innerhalb der beiden Einheitskugeln um 0, 0, $\pm a/2$, aber außerhalb der Einheitskugel um b, 0, $c - a/2$ liegt (vgl. Fig. 4). $\mathscr{I}_6$ ist deshalb Null für alle $a \geqq 2$.

Der Integrand selbst ist in beiden Fällen von y unabhängig und die Integration liefert nur die Differenz der Grenzen, die je nach der Zone, in der z liegt, zu wählen sind, nämlich Kreise um den Mittelpunkt 0, 0 oder 0, b. Die Integration über z ist nur in den Bereichen von z, in denen der Integrationsbereich rotationssymmetrisch bezüglich der z-Achse ist, analytisch möglich, anderenfalls muß auch hier auf numerische Verfahren zurückgegriffen werden.

$\mathcal{J}_5$ und $\mathcal{J}_6$ hängen im Gegensatz zu den früheren Integralen von drei Parametern ab. Eine Tabellierung kam deshalb hier nicht in Frage, sondern die Berechnung erfolgte einzeln. Dies ist möglich, da nur über maximal *eine* Variable numerisch zu integrieren ist.

5. Zusammenstellung der Terme

Die in der Störreihe für $E/(\Omega/a)$ eingehenden Terme sind im ersten Teil [1] abgeleitet worden und sollen nun nochmals der Übersichtlichkeit halber zusammengestellt werden. Bezüglich der Bedeutung der einzelnen Symbole wird auf die entsprechenden Gleichungen hingewiesen.

a) Die Energie pro Elementarzelle ist in nullter und erster Näherung

$$\frac{3m}{10}\,k_F^2+\frac{1}{2}\sum_i Z_i\left\{\sum_{\substack{i',j'\\ i\neq i',\ \text{wenn } j'\\ \text{die Basiszelle ist}}}\frac{Z_{i'}}{|r_i-r_{i'j'}|}-\frac{m}{a}\int\frac{dv'}{|r-r'|}\right\}-\frac{3mk_F}{4\pi}, \tag{11}$$

[Gl. (I. 10, 11, 27)].

b) In zweiter Näherung tritt hinzu

$$+\frac{8}{3m\pi^3}\sum_n S(n)\,S(-n)\,\frac{1}{n^4}\,\mathcal{J}_1(n)+V_E^2 \tag{12}$$

[Gl. (I. 29)].

c) Die dritte Näherung ist

$$\begin{aligned}&-\frac{64}{9m^2\pi^4k_F}\sum_{n_1n_2}S(-n_1)\,S(n_1-n_2)\,S(n_2)\,\frac{1}{n_1^2n_2^2(n_1-n_2)^2}\,[\mathcal{J}_5(n_1,n_2)-\mathcal{J}_6(n_1,n_2)]\\&-\frac{8}{3m\pi^5k_F}\sum_n S(n)\,S(-n)\,\frac{1}{n^4}\left\{\mathcal{J}_2(n)-\mathcal{J}_3(n)-\frac{4}{n^2}\,[\mathcal{J}_1(n)]^2\right\}+V_E^3\,.\end{aligned} \tag{13}$$

[Gln. (I. 32, 34, 37)]. Die Terme V_E^2 und V_E^3 lassen sich der Literatur entnehmen [3, 4].

Es bleibt schließlich die Frage, ob die Summen über die Gittervektoren endlich bleiben.

a) Gl. (12).

Die n-Summe im Diagramm V_K^2 enthält den Faktor n^{-4} und das Integral $\mathcal{J}_1$, das sich für große $|n|$ wie $1/n^2$ verhält. Die Zahl der Gittervektoren in einer Kugelschale wächst wie deren Oberfläche, d. h. mit n^2. Der Beitrag einer solchen Kugelschale verhält sich also wie $n^2\cdot n^{-4}\cdot n^{-2}=n^{-4}$. Derartige Summen bleiben endlich.

b) Gl. (13) 2. Term.

Der Faktor ist n^{-4} und die Integrale $\mathcal{J}_2$ bzw. $\mathcal{J}_3$ verhalten sich ebenfalls wie n^{-4}, so daß die Beiträge von Kugelschalen wie n^{-6} gehen und endlich bleiben.

c) Gl. (13) 1. Term.

Hier tritt der Faktor $n_1^{-2}n_2^{-2}(n_1-n_2)^{-2}$ auf und die Integrale $\mathcal{J}_4$ verhalten sich für große $|n_1|$ und $|n_2|$ wie $n_1^{-2}n_2^{-2}$. Für die Doppelsumme gilt, daß der Beitrag einer „neuen" Kugelschale $n_1=n+\Delta$, $n_2=n+\Delta$ sich wie $n^{-8}\cdot n^5\cdot n^{-2}=n^{-5}$

verhält und damit ebenfalls endlich bleibt (n^{-8} rührt von den Faktoren $n_1^{-2} n_2^{-2}$ im Vorfaktor und in $\mathcal{J}_4$ her, n^5 ist die Zahl der „neuen" Punktpaare und n^{-2} kommt aus dem Faktor $1/(n_1 - n_2)^{-2}$, der bewirkt, daß die meisten der Punktpaare nur einen verschwindenden Beitrag liefern).

Damit sind die Grundlagen für Proberechnungen geschaffen. Die Ergebnisse solcher Rechnungen für die einfachsten Systeme werden gesondert mitgeteilt werden.

Die numerischen Integrationen wurden im Deutschen Rechenzentrum, Darmstadt, durchgeführt. Ich möchte diesem Institut für die Möglichkeit hierzu danken. Die notwendigen finanziellen Mittel stellte der Sonderforschungsbereich „Theoretische Chemie" zur Verfügung.

Literatur

1. Reinsch, E. A.: Theoret. chim. Acta (Berl.) **23**, 155 (1971).
2. Bulirsch, R., Stoer, J.: Numer. Math. **6**, 413 (1964).
3. Gell-Mann, M., Brueckner, K. A.: Physic. Rev. **106**, 364 (1957).
4. Carr, W. J., Maradudin, A. A.: Physic Rev. A **133**, 371 (1964).

Dr. Ernst-Albrecht Reinsch
Institut für theoretische Chemie
Universität Frankfurt
D-6000 Frankfurt am Main
Robert-Mayer-Str. 11
Deutschland

Theoret. chim. Acta (Berl.) 24, 300—306 (1972)
© by Springer-Verlag 1972

Mass-Variation and Darwin Relativistic Corrections in Many-Electron Atoms*

B. W. N. LO, K. M. S. SAXENA, and S. FRAGA
Division of Theoretical Chemistry, Department of Chemistry, University of Alberta,
Edmonton 7, Alberta, Canada

Received June 7, 1971

The formulation for the evaluation of the matrix elements over the relativisitic mass-variation and Darwin operators is presented. Calculations of these corrections have been carried out, using available analytical Hartree-Fock functions, for the positive ions, neutral systems, and negative ions for all the atoms from He to Kr.

Die Formulierung der Matrix-Elemente des Operators der relativistischen Massen-Variation und des Darwin-Operators wird angegeben. Die Größe dieser Korrekturen wird unter Benutzung bekannter analytischer Hartree-Fock-Funktionen für die positiven Ionen, neutralen Systeme und negativen Ionen aller Atome von He bis Kr berechnet.

Introduction

In order to complete the general research project under way at this Laboratory on the properties and interactions of many-electron atoms, the contributions from two terms in the Breit-Pauli hamiltonian operator are now considered: the relativistic correction to the kinetic energy due to the variation of the mass of the electrons with the velocity and the so-called Darwin correction to the potential energy, characteristic of the Dirac theory but with no classical analogue.

The calculations on two-electron systems by Pekeris and co-workers [12, 16] have shown that these terms make an appreciable contribution to the relativistic energy. Work on these operators has also been carried out by Jones [7] and Rudzikas *et al.* [14, 15], but either the two-electron part of the Darwin operator was omitted [7] or its contribution evaluated only for the electrons in the outermost shell [15].

The purpose of this work is to present a complete analysis of these operators and determine the corresponding values for the positive ions, neutral systems, and negative ions from He to Kr.

Mathematical Formulation

The Darwin and mass-variation operators are defined (in a.u.) by

$$\begin{aligned}\mathscr{H}_d &= \mathscr{H}_{d1} + \mathscr{H}_{d2} \\ &= \frac{\pi\alpha^2}{2}\left\{Z\sum_i \delta(\boldsymbol{r}_i) - 2\sum_{i<j}\delta(\boldsymbol{r}_{ij})\right\},\end{aligned}$$

$$\mathscr{H}_p = -\frac{\alpha^2}{8}\sum_i \boldsymbol{p}_i^4 = -\frac{\alpha^2}{8}\sum_i \nabla_i^4,$$

---

* This work has been supported in part by the National Research Council of Canada.

respectively (see, e.g., Fontana and Meath [5]). Z represents the nuclear charge, $\boldsymbol{r}_i$ is the position vector of the i-th electron, associated with a linear momentum operator $\boldsymbol{p}_i$, and $\boldsymbol{r}_{ij}$ denotes the position vector of electron i relative to electron j; δ is a three-dimensional delta function and α is the fine structure constant. The summations extend over all the electrons in the system (with the restriction indicated).

The evaluation of the matrix elements of these three operators, $\mathscr{H}_{d1}$, $\mathscr{H}_{d2}$, and $\mathscr{H}_p$, is considered separately below.

One-Electron Darwin Operator

This interaction vanishes for all the orbitals with $l \neq 0$. For a single s-electron it is

$$\langle \Phi | \, \delta(\boldsymbol{r}) \, | \Phi \rangle = \varrho(0) \,,$$

where $\varrho(0)$ denotes the electron density at the nucleus. The total contribution is

$$E_{d1} = \tfrac{1}{2} \pi Z \alpha^2 \sum_i n_i \varrho_i(0) \,,$$

where the summation extends over all the occupied s-orbitals in the system; n_i represents the occupation number of the i-th orbital.

Two-Electron Darwin Operator

The intershell contribution may be evaluated, through the use of generalized coefficients of fractional parentage, from the basic two-electron matrix elements (de-Shalit and Talmi [4]),

$$\begin{aligned} &\langle l_a l_b L M_L S M_S | \, \mathscr{A}^{\dagger} \; \hbar_{d2} \mathscr{A} \, | l_a l_b L M_L S M_S \rangle \\ &\quad = -\tfrac{1}{4} \alpha^2 [1 + (-1)^S] \, (2l_a + 1)(2l_b + 1) \begin{pmatrix} l_a & l_b & L \\ 0 & 0 & 0 \end{pmatrix}^2 R_2(a, b) \,, \end{aligned}$$

given in terms of 3-j symbols and the radial integrals $R_2(a, b)$ (that appears in the formulation for the electron spin-spin contact interaction), defined by

$$R_2(a, b) = \int_0^{\infty} P_a^2(r) \, P_b^2(r) \, r^{-2} \, dr \;;$$

$P(r)$ is given by $rR(r)$, where $R(r)$ is the radial function of the shell under consideration. $\hbar_{d2}$ is the two-electron Darwin operator for the two electrons involved. The general formulation may be derived following the procedure described by Lo *et al.* [8] for the electron spin-spin contact interaction.

The interaction between the electrons of a given shell, characterized by a total quantum number Γ, may be expressed as

$$\langle l_a^n \Gamma | \, \mathscr{A}^{\dagger} \hbar_{d2} \mathscr{A} \, | l_a^n \Gamma \rangle = -\frac{\alpha^2}{4} R_2(a, a) \sum_k (2k + 1) f_k \,,$$

where f_k are the coefficients of the Slater-Condon integrals, F^k, in the expression of the electrostatic energy of the shell considered; these values have been tabulated by Nielson and Koster [11].

On the other hand, by an argument similar to that given by Armstrong [1] for the electron spin-spin contact interaction, the intrashell contribution may be also evaluated by

$$\langle l_a^n \Gamma | \mathcal{A}^\dagger k_{d2} \mathcal{A} | l_a^n \Gamma \rangle$$
$$= -\frac{\alpha^2}{4} R_2(a, a) \left| (2l_a + 1)(2l_a + 3)^{-1} \langle e_1(l_a) \rangle + \frac{7}{6435} \langle e_2(f) \rangle \delta_{3, l_a} \right| ,$$

which holds for $l_a \leqq 3$, and where e are the operators introduced by Racah [13] for the evaluation of the coulombic interactions. The matrix elements of e_2 have been tabulated by Nielson and Koster [11] and the matrix elements of e_1 are given by

$$\langle e_1(l) \rangle = \frac{1}{2}(2l + 3)(n - v) + \frac{v}{4}(v + 2) - S(S + 1)$$

where v is the seniority number and S the spin quantum number of the state under consideration.

It may be observed that the intrashell interaction is equal (with sign changed) to one half of the electron spin-spin contact interaction (Fraga and Thorhallsson [6]). In fact, when the general formulation for the intershell contributions is simplified for the special case of configurations with only one open shell, one finds the same relationship between the two-electron Darwin and electron spin-spin contact contributions as for the intrashell interaction.

Mass Variation

Taking into account that

$$\nabla^2 \Phi_{nl} = \frac{\partial^2 \Phi}{\partial r^2} + \frac{2}{r} \frac{\partial \Phi}{\partial r} - \frac{l(l + 1)}{r^2} \Phi ,$$

one can write, for a single electron,

$$\langle \Phi_{nl} | p^4 | \Phi_{nl} \rangle = \langle \nabla^2 \Phi_{nl} | \nabla^2 \Phi_{nl} \rangle$$
$$= I_{nl}(2, 2; 0) - 2l(l + 1) I_{nl}(2, 0; -2) + l^2(l + 1)^2 I_{nl}(0, 0; -4) ,$$

where $$I_{nl}(p, q; \beta) = \int_0^\infty \left(\frac{\partial^p P_{nl}}{\partial r^p} \right) r^\beta \left(\frac{\partial^q P_{nl}}{\partial r^q} \right) dr .$$

The total contribution is obtained by summation over all the occupied orbitals in the system, with consideration of the corresponding occupation numbers.

Results and Discussion

The calculations have been carried out using the analytical Hartree-Fock functions of Clementi [3] and Malli [9]; for the one-electron Darwin correction, the electronic densities at the nucleus have been taken from the work of Malli and Fraga [10].

The results for E_{d1} and E_p are presented in Tables 1 and 2, respectively; the values of E_{d2} may be obtained from those given by Lo *et al.* [8] for the electron spin-spin contact interaction.

The comparison made in Table 3 shows that, although the values of E_{d1} and E_p may be appreciable, the difference between the total contributions of the positive ion, neutral atom, and negative ion are small; in Br they are of the order of 0.2 eV. The same behavior is observed for the electron spin-spin contact interaction and consequently for E_{d2}.

Table 1. One-electron Darwin relativistic correction (in a.u.) for positive ions, neutral atoms, and negative ions

Configuration[a]	State	Positive ions		Neutral atoms		Negative ions	
		System	E_{d1}	System	E_{d1}	System	E_{d1}
$1s^2$	^1S	Li	0.00344	He	0.00060		
$2s^1$	^2S	Be	0.01180	Li	0.00347		
$2s^2$	^1S	B	0.03038	Be	0.01185	Li	0.00347
$2p^1$	^2P	C	0.06450	B	0.03008		
$2p^2$	^3P	N	0.12145	C	0.06399	B	0.02998
	^1D		0.12146		0.06398		0.03004
	^1S		0.12155		0.06405		0.03000
$2p^3$	^4S	O	0.20964	N	0.12059	C	0.06372
	^2D		0.20969		0.12069		0.06380
	^2P		0.20975		0.12076		0.06382
$2p^4$	^3P	F	0.33903	O	0.20866	N	0.12032
	^1D		0.33915		0.20871		0.12039
	^1S		0.33923		0.20874		0.12049
$2p^5$	^2P	Ne	0.52053	F	0.33765	O	0.20817
$2p^6$	^1S	Na	0.76685	Ne	0.51839	F	0.33678
$3s^1$	^2S	Mg	1.09715	Na	0.76661		
$3s^2$	^1S	Al	1.52603	Mg	1.09744	Na	0.76742
$3p^1$	^2P	Si	2.06880	Al	1.52468		
$3p^2$	^3P	P	2.74472	Si	2.06638	Al	1.52517
	^1D		2.74482		2.06653		1.52582
	^1S		2.74504		2.06667		1.52564
$3p^3$	^4S	S	3.57380	P	2.74168	Si	2.06702
	^2D		3.57293		2.74183		2.06689
	^2P		3.57494		2.74196		2.06789
$3p^4$	^3P	Cl	4.57875	S	3.57088	P	2.74210
	^1D		4.57986		3.57095		2.74203
	^1S		4.58010		3.57104		2.74262
$3p^5$	^2P	A	5.78349	Cl	4.57553	S	3.57176
$3p^6$	^1S	K	7.21205	A	5.77858	Cl	4.57672
$4s^1$	^2S	Ca	8.89708	K	7.21492		
$4s^2$	^1S			Ca	8.89869	K	7.21473
$3d^1$	^2D			Sc	10.86095		
$3d^2$	^3F	Sc	10.85295	Ti	13.12938	Sc	10.85599
$3d^3$	^4F	Ti	13.11990	V	15.73476	Ti	13.12280
$3d^4$	^5D	V	15.71815	Cr	18.71068	V	15.72703
$3d^5$	^6S	Cr	18.69686	Mn	22.08627	Cr	18.70822
$3d^6$	^5D	Mn	22.07164	Fe	25.89059	Mn	22.07664
$3d^7$	^4F	Fe	25.87280	Co	30.18592	Fe	25.87874
$3d^8$	^3F	Co	30.16532	Ni	34.98439	Co	30.17319

Table 1 (continued)

Configuration[a]	State	Positive ions		Neutral atoms		Negative ions	
		System	E_{d1}	System	E_{d1}	System	E_{d1}
$3d^9$	^2D	Ni	34.96177	Cu	40.33657		
$3d^{10}$	^1S	Cu	40.31049				
$4s^1$	^2S	Zn	46.26943	Cu	40.32028	Ni	34.96657
$4s^2$	^1S	Ga	52.85411	Zn	46.27901	Cu	40.31900
$4p^1$	^2P	Ge	60.12327	Ga	52.84791		
$4p^2$	^3P	As	68.16196	Ge	60.13149	Ga	52.84968
	^1D		68.16357		60.13261		52.85040
	^1S		68.16474				
$4p^3$	^4S	Se	76.94111	As	68.15581	Ge	60.12791
	^2D		76.94076		68.15608		60.12854
	^2P		76.94081		68.15682		60.12952
$4p^4$	^3P	Br	86.53040	Se	76.93409	As	68.15285
	^1D		86.53080		76.93328		68.15278
	^1S		86.53253		76.93528		68.15369
$4p^5$	^2P	Kr	97.00863	Br	86.52348	Se	76.92820
$4p^6$	^1S			Kr	96.99735	Br	86.51686

[a] The positive ions of the transition elements (from Sc through Cu) have configurations $4s^0\ 3d^n$.

Table 2. Relativistic correction (in a.u.) due to mass variation in positive ions, neutral atoms, and negative ions[a]

Configuration[b]	State	Positive ions		Neutral atoms		Negative ions	
		System	E_p	System	E_p	System	E_p
$1s^2$	^1S	Li	0.00410	He	0.00070		
$2s^1$	^2S	Be	0.01435	Li	0.00415		
$2s^2$	^1S	B	0.03723	Be	0.01439	Li	0.00415
$2p^1$	^2P	C	0.07969	B	0.03685		
$2p^2$	^3P	N	0.15109	C	0.07901	B	0.03671
	^1D		0.15106		0.07896		0.03680
	^1S		0.15119		0.07905		0.03674
$2p^3$	^4S	O	0.26242	N	0.14989	C	0.07863
	^2D		0.26242		0.15002		0.07873
	^2P		0.26250		0.15012		0.07874
$2p^4$	^3P	F	0.42678	O	0.26106	N	0.14950
	^1D		0.42694		0.26111		0.14959
	^1S		0.42698		0.26110		0.14973
$2p^5$	^2P	Ne	0.65874	F	0.42487	O	0.26034
$2p^6$	^1S	Na	0.97561	Ne	0.65562	F	0.42353
$3s^1$	^2S	Mg	1.40313	Na	0.97486		
$3s^2$	^1S	Al	1.96106	Mg	1.40327	Na	0.97642
$3p^1$	^2P	Si	2.67085	Al	1.95905		
$3p^2$	^3P	P	3.55871	Si	2.66702	Al	1.96024
	^1D		3.55882		2.66722		1.96144
	^1S		3.55897		2.66740		1.96090
$3p^3$	^4S	S	4.65181	P	3.55385	Si	2.66882
	^2D		4.65007		3.55400		2.66836
	^2P		4.65377		3.55417		2.67028
$3p^4$	^3P	Cl	5.98218	S	4.64733	P	3.55507
	^1D		5.98399		4.64740		3.55482

Table 2 (continued)

Configuration[b]	State	Positive ions System	Positive ions E_p	Neutral atoms System	Neutral atoms E_p	Negative ions System	Negative ions E_p
	^1S		5.98452		4.64743		3.55589
$3p^5$	^2P	A	7.58411	Cl	5.97771	S	4.64980
$3p^6$	^1S	K	9.49112	A	7.57683	Cl	5.98106
$4s^1$	^2S	Ca	11.74674	K	9.49617		
$4s^2$	^1S			Ca	11.74907	K	9.49595
$3d^1$	^2D			Sc	14.38126		
$3d^2$	^3F	Sc	14.36690	Ti	17.42976	Sc	14.37187
$3d^3$	^4F	Ti	17.41318	V	20.93745	Ti	17.41748
$3d^4$	^5D	V	20.90692	Cr	24.95282	V	20.92319
$3d^5$	^6S	Cr	24.92782	Mn	29.51192	Cr	24.94469
$3d^6$	^5D	Mn	29.48658	Fe	34.65538	Mn	29.49414
$3d^7$	^4F	Fe	34.62364	Co	40.48981	Fe	34.63348
$3d^8$	^3F	Co	40.45271	Ni	47.00052	Co	40.46618
$3d^9$	^2D	Ni	46.95903	Cu	54.28218		
$3d^{10}$	^1S	Cu	54.23631				
$4s^1$	^2S	Zn	62.36221	Cu	54.25142	Ni	46.97402
$4s^2$	^1S	Ga	71.34233	Zn	62.37778	Cu	54.24996
$4p^1$	^2P	Ge	81.30165	Ga	71.33870		
$4p^2$	^3P	As	92.34089	Ge	81.31519	Ga	71.34369
	^1D		92.34299		81.31675		71.34452
	^1S		92.34405				
$4p^3$	^4S	Se	104.4074	As	92.33386	Ge	81.31022
	^2D		104.4066		92.33448		81.31091
	^2P		104.4066		92.33467		81.31230
$4p^4$	^3P	Br	117.6005	Se	104.3989	As	92.32967
	^1D		117.6009		104.3977		92.32947
	^1S		117.6025		104.4003		92.33064
$4p^5$	^2P	Kr	132.0507	Br	117.5924	Se	104.3912
$4p^6$	^1S			Kr	132.0373	Br	117.5838

[a] All the values in this Table are negative.

[b] The positive ions of the transition elements (from Sc through Cu) have configurations $4s^0 3d^n$.

Table 3. Comparison of the orbital contributions to the relativistic corrections (in a.u.) in Br and its ions

	Correction for mass variation[a]			One-electron Darwin correction		
	$Br^+ (^3P)$	$Br (^2P)$	$Br^- (^1S)$	$Br^+ (^3P)$	$Br (^2P)$	$Br (^1S)$
1s	96.34546	96.34724	96.34673	77.56520	77.56668	77.56619
2s	12.07728	12.07627	12.07606	7.63681	7.63619	7.63603
3s	2.004271	2.00354	2.00313	1.20753	1.20709	1.20684
4s	0.20268	0.19035	0.18076	0.12086	0.11351	0.10780
2p	5.57172	5.57144	5.57156			
3p	1.03087	1.03083	1.03157			
4p	0.05414	0.05896	0.06031			
3d	0.31411	0.31379	0.31372			
Total	117.6005	117.5924	117.5838	86.53040	86.52348	86.51686
|Difference|		0.00860	0.00810		0.00692	0.00662

[a] In absolute value.

Table 4. Comparison of the relativistic corrections (in cm^{-1}) evaluated for He from various functions

Correction	Function				
	Hydrogenic[a]	Hartree[a]	Hartree-Fock[b]	Hylleraas[a]	Exact[c]
E_p	−118.45	−153.28	−154.31	−159.24	−158.03
E_{d1}	112.31	132.06	132.04	133.40	132.94
E_{d2}	− 7.02	− 6.90	− 7.00	− 8.30	− 3.91
Sum	− 13.16	− 28.11	− 29.27	− 34.14	− 29.00

[a] Evaluated by Sessler and Foley [17] and Bethe and Salpeter [2].

[b] This work.

[c] As given by Stewart [18] and Bethe and Salpeter [2].

A more detailed study of these interactions is made in Table 4 for He, where results obtained from different functions are available. In this connection it must be mentioned that all the values quoted from the work of Sessler and Foley [17] for E_{d2} have been multiplied by 2, as the operator used in their work is affected by a factor $\frac{1}{2}$, by comparison to the expressions usually accepted (see e.g., Fontana and Meath [5], Rudzikas [14], and Stewart [18]). The discrepancy observed for the value of E_{d2} obtained from the Hylleraas function cannot be explained; it should be similar to that obtained for the Pekeris function. In any case it may be concluded that Hartree-Fock functions provide a satisfactory description of these interactions in many-electron atoms.

References

1. Armstrong, L., Jr : Physic. Rev. **170**, 122 (1968).
2. Bethe, H. A., Salpeter, E. E.: Quantum mechanics of one- and two-electron atoms. New York: Academic Press 1957.
3. Clementi, E.: Tables of atomic functions. San Jose: IBM 1965.
4. De-Shalit, A., Talmi, I.: Nuclear shell theory. New York: Academic Press 1963.
5. Fontana, P. R., Meath, W. J., J. math. Physics **9**, 1357 (1968).
6. Fraga, S., Thorhallsson, J.: Physic. Rev. **178**, 70 (1969).
7. Jones, M.: J. Physics B **3**, 1571 (1970).
8. Lo, B. W. N., Saxena, K M. S., Fraga, S.: Theoret. chim. Acta (Berl.) (in press).
9. Malli, G · Canad J. Physics **44**, 3121 (1966).
10. - , Fraga, S.: Canad. J. Physics **44**, 3131 (1966).
11. Nielson, C. W., Koster, G. F.: Spectroscopic coefficients for the p^n, d^n and f^n configurations. Cambridge: MIT Press 1963.
12. Pekeris, C. L.: Physic. Rev. **112**, 1649 (1958).
13. Racah, G.: Physic. Rev. **76**, 1352 (1949)
14. Rudzikas, Z.: Liet. Fiz. Rinkinys **9**, 707 (1969).
15. - , Karaziya, R.: Liet. Fiz. Rinkinys **10**, 13 (1970).
16. Schiff, B., Lifson, H., Pekeris, C. L., Rabinowitz, P.: Physic. Rev. **140**, A 1104 (1965).
17. Sessler, A. M., Foley, H. M.: Physic. Rev. **92**, 1321 (1953).
18. Stewart, A. L.: Advan. Physics **12**, 299 (1963).

Prof. Dr. S. Fraga
Division of Theoretical Chemistry
University of Alberta
Edmonton 7, Alberta, Canada

Theoret. chim. Acta (Berl.) 24, 307–316 (1972)
© by Springer-Verlag 1972

The Electronic Structures and Energies of Borazine, Boronimide and Dimeric Boronimide

D. R. ARMSTRONG

Department of Pure and Applied Chemistry, University of Strathclyde, Glasgow, C. 1

D. T. CLARK

Department of Chemistry, The University, Durham

Received October 21, 1971

The electronic energies and structures of two proposed models of borazine have been examined by *ab initio* calculations using Gaussian-Type atomic orbitals. It is found that the planar D_{3h} model is energetically preferred. The electronic population analysis reveals that nitrogen and boron atoms in borazine possess a negative and positive charge, respectively. Calculations have also been performed on boronimide and dimeric boronimide. The trimerisation and dimerisation energy of boronimide is calculated to be −193.8 kcal/mole and −63.3 kcal/mole respectively. The reorganisation energy of boronimide in various configurations is obtained and used to discuss the energetics of formation of borazine and dimeric boronimide.

Unter Benutzung Gaußscher Atomorbitale wurden die Elektronenenergien und Strukturen zweier vorgeschlagener Modelle von Borazin mit *ab initio*-Rechnungen untersucht. Man fand, daß das ebene D_{3h}-Modell energetisch bevorzugt wird. Die Analyse der Elektronenbesetzung ergibt für Stickstoff- und Boratome im Borazin eine negative bzw. positive Ladung. Berechnungen wurden auch durchgeführt für Borimid und dimeres Borimid. Die Trimerisations- und Dimerisationsenergie von Borimid ergab sich zu −193,8 kcal/Mol bzw. −63,3 kcal/Mol. Die Umlagerungsenergie von Borimid in verschiedenen Konfigurationen wird berechnet und zur Diskussion der Bildungsenergien von Borazin und dimerem Borimid benutzt.

1. Introduction

Borazine has been the subject of both theoretical and experimental interest since the early structural studies established that borazine consisted of a planar hexagonal molecule with alternating B–H and N–H groups [2, 19]. The observed B–N bond distance of 1.44 Å [2, 19] indicated that it was intermediate between that expected for a single and double bond. Because of the isoelectronic and isosteric relationship, borazine was regarded as "inorganic benzene", and this relationship became more credible when a comparison of physical constants of benzene and borazine showed a striking similarity [14]. Furthermore, spectroscopic studies such as infra-red, raman [5, 18] and ultraviolet [11] could all be satisfactorily interpreted on the basis of a benzene like structure. It was, therefore, rather surprising when a recent redetermination of the structure by electron diffraction techniques [13] found that two models of borazine could fit the observed results. These were the "classical" D_{3h} model and a non-planar twist boat configuration of C_2 symmetry. In order to differentiate between these, we have carried out non-empirical LCAO–MO–SCF calculations on both models.

The electronic structure of borazine has been examined by many semi-empirical calculations. The earlier investigations [4, 15] were concerned with the π-electronic system and found that the ultraviolet spectrum could be interpreted on the basis of $\pi \rightarrow \pi$ transitions. The calculations also revealed that the π-electron population of the boron and nitrogen was 0.344 and 1.666 respectively, indicating a π-electron flow towards the boron [15]. Recent studies have covered both the σ- and π-electron systems in an attempt to gauge the extent of both σ- and π-electron movement. Extended Hückel [8] and CNDO [17, 6] calculations on borazine revealed that the classical picture of alternating B^- and N^+ atoms, directly comparable to the electronic situation in benzene, was totally misleading. Both methods showed that the valence electronic population on boron was positive and nitrogen possessed a negative charge. After a preliminary account of this work was published [1] an *ab initio* calculation on the excited states of borazine was reported [16].

2. Results and Discussion

2.1. Energies of the Two Models of Borazine

The first attempt to distinguish between the two models of borazine was made by CNDO SCF MO calculations. It was found that the planar D_{3h} model was energetically preferred by 1.6 kcal/mole. Considering the semi-empirical nature of the method, however, the difference in energy between the two models was too small for a definite assignment to be made of the preferred structure of borazine.

It was necessary, therefore, to resort to a non-empirical approach to distinguish between the proposed models of borazine. The calculations [20] were performed using a basis set of Gaussian-type atomic orbitals [3]. The basis set consisted of 7*s* and 3*p* atomic Gaussian functions for both boron and nitrogen atoms and 3*s* atomic Gaussian functions for the hydrogen atoms. The 114 primitive functions were then contracted to 42 functions comprised of 3*s* and 1*p* atomic orbitals for the heavy atoms and a 1*s* atomic orbital for each hydrogen. The nitrogen and boron orbital exponents and coefficients were obtained from the work of Whitman and Hornback [21] and the values for hydrogen from Ref. [10]. The total and orbital energies of the two models of borazine are presented in Table 1. It can be seen that the classical D_{3h} model is more stable by 40.5 kcal/mole and this large difference in energy effectively rules out the C_2 twisted model proposed by Bauer [2]. Twisting the N–H bonds out of the plane produces an increase in nuclear energy and this is coupled with a smaller decrease in the electronic energy.

The orbital energies of the two models have very similar values, with the highest filled orbitals showing the greatest difference in energy. The highest filled orbitals of the planar D_{3h} model is a doubly degenerate π-orbital (e'') which is composed mainly of the nitrogen π-orbitals. This orbital will therefore be most affected by the bending of the N–H bonds out of the plane. The UV photoelectron spectrum of borazine [12] confirmed that the highest filled orbital is of e'' symmetry. The lowest virtual orbital of planar borazine is also of e'' symmetry and is concentrated about the π-orbitals of the boron atoms.

Table 1. Total and orbital energies of the two models of borazine (in a.u.)

	Planar D_{3h} model	Twisted boat C_2 model
Electronic energy	-436.7149	-437.1257
Nuclear energy	196.1889	196.6742
Total energy	-240.5260	-240.4515
Virtual orbitals	0.4199 (e')	0.4129 (b)
		0.4093 (a)
	0.3365 (a_1')	0.3589 (a)
	0.2775 (a_2')	0.1996 (b)
		0.1343 (b)
	0.1316 (e'')	0.0810 (a)
Occupied orbitals	-0.4669 (e'')	-0.4583 (b)
		-0.4641 (b)
	-0.4994 (e')	-0.4949 (a)
	-0.5758 (a_1')	-0.5824 (a)
	-0.5783 (a_2')	-0.5858 (b)
		-0.6343 (b)
	-0.6335 (e')	-0.6375 (a)
	-0.6537 (a_1')	-0.6520 (b)
	-0.7687 (a_1')	-0.7583 (a)
		-0.7726 (b)
	-0.7792 (e')	-0.7798 (b)
		-1.1641 (b)
	-1.1662 (e')	-1.1679 (a)
	-1.2483 (a_1')	-1.2505 (a)
	-7.7739 (a_1')	-7.7682 (a)
		-7.7832 (a)
	-7.7743 (e')	-7.7836 (b)
	-15.6070 (e')	-15.5915 (b)
	-15.6072 (a_1')	-15.6050 (a)

2.2 Electronic Population Analysis of Borazine

The electronic population of planar borazine is presented in Table 2. This reveals that the nitrogen atoms possess a large negative charge (0.735) and the boron atoms have a positive charge (0.474). For the nitrogen atoms this charge arises from the bonded hydrogen atom (0.299) and from the boron atoms (0.436). The boron-to-nitrogen electron donation is interesting because it consists of a π-electron delocalisation from the nitrogen to the boron, however, this is coupled with a larger σ-electron polarisation from boron to nitrogen. This electronic description of borazine contradicts the classical picture in which the charges on boron and nitrogen atoms are -1 and $+1$, respectively. It explains, however, the chemical reactions of borazine in which the electrophilic reagent attacks the boron atoms and the nucleophiles react with the nitrogen atoms. Also included in Table 2 are the corresponding electronic population for the C_2 model of borazine. Comparison of the distributions reveals that producing twisted boat C_2 model has only a weak perturbing effect on its electronic population.

Table 2. Gross and overlap populations of the two models of borazine

		Planar D_{3h} model	Twisted boat C_2 model	
			A (out of plane)	B (on axis)
Nitrogen	s	3.529	3.532	3.533
	$p\sigma$	2.616	4.211	4.201
	$p\pi$	1.590		
	Total	7.735	7.743	7.734
Boron	s	2.738	2.761	2.749
	$p\sigma$	1.378	1.745	1.786
	$p\pi$	0.410		
	Total	4.526	4.506	4.535
Hydrogen				
(bonded to boron)		1.037	1.035	1.039
(bonded to nitrogen)		0.701	0.710	0.703
B N	σ	0.327		
	π	0.098		
	Total	0.425	0.420	
B H		0.446	0.442	
N H		0.364	0.358	
N N	σ	−0.024		
	π	−0.003		
	Total	−0.027	−0.298	
B B	σ	−0.108		
	π	0.003		
	Total	−0.105	−0.108	

2.3. π-Electronic Energy of Borazine

In benzene the π-electron system is of paramount importance as it determines the stability and reactivity of the molecule and its derivatives. The delocalisation of π-electrons in borazine is not as extensive as in benzene but is still quite considerable. A possible reason for the relative instability of the C_2 model of borazine is that the bending of the N-H bonds out of plane reduces the π-delocalisation of the lone pair of electrons on the nitrogen atoms. It was therefore of interest to estimate the π-electronic energy of borazine. This was achieved by calculating two models of borazine in which the π-electrons were artificially restricted to a) three boron-nitrogen localised π-bonds b) three nitrogen π-orbitals.

The energies of these models are presented in Table 3. It can be observed that localisation of the π-electrons on the nitrogen orbitals results in a loss of 119.1 kcal/mole, whereas restricting the π-electrons to three B-N localised bonds destabilises the total energy by only 13.1 kcal/mole. Hence, it appears that in borazine the nitrogen π-electrons prefer to be delocalised although the form of

Table 3. The total energies of localised and delocalised models of borazine (in u.a.)

	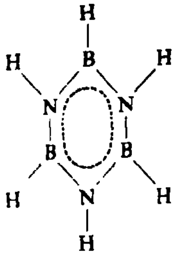	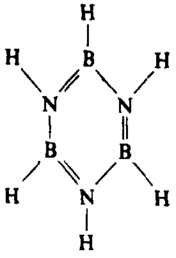	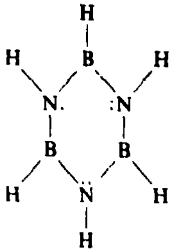
	Delocalised	Localised bond	Localised lone pair
Total energy	−240.5260	−240.5051	−240.3362
		$\xrightarrow{0.0209}$ $\xrightarrow{0.1689}$	
		$\xrightarrow{0.1898}$	

delocalisation is unimportant. The small value for the resonance energy suggests that localisation of the π-electrons into three bonds is a first step in a reaction process and, with electron bond polarisation, is a major reason why borazine is very reactive compared to benzene.

2.4. *Electronic Structure of Boronimide* HBNH

In 1948 Wiberg [22, 23] postulated that the formation of borazine from the reaction of diborane and ammonia should proceed stepwise according to

$$H_3N \cdot BH_3 \xrightarrow{-H_2} H_2N \cdot BH_2 \xrightarrow{-H_2} HB \cdot NH \longrightarrow \tfrac{1}{3}[HB.NH]_3 .$$

It was assumed that dehydrogenation led to boronimide as a reaction intermediate which rapidly trimerised to the thermodynamically favoured borazine. It was thought relevant that this intermediate should be examined and the energies involved in the trimerisation procedure estimated.

It was first necessary to calculate the equilibrium B-N bond distance for boronimide, as there has been no experimental or theoretical determination of this distance. The total energy of boronimide was calculated at various B N bond distances using the aforementioned basis set, and an optimum B N distance of 1.272 Å obtained. In order that trimerisation can occur, the boronimide molecule must reorganise into a non-linear molecule whose B·N bond length and N–B–H and B–N–H angles are equal to those in borazine. The total and orbital energies of boronimide in various configurations are presented in Table 4. The energy gained by the trimerisation of three molecules of boronimide to form one molecule of borazine is 193.8 kcal. The reorganisation energy of the boronimide is 66.6 kcals of which 23.4 kcals is the energy lost in stretching the B–N bond. The energy gained by the three reorganised molecules of boronimide on the formation of borazine is therefore (3 × 66.6 + 193.8) = 393.6 kcals and this energy will arise from the formation of the new B–N σ-bonds. The major term of the reorganisation

Table 4. The total and orbital energies of boronimide (in a.u.)

	a) Linear boronimide B–N = 1.272 Å	b) Linear boronimide B–N=B–N distance in borazine	c) Non-linear boronimide in the same configuration as in borazine	d) Non-linear boronimide bending the B–H bond only B–N=B–N distance in borazine	e) Non-linear boronimide bending the N–H bond only B–N=B–N distance in borazine	f) Non-linear boronimide in the same configuration as in dimeric boronimide
Electronic energy	−103.0609	−101.2075	−101.5711	−101.3873	−101.3873	−101.0295
Nuclear energy	22.9885	21.1724	21.6050	21.3920	21.3587	21.0483
Total energy	−80.0724	−80.0351	−79.9661	−79.9953	−80.0286	−79.9812
Virtual orbitals	0.285 (a)	0.242 (a)	0.145 (a'') (π)	0.142 (a'')	0.137 (a'')	0.136 (a')
	0.184 (e)	0.142 (a)	− 0.003 (a')	0.052 (a')	0.086 (a')	0.023 (a')
			− 0.405 (a'') (π)	− 0.407 (a'')	− 0.416 (a'')	− 0.398 (a'')
Filled orbitals	− 0.466 (e)	− 0.419 (e)	− 0.428 (a')	− 0.430 (a')	− 0.454 (a')	− 0.417 (a')
	− 0.611 (a)	− 0.610 (a)	− 0.591 (a')	− 0.577 (a')	− 0.606 (a')	− 0.593 (a'')
	− 0.747 (a)	− 0.715 (a)	− 0.678 (a')	− 0.727 (a')	− 0.686 (a')	− 0.689 (a')
	− 1.130 (a)	− 1.076 (a)	− 1.098 (a')	− 1.084 (a')	− 1.107 (a')	− 1.075 (a')
	− 7.785 (a)	− 7.792 (a)	− 7.799 (a')	− 7.781 (a')	− 7.798 (a')	− 7.797 (a')
	−15.613 (a)	−15.587 (a)	−15.564 (a')	−15.593 (a')	−15.584 (a')	−15.565 (a')

process is the energy required to bend the hydrogen bonds out of the boron-nitrogen plane. In order to determine which bending mode is the more energetic, two calculations were performed on boronimide in which only one hydrogen bond was bent out of the plane. From the results in Table 4 (d- e) it is found that 24.9 kcal/mole are required to bend the B-H bond and 4.1 kcal/mole needed to move the N-H bond out of the plane.

2.5. *The Electronic Energy of Dimeric Boronimide*

A very intriguing aspect of the production of borazine from boronimide is the absence of dimeric boronimide $(HBNH)_2$ in the process. It is therefore of interest to examine the electronic energies of the dimer of boronimide. In our calculation the boron-nitrogen framework was a square of length 1.47 Å [7] with the hydrogen atoms situated on a line extending along the diagonal by a distance equal to the corresponding hydrogen bond distance in borazine. The total and orbital energies of dimeric boronimide are presented in Table 5. It is found that the dimer is more stable than two molecules of boronimide by 63.3 kcal/mole. This is smaller than the corresponding 193.8 kcals/mole obtained for borazine and explains in part why the trimer is preferred to the dimeric form for boronimide (cf. Ref. [9]).

The energy required to reorganise boronimide into a configuration suitable for dimerisation was calculated to be 57.2 kcal/mole (Table 4a) and f)). This reorganisation energy to the dimer is smaller than to the trimer because of the greater bending of the bonds in the latter case (45° compared to 60°). We are now able to construct energy diagrams comparing the steps in the polymerisation processes.

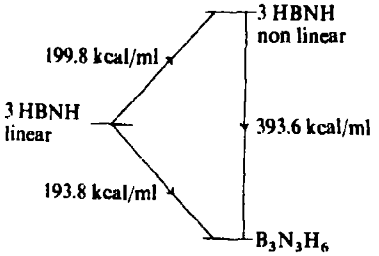

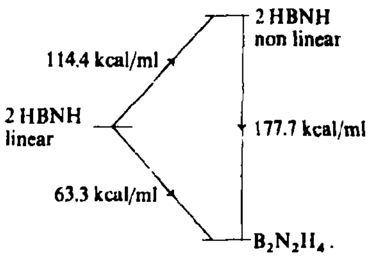

The difference between the two processes is the larger stabilisation energy gained by trimerisation than by dimerisation. If we can make the assumption that this stabilisation is due to the energy gained by the formation of new boron-nitrogen bonds, then the energy of the new boron-nitrogen bond is 131.2 kcal/mole and 88.8 kcal/mole for borazine and dimeric boronimide respectively. The difference between these two values represents to some extent the strain energy involved in the bonds of the dimeric species. From reorganisation energy considerations, it is expected that with certain boronimide derivatives the reorganisation term would be the most important and in these cases the dimeric boronimide derivative would be formed. This would obtain when the derivative

Table 5. The total and orbital energies of dimeric boronimide $(HBNH)_2$ (in a.u.)

Electronic energy	-256.1485
Nuclear energy	95.9027
Total energy	-160.2458
Virtual orbitals	0.228 (b_{1u}) π
	0.079 (b_{3g}) π
Filled orbitals	-0.400 (b_{2g}) π
	-0.500 (b_{3u})
	-0.555 (b_{1u}) π
	-0.570 (b_{1g})
	-0.575 (b_{2u})
	-0.602 (a_g)
	-0.733 (b_{3u})
	-0.769 (a_g)
	-1.082 (b_{2u})
	-1.252 (a_g)
	-7.796 (a_g)
	-7.796 (b_{3u})
	-15.560 (b_{2u})
	-15.561 (a_g)

is a bulky organic group or a group bonded strongly to the boron or nitrogen atoms.

The orbital energies of boronimide and dimeric boronimide listed in Tables 4 and 5 respectively, show that the highest filled orbital in both molecules is π-type and is largely concentrated about the nitrogen atoms. The π-electronic delocalisation energy of the dimeric boronimide is estimated by repeating the calculation with the π-electrons restricted to the nitrogen π-orbitals. The total energy of the localised model is -160.1177 a.u. which means that the π-delocalisation energy of dimeric boronimide is 80.3 kcal/mole. After adjustment for the differing number of π-electrons the delocalisation energy of dimeric boronimide is very similar to that of borazine. It would seem therefore that this value might be a constant transferable from molecule to molecule.

2.6. *The Electronic Population of Boronimide and Dimeric Boronimide*

The electronic population of boronimide is presented in Table 6. The electron densities are similar to the values in borazine, with the nitrogen and boron atoms possessing a large negative and positive charge, respectively. The B–N bond population, as expected, is greater in boromimide than in borazine, reflecting the shorter bond length and the involvement of more electrons in the B–N bond of the former. On examining the change in bond population of boromide with the change in configuration it is found that increasing the B–N bond length to that of borazine produces a small decrease in the B–N bond population ($\sigma = 0.351$, $\pi = 0.188$, $\pi' = 0.188$, total $= 0.727$). However, on moving the B–N and N–H bonds out of a linear configuration, there is a substantial decrease in the B–N bond population ($\sigma = 0.322$, $\pi = 0.208$, total $= 0.530$).

Table 6. The gross and overlap electronic populations of boronimide and dimeric boronimide

		Boronimide	Dimeric boronimide
Boron	S	2.767	2.815
	X	0.811	0.583
	Y	0.579 (π')	0.822
	Z	0.579 (π')	0.297 (π)
Total		4.736	4.517
Nitrogen	S	3.493	3.510
	X	1.288	1.288
	Y	1.421 (π')	1.278
	Z	1.421 (π)	1.703 (π)
Total		7.623	7.729
Hydrogen (B)		0.965	1.016
Hydrogen (N)		0.676	0.738
B-N	σ	0.321	0.323
	π	0.222	0.069
	π'	0.222	
Total		0.765	0.392
H-B		0.434	0.427
H-N		0.369	0.364

The electronic population of dimeric boronimide presented in Table 6 shows that the electronic charge pattern is the same as in borazine. The π-electronic drift towards the boron is not as great as in the trimer but this is offset by a smaller σ-electron polarisation. The boron-nitrogen overlap population, however, is lower in dimeric boronimide than in borazine entirely due to a smaller π-electron contribution in the former.

References

1. Armstrong, D. R., Clark, D. T.: J. chem. Soc. (London) (D) **1970**, 99.
2. Bauer, S. H.: J. Amer. chem. Soc. **60**, 524 (1938).
3. Boys, S. F.: Proc. Roy. Soc. (London) **200** A, 542 (1950).
4. Chalvet, O., Daudel, R., Kaufman, J. J.: J. Amer. chem. Soc. **87**, 339 (1965).
5. Crawford, B. L., Edsall, J. T.: J. chem. Physics 223 (1939).
6. Davies, D. W.: Trans. Faraday Soc. **64**, 2881 (1968).
7. Hess, H.: Angew. Chem. Intern. Ed. **6**, 419 (1967).
8. Hoffman, R.: J. chem. Physics **40**, 2474 (1964).
9. – J. chem. Soc. (London) (D) **1969**, 240.
10. Huzinaga, S.: J. chem. Physics **42**, 1293 (1965).
11. Jacobs, L. E., Platt, J. R., Schaeffer, G. W.: J. chem. Physics **16**, 248 (1948).
12. Lloyd, D. R., Lynaugh, N.: Phil. Trans. Roy. Soc. (London) A **268**, 97 (1970).
13. Marshbarger, W., Lee, G., Porter, R. F., Bauer, S. H.: Inorg. Chem. **8**, 1683 (1969).
14. Niedenzu, K., Dawson, J. W.: Boron-nitrogen compounds, p. 85. Berlin: Springer-Verlag 1965.
15. Perkins, P. G., Wall, D. H.: J. chem. Soc. (London) (A) **1966**, 235.
16. Peyerimhoff, S. G., Buenker, R. J.: Theoret. chim. Acta (Berl.) **19**, 1 (1970).
17. Pople, J. A., Segal, G. A., Santry, D. P.: J. chem. Physics **43**, S 129 (1965).

18. Price, W. C., Fraser, R. D. B., Robinson, T. S., Longuet-Higgins, H. C.: Discuss. Faraday Soc. **9**, 131 (1950).
19. Stock, A., Wierl, R.: Z. anorg. Allg. Chem. **203**, 228 (1931).
20. Veillard, A.: IBMOL Version 4, Special I.B.M. Technical Report, San Jose, California, 1968.
21. Whitman, D. R., Hornback, C. J.: J. chem. Physics **51**, 398 (1969).
22. Wiberg, E.: Naturwissenschaften **35**, 182 (1948).
23. - Naturwissenschaften **35**, 212 (1948).

Dr. D. R. Armstrong
Department of Pure and Applied Chemistry
University of Strathclyde
Glasgow, C. 1., Great Britain

Theoret. chim. Acta (Berl.) 24, 317–333 (1972)
© by Springer-Verlag 1972

Nature de la liaison dans l'ion tétraperoxochromate CrO_8^{3-} : une étude des structures cristalline et électronique

J. Fischer*, A. Veillard et R. Weiss*

Institut de Chimie, 1, rue Blaise Pascal, 67-Strasbourg, France

Reçu le 28 mai 1971

Nature of Bonding in the Chrome V Tetraperoxo Ion CrO_8^{3-}: *A Study of Crystal and Electronic Structure*

Refinement of the crystal structure of K_3CrO_8 points to a shortening of the O–O bond in the chrome *V* tetraperoxo ion CrO_8^{3-} with respect to its value in the peroxyde ion. An *ab-initio* calculation with a limited basis set of gaussian orbitals has been undertaken in order to explain the above result and to assess the nature of the metal-ligand bonding in the CrO_8^{3-} complex. The O–O overlap population is greater in the complex than in the peroxyde ion and the largest contribution to the metal-ligand bonding comes from the π^* antibonding orbitals of the ligands. This is in agreement with the experimental shortening of the O–O bond since the electron transfer from the ligand π^* antibonding orbital should strengthen the O–O bond. The stereochemistry of the complex with a dodecaedral surrounding of the oxygen atoms allows for an optimal overlap between the chromium $3d_{z^2}$ orbital and the ligand π^* orbitals. The $3b_1$ orbital corresponding to the unpaired electron is exclusively built up of $2p$ orbitals. This can be explained qualitatively on the basis of the charge transfer from the ligands to the metal.

Un nouvel affinement de la structure cristalline de K_3CrO_8 a permis de mettre en évidence un raccourcissement de la liaison O–O dans les ponts peroxyde de l'ion tétraperoxochromate CrO_8^{3-} par rapport à sa valeur dans l'ion O_2^{2-}. Afin d'interpreter ce résultat et de préciser la nature de la liaison métal-ligand dans le complexe CrO_8^{3-}, un calcul *ab-initio* a été effectué avec une base limitée d'orbitales gaussiennes. La population de recouvrement O–O est plus grande dans le complexe que dans l'ion peroxyde, la contribution la plus importante à la liaison métal-ligand étant due aux orbitales antiliantes π^*. Ceci est en accord avec le raccourcissement observé pour la liaison O–O, le transfert d'électrons π^* vers le métal à partir d'une orbitale antiliante du ligand entraînant un renforcement de la liaison O–O. La stéréochimie particulière du complexe (arrangement dodécaédrique des atomes d'oxygène autour du métal) permet un recouvrement optimal de l'orbitale $3d_{z^2}$ du chrome avec les orbitales π^* des ligands. L'orbitale $3b_1$ qui correspond à l'électron non apparié est exclusivement constituée d'orbitales $2p$ des ligands. Ce résultat s'interprête qualitativement en fonction du transfert de charge des ligands vers le métal.

Eine neue Bestimmung der Kristallstruktur von K_3CrO_8 spricht für eine Verkürzung der O–O-Bindungslänge im Chrom *V* tetraperox ion CrO_8^{3-} gegenüber dem Wert im Peroxidion. Eine *ab-initio* Rechnung mit einem limitierten Basissatz am Gauß-Orbitator wurde vorgenommen, um dieses Ergebnis zu erklären und die Natur der Metall-Liganden-Bindung im CrO_8^{3-}-Komplex zu untersuchen. Der Anteil der Überlappungsladungsdichte ist im Komplex größer als im Peroxidion, und der größte Anteil zur Metall-Liganden-Bindung stammt von den antibindenden π^*-Orbitalen des Liganden. Dies stimmt mit der experimentellen Verkürzung der O–O-Bindung überein, da der Elektronentransfer vom antibindenden π^*-Ligandenorbital die O–O-Bindung verstärken sollte. Die Stereochemie des Komplexes mit einer dodekaedrischen Umgebung des Sauerstoffatoms ermöglicht eine optimale Überlappung zwischen dem $3d_{z^2}$-Orbital und den π^*-Ligandenorbitalen. Das $3b_1$-Orbital, das dem ungepaarten Elektron entspricht, ist nur an $2p$-Orbitalen aufgebaut. Dies kann qualitativ mit der Ladungsübertragung von den Liganden zum Metall erklärt werden.

---

* Equipe de Recherche Associée au CNRS (ERA n° 8).

Introduction

La compréhension de la structure électronique dans les complexes des métaux de transition a successivement fait appel à la théorie du champ cristallin, à la théorie du champ des ligands et à la méthode des orbitales moléculaires dans différentes approximations semi-empiriques [1]. Dans la théorie du champ cristallin, les ligands sont représentés par des charges électriques ponctuelles et l'on étudie l'effet du potentiel créé par ces charges sur les niveaux d'énergie de l'atome de métal. Cette représentation schématique ne peut pas tenir compte des effets de covalence dans le complexe. La théorie du champ des ligands considère la fonction d'onde du système comme délocalisée sur l'ensemble du complexe et fait appel à la théorie des groupes pour prévoir quelles sont les orbitales des ligands susceptibles de se combiner avec les orbitales du métal. Le degré de covalence peut être estimé à partir de diverses données expérimentales telles que la structure hyperfine [2]. Un traitement purement théorique du problème est possible dans le cadre de la méthode des orbitales moléculaires (O.M.). En fait, l'étude des complexes métalliques par la méthode des O.M. est restée limitée jusqu'à maintenant à différentes approximations semi-empiriques telles que celle de Wolfsberg et Helmholtz [3]. Par suite de l'incertitude sur le choix des paramètres semi-empiriques, les résultats obtenus sont assez fréquemment contradictoires, l'étude de l'ion permanganate constituant un bon exemple de ces difficultés [4].

Il est maintenant possible d'étudier la structure électronique des complexes métalliques par les méthodes théoriques *ab-initio*, qui ne nécessitent pas l'introduction de paramètres semi-empiriques dans les données du calcul. Nous présentons ici le résultat d'une telle étude pour l'ion tétraperoxochromate CrO_8^{3-} (Fig. 1). Outre son intérêt sur le plan chimique puisque le chrome s'y trouve au degré d'oxydation V, ce système présente sur le plan structural la particularité d'une symétrie D_{2d} avec un arrangement dodécaédrique des atomes d'oxygène autour de l'atome central de chrome [5]. Le problème le plus intéressant soulevé par l'ion peroxochromate est relatif à la nature des liaisons dans ce complexe. Dans un système tel que l'ion tétracyanonickelate $[Ni(CN)_4]^{2-}$, les concepts chimiques habituels indiquent que la formation du complexe est liée à la présence d'une paire libre σ sur l'atome du ligand par lequel se fait la coordination. Un certain transfert d'électrons π en retour, du métal vers le ligand, peut éventuellement renforcer la liaison. Cette description qualitative est recoupée par les conclusions d'un travail théorique ab-initio [6]. Une situation différente se rencontre dans les composés du type ferrocène, pour lesquels on considère habituellement que la liaison est assurée par un transfert d'électrons π provenant d'orbitales délocalisées sur les ligands. Ces deux types de liaison peuvent être théoriquement envisagés dans le cas de l'ion tétraperoxochromate. On peut concevoir soit des liaisons mettant en jeu les paires libres σ du groupe peroxo (quoique l'orientation relative des atomes dans le complexe paraisse peu favorable à ce type de liaison) soit des liaisons mettant en jeu les électrons π du groupe peroxo. Une étude de la liaison chimique dans l'ion peroxochromate a été effectuée par Swalen et Ibers [7] en se basant d'une part sur un calcul de champ cristallin qui leur permet de préciser l'ordre relatif des orbitales d du métal, d'autre part sur un calcul du type champ des ligands qui leur permet de préciser le degré de covalence à partir de certaines données expérimentales. Ceci ne leur a toutefois pas permis d'estimer l'importance relative des deux types de liaison σ et π.

Géométrie de l'ion CrO_8^{3-}-Affinement de la structure cristalline de K_3CrO_8

La structure cristalline de K_3CrO_8 a été établie par Stomberg et Brosset [5]; avec les données expérimentales de cette détermination Swalen et Ibers [7] d'une part et Stomberg [8] d'autre part ont réaffiné cette structure.

Elle contient des anions CrO_8^{3-} et des cations K^+. Dans les anions, les atomes d'oxygène des quatre groupements peroxo sont disposés aux sommets d'un dodécaèdre régulier. Les valeurs des distances interatomiques trouvées dans les trois études citées plus haut sont très différentes (Tableau 1). Afin de préciser la géométrie de CrO_8^{3-} nous avons effectué, à partir de nouvelles données expérimentales, un nouvel affinement de la structure cristalline de K_3CrO_8.

Tableau 1. Distances interatomiques dans l'ion CrO_8^{3-}

	Réf. [5]	Réf. [7]	Réf. [8]
$Cr{-}O_I$	1,944 Å	1,944 Å	1,972 Å
$Cr{-}O_{II}$	1,895 Å	1,846 Å	1,874 Å
$O_I{-}O_{II}$	1,489 Å	1,405 Å	1,472 Å

Données cristallographiques: système quadratique, $a = b = 6,709$ (1), $c = 7,627$ (1)Å, groupe spatial I_{42} m (D_{2d}^{11}), $Z = 2$ ($\lambda K\alpha_1$ Mo $= 0,70926$ Å). Les valeurs des paramètres ont été obtenues par une méthode de moindres carrés à partir de 12 réflexions indépendantes mesurées à 20°C sur un diffractomètre à quatre cercles PICKER FACS-I.

Un cristal de dimensions 0,08 × 0,10 × 0,12 mm a été utilisé pour mesurer les intensités diffractées, avec la radiation $K\bar{\alpha}$ du molybdène monochromatisée par une lame de graphite. L'intensité de chaque réflexion a été mesurée par balayage $\theta - 2\theta$ à la vitesse de balayage de 1°/mn. La discrimination était réglée de façon à laisser passer 95% du faisceau transmis. Le détecteur était à 25 cm du cristal avec une ouverture de 4 × 4 mm. Le faisceau diffracté a été atténué avec des lames de cuivre.

Toutes les réflexions telles que $2\theta \leq 95°$ ont été mesurées. Trois réflexions intenses disposées sur les trois axes réciproques ont été utilisées comme intensités de référence et mesurées périodiquement (toutes les 32 réflexions). L'écart-type sur ces intensités de référence était de 0,009.

Les intensités brutes ont été corrigées des facteurs de Lorentz et de polarisation. Les facteurs de transmission ont été calculés par une méthode d'intégration numérique et ils sont compris entre 0,71 et 0,74; la correction d'absorption n'a en conséquence pas été appliquée.

405 réflexions indépendantes présentant un $\sigma(I)/I$ inférieur à 0,40 ont finalement été retenues.

La structure a été affinée par moindres carrés, au moyen d'un programme d'affinement à matrice totale [9], en partant des résultats du second affinement de Stomberg. Les facteurs de diffusion de Cromer et Waber [10] pour O^-, Cr^{2+} et K^+ ont été utilisés et la dispersion anomale des atomes de chrome et de potassium a été introduite dans le calcul. La pondération utilisée est dérivée de la formulation pour σ_F proposée par Ibers [11] avec $p = 0{,}02$.

Après six cycles d'affinements les variations des paramètres affinés étaient inférieures à la moitié des écarts-type correspondants. Le facteur R_1 est égal à 0.023 pour l'ensemble des 405 réflexions utilisées et 0,015 pour les 345 réflexions intervenant dans l'affinement; le facteur pondéré R_2 vaut respectivement 0,032 et 0,015. La quantité $|\Sigma\omega(F_0 - F_c)^2/(m-n)|^{1/2}$ vaut 1,00. Le facteur d'échelle de la correction d'extinction secondaire isotrope selon Zachariasen [12] est égal à $0{,}22 \cdot 10^{-9}$ ($\sigma = 0{,}18 \cdot 10^{-7}$).

Les résultats de l'affinement sont groupés dans les Tableaux 2, 3, 4 et 5. Les distances trouvées sont voisines de celles du deuxième affinement de Stomberg, mais la précision est nettement supérieure. Les corrections de dimensions dues aux effets de l'agitation thermique, calculées suivant la méthode de Schomacker

Tableau 2. Coordonnées atomiques relatives et écarts-type sur ces positions

	x	σ_x	y	σ_y	z	σ_z
Cr	0	0	0	0	0	0
K_I	0	0	0	0	0,5	0
K_{II}	0	0	0,5	0	0,25	0
O_I	0,2059	0,0002	0,2059	0,0002	0,0112	0,0002
O_{II}	0,1347	0,0002	0,1347	0,0002	0,1812	0,0002

Tableau 3. Facteurs d'agitation thermique anisotrope; les β_{ij} sont multipliés par 10^4

	β_{11}	β_{22}	β_{33}	β_{12}	β_{13}	β_{23}
Cr	38 (0,6)	38 (0,6)	37 (0,4)	0	0	0
K_I	76 (0,9)	76 (0,9)	61 (0,6)	0	0	0
K_{II}	73 (0,6)	73 (0,6)	143 (0,5)	0	0	0
O_I	75 (1)	75 (1)	86 (1)	-1 (1)	2 (2)	2 (2)
O_{II}	84 (2)	84 (2)	52 (1)	-5 (1)	-11 (1)	-11 (1)

Tableau 4. Distances interatomiques et angles de valence

Cr O_I	1,958 (0,6) Å	< O_I Cr- O_{II}	44,83 (0,04)
Cr O_{II}	1,882 (0,7) Å	< Cr O_I -O_{II}	64,97 (0,03°)
O_I O_{II}	1,466 (1) Å	< Cr- O_{II} O_I	70,30 (0,03°)
O_{II} O_{II}^1	2,560 (1) Å		
O_I O_I^2	2,771 (1) Å		
O_{II}-O_I^3	2,775 (1) Å		

Les numéros en exposant correspondent aux numéros de la Fig. 1.

Tableau 5 Facteurs de structure observés et calculés multipliés par 10: l'angle de phase α est exprimé en degrés

H	K	L	FC	α	FO	H	K	L	FC	α	FO	H	K	L	FC	α	FO	H	K	L	FC	α	FO
2	0	0	769	2,43	772	4	3	1	70	– 5,89	69	9	7	2	182	1,74	182	8	2	4	370	– 3,38	370
4	0	0	728	2,41	731	6	3	1	73	– 52,74	78	11	7	2	162	5,17	167	10	2	4	192	– 5,64	195
6	0	0	660	2,38	661	8	3	1	62	29,96	60	7	7	2	301	3,90	298	2	2	4	917	– 12,21	928
8	0	0	437	3,08	433	12	3	1	78	– 3,82	76	10	8	2	35	24,96	37	12	2	4	188	9,77	186
10	0	0	313	3,52	310	5	4	1	155	11,38	151	8	8	2	32	32,42	38	5	3	4	70	94,59	67
12	0	0	130	6,69	128	9	4	1	45	– 1,02	44	9	9	2	165	12,74	164	7	3	4	140	7,75	136
3	1	0	184	176.96	198	11	4	1	67	1,75	61	1	0	3	66	171,53	78	9	3	4	26	– 30,77	37
5	1	0	69	7,83	69	8	5	1	96	58,80	88	3	0	3	114	4,84	113	11	3	4	51	– 3,17	54
7	1	0	94	5,39	97	10	5	1	95	– 13,72	98	5	0	3	313	1,70	315	13	3	4	52	26,92	55
9	1	0	71	6,62	71	7	6	1	51	36,84	49	7	0	3	138	176,36	135	3	3	4	171	– 8,82	171
1	1	0	394	1.43	386	9	6	1	71	– 29.15	75	9	0	3	70	6,65	81	6	4	4	413	– 2.86	411
4	2	0	737	2,33	733	8	7	1	97	– 1.97	96	11	0	3	80	5,21	84	8	4	4	273	8,07	269
6	2	0	536	2.88	535	12	7	1	55	11.22	53	2	1	3	46	– 29,04	45	10	4	4	225	4,69	223
8	2	0	437	3.01	433	11	8	1	42	9.52	44	4	1	3	246	– 5,52	249	12	4	4	131	4,38	135
10	2	0	230	4,68	231	10	9	1	62	21.63	61	6	1	3	67	64,73	61	4	4	4	490	5.48	489
12	2	0	225	3.77	224	2	0	2	225	177.41	242	10	1	3	74	1,71	73	9	5	4	91	28,00	89
11	3	0	84	4,89	82	4	0	2	370	1.53	369	12	1	3	48	11,94	45	11	5	4	43	19.94	39
3	3	0	404	1,36	399	6	0	2	56	9,57	51	3	2	3	221	– 13,67	227	5	5	4	173	– 22,28	175
6	4	0	458	3,15	450	10	0	2	117	3,85	122	5	2	3	86	145,40	83	8	6	4	246	6,14	242
8	4	0	253	4,86	254	0	0	2	295	1,99	306	7	2	3	140	10,18	142	10	6	4	186	14,31	183
10	4	0	301	3,36	304	3	1	2	981	6.09	972	11	2	3	38	10,34	41	12	6	4	118	– 0,91	121
12	4	0	178	4,46	178	5	1	2	743	– 4.70	740	13	2	3	50	11.23	44	6	6	4	296	– 4,15	298
4	4	0	811	1,98	796	7	1	2	387	1,20	389	4	3	3	130	163,75	134	11	7	4	43	10,63	46
7	5	0	71	173.27	71	9	1	2	336	8.86	335	6	3	3	88	7,46	88	7	7	4	87	0,09	86
9	5	0	74	5,94	73	11	1	2	241	6,04	238	8	3	3	126	5,82	124	10	8	4	123	0.14	130
11	5	0	51	7,60	52	13	1	2	148	– 2,49	154	12	3	3	48	8,94	42	8	8	4	194	4,79	194
5	5	0	196	2.60	191	1	1	2	1110	15,50	1093	5	4	3	60	– 0,36	66	9	9	4	47	– 18,17	45
8	6	0	317	3,47	315	4	2	2	46	266.38	60	7	4	3	90	1.70	92	1	0	5	281	1,92	292
10	6	0	202	4.49	201	6	2	2	91	– 54.63	94	9	4	3	62	15,37	62	3	0	5	181	177,07	191
12	6	0	129	5,54	130	8	2	2	109	17.78	108	6	5	3	70	– 5,25	71	5	0	5	119	4,30	120
6	6	0	368	3,50	367	12	2	2	71	– 9.04	75	10	5	3	73	11.52	69	7	0	5	41	11,79	40
7	7	0	147	3,06	148	2	2	2	458	39.19	456	11	6	3	39	25.56	39	9	0	5	90	4,94	89
10	8	0	132	5,88	128	5	3	2	424	– 4.52	428	11	8	3	67	– 0,79	70	13	0	5	22	15,34	34
8	8	0	263	3.59	266	7	3	2	537	0.70	531	10	9	3	61	– 3,57	61	2	1	5	52	– 67,76	57

Tableau 5 (suite)

H	K	L	FC	α	FO	H	K	L	FC	α	FO	H	K	L	FC	α	FO	H	K	L	FC	α	FO
9	9	0	40	9,15	40	9	3	2	281	10,62	275	9	6	3	53	11,02	49	4	1	5	13	− 89,79	32
1	0	1	423	1,33	431	11	3	2	200	3,49	195	2	0	4	607	2,76	600	6	1	5	108	50,10	108
3	0	1	319	178,25	332	13	3	2	142	1,64	147	4	0	4	738	2,12	740	8	1	5	77	− 21,70	84
5	0	1	244	2,22	243	3	3	2	793	7,26	778	6	0	4	465	3,02	465	3	2	5	190	− 19,32	196
9	0	1	97	4,87	96	6	4	2	100	8,55	101	8	0	4	287	4,19	288	5	2	5	84	109,96	75
2	1	1	345	96,18	342	8	4	2	58	11,29	50	10	0	4	297	3,32	297	7	2	5	101	12,40	98
4	1	1	72	− 41,11	82	10	4	2	53	− 4,34	49	12	0	4	136	5,75	131	9	2	5	34	− 62,71	44
6	1	1	110	− 43,16	115	4	4	2	32	98,09	28	0	0	4	1140	1,47	1161	11	2	5	47	18,18	41
8	1	1	66	26,92	67	7	5	2	304	8,12	301	3	1	4	164	− 51,46	180	4	3	5	113	25,69	113
10	1	1	63	41,32	60	9	5	2	300	− 3,70	297	5	1	4	176	40,76	173	6	3	5	33	20,53	34
3	2	1	349	28,03	342	11	5	2	168	4,62	166	7	1	4	56	51,39	54	12	3	5	75	8,62	77
5	2	1	154	239,86	164	5	5	2	560	9,19	556	9	1	4	86	− 34,29	96	5	4	5	133	− 6,57	133
7	2	1	139	− 10,99	140	8	6	2	47	− 23,61	56	11	1	4	53	15,03	49	7	4	5	31	181,54	38
9	2	1	66	81,31	60	10	6	2	45	− 14,64	46	1	1	4	163	− 31,07	158	9	4	5	42	38,42	39
11	2	1	47	18,14	44	12	6	2	40	27,96	40	4	2	4	529	4,93	528	11	4	5	73	− 2,16	73
13	2	1	55	− 19,69	59	6	6	2	77	68,40	71	6	2	4	456	18,39	448	6	5	5	44	− 29,64	42
10	5	5	86	12,66	83	7	2	7	82	− 9,18	85	3	0	9	56	8,27	57	1	0	11	94	4,51	93
7	6	5	43	10,25	45	9	2	7	52	62,13	49	5	0	9	105	4,23	101	7	0	11	59	6,31	58
9	6	5	62	15,33	55	11	2	7	42	23,13	43	9	0	9	54	7,02	49	9	0	11	51	6,57	54
8	7	5	99	3,00	97	6	3	7	64	− 53,83	80	11	0	9	53	6,36	50	6	1	11	57	30,46	56
4	0	6	54	11,72	55	8	3	7	71	29,06	67	2	1	9	43	− 27,87	45	8	1	11	57	− 13,97	60
6	0	6	134	4,40	134	12	3	7	47	− 7,84	50	4	1	9	85	− 11,79	88	3	2	11	62	− 1,17	61
8	0	6	88	6,05	88	5	4	7	63	14,36	60	6	1	9	73	69,30	73	7	2	11	50	1,87	42
10	0	6	75	6,29	75	9	4	7	52	9,31	53	8	1	9	26	− 42,64	38	4	3	11	75	20,18	73
0	0	6	480	1,38	498	11	4	7	39	− 9,98	42	10	1	9	54	− 4,30	58	5	4	11	69	− 3,72	62
3	1	6	407	3,39	404	6	5	7	78	55,08	70	3	2	9	82	− 32,67	89	9	4	11	32	32,69	36
5	1	6	403	− 0,47	403	8	5	7	28	− 24,59	43	5	2	9	54	89,68	44	7	6	11	42	22,34	42
7	1	6	337	2,19	334	10	5	7	66	− 17,25	65	7	2	9	76	22,02	71	2	0	12	140	5,40	144
9	1	6	245	4,58	244	7	6	7	46	37,94	43	4	3	9	38	115,54	42	4	0	12	138	5,14	135
11	1	6	145	12,94	141	9	6	7	60	− 37,24	72	6	3	9	56	14,48	52	6	0	12	145	4,44	141
1	1	6	667	12,14	674	8	7	7	58	− 8,29	55	8	3	9	73	8,27	68	8	0	12	103	5,42	102
4	2	6	90	− 11,26	97	2	0	8	316	3,81	316	5	4	9	43	− 5,68	44	0	0	12	223	3,45	224
6	2	6	78	− 13,48	82	4	0	8	442	2,55	439	7	4	9	60	− 1,45	56	3	1	12	82	10,18	82
8	2	6	96	3,90	96	6	0	8	249	4,07	246	9	4	9	44	25,27	42	5	1	12	94	− 6,57	94

Tableau 5 (suite)

H	K	L	FC	α	FO	H	K	L	FC	α	FO	H	K	L	FC	α	FO	H	K	L	FC	α	FO
12	2	6	71	0,03	74	8	0	8	134	6,52	134	6	5	9	52	− 18,89	52	7	1	12	84	1,83	86
2	2	6	251	25,58	248	10	0	8	196	3,71	195	10	5	9	48	22,75	43	1	1	12	133	27,91	131
5	3	6	342	− 1,45	339	12	0	8	106	5.50	105	2	0	10	84	7.65	82	9	1	12	62	12,56	61
7	3	6	283	− 0,15	280	0	0	8	359	3,43	363	4	0	10	100	6,14	99	4	2	12	145	− 1,87	143
9	3	6	189	13,00	189	3	1	8	163	− 2,56	165	6	0	10	98	5,76	96	6	2	12	121	− 5,94	119
11	3	6	183	2,22	184	5	1	8	148	− 1,26	148	8	0	10	83	6,06	82	2	2	12	189	20,46	179
3	3	6	587	6,97	578	7	1	8	43	25,01	45	10	0	10	79	5,51	80	8	2	12	104	6,45	100
6	4	6	67	− 8,87	70	9	1	8	72	4,85	69	0	0	10	202	3,24	205	5	3	12	79	− 8,61	83
10	4	6	96	− 1,74	97	11	1	8	76	12.90	77	3	1	10	216	− 9,36	219	7	3	12	67	− 3,61	64
12	4	6	51	7.96	53	1	1	8	123	42.90	122	5	1	10	209	16,67	202	3	3	12	130	15,62	126
4	4	6	190	11,67	190	4	2	8	280	− 2,32	279	7	1	10	171	10.39	166	6	4	12	105	0,53	105
7	5	6	182	11,96	179	6	2	8	249	3.57	248	9	1	10	141	− 10,34	145	4	4	12	154	9,94	151
9	5	6	210	− 1.93	210	9	2	8	224	4.69	222	1	1	10	273	1,97	273	8	4	12	79	14,20	82
11	5	6	140	3.92	146	10	2	8	127	10.54	123	4	2	10	94	8,36	94	5	5	12	95	17,27	92
5	5	6	390	6.39	382	2	2	8	412	9.15	410	6	2	10	111	37,28	109	7	5	12	53	24,22	56
8	6	6	84	− 9,21	86	5	3	8	31	− 6.58	39	8	2	10	94	− 12,29	92	6	6	12	108	26,10	108
10	6	6	46	− 2,84	46	7	3	8	152	1,25	151	2	2	10	154	− 18,69	154	3	0	13	45	7,97	42
6	6	6	91	43,78	87	9	3	8	71	21,64	65	10	2	10	47	− 9.97	48	5	0	13	65	5,32	61
9	7	6	145	1.68	144	11	3	8	38	− 7,81	41	5	3	10	181	12,31	177	2	1	13	56	52,64	59
7	7	6	270	3,57	264	3	3	8	97	20.26	91	7	3	10	166	4,05	159	4	1	13	59	− 17,68	66
8	8	6	82	10,23	78	6	4	8	253	0,08	251	9	3	10	102	2,31	104	3	2	13	50	18,55	38
9	9	6	118	12.18	123	8	4	8	205	7,40	200	3	3	10	250	2.69	245	6	3	13	36	− 24,61	43
1	0	7	81	6.26	88	10	4	8	129	0.31	128	6	4	10	94	− 13,82	96	2	0	14	81	6,16	84
5	0	7	135	3,57	136	4	4	8	216	12.71	212	8	4	10	55	27.36	50	4	0	14	114	4,14	111
9	0	7	54	7.62	53	7	5	8	67	13,54	63	10	4	10	64	5,93	64	0	0	14	61	8,31	53
11	0	7	40	9,14	44	9	5	8	85	− 7.04	83	4	4	10	125	12,94	127	3	1	14	123	− 2,77	123
2	1	7	144	77,28	144	5	5	8	121	13,16	119	7	5	10	108	3,52	107	5	1	14	104	7,46	101
4	1	7	89	− 33,92	100	8	6	8	146	− 4,51	143	9	5	10	113	14,33	110	1	1	14	100	13,43	96
6	1	7	50	− 19,22	51	10	6	8	114	6.66	117	5	5	10	202	− 7,17	200	4	2	14	67	− 1,00	70
10	1	7	61	39,32	56	6	6	8	187	14.70	185	8	6	10	66	7,77	62	2	2	14	90	2,80	87
3	2	7	129	26,35	123	7	7	8	62	2,05	59	6	6	10	69	− 1.80	73	3	3	14	82	7,36	79
5	2	7	67	259,11	78	8	8	8	103	13.50	99	7	7	10	131	3,13	133	4	4	14	46	25,07	49
3	5	14	70	9,74	78	0	6	14	57	7,54	59	2	6	14	67	18,61	75	1	2	15	33	− 18,37	41
0	3	15	33	9,32	44																		

et Trueblood [26] sont très faibles et n'ont pas été appliquées. La distance O–O dans les ponts peroxydes est significativement différente de celle trouvée par Swalen et Ibers.

La Fig. 1 représente l'ion CrO_8^{3-} tracé au moyen d'un traceur de courbes Benson et du programme Ortep [13].

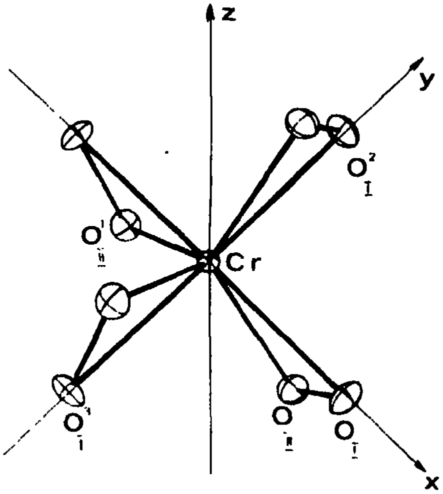

Fig. 1. L'ion $[\mathrm{CrO}_8]^{3}$ (ellipsoïdes à 20%)

La méthode théorique et les calculs

La fonction d'onde du système est exprimée par un produit antisymétrique d'orbitales moléculaires Φ_i ou déterminant de Slater [14]. Chaque orbitale moléculaire Φ_i est représentée par une combinaison linéaire d'orbitales atomiques (méthode LCAO-MO), les coefficients du développement étant déterminés par la résolution des équations du champ self-consistant [15]. La base d'orbitales atomiques utilisée comprend 166 fonctions gaussiennes dont les exposants ont été optimisés pour l'état fondamental des ions Cr^{2+} et O^-. La méthode d'optimisation utilisée sacrifie délibérément la qualité de la fonction d'onde près du noyau (c'est-à-dire des couches les plus internes en particulier) au profit d'une meilleure représentation des couches de valence. Pour cela, on optimise d'abord les exposants correspondant à une base de fonctions gaussiennes 9*s*, 5*p*, 3*d* pour l'ion Cr^{2+} [16]. Puis l'on élimine de la base la fonction *s* et la fonction *p* ayant l'exposant le plus élevé. Les fonctions gaussiennes décrivant les couches internes 1*s* et 2*p* de l'atome sont alors réoptimisées. Finalement deux fonctions *s* (d' exposants 0.18 et 0.08) et deux fonctions *p* (d'exposants 0,20 et 0,08) sont ajoutées à la base pour décrire les orbitales atomiques 4*s* et 4*p*. On aboutit ainsi à une base 10*s*, 6*p*, 3*d* pour l'ion Cr^{2+}. Un processus semblable conduit à une base 6*s*, 3*p* pour l'ion O^- à partir d'une base 7*s*, 4*p*. Les 166 fonctions gaussiennes sont ensuite transformées en 66 fonctions contractées [17], correspondant à une base contractée 5*s*, 3*p*, 2*d* pour l'ion Cr^{2+} et à une base «minimale» 2*s*, 1*p* pour l'ion O^-. La base contractée de l'ion Cr^{2+} correspond également à une base minimale sauf pour les orbitales $3d$ et $4s$ qui sont décrites par deux fonctions contractées. Un traitement plus satisfaisant nécessiterait l'emploi de deux fonctions contractées pour chacune des «orbitales de valence» (orbitale $2p$ de l'ion O$^-$, orbitales $3d$ et $4s$ de l'ion Cr^{2+}). Les limitations pratiques du calcul nous ont contraint à n'utiliser qu'une seule fonction contractée par orbitale $2p$ de l'ion O$^-$.

La géométrie utilisée est celle résultant de l'affinement décrit plus haut. Le choix d'axes est celui de la Fig. 1.

Les calculs ont été effectués avec la version IV du programme IBMOL [17, 18] sur les ordinateurs IBM 360/65 et 360/75. L'état fondamental de l'ion peroxochromate correspond à la configuration:

$$(10a_1)^2\,(9b_2)^2\,(2a_2)^2\,(11e)^2\,(3b_1)^1\,.$$

L'étude de la structure électronique de l'ion peroxochromate nécessite la connaissance de celle pour l'ion peroxyde O$_2^{2-}$. Nous avons étudié séparément cet ion avec la même base et la même contraction que celles utilisées pour le complexe. Pour juger de la signification des résultats obtenus avec cette base, nous avons effectué un autre calcul pour l'ion O$_2^{2-}$ avec une base plus large $9s$, $5p$ [19] contractée en $4s$, $2p$. Afin que les résultats obtenus pour l'ion peroxyde isolé puissent être comparés de manière significative à ceux du complexe, le calcul relatif à l'ion peroxyde a été effectué pour une distance interatomique O–O identique à celle obtenue dans le complexe.

Les résultats et leur discussion

Avant de discuter les résultats obtenus pour le complexe, nous allons d'abord examiner ceux relatifs à l'ion peroxyde O$_2^{2-}$. Dans le Tableau 6 sont indiquées les valeurs données par les deux calculs relatifs à l'ion O$_2^{2-}$ pour les énergies des orbitales, leur symétrie et les populations de recouvrement obtenues à partir de l'analyse de population de Mulliken [20]. L'ion peroxyde O$_2^{2-}$ est isoélectronique de la molécule de fluor F$_2$ avec dix-huit électrons et sa structure électronique dans l'état fondamental est représentée par la configuration:

$$1\sigma_g^2\,1\sigma_u^2\,2\sigma_g^2\,2\sigma_u^2\,1\pi_u^4\,3\sigma_g^2\,1\pi_g^4\,.$$

Les orbitales $2\sigma_g$, $1\pi_u$ et $3\sigma_g$, avec des populations de recouvrement positives, sont des orbitales liantes. Les orbitales $2\sigma_u$ et $1\pi_g$ ont des populations de recouvrement négatives et sont antiliantes. D'après le Tableau 6 les résultats fournis par les deux calculs avec des bases différentes sont en accord qualitatif.

L'ion peroxochromate a vingt neuf orbitales de valence outre les orbitales décrivant les électrons des couches internes: à chaque ion peroxyde correspondent en effet sept orbitales de valence (les orbitales dégénérées étant comptées deux fois) auxquelles s'ajoute l'électron de valence du Cr*V*. Le Tableau 7 indique pour chaque orbitale de valence du complexe la représentation irréducible correspondante du groupe D_{2d}, l'énergie de l'orbitale et la contribution de l'orbitale aux populations de recouvrement relatives aux liaisons Cr–O et O–O. Nous avons également fait figurer dans ce tableau les termes les plus importants dans le développement de chaque orbitale moléculaire par rapport aux fonctions contractées. Une caractéristique de chaque orbitale moléculaire du complexe

Tableau 6. Orbitales moléculaires de l'ion peroxyde O_2^{2-}

Orbitale	Energie (en u. a.)		Population de recouvrement	
	a	b	a	b
$1\pi_g$	0,28	0,30	−0,532	−0,482
$3\sigma_g$	0,15	0,17	0,029	0,038
$1\pi_u$	0,11	0,12	0,304	0,326
$2\sigma_u$	− 0,38	− 0,37	−0,107	−0,098
$2\sigma_g$	− 0,66	− 0,65	0,197	0,231
$1\sigma_u$	− 19,86	− 19,79	0	0
$1\sigma_g$	− 19,86	− 19,79	0	0
Total	−149,21	− 148,67	−0,110	−0,015

[a] Base 9s, 5p. [b] Base 6s, 3p.

est son lien de parenté avec les orbitales moléculaires du ligand, suivant qu'elle correspond à une orbitale σ ou π, liante ou antiliante. Cette parenté n'est pas absolue, puisque la symétrie propre au ligand peroxyde, qui permettait de distinguer entre orbitale σ et π, ne se retrouve plus dans le complexe. Une orbitale du complexe peut donc apparaître comme un mélange d'orbitales σ et π des ligands. C'est le cas par exemple pour l'orbitale $8a_1$ du complexe: elle s'apparente à une orbitale π du groupe peroxyde, avec un faible pourcentage d'orbitale 2s de l'oxygène. L'établissement d'un lien de parenté entre les orbitales du complexe et les orbitales σ, σ^*, π, π^* du ligand repose sur plusieurs critères tels que l'expression de l'orbitale moléculaire en fonction des orbitales atomiques, ou la valeur de l'énergie associée à l'orbitale moléculaire. En effet, les énergies des orbitales de valence du complexe se répartissent dans des intervalles bien définis. Les trois orbitales d'énergie comprises entre −0,96 u.a. et −0,94 u.a. correspondent à l'orbitale liante $2\sigma_g$ dont l'énergie est −0,66 u.a. dans le ligand. Les valeurs plus basses obtenues pour les énergies des orbitales dans le complexe par rapport à celles dans le ligand sont une conséquence de la stabilisation liée au transfert d'une fraction de la charge négative du ligand vers l'atome de métal (cf. *infra*). Un deuxième groupe de trois orbitales d'énergies −0,63 u.a. correspond à l'orbitale antiliante $2\sigma_u$ du ligand, d'énergie −0,38 u.a. Un troisième groupe de dix orbitales d'énergies comprises entre −0,21 u.a. et −0,03 u.a. correspond aux orbitales liantes $1\pi_u$ et $3\sigma_g$ du ligand, d'énergie +0,11 u.a. et +0,15 u.a. Enfin un dernier groupe de six orbitales d'énergies comprises entre +0,00 u.a. et +0,08 u.a.[1] correspond à l'orbitale antiliante $1\pi_g$ du ligand. Un troisième critère de filiation entre orbitale du ligand et orbitale du complexe est fourni par la valeur de la population de recouvrement O–O; une valeur négative correspond au caractère antiliant et inversement.

---

[1] L'énergie associée à ces orbitales est positive. Il en est de même pour les énergies des orbitales $1\pi_u$, $3\sigma_g$ et $1\pi_g$ de l'ion peroxyde. D'après le théorème de Koopmans pour les systèmes à couches complètes tels que l'ion peroxyde, à une énergie d'orbitale positive devrait correspondre l'autoionisabilité de ces orbitales. En fait, les valeurs positives de ces énergies d'orbitales représentent un artefact provenant de ce que l'on n'a pas tenu compte de l'influence des ions positifs voisins. Pour l'ion $CuCl_4^{2-}$, l'introduction des effets de cristal entraîne une stabilisation des énergies d'orbitales supérieure à 0,3 u. a. [25].

Tableau 7. Orbitales moléculaires de valence du complexe CrO_8^{3-}

Orbitale	Energie en (u. a.)	Population de recouvrement		Parenté	Termes principaux du développement[a]
		Cr–O	O–O		
$6a_1$	−0,960	−0,026	0,128	σ	$0{,}61\,S_1 + 0{,}67\,S_2$
$7a_1$	−0,629	0,006	−0,075	σ^*	$0{,}61\,S_1 - 0{,}77\,S_2$
$8a_1$	−0,163	−0,025	0,073	π	$0{,}52\,X_1 + 0{,}61\,X_2 - 0{,}26\,Z_1 - 0{,}33\,Z_2$
$9a_1$	−0,094	−0,004	0,014	σ	$0{,}52\,X_1 - 0{,}44\,X_2 + 0{,}38\,Z_1 - 0{,}42\,Z_2$
$10a_1$	0,005	0,044	−0,071	π^*	$0{,}53\,X_1 - 0{,}39\,X_2 - 0{,}46\,Z_1 + 0{,}63\,Z_2 + 0{,}19\,Z^2 + 0{,}22\,Z'^2$
$1a_2$	−0,055	0	0,088	π	$0{,}59\,Y_1 + 0{,}73\,Y_2$
$2a_2$	0,085	0	−0,118	π^*	$0{,}82\,Y_1 - 0{,}70\,Y_2$
$1b_1$	−0,212	0,028	0,033	π	$0{,}41\,XY + 0{,}40\,XY' + 0{,}46\,Y_1 + 0{,}38\,Y_2$
$2b_1$	−0,033	−0,035	0,042	π	$0{,}45\,XY + 0{,}43\,XY' - 0{,}53\,Y_1 - 0{,}42\,Y_2$
$3b_1$	0,054	0	−0,061	π^*	$0{,}76\,Y_1 - 0{,}86\,Y_2$
$5b_2$	−0,938	0,002	0,129	σ	$0{,}59\,S_1 + 0{,}67\,S_2$
$6b_2$	−0,635	0,003	−0,072	σ^*	$0{,}79\,S_1 - 0{,}74\,S_2$
$7b_2$	−0,138	0,023	0,068	π	$0{,}61\,X_1 + 0{,}45\,X_2 - 0{,}45\,Z_2$
$8b_2$	−0,061	−0,009	0,021	σ	$-0{,}31\,S_1 + 0{,}57\,X_2 - 0{,}56\,Z_1 + 0{,}40\,Z_2$
$9b_2$	0,023	0,017	−0,100	π^*	$0{,}61\,X_1 + 0{,}57\,X_2 - 0{,}35\,Z_1 + 0{,}50\,Z_2$
$5e$	−0,936	−0,046	0,266	σ	$0{,}61\,S_1 + 0{,}66\,S_2$
$6e$	−0,620	0,001	−0,155	σ^*	$0{,}80\,S_1 - 0{,}75\,S_2$
$7e$	−0,125	−0,050	0,144	π	$0{,}53\,X_1 + 0{,}43\,X_2 - 0{,}46\,Z_2$
$8e$	−0,113	0,012	0,144	π	$0{,}45\,X_5 + 0{,}62\,X_6 - 0{,}36\,Z_2$
$9e$	−0,033	0,012	0,080	σ	$0{,}48\,X_2 + 0{,}60\,Z_1 + 0{,}40\,Z_2$
$10e$	0,027	−0,008	−0,152	π^*	$0{,}76\,X_1 - 0{,}45\,X_2 + 0{,}44\,X_5$
$11e$	0,094	0,005	−0,247	π^*	$-0{,}29\,X_1 + 0{,}73\,X_5 - 0{,}75\,X_6$

[a] Les notations $S_1, S_2, X_1, Y_1, Z_1, Z^2$… désignent les orbitales de symétrie de chaque représentation irréductible, construites respectivement à partir des orbitales contractées $2s$ de l'atome O_1, $2s$ de l'atome O_2, $2px$ et $2py$ et $2pz$ de l'atome O_1, $3d_z2$ du chrome, etc. …

En se basant sur cette classification, il est possible de discuter *qualitativement* la nature de la liason dans le complexe peroxochromate. La population de recouvrement totale entre l'atome de chrome et un atome d'oxygène est de 0,046. Aucune signification absolue ne doit être attachée à cette valeur. Pour l'ion $CuCl_4^{2-}$, l'utilisation de bases de fonctions gaussiennes de plus en plus larges s'accompagne d'une augmentation de la population de recouvrement entre les atomes de cuivre et de chlore, qui passe d'une valeur faiblement négative à une valeur positive [21]. Plus significative est la décomposition de la population de recouvrement totale en contribution correspondant aux orbitales σ, σ^*, π et π^* (Tableau 8). La contribution des orbitales π^* et σ^* à la population de recouvrement totale est globalement positive tandis que celle des orbitales π et σ est globalement négative (avec certaines contributions individuelles de signe opposé, par exemple l'orbitale $9e$ de type σ à une contribution positive). La contribution la plus importante à la liaison métal-ligand est celle des orbitales π^*, le terme prédominant provenant de l'orbitale $10a_1$. Afin d'illustrer la nature de la liaison métal-ligand, Tableau 8. Populations de recouvrement

	Cr-O	O-O[a]	O-O[b]
σ	−0,071	0,638	0,269
π	−0,047	0,562	0,326
π^*	0,058	−0,749	−0,482
σ^*	0,010	−0,302	−0,098
Total	−0,050	0,147	0,015

[a] Dans le complexe.

[b] Dans la molécule de ligand (cf. Tableau 6).

nous avons représenté dans la Fig. 2 la densité électronique correspondant à l'orbitale $10a_1$ dans le plan xOz. Cette orbitale est représentée schématiquement dans la Fig. 3. Elle correspond au recouvrement de l'orbitale $3d_z^2$ du chrome avec deux orbitales π^* ($1\pi_g$) de deux molécules de ligands. Il apparait que seule *la géométrie particulière de ce complexe permet un recouvrement simultané du lobe positif de l'orbitale $3d_z^2$ avec les lobes positifs des orbitales π^* des ligands et du lobe négatif de l'orbitale $3d_z^2$ avec les lobes négatifs des orbitales π^* des ligands.*

La population de recouvrement entre les deux atomes d'oxygène d'une molécule de ligand passe de 0,015 pour le ligand isolé à 0,147 dans le complexe. On serait tenté d'expliquer cette augmentation par la contribution des orbitales π^* à la liaison métal-ligand, à laquelle doit correspondre un transfert d'électrons des orbitales π^* des ligands vers le métal donc une diminution du caractère antiliant de ces orbitales. La comparaison de la population de recouvrement O–O

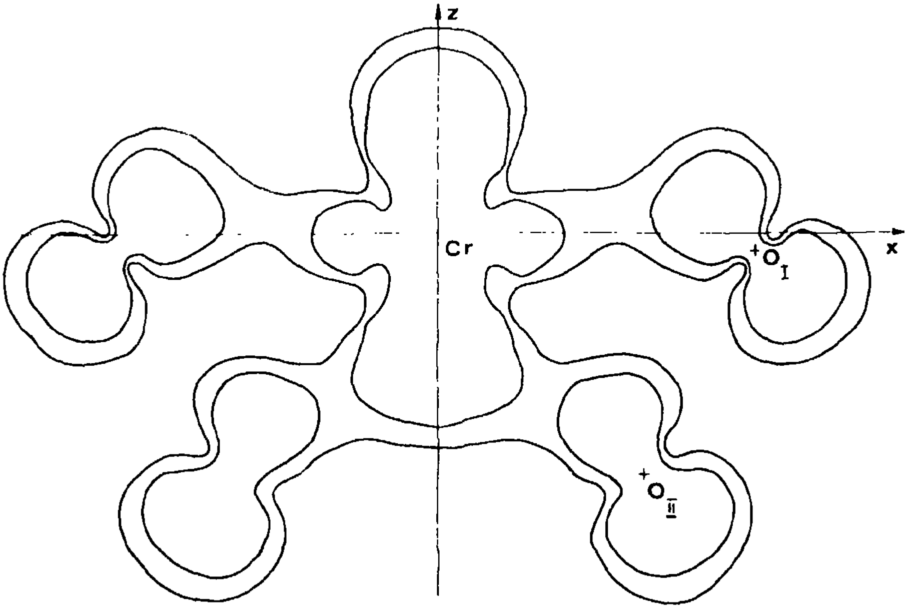

Fig. 2. Densité électronique de l'orbitale $10a_1$

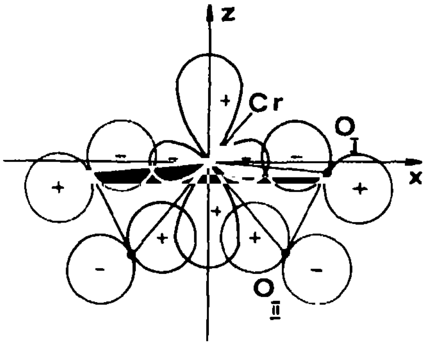

Fig. 3. Représentation schématique de l'orbitale $10a_1$ à partir de l'orbitale $3d_z2$ du chrome et des orbitales π* des ligands

par type d'orbitale fait apparaître une situation moins simple. Les orbitales liantes σ et π ont une population de recouvrement O–O plus grande dans le complexe que dans le ligand (Tableau 8). Simultanément la population de recouvrement correspondant aux orbitales antiliantes σ* et π* devient plus négative. La différence de ces deux effets correspond finalement à une légère augmentation de la population de recouvrement dans le complexe.

La nature de la liaison métal-ligand dans les complexes peroxo a été discutée par plusieurs auteurs sur des bases qualitatives. Selon Tuck et Walters [22], la formation de la liaison Cr-ligand résulte d'un transfert d'électrons de l'orbitale liante 2pπ du groupement peroxyde vers les orbitales *d* vides du métal. Griffith a rejeté ce modèle [23] en se basant sur le fait qu'un tel transfert d'électron devrait affaiblir la liaison O–O, donc se traduire par un allongement de la distance O–O. Expérimentalement on observe un raccourcissement de la liaison O–O. En outre, le modèle précédent ne permettrait pas d'interpréter la stéréochimie particulière des complexes peroxo. Griffith propose donc un autre modèle basé sur des liaisons courbes σ (Fig. 4), analogue au modèle classique du cyclopropane. Ultérieurement Stomberg a proposé un modèle proche de celui de Tuck et Walters, mais dans lequel le transfert d'électrons se fait de l'orbitale antiliante 2pπ* du groupement peroxyde vers les orbitales d_{xy} et $d_{x^2-y^2}$ du chrome [24] (Fig. 5), cette interprétation lui permettant d'expliquer le raccourcissement observé pour la liaison O–O puisque le transfert d'électron π vers le métal à partir d'une orbitale antiliante du ligand doit correspondre à un renforcement de la liaison O–O. Le modèle proposé par Stomberg est celui qui paraît le plus proche de nos résultats. En particulier et contrairement à la conception de Griffith, il paraît inexact de conclure que le modèle avec transfert d'électrons π ne permet pas d'expliquer la stéréochimie des complexes peroxydiques. Le schéma de la Fig. 3 fait apparaître au contraire que la possibilité d'une telle liaison par transfert d'électrons π repose sur la stéréochimie particulière du complexe. Toutefois la comparaison des Figs. 3 et 4 montre que la différence entre les conclusions du calcul et le modèle qualitatif de Griffith est moins grande que la terminologie utilisée ne le laisserait croire. Le modèle à liaisons courbes σ de Griffith correspond en effet à une disposition relative des orbitales peu différente de celle observée entre l'orbitale $3d_z^2$ du

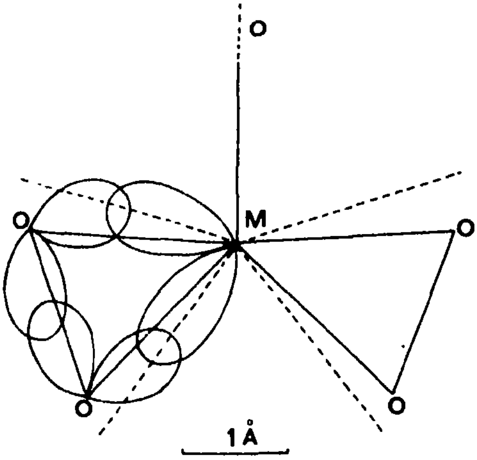

Fig 4

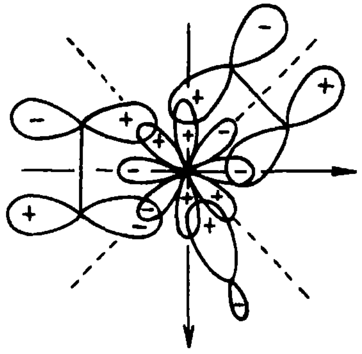

Fig. 5

Fig. 4. Modèle de liaison métal-pont peroxyde selon Griffith

Fig. 5. Modèle de liaison métal-pont peroxyde selon Stomberg

chrome et l'orbitale $2p\pi^*$ du ligand. Le schéma de la Fig. 3 représente donc un modèle de liaison qui réconcilie les conceptions apparemments opposées de Stomberg d'une part et de Griffith d'autre part.

Les résultats de l'analyse de population relatifs aux charges atomiques sont indiquées dans le Tableau 9. La charge formelle de l'atome de Cr est +2,58. On peut donc considérer que l'atome de chrome dans le degré d'oxydation *V* a reçu des ligands une charge électronique de 2,4 électrons. Effectivement, la population de chaque molécule de ligand dans le complexe n'est plus que de 17,39 électrons ce qui correspond bien au transfert de 0,6 électron *l* de chaque molécule de ligand vers le métal. Ces électrons gagnés par le métal se sont répartis dans les orbitales $3d$, les orbitales $4s$ et $4p$ ne paraissent jouer aucun rôle dans le complexe peroxochromate à la différence de ce que l'on observe pour les complexes du Ni et du Cu [6, 21]. On remarque en particulier que l'orbitale $3d_{xy}$ a une population de 2,0 électrons, ce résultat a une importance particulière qui apparaîtra dans la suite de la discussion (cf. *infra*).

Un point particulièrement important concerne la nature de l'orbitale $3b_1$ occupée par l'électron non apparié. Cette orbitale est entièrement constituée d'orbitale $2p$ des atomes d'oxygène sans aucune participation de l'orbitale $3d$ du

Tableau 9. Populations atomiques

	Total	s	p_x	p_y	p_z	d_{xy}	d_{xz}	d_{yz}	d_z2	$d_{x^2-y^2}$
Cr	21,42	5,98	3,95	3,95	4,02	2,00	0,40	0,40	0,51	0,18
O_I[a]	8,70 (9,00)	3,94 (3,90)	1,56 (1,80)	1,84 (2,00)	1,35 (1,29)					
O_{II}[a]	8,69 (9,00)	3,94 (3,90)	1,74 (1,80)	1,89 (2,00)	1,09 (1,29)					

[a] Les chiffres entre parenthèses correspondent à la molécule de ligand isolée.

métal. Ce résultat infirme l'hypothèse implicitement utilisée dans la théorie du champ des ligands, suivant laquelle l'orbitale décrivant l'électron non apparié à un caractère prédominant d'orbitale $3d_{xy}$ du métal ($3d_{xy}$ avec l'orientation d'axes choisie dans cet article, $3d_{x^2-y^2}$ avec l'orientation d'axes, à 45° de la nôtre, utilisée dans la Réf. [7]). Un résultat similaire a été obtenu pour l'ion tétracyanonickelate, dans lequel les plus hautes orbitales occupées sont également des orbitales π des ligands pratiquement pures [6]. Dans le cas de l'ion peroxochromate, il est possible de donner une interprétation simple de ce résultat en termes de transfert de charge et de populations d'orbitale. Les résultats de l'analyse de population indiquent que la formation du complexe à partir d'un ion Cr*V* et de quatre molécules de ligand se traduit par le transfert d'une charge correspondant à 2,4 électrons des ligands vers le métal, laissant l'atome de chrome avec une charge formelle de +2,6 (par analogie avec les résultats obtenus pour d'autres complexes [6], on peut prédire qu'un calcul utilisant une base plus large conduirait à une charge formelle plus faible donc à un transfert plus important). Les électrons transférés des ligands vers le métal se répartissent entre les différentes orbitales d du métal suivant leurs stabilités relatives dans le complexe, les populations correspondant aux différentes orbitales $3d$ dans l'ordre:

$$xy > z^2 > xz, yz > x^2 - y^2$$

qui est l'ordre de stabilité décroissante pour les orbitales d dans le champ des ligands [7]. La population de l'orbitale d_{xy} du métal atteint ainsi la valeur 2,00 dans le complexe. Ce résultat est obtenu par la formation de deux orbitales moléculaires, l'une liante ($1b_1$, représentée dans la Fig. 6) et l'autre antiliante

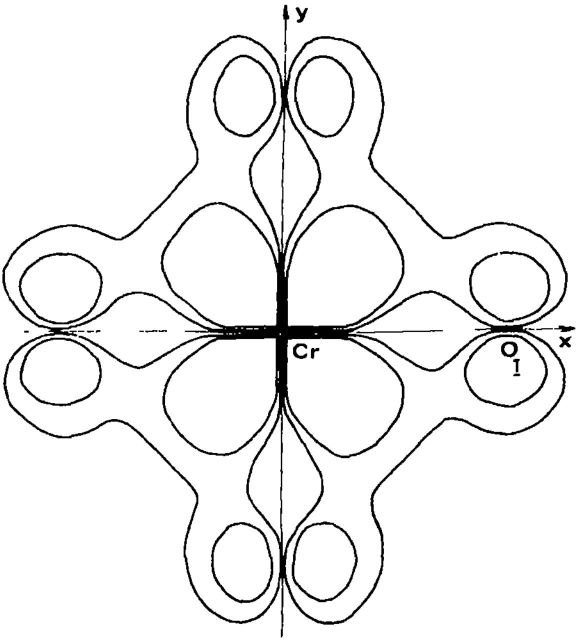

Fig. 6. Densité électronique de l'orbitale $1b_1$

($2b_1$) entre l'orbitale $3d_{xy}$ du métal et les orbitales $2p_y$ des ligands. L'orbitale $3d_{xy}$ ayant alors atteint sa population maximum ne peut plus être utilisée pour l'orbitale moléculaire qui décrit l'électron non apparié.

Conclusion

Un nouvel affinement de la structure cristalline de K_3CrO_8 confirme les conclusions du travail de Stomberg [8] avec une précision nettement supérieure et semble établir définitivement que la liaison O–O est plus courte dans l'ion tétraperoxochromate CrO_8^{3-} que dans l'ion peroxyde O_2^{2-}.

Un calcul ab-initio avec une base limitée de fonctions gaussiennes nous a permis d'interprêter ce résultat en relation avec la nature de la liaison métal-ligand dans le complexe. La contribution la plus importante à la liaison métal-ligand est due aux orbitales antiliantes π^* des ligands. Le transfert électronique de l'orbitale π^* du ligand vers le métal se traduit par une augmentation de la population de recouvrement O–O, c'est-à-dire par un renforcement de la liaison correspondant au raccourcissement observé expérimentalement. La formation de la liaison métal-ligand dans le complexe semble favorisée par l'arrangement dodécaédrique des atomes d'oxygène autour du métal qui correspond à un recouvrement optimal de l'orbitale $3d_z2$ du chrome avec les orbitales π^* des ligands. Le modèle de liaison proposé permet de réconcilier les conceptions apparement opposées de Stomberg et de Griffith.

Finalement l'orbitale $3b_1$ qui décrit l'électron célibataire est entièrement constituée d'orbitales $2p$ des atomes d'oxygène sans aucune participation des orbitales $3d$ du chrome. Ce résultat s'interprête qualitativement à partir des résultats de l'analyse de population qui mettent en évidence un transfert d'électrons des ligands vers les orbitales d du métal et plus particulièrement vers l'orbitale $3d_{xy}$. Celle-ci ne peut alors plus être utilisée pour l'orbitale moléculaire décrivant l'électron célibataire.

Remerciements. Les calculs ont été éffectués sur les ordinateurs des Centres de Calcul CNRS d'Orsay (C.I.R.C.E.) et de Strasbourg-Cronenbourg.

Bibliographie

1. Voir par exemple:
   (a) Ballhausen, C. J.: Introduction to ligand field theory. New York: McGraw Hill 1961.
   (b) Figgis, N. B.: Introduction to ligand fields. New York: Interscience Publishers 1966.
2. Voir par exemple: Réf. [1a], p. 163 et suivantes.
3. Wolfsberg, M., Helmholtz, L.: J. chem. Physics. **20**, 837 (1952).
4. Astier, M.: Molecular Physics **19**, 209 (1970).
5. Stomberg, R., Brosset, C.: Acta chem. scand. **14**, 441 (1960).
6. Demuynck, J., Veillard, A., Vinot, G.: Chem. Physics Letters **10**, 522 (1971).
7. Swalen, J. D., Ibers, J. A.: J. chem. Physics **37**, 17 (1962).
8. Stomberg, R.: Acta chem. scand. **17**, 1563 (1963).
9. Prewitt, C. T.: A Fortran IV Full-matrix Crystallographic Least Squares Program, SFLS-5.
10. International tables for X-ray cristallography. Vol. II. Birmingham, England: The Kynoch Press 1962.
11. Voir par exemple, Doedens, R. J., Ibers, J. A.: Inorg. Chem. **6**, 204 (1967).

12. Zachariasen, W. H.: Acta crystallogr. **16**, 1139 (1963).
13. Johnson, C. K.: Program ORTEP, ORNL 3794 (1965).
14. Slater, J. C.: Quantum theory of molecules and solids, Vol. 1, p. 43. New York: McGraw Hill 1963.
15. Roothaan, C. C. J.: Rev. mod. Physics **23**, 69 (1951); **32**, 179 (1960).
16. Roos, B., Veillard, A., Vinot, G.: Theoret. chim. Acta (Berl.) **20**, 1 (1971).
17. Clementi, E., Davis, D. R.: J. comput. Physics **2**, 223 (1967).
18. Veillard, A.: IBMOL Version IV, Special IBM Technical Report. San José 1968.
19. Huzinaga, S.: J. chem. Physics **42**, 1293 (1965).
20. Mulliken, R. S.: J. chem. Physics **23**, 1833 (1955).
21. Demuynck, J., Veillard, A.: Chem. Physics Letters **6**, 204 (1970).
22. Tuck, D. G., Walters, R. M.: Inorg. Chem. **2**, 428 (1963).
23. Griffith, W. P.: J. chem. Soc. (London) **1964**, 5248.
24. Stomberg, R.: Arkiv Kemi **24**, 283 (1965).
25. Wahlgren, U.: à paraître.
26. Schomacker, V., Trueblood, K. N.: Acta crystallogr. B **24**, 63 (1968).
27. Vannerberg, N. G.: Arkiv Kemi **14**, 99 (1959).

Dr. A. Veillard
Institut de Chimie
1, rue Blaise Pascal
F-67 Strasbourg, France

Theoret. chim. Acta (Berl.) 24, 334–345 (1972)
© by Springer-Verlag 1972

Polarization Functions and Geometry Optimization in *ab initio* Calculations of the Rotational Barrier in Hydrogen Peroxide

JOHN P. RANCK* and HELGE JOHANSEN
Chemical Laboratory IV, The H. C. Ørsted Institute, University of Copenhagen
Universitetsparken 5, 2100 Copenhagen Ø, Denmark

Received June 21, 1971

Ab initio calculations have been carried out for the hydrogen peroxide molecule with different size Gaussian basis sets in an attempt to determine the relative importance of carefully refined geometr and improvement of the wave function for calculation of the trans rotational barrier. *d*-type polarization functions on the oxygen atoms are found to be essential for calculation of a trans rotationa barrier Using the (O/7,3,1)(H/4,1) basis set, a trans rotational barrier of 0.63 kcal/mole is calculate (exp value, 1.1 kcal/mole). Except for refined calculations approaching the Hartree-Fock limi careful geometry optimization is found to be of secondary importance to the inclusion of *d*-typ functions on the oxygen atoms and may be carried out satisfactorily using a smaller basis set tha is used for the energy calculations. The (O/7,3)(H/4,1) basis set which includes *p*-type polarizatio functions on the hydrogen atoms yields geometrical parameters in good agreement with experimer as well as good charge distribution between the hydrogen and oxygen atoms.

Ab-initio Rechnungen für das Wasserstoffperoxidmolekül wurden mit Basissätzen verschiedene Große durchgeführt um den Einfluß einer genauen Geometrie und einer Verbesserung der Weller funktion auf die Berechnung der *trans*-Rotationsbarriere zu untersuchen. Es zeigte sich, daß *d*-Polar sationsfunktionen für solche Rechnungen außerst wichtig sind. Mit dem Basissatz (O/7,3,1)(H/4,1 wurde die Rotationsbarriere mit 0,63 kcal/Mol berechnet (exp.: 1.1 kcal/Mol). Außer bei Rechnunge nahe am Hartree-Fock-Limit zeigte sich, daß die Geometrieoptimisierung gegenüber der Mitnahm von *d*-Funktionen von sekundarer Bedeutung ist und daher mit einem kleineren Basissatz durchgeführt werden kann, als die Energieberechnung. Der (O/7,3)(H/4,1) Basissatz, der *p*-Funktione am Wasserstoffatom einschließt gibt die Geometrie und die Ladungsverteilung zwischen Wasserstoff- und Sauerstoffatom in guter Übereinstimmung mit dem Experiment

Introduction

In an attempt to explain barriers to internal rotation, a number of semiempirical and *ab initio* calculations have been performed using hydrogen peroxid as the simplest molecule having a barrier to internal rotation [1–6]. Althoug these attempts have quite generally predicted the trans conformation to be mor stable than the cis conformation, most have failed to predict the experimenta potential energy minimum at a dihedral angle of about 120° and show only monotonic decrease in energy as the dihedral angle is increased from 0 to 180 with the trans-planar conformation being the most stable. Veillard [6] ha carried out *ab initio* LCAO-MO-SCF calculations for the H_2O_2 molecule usin a large basis set of Gaussian-type functions including *d*-type functions for O and *p*-type functions for H, and has obtained energies approaching the Hartree-Fock limit. Further, he has minimized the energy with respect to variations in bond lengths and bond angles at each rotational angle calculated. These efforts have yielded a trans rotational barrier of 0.6 kcal/mole (experimental value, 1.1 kcal/mole) with a potential energy minimum at a dihedral angle of 123°. The rotation from 0° to 180° is also accompanied by a decrease of 0.025 Å in the O–O bond length and a decrease of 5.4° in the OOH bond angle. (The O–H bond length was not optimized.) From these results, Veillard has concluded that improvement of the wave function by using larger basis sets which include polarization functions and optimization of bond lengths and bond angles are equally important in achieving rotational barriers which approach the Hartree-Fock limit and he further states a belief that these two requirements must be satisfied simultaneously.

---

* On leave of absence from the Department of Chemistry, Elizabethtown College, Elizabethtown Pennsylvania 17022, USA.

An examination of Veillard's results shows clearly that the use of geometries which are in error by as much as 0.025 Å in O–O bond length and 5.4° in bond angle (such as would result from using the same bond lengths and bond angles for the cis- and trans-conformations of H_2O_2) would yield calculated energies on the order of 1.8 kcal/mole greater than the minimum energy calculated at the optimum geometry, an amount that is more than half again as large as the trans rotational barriers and that, indeed, refined calculations without geometry optimization would not be satisfactory.

It is not apparent from Veillard's results, however, what degree of expansion of basis sets is necessary to calculate satisfactory energy differences between two rotational conformations (as opposed to total energy of a single conformation) when the bond lengths and bond angles are optimized for each conformation; nor is it apparent whether a smaller basis set may be used for optimization of geometry prior to performing a single, good energy calculation with a larger basis set. (Forsén and Roos [7] have followed this procedure, but without particular justification, in their studies of the protonation of the carbon monoxide and the nitrogen molecule.) It is important to consider these possibilities which might allow geometry optimization, and perhaps energy calculations as well, with basis sets smaller than required to obtain total energies approaching the Hartree-Fock limit for the following reasons. (1) The number of two-electron integrals to be evaluated in an *ab initio* calculation increases roughly as the fourth power of the number of functions in the basis set. (2) In the IBMOL programs, evaluation of a two-electron integral involving one or more *d*-type functions requires approximately 4–8 times as long as evaluation of a two-electron integral involving only *s*- and *p*-type functions (only approximately 3 times as long if Roos's multiplication table [20] is used) and, thus, computation time may increase even more rapidly than the fourth power of the number of basis functions when the basis functions being added are *d*-type. (3) The number of points to be calculated in mapping a multi-dimensional energy surface sufficient to locate a local minimum increases rapidly with the size and complexity of the molecule. (Even with the small molecule H_2O_2 and assuming the two O–H bond lengths as well as the two OOH bond angles to be equal to each other, there are three coordinates to be varied at each torsional angle; a systematic search in three dimensions will *require the calculation of at least ten points and more will be required if the* initial values chosen are very far from the optimum values.) It is to these considerations and questions that this study is directed.

Calculations

The H_2O_2 molecule was used as a test case because (a) it is a small enough molecule that calculations using reasonably large basis sets are not prohibitive, (b) the trans rotational barriers is small and its successful prediction provides a fairly sensitive test of the method, and (c) Veillard's results [6] using a large basis set with calculated energies near the Hartree-Fock limit are available for comparison. Calculations were carried out at dihedral angles of 120° and 180° only.

The calculations are of the LCAO–MO–SCF type using basis sets of contracted Gaussian-type functions. The smallest basis set used was made up of five *s*-type and two *p*-type Gaussian functions for the oxygen atoms (O/5,2) and two *s*-type functions for the hydrogen atoms (H/2). This basis set will also be designated (5,2/2). This set was suggested by Sachs, Geller and Kaufman [8] as being the smallest basis set with which molecular geometries could be calculated with any degree of reliability. This basis set was contracted to two *s*-type and one *p*-type function for the oxygen atoms ⟨O/2,1⟩ and one *s*-type function for the hydrogen atoms ⟨H/1⟩. Contracted basis sets will be designated by brackets and, thus, this contracted basis set is designated ⟨2,1/1⟩. In studies of CF_2 with this basis set (uncontracted), Sachs *et al.* [8] calculated an equilibrium C–F bond length that is 2.4% longer than the experimental value and a FCF bond angle 1.0° larger than the experimental value. We are interested, however, in calculating bond lengths and bond angles that compare favorably, not so much with experimental values as with the optimum values calculated using a large basis set. If the comparison is no better than with the experimental values, it is probable that nothing can be gained by use of this small basis set, but if some of the systematic error introduced by using the small basis set also exists in calculations using the larger basis set, it may be possible to use the optimum geometrical parameters obtained with this small basis set for more refined calculations.

An intermediate-size basis set was constructed of seven *s*-type and three *p*-type functions for the oxygen atoms and four *s*-type functions for the hydrogen atoms (7,3/4); this set was contracted to ⟨4,2/2⟩. This set may be considered comparable to a Pople STO 2*G* set [9] which has been shown by Baird [10] to yield bond lengths generally within 0.01 Å of the experimental value for several diatomic and simple polyatomic molecules.

Roos and Siegbahn [11] have shown the necessity of adding polarization functions (*d*-type functions for O and *p*-type functions for H) before further increasing the (*s*, *p*/*s*) basis set. Accordingly, the third basis set used was (7,3,1/4,1) contracted to ⟨4,2,1/2,1⟩.

Finally, as results began to emerge, it became apparent that the *p*-type functions on hydrogen were, in many respects, more important than the *d*-type functions on oxygen. Since inclusion of *p*-type functions on hydrogen constitutes only a

Table 1. Gaussian basis functions used for hydrogen peroxide calculations

Atom	Basis set	Source	Type	Exponent	Expansion coefficients			Contraction coefficients
					1*s*	2*s*	2*p*	
H	(H/2)→⟨H/1⟩	Huzinaga [12]	*s*	1.66560[a]	0.27441			0.27441
				0.251909	0.82123			0.82123
	(H/4)→⟨H/2⟩	Huzinaga [12]	*s*	16.7019[a]	0.01906			0.01906
				2.51663	0.13424			0.13424
				0.567196	0.47449			0.47449
				0.154146	0.50907			0.50907
O	(O/5,2)→⟨O/2,1⟩	Whitman and Hornback [13]	*s*	736.6	0.0217	−0.0050		0.0217
				112.9	0.1447	−0.0316		0.1447
				26.04	0.4604	−0.1380		0.4604
				7.212	0.5061	−0.1698		0.5061
				0.5764	0.0215	1.0436		1.0436
			p	3.188			0.3503	0.3503
				0.5486			0.8005	0.8005
	(O/7,3)→⟨O/4,2⟩	Roos and Siegbahn [14]	*s*	2714.89	0.004324	−0.000975		0.004324
				415.725	0.032265	−0.007518		0.032265
				91.9805	0.156410	−0.037030		0.156410
				24.4515	0.447813	−0.130541		0.447813
				7.22296	0.481602	−0.204753		0.481602
				1.06314	0.042157	0.504708		0.504708
				0.322679	−0.011360	0.616743		0.616743
			p	7.75579			0.129373	0.129373
				1.62336			0.481269	0.481269
				0.365030			0.604484	0.604484

[a] Huzinaga's exponents for H atom multiplied by Wahlgren's scale factor of 1.25 as cited in Roos and Siegbahn [11].

slight expansion of the (7,3/4) basis set, a final set of calculations was carried out using a (7,3/4,1) basis set contracted to ⟨4,2/2,1⟩. For simplicity of discussion, henceforth, all these basis sets will be referred to with the uncontracted notation and the appropriate contractions will be understood.

The orbital exponents and expansion coefficients for different atoms and different-size Gaussian basis sets were taken from several sources and are listed, together with their sources, in Table 1. The common practice of using atomic expansion coefficients as contraction coefficients for molecular calculations has been discussed by Salez and Veillard [15] and that procedure has been followed in this work. The grouping of basis functions to form contracted functions was carried out observing Dunning's rules [16] and the groupings as well as the unnormalized contraction coefficients used are given in Table 1. The orbital exponents used for the *d*-type polarization functions added to the (O/7,3) basis set and the *p*-type polarization functions added to the (H/4) basis set were the optimum values found by Roos and Siegbahn [11], viz. 1.325 and 0.789, repsectively.

The calculations with the (5,2/2)→⟨2,1/1⟩ basis set were performed on an IBM 7094 computer using Version 2 of IBMOL [17, 18] (QCPE 92); the calculations with the (7,3/4)→⟨4,2/2⟩ basis set were performed on an IBM 360/75 computer using Version 4 of IBMOL [19]; all other energy calculations were performed on the 360/75 using the REFLECT program of Siegbahn [20]. Mulliken population analyses and dipole moment calculations were performed with the POPUL programs of Veillard [19]. Some times required for the calculation of the total energy of a single geometrical conformation using different basis sets, programs, and computers are shown in Table 2.

Table 2. Calculation times[a] in minutes for H_2O_2 using various basis sets, programs, and computers

Basis set	No. Basis functions Uncontracted	No. Basis functions Contracted	IBMOL(2)[b] (7094)	IBMOL(4)[b] (360/75)	REFLECT Non-planar case	REFLECT Planar case
(5,2/2)→⟨2,1/1⟩	26	12	12.2			
(7,3/4)→⟨4,2/2⟩	40	24	39.7	5.5		2.3
(7,3/4,1)→⟨4,2/2,1⟩	46	30			5.9	4.2
(7,3,1/4,1)→⟨4,2,1/2,1⟩	58	42		81.0	24.5	14.8

[a] CPU time except for 7094 which is elapsed time.

[b] IBMOL calculation times are for the non-planar case.

The search for optimum values for the geometrical parameters was conducted by varying the O–O and O–H bond lengths and the OOH bond angle in turn, holding all other parameters constant, and then fitting the calculated total energies to a quadratic or cubic equation. The optimum value thus found for one parameter was used as the constant value during the variation of the next parameter. In some cases, more than one cycle of variation of parameters was necessary to attain total energy constancy to eight figures.

Results and Discussion

The optimum values for the bond lengths and bond angle calculated with the different basis sets are given in Table 3. The values are seen to be highly dependent upon the basis set used.

The (5,2/2) basis set yields an O–O bond length that is 0.060 Å less than the experimental value and an O–H bond length that is 0.088 Å greater than the experimental value. Upon going to the (7,3/4) basis set, both these values improve significantly (errors equal to +0.006 Å and +0.024 Å, respectively). Addition of *p*-type functions to the H atoms brings the O–H bond length in very close agreement with the experiment value (error = 0.004 Å) and, as expected, has negligible effect upon the already good O–O bond length. Further addition of *d*-type functions to the O atom leaves the O–H bond length virtually unchanged, but reduces the O–O bond length to a value even less than that obtained with the (5,2/2) basis set.

The agreement of calculated bond angles with experiment is not very good in any case. All values are 5–7° too large which corresponds to a misplacement of the hydrogen atoms by about 0.1 Å. The range of the calculated values is about the same as the range of experimental uncertainty and corresponds to a range of misplacement of the hydrogen atoms by about ±0.015 Å, somewhat less than the range of the calculated values for the bond lengths.

These results are in general agreement with the conclusions of other workers [8–10, 24–26] – that calculations can be carried out using small basis sets to obtain bond lengths which agree with experimental values to within a few percent.

Table 3. Optimum geometries calculated for H_2O_2 with different basis sets

Parameter	Basis set	$\varphi = 120$	$\varphi = 180$	$\Delta[(\varphi = 120) - (\varphi = 180)]$
O–O	(5,2/2)	1.4145 Å	1.4228	−0.0103
	(7,3/4)	1.4812	1.4865	−0.0053
	(7,3/4,1)	1.4819	1.4876	−0.0057
	(7,3,1/4,1)	1.4038	1.4148	−0.0110
	(11,7,1/6,1)^a	1.475^b	1.475^b	0.000
	Experimental	1.475 ± 0.004^c		
O–H	(5,2/2)	1.0383	1.0339	+0.0044
	(7,3/4)	0.9739	0.9722	+0.0017
	(7,3/4,1)	0.9464	0.9458	+0.0006
	(7,3,1/4,1)	0.9442	0.9435	+0.0007
	(11,7,1/6,1)^a	–		
	Experimental	0.950 ± 0.005^c		
$\sphericalangle$OOH	(5,2/2)	101.85	100.22	+1.63
	(7,3/4)	100.63	99.43	+1.20
	(7,3/4,1)	99.64	98.66	+0.98
	(7,3,1/4,1)	101.11	99.71	+1.40
	(11,7,1/6,1)^a	101.3^b	100.2^b	+1.1
	Experimental	94.8 ± 2.0^c		

[a] (11,7,1/6,1)→⟨5,3,1/3,1⟩ [6].

[b] Veillard [6].

[c] Redington *et al.* [21].

Table 4a. Total energies[a] calculated for H_2O_2 with various basis sets and geometries

Basis set used for		$\varphi = 120°$	$\varphi = 180°$	$\Delta[(\varphi = 120°) - (\varphi = 180°)]$
Energy calculation	Geometry optimization			
(5,2/2)	(5,2/2)	−149.63690	−149.63643	−0.00047
	(11,7,1/6,1)[b]	−149.61610	−149.61735	+0.00125
(7,3/4)	(5,2/2)	−150.52717	−150.52895	+0.00178
	(7,3/4)	−150.53710	−150.53822	+0.00112
	(11,7,1/6,1)[b]	−150.53600	−150.53718	+0.00118
(7,3,1/4,1)	(5,2/2)	−150.59173	−150.59163	−0.00010
	(7,3/4)	−150.60217	−150.60149	−0.00068
	(7,3,1/4,1)	−150.60673	−150.60573	−0.00100
	(11,7,1/6,1)[b]	−150.60396	−150.60349	−0.00047
(11,7,1/6,1)[b]	(11,7,1/6,1)[b]	−150.79922[c]	150.79832[c]	−0.00090[c]
Experimental				−0.00175[d]

Table 4b

(7,3/4,1)	(5,2/2)	−150.55618	−150.55764	+0.00146
	(7,3,4)	−150.57360	−150.57395	+0.00035
	(7,3/4,1)	−150.57527	−150.57548	+0.00021
	(11,7,1/6,1)	150.57501	−150.57513	+0.00012
(7,3,1/4,1)	(7,3/4,1)	−150.60386	−150.60299	−0.00087
	(7,3,1/4,1)	150.60673	−150.60573	−0.00100

[a] Energies in hartrees.

[b] (11,7,1/6,1) → ⟨5,3,1/3,1⟩ [6].

[c] Veillard [6].

[d] Hunt *et al.* [22].

The (7,3/4,1) basis set, which is about the smallest "balanced" basis set one could construct to include *p*-type functions on the hydrogen atoms (cf. Roos and Siegbahn [11]), seems particularly good for this purpose. Also in agreement with the work of others [9, 24–26] we observe difficulty in calculating values for bond angles which agree well with experiment, even with the use of large basis sets.

Our primary interest, however is not the extent to which these optimum geometrical parameters agree or fail to agree with experiment, but the usefulness of the optimum values obtained with one basis set as geometrical parameters in an energy calculation with another basis set. Some total energies calculated for H_2O_2 in its skew conformation ($\varphi = 120°$) and in its trans-planar conformation ($\varphi = 180°$) using several basis sets and the optimum geometrical parameters obtained with the same and other basis sets are shown in Table 4a.

For any basis set, the lowest energy is calculated, of course, with the geometrical parameters as optimized with that same basis set. The improvement of total energies with increasing size and flexibility of the basis set also follows the well-known pattern. The last column in Table 4a gives the difference in total energy between the two conformations, i.e., the trans rotational barrier. Of particular interest is the observation that with the (7,3/4) basis set the energy of the 120° conformation is greater than the energy of the 180° conformation and, hence,

Table 5. Effect of polarization functions on the total energy[a] calculated for H_2O_2

Basis set	$\varphi = 120°$ [b]	$\varphi = 180°$ [b]	$\Delta[(\varphi = 120°) - (\varphi = 180°)]$
(7,3/4)	−150.53710	−150.53822	+0.00112
(7,3/4,1)	−150.57360	−150.57395	+0.00035
(7,3,1/4)	−150.58018	−150.57983	−0.00035
(7,3,1/4,1)	−150.60217	−150.60149	−0.00068

[a] Energies in hartrees.

[b] Geometry used for all calculations was the optimum geometry calculated with the (7,3/4) basis set.

no barrier to rotation is calculated, no matter which set of geometrical parameters is used; with the (7,3,1/4,1) basis set, however, a barrier to rotation is calculated, no matter which set of geometrical parameters is used. The best value for the barrier (obtained by using the (7,3,1/4,1) basis set for both optimization and energy calculations) is 57% of the experimental value and is the best value reported to date, though the improvement over Veillard's value (which is believed to approach the Hartree-Fock limit) should be regarded as accidental. Thus, at this level of refinement, we conclude that improvement of the basis set (especially by inclusion of polarization functions) is more important for calculation of the rotational barrier in hydrogen peroxide than the use of carefully optimized geometries.

Additional calculations were performed to determine the relative effects of the addition of *p*-type functions on the hydrogen atoms and *d*-type functions on the oxygen atoms. The optimum geometry as determined with the (7,3/4) basis set was used for all calculations. From the results (Table 5), it can be seen that using either *p*-type functions on the hydrogen atoms or *d*-type functions on the oxygen atoms will provide about two-thirds of the improvement in the total energy to be gained by using both types of polarization function together. However, the addition of *d*-type functions on the oxygen atoms alone results in an improvement in the energy difference equal to 82% of the amount to be gained by using both types of function, while use of *p*-type functions on the hydrogen atoms alone results in only 43% of the total improvement and the energy difference still has the wrong sign. Although the total energy of the molecule is determined by interactions among all four centers and improvement of the wave function in any region of the molecule must result in a lowering of the total energy, it is quite consistent with our ideas about localized chemical bonds that the greatest information about the potential function for rotation about the O–O "bond" can be gained by improving the wave function in this region.

These conclusions are further justified by the results of the Mulliken population analyses shown in Table 6a. All of these properties except the O–O overlap population are essentially an expression of the distribution of electronic charge between the hydrogen and the oxygen atoms. The *p*-type functions already included on the oxygen atoms provide sufficient flexibility for good charge distribution in this region and the greatest improvement is to be gained by addition of *p*-type orbitals on the hydrogen atoms. Addition of *d*-type functions to the oxygen atoms does not change the oxygen-hydrogen sharing, but only changes the distribution along the O–O bond. The effect of redistribution of

Table 6a. Population analyses for H_2O_2 calculated with various basis sets

Basis set used for		$\varphi = 120$							$\varphi = 180$						
Calculation	Geometry optimization	$n(H)^a$	$n(O)$	$o(OH)^b$	$o(OO)$	$q(H)^c$	$q(O)$	μ^d	$n(H)$	$n(O)$	$o(OH)$	$o(OO)$	$q(H)$	$q(O)$	μ
(5,2/2)	(5,2/2)	0.542	7.727	0.271	0.234	+0.209	−0.209	1.686	0.529	7.738	0.273	0.227	+0.217	−0.217	0.000
(7,3/4)	(7,3/4)	0.385	7.997	0.258	0.145	+0.377	−0.377	2.057	0.374	8.002	0.261	0.142	+0.384	−0.384	0.000
(7,3/4,1)	(7,3/4)	0.521	7.758	0.305	0.166	+0.201	−0.201	0.751	0.509	7.759	0.310	0.164	+0.205	−0.205	0.000
(7,3,1/4)	(7,3/4)	0.372	7.992	0.259	0.154	+0.387	−0.387	0.725	0.363	7.997	0.261	0.152	+0.392	−0.392	0.000
(7,3,1/4,1)	(7,3,1/4,1)	0.488	7.770	0.325	0.144	+0.212	−0.212	1.734	0.478	7.772	0.328	0.142	+0.217	−0.217	0.000

Table 6b

(7,3/4,1)	(7,3/4,1)	0.532	7.729	0.312	0.171	+0.183	−0.183	1.869	0.520	7.732	0.317	0.168	+0.189	−0.189	0.000
(7,3,1/4,1)	(7,3/4,1)	0.486	7.751	0.319	0.165	+0.214	−0.214	1.729	0.478	7.755	0.322	0.163	+0.219	−0.219	0.000

[a] Net atomic population

[b] Overlap population.

[c] Gross atomic charge.

[d] Dipole moment in Debyes. Experimental values reported. 2.26 D. 3.15 D. [23, 22].

charge along this bond is little betrayed in the O–O overlap population but is seen in the decrease in the total energy and the sensitivity of the total energy to changes – i.e., rotation – in the O O bond region.

These results suggest that a small basis set including *p*-type functions on hydrogen atoms but not *d*-type functions on first-row atoms could, indeed, be used for exploration of the potential surface as a function of geometrical distortions and for calculations of electron distribution in molecules involving only hydrogen and first-row atoms. Baird [10] has reached a similar conclusion regarding the use of the Pople-type STO 2G basis set for determining bond lengths, but a basis set including the flexibility of *p*-type functions on the hydrogen atoms, which the STO 2G set does not include, ought to be considerably superior. Pedersen and Morokuma [4] have noted that "hydrogen atom polarization appears to be significant for hydrogen peroxide and may be important for other molecules as well" and Forsén and Roos [7] used the (7,3/4,1) basis set to determine potential energy surfaces for HCO^+ and N_2H^+. Since the inclusion of these functions adds so little to the computation, there seems to be little justification for their continued exclusion in calculations using basis sets consisting of two contracted functions per atomic orbital.

These conclusions were further tested and borne out in the case of H_2O_2 with a complete set of calculations using the (7,3/4,1) basis set, the results of which are given in Tables 4b and 6b. With only the *p*-type polarization functions on the hydrogen atoms, the calculated barriers are bad, irrespective of the geometry; but the optimum geometry and the electron populations calculated with this basis set agree well with the results of calculations with larger basis sets. The use of the optimum geometry as determined with the (7,3/4,1) basis set in energy calculations with the (7,3,1/4,1) basis sets gives total energies within 0.00287 hartrees (1.80 kcal/mole) and a barrier energy within 0.00013 hartree (0.08 kcal/mole) of the best result obtained by optimizing the geometry with the (7,3,1/4,1) basis set itself.

The role of *d*-orbitals in bonds between first-row atoms is not sufficiently clarified in this study. Heteronuclear molecules such as H_2CNH ought to be examined more closely. Unfortunately Lehn *et al.* [27] have not included polarization functions in their basis sets for the study of the isoelectronic series H_2CCH^-, H_2CNH, H_2COH^+. The unusually bad value obtained for the O–O bond length in H_2O_2 when optimized with the (7,3,1/4,1) basis set indicates the need for better scaling. Roos and Siegbahn [11] have obtained their 3*d* orbital exponents for first and second-row atoms by minimization of the total energy alone. They have shown that, for first-row atoms, the total energy is only slightly dependent upon the value of the 3*d* orbital exponent, whereas gross atomic charge is highly dependent upon the value of the 3*d* exponent. Thus, charge distribution and other properties could also be important for choosing values for polarization exponents.

Conclusions

For small molecules involving only hydrogen and first-row atoms, Gaussian basis sets contracted to two functions per atomic orbital can effectively be used for the determination of equilibrium geometries and calculations of charge distribution. The (7,3/4,1) basis set, which is about the smallest balanced basis set which can be contructed to include *p*-type functions on the hydrogen atoms is particularly recommended. Inclusion of *p*-type functions on hydrogen atoms increases the complexity of the calculation very little, but results in a great improvement in the electron distribution in the X–H region (X is a first-row atom) and a significant improvement in the total energy.

In hydrogen peroxide (and probably in other molecules with first-row atoms bonded to each other), the inclusion of *d*-type functions on the oxygen atoms is essential for calculation of rotational potential barriers. The choice of a value for the 3*d* orbital exponent appears to be quite important, though the method of selection of good values is not yet clear.

In the calculation of small barriers to internal rotation, such as the trans barriers in hydrogen peroxide, some optimization of geometry is necessary so that the barrier is not obscured by gross errors. However, careful optimization of geometry is of secondary importance to the proper use of *d*-type polarization functions on the first-row atoms. For calculations approaching the Hartree-Fock limit, careful optimization of geometrical parameters is still necessary.

Acknowledgements. We thank the authors of the IBMOL and REFLECT programs, particularly the members of the Institute for Theoretical Physics at the University of Stockholm, for making their programs available to us. Computing facilities and time were provided by the Northern Europe University Computing Center at the Technical University of Denmark. One of us (JPR) is pleased to acknowledge the support of a Sabbatical-year half salary from Elizabethtown College, Elizabethtown, Pennsylvania, USA, and a National Science Foundation Science Faculty Fellowship.

References

1. Amako, Y., Giguère, P. A.: Canad. J. Chem. **40**, 765 774 (1962).
2. Kaldor, U., Shavitt, I.: J. chem. Physics **44**, 1823-1829 (1966).
3. Fink, W. H., Allen, L. C.: J. chem. Physics **46**, 2261 2275, 2276 2284 (1967).
4. Pedersen, L., Morokuma, K.: J. chem. Physics **46**, 3941-3947 (1967).
5. Palke, W. E., Pitzer, R. M.: J. chem. Physics **46**, 3948 -3950 (1967).
6. Veillard, A.: Chem. Physics Letters **6**, 51 52 (1969); Theoret. chim. Acta (Berl.) **18**, 21 33 (1970).
7. Forsén, S., Roos, B.: Chem. Physics Letters **6**, 128-132 (1970).
8. Sachs, L. M., Geller, M., Kaufman, J. J.: J. chem. Physics **51**, 2771 -2778 (1969).
9. Hehre, W. J., Stewart, R. F., Pople, J. A.: J. chem. Physics **51**, 2657-2664 (1969).
10. Baird, N. C.: Chem. Physics Letters **6**, 61- 63 (1970).
11. Roos, B., Siegbahn, P.: Theoret. chim. Acta (Berl.) **17**, 199--208 (1970).
12. Huzinaga, S.: J. chem. Physics **42**, 1293-1302 (1965).
13. Whitman, D. R., Hornback, C. J.: J. chem. Physics **51**, 398-402 (1969).
14. Roos, B., Siegbahn, P.: Theoret. chim. Acta (Berl.) **17**, 209-215 (1970).
15. Salez, C., Veillard, A.: Theoret. chim. Acta (Berl.) **11**, 441-451 (1968).
16. Dunning, T. H., Jr.: J. chem. Physics **53**, 2823-2833 (1970); - Chem. Physics Letters **7**, 423-427 (1970).
17. Clementi, E., Davis, D. R.: J. comput. Physics **2**, 223-244 (1967).
18. — Veillard, A.: IBMOL: Computation of wave functions for molecules of general geometry. An IBM 7094 program using the LCGO-MO-SCF Method. Version 2, San Jose, California, IBM Research Laboratory.
19. Veillard, A.: IBMOL: Computation of wave function for molecules of general geometry. Version 4, San Jose, California, IBM Research Laboratory.
20. Siegbahn, P.: Chem. Physics Letters **8**, 245-250 (1971).
21. Redington, R. L., Olson, W. B., Cross, P. C.: J. chem. Physics **36**, 1311-1326 (1962).

27. Hunt, R. H., Leacock, R. A., Peters, C. W., Hecht, K. T.: J. chem. Physics **42**, 1931–1946 (1965).
23. Massey, J. T., Bianco, D. R.: J. chem. Physics **22**, 442–448 (1954).
24. Newton, M. D., Lathan, W. A., Hehre, W. J., Pople, J. A.: J. chem. Physics **52**, 4064–4072 (1970).
25. Hehre, W. J., Ditchfield, R., Pople, J. A.: J. chem. Physics **53**, 932–935 (1970).
26. Pople, J. A.: Accts. Chem. Res. **3**, 217–233 (1970).
27. Lehn, J. M., Munsch, B., Millie, Ph.: Theoret. chim. Acta (Berl.) **16**, 351–372 (1970).

Prof. Dr. J. P. Ranck
Chemistry Department
Elizabethtown College
Elizabethtown, Pennsylvania 17022, USA

Theoret. chim. Acta (Berl.) 24, 346–370 (1972)
© by Springer-Verlag 1972

Porphyrins XXIV.
Energy, Oscillator Strength, and Zeeman Splitting Calculations (SCMO-CI) for Phthalocyanine, Porphyrins, and Related Ring Systems

A. J. McHugh* and Martin Gouterman
Department of Chemistry, University of Washington, Seattle, Washington 98105

Charles Weiss, Jr.*
Lawrence Radiation Laboratory, University of California, Berkeley, California 94720

Received May 17, 1971

Extensive CI calculations have been done on free base porphin and the metallo derivative of porphin, tetrazaporphin, phthalocyanine, various benzporphins, chlorin, and bacteriochlorin. The transition gradient operator gives good agreement with experimental intensities. Free base porphin may have a weak $\pi - \pi^*$ transition around 480 *nm*. Tetrabenzporphin and phthalocyanine are predicted to have much more intensity around 50000 cm^{-1} than porphin and tetrazaporphin due to benzenoid transitions, a prediction borne out by the available data. Magnetic effects are calculated for the low energy excited states. Q state angular momentum is calculated to be 4.35 h for porphin and 3.13 h for phthalocyanine. Although these numbers agree with some experimental results, the calculations show that the experimental analysis needs further refinement.

Es wurden ausführliche CI-Rechnungen für die freie Porphinbase und die Metallderivate von Porphin, Tetrazaporphin, Phthalocyanin, verschiedene Benzporphine, Chlorin und Bacteriochlorin durchgeführt. Der Operator des Übergangsgradienten zeigt gute Übereinstimmung mit experimentellen Intensitäten. Die freie Base Porphin hat höchstwahrscheinlich bei 480 *nm* einen schwachen $\pi - \pi^*$-Übergang. Mit Hilfe der vorhandenen Daten ist die Voraussage möglich, daß die benzoloiden Banden im Bereich um 50000 cm^{-1} im Falle von Tetrabenzporphin und Phthalocyanin intensiver als bei Porphin und Tetrazaporphin sind. Ferner werden die magnetischen Eigenschaften für angeregte Zustände niedriger Energie berechnet. Man erhält den Drehimpuls des Q-Zustandes zu 4,35 h für Porphin und 3,13 h für Phthalocyanin. Obwohl diese Werte mit einigen experimentellen Resultaten übereinstimmen, zeigen die Rechnungen, daß die experimentelle Analyse weiterer Verfeinerung bedarf.

1. Introduction

Gouterman and Wagnière [1] showed that the four orbital model could explain many of the observed features of porphyrin spectra. The model is based on the assumption that transitions between the two top filled orbitals and the two lowest empty are relatively well separated from the remainder. SCMO–PPP CI calculations (self-consistent molecular orbital-Pariser-Parr-Pople-configuration interaction) performed by Weiss, Kobayashi, and Gouterman [2] showed that the four orbital model was justified for the lowest energy transitions (Q bands) but was less justified for the near *uv* (Soret or B) transitions. These better calculations predicted various higher transitions; the main weakness was the overestimation of the $Q - B$ splitting and the gross overestimation of oscillator strength.

---

* Present address: See end of paper.

This paper extends the previous SCMO–PPP–CI study in the following ways: For porphin and tetrazaporphin (TAP), for which full CI has been reported, we have used the transition gradient operator [3] for the calculation of oscillator strength, obtaining good agreement with experiment. We also report a full CI treatment of phthalocyanine (Pc) and tetrabenzporphin (TBP), which were previously done only with the four-orbital model, and the mono, di, and tribenzporphins, which were previously not studied. Section 2 reports the results for the energy and oscillator strength calculations. Section 3 uses these wave functions to calculate Zeeman splitting integrals previously only reported within the four-orbital model [4]. For these latter calculations chlorin and bacteriochlorin are included.

2. SCMO–PPP–CI Energies and Oscillator Strengths

a) Method

The SCMO-PPP method was used to generate a basis for an extensive singly excited CI treatment. The choice of configurations was based on energetic considerations and was limited by the available core storage space in the 7094 computer. General policy was to include all configurations up to 66666 cm^{-1}, but for the larger molecules this was not practicable.

The choice of semiempirical parameters followed the "traditional" set espoused by Weiss *et al.* [2], mostly for consistency but also in the knowledge that this set has already given a good account of itself in previous calculations. The parameters are:

$$\begin{aligned} (ii|ii)_C &= 10.60\,\text{eV}, & (ii|ii)_N &= 13.31\,\text{eV}, \\ W_C &= -11.22\,\text{eV}, & W_N &= (-36.61 + 11.05p)\,\text{eV} \end{aligned} \tag{1}$$

where $p = 1$ for pyrrole, 1.5 for neutral porphyrin, and 2 for pyridine. The 1.5 value was used for the central N atoms except for the free base porphin calculation. The Mataga and Nishimoto [2, 5] formula for the Coulomb repulsion integrals γ_{ij} was used and the resonance integrals were given by

$$\beta_{ij} = \frac{-2.371\,S(R_{ij})}{S(1.39\,\text{Å})}\,\text{eV} \tag{2}$$

where $S(R_{ij})$ is the two center overlap integral. The geometry of Hoard *et al.* [6], artificially constrained to planar square symmetry, was used for porphin, tetrazaporphin, and the benzporphins [2]. Robertson's [7] geometry was used for phthalocyanine. After the MO's were obtained, the CI matrix elements were calculated among the allowed singly excited states.

Diagonalization of the resulting matrix gave our final allowed electronic states. Forbidden states were calculated separately in order to reduce the size of the matrices generated in the CI treatment. In calculating f_1 and f_2 we made use of Eqs. (7) and (8) of Ref. [3] using theoretical values for the energies. For the D_{4h} molecules reported in Table 1 and Figs. 1, 3, 4, and 7, the theoretical f values are for one transition of a degenerate pair. The experimental f values are obtained from

$$f = 4.33 \times 10^{-9} \int \varepsilon d\tilde{\nu}.$$

Thus for the D_{4h} cases theoretical f values must be doubled when comparing with experimental f values.

Some comparison of the parameters given above with the set more carefully worked out be the Stockholm group [9a, 9b, 9c] is in order. We find two principal differences: (i) The Stockholm one center parameters W_μ are 1.4 to 2 eV less negative than the ones we use; (ii) The Stockholm one center electron repulsion integrals $(ii|ii)_\mu$ are 1.4 to 2 eV more positive. The resonance integrals β_{ij} are not so different. The Stockholm value for the lowest ionization energy for free base porphin is ~6.5 eV [9c], while our value is ~8.5 eV [2]. Since the Stockholm parameter set was developed to fit among other data the ionization potentials of a set of small molecules, their value should be more reliable. Their calculations and ours give a rather similar account of the absorption spectra. The gap between visible and Soret bands, too large for both calculations, is somewhat smaller with our parameter set. Knop and Knop [9d] used values for W_μ and $(ii|ii)_\mu$ close to the values we have used except they used $(ii|ii)_N = 16.57$ eV and $\beta_{CN} = -1.8$ eV for pyrrole nitrogen. Their resulting free base porphin spectrum is rather similar to the one reported here.

b) Free Base Porphin (P)

Table 1 and Fig. 1 give energies and oscillator strengths for all transitions out to 60000 cm^{-1}. Three calculations are reported: $\Delta\alpha = 0$, 5.5 eV, and 11.05 eV, where $\Delta\alpha = \alpha_N$ (pyridine) $- \alpha_N$ (pyrrole). The last gives normal pyridine and pyrrole coulomb integrals to the central nitrogens of the free base, while the first corresponds to the metal. Several features are notable: (i) The f_2 (gradient) value for the near *uv* absorption agrees with experiment while the f_1 (dipole) value is large by a factor of 4. (ii) The gradient operator, but not the dipole operator, correctly predicts Q_y to be more intense than Q_x [8]. This last result can be obtained from the dipole operator if a somewhat different Hamiltonian is used [2, 9c]. (iii) At $\Delta\alpha = 5.5$ eV the B intensity is divided between three bands B_x, B_y, N_x. At $\Delta\alpha = 11.00$ eV the B intensity is primarily in the fourth and fifth excited states with the third band moderately intense. (See Table 1 and Fig. 1.) For both $\Delta\alpha$ values there is substantial splitting among the intense components of the B region. A similar result is found by Sundbom [9c] using somewhat different parameters.

Earlier interpretation of the porphin spectrum [10] assigned as B_x and B_y the two peaks of nearly equal intensity separated by 240 cm^{-1} observed by Rimington *et al.* [8] in the low temperature absorption spectrum. However this interpretation is incompatible with the calculated results for either $\Delta\alpha = 5.5$ eV or 11 eV. As shown in Table 1, for $\Delta\alpha = 0$ corresponding to a metal porphin, there are five principal bands Q, B, N, L, M calculated for $\lambda > 200$ nm. The Q band is expected to be very weak ($f_2 = 0.001$) while the B band is strong ($f_2 = 0.57$) [N.B.: These f_2 values refer to one component of a degenerate pair of transitions.] At $\Delta\alpha = 11$ eV the B band intensity appears in two transitions at 28370 cm^{-1} and 30310 cm^{-1} and an electronic band with $f_2 = 0.07$ is predicted to be between Q and B. Actually two pieces of data confirm the spreading of B band intensity: (i) Polarization data of Sevchenko, *et al.* [11] show positive and negative polarization regions of the B band separated by 600 cm^{-1}. (ii) The vapor and solution

Table 1. Oscillator strength for excited states of porphin as a function of α values

Metal	Energy	$\Delta\alpha = 0$[a]		Energy	$\Delta\alpha = 5.5$		Energy	$\Delta\alpha = 11.05$[b]	
State	(cm^{-1})	f_1	f_2	(cm^{-1})	f_1	f_2	(cm^{-1})	f_1	f_2
Q	15937	0.002	0.001	14989x	0.01	0.000	13553x	0.029	0.000
	x, y			16913y	0.000	0.002	17247y	0.005	0.004
B	28403	2.82	0.57	27524x	1.67	0.30	24930x	0.48	0.07
	x, y			28794y	3.06	0.67	28371y	2.73	0.58
N	33920	0.34	0.08	31667x	1.79	0.47	30307x	2.80	0.61
	x, y			35010y	0.19	0.08	32940y	0.38	0.10
L	37377	0.15	0.06	38423y	0.16	0.06	41965y	0.04	0.01
	x, y			40175x	0.11	0.06	42005x	0.12	0.06
	47563	0.02	0.001	47023x	0.11	0.05	43997x	0.34	0.14
	x, y			47599x	0.08	0.05	45358x	0.008	0.003
M	48007	0.07	0.05	47904y	0.02	0.001	46982y	0.001	0.001
	x, y			49118y	0.03	0.009	47947y	0.04	0.000
	50588	0.02	0.03	49905x	0.04	0.006	48788y	0.01	0.02
	x, y			50274y	0.001	0.006	49482x	0.02	0.03
	52208	0.07	0.01	52659x	0.000	0.008	52385x	0.03	0.03
	x, y			53539y	0.008	0.003	52808y	0.006	0.001
	53613	0.004	0.002	54513x	0.006	0.003	54214x	0.003	0.001
	x, y			56438y	0.06	0.02	56062y	0.19	0.11
	58297	0.09	0.03	59144x	0.11	0.03	57695x	0.09	0.04
	x, y			59553y	0.005	0.000	58176y	0.21	0.07
	59364	0.11	0.08	59665y	0.13	0.06	58713y	0.05	0.02

[a] Metal case; f values for one of the degenerate transitions.

[b] "Traditional" free base value.

spectra of Edwards [12] show unusual broadness of the Soret region in free base compared to metal complexes. Therefore we now assign the two peaks separated by 240 cm^{-1} observed by Rimington *et al.* [8] to a Shpol'skii or dimer splitting and believe the B intensity is spread among more widely separated electronic origins.

The facts known at present do not allow a clear choice between the $\Delta\alpha = 5.5$ eV and $\Delta\alpha = 11$ eV calculations. The vapor spectrum of Edwards [12] shows a very broad absorption between 25000 cm^{-1} and 32000 cm^{-1}, which contains the Soret intensity. A double L band ($f \sim 0.1$) is observed at 34250 and 37700 cm^{-1}. Finally an M band ($f \sim 0.3$) is observed at 44400 cm^{-1}. In addition we might note that a weak peak at $\sim$21000 cm^{-1} has been consistently observed by Longo and coworkers [13] in substituted free base tetraphenylporphins between $Q_y(1, 0)$ and the Soret band. It can also be observed in free base octaethylporphin [12a], and possibly one of the peaks in free base porphin in the region $\lambda \sim 485$ *nm* [8] is of the same origin. In the study of Longo *et al.* the intensity of this band depends on substituent, as might be expected for an electronic band. However its intensity is far less than $f_2 = 0.07$ predicted by the $\Delta\alpha = 11$ eV calculation for the band at 24930 cm^{-1} lying between the intense Soret bands and the two Q bands.

We can relate the $\Delta\alpha = 5.5$ eV calculation to the data as follows: (a) The "Longo" band at 21000 cm^{-1} is either Q (2, 0) or perhaps $n - \pi^*$; (b) the Soret intensity of Edwards is related to three intense calculated bands between 27520 cm^{-1} and 31670 cm^{-1}; (c) the L bands of Edwards are assigned to calcu-

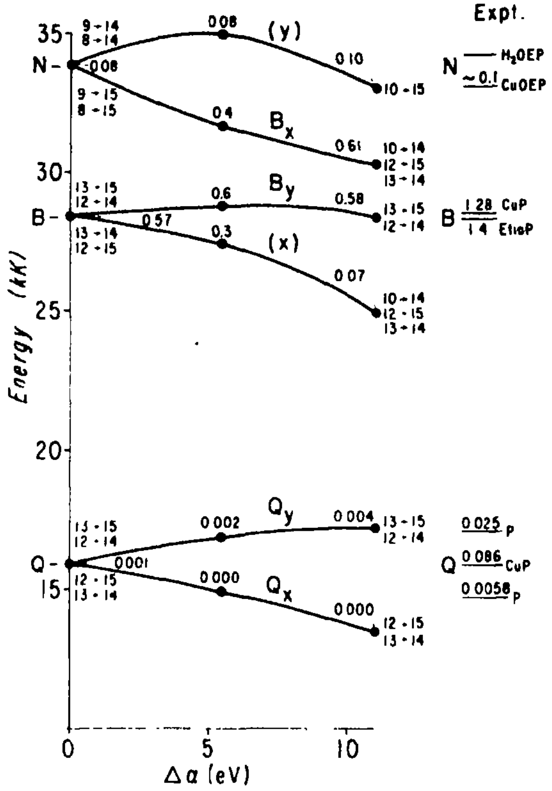

Fig. 1. Energy levels for porphin: $\Delta\alpha = 0$ corresponds to metal while $\Delta\alpha = 11.05$ eV to free ba (see Sect 2b) Orbitals 8, 9, 13 are b_{1u} symmetry; orbital 12 is a_u; orbital 14 is b_{2g} (nodal plane y orbital 15 is b_{3g} (nodal plane is xz). See Fig 9 for axes. Theoretical f_2 values are given. Experimen values of CuP and etioporphyrin from Ref. [33]. "Longo" band (see text) at 21000 cm^{-1} not sho

lated bands at 35010 cm^{-1} ($f_2 = 0.08$) and 38420 cm^{-1} ($f_2 = 0.06$); (d) tl Edwards M band is the three bands at ~47000 cm^{-1} with combined $f_2 \sim 0.$ (e) the calculated band at 40180 cm^{-1} ($f_2 = 0.06$) is probably the M regio Sundbom [9] gave a similar interpretation for the free base porphin spectrur placing two strong bands in the region 25000 to 31000 cm^{-1}. Her calculat $n - \pi^*$ transition is at 31600 cm^{-1}, rather to the blue of the "Longo" band.

We can relate the $\Delta\alpha = 11$ eV calculation to the data in a different way: (a) T "Longo" band is ascribed to the $\pi - \pi^*$ band ($f_2 = 0.07$) predicted to lie betwe the Soret and visible bands; (b) the Soret band of Edwards is related to the tv intense transitions calculated for 28370 cm^{-1} and 30310 cm^{-1}; (c) the Edwar L band is ascribed to the predicted band at 32940 cm^{-1} ($f_2 = 0.10$); (d) t Edwards M band is ascribed to the calculated band at 44000 cm^{-1} ($f_2 = 0.1$ (e) the calculated band at 42000 cm^{-1} ($f_2 = 0.06$) is probably in the M regic

An interpretation generally similar to this was proposed by Knop and Kn [9d], except they identified the strongest visible band (generally called Band I as the electronic transition between the visible bands and the Soret. Their prima

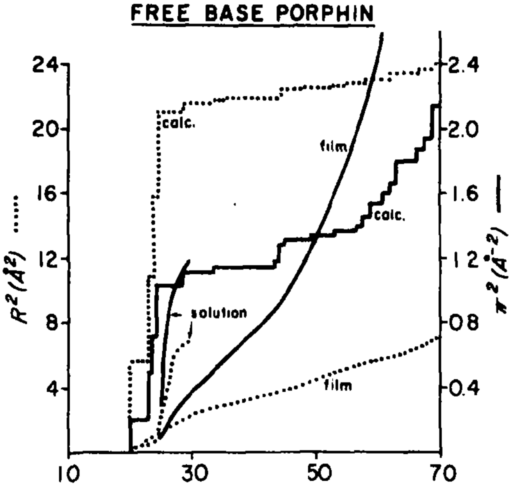

Fig. 2. Solution data [14], film data [15], and calculated values (from one-electron transitions) for R^2 (dotted lines) and Π^2 (solid lines). See Ref. [3] for detailed explanation of these plots

evidence for this was the positive fluorescence polarization. Since such polarization is predicted by vibronic considerations (see Ref. [32]), we do not find this argument compelling.

We can see that neither the calculations for $\Delta\alpha = 5.5$ eV nor those for $\Delta\alpha = 11$ eV match the vapor spectrum of free base porphin well enough for us to choose unambiguously between them. Both predict that the B intensity will be spread out and that beyond the B region there will not be much intensity. If substituent effects on intensity and polarization studies can establish that the "Longo" band at 21000 cm^{-1} represents the origin of a $\pi-\pi^*$ electronic transition, then the $\Delta\alpha = 11$ eV calculation will take precedence. As discussed below, MCD results are ambiguous on this point, and for the present the question remains unsettled.

Finally we compare the absolute value of calculated intensity to experiment in Fig. 2 using the cumulative total integrated absorption strength, a method of presentation used before [3]. The reported data come from solution data [14] and from recent data on protoporphyrin films [15]. There is considerable disagreement between these data sources, which might arise from errors in crystal thickness or density. The theoretical Π^2 value agrees well with the solution Π^2 value suggesting that Schechtman's crystal values are too low since there is considerable solution data. The calculated R^2 are much greater than experimental, as found for numerous aromatic hydrocarbons [3].

The rapid divergence between the film Π^2 and calculated Π^2 above 50000 cm^{-1} can be explained in terms of the presence of transitions to conducting states. Schechtman [15] has noted that continuum transitions appear at least as low as 30000 cm^{-1} in free base porphin. Conducting states are necessarily collective in nature and are outside the scope of the present isolated molecule calculations.

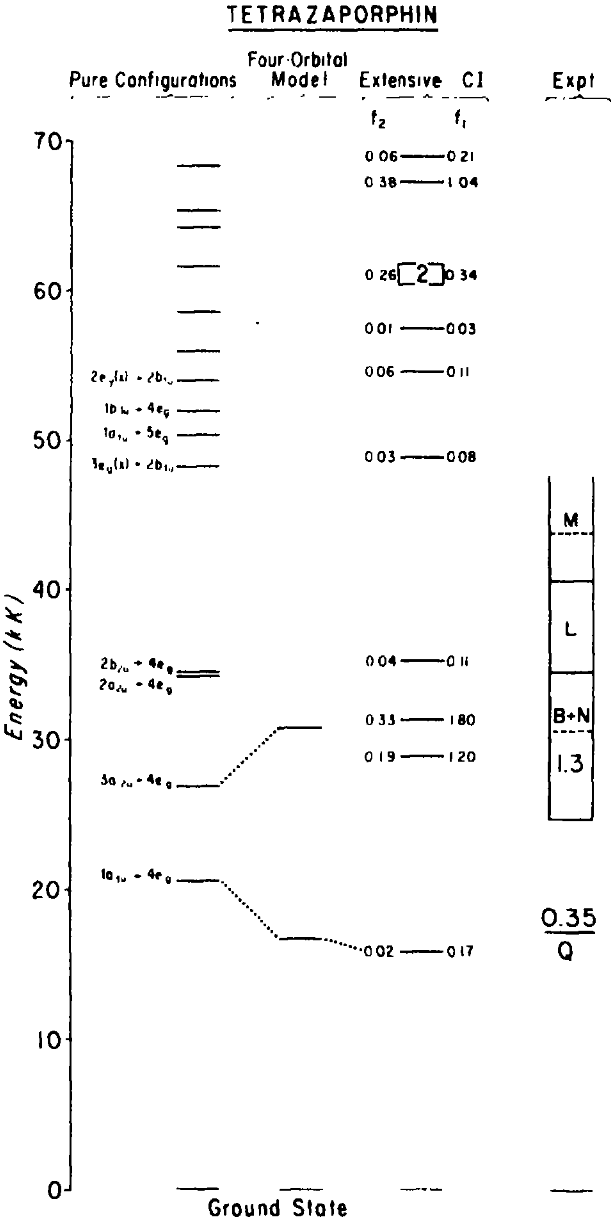

Fig. 3. Allowed transitions with and without CI with theoretical f_1 and f_2 values. Transitions w f_1 and f_2 below 0.01 are deleted. Integers in theoretical boxes give number of predicted leve Experimental data from Linstead [private communication] on MgTAP in methanol. Continuo absorption above 24.6 kK indicated by box: solid lines show minima and dashed lines peaks. Numb give experimental f values

c) Tetrazaporphin

The present SCMO–CI calculation employed a slightly higher cut-off energy than that of Weiss *et al.* [2], but the energy level diagram in Fig. 3 is very similar. Both transition gradient and dipole calculations predict a stronger N than B band. We believe the data supports this interpretation [14b], although our interpretation has been criticized (Ref. [11b], p. 167). The diffuseness of the composite B, N bands might be attributed to a strong vibronic interaction between the two. However, Hochstrasser and Marzzacco [16] have pointed out that interaction between $n-\pi^*$ and $\pi-\pi^*$ transitions is more effective in causing diffuseness than interaction between two $\pi-\pi^*$ transitions. Recent extended Hückel calculations on tetrazaporphin indicate the presence of $n-\pi^*$ transitions in the B, N region [17]. In view of the fact that the diffuseness of the B, N region in tetrazaporphin and phthalocyanine greatly exceeds that in the comparable region of porphin and tetrabenzporphin, where there is some overlapping of $\pi-\pi^*$ transitions, it seems likely that it is indeed underlying $n-\pi^*$ transitions that are responsible. The experimental spectrum of MgTAP in methanol shows bands at 39000 cm^{-1} and 44000 cm^{-1} [14b] which are indicated in Fig. 3. The second of these has no theoretical counterpart in the $\pi-\pi^*$ spectrum.

d) Phthalocyanine

Phthalocyanine energy levels, including those derived from vapor phase spectra of ZnPc and CuPc [18], are given in Fig. 4. An important experimental feature is the very high intensity of the Q band and the broadness of the B bands. The broad band at 3025 Å (33060 cm^{-1}) is probably the N band predicted to be at 35800 cm^{-1}. The f_2 calculation reported in Fig. 4 is in reasonably good agreement with the data, while the f_1 sum is grossly high. The energies of the stronger calculated transitions are in good agreement with the experimental values for the N, L, and C bands. As in TAP, the broadness of the B bands can be explained as due to underlying $n-\pi^*$ transitions [16]. Also, as shown in Fig. 9, there are forbidden $\pi-\pi^*$ transitions in the B region that may help to explain the broadness.

The cumulative absorption intensity plot for phthalocyanine is given in Fig. 5. There is more consistency here between the various reported experimental measurements than was the case in free base porphin. Once again it is found that Π^2 is a more satisfactory indicator of intensity than R^2.

An interesting feature of our calculations is the partial verification of the suggestion of Schechtman [15] that the benzene rings of phthalocyanine might play a semiautonomous part in determining the *uv* absorption. Schechtman assigns three peaks between 39000 and 59000 cm^{-1} to the benzenoid transitions. In Fig. 5 we see a steep rise in calculated intensity beginning at 57000 cm^{-1}. One way of deciding whether this rise is due to transitions of benzenoid character is to look at the transitions monopoles. For a one electron promotion $k \rightarrow l$, the product $C_{ik}C_{il}$ is the transition monopole and gives the contribution of atom i to the transition dipole, where C_{ik} is the MO coefficient of orbital k on atom i. The upper part of Fig. 6 shows the transition monopoles for $4e_g \rightarrow 4b_{1u}$, a typical contributing transition to the steep rise beyond 57000 cm^{-1}; the lower part of

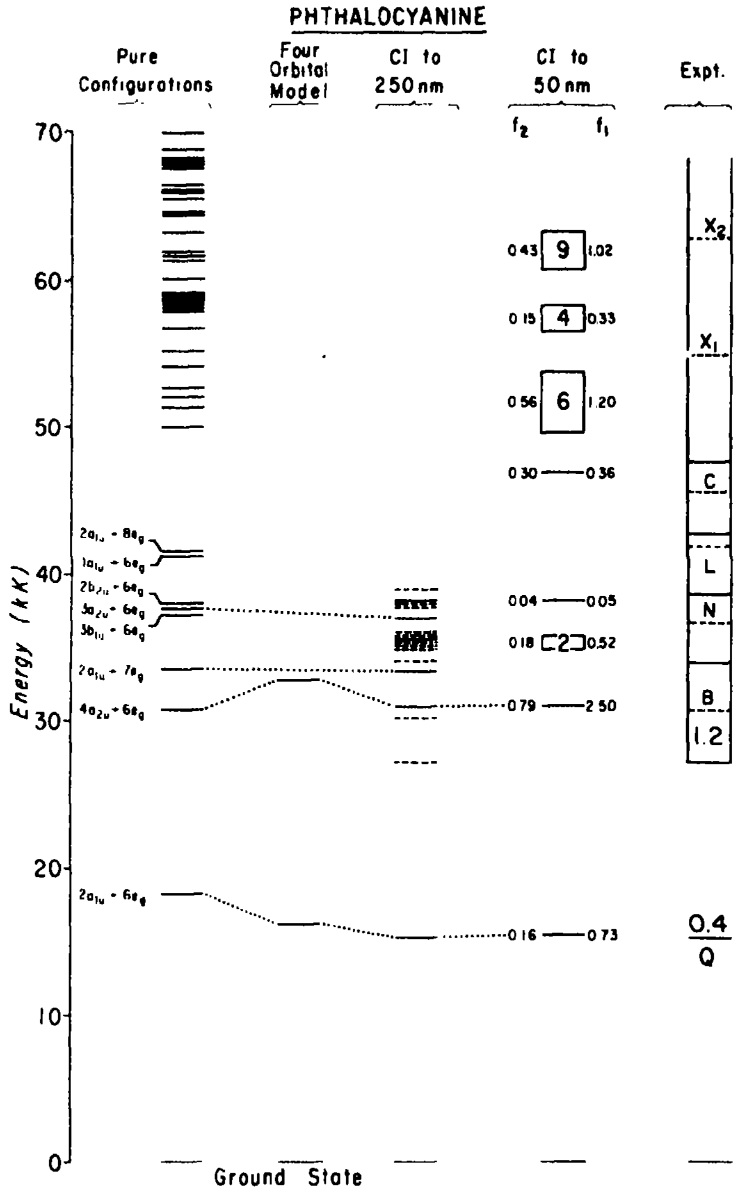

Fig. 4. See legend for Fig. 3. Forbidden levels in the region 20 to 40 kK shown as dotted lines. Experimental values based on ZnPc in vapor and solution [12a, 18b]

Fig. 6 shows the transition monopoles for $4a_{2u} \to 6e_g$ at 30570 cm^{-1}. One can see that the monopoles of the former transition are quite large on the atoms of the benzene rings, whereas the latter has monopoles overwhelmingly concentrated on the inner ring. For transitions between about 40000 and 50000 cm^{-1} we expect the excited states will be of mixed benzenoid and ring character. Beyond about 55000 cm^{-1}, benzenoid character will predominate.

e) Benzporphins

Fig. 7 shows the results of our calculations on the various benzporphin systems. Weiss *et al.* [2] reported on tetrabenzporphin (TBP), but only in the four-orbital model. To our knowledge, no previous SCMO calculation on the absorption spectrum of mono, di, or tribenzporphin has been reported. All of these should show a cluttered spectrum due to the splitting of the degeneracies of tetra-

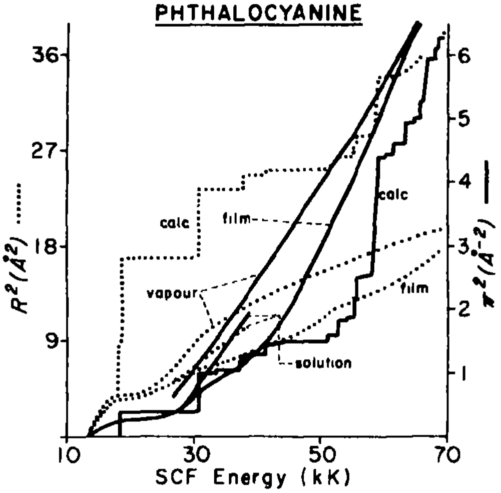

Fig. 5. Solution [14], film [15], and vapor [12] data compared with calculated values (from one-electron transitions) for R^2 (dotted lines) and Π^2 (solid lines)

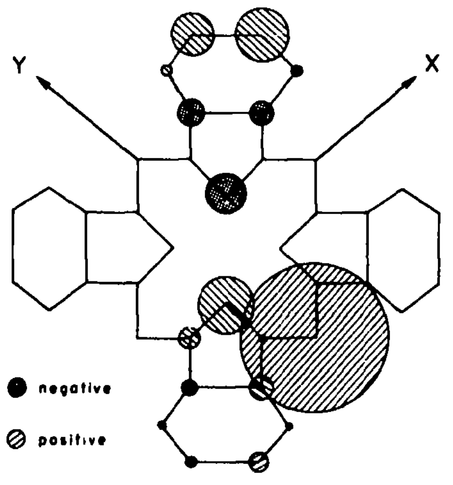

Fig. 6. Representation of $C_{ik}C_{il}$ as radius of circle about i for one-electron promotion $k \to l$. Lower part of diagram shows ring transition; upper part shows benzenoid transition (see text). Full diagrams obtained by symmetric rotation about y, antisymmetric rotation about x

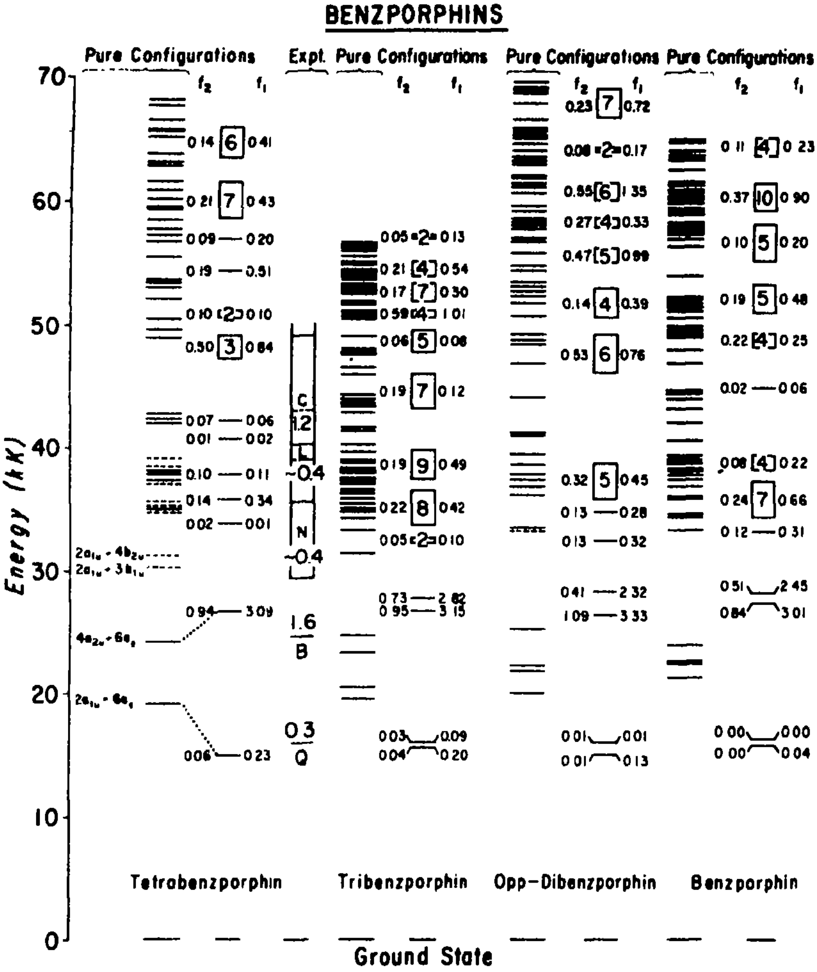

Fig. 7. See legend for Fig. 3. Experimental values for ZnTBP in vapor [12a] and octane pyridine [19]

benzporphin (TBP). All are predicted to have a greater B than Q splitting, with lower energy component in each case having greater intensity. Polarization of the bands is indicated in Table 4 given below.

Data on ZnTBP exists, and the theoretical calculation on TBP can be compared to experiment. We have recently remeasured the molar extinction coefficient in pyridine [19] and find somewhat higher values than those reported earlier [14c]. Also a weak band reported at 460 *nm* [14c] that has no theoretical counterpart has been shown by excitation spectra to be an impurity [19]. Vapor spectra have been taken down to $\lambda \gtrsim 200\,nm$ [12a]. We can determine wavelengths for all peaks in the vapor and relative f values. We can obtain absolute f values by assuming that the values for the Q and B bands measured in solution hold in vapor. The spectrum then consists of the following five bands: a clear Q band (16000 cm^{-1}, $f = 0.3$), a clear B band (24700 cm^{-1}, $f = 1.6$), a flattened N band

(~31200 cm^{-1}, $f \sim 0.4$), a fairly clear L band (39400 cm^{-1}, $f \sim 0.4$), and a clear C band (43400 cm^{-1}, $f \sim 1.2$.) We use "C" for this last band because of its relatively high intensity.

Let us now compare the data with the calculations. The calculated energies for the Q and B bands agree well with experiment, as shown in Fig. 7. The calculated f_2 values for Q and B sum to 1.0, which must be doubled *(vide ante)* to compare to the observed f sum of 1.9. Somewhat more than in the case of phthalocyanine, the f value of Q is underestimated by f_2, while the f value of B is overestimated. However the sum of the f_2 values for both bands agrees with the experimental sum value, while f_1 is high by a factor of 3.5. The experimental N band we identify with the two calculated transitions at 37000 cm^{-1} with $f_2 = 0.14$ and 0.10; the L band with the two transitions near 42000 cm^{-1} with $f_2 = 0.01$ and 0.07; the C band with the three transitions around 48000 cm^{-1} with $f_2 = 0.50$. Again these f_2 values must be doubled before comparing to experiment. This identification puts all experimental energies somewhat below the calculated ones. As in phthalocyanine, TBP transitions in the 48000 to 54000 cm^{-1} range are benzenoid in character. A notable point in the calculations is the far greater calculated intensity in phthalocyanine and TBP above 50000 cm^{-1} than in porphin and TAP. This intensity is attributable to the benzenoid transitions [15], and the data so far confirm this prediction [17, 15, 18b].

3. Calculations for Magneto-Optical Effects

a) Theory

Porphyrins and phthalocyanines are known to show large magneto-optical effects. Shashoua [20] reported on Faraday rotation, and Dratz [21] has measured magnetic circular dichroism. Malley, Feher, and Mauzerall [22] have reported Zeeman splitting. All of these observed effects are attributed to orbital angular momentum effects in the porphyrin and phthalocyanine excited states [4, 23]. In this section we use the SCMO-PPP CI wavefunctions to calculate these values.

We shall begin from the general treatment of Stephens *et al.* [4]. For a nondegenerate ground state, the magneto-optical effects for the transition $a \to j$ are determined by two parameters $A(a \to j)$ and $B(a \to j)$. The first term arises only for degenerate excited states, while the second arises in both degenerate and nondegenerate cases. Among the effects produced is magnetic circular dichroism (MCD), which we shall emphasize in our discussion. In this phenomenon there is an enhancement in the absorption of left circularly polarized light over right or vice versa. The types of circular dichroism that arise are shown in Fig. 8. We shall discuss the sign convention more fully below.

Stephens *et al.* express $A(a \to j)$ and $B(a \to j)$ in terms of complex wave functions. For computational purposes real wave functions are more convenient. We shall assume the molecule has at least C_{2v} symmetry, so that x and y polarized states have distinct symmetry, and shall consider interaction between a diamagnetic

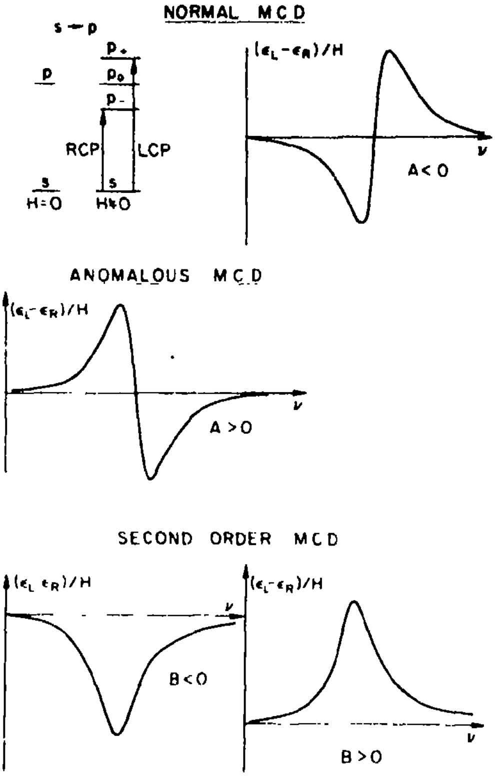

Fig. 8. Types of circular dichroism. Top panel shows $s \to p$ transition and normal MCD for degenerate states. Middle panel shows anomalous MCD for degenerate states. Bottom panel shows the two possible results of second order magnetic interactions. The quantity $[\theta]_M = 3300(\varepsilon_L - \varepsilon_R)/H$. See Ref. [26]

ground state $|a\rangle$ and a set of real excited states $|x_i\rangle$ (subscripts i and j) and $|y_k\rangle$ (subscripts j and k). For $\boldsymbol{m}$, the transition dipole operator, we shall define

$$\begin{aligned} \langle a|\boldsymbol{m}|x_i\rangle &\equiv eR_{xi}\hat{i} \\ \langle a|\boldsymbol{m}|y_k\rangle &\equiv eR_{yk}\hat{j} \\ \langle x_i|L_z|y_k\rangle &\equiv i\hbar M_{ik} = -\langle y_k|L_z|x_i\rangle\,. \end{aligned} \tag{3}$$

In this, L_z is the angular momentum component parallel to the unit vector $\hat{k}$ where $\hat{i}x\hat{j}\cdot\hat{k} = 1$. M_{ik} is real but its sign depends on the arbitrarily determined phases of $|x_i\rangle$ and $|y_k\rangle$. However, the triple $R_{xi}M_{ik}R_{yk}$ has a definite sign which is experimentally observable.

For a molecule with symmetry D_{2h} or lower, the term $A(a \to j)$ does not exist. The term $B(a \to j)$, which arises from the coupling of non-degenerate states by the magnetic field, consists of terms with energy denominators $W_k - W_i$ or $W_j - W_a$. In this i, j, k refer to excited states; a to the ground state. We shall in this paper neglect terms with the much larger denominators $W_j - W_a$ and keep only the former terms. Thus from Stephens *et al.* more general expression we derive

$$B(a\to i) = e^2\beta \sum_k R_{xi}M_{ik}R_{yk}(W_k - W_i)^{-1}, \tag{4a}$$

where β is the Bohr magneton. We note that the subscript i refers to an x polarized state and k to a y polarized one. For y polarized states we derive

$$B(a\to k) = e^2\beta \sum_i R_{yk}M_{ik}R_{xi}(W_i - W_k)^{-1}. \tag{4b}$$

We note that if there is only one state $|x_i\rangle$ and one state $|y_k\rangle$ then $B(a\to i) = -B(a\to k)$, as is expected.

For a molecule where the z axis is a symmetry axis for a rotation group with degeneracy, the allowed states will be associated in degenerate pairs $|x_j\rangle$ and $|y_j\rangle$. In this case the $A(a\to j)$ term is

$$A(a\to j) = e^2\beta\, R_{xj}M_{jj}R_{yj} \tag{5}$$

while

$$B(a\to j) = e^2\beta \sum_{l\neq j} 2R_{xj}M_{jl}R_{yl}(W_l - W_j)^{-1}. \tag{6}$$

In this last expression the summation is taken over all energy levels and the factor of two takes account of degeneracy.

When making comparisons between theory and experiment, it is common to divide $A(a\to j)$ and $B(a\to j)$ by the dipole strength. Again we follow Stephens *et al.* [4] and define the dipole strength for the non-degenerate case as

$$D(a\to i) = e^2 R_{xi}^2 \tag{7}$$

and obtain the expression for x polarized states

$$\frac{B(a\to i)}{D(a\to i)} = \beta \sum_k M_{ik}(R_{yk}/R_{xi})(W_k - W_i)^{-1}. \tag{8a}$$

Similarly for y polarized states

$$\frac{B(a\to k)}{D(a\to k)} = \beta \sum_i M_{ik}(R_{xi}/R_{yk})(W_i - W_k)^{-1}. \tag{8b}$$

In the degenerate case we note that $D(a\to j) = 2e^2R_{xj}^2 = 2e^2R_{yj}^2$ so that

$$\frac{2A(a\to j)}{D(a\to j)} = \beta M_{jj}(R_{yj}/R_{xj}) \tag{9}$$

while

$$\frac{B(a\to j)}{D(a\to j)} = \beta \sum_{l\neq j} M_{jl}(R_{yl}/R_{xj})(W_l - W_j)^{-1}. \tag{10}$$

The terms B/D and $2A/D$ are experimental observables, where the A and B values are determined either from MCD or from MORD (magnetic optical rotatory dispersion) and D is determined from the absorption coefficient. A convenient way to express the results of our calculations is in terms of dimensionless quantities

$$\begin{aligned}\mathcal{M}_{ik}^{(x)} &\equiv M_{ik}(R_{yk}/R_{xi})\\ \mathcal{M}_{ik}^{(y)} &\equiv M_{ik}(R_{xi}/R_{yk}).\end{aligned} \tag{11}$$

For an x polarized state the B/D term is simply $\beta \sum_k \mathcal{M}_{ik}^{(x)} (W_k - W_i)^{-1}$. From a matrix of $\mathcal{M}_{ik}^{(x)}$ one can see how strongly this series will converge. Moreover, one can use either experimental or theoretical energy denominators. Similarly for a y polarized state $B/D = \beta \sum_i \mathcal{M}_{ik}^{(y)} (W_i - W_k)^{-1}$. In the case of degeneracy it is easy to show that $\mathcal{M}_{ik}^{(x)} = \mathcal{M}_{ki}^{(y)}$ so that B/D sums are the same for both components, while $2A/D = \beta \mathcal{M}_{jj}^{(x)} = \beta \mathcal{M}_{jj}^{(y)}$. Thus it is necessary to tabulate only one of these matrices. The Zeeman splitting of an orbitally degenerate state will be $2 \mathcal{M}_{jj}^{(x)} \beta H_z$, where H_z is the magnetic field along the z axis.

The method of calculation for the SCMO-PPP-CI states is relatively straightforward. The excited states are taken as a sum of singly excited states. For singlet states $\psi(\nu \to n)$ and $\psi(\mu \to m)$ we have $\langle \psi_u | \boldsymbol{m} | \psi(\nu \to n) \rangle = \sqrt{2} \langle \nu | \boldsymbol{m} | n \rangle$

$$\langle \psi(\nu \to n) | L_z | \psi(\mu \to m) \rangle = \delta_{\nu\mu} \langle n | l_z | m \rangle + \delta_{mn} \langle \nu | l_z | \mu \rangle . \tag{12}$$

Combination of these one-electron integrals with the CI expansion coefficients yields values of M_{ik}, R_{xi}, R_{yk}, from which $\mathcal{M}_{ik}^{(x)}$ and $\mathcal{M}_{ik}^{(y)}$ are determined.

The most important terms for $\mathcal{M}_{ik}^{(x)}$ are the orbital l_z values. It is simple enough to show that

$$\langle n | l_z | m \rangle = \sum_a \sum_{a < b} (C_{na} C_{mb} - C_{nb} C_{ma}) \langle \chi_a | l_z | \chi_b \rangle \tag{13}$$

where C_{nb}, etc., are the expansion coefficients of the molecular orbital n onto the π atomic orbital χ_b on center b. The integral on the atomic orbitals can further be written [4, 24]

$$\langle \chi_a | l_z | \chi_b \rangle = -i\hbar T(a, b) [\xi_a \eta_b - \eta_a \xi_b] \tag{14}$$

where (ξ_a, η_a) and (ξ_b, η_b) are the x, y coordinates of the two centers in a.u. $T(a, b)$ has a form like an overlap integral and is given in Appendix 1 for equal and unequal exponents. We used exponents of 1.5679 for carbon and 1.9170 for nitrogen.

Table 2. Orbital zeeman terms[a]

Compound	Top filled $\hbar^{-1} (a_{1u} \| l_z \| a_{2u})$	Lowest empty $\hbar^{-1} (e_{gx} \| l_z \| e_{gy})$
Porphin	2.27	2.09
(Simple Hückel)[b]	(1.67)	(1.29)
(Extended Hückel)[c]	(2.37)	(2.39)
TAP	2.17	1.90
TBP	1.99	1.92
Pc	2.12	1.82
H_2 Porphin	2.24	2.08
Chlorin	2.06	1.84
Bacterio	2.05	2.03
MBP	2.05	1.95
OPP DBP	2.03	1.96
TRIBP	1.99	1.92

[a] Symmetry labels apply to D_{4h} systems. Analogous orbitals chosen for molecules of lower symmetry. Orbital phases chosen to give positive values.

[b] Obtained with $\alpha_N = \alpha_C$. See Ref. [34]. Only nearest neighbor l_z integrals included.

[c] See Ref. [35]. All two center l_z integrals included.

Only nearest neighbor integrals were included to be consistent with the zero differential overlap assumption inherent in the PPP wavefunctions. In Table 2 we have tabulated the orbital angular momentum integrals for top filled and lowest empty orbitals. These are the largest such integrals, but the others are not negligible.

b) Degenerate Case $A(a \to j)$ Term

The four D_{4h} molecules are presented in Table 3. The diagonal entries are $\mathcal{M}_{jj}^{(x)} = 2\beta^{-1} A/D$. The sign is a genuine observable. To clarify it we shall use as a reference an atomic transition $s \to p$. In a magnetic field the energy levels for $m = \pm 1, 0$ will be shifted by $\pm \beta H, 0$. For light incident parallel to H, only transitions to $\pm \beta H$ occur. The transition to $m = +1$ requires left circularly polarized light, by which we mean the electric vector portrays a right-hand helix [25a][1]. The transition to $m = -1$ requires right circularly polarized light. The expected circular dichroism is shown in Fig. 8. By our convention $\mathcal{M}_{jj}^{(x)} = -1$ and $A < 0$ for $s \to p$. It is convenient in D_{4h} cases to refer to bands with $A < 0$ as "normal MCD" and cases with $A > 0$ as "anomalous MCD."

We shall here consider whether normal or anomalous MCD occurs in the Q(0, 0) and B(0, 0) bands of D_{4h} porphyrin. We note that Table 3 predicts normal MCD for all Q(0, 0) bands and for all B(0, 0) bands except unsubstituted porphin. Experimentally $A < 0$ has been found for all Q(0, 0) and B(0, 0) bands that have been investigated in D_{4h} cases [4, 22, 26, 27]. This includes octalkylporphin, tetraphenylporphin, porphin, and phthalocyanine. (Although Dratz [21] reported anomalous MCD in metalloporphyrins, he did not determine sign absolutely, and we believe he erred on this point.) We are not disturbed that the B(0, 0) band of metalloporphyrins so far studied show $A < 0$, although Table 3 predicts $\mathcal{M}_{BB}^{(x)} = +0.030$. This small value is essentially a difference between the MO contributions of top filled and lowest empty orbitals (Table 2) plus many small terms. It might vary quite strongly with small changes of parametrization. That the B band is sensitive to parametrization has been shown by the calculations of Stephens *et al.* [28] on triphenylene and coronene B bands. Sooner or later a D_{4h} porphyrin may be found with substituents such that $A > 0$ for the B band.

Table 3. Matrix of $\mathcal{M}_{ik}^{(x)}$ value for (Porphin, TAP/TBP, Phthalocyanine)[a] and dipole strengths

R_{xl}^2(Å^2)			Q_y		B_y		N_y		L_y	
0.012	0.971	Q_x	−4.347	−3.835	6.109	0.584	−4.812	2.527	−1.130	0.198
1.421	4.412		−3.684	−3.134	2.133	1.768	0.035	0.0163	−0.001	0.091
9.154	3.809	B_x	0.008	0.147	0.030	−0.258	0.141	0.014	0.144	0.400
10.710	7.519		0.283	1.077	−0.275	−0.632	0.003	0.013	0.165	0.013
0.982	5.308	N_x	−0.063	0.464	1.396	0.011	0.302	0.376	−1.256	−0.274
0.032	0.012		1.546	−2.766	−0.734	−6.362	1.752	−1.236	−0.693	−1.833
0.380	0.290	L_x	−0.036	0.663	3.485	5.247	−3.048	−5.021	−0.043	−0.020
0.022	0.166		−0.022	1.893	1.657	0.573	−1.038	0.148	1.141	1.301

[a] Order of entries in Table: Porphin, TAP top line; TBP, phthalocyanine lower line. Thus $\mathcal{M}_{QQ}^{(x)} = -4.347$, $\mathcal{M}_{QB}^{(x)} = 6.109$, and $\mathcal{M}_{BB}^{(x)} = 0.030$ for porphin.

---

[1] We might note that an opposite definition for left circularly polarized light has been given [25b].

The absolute magnitude of $\mathcal{M}^{(x)}_{QQ}$ calculated for porphin can be compared to the experimental MCD numbers of Dratz [21]. He studied six metal deuteroporphyrins and obtained values from 4.44 for the cobalt complex to 6.52 for the zinc complex, a range of variation he can explain by perturbation theory. Stephens *et al.* [28] analyzing zinc hematoporphyrin MORD find 6.94. For zinc coproporphyrin by MCD Dratz obtains 6.5 ± 0.5. On this same compound Malley *et al.* [22] by direct Zeeman studies obtain 9.5 ± 0.6 at room temperature and 6.4 ± 0.6 at 77° K. Recently Sutherland *et al.* [29] have explained the discrepancy between the MCD value and the direct Zeeman value by postulating a zero-field splitting of the orbital degeneracy and an inequality of the two transition dipoles. According to this explanation, the MCD value should be a more accurate measurement of the orbital Zeeman splitting. Our calculated value of 4.35 agrees reasonably well with the measured MCD value of cobalt deuteroporphyrin.

Can our calculated magnitude of 4.35 be raised while retaining a reasonable set of parameters? The basic ingredients for the calculation are: (i) the coefficients of the π electron wavefunction, (ii) the exponents of the atomic orbitals, and (iii) the molecular geometry. Several calculations for orbital angular momentum were carried out using other sets of MO coefficients. (Two such calculations for porphin are shown in Table 2.) In no case did we obtain values significantly larger than those listed. The atomic orbitals affect $T(a, b)$, which is maximized by an orbital exponent of $\zeta = 1.3$. Use of such a smaller exponent agrees with the double-zeta carbon $2p_z$ orbital of Clementi [30] and has been justified in another context by Silverstone *et al.* [31]. This could raise $\mathcal{M}^{(x)}_{QQ}$ by about 10%. If all bond lengths are reduced by 0.06 Å another increase of 10% can be obtained. All effects taken together would be unlikely to increase $\mathcal{M}^{(x)}_{QQ}$ much above 5.5 to 6. This agrees with the larger MCD values of Dratz and supports the conclusion of Sutherland *et al.* [29] that the room temperature Zeeman value of Malley *et al.* [22] is high.

Experimental comparison can also be made between the calculated value $\mathcal{M}^{(x)}_{QQ} = -3.134$ for phthalocyanine (Pc) and values obtained from experiment. Stephens *et al.* [4] analyzed Shashoua's MORD data on MgPc [20] and obtained $\mathcal{M}^{(x)}_{QQ} = -8.16$. Pershan *et al.* [23] analyzed Shashoua's MORD data on ZnPc and obtained a value of -1.3, an enormous discrepancy. We have carefully reconsidered the Pershan *et al.* calculation and found errors in the values for magnetic molar rotation and angular frequency halfwidth. With correct values $\Phi_s(\max) = -5.95 \times 10^{-3}$ cm^3/gauss mole and $\Gamma = 6.1 \times 10^{13}$/sec, a value of $\mathcal{M}^{(x)}_{QQ} = -1.9$ is obtained. (For definitions of $\Phi_s(\max)$ and Γ, see Ref. [23].) A further correction of $\pi/2$ arises from the Pershan *et al.* assumption of Lorentzian shape, giving $\mathcal{M}^{(x)}_{QQ} = -3.0$[2]. However the remaining difference arises from the data. Comparison of MgPc with ZnPc shows that both have similar values for D, while MgPc has a value of $\Phi_s(\max)$ that is 0.88 times the ZnPc value, and a line width 1.75 times that ZnPc value. From the Pershan *et al.* formulas we expect $\mathcal{M}^{(x)}_{QQ} = -3.0 \times 0.88 \times (1.75)^2 = -8.1$. The data show that CuPc also has a comparable value of D, a value of $\Phi_s(\max)$ that is only 0.24 times the ZnPc value, and a linewidth 1.3 the ZnPc value. Thus we roughly expect $\mathcal{M}^{(x)}_{QQ} = -3.0 \times 0.24 \times (1.3)^2 = -1.2$. Thus analysis of the Shashoua data gives $\mathcal{M}^{(x)}_{QQ} = -8.1$, -3.0, and -1.2

---

[2] With a Lorentzian line shape $\int \varepsilon(\omega)\, d\omega = \pi \varepsilon(\max)\, \Gamma/2$; however experimental shapes are such that $\varepsilon(\max)\, \Gamma$ is a better estimate of integrated intensity.

for McPc, ZnPc, and CuPc respectively, all of which should be -3.1 according to our calculations.

This range of values cannot be explained by perturbation theory such as that used by Dratz [21] for the metal prophyrins. The broad band of MgPc suggests peculiar complexing phenomena are occurring. Such phenomena are not explicitly considered in the theory of band shape used to extract the value of $\mathcal{M}^{(x)}_{QQ}$ from MORD data. We tend to believe that the naive treatment of band shape has led to an incorrect "experimental" value of $\mathcal{M}^{(x)}_{QQ}$ for MgPc. More experiments on phthalocyanine varying metal, solvent, and temperature are needed. We also need more theoretical analyses, such as that of Sutherland *et al.* [29], on how solvent effects on band shape and how orbital degeneracy will affect the $\mathcal{M}^{(x)}_{QQ}$ values extracted from the data.

c) Degenerate Case $B(a \to j)$ Term

The value of $\beta^{-1}B/D = \sum_k \mathcal{M}^{(x)}_{lk}(W_k - W_l)^{-1}$. As can be seen from Fig. 8, the sign of this quantity is an observable. Thus for the Q band where $A<0$, a value $B<0$ will enhance the longwavelength minimum while $B>0$ will enhance the shortwavelength maximum. Our calculation for the Q state of porphin (Table 3) shows that interaction with the B state gives a positive contribution to the sum while the N state gives a negative contribution about half the size. The net positive contribution should enhance the shortwavelength maximum.

The experimental information is ambiguous. Dratz [21] finds different results for different systems: The longwavelength Q band dichroism is enhanced for Zn coproporphyrin III, Fe (II) protoporphyrin IX in H_2O, bovine oxyhemoglobin, cytochrome *c*; while the shortwavelength is enhanced for Ni, Cu, Zn deuteroporphyrin IX and Fe (III) protoporphyrin IX in pyridine. The experimental sign of the B term thus appears to be quite variable. As a sum of terms from many states, this is not so surprising. Because the energy denominators are several thousand wavenumbers, the overall magnitude of $\beta^{-1}B/D \sim 10^{-3}$ cm. Stephens *et al.* [4] determined an experimental value of -3.9×10^{-3} cm for Zn hematoporphyrin, which by the above arguments means enhanced longwavelength dichroism, although their experimental data showed enhanced shortwavelength dichroism. They report the impossibly large value of -72×10^{-3} cm for MgPc. As suggested above, the value $\mathcal{M}^{(x)}_{QQ} = -8.1$ obtained for MgPc is far too large in magnitude when compared to theory and seems due to an inadequate treatment of the anomalously large bandwidth. We believe that the impossibly large value for $\beta^{-1}B/D$ comes from this same inadequacy.

As noted in the previous paragraph, a non-zero B value when added to a non-zero A value can give asymmetry to the MCD curve of degenerate molecules, even though there is no lifting of degeneracy. Sutherland *et al.* [29] note that if the x and y transition dipoles are not equal and there is zero field splitting, a similar asymmetry will occur. Thus experimentally observed asymmetries may be due to this effect as well as to non-zero $\beta^{-1}B/D$, and extraction of $\beta^{-1}B/D$ from the data must proceed with caution.

d) Non-Degenerate Case B(a→j) Terms

The results for the non-degenerate molecules are given in Table 4. The axis convention is given in Fig. 9. These systems are closely related to the degenerate systems given in Table 3. This relation is manifest in Table 2, which shows that the

Table 4a. Matrix of $\mathcal{M}_{ik}^{(x)}$ values for (free base porphin, chlorin/bacteriochlorin, MBP/OPP-DBP, TRIBP)[a,b] and dipole strengths

R^2_{xl}(Å^2)			Q_y		B_y		N_y		L_y	
0.077	0.143	Q_x	0.635	−0.133	−0.477	5.371	−0.575	0.082	−0.857	−0.247
0.573	0.020		−8.702	−13.976	5.283	7.048	0.035	0.038	0.126	0.124
0.049	0.536		15.820	−5.606	9.272	3.201	0.989	−0.004	0.306	0.003
5.584	7.500	B_x	−0.014	0.135	−0.279	−0.406	0.448	−0.020	0.089	0.033
1.963	10.169		1.431	−0.010	−0.101	−0.113	−0.153	−0.001	−0.046	0.060
11.687	10.951		−0.010	0.122	−0.121	0.136	0.057	−0.173	0.085	−0.007
5.211	0.697	N_x	0.010	−0.695	0.833	−1.327	−0.451	−0.016	0.048	0.015
5.580	0.014		0.068	0.219	−0.428	10.211	0.046	−0.006	0.033	−12.885
0.903	0.172		0.655	−0.066	0.587	−2.470	0.290	0.557	0.234	0.024
0.254	0.514		0.017	−0.291	2.185	−1.207	0.205	0.028	−2.506	−0.683
0.016	0.866	L_x	4.876	0.337	−4.785	0.616	−1.812	−0.010	1.745	0.370
0.744	0.099		0.283	0.373	2.464	2.236	−1.145	−0.139	−0.654	0.236
$E^{(y)}$			16.91	16.17	28.79	28.75	35.01	32.54	38.42	35.68
(calc.)			14.93	15.89	32.57	28.16	43.28	32.59	43.77	34.29
			15.12	15.69	28.33	27.61	35.82	30.67	36.97	33.59

[a,b] See footnotes for Table 4b.

Table 4b. Matrix of $\mathcal{M}_{ik}^{(y)}$ values for (free base porphin, chlorin/bacteriochlorin, MBP/OPP-DBP, TRIBP)[a,b] and dipole strengths

R^2_{yl}			Q_x		B_x		N_x		L_x	
0.0017	0.802	Q_y	28.956	−1.624	−45.813	1.266	29.674	−0.603	2.519	−0.187
3.238	0.250		−1.539	−1.119	0.867	−0.413	0.118	0.012	0.025	1.168
0.820	1.187		−0.952	−2.530	−0.133	1.252	0.722	−0.010	0.257	0.031
9.807	7.473		−0.004	0.102	−0.159	−0.407	0.442	−0.124	0.057	−0.083
8.244	8.031	B_y	0.367	0.018	−0.024	−0.143	−0.289	0.017	−0.009	0.066
7.565	9.417		0.060	0.182	−0.187	−0.201	0.070	−0.045	0.242	0.023
0.489	0.106	N_y	−0.089	0.110	5.019	−1.387	−4.716	−0.106	0.105	0.136
0.025	0.003		0.808	0.232	−12.168	−3.418	10.284	−0.024	−1.196	−2.636
0.272	0.008		0.179	−0.281	2.463	−9.025	0.964	11.382	−3.131	−1.630
0.379	0.189	L_y	−0.174	−0.186	1.322	1.310	0.658	0.054	−1.680	−1.859
0.056	0.434		1.297	0.006	−1.575	1.396	3.330	−0.402	0.513	0.739
0.290	0.001		0.052	1.609	3.433	−10.172	0.729	3.749	−1.682	21.308
$E^{(x)}(kK)$			14.99	17.71	27.52	28.58	31.67	32.84	40.18	35.19
(calc.)			17.12	16.38	30.23	27.26	32.00	31.71	48.35	33.15
			15.92	15.92	26.27	26.55	32.45	32.21	34.86	32.60

[a] Order of entries in Table indicated by slashes as for Table 3. Free base uses $\Delta\alpha = 5.5$ eV.

[b] Abbreviations: MBP (monobenzporphin); OPP-DBP (opposite dibenzporphin);
TRIBP (tribenzporphin).

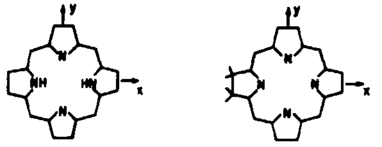

Free Base Porphin

Chlorin

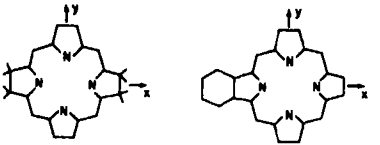

Bacteriochlorin

Monobenzporphin

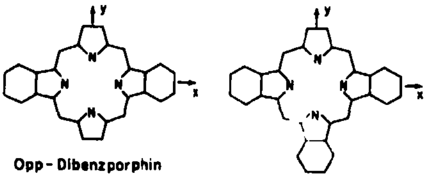

Opp-Dibenzporphin

Tribenzporphin

Fig. 9. Orientation of molecules of D_{2h} and C_{2v} symmetry

angular momenta of top filled and lowest empty orbitals is much the same for all systems. Nonetheless the absolute values of $\beta^{-1}B/D$ can be quite different for two quasidegenerate bands. Thus for chlorin Q_x and Q_y we get:

$$10^3\beta^{-1}B/D[Q_y] = -1.624\,(1.54)^{-1} + 1.266\,(12.41)^{-1} - 0.603\,(15.50)^{-1}$$
$$-0.187\,(19.02)^{-1} = -1.001\text{ cm},$$
$$10^3\beta^{-1}B/D[Q_x] = -9.133\,(-1.54)^{-1} + 5.371\,(11.04)^{-1} + 0.082\,(14.83)^{-1}$$
$$-0.247\,(17.97)^{-1} = 6.409\text{ cm}.$$

We see from these calculations and Fig. 9 that the longwavelength Q_y transition should show RCP (right circular polarization) while the shorter wavelength Q_x band should show LCP. The main contribution arises from the magnetic interaction between Q_y and Q_x, although the other terms are not negligible.

In analogy to our earlier definition of normal and anomalous MCD in D_{4h} systems, it is convenient to call RCP ($B<0$) "normal longwavelength MCD" and LCP ($B>0$) "anomalous longwavelength MCD" in systems of D_{2h} or lower symmetry. Examination of Table 4 shows that all the D_{2h} molecules except free base porphin are calculated to show normal longwavelength MCD. However measurements of the free bases of octalkylporphin, tetraphenylporphin, and unsubstituted porphin [21, 26, 27b] do show normal longwavelength MCD. On the other hand measurements of the dication and the free base of tetraphenylchlorin show anomalous longwavelength MCD [27b]. This is the reverse of the predictions in Table 4. The sign of longwavelength MCD in molecules of D_{2h} or lower symmetry depends quite delicately on the wavefunctions. In the next section we take up this problem.

Table 5. Transition gradient and oscillator strength for chlorin and bacteriochlorin[a]

State Energy	(kK)	$\Pi_x(\text{Å})^{-1}$	$\Pi_y(\text{Å})^{-1}$	f_2
A. Chlorin				
Q_y	16.17		0.105	0.028
Q_x	17.71	−0.019		0.001
B_x	28.58	0.610		0.534
B_y	28.75		−0.638	0.580
N_y	32.54		−0.100	0.013
N_x	32.84	0.261		0.085
L_x	35.19	−0.233		0.063
L_y	35.68		0.176	0.036
B. Bacteriochlorin[a]				
Q_y	14.93		0.138	0.052
Q_x	17.12	0.062		0.009
B_x	30.23	0.285		0.110
N_x	32.00	0.599		0.460
B_y	32.57		0.731	0.673
N_y	43.28		0.021	0.001
L_y	43.76		0.109	0.011
L_x	48.35	0.066		0.004

[a] Opposite tetrahydroporphin.

e) Further Discussion of Normal and Anomalous MCD

A considerable insight into the observed MCD of porphyrins and related systems can be obtained by discussing the basis of normal and anomalous MCD in degenerate systems and normal and anomalous longwavelength MCD in non-degenerate systems.

The fact that Q(0′, 0″) bands in D_{4h} porphyrins must show normal MCD can be understood as follows. The phase of the wavefunctions can be chosen so that

$$\begin{aligned} C_4 Q_x &= Q_y \\ C_4 Q_y &= -Q_x \end{aligned} \tag{15}$$

where C_4 is a rotation that sends the x axis into the y axis. In this case $\mathrm{M}(Q_x, Q_y)$ defined as

$$i\hbar \mathrm{M}(Q_x, Q_y) = \langle Q_x | L_z | Q_y \rangle \tag{16}$$

will be a negative number ~ -2 to -4. With this choice of phase for the wavefunctions, the transition dipoles

$$\begin{aligned} \langle a | er | Q_x \rangle &= eR_x \hat{i} \\ \langle a | er | Q_y \rangle &= eR_y \hat{j} \end{aligned} \tag{17}$$

must relate as

$$\begin{aligned} C_4 R_x \hat{i} &= R_y \hat{j} \\ C_4 R_y \hat{j} &= -R_x \hat{i}\,. \end{aligned} \tag{18}$$

The consequence of Eqs. (18) is that either R_x, R_y are both positive or are both negative. The triple $R_x \mathrm{M}(Q_x, Q_y) R_y < 0$. This triple determines that the sign of $A < 0$. For the B(0′, 0″) band Eqs. (18) still hold on symmetry grounds. However as already noted [*vide ante*] the value of $\mathrm{M}(B_x, B_y)$ defined by an equation analogous to Eq. (16) is the difference between two numbers of comparable size. The difference might make $M(B_x, B_y)$ a small positive number giving rise to anomalous MCD.

What will be the A value for vibrational overtones of the Q and B bands of degenerate porphyrins? Although Stephens *et al.* [4] noted that $\mathcal{M}_{jj}^{(x)} = 2\beta^{-1}A/D$ should have the same magnitude for vibrational bands $Q(v', 0'')$ as for the $Q(0', 0'')$ band, they failed to note, that the sign of $\mathcal{M}_{jj}^{(x)}$ depends on the symmetry of the vibration, a fact noted elsewhere [32]. It can be shown by group theory that the transition dipoles $R_x(v', 0'')$, $R_y(v', 0'')$ will transform according to Eq. (18) if v' is a vibration of α_{1g} or α_{2g} symmetry but will transform as

$$\begin{aligned} C_4 R_x(v', 0'')\,\hat{i} &= -R_y(v', 0'')\hat{j} \\ C_4 R_y(v', 0'')\hat{j} &= R_x(v', 0'')\,\hat{i} \end{aligned} \qquad (19)$$

if v' if of β_{1g} or β_{2g} symmetry. Eq. (19) will result in anomalous MCD. It has been noted [32] that the experimental Q(1, 0) bands of metalloporphyrins are a composite of $Q(v', 0'')$ bands with several different v' vibrations [32]. It is therefore not surprising that both signs of A are observed, and MCD is complex [21, 27]. For ZnTPP the Q(1, 0) shows little resolution and appears as a single $A < 0$ band [26]. However, since the unresolved band has contributions with both $A > 0$ and $A < 0$, we can understand why the value of A/D is not as extreme for Q(1, 0) as for Q(0, 0).

Consider now porphyrins where substituents or free base formation break the D_{4h} symmetry. Suppose we label the lower energy transition Q_x. (The argument, of course, does not depend on choice of x instead of y.) The sign of MCD will depend mainly on $R_x M(Q_x, Q_y) R_y$, since the Q_x, Q_y magnetic interaction will be the predominant term in Eq. (4a). If the perturbation from D_{4h} symmetry is small, this term will maintain the same sign as in the D_{4h} case, *i.e.* negative. The result will be $B < 0$ for the $Q_x(0', 0'')$ band, and normal longwavelength MCD will occur. Since $M(Q_x, Q_y)$ has relatively large magnitude its sign will persist as the perturbation from D_{4h} symmetry increases. However the transition dipoles are no longer symmetry related. If the symmetry is at least C_{2v}, we will have

$$\begin{aligned} C_4 R_x \hat{i} &= \eta R_y \hat{j} \\ C_4 R_y \hat{j} &= -\eta^{-1} R_x \hat{i} \end{aligned} \qquad (20)$$

replacing Eq. (18). If the perturbation from D_{4h} symmetry is small, η may remain close to unity as in Eq. (18). However for certain large perturbations a negative η may occur. For such a case the sign of $R_x M(Q_x, Q_y) R_y > 0$, and we will observe anomalous longwavelength MCD.

We therefore see that normal longwavelength MCD will be expected for substituted D_{2h} porphyrins such that in the compound itself and in the closest related D_{4h} compound the Q_x and Q_y bands are moderately intense. This explains the observation that the free bases of octalkylporphin [21, 27b], tetraphenylporphin [26], and phthalocyanine [27a] show normal longwavelength MCD. In unsubstituted free base porphin, although the intensity of $Q_x(0, 0)$ and $Q_y(0, 0)$ is relatively weak, the MCD remains normal [27b]. Djerassi *et al.* have found anomalous longwavelength MCD in a number of dihydroporphins (chlorins) and in some low symmetry substituted free base porphyrins [27]. We note that in chlorins the higher energy $Q_x(0, 0)$ band is usually quite weak so that a negative η

value is not so surprising. Very detailed consideration of the effect of the substituents on excited state wavefunctions will be needed to predict whether in a given case longwavelength MCD should be normal or anomalous. However theory makes clear why both behaviors can be obtained.

Some comments can be made about the sign of the B values for the vibronic bands $Q_x(v', 0'')$ and $Q_y(v', 0'')$ in cases where D_{4h} symmetry is lifted by a free base perturbation. If we assume the perturbation is too weak to substantially change the character of these states but merely lifts their degeneracy, then the B term of a band like $Q_x(v', 0'')$ will be dominated by its interaction with $Q_y(v', 0'')$. Just as $Q(v', 0'')$ bands of degenerate porphyrins can show A values of either sign depending on the symmetry of v', bands $Q_x(v', 0)$ can show B values of either sign. Alternation of sign of B values is in fact observed in different regions of the $Q_x(1, 0)$ and $Q_y(1, 0)$ bands [26, 27b]. This is expected, since it has been known that such bands contain vibrations of different symmetry. If the individual vibrational components of $Q_x(1, 0)$ and $Q_y(1, 0)$ are not resolved, the observed B/D is due to the combined effect of several vibrations and will reach a less extreme value than in the corresponding $Q_x(0, 0)$ and $Q_y(0, 0)$ bands.

Finally we note that Kobayashi *et al.* [27] find no MCD in the "Longo" band at 21000 cm^{-1}. The absence of MCD could be explained for a Q(2, 0) band if it were a composite band of vibrational symmetries with cancelling B values. It could also be explained as an electronic origin with small and cancelling magnetic interactions with electronic transitions to higher and lower energy, a situation that is quite likely according to our numbers in Table 4. Thus MCD does not provide an unequivocal identification of the Longo band.

Summary

The calculations reported in this paper have given a number of results for porphyrin and some related compounds that we now summarize:

(1) For an excited state built as a linear combination of single excitations, transition gradient operators predict intensities with reasonable accuracy even though transition dipole operators predict intensities high by about a factor of three to four.

(2) The B band intensity of free base porphyrin is spread over a range of 1000 cm^{-1} or more. Conceivably there is a $\pi-\pi^*$ transition between $Q_y(1, 0)$ and the main Soret band in the free base.

(3) The compounds tetrabenzporphin and phthalocyanine show far stronger absorption than porphin and tetrazaporphin in the range $\lambda < 200$ nm due to benzenoid transitions.

(4) Very likely the cause of the anomalously broad Soret absorption in tetrazaporphin and phthalocyanine compared to porphin and tetrabenzporphin is underlying $n-\pi^*$ transitions.

(5) Theory seems to be giving the correct order of magnitude for magnetic effects due to orbital angular momenta. For porphin a theoretical value of 4.35 $\hbar$ calculated for the Q state compares to experimental values from MCD between 4.4 and 6.9 $\hbar$. For phthalocyanine the "experimental" values cover the range 1.2 to 8.1, while theory is 3.1 $\hbar$. It is suggested that the "experimental" values may be in error due to improper treatment of the bandshape.

(6) The MCD for the Q(0′, 0″) of D_{4h} porphyrins must be normal, *i.e.* have $A<0$. Bands B(0′, 0″) may sometimes show $A>0$.

(7) Vibrational bands Q(v', 0″) will have $2\beta^{-1}A/D$ values of the same magnitude as Q(0′, 0″), however $A<0$ for v' of α_{1g} or α_{2g} symmetry (normal MCD) but $A>0$ for v' of β_{1g} or β_{2g} symmetry (anomalous MCD). Experimental Q(1, 0) bands are composites of several Q(v', 0″) bands with both signs of A present.

(8) In degenerate cases the value of $\beta^{-1}B/D$, which introduces asymmetry to the A term MCD, should be in the range $\pm 3\times 10^{-3}$ cm. Magnitude grossly larger than this indicate errors in the experimental analysis.

(9) In non-degenerate porphyrins where the Q_x(0′, 0″) and Q_y(0′, 0″) bands are moderately intense and the perturbation lifting D_{4h} symmetry is small, longwavelength MCD will be "normal", *i.e.* RCP. In cases where one or both bands are very weak or the perturbation lifting D_{4h} symmetry is large, the longwavelength MCD may be "anomalous", *i.e.* LCP.

(10) Vibrational bands Q_x(v', 0″) and Q_y(v', 0″) in non-degenerate cases will (to zeroth order) have B values of equal magnitude and opposite sign. The absolute sign will depend on the symmetry of v'. Experimental Q_x(1, 0) and Q_y(1, 0) bands will contain various v' vibrations, so both signs of B occur. The observed MCD may result from the sum of B values of both signs.

Acknowledgements. This research was supported in part by Public Health Services Grant GM 14292 from the Division of General Medical Sciences and by AEC Contract W-7405-ENG-48. One of us (MG) acknowledges fruitful discussion with Drs. V. E. Shashoua and E. A. Dratz on magneto-optical effects in porphyrins. C. W. thanks the National Institutes of Health for a post-doctoral fellowship.

Prof. C. Djerassi of Stanford University kindly supplied us with some previously unpublished MCD spectra.

Appendix 1 — $T(a, b)$

For the case of orbitals a and b having equal exponents, it can be shown [4, 24] that

$$T(a,b)=0.2\zeta^2 e^{-\varrho}[1+\varrho+(\varrho^2/3)]\,.$$

In the case of unequal exponents

$$T(a,b)=0.2\,\zeta^2 e^{-\varrho}[1+\varrho+(\varrho^2/3)]\,(1-\tau^2)^{7/2}B\,.$$

In these expressions

$$\zeta=(\zeta_a+\zeta_b)/2$$

$$\tau=(\zeta_a-\zeta_b)/(\zeta_a+\zeta_b)$$

$$\varrho=\zeta R$$

$$B=15[(\tau\varrho)^2\sinh(\tau\varrho)-3\tau\varrho\cosh(\tau\varrho)+3\sinh(\tau\varrho)]/(\tau\varrho)^5\,.$$

References

1. Gouterman, M., Wagnière, G. H.: J. molecular Spectroscopy 11, 108 (1963), (Paper II).
2. Weiss, C., Kobayashi, H., Gouterman, M.: J. molecular Spectroscopy 16, 415 (1965), (Paper III).
3. McHugh, A. J., Gouterman, M.: Theoret. chim. Acta (Berl.) 13, 249 (1969).
4. Stephens, P. J., Suëtaka, W., Schatz, P. N.: J. chem. Physics 44, 4592 (1966).
5. Mataga, N., Nishimoto, K.: Z. physik. Chem. (Frankfurt) 13, 140 (1957).
6. Hoard, J. L., Hamor, M. J., Hamor, T. A.: J. Amer. chem. Soc. 85, 2334 (1963).
7. Robertson, J. M., Woodward, I.: J. chem. Soc. (London) 1837, 219.
8. Rimington, C., Mason, S. F., Kennard, O.: Spectrochim. Acta 12, 65 (1958).

9. a Roos, B., Skancke, P. N.: Acta chem. scand. **21**, 607, (1967).
   b Fischer-Hjalmars, I., Sundbom, M.: Acta chem. scand. **22**, 607 (1967).
   c Sundbom, M.: Acta chem. scand. **22**, 1317 (1967).
   d Knop, J. V., Knop, A.: Z. Naturforsch. **25a**, 1720 (1970).
10. a Gouterman, M.: J. chem. Physics **30**, 1139 (1959).
   b Gouterman, M.: J. molecular Spectroscopy **6**, 138 (1961), (Paper I).
11. a Sevchenko, A. N., Solov'ev, K. N., Mashenkov, V. A., Shkirman, S. F.: Soviet Phys.-Dokl. **10**, 778 (1966).
   b Gurinovich, G. P., Sevchenko, A. N., Solov'ev, K. N.: Spectroscopy of chlorophyll and related compounds. (Izdatel'stvo Nauka i Tekhnika, Minsk, 1968; Eng. trans.: National Technical Information Service, U.S. Dept. of Commerce, Springfield, Virginia 22151).
12. a Edwards, L.: Ph. D. Thesis, Committee on Chemical Physics, Harvard University (1969).
   b Paper XVII: — Dolphin. D. H., Gouterman, M., Adler, A. D.: J molecular Spectroscopy **38**, 16 (1971).
13. Kim, J. B., Leonard, J. J., Longo, F R.: J. Amer. chem. Soc. [in press 1972].
14. a Eisner, U., Linstead, R. P.: J. chem. Soc (London) **1955**, 3749.
   b Linstead, R. P.: J. chem. Soc. (London) **1952**, 4839.
   c unpublished spectra some of which are reproduced in Ref. [**10b**].
15. a Schechtman, B. H.: Technical Report No. 5207-2, Solid State Laboratory, Stanford University (1968).
   b , Spicer, W. E.: J. molecular Spectroscopy **33**, 28 (1969).
16. Hochstrasser, R. M., Marzzacco, C.: J. chem. Physics **49**, 971 (1968).
17. Schaffer, A. M.: Ph D. thesis, Department of Chemistry, University of Washington, Seattle (1972).
18. a Eastwood, D., Edwards, L., Gouterman, M., Steinfeld, J.: J. molecular Spectroscopy **20**, 381 (1966), Paper VII.
   b Edwards, L., Gouterman, M.: J. molecular Spectroscopy **33**, 292 (1969), Paper XV.
19. Bajema, L., Gouterman, M., Rose, C B.: J. molecular Spectroscopy **39**, 421 (1971), Paper XXIII.
20. Shashoua, V. E.: J. Amer. chem. Soc. **86**, 2109 (1964); **87**, 4044 (1965).
21. Dratz, E. A.: Ph. D. Thesis, University of California, Berkeley [Radiation Lab. Report UCRL-17200], (1966)
22. a Malley, M, Feher, G., Mauzerall, D.: J. molecular Spectroscopy **26**, 320 (1968).
   b Private communication.
23. Pershan, P. S., Gouterman, M., Fulton, R. L.: Molecular Physics **10**, 397 (1966).
24. Chong, D. P.: Molecular Physics **14**, 275 (1968).
25. a Ditchburn, R. W.: Light, p. 469. New York: Interscience (1963).
   b Bernheim, R.: Optical Pumping, p. 6. New York: W. A. Benjamin (1965).
26. Kobayashi, H., Shimizu, M., Fujita, I.: Bull. chem. Soc. Japan **43**, 2335 (1970).
27. a Briat, B., Schooley, D. A., Records, R., Bunnenberg, E., Djerassi, C.: J. Amer. chem. Soc. **89**, 6170 (1967).
   b Djerassi, C.: Private communication.
28. Stephens, P J., Schatz, P. N., Ritchie, A. B., McCaffery, A. J.: J. chem. Physics **48**, 132 (1968).
29. Sutherland, J. C., Axelrod, D., Klein, M. P.: J. chem. Physics **54**, 2888 (1971).
30. Clementi, E.: J. chem. Physics **40**, 1944 (1964), and IBM Tech. Rept. RJ-256, August, (1963).
31. Silverstone, H. J., Joy, H. W., Orloff, M. K.: J. Amer. chem. Soc. **88**, 1325 (1966).
32. Perrin, M. H., Gouterman, M., Perrin, C. L.: J. chem. Physics **50**, 4137 (1969).
33. Stern, A., Pruckner, F.: Z. Physik. Chem. **178 A**, 420 (1937).
34. Longuet-Higgens, H. C., Rector, C. W., Platt, J. R.: J. chem. Physics **18**, 1174 (1950).
35. Zerner, M., Gouterman, M.: Theoret. chim. Acta (Berl.) **4**, 44 (1966), Paper IV.

Dr. A. J. McHugh
130 Jiddens Wharf Rd.
Killara, NSW 2071
Australia

Prof. Dr. Martin Gouterman
Department of Chemistry
University of Washington
Seattle, Washington 98105
USA

Dr. C. Weiss, Jr.
International Bank
for Reconstruction and Development
1818 H Street, N.W.,
Washington, DC 20433, USA

Theoret. chim. Acta (Berl.) 24, 371—381 (1972)
© by Springer-Verlag 1972

Zur Quantenchemie zyklischer und linearer Kohlenwasserstoffe*

P. Raeber
Institut für Theoretische Physik der Universität Zürich

Eingegangen am 4. November 1971

Quantum Chemistry of Cyclic and Linear Hydrocarbons

Binding energies and interatomic distances (bond lengths) are determined for simple cyclic and linear hydrocarbons, such as benzene, C_nH_{2n}, $n = 4, 5, 6$, butadiene and the molecules C_2H_m, $m = 2, 4, 6$, using the method of interacting atoms in particular atomic states and the concept of valence structures (Heitler, Rumer *et al.*). Furthermore, qualitatively correct predictions about the most stable three-dimensional shapes of some ring compounds are made. The energies and the bond lengths can be read off from the minima of potential curves $E(R)$ (energy as function of distance) calculated for each molecule, which are given in terms of Coulomb and exchange integrals. For the C—C interaction, the distance dependence can be determined semiempirically. For the C—H interaction, a fixed atomic distance is assumed and therefore constant values of the related integrals are introduced in $E(R)$. The results are in most cases in very good agreement with the experimental data.

Ausgehend von der Vorstellung wechselwirkender ganzer Atome in bestimmten Quantenzuständen werden für einfache zyklische und lineare Kohlenwasserstoffe sowohl die Bindungsenergien als auch die Atomabstände mit einer modifizierten VB-Methode berechnet. Außerdem läßt sich die stabilste räumliche Anordnung der Kohlenstoff-Atome in einigen Ringverbindungen richtig voraussagen. Neben den Ringen Benzol und C_nH_{2n}, $n = 4, 5, 6$ werden lineare Ketten wie Butadien und die Moleküle C_2H_m, $m = 2, 4, 6$, untersucht. Die Bindungsenergien und Abstände ergeben sich unmittelbar aus den Minima von Potentialkurven $E(R)$, die für jedes Molekül berechnet werden (Energie als Funktion des Nachbarabstandes). Da höhere Austausch-Terme und die Überlappungsintegrale vernachlässigt werden, ist $E(R)$ durch Einfachaustausch-Integrale und Coulombintegrale bestimmt. Für die C—C-Wechselwirkung kann die Abstandsabhängigkeit dieser Funktionen semiempirisch bestimmt werden. Dagegen wird ein fester C—H-Abstand angenommen, so daß konstante Werte für die entsprechenden Integrale in $E(R)$ eingehen. Die Resultate sind in den meisten Fällen in sehr guter Übereinstimmung mit der Erfahrung.

Einleitung

In der Theorie der chemischen Bindung haben sich schon früh zwei wesentlich verschiedene Standpunkte herausgebildet: die MO- (molecular orbital) Näherung und die VB- (valence bond) oder HL- (Heitler-London) Methode. Das MO-Verfahren weist bei völligem Verzicht auf das chemische Bild mathematische Vorteile auf (orthogonale Orbitale) und wurde in den letzten Jahren fast ausschließlich angewandt. Die VB-Näherung ist dagegen für den Chemiker anziehender und ermöglicht auch Aussagen über chemische Reaktionen (Aktivierungs-Energie). Will man jedoch zu einem wirklichen Verständnis der chemischen Bindung kommen, kann man es sich nicht leisten, den einen oder andern Standpunkt zu ignorieren; beide Methoden ergänzen einander. Außerdem sind die wegen der

---

* Work supported by the Swiss National Foundation.

Kompliziertheit der Probleme notwendigen Vernachlässigungen im MO-Verfahren mindestens so einschneidend wie in der VB-Methode.

In der vorliegenden Arbeit soll die Theorie der Molekülbildung vom Standpunkt der VB-Methode (Heitler, London, Rumer *et al.* [1, 2]) auf eine Reihe von *Kohlenwasserstoffen* angewendet werden. Die Wechselwirkung von Atomen in *bestimmten Quantenzuständen* wird in Funktion ihrer Abstände mit Störungstheorie in 1. Ordnung berechnet. Da die 4-Wertigkeit von Kohlenstoff im wesentlichen auf dem angeregten Zustand ^5S beruht, wird nur dieser Term berücksichtigt. Das bedeutet natürlich nicht, daß das C-Atom vor der Molekülbildung in dieses Niveau angeregt werden muß [3, 4].

Bei der Berechnung der Bindungsenergien mit der HL-Methode stößt man auf eine charakteristische Schwierigkeit: wegen der Nichtorthogonalität der Atom-Orbitale tritt im Energieausdruck eine riesige Zahl von Austausch- und Überlappungsintegralen auf. Diese werden üblicherweise bis auf die Beiträge von einfachen Elektronen-Transpositionen vernachlässigt. Nun geben zwar die höheren Austausch-Terme für mittlere und große Abstände einzeln nur kleine Beiträge [5], sind jedoch derart zahlreich, daß man nicht von vorneherein hoffen darf, der Fehler aus dieser Näherung sei klein. Diese scheinbare Inkonsistenz ist in der Literatur unter dem ominösen Ausdruck „Nichtorthogonalitäts-Katastrophe in der HL-Theorie" bekannt. Mizuno u. Izuyama konnten jedoch zeigen, daß diese Schwierigkeit nie auftritt [6]. Das Weglassen aller Überlappungen kompensiert näherungsweise immer den Fehler, der von der Vernachlässigung der höheren Austausch-Integralen herrührt. Kritik an der Theorie in diesem Sinne [7, 8] ist deshalb nicht stichhaltig [9].

Die Coulomb- und Austauschintegrale der C—C- und der C—H-Wechselwirkung wurden schon in früheren Arbeiten semiempirisch bestimmt, da kaum Hoffnung besteht, sie direkt aus den Wellenfunktionen der Atome zu berechnen [10]. Kohlenwasserstoffe sind für diesen Zweck besonders geeignet, da die gleichen Integrale in verschiedenen Kombinationen in vielen Verbindungen vorkommen. Bis jetzt waren die folgenden Approximationen üblich:

a) Vernachlässigung der Nichtnachbar-Wechselwirkungen.
b) Die Berechnungen bezogen sich nur auf die Potentialminima und die C-C-Abstände wurden in allen Verbindungen gleichgesetzt.
c) Nur Zweier-Elektronenaustausche konnten berücksichtigt werden.
d) In der Behandlung komplizierterer Moleküle wurden häufig nur einige wenige Valenzstrukturen in Betracht gezogen.

In dieser Arbeit werden nun alle aufgeführten Näherungen bis auf Punkt c) fallengelassen: bei den zyklischen Verbindungen berechnen wir die volle Wechselwirkung, auch zwischen *Nicht-Nachbarn*. Außerdem wird immer der *vollständige Satz* linear unabhängiger Valenzstrukturen verwendet.

Die *Abstandsabhängigkeit* der Integrale zur Kohlenstoff-Kohlenstoff-Wechselwirkung wird halbempirisch bestimmt. Eine wesentliche Hilfe ist die Form der Nichtnachbar-W.W., die sich als stark *abstoßend* erweist.

Die Resultate sind die Folgenden: neben den *Bindungsenergien*, die bisher fast ausschließlich Gegenstand der Berechnungen waren, können nun auch die *Atomabstände* für C—C aus den Minima der Potentialkurven ermittelt werden. Wir können damit die verschiedenen Bindungslängen der Einfach-, Doppel- und

Dreifachbindung C–C, C=C und C≡C erklären. Sogar die bevorzugte dreidimensionale Struktur gewisser Ringverbindungen läßt sich qualitativ verstehen. Die theoretischen Ergebnisse sind in guter Übereinstimmung mit der Erfahrung.

Untersucht wurden die Ringe Benzol, Cyclohexan, Cyclopentan und Cyclobutan, einige lineare Kohlenwasserstoffe wie z. B. Butadien und die einfachen Verbindungen C_2H_{2n}, $n = 1, 2, 3$.

Bindungsenergie von Benzol C_6H_6

Unmittelbarer Ausgangspunkt zur Berechnung von Molekül-Bindungsenergien nach der Methode der Valenzstrukturen [1, 2] ist das lineare System der Bindungsgleichungen. Werden nur Elektronen-Transpositionen berücksichtigt und alle Überlappungs-Integrale vernachlässigt (vgl. dazu Bemerkung in der Einleitung), ergibt sich als Lösbarkeitsbedingung:

$$\left|\left(E - C + \sum_{a,b} (\mathrm{AB})\, t_{ab}\right) \varphi_i\right| = 0, \qquad i = 1 \ldots n. \qquad (1)$$

Summiert wird über alle Atompaare A, B. Die φ_i bilden einen vollständigen Satz von linear unabhängigen Valenzstrukturen, Spinwellenfunktionen zum Gesamtspin Null, mit lokalisierten Bindungen (d. h. antiparallelen Spinpaaren) zwischen je zwei Atomen A, B, ... Diese Bindungen werden graphisch durch Valenzpfeile symbolisiert.

$C = C_{ab} + C_{ac} + \cdots$ ist das totale Coulomb-Integral, (AB) das Austausch-Integral zwischen A und B:

$$(\mathrm{AB}) = (u_a u_b \ldots V T_{ab} u_a u_b \ldots), \qquad (2)$$

Unter den Bahnwellenfunktionen $u_a, u_b, \ldots$ der Atome sind im Falle von Kohlenstoff diejenigen des *Terms* ^5S zu verstehen (vgl. Einleitung). T_{ab} vertauscht irgend ein Valenzelektron von A mit einem solchen von B. Die Summe aller dieser Vertauschungen ergibt den Operator t_{ab}. Er erzeugt aus den φ_i Linearkombinationen von Valenzstrukturen, welche immer auf die einmal gewählte Basis zurückgeführt werden können [2].

E und V bezeichnen die Bindungsenergie des Systems und die Störung (reine Coulomb-Wechselwirkung verschiedener Atome).

Um das Gleichungssystem (1) auf die zyklische Verbindung Benzol praktisch anwenden zu können, sind weitere Annahmen erforderlich: Wir denken uns nur die C–C-Bindungen beweglich und die H-Atome fest an „ihre" C-Atome gebunden. Jedes CH-Radikal wird also als 3-valentiges „Atom" aufgefaßt. Damit verkleinert sich die Zahl der Valenzstrukturen drastisch von über 3000 auf nurmehr *34*. Das Vorgehen ist gerechtfertigt, da die CH-Energie verglichen mit der C–C-Energie relativ groß ist.

Es sollen nun *alle* Strukturen in die Rechnung einbezogen werden. In früheren Approximationen wurde der Ring dagegen meistens zu einem 6-Elektronen-System vereinfacht, für das 5 kanonische Strukturen (2 Kekulé und 3 Dewar) existieren. Ein Ring lokalisierter Einfachbindungen wurde als fest angenommen [3].

In der vollständigen Basis der 34 Valenzstrukturen kommen neben den geläufigen Strichbildern 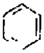 (Kekulé) und 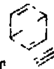 (Dewar) eine große Zahl mehr oder weniger „exotischer“ Strukturen wie 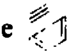, 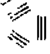 und 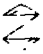 vor. Die Dimension des Säkularproblems läßt sich aber mit Hilfe der Punktsymmetrie des Moleküls (D_{6h}) auf 8 reduzieren.

Berechnung der Bindungsenergie

Aus Symmetriegründen läßt sich der Operator in (1) wie folgt schreiben:

$$\sum_{a,b} (AB)\, t_{ab} = X \cdot T_x + Y \cdot T_y + Z \cdot T_z .$$

Hier bedeuten

$$T_x = t_{ab} + t_{bc} + t_{cd} + t_{de} + t_{ef} + t_{fa}$$

$$T_y = t_{ac} + t_{bd} + t_{ce} + t_{fd} + t_{ae} + t_{fb}$$

$$T_z = t_{ad} + t_{eb} + t_{fc} .$$

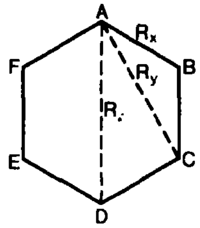

Fig. 1

In der üblichen Notation nennen wir das Austauschintegral zwischen Kohlenstoff-Atomen (genauer: zwischen CH-Gruppen) (CC)(R). X, Y und Z sind seine Werte für die Abstände R_x, R_y und R_z (Fig. 1). Sei $C_{CC}(R)$ das entsprechende Coulombintegral. Beide Integrale werden also explizit als Funktionen des Atomabstandes R betrachtet. Sie sollen zudem für mittlere und große R stets *negativ* sein [10].

Die Säkulardeterminante (1) wird durch Anwendung der Austausch-Operatoren t_{ab}, t_{ac}, ... auf die Valenzstrukturen φ_i erhalten:

$$\det((E - C)\,\delta_{ik} + a_{ik} \cdot X + b_{ik} \cdot Y + c_{ik} \cdot Z) = 0 \qquad i, k = 1 \dots 8 \qquad (3)$$

a_{ik}, b_{ik} und c_{ik} sind ganzzahlige Faktoren. Erste Anhaltspunkte über den Verlauf von (CC)(R) ergeben sich durch Einsetzen wachsender Verhältnisse Y/X und Z/X in die Determinante (3) nach Division der Zeilen durch X. Wir setzen $(E - C)/X = x$, eine Zahl, die für das stabile Molekül *positiv* sein muß. Die höchste Lösung von (3) für α entspricht also offensichtlich dem Grundzustand des Moleküls, wir nennen sie deshalb $\alpha_g(Y/X, Z/X)$. Diese Funktion ist in Fig. 2 für drei Werte von Z/X dargestellt; aus ihrem Verlauf ist der Charakter der Nichtnachbar-Wechselwirkung unmittelbar ersichtlich: Nicht verschwindende Y und Z geben *stark abstoßende* Beiträge zur Bindungsenergie. Es wird sich herausstellen, daß bei vernünftigen Werten von X nur die Kurve $Z/X = 0$ eine Rolle spielt, da schon $Y = (CC)(R_y)$ praktisch Null sein muß.

Betrachten wir kurz den Spezialfall $Y = Z = 0$, also vorläufige Vernachlässigung der Nichtnachbar-Austauschwechselwirkung. Auch die entsprechenden Coulomb-Integrale C_{ac}, C_{bd} ... sollen verschwinden. Dies war eine übliche Näherung bei früheren Rechnungen. Wir erhalten $\alpha_g(0, 0) = \alpha_g^0 = 7{,}79$[1]. Für die volle

---

[1] Für die Berechnungen wurde ein Computer IBM 360-40 benutzt.

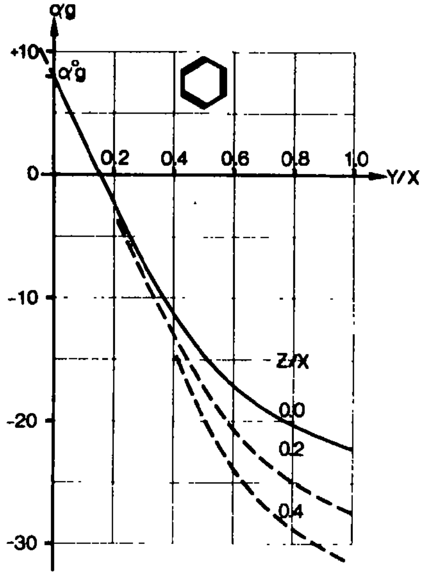

Fig. 2

Bindungsenergie müssen natürlich die additiven Beiträge der CH-Gruppen und die Anregungsenergie von ^5S, $\varepsilon = 4{,}16$ eV, berücksichtigt werden:

$$E = \alpha_g^0 \cdot X + 6(C_{CC} + C_{CH}) + 6(CH) + 6\varepsilon . \qquad (4)$$

Die Größen in (4) sind zuerst von Heitler [10] halbempirisch unter Benutzung der experimentell bekannten Dissoziationsenergien einfacher Kohlenwasserstoffe ur Anpassung der Integrale bestimmt worden. Es wurde allerdings nicht berückichtigt, daß die C–C-Abstände von 1,20 Å im Falle der Dreifachbindung bis ,55 Å für die Einfachbindung variieren.

Heitler erhielt folgende Werte für die Integrale (in eV): $X = (CC) = -3{,}80$, $CH) = -2{,}75$, $C_{CC} = -1{,}90$, $C_{CH} = -3{,}35$. Eingesetzt in (4) wird die Bindungsnergie von Benzol $-52{,}7$ eV. Demgegenüber ist der experimentelle Wert -58 eV. Angesichts der vielen Näherungen darf die Übereinstimmung als ziemlich befriedigend bezeichnet werden.

Die Auswertung der Determinanten (3) unter Berücksichtigung der vollen Wechselwirkung, also auch der *Nichtnachbarn*, gibt uns eine Möglichkeit, die Methode von Heitler [10] zu verbessern und über die bloße Berechnung der Bindungsenergie hinauszugehen. Die oben angegebenen Werte für die Integrale ind gewissermaßen für einen mittleren Gleichgewichtsabstand der Atome gültig. Wir werden nun aber bei (CC) und C_{CC} die Abstandsabhängigkeit *semiempirisch* bestimmen. Die in allen Kohlenwasserstoffen praktisch gleichen C–H-Abstände assen wir fest, so daß konstante Werte für die betreffenden Integrale genügen.

Für weitere Ringverbindungen berechnen wir nun die Funktionen α_g. Mit ihrer Hilfe lassen sich sowohl die *Bindungsenergien* als auch die *Atomabstände* R_x durch eeignete Wahl von (CC)(R) und $C_{CC}(R)$ anpassen. Um eine praktisch eindeutige

Lösung zu erhalten, genügen unter gewissen Einschränkungen die Daten von *drei* Verbindungen; wir haben neben *Benzol Cyclobutan* (C_4H_8) und *Cyclopentan* (C_5H_{10}) gewählt. Es ist jedoch keineswegs trivial, daß Energien *und* Abstände gut angepaßt werden können. Aus Gründen, die wir im nächsten Abschnitt anführen werden, ist eine perfekte Übereinstimmung tatsächlich unmöglich. Es muß schon als Erfolg der Theorie gewertet werden, daß weitgehende Anpassung erzielt werden konnte.

Die Rechnungen für C_5H_{10} und C_4H_8 führen zu ähnlichen Ergebnissen wie bei Benzol. Beide Ringe behandeln wir zunächst als *ebene*, reguläre Polygone, in denen die CH_2-Radikale als 2-valentige „Atome" aufgefaßt werden.

Die Faktoren $\alpha_g(Y/X)$, welche wieder die Energie wesentlich bestimmen, nehmen linear mit Y/X ab (Abstoßung von Nichtnachbarn, vgl. Fig. 2). Vernachlässigt man in erster Näherung die Nichtnachbar-W.W. ($Y=0$), so findet man unter Verwendung der Integrale von Heitler (S. 7):

$$C_5H_{10}: E = -58{,}8\,\text{eV} \quad (-60{,}5\,\text{eV})$$

$$C_4H_8\ : E = -53{,}0\,\text{eV} \quad (-48{,}5\,\text{eV}).$$

In Klammern stehen die experimentellen Werte. Die Übereinstimmung ist, wenigstens bei C_5H_{10}, recht gut. Die zu große Bindungsenergie von Cyclobutan läßt vermuten, daß hier der Abstoßungseffekt diametral liegender Atome wirksam werden muß. Wir erwarten deshalb nichtverschwindende Y-Werte bei Cyclobutan.

Die Integrale (CC) (R) und $C_{CC}(R)$

Wir setzen voraus, daß diese Funktionen für mittlere und große Abstände stets negative Werte annehmen. Zudem müssen die Minima von der Größenordnung der Heitlerschen Zahlen sein (S. 7), da sich andernfalls Widersprüche zu seinen Resultaten ergeben würden. Diese Bedingungen garantieren bereits die Eindeutigkeit der Lösung.

In einem ersten Schritt zeichnet man sich ein Paar von Versuchsfunktionen auf, deren ungefährer Verlauf vor allem durch die α_g der drei Ringe Benzol, Cyclobutan und Cyclopentan nahegelegt wird. Damit lassen sich die Potentialkurven $E(R_x)$ für alle drei Verbindungen berechnen. Zu jedem Wert von R_x gehören bei Benzol zwei Quotienten Y/X und Z/X, bei den beiden andern Ringen je ein Y/X. Diese werden der *Versuchskurve* (CC) (R) entnommen und bestimmen ihrerseits den zugehörigen Funktionswert von α_g (bei Benzol nach Fig. 2). Zusammen mit den additiven Beiträgen des Coulomb-Integrals und der Radikale ergibt sich die Bindungsenergie. Die Gleichgewichtsabstände sind durch die Minima der Kurven $E(R_x)$ definiert. Bis zur optimalen Übereinstimmung mit der Erfahrung müssen (CC) (R) und $C_{CC}(R)$ schrittweise verbessert werden.

Die Integrale der bestmöglichen Approximation zeigt Fig. 3. Die nebenstehende Tabelle vergleicht die Bindungsenergien und Atomabstände, welche mit diesen Kurven gewonnen wurden, mit den exp. Daten. Wir sehen, daß die Bindungsenergien gegenüber den Ergebnissen der alten Näherung (S. 7, 8) beträchtlich verbessert werden konnten und die Gleichgewichtsabstände der Radikale bis auf ca. 1 % mit der Erfahrung übereinstimmen.

	C_6H_6	C_5H_{10}	C_4H_8
E^{th}	−55,3	−60,7	−49,0
E^{exp}	−58,0	−60,5	−48,5
R_x^{th}	1,405	1,50	1,575
R_x^{exp}	1,395	1,52	1,56

(Werte in eV resp. Å)

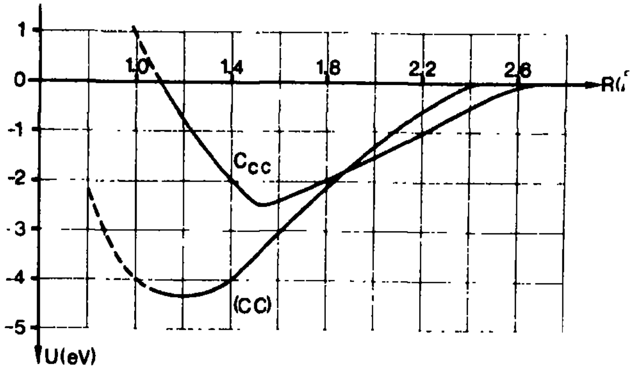

Fig. 3

Die Funktionen von Fig. 3 stellen allerdings nur sehr angenähert die Integrale *C* und (AB) dar, wie sie ursprünglich im vorigen Abschnitt definiert wurden. Hier handelt es sich eigentlich um die Wechselwirkung ganzer Radikale, CH im Falle von Benzol, CH_2 bei den beiden andern Ringen. Daß man in beiden Näherungen die *gleichen* Funktionen benützen kann, ist nicht von vornherein selbstverständlich. Tatsächlich weicht bei *Cyclopentadien* (C_5H_6), wo beide Radikale vorkommen, die Energie um ca. 20% vom richtigen Wert ab.

Wir wenden uns nun einer zusätzlichen Prüfung der Integrale zu, nämlich der *Planarität* von Ringverbindungen.

Nicht-planare Systeme

Bei einigen zyklischen Kohlenwasserstoffen sind nicht-planare räumliche Anordnungen der C-Atome energetisch günstiger, z. B. beim Cyclohexan (C_6H_{12}). Vor allem zwei Effekte sind dafür verantwortlich:

1. Bei ebenen Ringen ist der Valenztetraeder i.a. deformiert, was eine beträchtliche Spannung im Molekül erzeugt. In unseren Rechnungen zeigen sich aber keine Richtungseigenschaften der Valenzen (nur ^5S!). Diese ergeben sich erst, wenn mehrere Atomterme von Kohlenstoff kombiniert werden, z. B. ^3P mit ^5S [11], oder wenn man höhere Austausch-Terme berücksichtigt [12].

2. In unserer Theorie ist eine eventuelle Nichtplanarität, z. B. von C_6H_{12}, allein eine Konsequenz der Nichtnachbar-Wechselwirkung, d. h. sie folgt aus der Funktion α_g sowie aus der Form von Coulomb- und Austauschintegral. Für andere räumliche Strukturen (mit i.a. niedrigeren Symmetrien) berechnen wir die zugehörigen Funktionen α_g und daraus die Bindungsenergien. Die möglicherweise tieferliegenden neuen Gleichgewichtszustände werden durch das Zusammenwirken von Coulomb-Anziehung und Austausch-Abstoßung bestimmt.

Bei Sechser-Ringen können die Winkel des freien Valenztetraeders von je 109,5° in zwei nicht-planaren Strukturen, dem sog. „Sessel“ und der „Wanne“, realisiert werden. Anschaulich gehen beide aus der ebenen Form ($\sphericalangle\, CCC \equiv \varphi = 120°$) durch Faltung des Ringes unter stetiger Verkleinerung von φ hervor. Im folgenden vergleichen wir den Einfluß dieser Deformation auf die Bindungsenergie in den Fällen Benzol und Cyclohexan.

Die Bindungsenergie ist nun in Funktion von φ, mit dem Nachbarabstand R_x als Parameter, zu berechnen. Für jedes R_x erhalten wir so eine Kurve $E(\varphi, R_x)$, die ihr Minimum bei einem bestimmten Winkel $\varphi_{\min}(R_x)$ annimmt. Die Ergebnisse werden besonders anschaulich, wenn diese Minimalenergien für alle R_x mit der Potentialkurve des ebenen Moleküls verglichen werden. Dies zeigt Fig. 4 (Benzol) und Fig. 5 (Cyclohexan).

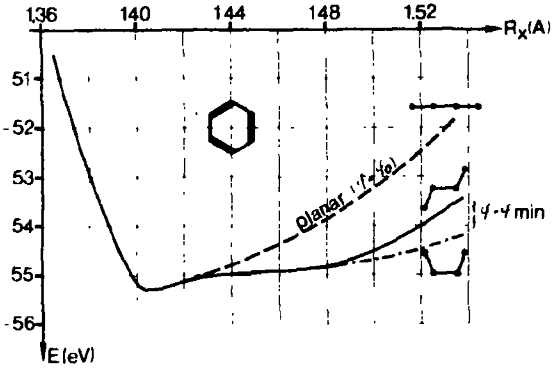

Fig. 4

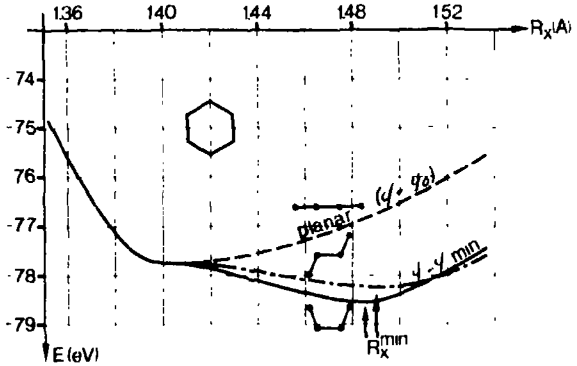

Fig. 5

Wir sehen, daß bei C_6H_6 die tiefste Energie im ebenen Molekül angenommen wird; infolge der starren Doppelbindungen ist Benzol tatsächlich streng eben. Wesentlich anders ist dagegen die Situation bei Cyclohexan. Dreierlei ist hier bemerkenswert: 1. Sessel und Wanne sind wirklich stabiler als das ebene Molekül für irgend ein R_x. – 2. Der Gleichgewichtsabstand hat sich von 1,41 Å (planar) nach 1,49 Å (Sessel) verschoben. Das ist sehr befriedigend, geben die Messungen doch 1,53 Å. – 3. Als Bindungswinkel φ erhalten wir fast genau 109,5°. Cyclohexan ist in Wirklichkeit auch frei von Winkelspannungen [13]. Nach der Erfahrung liegt allerdings der Sessel um ca. 0,25 eV tiefer als die Wanne; hier ist es gerade umgekehrt. Derart kleine Energiedifferenzen sind aber außerhalb der Genauigkeit der Theorie. Es ist jedoch offensichtlich, daß die Nichtnachbar-W.W. für die

Nichtplanarität eines Ringes ebenso verantwortlich ist wie die Tetraeder-Struktur der Kohlenstoff-Valenzen.

Cyclohexan „klappt" bereits bei Zimmertemperatur rapide von der Sesselform zu ihrem Spiegelbild um [13]. Die quasistabile Wanne ist durch eine Potentialbarriere vom Sessel getrennt. Für diese Energieschwelle erhält man eine Majorante, nennen wir sie ΔE, wenn eine *hypothetische* Übergangsform angenommen wird: der Sessel werde zur Wanne, indem seine „Lehne" auf die andere Seite klappt [13]. – Wir fassen die Ergebnisse für Cyclohexan in der folgenden Tabelle zusammen:

C_6H_{12}	E_{Sessel}	E_{Wanne}	$(R_x)_{\min}$	$\varphi_{\min}$	ΔE(Sessel ↔ Wanne)
Theorie	– 78,3 eV	– 78,6 eV	1,49 Å	109,5°	~ 0,9 eV
Experiment	– 73,3 eV	– 73,0 eV	1,53 Å	109,5°	~ 0,5 eV

Entsprechende Rechnungen bei Cyclopentan und Cyclobutan entscheiden in beiden Fällen zugunsten der *ebenen* Form. Die schwache Nichtplanarität der Ringe beruht hauptsächlich auf der Abstoßung von H-Atomen *verschiedener* Radikale. Insbesondere ist Cyclopentan praktisch frei von Winkelspannungen ($\varphi = 108°$!).

Lineare Verbindungen

Nach den Ergebnissen der letzten Abschnitte liegt es nahe, die Untersuchung auf einfache lineare Ketten auszudehnen und so die Gültigkeit der beiden Integrale strenger zu prüfen. Zunächst sollen die folgenden Strukturen betrachtet werden:

a) 1,3-Butadien C_4H_6 : $(CH_2)\overset{R_x}{=\!=}(CH)\overset{R_y}{-\!-}(CH)\overset{R_x}{=\!=}(CH_2)$,

b) 1,2-Butadien C_4H_6 : $(CH_3)-\!-(CH)=\!=(C)=\!=(CH_2)$,

c) 1-Buten C_4H_8 : $(CH_3)-\!-(CH_2)-\!-(CH)=\!=(CH_2)$.

Im Einklang mit den Näherungen bei den zyklischen Verbindungen werden wieder ganze Atomgruppen als Bausteine der Moleküle angenommen, um die Zahl der Valenzstrukturen in Grenzen zu halten. Die Radikale sollen auf *Geraden* liegen und die Abstände so variiert werden, daß Einfach- *resp.* Doppelbindungen unter sich stets gleich lang bleiben. Die Bindungsenergie ist also einfach eine Funktion von R_x und R_y.

In Wirklichkeit sind die Ketten etwas geknickt. Es ist sehr wahrscheinlich, daß Bindungswinkel kleiner als 180° aus den gleichen Gründen stabilere Zustände ergeben würden, die für die Nichtplanarität von C_6H_{12} verantwortlich sind. Linearität ist hier eine erste Näherung. – Die nachfolgende Tabelle erlaubt einen Vergleich der Theorie mit der Erfahrung. Der Unterschied zwischen Einfach- und Doppelbindungslänge erscheint sehr schön, und die Fehler in den Energien liegen unterhalb von 2,3%.

	1,3-Butadien		1,2-Butadien		1-Buten	
	Theorie	Experiment	Theorie	Experiment	Theorie	Experiment
E	−41,7 eV	−42,1 eV	−42,0 eV	−41,6 eV	−48,9 eV	−47,8 eV
R_z	1,45 Å	1,46 Å	1,47 Å	1,48 Å	1,48 Å	1,50 Å?
R_v	1,36 Å	1,35 Å	1,36 Å	1,33 Å	1,36 Å	1,34 Å?

Zum Schluß untersuchen wir noch die einfachsten Kohlenwasserstoffe der Formel C_2H_{2n}, $n = 1, 2, 3$ [10, 14]. Was deren Dissoziationsenergien betrifft, konnte von Heitler [10] mit Hilfe von angepaßten Integralen eine ausgezeichnete Übereinstimmung erreicht werden. Diese Integrale waren Konstante (vgl. S.) und die Bindungslängen standen nicht zur Diskussion.

Für die C–C-Wechselwirkung führen wir nun wieder unsere Funktionen $(CC)(R)$ und $C_{CC}(R)$ von Fig. 3 ein und halten nur den C–H-Abstand fest. Die bis jetzt verwendete Näherung, die Atome durch Radikale CH, ... zu ersetzen, ist sicher dem Problem nicht mehr angemessen. Die Rechnungen bleiben aber einfach, wenn statt dessen die H-Atome in jeder CH_2- (CH_3-)Gruppe wie *ein* Atom mit zwei (drei) parallelen Spins behandelt werden.

Für die Dissoziationsenergien der Moleküle und für die Bindungslängen C–C, C=C, C≡C ergeben sich die Werte der untenstehenden Tabelle. Die Resultate der Anpassung von Heitler stehen in Klammern. $\Delta E = E_{\min} - E(R^{\text{exp}})$ ist die Energiedifferenz zwischen dem Minimum der Potentialkurven $E(R)$ und der Energie für den experimentell bestimmten Atomabstand R^{exp}.

	C_2H_2		C_2H_4		C_2H_6	
	Theorie	Exp.	Theorie	Exp.	Theorie	Exp.
E (eV)	−17,5 (17,0)	−17,0	23,8 (−23,7)	−23,5	−28,9 (−29,1)	−29,1
R (Å)	1,30 (−)	1,206	1,345 (−)	1,337	1,38 (−)	1,53
ΔE (eV)	~ 0,3 (−)	–	~ 0 (−)	–	~ 0,7 (−)	–

Die Übereinstimmung in der Energie ist sehr gut. Die Bindungslängen erscheinen in der richtigen Reihenfolge ($R_{C_2H_2} < R_{C_2H_4} < R_{C_2H_6}$), weichen jedoch mit Ausnahme von C_2H_4 ziemlich stark von den richtigen Werten ab. Es zeigt sich aber, daß die Energiekurven im Gegensatz zu denjenigen der zyklischen Verbindungen sehr flach verlaufen. Opfert man etwas Genauigkeit in der Energie, ergeben sich korrekte Distanzen. Dies wird durch die Größe ΔE illustriert, die in keinem Fall mehr als 2–3 % der totalen Energie ausmacht.

Zwei weitere Punkte müssen beachtet werden: Die Integrale $(CC)(R)$ und $C_{CC}(R)$ sind graphisch gegeben. Die Lagen der Energieminima hängen aber außerordentlich empfindlich von diesen Funktionen ab. Es ist deshalb kaum möglich, die Potentialkurven mit der großen Genauigkeit zu berechnen, welche für eine exakte Bestimmung der Minima notwendig wäre. Zudem muß daran erinnert werden, daß $(CC)(R)$ und $C_{CC}(R)$ aus der Wechselwirkung von Radikalen hergeleitet wurden, hier jedoch auf die bloße C–C-Wechselwirkung angewendet werden.

Schlußbemerkungen

Mit den beiden angepaßten Integralen (CC) (R) und $C_{CC}(R)$ lassen sich offensichtlich die Bindungsenergien und die Bindungsabstände verschiedener Kohlenwasserstoffe recht gut verstehen. Die Unterschiede in den Bindungslängen von C–C, C=C und C≡C ergeben sich richtig und selbst feinere Details, wie die Nichtplanarität von Cyclohexan, können qualitativ erklärt werden.

Daß unsere Resultate mit der Erfahrung nicht völlig übereinstimmen, darf angesichts der zum Teil doch recht groben Näherungen nicht verwundern. Es ist im Gegenteil bemerkenswert, daß nur zwei Funktionen genügen, um so verschiedenartige Moleküleigenschaften zu erklären. Es ist jedoch plausibel anzunehmen, daß mindestens einige der Vernachlässigungen ihren Niederschlag in den angepaßten Integralen gefunden haben.

Meinem verehrten Lehrer, Herrn Prof. Dr. W. Heitler, möchte ich an dieser Stelle für seine Anregungen und sein stetes Interesse an meiner Arbeit herzlich danken.

Literatur

1. Heitler, W., London, F.: Z. Physik **44**, 455 (1927).
2. — Rumer, G.: Z. Physik **68**, 12 (1931).
3. — Int. Journal of Quantum Chemistry **1**, 13–36 (1967).
4. – Arkiv för Fysik **10**, 13 (1955).
5. Bärlocher, M. A.: Helv. chim. Acta **43**, 3 (1960).
6. Mizuno, Y., Izuyama, T.: Prog. theoret. Physics Kyoto **22**, 3 (1959).
7. Inglis, D. R.: Physic. Rev. **46**, 135 (1934).
8. McWeeny, R.: Proc. Roy. Soc. (London) A **223**, (1954).
9. Van Vleck, J. H.: Physic. Rev. **49**, 232 (1936).
10. Heitler, W.: Helv. chim. Acta **38**, 5 (1954).
11. Nordheim-Pöschl, G.: Ann. Physik **26**, 258 (1936)
12. Artmann, K.: Z. Physik **137**, 137 (1954).
13. Lambert, J. B.: Scientific American **1**, (1970).
14. Hellmann, H.: Z. Physik **82**, 192 (1933).

Dr. P. Raeber
Institut für Theoretische Physik
der Universität Zürich
CH-8001 Zürich, Schönberggasse 9

Theoret. chim. Acta (Berl.) 24, 382—388 (1972)
© by Springer-Verlag 1972

Relationes

Spectral Variational Principle for Green's Functions

S. M. Blinder*

Centre de Mécanique Ondulatoire Appliquée, 23 rue du Maroc, Paris 19^e, France
and
Mathematical Institute, University of Oxford, 24–29 St Giles, Oxford OX1 3LB, Great Britain

Received September 27, 1971

For a suitable approximation $\tilde{K}(q, q', \tau)$ to the Dirac-Feynman Green's function of a quantum-mechanical system, the parameter $\Delta \equiv \mathrm{tr}[\mathscr{S}\tilde{K} \cdot (\mathscr{S}\tilde{K})^*]$ is defined, where $\mathscr{S} \equiv i\partial/\partial\tau - \mathscr{H}$. It is shown that $\Delta \geqq 0$ and $\Delta \to 0$ as $\tilde{K} \to K$, the exact Green's function, thus providing a criterion on approximate Green's functions analogous in its role to the variational principle for wavefunctions. A second somewhat weaker criterion is also proposed, based on $\Sigma \equiv [\mathrm{tr}\tilde{K}^* \mathrm{tr}\mathscr{S}^2\tilde{K} - |\mathrm{tr}\mathscr{S}\tilde{K}|^2]_{\tau\,\mathrm{avg}} \geqq 0$. Recipes are given for projecting out continuum contributions to Δ or Σ and for analyzing for the discrete eigenvalue spectrum.

Um zu Näherungen $\tilde{K}(q, q', \tau)$ für die Dirac-Feynman-Greensche Funktion eines quantenmechanischen Systems zu gelangen, wird der Parameter $\Delta \equiv \mathrm{tr}[\mathscr{S}\tilde{K} \cdot (\mathscr{S}\tilde{K})^*]$ definiert, wobei $\mathscr{S}$ für $i\partial/\partial\tau - \mathscr{H}$ steht. Es wird gezeigt, daß $\Delta \geqq 0$ und $\Delta \to 0$ wenn $\tilde{K} \to K$, so daß damit ein Kriterium für Näherungen der Green'schen Funktion analog dem Variationsprinzip für Wellenfunktionen gefunden ist. Als zweites, wenn auch schwächeres Kriterium gründet sich auf

$$\Sigma \equiv [\mathrm{tr}\tilde{K}^* \mathrm{tr}\mathscr{S}^2\tilde{K} - |\mathrm{tr}\mathscr{S}\tilde{K}|^2]_{\tau\,\mathrm{avg}} \geqq 0 .$$

Hinweise für das Herausprojizieren der Beträge des Kontinuums aus Δ bzw. Σ und für die Analyse des diskreten Spektrums werden gegeben.

1. Properties of Exact Green's Functions

The Dirac-Feynman Green's function or propagator for a quantum-mechanical system is given by

$$K(q, q', \tau) \equiv \langle q' t' | q t \rangle = \langle q' | \mathscr{T}(\tau) | q \rangle , \tag{1}$$

where $\tau = t - t'$. For time-independent Hamiltonian, the evolution operator takes the simple form

$$\mathscr{T}(\tau) = e^{-i\tau\mathscr{H}} \tag{2}$$

so that the Green's function has the following spectral representation in terms of the energy eigenstates:

$$K(q, q', \tau) = \sum_n \psi_n(q)\, \psi_n^*(q')\, e^{-i\omega_n \tau} . \tag{3}$$

In principle therefore, if K is known, the complete spectrum of eigenstates is accessible by fourier analysis [1].

---

* National Science Foundation Senior Postdoctoral Fellow 1970–1971. Permanent address: Department of Chemistry, University of Michigan, Ann Arbor, Michigan 48104.

The Green's function is a solution of the time-dependent Schrödinger equation in both unprimed and primed coordinates:

$$\mathscr{S}\,K(q,q',\tau)=\mathscr{S}'^{\dagger}K(q,q',\tau)=0 \tag{4}$$

with the initial condition

$$K(q,q',0)=\delta(q-q'). \tag{5}$$

For convenience, we have defined the "Schrödinger operator"

$$\mathscr{S}\equiv i\frac{\partial}{\partial t}-\mathscr{H}=i\frac{\partial}{\partial\tau}-\mathscr{H}. \tag{6}$$

Accordingly, $\mathscr{S}'=i\partial/\partial t'-\mathscr{H}'=-i\partial/\partial\tau-\mathscr{H}'$ and $\mathscr{S}'^{\dagger}=i\partial/\partial\tau-\mathscr{H}'$. We note, incidentally, that $K(q,q',\tau)$ is technically the Green's function for the inverse evolution operator, i.e.

$$\mathscr{T}^{\dagger}(\tau)\,K(q,q',\tau)=\delta(q-q'). \tag{7}$$

Better known in the quantum theory of scattering are time-dependent Green's functions which are solutions of

$$\mathscr{S}\,G(q,q',\tau)=\delta(\tau)\,\delta(q-q'). \tag{8}$$

These are evidently related to K as follows:

$$\begin{aligned} G_{\text{ret}}(q,q',\tau)&=-i\Theta(\tau)\,K(q,q',\tau),\\ \text{or}\qquad G_{\text{adv}}(q,q',\tau)&=i\Theta(-\tau)\,K(q,q',\tau),\end{aligned} \tag{9}$$

where $\Theta(\tau)$ is the unit step function. Conversely,

$$K(q,q',\tau)=i\left[G_{\text{ret}}(q,q',\tau)-G_{\text{adv}}(q,q',\tau)\right]. \tag{10}$$

2. Approximate Green's Functions

Supposing the exact Green's function for a particular quantum system to be unavailable, we should like to deal with approximation functions $\tilde{K}(q,q',\tau)$ with a view toward extracting approximate eigenvalues and eigenfunctions. Primarily, we shall focus on the discrete eigenvalue spectrum.

Accordingly, let an otherwise arbitrary function $\tilde{K}(q,q',\tau)$ conform to the following conditions (which all apply to exact Green's functions):

i) $\tilde{K}(q,q',\tau)$ obeys the same analyticity, continuity, boundary, permutation and symmetry conditions as are appropriate to $K(q,q',\tau)$.

ii) $\tilde{K}^{*}(q,q',\tau)=\tilde{K}(q',q,-\tau)$.

iii) $\tilde{K}(q,q'',\tau_1)\cdot\tilde{K}(q'',q',\tau_2)=\tilde{K}(q,q',\tau_1+\tau_2)$, scalar product signifying integration over q''.

iv) $\tilde{K}(q,q',0)=\delta(q-q')$.

As shown in the Appendix, conformity with (i)–(iv) specifies a function possessing the formal structure

$$\tilde{K}(q,q',\tau)=\sum_{n}\phi_n(q)\,\phi_n^{*}(q')\,e^{-i\lambda_n\tau} \tag{11}$$

in which $\{\phi_n(q)\}$ represents some complete orthonormal set spanning the same function space as the eigenfunctions $\{\psi_n(q)\}$ and $\{\lambda_n\}$ is some associated set of real numbers.

Presuming that $\mathscr{S}\tilde{K} \neq 0$, so that $\tilde{K}$ is not the exact Green's function, define the parameter

$$\Delta \equiv \operatorname{tr}[\mathscr{S}\tilde{K} \cdot (\mathscr{S}\tilde{K})^*] . \tag{12}$$

By writing this in the redundant form

$$\Delta = \operatorname{tr}[\tilde{K}^* \cdot \mathscr{S}\tilde{K} \cdot (\mathscr{S}\tilde{K})^* \cdot \tilde{K}] \tag{13}$$

it follows most directly that Δ has the formal structure

$$\Delta = \sum_m \sum_n |\lambda_n \delta_{mn} - H_{mn}|^2 \tag{14}$$

with

$$H_{mn} \equiv (\phi_m, \mathscr{H} \phi_n) . \tag{15}$$

By reduction of (14), or directly from (12), we find alternatively

$$\Delta = \sum_n [\lambda_n^2 - 2\lambda_n H_{nn} + (H^2)_{nn}] = \sum_n [(\lambda_n - H_{nn})^2 + \sigma_n^2] , \tag{16}$$

where each σ_n represents an energy variance, i.e.

$$\sigma_n^2 \equiv (H^2)_{nn} - (H_{nn})^2 = (\phi_n, [\mathscr{H} - H_{nn}]^2 \phi_n) \geqq 0 . \tag{17}$$

Equivalent forms for Δ, as suggested by (16), are

$$\Delta = \operatorname{tr} \mathscr{S}^2 \tilde{K}|_{t=0} = [\operatorname{tr} \tilde{K}^* \operatorname{tr} \mathscr{S}^2 \tilde{K}]_{t\,\mathrm{avg}} \tag{18}$$

and, in any case,

$$\Delta \geqq 0 . \tag{19}$$

The summation (14) runs over the elements of the infinite secular determinant for the Hamiltonian in the basis $\{\phi_n(q)\}$. Clearly, Δ can vanish only if $\{\phi_n\}$ diagonalizes $\mathscr{H}$, which means that $\phi_n = \psi_n$, $\lambda_n = \omega_n$, for all n. Alternatively, from (16), it follows that Δ can vanish only if each $\sigma_n = 0$. This, in turn, implies that each $H_{nn} = \omega_n$, the corresponding exact eigenvalue, and that each $\lambda_n = \omega_n$.

Comparing (11) with (3), it follows that, as $\Delta \to 0$, $\tilde{K} \to K$, the true Green's function. Failure of Δ, as defined, to exist indicates that $\tilde{K}$ deviates too greatly from K for the sums over n to converge. Should $\tilde{K}$ depend on one or more adjustable parameters, the minimization condition

$$\delta\Delta = 0, \qquad \delta^2 \Delta > 0 \tag{20}$$

would provide an optimization criterion on $\tilde{K}$ analogous to the variational principle for wavefunctions:

Eq. (20) can, in a more abstract sense, be treated as a condition on the functional $\Delta(\tilde{K})$. Applied to (12),

$$\delta\Delta(\tilde{K}) = \operatorname{tr}[\mathscr{S}\delta\tilde{K} \cdot (\mathscr{S}\tilde{K})^*] + \operatorname{tr}[\mathscr{S}\tilde{K} \cdot (\mathscr{S}\delta\tilde{K})^*] = 0 \tag{21}$$

with respect to unrestricted variation in $\tilde{K}$ (consistent however with (i)–(iv) above). Eq. (21) is fulfilled only if $\mathscr{S}\tilde{K}=0$, wherein $\tilde{K}=K$. Eq. (20) thereby represents the variational counterpart of the differential equation $\mathscr{S}K=0$ – being therefore analogous to the Ritz variational theorem for wavefunctions.

It might also be of interest to consider the alternative parameter

$$\Sigma \equiv [\operatorname{tr}\tilde{K}^* \operatorname{tr}\mathscr{S}^2\tilde{K} - |\operatorname{tr}\mathscr{S}\tilde{K}|^2]_{\tau\,\mathrm{avg}} \tag{22}$$

which represents the sum of the squares of the energy variances:

$$\Sigma = \sum_n \sigma_n^2 . \tag{23}$$

In place of $\mathscr{S}$ in (22), $\mathscr{H}$ can be written, since dependence on the λ_n cancels out. Clearly, $\Sigma \to 0$ as $\tilde{K} \to K$. Vanishing of Σ is not however a sufficient condition for an exact Green's function: for example, a function having the structure

$$\tilde{K}(q, q', \tau) = \sum_n \psi_n(q)\, \psi_n^*(q')\, e^{-i\lambda_n\tau} \tag{24}$$

in which $\lambda_n \neq \omega_n$ for at least one n, also gives $\Sigma = 0$.

One convenient way to ensure that $\tilde{K}$ has the requisite structure (11) is to employ a known Green's function, say K_0, for a related "unperturbed" Hamiltonian $\mathscr{H}_0$, such that

$$\mathscr{H} = \mathscr{H}_0 + \mathscr{V} . \tag{25}$$

The corresponding Schrödinger operator is then of the form

$$\mathscr{S} = \mathscr{S}_0 - \mathscr{V} , \tag{26}$$

wherein

$$\mathscr{S}_0 K_0 = 0 . \tag{27}$$

Under this simplification, we can write

and

$$\begin{aligned} \Delta &= \operatorname{tr}[\mathscr{V}K_0 \cdot (\mathscr{V}K_0)^*] \\ \Sigma &= [\operatorname{tr}K_0^* \operatorname{tr}\mathscr{V}^2 K_0 - |\operatorname{tr}\mathscr{V}K_0|^2]_{\tau\,\mathrm{avg}} , \end{aligned} \tag{28}$$

in effect, a transformation to interaction picture.

3. Projecting out the Continuum

Convergence of Δ and Σ might be promoted by eliminating continuum contributions in the corresponding summations. This would be particularly desirable if one were interested only in the discrete spectrum. How to do this is suggested by the asymptotic behavior of continuum eigenfunctions. The limit

$$\lim_{\Delta Q \to \infty} \int_{\Delta Q} |\psi_\nu(q)|^2 \,\mathrm{d}q \tag{29}$$

will not, of course, exist owing to the δ-function normalization of $\psi_\nu(q)$. However for any wavefunction whose asymptotic behavior approaches that of a free particle

$$\int_{\Delta Q} |\psi_\nu(q)|^2 \,\mathrm{d}q = O[(\Delta Q)^N] \tag{30}$$

as $\Delta Q \to \infty$ for some N (not necessarily an integer). This suggests the following definition of the principal part of an improper integral:

$$\mathscr{P}\int F(q)\,\mathrm{d}q \equiv \lim_{\Delta Q\to\infty} \int_{\Delta Q} [F(q)-(\Delta Q)^{N-1}F_N]\,\mathrm{d}q\,, \tag{31}$$

where

$$F_N \equiv \lim_{\Delta Q\to\infty} \left[(\Delta Q)^{-N}\int_{\Delta Q} F(q)\,\mathrm{d}q\right]. \tag{32}$$

Should (31) itself diverge as $O[(\Delta Q)^{N'}]$ $(N'<N)$, the definition can obviously be generalized to

$$\mathscr{P}\int F(q)\,\mathrm{d}q \equiv \lim_{\Delta Q\to\infty} \int_{\Delta Q} \left[F(q)-\sum_N (\Delta Q)^{N-1}F_N\right]\mathrm{d}q\,. \tag{33}$$

The latter is likely to pertain to expectation value integrals of the form

$$\int \psi_\nu^*(q)\,\mathscr{A}\,\psi_\nu(q)\,\mathrm{d}q\,. \tag{34}$$

Convergent integrals over normalizable eigenfunctions are retained under the projection operation represented by (31) or (33).

One can generalize further for asymptotic behavior such as $O(e^{\alpha\Delta Q})$ or the like but such instances are unlikely in the present application. The technique will, in fact, fail only if isolated singularities cause $\int_{\Delta Q} F(q)\,\mathrm{d}q$ itself to diverge.

In the case of the free particle itself, the integral (30) goes as $O(V)$ in cartesian coordinates or as $O(V^{1/3})=O(r)$ in spherical polar coordinates. In either case, the principal part (31) equals zero. Likewise for coulomb wavefunctions, such as hydrogen atom continuum eigenfunctions, the projected overlap integral vanishes.

We assert therefore that application of (33) to a Green's function with the general structure (11) gives

$$\mathscr{P}\,\mathrm{tr}\,\mathscr{A}\tilde{K} = \sum_n A_{nn}e^{-i\lambda_n\tau} \tag{35}$$

the original summation having become truncated such as to retain only its discrete components. Of course, the sum (35) might still diverge. But application of this projection technique to calculation of Δ and Σ cannot fail to facilitate convergence. We define accordingly

$$\begin{aligned} \Delta' &\equiv \mathscr{P}\mathrm{tr}[\mathscr{S}\tilde{K}\cdot(\mathscr{S}\tilde{K})^*] = \sum_n [(\lambda_n - H_{nn})^2+\sigma_n^2] \\ \Sigma' &\equiv [\mathscr{P}\mathrm{tr}\tilde{K}^*\mathscr{P}\mathrm{tr}\mathscr{S}^2\tilde{K} - |\mathscr{P}\mathrm{tr}\mathscr{S}\tilde{K}|^2]_{\tau\,\mathrm{avg}} = \sum_n \sigma_n^2\,. \end{aligned} \tag{36}$$

As $\Delta' \to 0$, the approach of $\tilde{K}$ to K is implied with certainty only with regard to discrete spectral content. But this will be adequate in the applications we propose.

4. Spectral Analysis

Once a Green's function has been optimized in accordance with the foregoing procedures, one can fourier analyze to obtain approximate eigenfunctions and eigenvalues. Specifically, for the discrete eigenvalue spectrum, it is convenient to compute $\operatorname{tr}\tilde{K}$ before spectral analysis. In fact,

$$\mathscr{P}\operatorname{tr}\tilde{K} = \sum_n e^{-i\lambda_n\tau} = \sum_j g_j e^{-i\lambda_j\tau} \tag{37}$$

in which the latter form takes explicit account of degeneracies. Note also that

$$\mathscr{P}\operatorname{tr}\mathscr{H}\tilde{K} = \sum_n H_{nn} e^{-i\lambda_n\tau} \tag{38}$$

and

$$\mathscr{P}\operatorname{tr}\mathscr{H}^2\tilde{K} = \sum_n (H^2)_{nn} e^{-i\lambda_n\tau}. \tag{39}$$

By fourier analysis of (38), one can extract both the λ_n as frequencies and the H_{nn} as weight factors. Coupled with analysis of (39), this provides sufficient data to determine the energy variances σ_n(cf. (17)). By Weinstein's theorem [2], some exact eigenvalue must be bracketed by each $H_{nn} \pm \sigma_n$. Stronger bracketing conditions can be deduced by making use of the distribution of neighboring eigenvalues. There does not appear to be any condition relating the λ_n to exact eigenvalues. The best choice of approximate energy eigenvalues is evidently provided by $\tilde{\omega}_n = H_{nn}$, obtained from (38).

The summations (37), (38) and (39) have the form of Dirichlet series for almost periodic functions. It has been assumed in the preceding that they do indeed exist - expecting, at most, a countable set of points τ. This assumption certainly merits further discussion, which we shall defer however until specific cases – e.g. atomic eigenvalue spectra – are taken up.

Acknowledgements. I should like to thank Professor R. Daudel in Paris and Professor C. A. Coulson in Oxford for their very generous hospitality during the progress of this work. The National Science Foundation provided financial support through a Senior Postdoctoral Fellowship for the academic year 1970–1971.

Appendix

Structure of $\tilde{K}(q, q', \tau)$

A function obeying condition (i) can be formally expanded in the eigenfunctions of $\mathscr{H}$ as follows:

$$\tilde{K}(q, q', \tau) = \sum_n C_n(q', \tau)\, \psi_n(q). \tag{A.1}$$

By virtue of (ii) however

$$\tilde{K}(q, q', \tau) = \tilde{K}^*(q', q, -\tau) = \sum_n C_n^*(q, -\tau)\, \psi_n^*(q'). \tag{A.2}$$

Eqs. (A.1) and (A.2) are therefore consistent with the general bilinear expansion

$$\tilde{K}(q, q', \tau) = \sum_m \sum_n c_{mn}(\tau)\, \psi_n(q)\, \psi_m^*(q') \tag{A.3}$$

with

$$c_{mn}(-\tau) = c_{nm}^*(\tau). \tag{A.4}$$

Property (iii) implies the following composition rule among the coefficients:

$$\sum_k c_{mk}(\tau_1)\, c_{kn}(\tau_2) = c_{mn}(\tau_1 + \tau_2) = \sum_k c_{mk}(\tau_2)\, c_{kn}(\tau_1). \tag{A.5}$$

The c-matrices for different τ evidently commute among themselves. They can accordingly be diagonalized by the same unitary transformation. Let $\{\phi_n(q)\}$ represent the basis set arrived at by the corresponding unitary transformation on the eigenfunctions. The expansion (A.3) can therefore be specialized to a quadratic form

$$\tilde{K}(q, q', \tau) = \sum_n c_n(\tau)\,\phi_n(q)\,\phi_n^*(q'), \tag{A.6}$$

whereas (A.5) simplifies to

$$c_n(\tau_1)\,c_n(\tau_2) = c_n(\tau_1 + \tau_2). \tag{A.7}$$

The last relation can only be fulfilled by linear exponential dependence on τ. Consistent with (A.4), in fact,

$$c_n(\tau) = e^{-i\lambda_n\tau}, \tag{A.8}$$

having written $-\lambda_n$ for an arbitrary real constant. Condition (iv) requires lastly that the above summations run over the complete set of basis functions, consistent with the closure relation

$$\sum_n \phi_n(q)\,\phi_n^*(q') = \delta(q - q'). \tag{A.9}$$

We arrive finally at Eq. (11), showing $\tilde{K}$ to have a formal structure analogous to that of K.

The same result can be demonstrated more compactly as follows. Condition (i) implies that there exists some operator $\tilde{\mathscr{T}}(\tau)$ on the same function space as $\mathscr{T}(\tau)$ having the configuration representative

$$\tilde{K}(q, q', \tau) = \langle q'|\tilde{\mathscr{T}}(\tau)|q\rangle \tag{A.10}$$

analogous to (1). If $\tilde{\mathscr{T}}$ is required to be unitary and to obey the composition relation

$$\tilde{\mathscr{T}}(\tau_1)\,\tilde{\mathscr{T}}(\tau_2) = \tilde{\mathscr{T}}(\tau_1 + \tau_2) = \tilde{\mathscr{T}}(\tau_2)\,\tilde{\mathscr{T}}(\tau_1) \tag{A.11}$$

then, by the Stone-von Neumann theorem, it must have the structure

$$\tilde{\mathscr{T}}(\tau) = e^{-i\tau\mathscr{A}}, \tag{A.12}$$

where $\mathscr{A}$ is an hermitian operator on the same space. If λ_n and $\varphi_n(q)$ are, respectively, the eigenvalues and eigenfunctions of $\mathscr{A}$, then $\tilde{\mathscr{T}}(\tau)$ has the spectral representation corresponding to Eq. (11).

References

1. Blinder, S. M.: Int. J. Quant. Chemistry **1**, 285 (1967).
2. Weinstein, D. H.: Proc. Nat. Acad. Sci. **20**, 529 (1934).

Prof. S. M. Blinder
Department of Chemistry,
University of Michigan,
Ann Arbor, Michigan 48104, USA

Theoret. chim. Acta (Berl.) 24, 389—392 (1972)
© by Springer-Verlag 1972

CNDO/2 Calculation of Prototropic Rearrangement in Cyclopentadiene

G. A. Shchembelov and Yu. A. Ustynyuk

NMR Laboratory, Chemical Division, M.V. Lomonosov State University, Moscow B-234

Received July 13, 1971

A self-consistent procedure has been worked out for the optimisation of geometrical parameters of ground and transition states of molecular systems and chemical reactions. For cyclopentadiene molecule, the CNDO/2 method is used to calculate a number of the geometrical configurations which lie at the reaction co-ordinates corresponding to possible channels of the proton migration.

Deuteriated cyclopentadienes, as well as sigma-cyclopentadienyl compounds, were reported to rearrange through the 1,2 migration of proton or deuterium [1–3]. The rearrangement was proved to be intramolecular [4].

Various multi-centre mechanisms of the migration may be assumed. E.g., proton or deuterium may migrate in sigma-cyclopentadienyl compounds via the formation of two-centre (2C), three-centre (3C), and five-centre (5C) bonds between a hydrogen and the ring carbons.

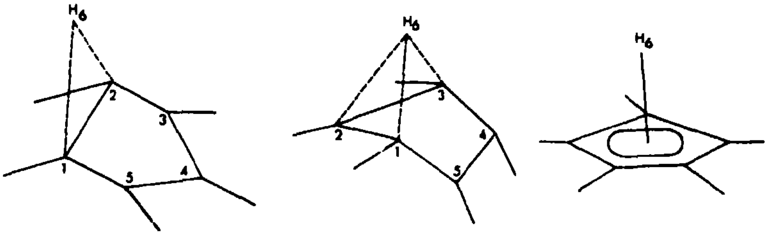

(2C) (3C) (5C)

Fig. 1

The 3C and 5C transition states require that a usual carbon-hydrogen bond become much longer, hence a priori they must have greater energies.

Other transition states may also be possible, e.g. the 3CA state:

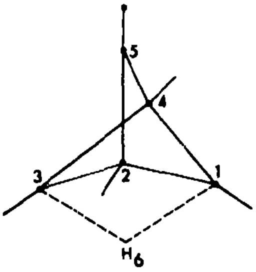

(3CA)

Fig. 2

In structural chemistry terms, however, the structures such as 3CA must have very high energies, in other words, the resulting C–C bonds would be subject to noticeable strain.

Cyclopentadiene is a simplest sigma-cyclopentadienyl molecule in which a prototropic rearrangement is possible.

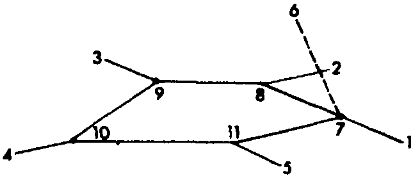

(2)

Fig. 3.

We have calculated the ground state (GS) and the states 2C, 3C, and 5C, of the molecule by using a self-consistent optimisation of the geometrical parameters [5] with the total energy minimum obtained through CNDO/2 (Ref. [6]) serving as the criterion. GS has been approximated to have the C_{2v} symmetry, 2C and 3C states the plane of symmetry perpendicular to the lines C_1C_2 (for 2C) and $C_1C_1C_3$ (for 3C), the state 5C the C_{5v} symmetry.

The results are summarised in the Table. The Table also includes the microwave spectroscopy data [7]. When comparing these with the experiment, one comes to the conclusion (cf. the calculations by Fischer and Kollmar [8]) that CNDO/2 gives too low values for the C–C single bond while the calculation of shorter (double, one and one half) C–C bonds fits with the experiment somewhat better.

As for calculated CH bond lengths, they were reported to be on the average 0.01 Å higher than the experimental values [8]. This is the case with our calculation as well.

The 3C and 5C states are specific in that their H_6 atom is slightly attracted by the nearest hydrogen. E.g., H_2 in 3C declines from the $C_1C_3C_4C_5$ plane by ca. 2.1° towards the proton H_6. H_2, H_3, H_4, H_5, H in 5C decline along the same direction by 1.1°. For the 2C state the situation is as follows. The perpendicular dropped from the point H_6 to the line C_1C_2 forms the angle of 92.2° with the plane $H_2C_1C_2H_3$, the analogous angle is equal to 104.3° for the plane $C_5C_1C_2C_3$, and the H_6 atom is repulsed by the ring plane much stronger than it is by the hydrogens H_2 and H_3.

Further, the C_1C_2 bond length calculated for the 2C state is nearly equal to that for GS.

Total energy values listed in the Table show that proton is much more likely to migrate via the 2C state as compared with the states 3C and 5C, in other words, the migration consists in successive 1,2 shifts. These were verified experimentally. We plan to program the automatic search of the transition state responsible for the shift. This state is anticipated to resemble, or coincide with, the 2C state.

The 3C state is located, most probably, at the reaction co-ordinate responsible for the proton migration to the state 5C. This needs not be discussed in more

Table 1. The calculated geometry of various configurations of cyclopentadiene[a]

Variable	GS calcd.	GS exptl.	2C	3C	5C
1. (*m*, *n*)[b]					
(1, 7)	1.122	–	1.114	1.109	1.111
(2, 8)	1.112	–	1.111	1.114	1.111
(3, 9)	1.112	–	1.111	1.110	1.111
(6, 7)	1.122	–	1.595	1.229	1.477
(6, 8)	2.152	–	2.215	1.556	1.477
(6, 9)	3.080	–	1.279	1.840	1.477
(7, 8)	1.467	1.509	1.393	1.424	1.418
(8, 9)	1.348	1.342	1.404	1.413	1.418
(9, 10)	1.446	1.469	1.470	1.406	1.418
2. (*p*, *q*, *r*)[c]					
(1, 7, 6)	106.2	–	157.6	123.0	–
(1, 7, 8)	111.7	–	124.6	116.0	–
(7, 8, 2)	122.6	–	126.9	126.5	126.0
(2, 8, 9)	127.9	–	125.6	125.8	126.0
(3, 9, 10)	124.0	–	125.5	127.3	126.0
(3, 9, 8)	127.3	–	126.0	124.2	126.0
(11, 6, 8)	64.7	–	62.4	95.4	–
(10, 6, 9)	27.2	–	70.2	44.9	–
(11, 7, 8)	103.8	102.5	110.9	107.9	108.0
(7, 8, 9)	109.5	109.2	107.5	107.1	108.0
(8, 9, 10)	108.7	109.2	107.1	108.5	108.0
3. (*m*, *n*) (*p*, *q*, *r*)[d]					
(7, 1) (11, 7, 8)	53.1	–	– 0.8	– 0.2	1.1
(8, 2) (10, 8, 9)	0	–	– 0.6	2.1	1.1
(9, 3) (10, 8, 9)	0	–	– 10.5	0.4	1.1
4. (*p*, *q*, *r*) (*s*, *t*, *u*)[e]					
(6, 9, 10) (10, 9, 8)	–	–	104.3	–	–
(7, 8, 11) (11, 8, 9)	0	–	0.4	9.4	0
5. $-g$[f]					
	1088.67	–	1088.21	1086.02	1084.28

[a] Distances are in Å, angles in degrees. The atoms are numbered in the scheme (2).

[b] The internuclear distance between atoms numbered by *m* and *n*.

[c] The planar angle.

[d] The angle formed by bond (*mn*) and plane (*p*, *q*, *r*). The angle is arbitrarily assumed positive when the bond deviates towards H_6.

[e] The dihedral angles.

[f] Total energy multiplied by – 1, eV.

detail since the total energies demonstrate that the 3C and 5C state are, in usual conditions, rather improbable.

Acknowledgements. The authors heartily appreciate the co-operation of I. P. Gloriozov, V. V. Sushchenko, and A. A. Zenkin who helped in the programming; thanks are also due to A. V. Grib and Yu. G. Bundel' for their interest in the work and for the valuable discussion.

References

1. Mironov, V. A., Sobolev, E. V., Elizarova, A. N.: Tetrahedron **19**, 1939 (1963).
2. Roth, W.: Tetrahedron Letters **1964**, 1009.
3. Avramenko, G. I., Sergeyev, N. M., Ustynyuk, Yu. A.: J. organomet. Chem. (in press).
4. McLean, S., Haynes, P.: Tetrahedron **21**, 27 (1965).
5. Shchembelov, G. A., Ustynyuk, Yu. A.: To be published.
6. Pople, I. A., Segal, G. A.: J. chem. Physics **44**, 3289 (1966).
7. Sharpen, L. H., Laurie, V. W.: J. chem. Physics **43**, 2760 (1965).
8. Fischer, H., Kollmar, H.: Theoret. chim. Acta (Berl.) **13**, 213 (1969).

Dr. G. A. Shchembelov
NMR Laboratory
Chemical Division
M.V. Lomonosov State University
Moscow B-234, USSR

Theoret. chim. Acta (Berl.) 24, 393—395 (1972)
© by Springer-Verlag 1972

SCF MO INDO Calculation of Anisotropic Hyperfine Coupling Tensors for σ-Type Radicals

TETSUO MORIKAWA and OSAMU KIKUCHI
Department of Chemistry, Tokyo Kyoiku University, Otsuka, Tokyo, Japan

KAZUO SOMENO
Government Chemical Industrial Research Institute, Tokyo, Shibuya, Tokyo, Japan

Received October 21, 1971

The anisotropic hyperfine coupling tensors for some σ-type radicals (HCO, FCO, NO_2, CO_2^-, CN, phenyl, vinyl) were calculated. The calculation was performed with an all-valence-electron approximate open-shell MO method using the INDO approximation and with the dipolar integrals evaluated over Slater-type AO's. The diagonalyzed tensors were in reasonable agreement with the available data of experiment.

There have been relatively few theoretical studies of the anisotropic hyperfine coupling constants. Some of the reasons for this may be: (a) the experimental data of anisotropic hyperfine structure are less abundant than those for isotropic cases, (b) the theoretical evaluation of anisotropic interaction requires the appropriate theoretical formula in addition to the spin density calculation. The anisotropic term of the hyperfine interaction gives valuable information about the electronic structure of the paramagnetic species, for it is possible from the anisotropic term to estimate both the *p*-character of the odd-orbital centered on the atom of which the nucleus interacts with an unpaired electon and the *s*- and *p*-character of the odd-orbitals on the neighbouring atoms. A theoretical study on this subject will be useful in predicting magnitudes and signs of hyperfine coupling constants, and in interpreting known hyperfine coupling constants in terms of the electronic structure of the species.

Table 1. Contribution of each atom to the hyperfine tensor for HCO (MHz)

Nucleus	Atom	A_{XX}	A_{XY}	A_{YY}	A_{ZZ}[a]
^1H	H	0.0	0.0	0.0	0.0
	C	− 7.1	6.6	20.8	−13.7
	O	4.2	3.5	− 1.0	− 3.2
	Total	− 2.8	10.1	19.8	−16.9
^{13}C	H	− 0.5	2.5	2.5	− 1.9
	C	− 8.3	−30.4	32.8	−24.4
	O	5.5	1.3	− 2.2	− 3.3
	Total	− 3.4	−26.6	33.1	−29.7
^{17}O	H	− 0.3	− 0.3	0.1	0.2
	C	− 2.3	1.1	0.8	1.6
	O	26.6	27.7	−66.0	36.8
	Total	29.3	28.5	−65.2	38.6

[a] The molecular axes *X*, *Y*, and *Z* are along the C—O bond and perpendicular to *X* and *Z*, and to the molecular plane, respectively. All A_{XZ} and A_{YZ} are equal to zero.

The anisotropic hyperfine coupling tensor for the nucleus N of a radical, $A_{ij}(\mathrm{N})$ $(i, j = X, Y, Z)$, may be derived from the expectation value $\langle \Psi_g | H | \Psi_g \rangle$, where Ψ_g is an all-antisymmetrized wave function [1], and H is the Hamiltonian of anisotropic hyperfine interaction. Molecular orbitals ϕ_i are expressed as linear combinations of atomic orbitals $\chi_\mu : \phi_i = \Sigma \chi_\mu C_{\mu i}$. Thus,

$$A_{ij}(\mathrm{N}) = -g\beta\hbar\gamma_{\mathrm{N}} \sum_{\mu,\nu} C_{\mu m} C_{\nu m} t_{ij}(\chi_\mu \chi_\nu) ,$$
$$t_{ij}(\chi_\mu \chi_\nu) = \langle \chi_\mu | r^{-5}(r^2 \delta_{ij} - 3 r_i r_j) | \chi_\mu \rangle . \tag{1}$$

The dipolar integrals $t_{ij}(\chi_\mu \chi_\nu)$, were evaluated at the level of approximation corresponding to that employed in the INDO calculation of Ψ_g. Namely, all three-

Table 2. Calculated principal values (MHz) for some σ-radicals (data in parentheses are experimental)

Radical	Nucleus	A_{xx}	A_{yy}	A_{zz}	Ref.
HCO	^{1}H	24	− 7	− 17	
		(15)	(− 2)	(− 14)	[2]
		(25)	(− 8)	(− 17)	[3]
	^{13}C	− 17	47	− 30	
		(− 39)	(50)	(− 12)	[2]
		(− 48)	(72)	(− 24)	[3]
	^{17}O	35	− 73	39	
		—	—	—	
FCO	^{13}C	38	− 13	− 25	
	^{17}O	− 73	35	38	
		—	—	—	
	^{19}F	389	−191	−198	
		(534)	(−267)	(−267)	[2]
NO$_2$	^{14}N	− 8	22	− 14	
		(− 22)	(37)	(− 15)	[4]
	^{17}O	− 68	32	36	
		(− 97)	(52)	(45)	[4]
CO$_2$	^{13}C	− 12	44	− 32	
		(− 47)	(79)	(− 33)	[5]
	^{17}O	− 54	26	28	
		(− 53)	(25)	(28)	[5]
CN	^{13}C	− 36	72	− 36	
		(− 45)	(90)	(− 45)	[6]
	^{14}N	− 14	29	− 14	
		(− 15)	(31)	(− 15)	[6]
Phenyl	^{13}C$_1$	− 40	84	− 44	
		—	—	—	
	^{13}C$_2$	11	− 3	− 7	
		—	—	—	
	^{1}H$_2$	− 4	11	− 7	
		(− 6)	(13)	(− 7)	[7]
CH$_2$=CH	^{13}C$_1$	− 46	96	− 49	
		—	—	—	
	^{1}H$_1$	34	− 7	− 26	
		(38)	(− 11)	(− 27)	[8]

center integrals and all two-center integrals involving the product $\chi_\mu \chi_\nu$ in which μ and ν belong to different atoms were assumed to be negligible, and the remaining two-center and one-center integrals were analytically evaluated over Slater orbitals. An approximate open-shell SCF MO INDO method used for the calculation of spin density has been reported in elsewhere [1].

The hyperfine tensor for the magnetic nucleus is obtained from the total of contribution of each atom, according to Eq. (1). The calculated results of the formyl radical HCO shown in Table 1 indicate that to the tensor for the carbon-13 or oxygen-17 nucleus the orbitals centered on the same nucleus mainly contribute, and to the tensor for the proton the orbitals of oxygen atom do to some extent. The three tensors were diagonalyzed and the results compared with the available data of experiment in Table 2, where x, y, and z denote the principal axes. The agreement is satisfactory for the proton, but not quantitatively satisfactory for the carbon-13, especially for A_{xx}. The orientation of the principal axes with respect to the molecular frame can be estimated by the direction cosines obtained. The angle between x and C—H bond for ^{1}H or ^{13}C is 69° or 28°, respectively. The dependence of the principal values for HCO on H—C—O angle is not large, e.g., A_{xx}(H), A_{yy}(H), and A_{zz}(H) in MHz units are 27, -9, and -18 for 130°, 24, -7, and -17 for 120°, 20, -5, and -16 for 110°, respectively.

Calculated principal values for other σ-type radicals are shown in Table 2. No signs of anisotropic hyperfine splitting can be determined by ESR experiment. It may be noted that the signs of some observed data are assigned by the calculated results and listed in Table 2. The calculated tensors for nuclei which are one or more bonds away from the radical-center are in relatively satisfactory agreement with the observed values, e.g., for the proton of vinyl or phenyl, for the nitrogen-14 of CN.

References

1. Morikawa, T., Kikuchi, O., Someno, K.: Theoret. chim. Acta (Berl.) **22**, 224 (1971).
2. Cochran, E. L., Adrian, F. J., Bowers, V. A.: J. chem. Physics **44**, 4626 (1966).
3. Holmberg, R. W.: J. chem. Physics **51**, 3255 (1969).
4. Luz, Z., Reuveni, A., Homverg, R. W., Silver, B. L.: J. chem. Physics **51**, 4017 (1969).
5. Schlick, S., Silver, B. L., Luz, Z.: J. chem. Physics **54**, 867 (1971).
6. Easley, W. C., Weltner, W., Jr.: J. chem. Physics **52**, 197 (1970).
7. Kasai, P. H., Hedaya, E., Whipple, E. B.: J. Amer. chem. Soc. **91**, 4364 (1969).
8. Iwasaki, M., Eda, B.: J. chem. Physics **52**, 3837 (1970).

Dr. T. Morikawa
Department of Chemistry
Tokyo Kyoiku University
Otsuka, Tokyo, Japan